

Ecological restoration in drylands: Towards land degradation neutrality

Edited by

Guang-Lei Gao, Jifeng Deng, Shengbo Xie
and Hamid Gholami

Published in

Frontiers in Environmental Science



FRONTIERS EBOOK COPYRIGHT STATEMENT

The copyright in the text of individual articles in this ebook is the property of their respective authors or their respective institutions or funders. The copyright in graphics and images within each article may be subject to copyright of other parties. In both cases this is subject to a license granted to Frontiers.

The compilation of articles constituting this ebook is the property of Frontiers.

Each article within this ebook, and the ebook itself, are published under the most recent version of the Creative Commons CC-BY licence. The version current at the date of publication of this ebook is CC-BY 4.0. If the CC-BY licence is updated, the licence granted by Frontiers is automatically updated to the new version.

When exercising any right under the CC-BY licence, Frontiers must be attributed as the original publisher of the article or ebook, as applicable.

Authors have the responsibility of ensuring that any graphics or other materials which are the property of others may be included in the CC-BY licence, but this should be checked before relying on the CC-BY licence to reproduce those materials. Any copyright notices relating to those materials must be complied with.

Copyright and source acknowledgement notices may not be removed and must be displayed in any copy, derivative work or partial copy which includes the elements in question.

All copyright, and all rights therein, are protected by national and international copyright laws. The above represents a summary only. For further information please read Frontiers' Conditions for Website Use and Copyright Statement, and the applicable CC-BY licence.

ISSN 1664-8714
ISBN 978-2-8325-4758-8
DOI 10.3389/978-2-8325-4758-8

About Frontiers

Frontiers is more than just an open access publisher of scholarly articles: it is a pioneering approach to the world of academia, radically improving the way scholarly research is managed. The grand vision of Frontiers is a world where all people have an equal opportunity to seek, share and generate knowledge. Frontiers provides immediate and permanent online open access to all its publications, but this alone is not enough to realize our grand goals.

Frontiers journal series

The Frontiers journal series is a multi-tier and interdisciplinary set of open-access, online journals, promising a paradigm shift from the current review, selection and dissemination processes in academic publishing. All Frontiers journals are driven by researchers for researchers; therefore, they constitute a service to the scholarly community. At the same time, the *Frontiers journal series* operates on a revolutionary invention, the tiered publishing system, initially addressing specific communities of scholars, and gradually climbing up to broader public understanding, thus serving the interests of the lay society, too.

Dedication to quality

Each Frontiers article is a landmark of the highest quality, thanks to genuinely collaborative interactions between authors and review editors, who include some of the world's best academicians. Research must be certified by peers before entering a stream of knowledge that may eventually reach the public - and shape society; therefore, Frontiers only applies the most rigorous and unbiased reviews. Frontiers revolutionizes research publishing by freely delivering the most outstanding research, evaluated with no bias from both the academic and social point of view. By applying the most advanced information technologies, Frontiers is catapulting scholarly publishing into a new generation.

What are Frontiers Research Topics?

Frontiers Research Topics are very popular trademarks of the *Frontiers journals series*: they are collections of at least ten articles, all centered on a particular subject. With their unique mix of varied contributions from Original Research to Review Articles, Frontiers Research Topics unify the most influential researchers, the latest key findings and historical advances in a hot research area.

Find out more on how to host your own Frontiers Research Topic or contribute to one as an author by contacting the Frontiers editorial office: frontiersin.org/about/contact

Ecological restoration in drylands: Towards land degradation neutrality

Topic editors

Guang-Lei Gao — Beijing Forestry University, China

Jifeng Deng — Shenyang Agricultural University, China

Shengbo Xie — Northwest Institute of Eco-Environment and Resources, Chinese Academy of Sciences (CAS), China

Hamid Gholami — University of Hormozgan, Iran

Citation

Gao, G.-L., Deng, J., Xie, S., Gholami, H., eds. (2024). *Ecological restoration in drylands: Towards land degradation neutrality*. Lausanne: Frontiers Media SA. doi: 10.3389/978-2-8325-4758-8

Table of contents

- 05 **Editorial: Ecological restoration in drylands: toward land degradation neutrality**
Jifeng Deng, Shengbo Xie, Guanglei Gao and Hamid Gholami
- 08 **Effect of the Type of Wind Data on Regional Potential Wind Erosion Estimation**
Li Zhang, Zhongling Guo, Jifeng Li, Chunping Chang, Rende Wang and Qing Li
- 22 **The Natural Suitability of Human Settlements and Their Spatial Differentiation in the Nenjiang River Basin, China**
Yang Zhao and Junling Zhang
- 32 **Microbial Residual Nitrogen Distribution in Brown Earth's Aggregates as Affected by Different Maize Residues and Soil Fertility Levels**
Pingluo Xue, Jiubo Pei, Nan Ma and Jingkuan Wang
- 45 **Ectomycorrhizal Fungi Associated With *Pinus sylvestris* var. *mongolica* Were Altered by Soil Environments With Aging Plantation in a Semi-arid Desert**
Yue Ren, Mishan Guo, Guodong Ding and Yue Wang
- 57 **Artificial Regulation Effect of Plant Retardants on Leaf Anatomical Characteristics of *Elaeagnus Angustifolia***
Chao Zhang, Wanjiao Li, Yong Gao, Zhengzheng Xu and Xiaoning Tian
- 66 **The Optimum Calcium Concentration for Seedling Growth of Mongolian Pine (*Pinus Sylvestris* Var. *Mongolica*) Under Different Soil Types in Northern Semi-Arid Areas of China**
Hui Li, Xiangjun Li, Guangqi Zhang, Xiaohang Weng, Shenglan Huang, Yongbin Zhou, Songzhu Zhang, Liying Liu and Jiubo Pei
- 76 **Spatio-Temporal Evolution of Sandy Land and its Impact on Soil Wind Erosion in the Kubuqi Desert in Recent 30 Years**
Xiaohong Dang, Ya Na, Wenfeng Chi, Jiangjia Zhao, Yuanyuan Zhao, Yue Wang, Xiaoguang Wu and Yuetian Wang
- 90 **Characteristics of Canopy Conductance and Environmental Driving Mechanism in Three Monsoon Climate Regions of China**
Rui-Qiao Wu, Jian-Bo Jia, Wen-De Yan, Lei Hu, Yi-Fan Wang and Yu Chen
- 104 **Characteristics of Energy Distribution in a Desert Ecosystem in Inner Mongolia, Northern China**
Yumeng Pan, Huijie Xiao, Zhiming Xin, Junran Li, Abbas Miri and Qiqi Cao
- 119 **Microclimate and Wind Regime of Three Typical Landscapes in the Northeastern Ulan Buh Desert**
Fengmin Luo, Huijie Xiao, Junliang Gao, Yuan Ma, Xing Li, Junran Li, Abbas Miri, Qiqi Cao and Zhiming Xin

- 129 **Soil Seed Bank Characteristics of *Nitraria tangutorum* *Nebkhas* in a Desert–Oasis Ecotone**
Min Li, Huijie Xiao, Zhiming Xin, Xing Li, Junran Li, Abbas Miri and Qiqi Cao
- 140 **Evapotranspiration and land surface temperature of typical urban green spaces in a semi-humid region: Implications for green management**
Xinhao Li, Yiran Li, Suchuang Di, Yong Niu and Chuanjie Zhang
- 151 **Short-term land degradation driven by livestock grazing does not affect soil properties in semiarid steppe rangelands**
Amale Macheroum and Haroun Chenchouni
- 168 **The branching architecture of *artemisia ordosica* and its resistance to wind erosion**
Zhiqiang Qu, Zhiguo Li, Linxi Hu, Lianyou Liu, Xia Hu, Guoming Zhang, Yanli Lv, Lanlan Guo, Yanyan Yang, Ziqiong Yang and Guodong Han
- 178 **Carbon dioxide fluxes of cyanobacterial crusts and underlying soil under different precipitation patterns in the Ulan Buh Desert, China**
Lili Wang, Ying Gao, Xiaoming Cao and Weiwei Lu
- 188 **Relationship between species distribution of sandy alpine grasslands and microtopography in the source regions of Yangtze river**
Peng Zhao, Xianying Xu, Jinnian Tang and Shengxiu Jiang
- 199 **The relationship between succession and reclamation of desertified areas in artificial forests of *Calligonum* spp. in an arid desert of southeastern Iran**
Mahdieh Ebrahimi and Morteza Saberi
- 213 **Monitoring the severity of degradation and desertification by remote sensing (case study: Hamoun International Wetland)**
Farhad Zolfaghari, Hossein Azarnivand, Hasan Khosravi, Gholamreza Zehtabian and Shahram Khalighi Sigaroudi



OPEN ACCESS

EDITED AND REVIEWED BY
Niall Patrick Hanan,
New Mexico State University, United States

*CORRESPONDENCE
Jifeng Deng,
✉ jifeng-deng@syau.edu.cn

RECEIVED 09 January 2024
ACCEPTED 17 January 2024
PUBLISHED 25 March 2024

CITATION
Deng J, Xie S, Gao G and Gholami H (2024),
Editorial: Ecological restoration in drylands:
toward land degradation neutrality.
Front. Environ. Sci. 12:1367580.
doi: 10.3389/fenvs.2024.1367580

COPYRIGHT
© 2024 Deng, Xie, Gao and Gholami. This is an
open-access article distributed under the terms
of the [Creative Commons Attribution License](#)
(CC BY). The use, distribution or reproduction in
other forums is permitted, provided the original
author(s) and the copyright owner(s) are
credited and that the original publication in this
journal is cited, in accordance with accepted
academic practice. No use, distribution or
reproduction is permitted which does not
comply with these terms.

Editorial: Ecological restoration in drylands: toward land degradation neutrality

Jifeng Deng^{1,2,3*}, Shengbo Xie^{4,5}, Guanglei Gao⁶ and
Hamid Gholami⁷

¹College of Forestry, Shenyang Agricultural University, Shenyang, Liaoning Province, China, ²Key Laboratory of Forest Tree Genetics and Breeding of Liaoning Province, Shenyang, Liaoning Province, China, ³Liaoning Fengyu Ecological Technology Co. Ltd., Shenyang, Liaoning Province, China, ⁴Northwest Institute of Eco-Environment and Resources, Chinese Academy of Sciences (CAS), Lanzhou, China, ⁵Key Laboratory of Desert and Desertification, Northwest Institute of Eco-Environment and Resources, Chinese Academy of Sciences (CAS), Lanzhou, China, ⁶Key Laboratory of State Forestry and Grassland Administration on Soil and Water Conservation, Beijing Forestry University, Beijing, China, ⁷Department of Natural Resources Engineering, University of Hormozgan, Bandar-Abbas, Hormozgan Province, Iran

Land degradation neutrality (LDN) has been defined as “a state whereby the amount and quality of land resources necessary to support ecosystem functions and services remains stable or increases within specified temporal and spatial scales and ecosystems.” In practice, the application and success of LDN in drylands vary greatly depending on the targeted ecosystem services and the impacts of environmental conditions and various restoration methods on the efficacy and sustainability of restoration. In this editorial, we summarize the most viewed and downloaded articles contributing to the Research Topic “*Ecological Restoration in Drylands: Toward Land Degradation Neutrality*” of the journal *Frontiers in Environmental Science*.

KEYWORDS

land degradation, ecological restoration, biodiversity, ecosystem services, land degradation neutrality

Editorial on the Research Topic

Ecological restoration in drylands: towards land degradation neutrality

1 Spatiotemporal evolution of drylands and its impact on soil erosion: observations

Given the increasing degradation trend of drylands, continuous remote sensing monitoring of sand or precipitation in drylands is one of the main concerns for governments. In addition, exploration of the spatiotemporal evolution characteristics of soil erosion has great scientific value for desertification and degradation prevention and ecological restoration. This theme is represented by the case study reported by [Dang et al.](#) who showed that differences in sand types contributed most to the reduction of soil–wind erosion intensity, while ecological restoration played a key role in reducing soil erosion

intensity. Their study also indicated that the increase in forest and grass vegetation cover and agricultural oases play a positive role in soil restoration and wind-proofing sand and that the pattern of dryland changes in desert areas is closely related to the ecological construction policy and the impact of climate change. Furthermore, detecting the areas subjected to desertification and degradation requiring management within the shortest time and at the lowest cost is a necessity, especially in border areas. This Research Topic is represented by the case study by Zolfaghari et al. who showed that when the surface of a wetland dries, the land surface, which is free of moisture and vegetation, should be classified as being under extreme degradation; when the wetland is flooded, the area of degradation is highly reduced, but contrary to expectations, the land area without any degradation also increased due to temporarily supported vegetation. All these studies address the needs of target 15.3 in the LDN initiative (an accelerator of the Sustainable Development Goal 15): Goal 15 aims to conserve life on land, protect and restore terrestrial ecosystems, sustainably manage forests, combat desertification, and halt and reverse land degradation and stop biodiversity loss; by 2030, Goal 15.3 aims to combat desertification, restore degraded land and soil, including land affected by desertification, drought, and floods, and strive to achieve a land degradation-neutral world (United Nations, Sustainable Development Goals, 2015).

2 Soil and vegetation relationships: experiments

In recent decades, soil restoration and sand transformation methods, including mechanical sand barriers (Bo et al., 2015), biological soil crusts (Li et al., 2011), and afforestation (Deng et al., 2021), have been implemented. In particular, afforestation, plantation, and vegetation methods have been successfully established as feasible methods of environmental management for desertification control in drylands (Tang and Li, 2018; Song et al., 2020). Li et al. conducted a survey in the field and a seed germination experiment in the laboratory to investigate the characteristics of soil seed banks of different sizes and parts of nebkhas and examine their relationship with aboveground vegetation. Ren et al. described a case of ectomycorrhizal fungal communities associated with *Pinus sylvestris* var. *mongolica* that were altered by soil environments with aging plantation in drylands in China. These experiments provide a better understanding of the relationship between soil properties and vegetation, which is critical to sustainable forest management and biodiversity restoration in the future. The work mentioned above meets the needs of the Aichi Biodiversity Targets in LDN (ways LDN can support each of the strategic goals for biodiversity conservation): “enhance benefits to all from biodiversity and ecosystem services.”

3 Characteristics of water–carbon exchanges and environmental driving mechanisms in drylands: modeling

We are now familiar with the implementation of observations and experiments in ecological restoration in drylands and have

found that vegetation plays a key role in soil transformation. In general, the canopy is the core location of water vapor and carbon exchanges between plants and the atmosphere in the soil–plant–atmosphere continuum. However, more research studies should focus on the characteristics of water–carbon exchanges and their environmental driving mechanisms in drylands. Wu et al. indicated that temperature is an important factor limiting and driving canopy conductance in different climate regions and that there is a synergistic effect between moisture and temperature factors jointly driving the change in canopy conductance. They also showed that the synergistic driving effects on different climatic regions all had a certain threshold and indicated that modeling of these factors can be useful for predicting water–carbon exchanges in drylands in the future. In another case study, Wang et al. found that changes in precipitation amount and frequency caused by global climate change will increase carbon emissions of cyanobacterial crusts and underlying soil, suggesting that cyanobacteria should be considered in projections of the future carbon budget.

4 Final considerations

In conclusion, these studies promise to improve our knowledge of ecological restoration in drylands and foster land degradation neutrality through observations, experiments, and modeling. This Research Topic included reports that provided useful additional insights into research in these directions. In addition to the papers highlighted herein, many other high-quality studies on this Research Topic, which well deserve discussion, including those on urban green spaces, natural suitability of human settlements, and microclimate and wind regime of typical landscapes in drylands, have been published. This series “*Ecological Restoration in Drylands: Toward Land Degradation Neutrality*” spans a wide range of important subjects.

Author contributions

JD: conceptualization, supervision, writing–original draft, and writing–review and editing.

Conflict of interest

Author JD was employed by Liaoning Fengyu Ecological Technology Co., Ltd.

The remaining authors declare that the research was conducted in the absence of any commercial or financial relationships that could be construed as a potential conflict of interest.

Publisher’s note

All claims expressed in this article are solely those of the authors and do not necessarily represent those of their affiliated organizations, or those of the publisher, the editors, and the reviewers. Any product that may be evaluated in this article, or claim that may be made by its manufacturer, is not guaranteed or endorsed by the publisher.

References

- Bo, T. L., Ma, P., and Zheng, X. J. (2015). Numerical study on the effect of semi-buried straw checkerboard sand barriers belt on the wind speed. *Aeolian Res.* 16, 101–107. doi:10.1016/j.aeolia.2014.10.002
- Deng, J. F., Yao, J. Q., Zheng, X., and Gao, G. L. (2021). Transpiration and canopy stomatal conductance dynamics of Mongolian pine plantations in semiarid deserts, Northern China. *Agr. Water Manage.* 249, 106806. doi:10.1016/j.agwat.2021.106806
- Li, X. R., Ji, R. L., Chen, Y. W., Huang, L., and Zhang, P. (2011). Association of ant nests with successional stages of biological soil crusts in the Tengger Desert, Northern China. *Appl. Soil Ecol.* 47, 59–66. doi:10.1016/j.apsoil.2010.10.010
- Song, L., Zhu, J., Zheng, X., Wang, K., Lü, L., Zhang, X., et al. (2020). Transpiration and canopy conductance dynamics of *Pinus sylvestris* var. *mongolica* in its natural range and in an introduced region in the sandy plains of Northern China. *Agr. For. Meteorol.* 281, 107830. doi:10.1016/j.agrformet.2019.107830
- Tang, Y., and Li, X. (2018). Simulating effects of precipitation and initial planting density on population size of Mongolian pine in the Horqin Sandy Land, China. *Agroforest Syst.* 92, 1–9. doi:10.1007/s10457-016-0004-2
- United Nations, Sustainable Development Goals (SDGs) (2015). The 17 Goals: sustainably manage forests, combat desertification, halt and reverse land degradation, halt biodiversity loss. Available at: <https://www.un.org/sustainabledevelopment/biodiversity/>.



Effect of the Type of Wind Data on Regional Potential Wind Erosion Estimation

Li Zhang¹, Zhongling Guo^{1*}, Jifeng Li^{1*}, Chunping Chang¹, Rende Wang² and Qing Li²

¹School of Geographical Sciences/Hebei Key Laboratory of Environmental Change and Ecological Construction, Hebei Normal University, Shijiazhuang, China, ²Institute of Geographical Sciences, Hebei Academy Sciences/Hebei Engineering Research Center for Geographic Information Application, Shijiazhuang, China

OPEN ACCESS

Edited by:

Guang-Lei Gao,
Beijing Forestry University, China

Reviewed by:

Yuanyuan Zhao,
Beijing Forestry University, China
Dongwei Liu,
Inner Mongolia University, China
Heqiang Du,
Northwest Institute of Eco-
Environment and Resources (CAS),
China

*Correspondence:

Zhongling Guo
gzldhr@hebtu.edu.cn
Jifeng Li
ljfgjs@163.com

Specialty section:

This article was submitted to
Drylands,
a section of the journal
Frontiers in Environmental Science

Received: 01 January 2022

Accepted: 02 February 2022

Published: 04 March 2022

Citation:

Zhang L, Guo Z, Li J, Chang C, Wang R
and Li Q (2022) Effect of the Type of
Wind Data on Regional Potential Wind
Erosion Estimation.
Front. Environ. Sci. 10:847128.
doi: 10.3389/fenvs.2022.847128

The Agro-Pastoral Ecotone of Northern China (APEC) is a transitional area suffering from severe wind erosion. The wind data used in wind erosion modeling generally have different temporal resolutions and spatial station distributions. Previous studies have suggested that the temporal wind speed resolution influences the prediction of wind erosion events at the field scale. To date, no studies have been conducted to assess the impact of the type of wind data on regional wind erosion estimation. In this study, the Revised Wind Erosion Equation (RWEQ) and the Integrated Wind Erosion Modeling System (IWEMS) were used to evaluate the regional potential wind erosion in the Agro-Pastoral Ecotone of Northern China (APEC) during 2000 and 2012 based on four wind data type scenarios, including basic weather stations with daily wind statistics, basic weather stations with four wind speed measurements per day, reference climatological stations with daily wind statistics, and reference climatological stations with four wind speed measurements per day. The principal results reveal that the potential wind erosion estimates evaluated using the two models are closely correlated with the measured wind erosion data reported in the published literature, but the predicted values are generally lower than the observed values for the different scenarios. The magnitudes of the mean potential wind erosion ranged from 15.73 to 27.33 t ha⁻¹ a⁻¹ by RWEQ and changed between 61.77 and 98.54 t ha⁻¹ a⁻¹ by IWEMS for different scenarios. The spatial distribution and temporal trends of the annual or seasonal potential wind erosion obtained using the two models were similar for the different scenarios. This study revealed that wind speed is the most sensitive input, and hourly wind speed generated by the different temporal interpolation can significantly affect regional wind erosion estimation. Some studies involving precise regional wind erosion estimation, such as the impacts of landscape changes (land use/cover) on wind erosion, ecosystem service evaluation of reducing soil erosion, soil carbon sequestration and emissions through wind erosion, and wind erosion induced surface soil nutrient loss (e.g., nitrogen and phosphorus), may have been influenced by conducting regional wind erosion modeling based on different types of wind data. The users need to calibrate and validate the selected models for precise wind erosion prediction.

Keywords: wind data, wind erosion modeling, potential wind erosion, RWEQ, IWEMS

INTRODUCTION

Land degradation due to wind-induced soil erosion is an important surface process in arid and semi-arid regions (Dong and wang, 2000; Song et al., 2005; Guo et al., 2014; Webb et al., 2020; Borrelli et al., 2021). In China, according to the First National Bulletin on Water and Soil Conservation in the National Water Resources Survey (MWRPRC, 2013), the total land area affected by wind erosion is approximately $165.59 \times 104 \text{ km}^2$, accounting for 17.24% of the national territory. Wind erosion has a significant impact on agricultural activities and human beings (Zobeck et al., 2000). Therefore, determining a method of reducing the damage caused by wind erosion is an important challenge for governments in arid and semi-arid areas (O’Loingsigh et al., 2014; Du et al., 2015a).

Many wind erosion models have been developed to quantify wind erosion since the 1960s. These models mainly include the Wind Erosion Equation (WEQ) (Woodruff and Siddoway, 1965), the Revised Wind Erosion Equation (RWEQ) (Fryrear et al., 2000), the Wind Erosion Prediction System (WEPS) (Hagen, 1991), the Texas Tech Erosion Analysis Model (TEAM) (Gregory et al., 2004), the Wind Erosion on European Light Soil (WEELS) (Böhner et al., 2003), and the Wind Erosion Stochastic Simulator (WESS) (Potter et al., 1998) at the field scale, and the Integrated Wind-Erosion Modeling System (IWEMS) (Lu and Shao, 2001; Shao, 2001) and the AUStralian Land Erodibility Model (AUSLEM) (Webb et al., 2009) at a regional scale. Basically, these models include empirical (e.g., WEQ, RWEQ) or physical scheme (e.g., WEPS, IWEMS). In China, several studies have been conducted to build wind erosion models for different target regions at various scales since the 1990s (e.g., Dong, 1998; Zhao et al., 2011; Zou et al., 2015). To meet the demand of the first national wind erosion survey of China, the National Wind Erosion Survey Model of China (NWESMC) was developed in 2012 (Li et al., 2013). Wind erosion models play an important role in evaluating regional on-site wind erosion and off-site dust emissions. The inputs of a wind erosion model include soil properties (e.g., soil texture and moisture), meteorological factors (e.g., wind speed and precipitation), ground surface characteristics (e.g., roughness and vegetation cover), and anthropogenic activities (e.g., land management) (Wang et al., 2018; Fattahi et al., 2020; Zhang et al., 2020; Liu et al., 2021). Wind data (speed, direction, and turbulence) are generally considered to be the most sensitive parameters in wind erosion modeling (Lin et al., 2020; Webb et al., 2020).

In China, there are 2425 meteorological observing stations (reference and basic stations), of which 756 are national reference climatological stations (reference stations) (MBPRC, 2019). Correspondingly, previous wind erosion modeling studies have used either the wind data from the basic (e.g., Chi et al., 2019; Wang et al., 2020) or reference (e.g., Guo et al., 2013; Du et al., 2015a; Du et al., 2018) stations. Evaluations of regional wind erosion require a detailed representation of the wind data. However, only limited wind data (e.g., daily wind statistics) are available for many locations where wind erosion is occurring (van Donk et al., 2008; Guo et al., 2012; Liu et al., 2013). Consequently, the daily wind statistics and four wind

records per day documented at meteorological observing stations have been extensively used in regional wind erosion research. For instance, the NWESMC and RWEQ were used to estimate the potential wind erosion in the Agro-Pastoral Ecotone of Northern China (APEC) using four wind records per day (Guo et al., 2013; Wang et al., 2020). The average and maximum wind speeds per day were used to predict the soil loss due to wind in Northern China (Du et al., 2015a; Du et al., 2018). The daily average wind speed was used to assess the wind erosion in Inner Mongolia, China (Lyu et al., 2021). To improve the accuracy of wind erosion modeling, several methods have been developed to generate detailed wind data (e.g., hourly wind speeds) from limited wind data (e.g., daily wind statistics) (e.g., Skidmore and Tatarko, 1990; van Donk et al., 2008; Donatelli et al., 2009; Yuan et al., 2018). Further studies have also revealed that the averaging time has a significant impact on wind erosion estimations, and it may influence single-event and period (e.g., seasonal and annual) wind erosion evaluations (van Donk et al., 2005; Panebianco and Buschiazzo, 2013; Guo et al., 2016; Yizhaq et al., 2020). Generally, the effect of the type of wind data on regional wind erosion modelling has been neglected. In this study, the widely-used empirical RWEQ and process-based IWEMS were selected to explore how the type of wind data (basic weather/reference climatological stations and wind data with different temporal resolutions) influences regional potential wind erosion estimation.

MATERIALS AND METHODS

Study Area

The APEC is located in the transition zone between the monsoon region in eastern China and the arid and semi-arid regions in northwestern China (Guo et al., 2013). The APEC includes parts of Inner Mongolia, Liaoning, Jilin, Hebei, Shanxi, Shaanxi, and Ningxia Provinces ($36^{\circ}30' - 46^{\circ}42' \text{N}$, $106^{\circ}16' - 124^{\circ}51' \text{E}$) (Figure 1B). Most of the APEC is semi-arid. The annual precipitation distribution is uneven and is concentrated in summer and autumn. The average annual precipitation is 300–450 mm and the annual average temperature is $2.4 - 11.5^{\circ}\text{C}$. Strong winds are frequent and mainly occur in spring (March–April–May). The annual average wind speed ranges from 1.3 to 3.9 m s^{-1} , with an average maximum wind speed of $16 - 24 \text{ m s}^{-1}$. The land uses are diverse and the sandy land (including the Mu Us Sandy Land, Hunshan Lake Sandy Land, and Horqin Sandy Land), grassland, and farmland have staggered distributions in the APEC. In addition, agricultural and animal husbandry activities are still intensive in some region with a fragile ecology, and the human activities and severe wind erosion continuously decrease the local soil productivity in these areas.

Data Preparation

In this study, we collected meteorological data, vegetation data, land uses/cover data, Digital Elevation Model (DEM) data, and soil data to calculate the wind erosion in the APEC (Table 1). The data from all of the meteorological stations from 2000 to 2012

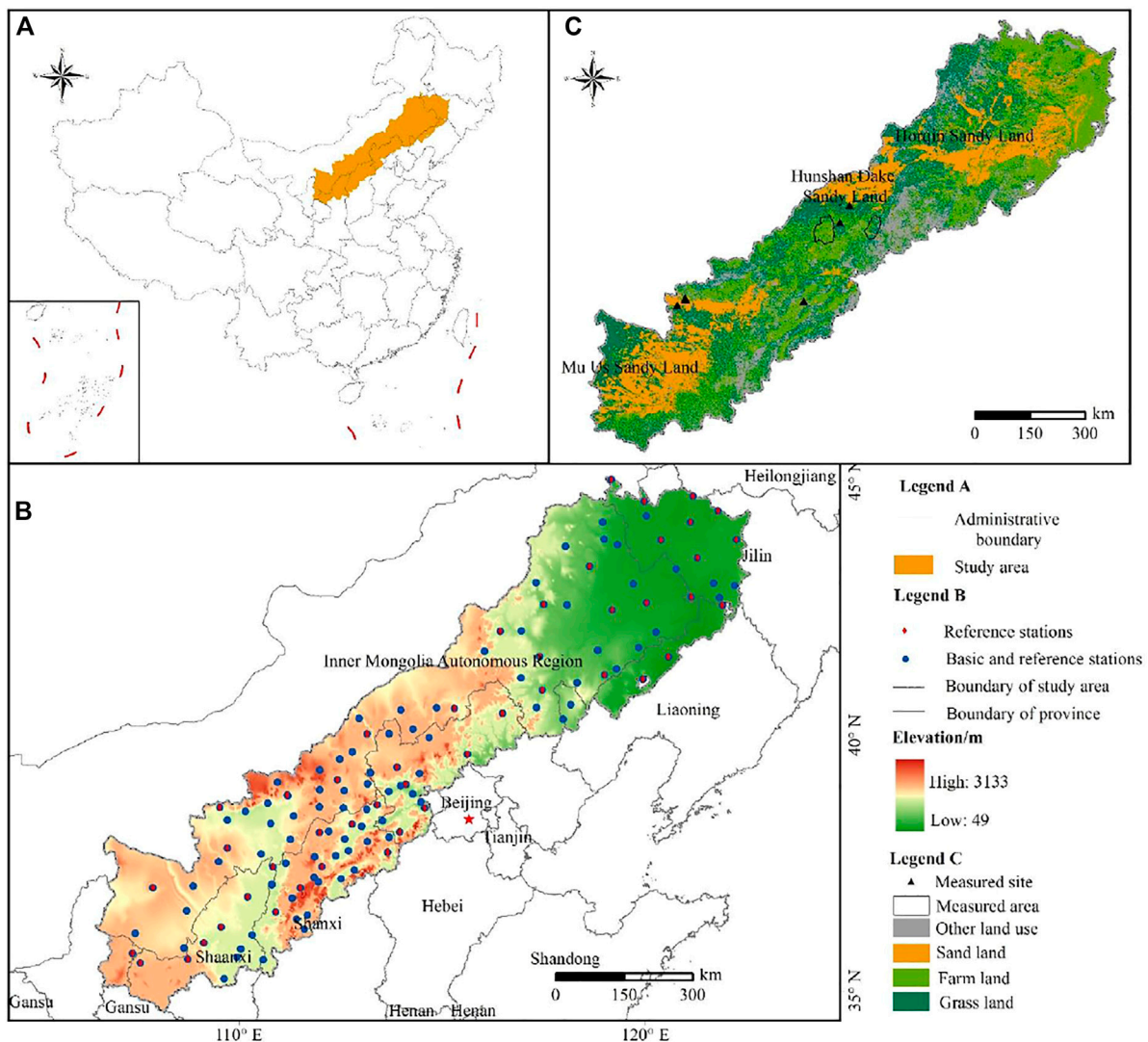


FIGURE 1 | (A) Location of the Agricultural Pastoral Ecotone in northern China (APEEC); **(B)** Distribution of the reference climatological stations and basic weather stations; and **(C)** Distribution of the measured wind erosion sites from published documents.

TABLE 1 | Required data for wind erosion modeling.

Data types	Temporal resolution	Spatial resolution
Meteorological data	Daily/Hourly	N/A
Soil data	N/A	1000 m
Normalized Difference Vegetation Index (NDVI)	16 days	1000 m
Digital Elevation Model (DEM)	N/A	1000 m
Land use/cover data	Annual	1000 m

N/A denotes not available.

were obtained from the China Meteorological Science Data Sharing Service Network (<http://data.cma.cn>). These meteorological data included wind speed, temperature, precipitation, sunshine duration, and other variables. Two wind databases are available, one dataset contains four wind

records per day (UTC+8 2:00, UTC+8 8:00, UTC+8 14:00, and UTC+8 20:00), and the other contains two wind records (average and maximum). The hourly wind speed data were generated from the four wind records per day using the linear interpolation method (Li et al., 2013) and from the two wind records per day

using WINDGEN (Skidmore and Tatarko, 1990). The Normalized Difference Vegetation Index (NDVI) data were derived from Moderate Resolution Imaging Spectroradiometer (MODIS) data products obtained from the United States Geological Survey's website (<https://www.usgs.gov>), and the MOD13A2, MOD11A2, and MOD09A1 products were mainly used. The 1 km resolution land use/cover data of 2010 was obtained from the Resource and Environment Data Center, Chinese Academy of Sciences (<http://www.resdc.cn>). The DEM data (China 1 km Low Range Model Data Set) were provided by the Science Data Centre for Cold and Arid Areas (<http://westdcwestgis.ac.cn>). The soil data were mainly obtained from the world soil database (HWSD) and were provided by the Scientific Data Center (<http://westdcwestgis.ac.cn>) for Cold and Arid Regions. These data were used to calculate the surface soil factors in the different regions. Farmland, grassland and sands (or desert) were selected to evaluate regional potential wind erosion.

Model Description

RWEQ Model

The RWEQ was proposed by the United States Department of Agriculture (USDA) to estimate soil wind erosion in farmland in the United States (Fryrear et al., 1998). The RWEQ is an empirical wind model that has been widely used to estimate wind erosion at the field scale. The main factors include climatic parameters, soil properties, surface roughness, and vegetation cover (Fryrear et al., 2000; Fryrear et al., 2001). The principal equations of the RWEQ are (Fryrear et al., 2000)

$$Q_x = Q_{max} \left[1 - e^{\left(\frac{x}{s} \right)^2} \right] \quad (1)$$

$$s = 150.71 (WF \times EF \times SCF \times K' \times C)^{-0.3711} \quad (2)$$

$$Q_{max} = 109.8 (WF \times EF \times SCF \times K' \times C) \quad (3)$$

where Q_x is the sediment flux at block length x (distance from the upwind direction) (kg m^{-1}); Q_{max} is the maximum sediment transport capacity of the wind force (kg m^{-1}); and s is the key block length (m). WF is the weather factor (kg m^{-1}); EF is the erodible soil fraction (dimensionless); SCF is the soil crust factor (dimensionless); K' is the soil roughness factor (dimensionless); and C is the vegetation cover factor (dimensionless).

The weather factor (WF) can be calculated using:

$$WF = \sum_{i=1}^N \rho \frac{(U_2 - U_t)^2 U_2}{gN} \times N_d \times SW \times SD \quad (4)$$

where U_2 is the wind speed (m s^{-1}) at a height of 2 m, and it can be converted from the wind speed observed at standard anemometer heights using Elliot's method (Elliot, 1979). U_t is the threshold wind speed (m s^{-1}) at a height of 2 m, and the threshold wind speed is assumed to be 5 m s^{-1} in the RWEQ (Fryrear et al., 2000). N is the number of wind speed observations during the period; N_d is the number of observation days in the study; g is the acceleration of gravity (m s^{-2}); SW is the soil moisture factor (dimensionless); and SD is the snow-cover factor (dimensionless).

The soil erodible factor (EF) and the soil crust factor (SCF) are calculated using Eqs 5, 6:

$$EF = \frac{29.9 + 0.31Sa + 0.17Si + 0. + 33Sa/Cl - 2.59OM - 0.95CaCO_3}{100} \quad (5)$$

$$SCF = \frac{1}{1 + 0.0066(Cl)^2 + 0.021(OM)^2} \quad (6)$$

where Sa is the sand content of the soil (%), Si is the silt content of the soil (%), Sa/Cl is the ratio of the sand to clay contents of the soil (%), OM is the organic-matter content of the soil (%), and $CaCO_3$ is the calcium carbonate content of the soil (%).

The combined vegetation factor (C) is the product of three factors: the crop canopy (SLR_c), flat-residues factor (SLR_f), and standing residues factor (SLR_s). However, the crop residues are normally used and most of the agricultural land is exposed in the research area (Guo et al., 2013). Therefore, the combined vegetation factor (C) was adjusted and is expressed as follows:

$$SLR_c = e^{-5.614(cc^{0.7366})} \quad (7)$$

where cc is the growing vegetation cover.

The surface roughness factors include the directional roughness and random roughness. Tillage measures produce roughness, while climatic factors such as rainfall gradually reduce the roughness factors. The surface roughness factor is calculated as follows (Shen et al., 2016):

$$K' = \cos \alpha \quad (8)$$

where α is the slope of the terrain, which was extracted from DEM data (Table 1) using ArcGIS 10.2.

IWEMS Model

The Integrated Wind Erosion Modelling System (IWEMS) was proposed by Shao (2001). This model has been widely used to estimate the wind erosion in China (Song, 2004; Du et al., 2018). The horizontal saltation flux $Q(d_s)$ ($\text{kg m}^{-1} \text{s}^{-1}$) for a soil with a uniform particle size d_s can be estimated using Owen's (1964) model:

$$Q(d_s) = \begin{cases} \frac{c_o A_c \rho_a u_*^3}{g} \left[1 - \left(\frac{u_{*t}(d_s)}{u_*} \right)^2 \right], & u_* \geq u_{*t} \\ 0, & u_* < u_{*t} \end{cases} \quad (9)$$

where A_c is the fraction of the erodible area, and c_o is the Owen coefficient. In theory, c_o is not a constant; and it was set equal to $0.25 + \omega_t(d_s)/3u_*$ in Owen's original formulation, where ω_t (m s^{-1}) is the terminal velocity of the salted particles (Owen, 1964).

The threshold fraction velocity u_{*t} is (Du et al., 2015b)

$$u_{*t}(d_s; \lambda; \theta) = u_{*t}(d_s) f_\lambda(\lambda) f_\theta(\theta) \quad (10)$$

where $u_{*t}(d_s; \lambda; \theta)$ (m s^{-1}) is the threshold friction velocity of sand particles with diameter d_s in the presence of vegetation and soil moisture; λ (m^2) is the frontal area of the roughness element; $f_\lambda(\lambda)$ is a function that modifies the threshold friction velocity to reflect the roughness elements; θ (m^3/m^3) is the volumetric soil moisture

($\text{m}^3 \text{m}^{-3}$); and $f_w(\theta)$ is a function that corrects the threshold friction velocity for soil moisture.

The $u_{*t}(d_s)$ is the threshold friction velocity under ideal conditions in which the surface is covered by loose sand particles that are uniform and spherical. The threshold friction velocity under the ideal conditions $u_{*t}(d_s)$ can be expressed by the equation proposed by Shao (2001):

$$u_{*t}(d_s) = \sqrt{a_1 \left(\frac{\rho_p}{\rho_a} g d_s + \frac{a_2}{\rho_a d_s} \right)} \quad (11)$$

where ρ_a and ρ_p are the densities of the air and sand particles, 1.29 and 2,600 kg m^{-3} , respectively; g is the acceleration of gravity (9.8 m s^{-2}); a_1 is a dimensionless parameter and a_2 is a dimension parameter, Shao (Lu and Shao, 2001; Shao, 2001) suggested values of $a_1 = 0.0123$ and $a_2 = 3 \times 10^{-4} \text{ kg s}^{-2}$.

The roughness element correction function f_λ proposed by Raupach et al. (1993) represents the ratio between the threshold friction velocity with roughness elements $u_{*t}(d_s; \lambda)$ and the velocity without roughness elements $u_{*t}(d_s)$. The equation for $f_\lambda(\lambda)$ is:

$$f_\lambda(\lambda) = \frac{u_{*t}(d_s, \lambda)}{u_{*t}(d_s)} = (1 - m_r \sigma_r \lambda)^{1/2} (1 + m_r \sigma_r \lambda)^{1/2} \quad (12)$$

where m_r is a tuning parameter with a value of less than one, which accounts for the non-uniformities in the surface stress distribution; σ_r is the ratio of the basal to frontal areas $\sigma_r = \eta/\lambda$ of the roughness elements; and $\beta_r = C_r/C_S$ is the ratio of the pressure-drag coefficient to the friction-drag coefficient (Raupach et al., 1993). The recommended values are $\beta_r \approx 90$, $m_r \approx 0.5$, and $\sigma_r \approx 1$.

The soil moisture correction function $f_w(\theta)$ was calculated using the simple method proposed by Fecan et al. (1998):

$$f_w(\theta) = [1 + A(\theta - \theta_r)^b]^{1/2} \quad (13)$$

where θ_r is the air-dry soil moisture ($\text{m}^3 \text{m}^{-3}$), and A and b are dimensionless parameters. The daily soil moisture was calculated using the Bridge Event and Continuous Hydrological (BEACH) model proposed by Sheikh et al. (2009).

The typical value of c_0 is approximately one and is regarded as a constant. u_* was calculated using the wind profile equation (Bagnold, 1941):

$$u_* = \frac{ku_z}{\ln\left(\frac{z-d}{z_0}\right)} \quad (14)$$

where u_z (m s^{-1}) is the wind velocity at height z , k is Von Karman's constant (0.4), z (m) is the measurement height, d (m) is the zero-plane displacement, and z_0 (m) is the aerodynamic roughness length.

Sensitivity Analysis

Sensitivity analysis is generally used to determine the main sensitive factors of a wind and water erosion model (Hagen et al., 1999; Feng and Sharratt, 2005). The sensitivity parameter, SS, is calculated by:

TABLE 2 | The spatial resolution of the climatological stations and temporal resolution of the wind speed for different scenarios.

Scenarios	Stations density	Wind speed resolution
Scenario 1	130	Daily average and maximum wind speed
Scenario 2	130	Four wind speeds per day
Scenario 3	47	Daily average and maximum wind speed
Scenario 4	47	Four wind speeds per day

The four wind speeds per day include the UTC+8:00, UTC+8 8:00, UTC+8 14:00, and UTC+8 20:00 wind speeds.

$$SS = \frac{O_2 - O_1}{O_{12}} / \frac{I_2 - I_1}{I_{12}} \quad (15)$$

where I_1 and I_2 are the least and greatest values of input parameters; O_1 and O_2 are the output values correspond to inputs values; I_{12} and O_{12} are the average of input and output values.

Temporal Interpolation of Wind Speed

WINDGEN (Wind-generator) is a subsystem of WEPS developed by United States Department of Agriculture (Skidmore and Tatarko, 1990). WINDGEN is a sub-daily wind speed generator and can reproduce the hourly wind speed. Wind speed for any hour of the day $u(i)$ can be simulated by:

$$u(i) = u_{rep} + 0.5(u_{max} - u_{min})\cos[2\pi(24 - h_{max} + i)/24] \quad (16)$$

where $u(i)$ is the wind speed for any hour (i) of the day; u_{rep} is the daily mean representative wind speed; u_{max} and u_{min} are the maximum and minimum wind speed for the day; h_{max} is the hour of the day when wind speed is maximum.

Linear interpolation method refers to the wind speed estimation data obtained 24 times per day by calculating the wind speed at 2 adjacent integer points, and the equation is expressed as (Li et al., 2013):

$$u_{ti} = \frac{|u_{t2} - u_{t1}|}{t_2 - t_1} (t_2 - t_1) + u_{t1} \quad (17)$$

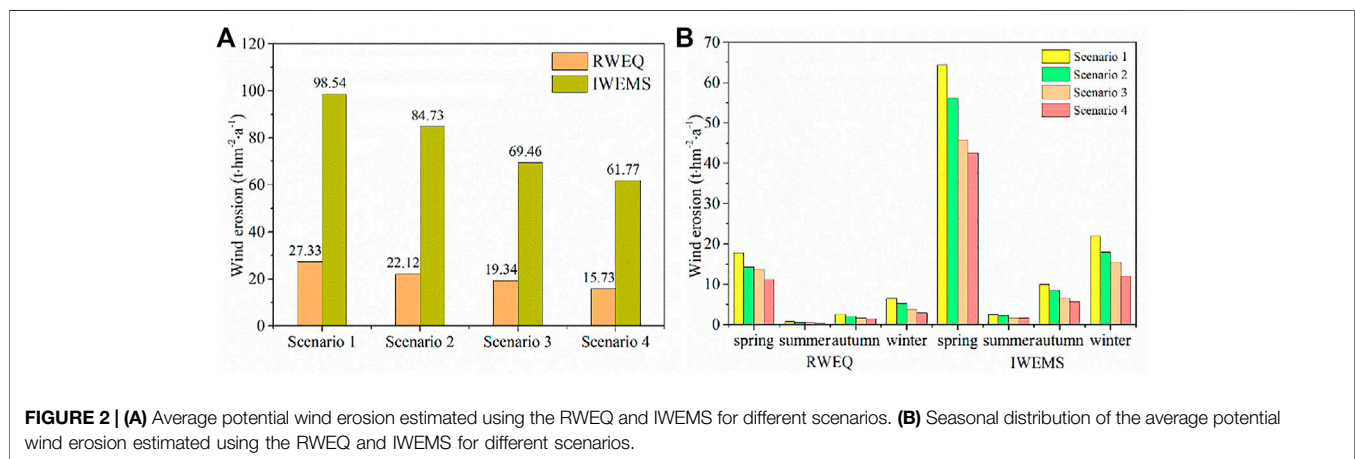
where t_1 and t_2 are the hours of two adjacent wind speed in four wind speeds on day (02:00, 08:00, 14:00 and 20:00); t_i is the hour between t_1 and t_2 ; u_{ti} , u_{t1} and u_{t2} are the wind speed correspond to t_i , t_1 and t_2 .

Scenario

In the APEC, there are 130 meteorological observing stations (reference and basic stations), of which 47 are reference climatological stations (reference stations). The four wind speeds per day (UTC+8 2:00, UTC+8 8:00, UTC+8 14:00, and UTC+8 20:00) or the daily wind statistics (average and maximum) per day are generally available in China. Based on the characteristics of the available wind data, four scenarios regarding the selection of the type of wind data were used to model the regional potential wind erosion (Table 2). In Scenario 1, 130 meteorological observing stations (reference and basic stations) with daily average and maximum wind speed data were used. In Scenario 2, 130 meteorological observing stations

TABLE 3 | The values of testing parameters, base values, input values and sensitivity values in RWEQ and IWEMS.

Model	Parameters	Units	Base value	Input 1	Input 2	Sensitivity values	Rank
RWEQ	Wind speed	m s ⁻¹	12.00	6.00	24.00	1.66	1
	Snow cover	-	0.98	0.70	1.00	1.00	2
	NDVI	%	16.00	0.00	100.00	-0.99	3
	Clay content	%	4.75	0.00	25.20	-0.81	4
	Rain	mm	10.21	0.00	111.40	-0.68	5
	CaCO ₃ content	%	20.60	5.00	39.30	-0.47	6
	Sand content	%	44.39	5.50	93.60	0.38	7
	Topography slope (α)	°	0.97	0.00	45.00	-0.31	8
	Organic matter	%	1.78	0.18	4.79	-0.23	9
	Rain day	d	2.60	0.00	11.00	-0.19	10
	Silt content	%	35.01	0.50	69.50	0.15	11
	Duration	h	8.40	0.00	14.30	0.11	12
	Temperature	°C	8.60	-29.20	39.80	-0.01	13
IWEMS	Wind speed	m.s ⁻¹	12	8	24	2	1
	NDVI	%	16.00	0	100	-1	2
	Silt	mm	0.38	0.002	0.05	0.87	3
	Soil moisture	%	11.28	0	19.32	0.69	4
	Sand	mm	0.54	0.05	2.00	0.65	5
	Air-dry soil moisture	%	4.10	0.52	11.28	0.15	6
	clay	mm	0.001	0.00	0.002	0.00	7

**FIGURE 2 | (A)** Average potential wind erosion estimated using the RWEQ and IWEMS for different scenarios. **(B)** Seasonal distribution of the average potential wind erosion estimated using the RWEQ and IWEMS for different scenarios.

(reference and basic stations) with four wind records per day were used. In Scenario 3, 47 reference climatological stations (reference stations) with daily average and maximum wind speed data were used. In Scenario 4, 47 reference climatological stations (reference stations) with four wind records per day were used. The “Standards for Classification and Gradation of Soil Erosion” were used to classify the potential wind erosion hazard (weak, slight, moderate, severe, very severe, and catastrophic) (MWRPRC, 2007).

RESULTS

Sensitivity Analysis of Model Parameters

The parameters testing, the base values, the input values, and the sensitivity values are presented in Table 3. Overall, wind speed is the most sensitive parameters of the two models. Generally, wind

erosion intensity is remarkably affected by threshold wind speed. The wind speed data with high spatial and temporal resolution is thus important for regional wind erosion simulation. Besides wind speed, for RWEQ, snow cover and vegetation cover can effectively control wind erosion, and the climatic factors have apparent seasonality. Several soil properties, such as the clay content and soil moisture can also reduce the wind erosion. However, the least sensitivity was observed for the inputs of temperature, precipitation days and sunshine time. For IWEMS, the wind speed is also the most sensitive inputs for wind erosion modeling.

Potential Wind Erosion for Different Scenarios

The average potential wind erosion values from 2000 to 2012 for the different scenarios are presented in Figure 2A. For the

TABLE 4 | Comparison of wind erosion in sites among different studies.

No.	Longitude	Latitude	References	Wind erosion ($t\text{ hm}^{-2}\text{ a}^{-1}$)	RWEQ simulates wind erosion ($t\text{ hm}^{-2}\text{ a}^{-1}$)				IWEMS simulates wind erosion ($t\text{ hm}^{-2}\text{ a}^{-1}$)			
					Scenario 1	Scenario 2	Scenario 3	Scenario 4	Scenario 1	Scenario 2	Scenario 3	Scenario 4
1	115.14	41.93	Hu et al. (2005)	77.76	23.51	20.2	11.91	8.53	137.24	127.36	118.49	108.39
2	113.62	40.05	Jiang, (2010)	56.36	13.47	14.19	23.52	20.63	79.68	55.43	101.57	63.52
3	115.55	42.33	Liu et al. (2008)	3.51	2.99	2.41	1.11	0.89	23.48	7.75	9.08	3.83
4	109.72	40.35	Li et al. (2016)	3.2	2.74	2.54	1.23	1.26	27.53	11.72	14.69	5.16
5	109.45	40.21		48.5	30.88	26.96	15.54	15.48	227.13	189.98	140.74	107.59
6	109.74	40.35		6.2	2.06	1.92	0.9	0.92	18	7.8	9.37	3.44
7	109.72	40.39		59	32.2	27.7	13.61	13.9	172.59	146.13	83.18	63.39

RWEQ, the highest average potential wind erosion values were 27.33, 22.12, 19.34, and 15.73 $t\text{ hm}^{-2}\text{ a}^{-1}$ for scenarios 1, 2, 3, and 4, respectively. For the IWEMS, the average annual potential wind erosion values were 98.54, 84.73, 69.46, and 61.77 $t\text{ hm}^{-2}\text{ a}^{-1}$ for scenarios 1, 2, 3, and 4, respectively. As is shown in **Figure 2B**, most of the severe wind erosion occurred in spring and the wind erosion was the lowest in summer. **Table 4** presents the potential wind erosion with different erosion hazards from 2000 to 2012 for the different scenarios. For the RWEQ, the percentage of the area with weak and slight erosion hazards accounted about 80% of the total area. The percentages of the areas with weak erosion hazards were 27.52, 41.10, 39.43, and 47.82% for scenarios 1, 2, 3, and 4, respectively, and the percentages of the areas with slight erosion hazards were 50.75, 39.21, 45.36, and 38.97%, respectively. For the IWEMS, the areas with weak and slight erosion hazards were remarkably smaller than those for the RWEQ, and the weak and slight erosion hazard areas occupied the large proportion (~50%) of the total area. In contrast, the percentages of the areas with severe, very severe, and catastrophic erosion hazards were high for all of the scenarios, i.e., 41.37, 32.82, 33.07, and 25.83% for scenarios 1, 2, 3, and 4, respectively. The areas with severe, very severe, and catastrophic erosion hazards decreased and the areas with weak and slight erosion hazards increased from scenario 1 to scenario 4. In summary, weak and slight erosion hazards were predominant in the APEC. Moreover, the potential wind erosion estimated using the IWEMS model is higher than that estimated using the RWEQ, and the four scenarios produce different results.

Spatiotemporal Distribution of Potential Wind Erosion

Figure 3 shows the spatial patterns of the potential wind erosion estimated using the RWEQ and IWEMS for the different scenarios. For the RWEQ, the area of very severe and catastrophic erosion hazards markedly decreased from scenarios 1 to 4 in the Horqin Sandy Land and the Hunshan Dake Sandy Land, and no catastrophic erosion hazards were scattered in the Hunshan Dake Sandy Land for scenario 4. Moderate erosion hazards dominated the Mu Us Sandy Land for all of the scenarios, and severe erosion hazards occurred in small regions for scenarios 1 and 2. For the IWEMS, the Horqin Sandy Land, the Hunshan Dake Sandy Land, and the Mu Us

Sandy Land exhibited very severe and catastrophic erosion hazards for all of the scenarios. The very severe and catastrophic erosion hazards decreased remarkably from scenarios 1 to 4 in the Horqin Sandy Land and the Hunshan Dake Sandy Land. In summary, the geographic distributions of the potential wind erosion were similar, and the wind erosion hotspots were mainly located in the Horqin Sandy Land, the Hunshan Dake Sandy Land, and the Mu Us Sandy Land.

The results show that there were seasonal variations and annual fluctuations in the potential wind erosion. **Figure 2B** shows the average seasonal potential wind erosion in the APEC. Wind erosion occurred during all of the seasons, and the seasonal variation of the potential wind erosion was as follows for all of the scenarios: spring > winter > autumn > summer. The potential wind erosion exhibited obvious annual fluctuations from 2000 to 2012 (**Figure 4**). The trends of the inter-annual variations in the average potential wind erosion were similar between 2000 and 2012 for all of the scenarios. The average potential wind erosion was the highest in 2001 for all of the scenarios; and it was the lowest in 2011, except for scenarios 3 and 4 for the IWEMS, in which they occurred in 2005 and 2008, respectively. Overall, the potential wind erosion significantly decreased from 2000 to 2012.

DISCUSSION

Model Applicability and Verification

Several methods often employed in soil wind erosion evaluation, particularly the common radioisotope ^{137}Cs monitoring method have high degree of precision for wind erosion monitoring in field surface experiments and observations in different model (Gharibreza et al., 2020). The verification of the models was investigated based on collected measured wind erosion data. Here, the seven sites and two regional areas of measured wind erosion were obtained using radioisotope ^{137}Cs method from the literatures (**Tables 5, 6**). The locations of the observation are presented in **Figure 1C**. We compared our results in all scenarios with previous findings by using radioisotope ^{137}Cs method. From **Table 5**, the simulated results were generally in agreement with the wind erosion sites reported in the literature in two models. For all the sites, the results of simulated wind erosion are usually over the measured wind erosion in IWEMS, except for Datong county

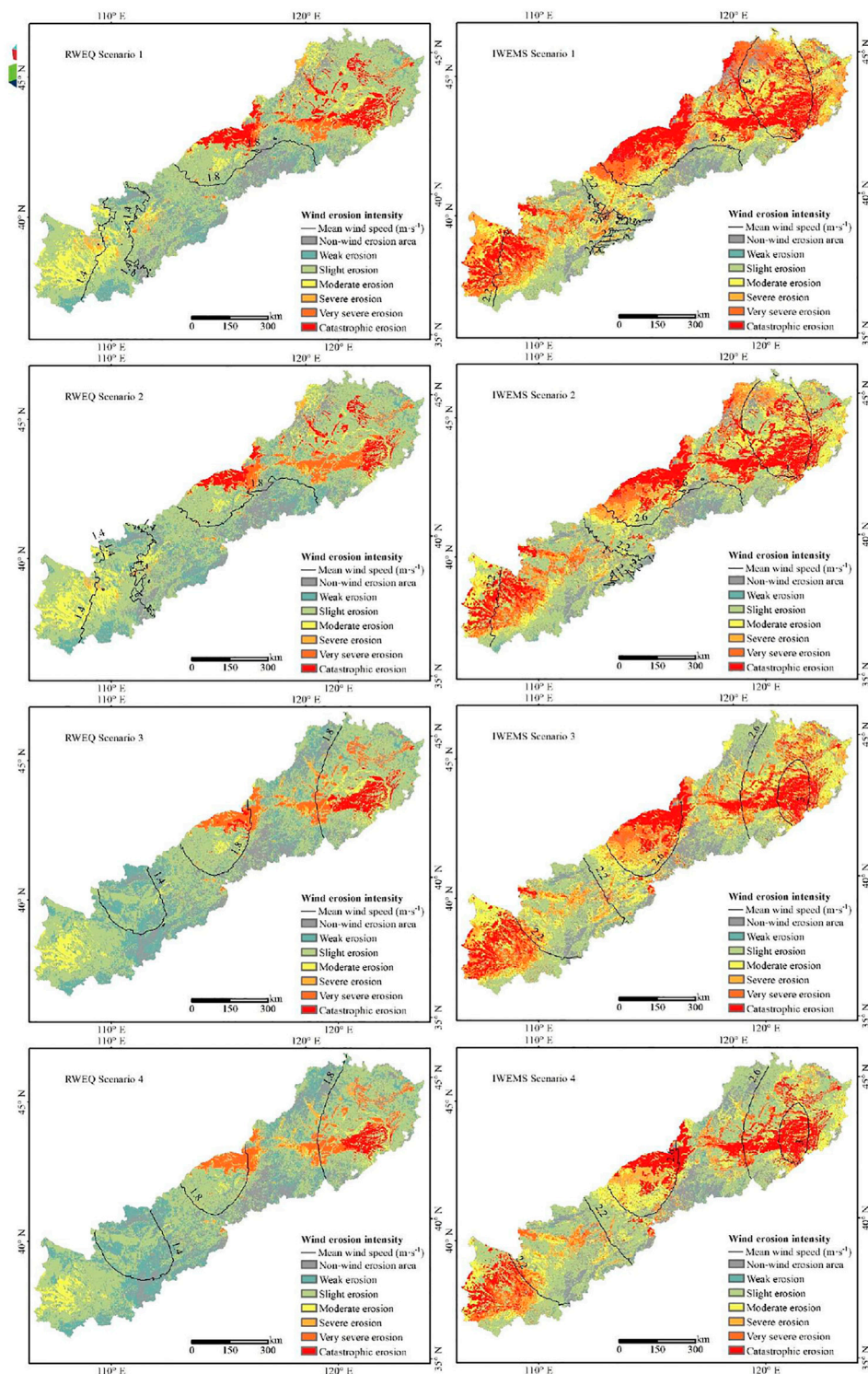


FIGURE 3 | Spatial distribution of the wind erosion hazards for the different scenarios. Note: Mean wind speed in RWEQ at 2 m height and in IWEMS at 10 m height.

and Dalad Banner in scenario 2 and scenario 4, respectively. However, RWEQ modeling results generally larger than previous measured values using ^{137}Cs in scenario 1 and scenario 2, meanwhile, simulated results less than the measured in

scenario 3 and scenario 4. We also compared our results in regional range with previous study of radioisotope ^{137}Cs in Kangbao and Fengning, Hebei of china (**Table 6**). On the whole, simulated results with IWEMS larger than RWEQ,

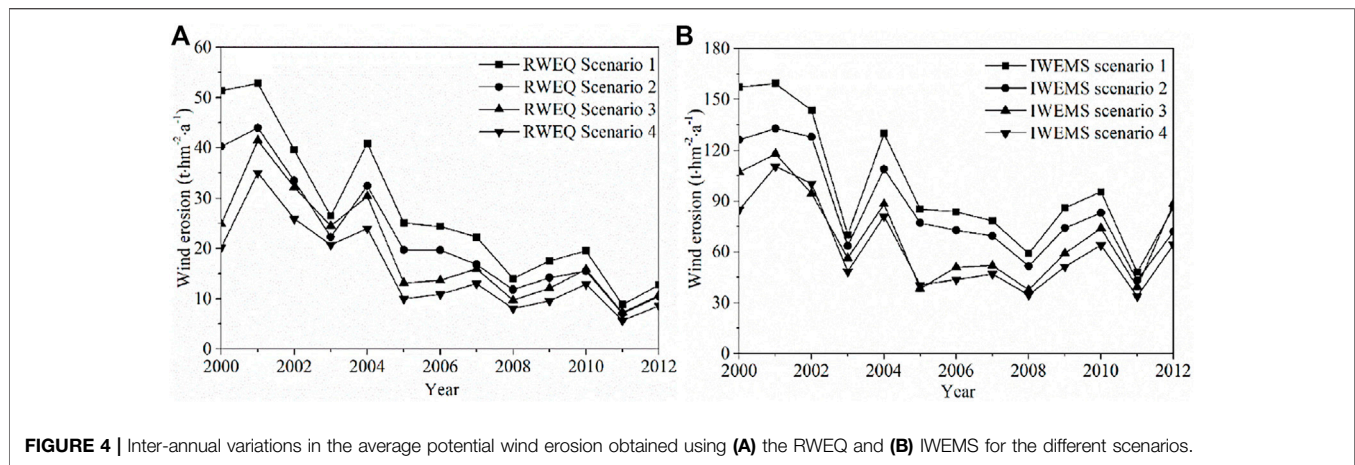


FIGURE 4 | Inter-annual variations in the average potential wind erosion obtained using (A) the RWEQ and (B) IWEMS for the different scenarios.

particularly in Kangbao county. And maximum values of the simulated over the maximum from observed values.

Influence of the Type of Wind Data on Regional Potential Wind Erosion Evaluation

Herein, the average potential wind erosion was found to be significantly lower for scenarios 1 to 4 for both models. For the same basic spatial meteorological data (scenarios 1 and 2 and scenarios 3 and 4), the average potential wind erosion estimated from the daily average and maximum wind speeds was higher than that calculated using four wind speeds per day (Figure 2). This is due to the fact that the methods of generating the hourly wind speed were different. WINDGEN was used to reproduce the hourly wind speed based on the daily average and maximum wind speeds, whereas the four wind speed measurements per day were interpolated using the linear interpolation method to obtain the hourly wind speed Wagner et al., 1992. Table 7 presents the average wind speed and the percentage of erosive wind ($>5 \text{ m s}^{-1}$ wind speed at a height of 2 m). Clearly, the average wind speed and the percentage of erosive wind generated using WINDGEN are greater than those generated using the linear interpolation method. High temporal resolution wind speeds are generally required to generate a precise wind erosion model (van Donk et al., 2008; Guo et al., 2012; Panebianco and Buschiazzo, 2013). Since detailed wind data may be unavailable for some regions, several temporal wind data interpolation methods have been developed (Donatelli et al., 2009). It is suggested that the users need to access the prediction errors of the different temporal interpolation methods when modeling regional wind erosion.

For the same temporal meteorological data (scenarios 1 and 3 and scenarios 2 and 4), the average regional wind erosion obtained from the 130 meteorological stations was higher than that obtained from the 47 meteorological stations (Figure 2). Point meteorological data are generally interpolated into regional raster data for regional geographical and environmental modeling (Mauger et al., 2013; Li and Heap, 2014). Mathematically, the factors affecting the performances of spatial interpolation methods include the sampling design, the spatial distribution of the samples, the nature and quality of the data, the correlation between the primary and secondary variables, and the interactions among the factors (Shepard,

1968; Li and Heap, 2014). Here the kriging method was used to upscale the wind data. As the number of meteorological stations and the measured accuracy increase, the performance of the kriging interpolation tends to increase (MacEachren and Davidson, 1987; Luo et al., 2008; Martin et al., 2016). In addition, the locations and distribution of the meteorological stations within the study area also affect the accuracy of the kriging interpolation (MacEachren and Davidson, 1987; Keskin et al., 2015; Ozturk and Kilic, 2016).

Implications for the Impacts of Climate Change on Wind Erosion

Climate change is an important contributor to wind and water erosion. It can accelerate or decelerate the rates of wind and water erosion and can further alter the soil's health, productivity, and surface cover (Gao et al., 2002; Sharratt et al., 2015; Webb et al., 2020). The influences of historical climate changes on wind erosion have been extensively studied. The variations in the historical wind speed, precipitation, and temperature have generally been summarized as the main factors affecting temporal wind erosion trends (e.g., Haiyan Zhang et al., 2018; Edwards et al., 2019; Lin et al., 2020). Recently, the effects of future climate change scenarios on wind erosion have also been explored. For example, Sharratt et al. (2015) reported that the soil and PM_{10} losses via wind erosion will be 25–84% lower under the mid-21st century climate (2035–2064) on the Columbian Plateau, USA, compared with the baseline scenario (1970–1999). Li et al. (2020) reported that projected climate changes (2006–2099) will decrease the regional wind erosion by 10.71–33.74% in Central Asia. These studies generally used different types of wind data (e.g., daily or hourly data) and various wind erosion models (e.g., the RWEQ and WEPS). Mathematically, the magnitude of the wind erosion variations due to climate change may be similar to the effects of using different types of wind data (e.g., Munson et al., 2011; Zhang et al., 2019). The discrepancy in the wind erosion modeling caused by using different types of wind data or different wind erosion models may interfere with characterizing the effect of climate change on wind erosion. Therefore, determining a method of selecting a type of wind data in terms of the temporal resolution (daily or hourly data) and spatial network (basic or reference

TABLE 5 | Comparison of wind erosion in regional range among different studies.

No.	Longitude	Latitude	References	Wind erosion ($t\ km^{-1}\ a^{-1}$)	RWEQ simulates wind erosion ($t\ km^{-2}\ a^{-1}$)				IWEMS simulates wind erosion ($t\ km^{-2}\ a^{-1}$)			
					Scenario 1	Scenario 2	Scenario 3	Scenario 4	Scenario 1	Scenario 2	Scenario 3	Scenario 4
Kangbao county	113.78–116.20	40.08–42.05	Zhang et al. (2010)	83.62	16.60	13.50	8.18	6.37	100.65	51.17	64.64	43.09
				280.00	308.68	252.12	152.66	116.13	1287.08	785.47	1128.91	843.65
Fengning county	116.08–116.25	41.5–41.58	Zhao et al. (2005)	20.00	0.07	0.06	0.03	0.02	30.60	16.44	9.26	6.76
				28.97	21.17	17.71	17.31	12.38	56.86	58.32	50.78	70.41
				50.192	252.89	210.50	210.12	146.77	232.41	231.92	268.61	318.90
				24.86	0.02	0.02	0.02	0.01	2.76	1.45	2.21	2.07

stations) is vital to quantifying the effects of historical or future climate change on regional wind erosion.

Moreover, many studies involving correlations with wind erosion, such as the impacts of landscape changes (land use/cover) on wind erosion (e.g., Chunlai Zhang et al., 2018; Chi et al., 2019), ecosystem services evaluation of reducing soil erosion (e.g., Hao et al., 2017; Zhao et al., 2017), soil CO₂ sequestration and emissions due to wind erosion (e.g., Webb et al., 2012; Chappell et al., 2019), and wind erosion-induced surface soil nutrient loss (e.g., nitrogen and phosphorus) (e.g., Du et al., 2019; Song et al., 2019), have generally neglected the effect of the type of wind data on precise wind erosion modeling.

Limitations and Future Perspectives

Soil loss due to wind erosion at the field or regional scales can be simulated by wind erosion models. However, the models' predictions are widely underestimated or overestimated (Pi et al., 2017). For instance, Buschiazzo and Zobeck (2008) found that the RWEQ and WEPS underestimated the soil mass transport by 45 and 40%, respectively, in a bare agriculture field. Several studies have demonstrated the underestimation of the maximum sediment transport (Q_{max}) and field soil loss (SL) and the overestimation of the critical field length (S) when using the RWEQ model at multiple sites (Zobeck et al., 2001; VanPelt et al., 2004).

To improve the accuracy of wind erosion models, calibration of the sensitive inputs of the models is necessary. At the field scale, measured wind erosion data can be relatively easily determined (Jarrah et al., 2020). Several studies have concluded that the prediction accuracy of wind erosion models (e.g., the RWEQ and WEPS) can be remarkably improved by calibrating some of the key parameters (Visser et al., 2005; Fryrear et al., 2008; Youssef et al., 2012; Xing et al., 2018). At the regional scale, the calibration of wind erosion models requires more standard long-term observation data (Jarrah et al., 2020). Du et al. (2018) calibrated the IWEMS model to enhance its performance using data from 452 passive sand traps from 2009 to 2011. Song et al. (2019) predicted the soil organic carbon and nutrient losses resulting from aeolian dust emissions after calibrating the IWEMS using data from 293 field experimental sites from 2014 to 2015. The RWEQ was upscaled to the regional scale and calibrated using measured wind erosion data, and then, it was further used to access the wind erosion risk in the Yellow River watershed, China (Du et al., 2015a; Du et al., 2015b). Several other studies have focused on validating wind erosion models. The soil loss through wind erosion determined using the ¹³⁷Cs method was used to validate the upscaled RWEQ (e.g., Chunlai Zhang et al., 2018; Chi et al., 2019; Wu et al., 2021). Published wind erosion data have also been used to verify wind erosion models (e.g., Wang et al., 2020; Zhou et al., 2020). Nevertheless, many studies have directly assessed regional wind erosion, but no calibration or verification of the wind erosion models were conducted (e.g., Feng and Sharratt, 2005; Guo et al., 2013; Borrelli et al., 2017; Fenta et al., 2020; Lin et al., 2020). Our study indicates that the type of wind data has a significant influence on the potential wind erosion estimation obtained using the RWEQ and IWEMS. Therefore, it is necessary to systematically calibrate and validate these models to achieve precise wind erosion modeling.

TABLE 6 | The area and percentage of the wind erosion hazards determined using the RWEQ and IWEMS for different scenarios.

Wind erosion hazards/Range ($\text{t hm}^{-1} \text{a}^{-1}$)		Area of the class (km^2)/Percentage of total area for the class (%)			
		Scenario 1	Scenario 2	Scenario 3	Scenario 4
RWEQ	Weak/0–2	149.047/27.52	222.587/41.10	213.506/39.43	258.935/47.82
	Slight/2–25	274.827/50.75	212.305/39.21	245.654/45.36	211.050/38.97
	Moderate/25–50	54.649/10.09	49.746/9.19	29.495/5.45	20.661/3.82
	Severe/50–80	10.473/1.93	7.199/1.33	5.058/0.94	8.910/1.65
	Very severe/80–150	15.082/2.79	26.640/4.92	30.879/5.71	32.187/5.95
	Catastrophic/>150	37.439/6.91	23.040/4.25	16.925/3.13	9.774/1.81
IWEMS	Weak/0–2	134.904/24.90	156.514/28.89	107.568/19.85	136.838/25.24
	Slight/2–25	99.301/18.33	11.5416/21.30	162.530/29.99	182.699/33.69
	Moderate/25–50	83.387/15.39	92.043/16.99	92.632/17.09	82.666/15.25
	Severe/50–80	64.104/11.83	49.536/9.14	53.556/9.88	31.294/5.77
	Very severe/80–150	59.982/11.07	36.100/6.66	51.495/9.50	36.608/6.75
	Catastrophic/>150	100.051/18.47	92.218/17.02	74.211/13.69	72.134/13.30

TABLE 7 | Mean wind speed and percentage of wind speeds greater than the threshold wind speed (5 m s^{-1}) estimated by the WINDGEN and Linear interpolation methods.

Wind speed interpolation method	130 climatological stations		47 climatological stations	
	Mean wind speed (m s^{-1})	Mean percentage (%)	Mean wind speed (m s^{-1})	Mean percentage (%)
WINDGEN	2.37	8.83	2.45	9.51
Linear interpolation	2.35	8.00	2.43	8.67

CONCLUSION

To quantitatively determine the effect of wind data with different temporal resolutions or spatial station distributions on regional wind erosion modeling, the Revised Wind Erosion Equation and the Integrated Wind Erosion Modeling System were used to evaluate the regional potential wind erosion in the APEC during 2000–2012 based on four scenarios with different types of wind data (Table 2). The principal conclusions of this study are as follows.

- 1) The potential wind erosion evaluated using the two models are closely correlated with the measured wind erosion documented in the literature, but the observed values were generally lower than the predicted values for all four scenarios.
- 2) The magnitudes of the mean potential wind erosion ranged from 15.73 to $27.33 \text{ t ha}^{-1} \text{a}^{-1}$ by RWEQ and changed between 61.77 and $98.54 \text{ t ha}^{-1} \text{a}^{-1}$ by IWEMS, but the spatial distributions and temporal trends of the annual and seasonal potential wind erosion for the two models were similar for the different scenarios.
- 3) The impacts of landscape changes (land use/cover) on wind erosion, ecosystem service evaluation of reducing soil erosion, CO_2 soil sequestration and emissions through wind erosion, and wind erosion induced surface soil nutrient loss (e.g., nitrogen and phosphorus) may be influenced by regional wind erosion modeling based on different types of wind data (Shepard, 1968; Wagner et al., 1992).

In this study, it was determined that the type of wind data can significantly affect regional wind erosion estimation. Users need

to calibrate and validate their selected model to achieve precise wind erosion prediction.

DATA AVAILABILITY STATEMENT

The original contributions presented in the study are included in the article/Supplementary Material, further inquiries can be directed to the corresponding authors.

AUTHOR CONTRIBUTIONS

ZG and JL initialed and designed the work. LZ and ZG wrote the original draft. CC, RW, and QL reviewed and edited the manuscript.

FUNDING

This research was funded by the National Science Foundation of China (41877066, 41901001), Natural Science Foundation of Hebei Province (D2018205192, D2018205212), and Young Talents Foundation in Hebei Province (13505197).

ACKNOWLEDGMENTS

The authors thank reviewers and the editors for their suggestions on improving the manuscript.

REFERENCES

- Bagnold, R. A. (1941). *The Physics of Blown Sand and Desert Dunes*. London: Chapman & Hall. doi:10.1038/148480a0
- Böhner, J., Schäfer, W., Conrad, O., Gross, J., and Ringeler, A. (2003). The WEELS Model: Methods, Results and Limitations. *Catena* 52 (3-4), 289–308. doi:10.1016/S0341-8162(03)00019-5
- Borrelli, P., Alewell, C., Alvarez, P., Anache, J. A. A., Baartman, J., Ballabio, C., et al. (2021). Soil Erosion Modelling: A Global Review and Statistical Analysis. *Sci. total Environ.* 780, 146494. doi:10.1016/j.scitotenv.2021.146494
- Borrelli, P., Lugato, E., Montanarella, L., and Panagos, P. (2017). A New Assessment of Soil Loss Due to Wind Erosion in European Agricultural Soils Using a Quantitative Spatially Distributed Modelling Approach. *Land Degrad. Develop.* 28 (1), 335–344. doi:10.1002/ldr.2588
- Buschiazzo, D. E., and Zobeck, T. M. (2008). Validation of WEQ, RWEQ and WEPS Wind Erosion for Different Arable Land Management Systems in the Argentinean Pampas. *Earth Surf. Process. Landforms* 33 (12), 1839–1850. doi:10.1002/esp.1738
- Chappell, A., Webb, N. P., Leys, J. F., Waters, C. M., Orgill, S., and Eyres, M. J. (2019). Minimising Soil Organic Carbon Erosion by Wind Is Critical for Land Degradation Neutrality. *Environ. Sci. Pol.* 93, 43–52. doi:10.1016/j.envsci.2018.12.020
- Chi, W., Zhao, Y., Kuang, W., and He, H. (2019). Impacts of Anthropogenic Land Use/cover Changes on Soil Wind Erosion in China. *Sci. total Environ.* 668, 204–215. doi:10.1016/j.scitotenv.2019.03.015
- Chunlai Zhang, C., Song, C., Wang, Z., Zou, X., and Wang, X. (2018). Review and prospect of the Study on Soil Wind Erosion Process. *Adv. Earth Sci.* 33, 27–41. doi:10.11867/j.issn.1001-8166.2018.01.0027
- Donatelli, M., Bellocchi, G., Habyarimana, E., Confalonieri, R., and Micale, F. (2009). An Extensible Model Library for Generating Wind Speed Data. *Comput. Elect. Agric.* 69 (2), 165–170. doi:10.1016/j.compag.2009.07.022
- Dong, Z. (1998). Establishing Statistic Model of Wind Erosion on Small Watershed Basis. *Bull. Soil Water Conservation* 18, 55–62. doi:10.3969/j.issn.1000-288X.1998.05.013
- Dong, Z., Wang, X. M., and Liu, L. Y. (2000). Wind Erosion in Arid and Semiarid China: an Overview. *Soil & Water Conservation* 55 (4), 439–444. doi:10.3321/j.issn:1000-694X.2000.02.007
- Du, H., Wang, T., Xue, X., and Li, S. (2018). Modelling of Sand/dust Emission in Northern China from 2001 to 2014. *Geoderma* 330, 162–176. doi:10.1016/j.geoderma.2018.05.038
- Du, H., Wang, T., Xue, X., and Li, S. (2019). Estimation of Soil Organic Carbon, Nitrogen, and Phosphorus Losses Induced by Wind Erosion in Northern China. *Land Degrad. Dev.* 30 (8), 1006–1022. doi:10.1002/ldr.3288
- Du, H., Xue, X., Wang, T., and Deng, X. (2015a). Assessment of Wind-Erosion Risk in the Watershed of the Ningxia-Inner Mongolia Reach of the Yellow River, Northern China. *Aeolian Res.* 17, 193–204. doi:10.1016/j.aeolia.2015.04.003
- Du, H., Xue, X., Wang, T., and Deng, X. (2015b). Wind Erosion Modulus and Quantity Evaluation of Aeolian Sediment Feed into River in Watershed of Ningxia-Inner Mongolia Reach of Yellow River from 1986 to 2013. *Trans. Chin. Soc. Agric. Eng.* 31, 142–151. doi:10.11975/j.issn.1002-6819.2015.10.019
- Edwards, B. L., Webb, N. P., Brown, D. P., Elias, E., Peck, D. E., Pierson, F. B., et al. (2019). Climate Change Impacts on Wind and Water Erosion on US Rangelands. *J. Soil Water Conservation* 74 (4), 405–418. doi:10.2489/jswc.74.4.405
- Elliot, D. L. (1979). “Adjustment and Analysis of Data for Regional Wind Energy Assessments,” in *Paper Presented at the Workshop on Wind Climate* (Asheville, NC), 121–213.
- Fattahi, S. M., Soroush, A., and Huang, N. (2020). Wind Erosion Control Using Inoculation of Aeolian Sand with Cyanobacteria. *Land Degrad. Dev.* 31, 2104–2116. doi:10.1002/ldr.3590
- Fécan, F., Marticorena, B., and Bergametti, G. (1998). Parametrization of the Increase of the Aeolian Erosion Threshold Wind Friction Velocity Due to Soil Moisture for Arid and Semi-arid Areas. *Ann. Geophys.* 17 (1), 149–157. doi:10.1007/s00585-999-0149-7
- Feng, G., and B. Sharratt, B. S. (2005). Sensitivity Analysis of Soil and PM10 Loss in WEPS Using the LHS-OAT Method. *Trans. ASABE* 48 (4), 1409–1420. doi:10.13031/2013.19198
- Fenta, A. A., Tsunekawa, A., Haregeweyn, N., Poesen, J., Tsubo, M., Borrelli, P., et al. (2020). Land Susceptibility to Water and Wind Erosion Risks in the East Africa Region. *Sci. Total Environ.* 703, 135016. doi:10.1016/j.scitotenv.2019.135016
- Fryrear, D. W., Saleh, A., Bilbro, J. D., Schomberg, H. M., Stout, J. E., and Zobeck, T. M. (1998). “Revised Wind Erosion Equation (RWEQ). Wind Erosion and Water Conservation Research Unit,” in *USDA-ARS, Southern Plains Area Cropping Systems Research Laboratory* (Lubbock: Technical Bulletin No. 1).
- Fryrear, D. W., Bilbro, J. D., Saleh, A., Schomberg, H. M., Stout, J. E., and Zobeck, T. M. (2000). RWEQ: Improved Wind Erosion Technology. *Soil and Water Conservation* 55 (2), 183–189.
- Fryrear, D. W., Sutherland, P. L., Davis, G., Hardee, G., and Dollar, M. (2001). Wind Erosion Estimates with RWEQ and WEQ. *CO KS Assembly St.* 67401, 760–765.
- Fryrear, D. W., Wassif, M. M., Tadrus, S. F., and Ali, A. A. (2008). Dust Measurements in the Egyptian Northwest Coastal Zone. *Trans. ASABE* 51 (4), 1255–1262. doi:10.13031/2013.25242
- Gao, Q., Ci, L., and Yu, M. (2002). Modeling Wind and Water Erosion in Northern China under Climate and Land Use Changes. *Soil & Water Conservation* 57 (1), 46–55.
- Gharibreza, M., Zaman, M., Porto, P., Fulajtar, E., Parsaei, L., and Eisaei, H. (2020). Assessment of Deforestation Impact on Soil Erosion in Loess Formation Using 137Cs Method (Case Study: Golestan Province, Iran). *Int. Soil Water Conservation Res.* 8 (4), 393–405. doi:10.1016/j.iswcr.2020.07.006
- Gregory, J., Wilson, G., Singh, U., and Darwish, M. (2004). TEAM: Integrated, Process-Based Wind-Erosion Model. *Environ. Model. Softw.* 19 (2), 205–215. doi:10.1016/S1364-8152(03)00124-5
- Guo, Z., Zobeck, T. M., Stout, J. E., and Zhang, K. (2012). The Effect of Wind Averaging Time on Wind Erosivity Estimation. *Earth Surf. Process. Landforms* 37 (7), 797–802. doi:10.1002/esp.3222
- Guo, Z., Zobeck, T. M., Zhang, K., and Li, F. (2013). Estimating Potential Wind Erosion of Agricultural Lands in Northern China Using the Revised Wind Erosion Equation and Geographic Information Systems. *J. Soil Water Conservation* 68 (1), 13–21. doi:10.2489/jswc.68.1.13
- Guo, Z., Huang, N., Dong, Z., Van Pelt, R., and Zobeck, T. (2014). Wind Erosion Induced Soil Degradation in Northern China: Status, Measures and Perspective. *Sustainability* 6 (12), 8951–8966. doi:10.3390/su6128951
- Guo, Z., Chang, C., and Wang, R. (2016). A Novel Method to Downscale Daily Wind Statistics to Hourly Wind Data for Wind Erosion Modelling. *Geo-Informatics Resource Manag. Sust. Ecosystem* 569, 611–619. doi:10.1007/978-3-662-49155-3_64
- Hagen, L. J., Wagner, L. E., and Skidmore, E. L. (1999). Analytical Solutions and Sensitivity Analyses for Sediment Transport in WEPS. *Anal. solutions sensitivity analyses sediment transport WEPS. Transactions Asae* 42 (6), 1715–1722. doi:10.13031/2013.13334
- Hagen, L. J. (1991). A Wind Erosion Prediction System to Meet User Needs. *J. Soil Water Conservation* 46 (2), 106–111.
- Haiyan Zhang, H., Fan, J., Cao, W., Harris, W., Li, Y., Chi, W., et al. (2018). Response of Wind Erosion Dynamics to Climate Change and Human Activity in Inner Mongolia, China during 1990 to 2015. *Sci. Total Environ.* 639, 1038–1050. doi:10.1016/j.scitotenv.2018.05.082
- Hao, R., Yu, D., Liu, Y., Liu, Y., Qiao, J., Wang, X., et al. (2017). Impacts of Changes in Climate and Landscape Pattern on Ecosystem Services. *Sci. Total Environ.* 579, 718–728. doi:10.1016/j.scitotenv.2016.11.036
- Hu, Y., Liu, J., Zhuang, D., Cao, H., Yan, H., and Yang, F. (2005). Distribution Characteristics of 137Cs in Wind-Eroded Soil Profile and its Use in Estimating Wind Erosion Modulus. *Chin. Sci. Bull.* 50 (11), 1155–1159. doi:10.1360/04wd0312
- Jarrah, M., Mayel, S., Tatarko, J., Funk, R., and Kuka, K. (2020). A Review of Wind Erosion Models: Data Requirements, Processes, and Validity. *Catena* 187, 104388. doi:10.1016/j.catena.2019.104388
- Jiang, H. (2010). *Study on Soil Erosion in Agro Pastoral Ecotone of Northern China Based on ¹³⁷Cs Technology*. Huhehaote: Inner Mongolia Normal University.

- Keskin, M., Dogru, A. O., Balcik, F. B., Cigdem, G., Ulugtekin, N., and Sozen, S. (2015). Comparing spatial interpolation methods for mapping meteorological data in Turkey. *Energy Syst. Manage.* 26, 33–42. doi:10.1007/978-3-319-16024-5_3
- Li, J., and Heap, A. D. (2014). Spatial Interpolation Methods Applied in the Environmental Sciences: A Review. *Environ. Model. Softw.* 53, 173–189. doi:10.1016/j.envsoft.2013.12.008
- Li, Z., Zou, X., and Cheng, H. (2013). Method of Wind Erosion Sampling Survey in China. *Sci. Soil Water Conservation* 11 (4), 17–21. doi:10.3969/j.issn.1672-3007.2013.04.003
- Li, M., Yao, W., Shen, Z., Yang, J., and Yang, E. (2016). Erosion Rates of Different Land Uses and Sediment Sources in a Watershed Using the ¹³⁷Cs Tracing Method: Field Studies in the Loess Plateau of China. *Environ. Earth Sci.* 75 (7), 591. doi:10.1007/s12665-015-5225-6
- Li, J., Ma, X., and Zhang, C. (2020). Predicting the Spatiotemporal Variation in Soil Wind Erosion across Central Asia in Response to Climate Change in the 21st century. *Sci. Total Environ.* 709, 136060. doi:10.1016/j.scitotenv.2019.136060
- Lin, J., Guan, Q., Pan, N., Zhao, R., Yang, L., and Xu, C. (2020). Spatiotemporal Variations and Driving Factors of the Potential Wind Erosion Rate in the Hexi Region, PR China. *Land Degrad. Dev.* 32 (1), 139–157. doi:10.1002/ldr.3702
- Liu, J., Qi, Y., Shi, H., Zhuang, D., and Hu, Y. (2008). Estimation of Wind Erosion Rates by Using ¹³⁷Cs Tracing Technique: A Case Study in Tariat-Xilin Gol Transect, Mongolian Plateau. *Chin. Sci. Bull.* 53, 751–758. doi:10.1007/s11434-008-0007-0
- Liu, B., Qu, J., and Wagner, L. E. (2013). Building Chinese Wind Data for Wind Erosion Prediction System Using Surrogate US Data. *J. Soil Water Conservation* 68 (4), 104A–107A. doi:10.2489/jswc.68.4.104A
- Liu, X. M., Song, H. Q., Lei, T. J., Liu, P. F., Xu, C. D., Wang, D., et al. (2021). Effects of natural and anthropogenic factors and their interactions on dust events in Northern China. *Catena* 196, 104919. doi:10.1016/j.catena.2020.104919
- Lu, H., and Shao, Y. (2001). Toward Quantitative Prediction of Dust Storms: an Integrated Wind Erosion Modelling System and its Applications. *Environ. Model. Softw.* 16 (3), 233–249. doi:10.1016/S1364-8152(00)00083-9
- Luo, W., Taylor, M. C., and Parker, S. R. (2008). A Comparison of Spatial Interpolation Methods to Estimate Continuous Wind Speed Surfaces Using Irregularly Distributed Data from England and Wales. *Int. J. Climatol.* 28 (7), 947–959. doi:10.1002/joc.1583
- Lyu, X., Li, X., Wang, H., Gong, J., Li, S., Dou, H., et al. (2021). Soil Wind Erosion Evaluation and Sustainable Management of Typical Steppe in Inner Mongolia, China. *J. Environ. Manage.* 277, 111488. doi:10.1016/j.jenvman.2020.111488
- MacEachren, A. M., and Davidson, J. V. (1987). Sampling and Isometric Mapping of Continuous Geographic Surfaces. *The Am. Cartographer* 14 (4), 299–320. doi:10.1559/152304087783875723
- Martin, R., Aler, R., Valls, J. M., and Galvan, I. M. (2016). Machine Learning Techniques for Daily Solar Energy Prediction and Interpolation Using Numerical Weather Models. *Concurrency Computat.: Pract. Exper.* 28 (4), 1261–1274. doi:10.1002/cpe.3631
- Mauger, G. S., Bumbaco, K. A., Hakim, G. J., and Mote, P. W. (2013). Optimal Design of a Climatological Network: beyond Practical Considerations. *Geosci. Instrum. Method. Data Syst.* 2 (2), 199–212. doi:10.5194/gi-2-199-2013
- Meteorological Bureau of the People's Republic of China (MBPRC) (2019). *Classification and Rules of Nomenclature for Meteorological Observing Stations*. Beijing, China: China Meteorological Press.
- Ministry of Water Resources of the People's Republic of China (MWRPRC) (2007). *Standards for Classification and Gradation of Soil Erosion*. Beijing, China: China Water Power Press.
- Ministry of Water Resources of the People's Republic of China (MWRPRC) (2013). *The First National Bulletin on Water and Soil Conservation in the National Water Resources Survey*. Beijing, China: Soil and Water Conservation in China.
- Munson, S. M., Belnap, J., and Okin, G. S. (2011). Responses of Wind Erosion to Climate-Induced Vegetation Changes on the Colorado Plateau. *Proc. Natl. Acad. Sci.* 108 (10), 3854–3859. doi:10.1073/pnas.1014947108
- O'Loingsigh, T., McTainsh, G. H., Tews, E. K., Strong, C. L., Leys, J. F., Shinkfield, P., et al. (2014). The Dust Storm Index (DSI): A Method for Monitoring Broad-scale Wind Erosion Using Meteorological Records. *Aeolian Res.* 12, 29–40. doi:10.1016/j.aeolia.2013.10.004
- Owen, P. R. (1964). Saltation of Uniform Grains in Air. *J. Fluid Mech.* 20 (02), 225–242. doi:10.1017/S00222112064001173
- Ozturk, D., and Kilic, F. (2016). Geostatistical Approach for Spatial Interpolation of Meteorological Data. *Acad. Bras. Ciênc.* 88 (4), 2121–2136. doi:10.1590/0001-3765201620150103
- Panebianco, J., and Buschiazio, D. (2013). Effect of Temporal Resolution of Wind Data on Wind Erosion Prediction with the Revised Wind Erosion Equation (RWEQ). *Ciencia Del Suelo* 31 (2), 189–199.
- Pi, H., Sharratt, B., Feng, G., and Lei, J. (2017). Evaluation of Two Empirical Wind Erosion Models in Arid and Semi-arid Regions of China and the USA. *Environ. Model. Softw.* 91 (MAY), 28–46. doi:10.1016/j.envsoft.2017.01.013
- Potter, K. N., Williams, J. R., Larney, F. J., and Bullock, M. S. (1998). Evaluation of EPIC's Wind Erosion Submodel Using Data from Southern Alberta. *Can. J. Soil Sci.* 78 (3), 485–492. doi:10.4141/S97-091
- Raupach, M. R., Gillette, D. A., and Leys, J. F. (1993). The Effect of Roughness Elements on Wind Erosion Threshold. *J. Geophys. Res.* 98 (D2), 3023–3029. doi:10.1029/92JD01922
- Shao, Y. (2001). A Model for mineral Dust Emission. *J. Geophys. Res.* 106 (D17), 20239–20254. doi:10.1029/2001JD900171
- Sharratt, B. S., Tatarko, J., Abatzoglou, J. T., Fox, F. A., and Huggins, D. (2015). Implications of Climate Change on Wind Erosion of Agricultural Lands in the Columbia Plateau. *Weather Clim. Extremes* 10 (PA), 20–31. doi:10.1016/j.wace.2015.06.001
- Sheikh, V., Visser, S., and Stroosnijder, L. (2009). A Simple Model to Predict Soil Moisture: Bridging Event and Continuous Hydrological (BEACH) Modelling. *Environ. Model. Softw.* 24 (4), 542–556. doi:10.1016/j.envsoft.2008.10.005
- Shen, L., Tian, M., and Gao, J. (2016). Analysis on Wind Erosion and Main Factors in Desertification Control Ecological Function Area of Hunshandake Using the Revised Wind Erosion Equation Model. *Res. Soil Water Conservation* 23 (06), 90–97. doi:10.13869/j.cnki.rswc.2016.06.010
- Shepard, D. (1968). "A Two-Dimensional Interpolation Function for Irregularly-Spaced Data," in Proceedings of the 1968 23rd ACM national conference on, January 1968, 517–524. doi:10.1145/800186.810616
- Skidmore, E. L., and Tatarko, J. (1990). Stochastic Wind Simulation for Erosion Modeling. *Trans. ASAE Am. Soc. Agric. Eng.* 33 (6), 1893–1899. doi:10.13031/2013.31555
- Song, Y., Liu, L., Yan, P., and Cao, T. (2005). A Review of Soil Erodibility in Water and Wind Erosion Research. *J. Geogr. Sci.* 15 (2), 167–176. doi:10.1007/BF02872682
- Song, H., Zhang, K., Piao, S., Liu, L., Wang, Y.-P., Chen, Y., et al. (2019). Soil Organic Carbon and Nutrient Losses Resulted from spring Dust Emissions in Northern China. *Atmos. Environ.* 213, 585–596. doi:10.1016/j.atmosenv.2019.06.043
- Song, Z. (2004). A Numerical Simulation of Dust Storms in China. *Environ. Model. Softw.* 19 (2), 141–151. doi:10.1016/S1364-8152(03)00116-6
- van Donk, S. J., Wagner, L. E., Skidmore, E. L., and Tatarko, J. (2005). Comparison of the Weibull Model with Measured Wind Speed Distributions for Stochastic Wind Generation. *Soil Water Division. ASABE* 48, 503–510. doi:10.13031/2013.18324
- van Donk, S. J., Liao, C., and Skidmore, E. L. (2008). Using Temporally Limited Wind Data in the Wind Erosion Prediction System. *ASABE* 51 (5), 1585–1590. doi:10.13031/2013.25315
- Vanpelt, R., Potter, K., Stout, J., Popham, T., and Zobeck, T. (2004). Validation of the Wind Erosion Stochastic Simulator (WESS) and the Revised Wind Erosion Equation (RWEQ) for Single Events. In *Proceedings of the International Symposium on Soil Erosion Research for the 21st Century, Honolulu, January 3–5*, 471–474. doi:10.1016/S1364-8152(03)00122-1
- Visser, S. M., Sterk, G., and Karssenbergh, D. (2005). Wind Erosion Modelling in a Sahelian Environment. *Environ. Model. Softw.* 20 (1), 69–84. doi:10.1016/j.envsoft.2003.12.010
- Wagner, L. E., Tatarko, J., and Skidmore, E. L. (1992). *WIND-GEN: A Statistical Database and Generator for Wind Data*. Paper-American Society of Agricultural Engineers USA.
- Wang, X., Guo, Z., Chang, C., Wang, R., Li, J., Li, Q., et al. (2020). Spatiotemporal Distribution of Soil Wind Erosion Modulus in the Agro-Pastoral Ecotone of north China. *J. Desert Res.* 40 (1), 12–22. doi:10.7522/j.issn.1000-694X.2019.00030

- Wang, X., Liu, J., Che, H., Ji, F., and Liu, J. (2018). Spatial and Temporal Evolution of Natural and Anthropogenic Dust Events over Northern China. *Sci. Rep.* 8 (5), 241–257. doi:10.1038/s41598-018-20382-5
- Webb, N. P., McGowan, H. A., Phinn, S. R., Leys, J. F., and McTainsh, G. H. (2009). A Model to Predict Land Susceptibility to Wind Erosion in Western Queensland, Australia. *Environ. Model. Softw.* 24 (2), 214–227. doi:10.1016/j.envsoft.2008.06.006
- Webb, N. P., Chappell, A., Strong, C. L., Marx, S. K., and McTainsh, G. H. (2012). The Significance of Carbon-Enriched Dust for Global Carbon Accounting. *Glob. Change Biol.* 18 (11), 3275–3278. doi:10.1111/j.1365-2486.2012.02780.x
- Webb, N. P., Kachergis, E., Miller, S. W., McCord, S. E., Bestelmeyer, B. T., Brown, J. R., et al. (2020). Indicators and Benchmarks for Wind Erosion Monitoring, Assessment and Management. *Ecol. indicators* 110, 105881. doi:10.1016/j.ecolind.2019.105881
- Woodruff, N. P., and Siddoway, F. H. (1965). A Wind Erosion Equation. *Proc. Soil Ence Soc. America* 29 (5), 602–608. doi:10.2136/sssaj1965.03615995002900050035x
- Wu, X., Fan, J., Sun, L., Zhang, H., Xu, Y., Yao, Y., et al. (2021). Wind Erosion and its Ecological Effects on Soil in the Northern piedmont of the Yinshan Mountains. *Ecol. Indicators* 128, 107825. doi:10.1016/j.ecolind.2021.107825
- Xing, C., Guo, Z., Chang, C., Wang, R., and Zhang, Z. (2018). Validation of RWEQ Model in the Bashang Area, Hebei, China. *J. Desert Res.* 38 (06), 1180–1192. doi:10.7522/j.issn.1000-694X.2018.00014
- Yizhaq, H., Xu, Z., and Ashkenazy, Y. (2020). The Effect of Wind Speed Averaging Time on the Calculation of Sand Drift Potential: New Scaling Laws. *Earth Planet. Sci. Lett.* 544, 116373. doi:10.1016/j.epsl.2020.116373
- Youssef, F., Visser, S., Karssen, D., Bruggeman, A., and Erp, G. (2012). Calibration of RWEQ in a Patchy Landscape; a First Step towards a Regional Scale Wind Erosion Model. *Aeolian Res.* 3 (4), 467–476. doi:10.1016/j.aeolia.2011.03.009
- Yuan, Y., Yin, S., Xie, Y., and Guo, Z. (2018). Temporal and Spatial Characteristics of Diurnal Variations of Wind Speed in Wind Erosion Areas over China. *Arid Land Geogr.* 41 (3), 480–487. doi:10.13826/j.cnki.cn65-1103/x.2018.03.006
- Zhang, J., Zou, X., Zhang, C., Yang, S., Pan, X., and Liu, Y. (2010). *Evaluating farmland Soil Erosion by Wind in Bashang of Zhangjiakou with ¹³⁷Cs as a Tracer*, 46. Natural Science: Journal of Beijing Normal University, 724–728.
- Zhang, G., Azorin-Molina, C., Shi, P., Lin, D., Guijarro, J. A., Kong, F., et al. (2019). Impact of Near-Surface Wind Speed Variability on Wind Erosion in the Eastern Agro-Pastoral Transitional Zone of Northern China, 1982–2016. *Agric. For. Meteorology* 271, 102–115. doi:10.1016/j.agrformet.2019.02.039
- Zhang, D., Liang, P., Yang, X., and Li, H. (2020). The Control of Wind Strength on the Barchan to Parabolic Dune Transition. *Earth Surf. Process. Landforms* 45 (10), 2300–2313. doi:10.1002/esp.4881
- Zhao, Y., Yue, J., Xu, C., Du, C., and Chang, Y. (2005). Application of ¹³⁷Cs Tracer Technique to Estimate the Wind Erosion Rate of Castanet in Luanhe River Source Area. *Acta Scientiae Circumstantiae* 2005 (4), 562–566. doi:10.3321/j.issn:0253-2468.2005.04.024
- Zhao, Y., Pei, Y. S., and Zhai, Z. J. (2011). Distributed Simulation of Soil Wind Erosion and its Application to the Tuhaimajia River basin. *Hydraulic Eng.* 42 (05), 554–562. doi:10.13243/j.cnki.slx.2011.05.009
- Zhao, Y., Wu, J., He, C., and Ding, G. (2017). Linking Wind Erosion to Ecosystem Services in Drylands: a Landscape Ecological Approach. *Landscape Ecol.* 32 (12), 2399–2417. doi:10.1007/s10980-017-0585-9
- Zhou, Z., Zhang, Z., Zou, X., Zhang, K., and Zhang, W. (2020). Quantifying Wind Erosion at Landscape Scale in a Temperate Grassland: Nonignorable Influence of Topography. *Geomorphology* 370, 107401. doi:10.1016/j.geomorph.2020.107401
- Zobeck, T. M., Parker, N. C., Haskell, S., and Guoding, K. (2000). Scaling up from Field to Region for Wind Erosion Prediction Using a Field-Scale Wind Erosion Model and GIS. *Agriculture, Ecosystems, Environ.* 82 (1–3), 247–259. doi:10.1016/S0167-8809(00)00229-2
- Zobeck, T. M., Van Pelt, S., Stout, J. E., and Popham, T. W. (2001). Validation of the Revised Wind Erosion Equation (RWEQ) for Single Events and Discrete Periods. *Soil Erosion*, 471–474. doi:10.13031/2013.4579
- Zou, X., Zhang, C., Cheng, H., Kang, L., and Wu, Y. (2015). Cogitation on Developing a Dynamic Model of Soil Wind Erosion. *Sci. China Earth Sci.* 58 (3), 462–473. doi:10.1007/s11430-014-5002-5

Conflict of Interest: The authors declare that the research was conducted in the absence of any commercial or financial relationships that could be construed as a potential conflict of interest.

Publisher's Note: All claims expressed in this article are solely those of the authors and do not necessarily represent those of their affiliated organizations, or those of the publisher, the editors, and the reviewers. Any product that may be evaluated in this article, or claim that may be made by its manufacturer, is not guaranteed or endorsed by the publisher.

Copyright © 2022 Zhang, Guo, Li, Chang, Wang and Li. This is an open-access article distributed under the terms of the Creative Commons Attribution License (CC BY). The use, distribution or reproduction in other forums is permitted, provided the original author(s) and the copyright owner(s) are credited and that the original publication in this journal is cited, in accordance with accepted academic practice. No use, distribution or reproduction is permitted which does not comply with these terms.



The Natural Suitability of Human Settlements and Their Spatial Differentiation in the Nenjiang River Basin, China

Yang Zhao and Junling Zhang*

College of Landscape Architecture, Northeast Forestry University, Harbin, China

OPEN ACCESS

Edited by:

Jifeng Deng,
Shenyang Agricultural University,
China

Reviewed by:

Xiaoyu Li,
Northeast Institute of Geography and
Agroecology (CAS), China
Liping Rong,
Yanbian University, China

*Correspondence:

Junling Zhang
zy1594858050@163.com

Specialty section:

This article was submitted to
Drylands,
a section of the journal
Frontiers in Environmental Science

Received: 24 January 2022

Accepted: 02 March 2022

Published: 04 April 2022

Citation:

Zhao Y and Zhang J (2022) The Natural
Suitability of Human Settlements and
Their Spatial Differentiation in the
Nenjiang River Basin, China.
Front. Environ. Sci. 10:861027.
doi: 10.3389/fenvs.2022.861027

The natural suitability of human settlements (NSHS) of the Nenjiang River Basin was carried out by evaluation indices such as terrain characteristics, vegetation, hydrology, and climate of the region. The NSHS model is built using a GIS spatial analysis platform to reveal the suitability zoning and spatial differentiation (SD) characteristics of human settlements in the study area. The results show that the NSHS index of the study area ranges from 0.31 to 0.92, with an average of 0.54, indicating that the values show a gradual increase from northwest to southeast and from mountainous and hilly areas to plains. The most suitable and generally suitable areas constitute nearly 41.81% of the basin, and the population of these terrain accounts for about 84.25% of the total population of the basin. The suitable area category covers the largest area among all other categories accounting for about 25.16%, and the population of these regions accounts for about 12.46%. The critical suitable area category accounts for 21.70% of the basin, whereas unsuitable areas account for 11.32%, constituting the smallest areas compared to other categories. It is also evident that diverse limiting factors of NSHS characterize distinct areas in the study area. For example, high NSHS index, the normalized difference vegetation index (NDVI), and water resource index (WRI) are the main limiting factors in plane areas, low NSHS index, the relief degree of land surface (RDLS) index, and temperature-humidity index (THI) are the major limiting factors in the mountainous, hilly and plateau areas.

Keywords: GIS, human settlements, natural suitability, spatial differentiation, Nenjiang River basin

1 INTRODUCTION

The natural environment is recognized as the framework for human existence, productivity, and life. The natural suitability of human settlements (NSHS) directly influences the distribution, migration, and population density of an area under natural conditions and affects the degrees of regional and socio-economic development, living comfort, and rational utilization of resources.

Several researchers have traditionally focused on diverse aspects of human settlement environment assessment (HSEA), including HSEA with cities [(Li and Ni, 2009; Sui et al., 2013; Qing et al., 2018), etc.], HSEA with rural areas [(Li et al., 2015; Wu D. et al., 2016; Zeng et al., 2016)], etc. The mainstream evaluation methods of HSEA are mostly comprised of questionnaire surveys, structural models, analytic hierarchy processes, fuzzy comprehensive

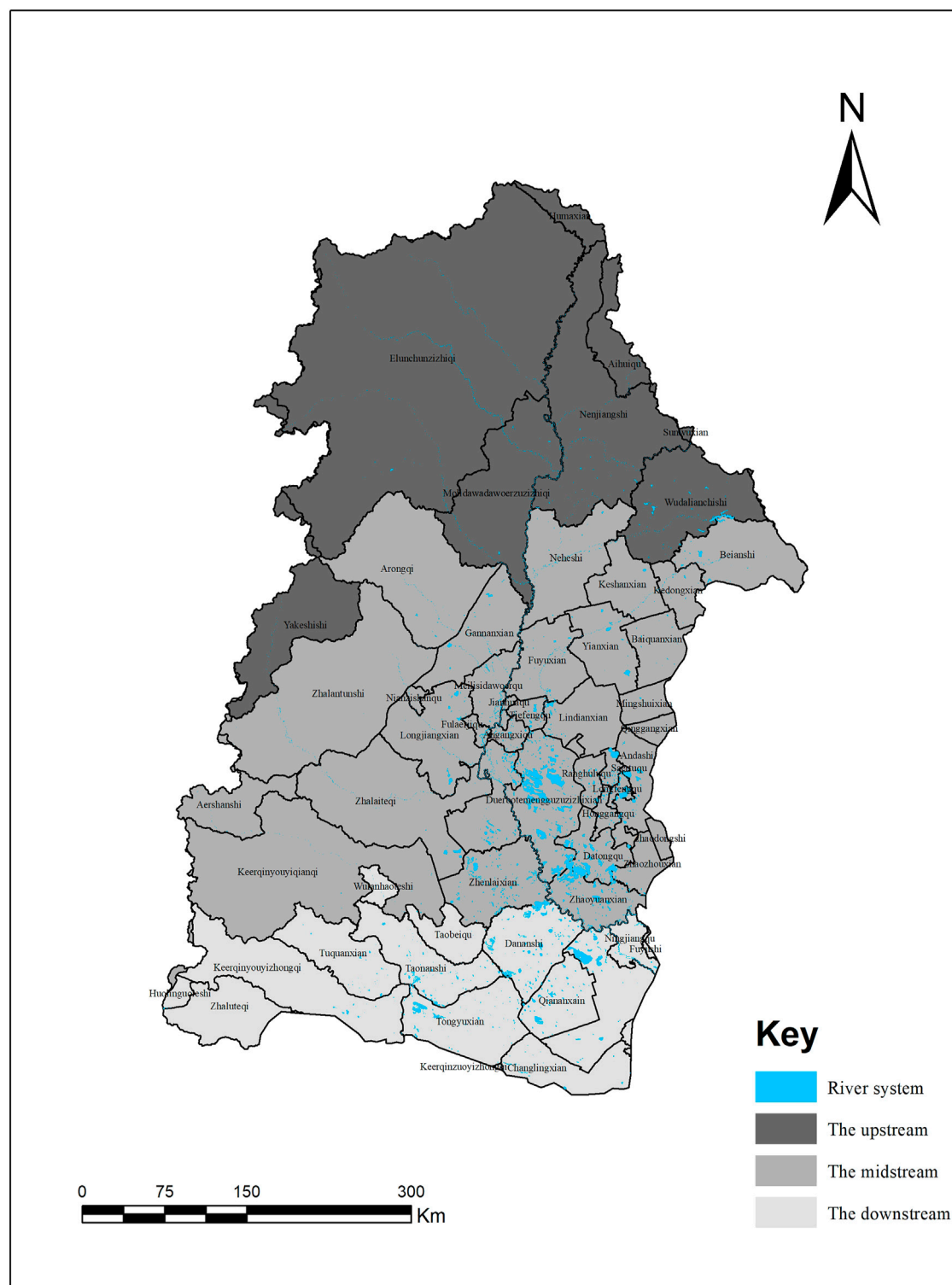
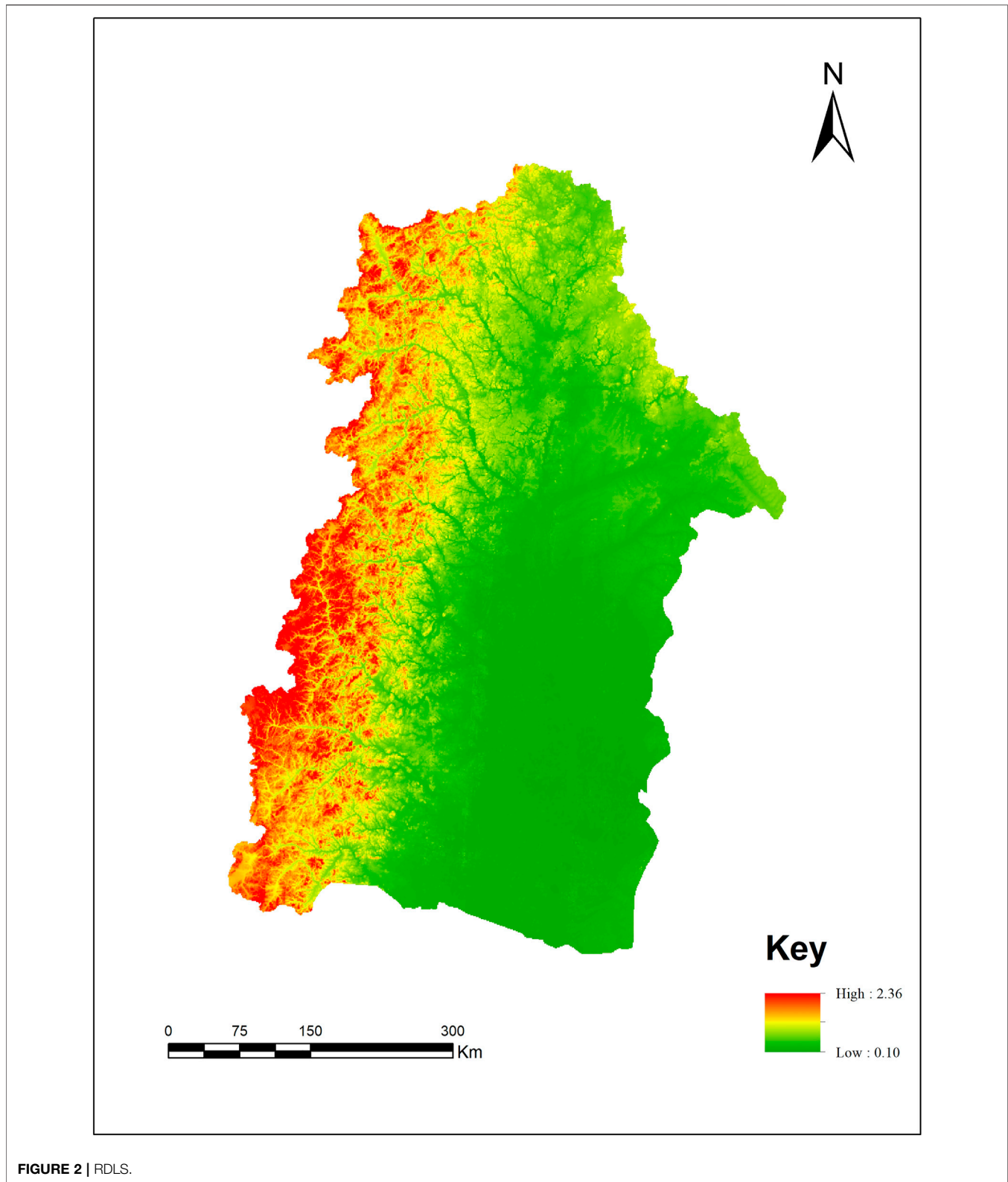


FIGURE 1 | Nenjiang river basin.

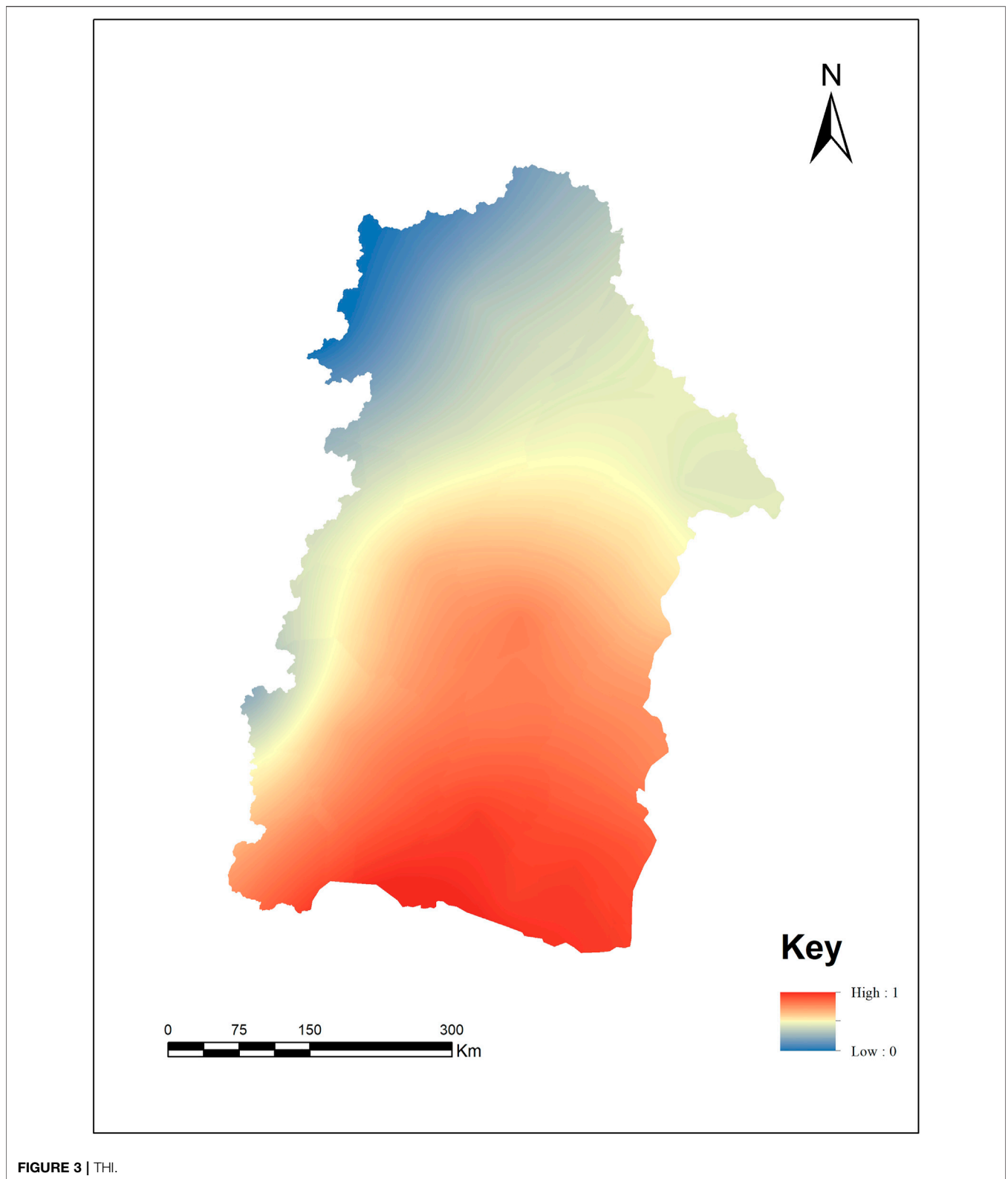
evaluation, GIS analyses, etc. (Liu and Zhang, 2014). Several domestic researchers have conducted numerous HSEAs at various levels (Xu et al., 2007; Li et al., 2010; Li et al., 2011;

Min et al., 2012; Gu et al., 2015; Wu H. et al., 2016; Wang and Wang, 2019), including those conducted across different countries, regions, provinces, and cities. The earlier



research in the Nenjiang River Basin related to HSEA are unilaterally focused on climate, topography, vegetation, and hydrology (De Freitas, 1979; Wu et al., 2019; Li et al., 2020;

Wang X. et al., 2020; Wang Z. et al., 2020). However, a comprehensive HSEA based on the aforementioned natural factors has not been reported so far, and hence adequate



research on NSHS evaluation of the study areas needs utmost importance. In this context, the present study builds the human settlements index (HSI) model for the Nenjiang

River Basin in terms of various factors such as topography, climate, vegetation, hydrology, and soil using GIS. The study also highlights the spatial adaptability and geographical

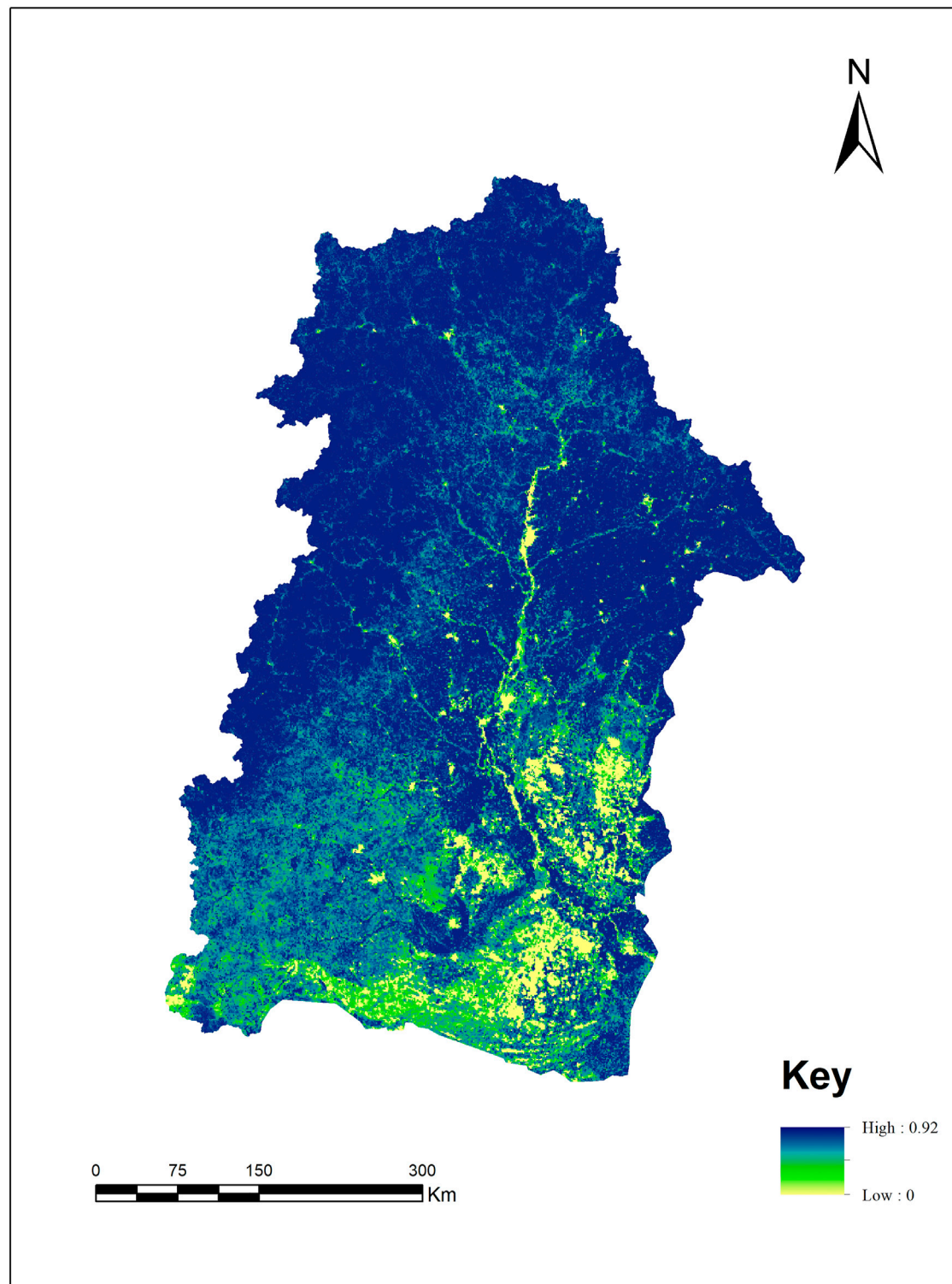


FIGURE 4 | NDVI.

distribution features of human settlements in the study area. It provides a scientific basis and decision-making reference for population distribution planning, resources efficiency and

rationality, environmental protection, and improvement of NSHS. The present paper evaluates the adequacy of natural conditions and living environment in the Nenjiang River

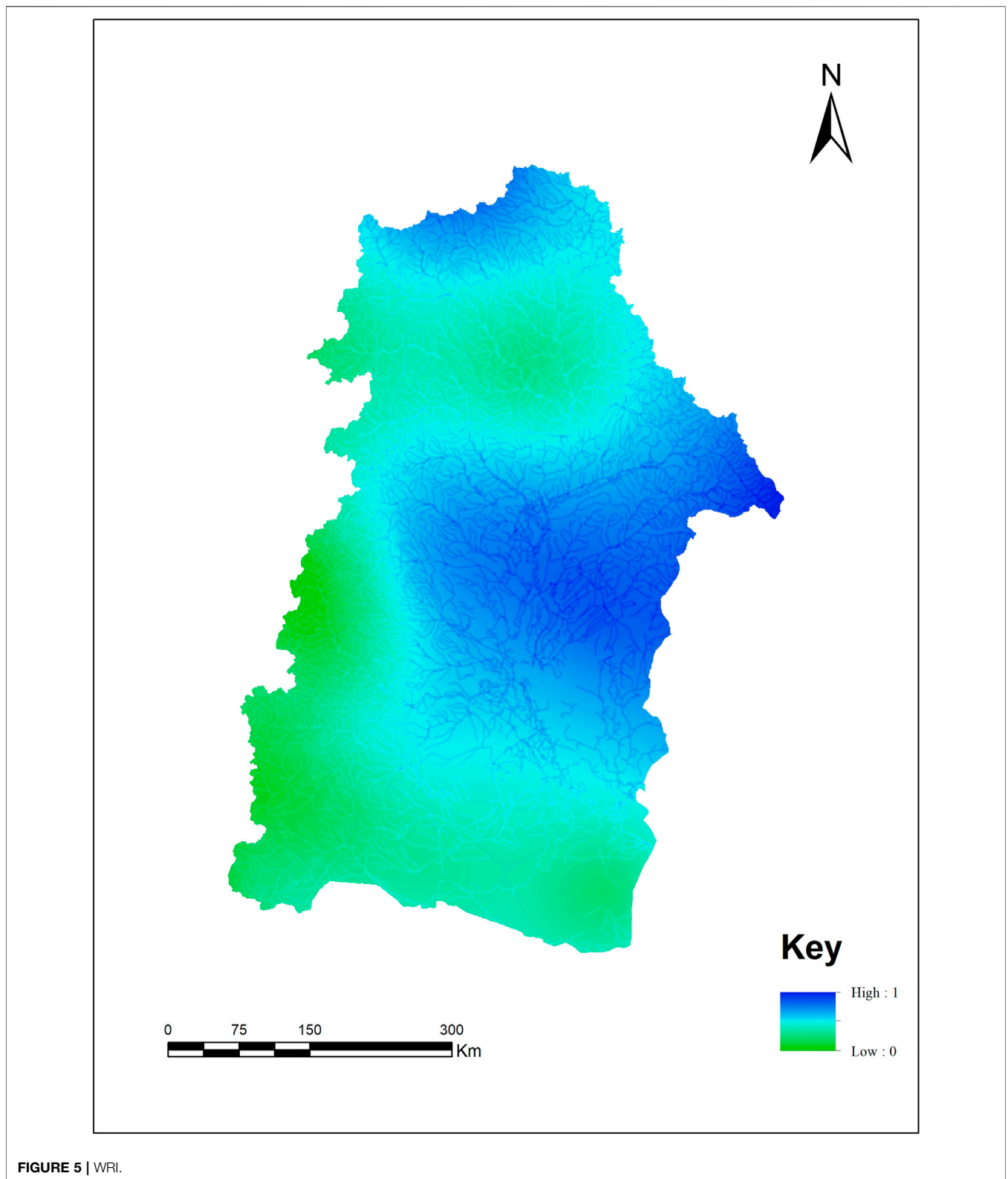


FIGURE 5 | WRI.

Basin, China. This study helps to rejuvenate the northeast by providing a theoretical foundation for rational population distribution planning, efficient and rational utilization of

resources, regional natural environmental protection, rational social infrastructure construction, and improvement of NSHS.

2 MATERIALS AND RESEARCH METHODS

2.1 Overview of the Study Area

This region is located at 119°15′–127°40′E and 44°26′–51°37′N. Originating from the south foot of Yilehuli Mountain in Greater Khingan Mountains, the river flows through Nenjiang, Erlunchun, Nehe, and other counties (cities and banners) from north to south. It merges with the main stream of Songhua River at Sancha estuary, with a total length of 1,370 km and a drainage area of 297,000 km². The region is in the northern edge of East Asian monsoon region, with the semi-humid continental climate of cold temperate zone. It has long and cold winter, short and rainy summer, with the annual average temperature of 1°–4°. Its historical minimum temperature is –39.5°C, while the maximum temperature is 40.1°C. The region's main geomorphic types include plateaus, mountains, hills, and plains. It covers Hailar City, Ulanhot City, Huolingol City, and Tongliao City in Inner Mongolia Autonomous Region, Heihe City, Qiqihar City, Daqing City, Suihua City, and Harbin City in Heilongjiang Province, Baicheng City and Fuyu City in Jilin Province. The region can be divided into three sections on the basis of the natural characteristics: the upstream, the midstream and the downstream, as shown in Figure 1.

2.2 Data Source and Processing

2.2.1 Data Sources

The remote sensing data and images of the study area, including 30 m × 30 m DEM, were generated using the topographic map from the China Geospatial data Cloud of the Chinese Academy of Sciences. The meteorological data such as temperature, humidity, and precipitation in the basin from the basic observation data of 16 meteorological stations as part of the China Meteorological data Network. The vegetation data of the area from July to September 2015 were collected from the remote sensing data captured by Landsat 8. The demographic population data in 2017 was collected from the economic and social statistical yearbook for the study area.

2.2.2 Data Preprocessing

A uniform projection coordinate system was established by projecting and transforming the remote sensing and DEM data. Further, relief features such as slope, elevation variation, average altitude, and other relevant data were extracted from the DEM. The normalized difference vegetation index (NDVI) and modified normalized difference water index (MNDWI) of the basin were extracted using ENVI software. A comprehensive evaluation of the natural factor data precipitation, temperature, and humidity in the basin was carried out by generating their index data layers through density calculation and kriging interpolation using the spatial analysis tool of the ArcGIS software. Further, the HSEA model was built to develop the NSHS index map and to examine the SD characteristics of the study area.

2.3 Research Methods

2.3.1 RDLS

The land surface is the foundation for human existence and development, and hence, the human activities of an area are

significantly influenced by the topographic variations and geomorphic features. The relief degree of the land surface (RDLS) of the study area has been calculated based on Feng et al. (2008), and the following equation is used for the calculation.

$$RDLS = \frac{ALT}{1000} + \{[Max(H) - Min(H)] \times [1 - P(A)/A]\} \times /500$$

Where: *Max(H)* and *Min(H)* represent the highest and the lowest altitudes respectively in the study area; *A* is the total area, and *P(A)* is the area of flat land. The RDLS is computed using the unique topography and landform of the basin as the basis of this study, with a 1 km × 1 km grid as the fundamental evaluation unit (*A* is 1 km²). The calculation results of RDLS are shown in Figure 2.

2.3.2 THI

Climate patterns have a significant impact on human activity. Tome's discomfort index, commonly known as the temperature-humidity index (THI), measures the degree of humidity in the absence of wind. The following equation is used for the calculation of THI.

$$THI = T - 0.55 \times (1 - f)(T - 58)$$

$$T = 1.8t + 32$$

$$K = -(10\sqrt{v} + 10.45 - v)(33 - t) + 8.55S$$

Where *THI* represents the temperature-humidity index, *K* represents the wind efficiency index, *t*, and *T* represent the monthly averages of temperatures in °C and °F respectively, *f* represents the monthly average relative humidity of air (%), *v* represents the average wind speed (m/s) at the height of 10 m above the ground, and *S* represents the sunshine hours (h/d). The calculation results of THI are shown in Figure 3.

2.3.3 NDVI

The height of vegetation cover is considered as one of the essential indices for determining the living environment and is used to evaluate ecological conditions of human production and life. The normalized difference vegetation index (NDVI) is the standard way to represent the vegetation index (Wei et al., 2012). The following equation is used to calculate the NDVI.

$$NDVI = (NIR - R)/(NIR + R)$$

Where *NIR* and *R* are the reflectances of the near-infrared and red bands, respectively. The estimated values of NDVI are in Figure 4.

2.3.4 WRI

The quality of hydrological conditions is particularly significant to the NSHS in the basin since water resources are essential natural resources for survival and development. One of the most often used indices for assessing the regional hydrological conditions is the water resource index (WRI) (Wei et al., 2012). The equation used for the calculation of WRI is as follows.

$$WRI = \alpha P + \beta WPM$$

Where *WRI* is the water resource index, *P* is normalized precipitation; *WPM* is the normalized water production modulus, and α and β are the weight values of precipitation and water production modulus, respectively. The estimated values of *WRI* for the basin are shown in **Figure 5**.

2.3.5 HEI Model

$$HEI = \alpha \times NRDLS + \beta \times NTHI + \gamma \times NWRI + \delta \times NLCI$$

Where *HEI*, *NRDLS*, *NTHI*, *NWRI*, and *NLCI* represent human settlements environment index, normalized relief degree of the land surface, normalized temperature-humidity index, normalized water resource index, and normalized land-cover index. The symbols α , β , γ , and δ represent the weights of *NRDLS*, *NTHI*, *NWRI*, and *NLCI*, respectively. The maximum, minimum, and optimum values corresponding to each index in standardization procedures are based on the research findings reported by Feng et al. (2008), Wei et al. (2012), and Li and Zheng (2018). The correlation between these four indices and the grid layer of population density was examined using the spatial analysis tool of ArcGIS. The correlation coefficients were subsequently inverted and normalized using SPSS statistical software. The weights of NSHS evaluation indices in the basin, α , β , γ , and δ were estimated as 0.387, 0.153, 0.275, and 0.185, respectively. Based on the NSHS values, the study area has been divided into five categories: most suitable, generally suitable, suitable, critical suitable, and unsuitable areas. The SD and regional characteristics of these categories were analyzed based on the results of earlier research on the human settlements index model (Ma et al., 2007; Hao and Ren, 2009; Wei et al., 2012; Li and Zheng, 2018).

3 RESULTS AND ANALYSIS

3.1 NSHS Evaluation in Nenjiang River Basin

The results of the calculations (**Figure 3**) demonstrate that the NSHS indices of the Nenjiang River Basin vary from 0.3 to 0.92, with an average of 0.54. The relative suitability progressively improves from northwest to southeast and from mountainous and hilly areas towards plains. The north of Songnen and Liaohe Plains, with flat topography, excellent hydrothermal conditions, convenient transportation, a high level of economic development, and large population density, is characterized by high NSHS indices. The area falling under the suitable category of NSHS indices occupies most part of the basin, accounting for 25.16% of the total area of the basin. The details of different categories of NSHS indices of the basin are discussed in the following subheads.

- 1) Most suitable area: The areas under the most suitable category are characterized by NSHS indices from 0.68 to 0.90, covering an estimated land area of 56,161.05 km², accounting for 19.35% of the basin area. The settlements of the area are mainly concentrated in the Songnen Plain and the northern parts of Liaohe plain with a population of 3,563,250, which is 61.54% of the total population of the basin and the population

density of 63 people/km². These areas mark the economic powerhouse of the Nenjiang River Basin due to ideal natural conditions. However, the shortage of water resources and severe deterioration of vegetation in the area limits the NSHS in terms of population and natural conditions.

- 2) Generally suitable area: The NSHS indices of the generally suitable category of areas range from 0.59 to 0.69, covering a land area of 65,188.41 km², which account for about 22.46% of the basin area. These zones are mainly focused in the southeastern parts of the Greater Khingan Mountains and nearby areas with a population of 1,315,187, which is 22.71% of the total population of the basin, and a population density of 20 people/km². Agricultural production lands mainly dominate these areas where the topography is flat.
- 3) Suitable areas: The NSHS indices of the suitable category of land range from 0.47 to 0.59, covering a land area of 73,028.45 km², which is about 25.16% of the basin area. The category is mainly distributed in the Greater Khingan Mountains areas, where the population is 721,493, which accounts for 12.46% of the total population of the basin, with a population density of 10 people/km². These areas are described as agricultural lands with modest residual mountains and hills.
- 4) Critical suitable area: The NSHS indices of the critical suitable area category ranges from 0.36 to 0.47, occupying nearly 62,969.82 km² of land area, which accounts for 21.70% of the basin area. This zone covers the northwestern parts of the Greater Khingan Mountains, where the population is 150,359, which is 2.60% of the total population of the basin, with a population density of 2 persons/km². This zone is characterized by larger RDLS with poor human settlements and is unsuitable for living due to its relatively sparse population.
- 5) Unsuitable areas: The NSHS indices of the unsuitable category of the basin range from 0.13 to 0.36, covering a land area of 32,864.03 km², accounting for about 11.32% of the basin area. This zone is occupied in the eastern part of Hulunbuir plateau, where the population is 40,211, which is nearly 0.69% of the total population of the basin and the population density is 1 person/km². The area is characterized by steep slopes with low THI and poor environment and hence unsuitable for living.

3.2 Single-Factor Analysis of NSHS in the Study Area

The superimposition of each evaluation factor and the NSHS using the spatial analysis tool in ArcGIS indicates that the dominant limiting factors of human settlements vary spatially with greater spatial differentiation.

- 1) RDLS factor analysis: The NSHS of the study area is essentially associated with RDLS in space, with a significant negative correlation, indicating lower values of RDLS for better NSHS and vice versa. RDLS has a significant impact on the population distribution of an area. A lesser percentage of the population occupy steep and hilly areas, while most of the population lives in plane lands.
- 2) NDVI factor analysis: The NDVI index directly impacts the perception of people on NSHS, and there is a positive

TABLE 1 | The grading standards of biometeorology suitability assessment.

THI		K		Grade
Range	Degree of sensation	Range	Degree of sensation	
<40	Extremely cold, extremely uncomfortable	<-1,200	Severe cold, extremely uncomfortable	e
40–45	Cold, uncomfortable	-1,200~-1,000	Cold, uncomfortable	d
45–55	Slightly cold, rather uncomfortable	-1,000~-800	Cold and icy, rather uncomfortable	c
55–60	Clear and cool, comfortable	-800~-600	Clear and cool, comfortable	b
60–65	Cool, very comfortable	-600~-300	Cool, very comfortable	A
65–70	Warm, comfortable	-300~-200	Warm, comfortable	B
70–75	Slightly heat, rather comfortable	-200~-50	Warmly heat, rather comfortable	C
75–80	Muggy, uncomfortable	-50~80	Hot, uncomfortable	D
>80	Extremely muggy, extremely uncomfortable	>80	Scorching hot, extremely uncomfortable	E

correlation between these two factors. However, the correlation is generally lower in densely populated areas with higher NSHS, while it is higher in sparsely populated mountainous and hilly areas, especially between NVDI and RDLS factors. This is one of the most important elements affecting the NSHS on the plain.

- 3) THI factor analysis: The THI indices of the Nenjiang River Basin rises substantially from northwest to southeast and from areas with higher altitudes to low altitudes, and the values are shown in **Table 1**. Based on the spatial variations in THI, the basin has been divided into three categories with THI values < 40, 40–45, and 45–55. Extreme areas are also distributed in the basin, especially in the northwestern parts, accounting for 36.3% of the basin area. Hence, THI can be considered as one of the important factors affecting the NSHS values. It is also observed that the THI indices are negatively correlated with RDLS.
- 4) WRI Factor analysis. The WRI and NSHS indices of the Nenjiang River basin are positively correlated with a correlation coefficient of 0.1848. The overall WRI index of the basin increases in the east and decreases towards the west along the Nenjiang River. This is one of the major challenges that limit the improvement in NSHS in the plain to a certain extent.

4 DISCUSSION

The present study investigates the suitability zoning and spatial differentiation (SD) characteristics for human settlements in the Nenjiang River Basin using NSHS as an evaluation index by considering the terrain features, climate, vegetation, and hydrology. The NSHS model of the area was built using the GIS spatial analysis platform. The Nenjiang River is a tributary of Songhua River and serves various purposes, including water conservation, soil and water conservation, economic development, and human survival. Hence, understanding the NSHS and SD of the basin offers both theoretical and practical relevance.

It may be used to provide theoretical and empirical justification for a follow-up ecological compensatory mechanism to analyze the NSHS of the basin using a quantitative approach. The most suitable areas are often economically established, with significant environmental carrying capacities, whereas the unsuitable areas are often economically underdeveloped, with limited environmental carrying capacities. As a result, it is necessary to

establish a reasonable and appropriate upstream-midstream-downstream ecological compensation mechanism must be established and the ecological compensation priority and compensation criteria of each basin section must be calculated. The goal of the present study is to use the ecological compensation mechanism to limit human activities in unsuitable areas and develop a green industry. Furthermore, the selection of indices and weighting procedures involved in the study need to be discussed further in view of the complex social and natural environment of the study area. As a consequence of long term and historical effects, certain phenomena in the study area are incongruous with the research conclusion in the present study, which needs detailed investigations in the future. At the same time since the natural foundation, social foundation, and ecological background involved in human settlements make a complex system to accurately express the suitability of human settlements, the selection of indicators and determination of parameters of the model still need to be deeply investigated.

5 CONCLUSION

- 1) The NSHS values gradually decrease from southeast to northwest and from plain to mountainous and hilly areas. The most suitable category covers nearly 56,161.05 km² of area, which accounts for 19.35% of basin area, whereas the generally suitable category covers an area of 65,188.41 km², which accounts for 22.46% of the basin areas. The suitable category areas cover 73,028.45 km² of land, accounting for about 25.16% of basin area, while the critically suitable areas cover 62,969.82 km² of land, accounting for about 21.70% of the basin area. Further, the unsuitable areas cover nearly 32,864.03 km² of land, accounting for 11.32% of the basin area.
- 2) The major limiting factors of NSHS vary spatially, with high NSHS THI index and WRI index values in plane areas. The limiting factors in the mountainous and hilly areas include low NSHS and RDLS indices. The NDVI index has a negligible effect on the SD of NSHS in the study area.
- 3) The SDs of NSHS in the study area are highly correlated with RDLS values, which greatly affect the population distribution of the basin. The majority of the population is occupied in the northern parts of Songnen and Liaohe plains.
- 4) With the help of GIS platform, the calculation, statistics, and analysis methods of GIS are used to determine the influencing

factors of human settlement suitability in Nenjiang River Basin. Based on grid data and spatial patterns, which can better quantitatively reflect the regional differences in the basin, it can guide the rational distribution and flow of population, and is of great significance to promote the coordinated development of population, resources and environment. It is a research method worthy of reference and utilization.

DATA AVAILABILITY STATEMENT

The original contributions presented in the study are included in the article/Supplementary Material, further inquiries can be directed to the corresponding author.

REFERENCES

- De Freitas, C. R. (1979). Human Climates of Northern China. *Atmos. Environ.* 13, 71–77. doi:10.1016/0004-6981(79)90246-4
- Feng, Z., Tang, Y., Yang, Y., and Zhang, D. (2008). The Establishment and Application of China's Human Settlement Index Model Based on GIS. *Acta Geogr. Sin.* 63, 1327–1336. doi:10.3321/j.issn:0375-5444.2008.12.010
- Gu, Y., Yang, J., Feng, X., Li, C., and Li, X. (2015). Research on the Spatial Differentiation of Human Settlement Suitability in Typical Tourist Cities in China. *Geogr. Sci.* 35, 410–418. doi:10.13249/j.cnki.sgs.2015.04.004
- Hao, H., and Ren, Z. (2009). Evaluation of the Natural Suitability of Human Settlements in Shaanxi Province Based on Raster Data. *Acta Geogr. Sin.* 64, 498–506. doi:10.11821/xb200904012
- Li, B., and Zheng, S. (2018). Evaluation of Human Settlement Environment Suitability and Spatial Differentiation in Fenhe River Basin. *Arid Land Resour. Environ.* 32, 87–92. doi:10.13448/j.cnki.jalre.2018.240
- Li, H., Yang, W., and Li, F. (2020). Analysis of Temporal and Spatial Distribution of Precipitation Characteristics in Nenjiang River Basin. *J. Northwest. Univ. Nat. Sci. Ed.* 50, 427–437. doi:10.16152/j.cnki.xdxbzr.2020-03-013
- Li, P., Chen, C., and Chen, J. (2015). Research on the Evolution and Influencing Factors of the Multi-Functional Spatio-Temporal Pattern of Rural Areas: Taking Jiangsu Province as an Example. *Geogr. Sci.* 35, 845–851. doi:10.13249/j.cnki.sgs.2015.07.006
- Li, X., and Ni, Y. (2009). Evaluation of the Coordinated Development of Urbanization and Urban Human Settlements in My Country's Excellent Livable Cities in the Past Ten Years. *Arid Land Resour. Environ.* 23, 8–14. doi:10.13448/j.cnki.jalre.2009.03.025
- Li, Y., Liu, C., Zhang, H., and Gao, X. (2011). Evaluation on the Human Settlements Environment Suitability in the Three Gorges Reservoir Area of Chongqing Based on RS and GIS. *J. Geogr. Sci.* 21, 346–358. doi:10.1007/s11442-011-0849-2
- Li, Y., Liu, S., and Li, X. (2010). GIS-based Evaluation of Human Settlements in the Nuijiang Canyon — Taking Lushui County as an Example. *Adv. Geogr. Sci.* 29, 572–578. doi:10.11820/dlkxjz.2010.05.009
- Liu, J., and Zhang, W. (2014). A Review of Research on Human Settlement Environment Evaluation Methods. *Urban Dev. Res.* 21, 46–52. doi:10.1007/s11356-014-2843-6
- Ma, L., Sun, G., Li, F., and Wang, B. (2007). Evaluation of Tourism Climate Comfortableness in Shanxi Province. *Resour. Sci.* 29, 40–44. doi:10.3321/j.issn:1007-7588.2007.06.006
- Min, J., Liu, C., and Li, Y. (2012). Nature Suitability for Human Settlement Based on GIS Technology. *Resour. Environ. Yangtze River Basin* 21, 1006–1012.
- Qing, F., Xia, X., and Jiang, Z. (2018). Evaluation of Human Settlement Environment Suitability in Xindu District of Chengdu Based on RS and GIS. *J. Qiqihar Univ. (Nat. Sci. Ed.)* 34, 7689–7780. doi:10.3969/j.issn.1007-984X.2018.02.015
- Sui, Y., Shi, J., Cui, L., and Liang, P. (2013). Comprehensive Evaluation of the Ecological Quality of Urban Human Settlements in Shanghai. *Resour. Environ. Yangtze River Basin* 22, 965–971.

AUTHOR CONTRIBUTIONS

YZ and JZ contributed to conception and design of the study. YZ organized the database, performed the statistical analysis. YZ wrote the first draft of the manuscript, wrote sections of the manuscript. All authors contributed to manuscript revision, read, and approved the submitted version.

FUNDING

This work was supported by the Science Foundation of Heilongjiang Province (Grant No. LH2020E008).

- Wang, X., Liu, H., and Lu, J. (2020). *Analysis on the Characteristics of Wetland Changes in the Nenjiang River Basin*. China Soil Water Conserv, 59–62.
- Wang, Z., Li, Y., Luo, J., Liu, F., Wang, Y., and Li, H. (2020). The Evolution of the Spatial and Temporal Pattern of Habitat Quality in the Nenjiang River Basin Based on the InVEST Model. *Environ. Ecol.* 2, 19–26.
- Wang, X., and Wang, C. (2019). Natural Suitability Analysis of Human Settlement Environment in Liaoning Province Based on GIS Spatial Analysis Modeling. *For. Sci. Technol. Inform.* 51, 133–136.
- Wei, W., Shi, P., Feng, H., and Wang, X. (2012). Suitability Assessment of Human Settlements in Arid Inland River Basins — Taking Shiyang River Basin as an Example. *J. Nat. Resour.* 27, 1940–1950. doi:10.1007/s11442-013-1013-y
- Wu, D., Li, Y., and Li, S. (2016). The Characteristics of Spatial Distribution and Human Settlement Suitability of Residential Areas in the Hexi Small Watershed of Miyun County under the Influence of Natural Factors. *J. China Agr. Univ.* 21, 129–136. doi:10.11841/j.issn.1007-4333.2016.04.17
- Wu, H., Wang, X., Shahid, S., and Ye, M. (2016). Changing Characteristics of the Water Consumption Structure in Nanjing City, Southern China. *Water* 8, 314. doi:10.3390/w8080314
- Wu, Y., Zhang, G., Qi, P., Rousseau, A. N., Hu, B., Song, Z., et al. (2019). Simulation Efficiency Evaluation of Watershed Hydrological Model Coupled with Wetland Module. *Adv. Water Sci.* 30, 326–336. doi:10.14042/j.cnki.32.1309.2019.03.003
- Xu, C., Liu, M., Zhang, C., An, S., Yu, W., and Chen, J. M. (2007). The Spatiotemporal Dynamics of Rapid Urban Growth in the Nanjing Metropolitan Region of China. *Landscape Ecol.* 22, 925–937. doi:10.1007/s10980-007-9079-5
- Zeng, J., Yang, Q., Liu, Y., Zhao, C., and Li, B. (2016). The Evolution and Influence Mechanism of the Rural Human Settlement Environment in the National Key Ecological Function Zone: Taking Lichuan City, Hubei Province as an Example. *Hum. Geogr.* 31, 81–88. doi:10.13959/j.issn.1003-2398.2016.01.011

Conflict of Interest: The authors declare that the research was conducted in the absence of any commercial or financial relationships that could be construed as a potential conflict of interest.

Publisher's Note: All claims expressed in this article are solely those of the authors and do not necessarily represent those of their affiliated organizations, or those of the publisher, the editors and the reviewers. Any product that may be evaluated in this article, or claim that may be made by its manufacturer, is not guaranteed or endorsed by the publisher.

Copyright © 2022 Zhao and Zhang. This is an open-access article distributed under the terms of the Creative Commons Attribution License (CC BY). The use, distribution or reproduction in other forums is permitted, provided the original author(s) and the copyright owner(s) are credited and that the original publication in this journal is cited, in accordance with accepted academic practice. No use, distribution or reproduction is permitted which does not comply with these terms.



Microbial Residual Nitrogen Distribution in Brown Earth's Aggregates as Affected by Different Maize Residues and Soil Fertility Levels

Pingluo Xue, Jiubo Pei*, Nan Ma and Jingkuan Wang

College of Land and Environment, Shenyang Agricultural University, National Engineering Research Center for Efficient Utilization of Soil and Fertilizer Resources, National Development and Reform Commission, Northeast Key Laboratory of Cultivated Land Conservation, Ministry of Agriculture and Rural Affairs, Shenyang, China

OPEN ACCESS

Edited by:

Shengbo Xie,
Northwest Institute of Eco-
Environment and Resources (CAS),
China

Reviewed by:

Bin Zhang,
Nanjing University of Information
Science and Technology, China
Haixia Tian,
Northwest A&F University, China

*Correspondence:

Jiubo Pei
peijiubo@syau.edu.cn

Specialty section:

This article was submitted to
Drylands,
a section of the journal
Frontiers in Environmental Science

Received: 08 March 2022

Accepted: 21 March 2022

Published: 14 April 2022

Citation:

Xue P, Pei J, Ma N and Wang J (2022)
Microbial Residual Nitrogen
Distribution in Brown Earth's
Aggregates as Affected by Different
Maize Residues and Soil
Fertility Levels.
Front. Environ. Sci. 10:892039.
doi: 10.3389/fenvs.2022.892039

Brown earth is one of the typical soils in the dryland areas of Northeast China, and its degradation is closely related to food security in the local. Effectively preventing soil nitrogen (N) loss can promote the soil fertility supply. As the hub of nitrogen cycling, microorganisms play an important role in N transformation and accumulation. Soil aggregates are important in improving soil fertility and preventing soil degradation because they are an important index to maintain soil fertility. However, the allocation of microbial residual N and its contribution to total N in brown earth's aggregates are still limited, especially the effects of different maize residue types' return and soil fertility levels. Focusing on this, a 360-day laboratory incubation experiment at 25°C was carried out induced by adding maize roots and shoots into brown earth with low (L) and high (H) fertility, respectively. Randomized soil samples were taken on the incubation day of 0, 30, 60, 180, and 360, and then, they were divided into macroaggregates (>250 µm) and microaggregates (<250 µm) using a dry-sieved method. The relative contributions of fungal and bacterial residual N to soil total N were calculated by the amino sugar content to examine the accumulated differences of microbial residual N in brown earth's aggregates with the addition of different parts of maize residues and fertility levels. The results showed that maize residue types had different effects on the fungal and bacterial residual N enrichment in soil aggregates. In macroaggregates, maize roots promoted the accumulation of fungal residual N. The fungal residual N contributions to total nitrogen with root treatments were 1.03 times more than those with shoot treatments. However, in microaggregates, the bacterial residual N contributions to total nitrogen with shoot treatments were 1.01 times more than those with root treatments. These indicated that maize roots should be more beneficial to the accumulation of bacterial residual N in microaggregates. Moreover, the high fertility soil could sequester more microbial residual N than the low fertility soil, showing the content of microbial residual N in high fertility was 1.12–1.18 times more than that in low fertility. Furthermore, the fungal residual N was more beneficially accumulated in low fertility soil. Regardless of the level of fertility, the proportion of N in total N with shoot treatment was higher than that with root treatment, indicating that

the above ground maize residues could better promote the metabolic process of microorganisms than the below ground ones. These could provide a theoretical basis for studying the microbial transformation mechanism of nitrogen after maize straw returning to the field, which could be of great significance to main soil fertility.

Keywords: maize residues, fungal residual nitrogen, bacterial residual nitrogen, soil aggregates, soil fertility

HIGHLIGHTS

Microbial residual N was quantified using amino sugar analysis.

Maize residues returning could increase microbial residual N in soil aggregates.

Residue types had different effects on the accumulation of residual nitrogen in aggregates.

High fertility soil could sequester more microbial residual N than low fertility soil.

Bacterial residual N was more accumulated in high fertility soil, while fungal N in low fertility soil.

INTRODUCTION

It is an important grain production base for the dryland in Northeast China, whose area accounts for over 85% of the local region, guaranteeing national grain security (Han and Li, 2018). Brown earth (Hapli-Udic Cambisol, FAO Classification) is one of the important dryland soils of black land in Northeast China. However, for a long time, unreasonable agricultural production and management have caused serious soil degradation in the local (Liu et al., 2010). As a result, the nutrient ratio of dryland brown earth in Northeast China is unbalanced, with nitrogen loss and organic matter decreasing year by year.

Nitrogen is always considered to be the element with rapid turnover and loss in soil, and preventing its loss can promote soil fertility supplied to plants (Schlesinger et al., 1990; Wang et al., 2019). In addition, microorganisms can not only provide the driving force for nitrogen cycling and transformation but also act as the “source” and “sink” of nitrogen internal cycling (Jawson et al., 1989). Moreover, as an important indicator of soil fertility, soil aggregates contain a large amount of nitrogen and play an important role in regulating the dynamic change of soil nitrogen (Six et al., 2004). Likewise, they also influence the microenvironment in which microorganisms live to a certain extent (such as water and gas conditions and porosity), thereby affecting the microbial metabolic activities (Schutter and Dick, 2002; Ruamps et al., 2011). Thus, soil microorganisms, aggregates, and nitrogen are allowed to interact with each other, maintaining a certain balance in soil ecosystems to resist soil degradation.

For the farmland ecosystems, the addition of exogenous organic matter, such as maize (*Zea mays* L.) residues, would disturb this balance. Meanwhile, microbial decomposition of maize residues is an important process, showing parts of the nitrogen from maize residues would be assimilated by

microorganisms, and the most of the assimilated nitrogen could be stored and accumulated in the dead microbial residual components (such as amino sugars), becoming an important reservoir of nitrogen in the soil (Engelking et al., 2007; Ding et al., 2011). Compared with the living microorganisms, the dead microbial residues may have a more lasting promoting effect on the formation and stability of aggregates to improve soil fertility (Tisdall and Oades, 1982; Chantigny et al., 1997). Therefore, understanding the distribution of the microbial residual nitrogen in soil aggregates after maize residues' return, and further study on the role of microorganisms in nitrogen accumulation in aggregates is of great significance in the rational management of dryland nitrogen nutrients and soil fertility improvement.

As one of the major contributors to mineral nitrogen, amino sugars from microorganisms account for 5–10% of organic nitrogen (Roberts et al., 2007; Liang et al., 2019). They are the residues of microbial cell walls, relatively stable in the soil, representing the long-term remaining effects of dead microorganisms (Amelung et al., 2001). Among them, glucosamine mainly comes from fungi, while muramic acid only comes from bacteria (Joergensen, 2018; Lu et al., 2021). Due to the heterogeneity of glucosamine and muramic acid, the relative contribution of fungal and bacterial nitrogen to total nitrogen in soil aggregates can be calculated by the contents of glucosamine and muramic acid (Joergensen, 2018; Lu et al., 2021). Previous studies provide a methodological support for exploring the microbial mechanism of soil nitrogen accumulation by the combined ecosystem approaches with elemental carbon and nitrogen stoichiometry using amino sugar data published between 1996 and 2018 (Liang et al., 2019). Consequently, amino sugars were selected as a marker to study the dynamic changes of microbial residual nitrogen in soil.

Due to the different chemical compositions of carbon and nitrogen in different parts of maize residues (such as roots and shoots), they can cause microbial disturbance differences after the ones returned to the field (Abiven et al., 2005). The Microbial Efficiency-Matrix Stabilization (MEMS) framework indicated that the quality of plant litter could affect microbial biomass; high quality litters have a high microbial catabolism ratio, resulting in more microbial residues per amount of plant litter metabolism; low quality litters have a relatively low microbial biomass, resulting in fewer microbial residues per amount of plant litter metabolism (Castellano et al., 2015). Moreover, different soil fertility levels will have different effects on metabolic activities of soil microorganisms due to the different substrates in physicochemical properties and microbial community structures, resulting in the varied distributions of microbial residues in soil aggregates (An et al., 2015; Bonanomi

et al., 2017; Xu et al., 2019). Some studies reported that high fertility soil had higher microbial biomass, larger aggregate ratio, enzyme activity, and different microbial community compositions than low fertility soil, which could influence the assimilation of microbial residues (Paul et al., 2002; Marschner et al., 2003; Fontaine et al., 2011; Wang et al., 2017; Xu et al., 2020).

From the previously stated facts, at present, there are few comprehensive studies on the change of residual nitrogen in soil aggregates with different fertility under the different types of maize residues by using amino sugars as microbial markers to reflect the changes of residual nitrogen. Some of them have shown that the portion of microbially derived soil organic N (SON) to total SON was higher than the portion of microbially derived SOC to total SOC, indicating the importance of microbially derived N to soil N cycling (Simpson et al., 2007; Chao Wang et al., 2020). Therefore, to examine the microbial residual nitrogen accumulation in the dryland soil aggregates, the relative contribution of fungal and bacterial-derived residual nitrogen to the total nitrogen of aggregates should be figured out; we conducted an experiment to monitor the variations of amino sugars with different maize residues' parts (roots and shoots) added into the dryland brown earth with high and low fertility. We hypothesized that (1) maize residue types differed in the accumulation of microbial residues (fungal and bacterial residues) in different aggregates; (2) shoots should be more favorable for the accumulation of microbial residues in aggregates because the nutrient in shoots is easier to be utilized by microorganisms than that by roots; and (3) fertility level and residue types would interact with the accumulation of microbial residual nitrogen in aggregates.

MATERIALS AND METHODS

Tested Materials

Tested Soil

The topsoil (0–20 cm) with high and low fertility was collected from the brown earth long-term positioning experimental station of Shenyang Agricultural University (41°49' N, 123°34' E, elevation of 75 m), which was established in 1987. The typical local soil is brown earth (Hapli-Udic Cambisol, FAO Classification) with loess parent material. The climate is a northern temperate continental monsoon climate with an average annual temperature of 7–8°C and an average annual rainfall of 730 mm that is concentrated in summer. Maize (*Zea mays* L.) is a long-term continuous cropping crop in this station. It is usually fertilized and sown in early May and harvested in late September per year. The high fertility soil (HF) was treated with a high amount of organic fertilizer (annual application of manure fertilizer was equivalent to 135 kg N hm⁻², and the manure was the pig compost that contained 150 g kg⁻¹ organic carbon, 10 g kg⁻¹ N, 4.4 g kg⁻¹ phosphorus (P), and 3.3 g kg⁻¹ potassium (K) on a dry weight basis) combined with chemical N and P fertilizers (chemical fertilizers with urea N 75 kg hm⁻² and P₂O₅ 67.5 kg hm⁻²). The low fertility soil was the control

treatment without fertilization (LF). The detailed differences between the treatments of high and low fertility soils are shown in **Table 1**. The collected brown earth sample was air-dried at room temperature by the combination of five random sampling points and then removed the visible roots and gravel. The soil was screened through a 2-mm sieve for the next step use. The basic physicochemical properties of the tested soil are shown in **Table 1**.

Tested Maize Residues

The tested maize materials were maize roots and shoots (including stem and leaf). After harvest, the maize residues collected in the field were first oven-dried at 105°C for 30 min and then oven-dried at 60°C for 8 h. After separating the roots from the shoots, they were respectively cut into 2-cm sections, ground with a grinder, and then passed through a 40-mesh sieve. The basic physicochemical properties are shown in **Table 2**.

Incubation Experiment

The samples of 250 g with 2 mm air-dried soil (drying weight) were weighed and placed in a 1000-ml incubation flask. The soil moisture content was adjusted to 40% of field water capacity for pre-active microorganisms, and the lid with holes (the diameter of the lid was 11 cm, and 20 pores of the same size were tied evenly) was put on the incubation flask to seal at the incubation temperature of 25°C for 7 days without light. After the pre-incubation time, the maize residue samples (roots and shoots) of 5 g (2% of air-dried soil weight) were thoroughly mixed with the pre-incubation soil, and then, the samples were sealed and placed in an incubator (25°C) for 360 days. During incubation time, the soil water content was kept at 60% of field capacity using the weighing method. There were six treatments in this incubation experiment (**Figure 1**): (1) low fertility brown earth with maize roots (LF + R), (2) low fertility brown earth with maize shoots (LF + S), (3) high fertility brown earth with maize roots (HF + R), (4) high fertility brown earth with maize shoots (HF + S), and (5) low (LF) or (6) high (HF) fertility brown earth without any maize residues. Each treatment was repeated three times. The samples were randomly taken on the 30, 60, 180, and 360 days after incubation. The aggregates of them were sieved at two levels (>250 µm and <250 µm) and weighed using a dry-sieving method (Dorodnikov et al., 2009; Gunina and Kuzyakov, 2014). Then, these aggregate samples were air-dried; one part was sieved through a 100-mesh sieve for soil carbon and nitrogen content determination, and the other part was extracted to determine amino sugars.

Soil Aggregates Separation

The moisture contents of fresh soil samples were uniformly regulated to about 10% using the air-dried method at 4°C. A 100 g soil sample was placed in an automatic sieving apparatus (Retsch AS 200, Germany) with a sieve hole size of 250 µm. The sample was sieved into macroaggregates (>250 µm) and microaggregates (<250 µm) with a vibration amplitude of 1.5 mm for 2 min (Dorodnikov et al., 2009; Gunina and Kuzyakov, 2014).

TABLE 1 | Basic characteristics of the tested soil.

Soil fertility level	Soil organic matter (g kg ⁻¹)	Total nitrogen (g kg ⁻¹)	C/N	Alkaline nitrogen (mg kg ⁻¹)	Available phosphorus (mg kg ⁻¹)	Available potassium (mg kg ⁻¹)
Low fertility	10.8	1.1	9.8	82.6	11.0	50.7
High fertility	15.0	1.7	8.8	196.0	266.0	150.7

TABLE 2 | Basic characteristics of maize residues.

Residue type	Total carbon (g kg ⁻¹)	Total nitrogen (g kg ⁻¹)	C/N
Roots	444.46 ± 0.48	6.14 ± 0.03	72.51 ± 3.02
Shoots	407.54 ± 0.97	8.49 ± 0.06	48.14 ± 2.06

Soil Sample Analysis

The Contents of Soil Organic Carbon and Total Nitrogen

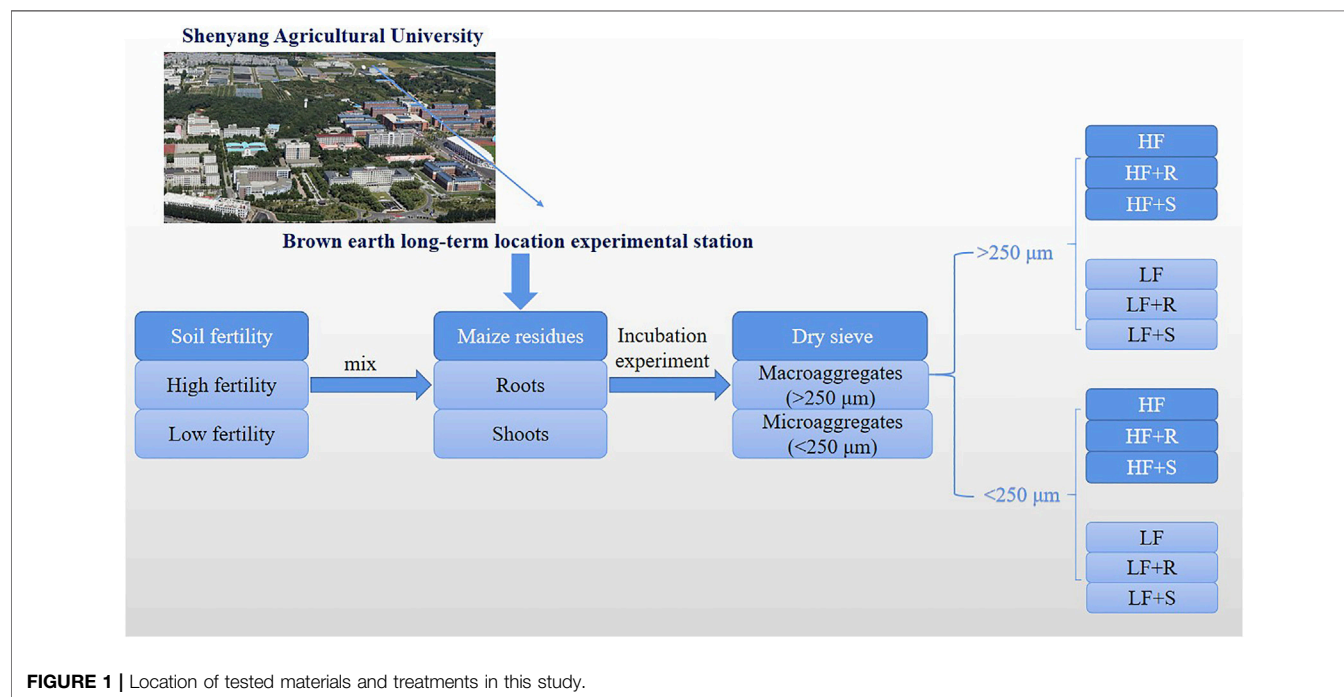
The soil samples were air-dried and passed through a 100-mesh sieve, and the contents of total organic carbon and total nitrogen in soil were determined using an elemental analyzer (EA, Germany).

Soil Amino Sugars

The content of amino sugars in soil samples was determined using Zhang's method (Zhang and Amelung, 1996). The brief steps are as follows: 0.4 mg nitrogen of soil samples were placed in the hydrolyzing flask and hydrolyzed at 105°C for 8 h. The cooled samples were successively steamed, and the pH of the dissolved solution was adjusted to neutral with

0.4 mol L⁻¹ KOH and dilute HCL. Those solutions were centrifuged (3000rpm min⁻¹ for 10 min) and rotated; then, the supernatant (amino sugar part) obtained was transferred to a 5-ml derivative bottle for nitrogen blowing (to remove anhydrous methanol), and 1 ml DDI water and 100 µL of n-methylglucosamine (internal standard 2) were added to the dried supernatant. Then, the derivative bottles were tightened with a sealing film, and the substance was shaken in the derivative bottle well by hand. Three 5 ml derived vials were taken as standard samples, and 100 µL of cytotoc acid was added to each of them. After nitrogen blowing, 100 µL of mixed standard (D-(+) -glucosamine, D-(+) -galactosamine, D-(+) -mannosamine), 100 µL of inositol, 100 µL of n-methylglucosamine, and 1 ml of DDI water were added. After sealing and shaking well, the samples were allowed for freeze drying.

The 300 µL of derivative reagents (cyanidation reaction) were added to each dried derivative bottle, followed by two water baths of duration 30 min and 60 min. During the two water baths, 1 ml of acetic anhydride and 1.5 ml of dichloromethane were added sequentially. Then, 1 ml 1 mol L⁻¹ HCl and 3 ml DI water (1 ml per time) were used to extract the organic phase. In the final extraction, water was



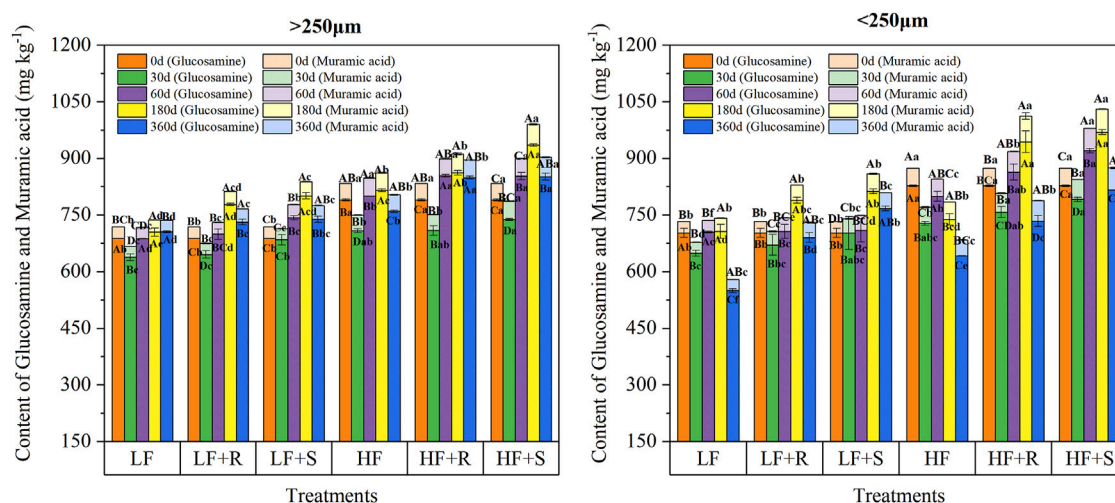


FIGURE 2 | Contents of glucosamine and muramic acid in soil aggregates with different fertility levels after the addition of different parts of maize residues. Note: LF means low fertility, LF + R means low fertility + roots, and LF + S means low fertility + Shoots; HF means high fertility, HF + R means high fertility + roots, and HF + S means high fertility + Shoots. Uppercase letters represent differences between different periods in the same treatment, and lowercase letters represent differences between different treatments at the same period. Uppercase letters represent differences between different periods in the same treatment, and lowercase letters represent differences between different treatments at the same period.

removed as much as possible. The extracted organic phase was dried with nitrogen at 45°C, and 200 µL ethylacetate-n-hexane mixture (1:1) liquids were added to dissolve the dry matter. Then, those were transferred into a gas chromatographic bottle with a liner for use.

Calculations

The formula for calculating the nitrogen content of microbial residues in each grain size of soil is as follows (Liang et al., 2019):

Microbial residual nitrogen content (g kg^{-1}) = fungal residual nitrogen + bacterial residual nitrogen, where fungal residual nitrogen (g kg^{-1}) = (glucosamine (mmol)/179.17–2 × muramic acid (mmol)/251.23) × 179.17 × 1.4 and bacterial residual nitrogen (g kg^{-1}) = muramic acid (mmol) × 6.67.

Assuming the molar ratio of glucosamine to wall acid in bacterial cells is 2:1. Among them, 179.17 was the molecular weight of glucosamine, 251.23 was the molecular weight of muramic acid, 1.4 was the conversion coefficient of glucosamine to fungal residual nitrogen, and 6.67 was the conversion coefficient of muramic acid to bacterial residual nitrogen.

Statistics

The software of Origin 2019 and Microsoft Office Excel 2013 were used to process and plot the experimental data, and SPSS 25.0 software was used to analyze the variance of the experimental results. Repeated measurement analysis of variance was used for significance among different treatments, and the significance level was $p < 0.05$. Multiple linear regression analysis was conducted to partition the effects of carbon content, nitrogen content, and aggregate composition on the content of microbial, fungal, and bacterial residues of nitrogen.

RESULTS

Contents of Glucosamine and Muramic Acid in Soil Aggregates

The contents of glucosamine and muramic acid in macro- and micro-aggregates with maize residue addition were different (Figure 2), showing the contents of glucosamine in macro- and micro-aggregates were $638.32\text{--}935.70 \text{ mg kg}^{-1}$ and $550.14\text{--}969.55 \text{ mg kg}^{-1}$, respectively. Moreover, the contents of muramic acid in macro- and micro-aggregates were $29.00\text{--}54.87 \text{ mg kg}^{-1}$ and $28.87\text{--}68.16 \text{ mg kg}^{-1}$, respectively.

Nitrogen Contents of Microbial Residues in Soil Aggregates

The soil fertility level and type of maize residues had extremely significant effects on the content of microbial, fungal, and bacterial residues of nitrogen ($p < 0.001$) (Figure 3, Figure 4 and Figure 5). The aggregate level had a significant effect on the content of microbial and bacterial residual nitrogen ($p < 0.05$). The contents of microbial and fungal residual nitrogen added with maize residues showed a decreasing trend at the early stage of incubation time in all levels of aggregates, showing the lowest on 30 days and then gradually increasing to the peak on 180 days. Those were still significantly higher than that of the control treatment on 360 days ($p < 0.05$). The content of microbial and fungal residual nitrogen in aggregates was higher in microaggregates than that in macroaggregates at the beginning of incubation time. Meanwhile, they were higher in macroaggregates than that in microaggregates from 180 days to the end of incubation, and the content of fungal residues of nitrogen in macroaggregates was significantly higher than that in

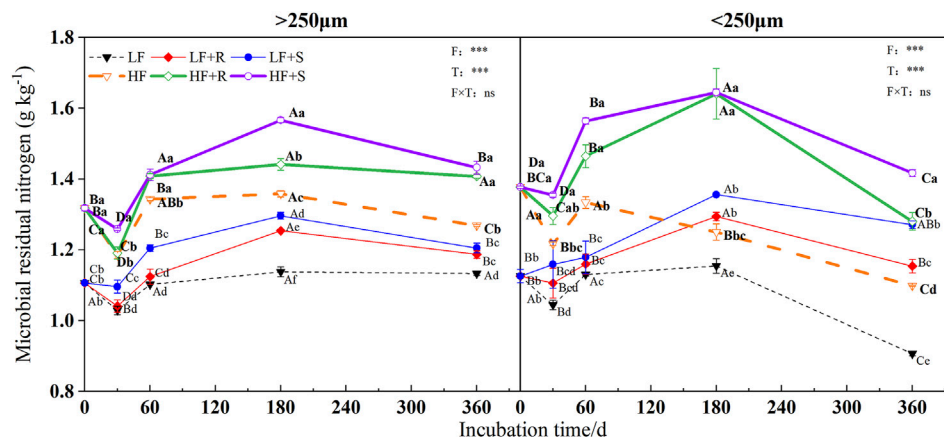


FIGURE 3 | Microbial residual nitrogen in soil aggregates with different fertility levels after the addition of different parts of maize residues. Note: LF means low fertility, LF + R means low fertility + roots, and LF + S means low fertility + Shoots; HF means high fertility, HF + R means high fertility + roots, and HF + S means high fertility + Shoots. Uppercase letters represent differences between different periods in the same treatment, and lowercase letters represent differences between different treatments at the same period. For the ANOVA, F means fertility level, T means the type of maize residues, and F × T means fertility level × type of maize residues. *, **, and *** mean $p < 0.05$, 0.01 , and 0.001 , respectively. ns means no significance.

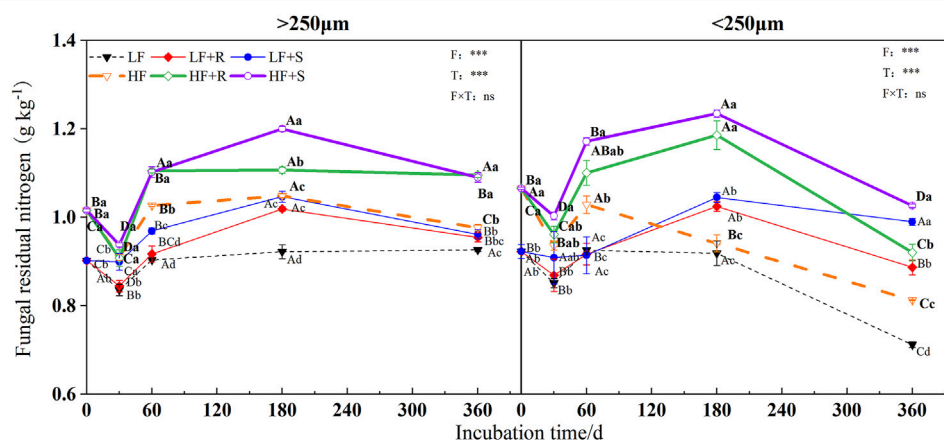


FIGURE 4 | Fungal residual nitrogen in soil aggregates with different soil fertility levels after the addition of different parts of maize residues. Note: LF means low fertility, LF + R means low fertility + roots, and LF + S means low fertility + Shoots; HF means high fertility, HF + R means high fertility + roots, and HF + S means high fertility + Shoots. Uppercase letters represent differences between different periods in the same treatment, and lowercase letters represent differences between different treatments at the same period. For the ANOVA, F means fertility level, T means the type of maize residues, and F × T means fertility level × type of maize residues. *, **, and *** mean $p < 0.05$, 0.01 , and 0.001 , respectively. ns means no significance.

microaggregates at the end of incubation ($p = 0.001$). However, the content of bacterial residual nitrogen increased briefly and then decreased in the treatment with shoots in the macroaggregates of high fertility soil. It maintained an increasing trend in the microaggregates until reaching the peak on 180 days and then gradually decreased until the end of incubation. The contents of bacterial residual nitrogen in all aggregates showed macroaggregates > microaggregates. There were significant differences on the 30, 60, and 360 days ($p < 0.05$).

After 1 year incubation, compared with the control, the addition of maize residues increased the content of microbial,

fungal, and bacterial residual nitrogen in aggregates with high and low fertility levels to different degrees. The content of residual nitrogen in aggregates at all levels showed HF > LF ($p < 0.05$). In the macroaggregates, the contents of microbial residual nitrogen were 1.42 g kg^{-1} (HF) and 1.20 g kg^{-1} (LF). The nitrogen contents of fungal residues were 1.09 g kg^{-1} (HF) and 0.96 g kg^{-1} (LF) and those of bacterial residues were 0.33 g kg^{-1} (HF) and 0.25 g kg^{-1} (LF). In the microaggregates, the contents of microbial residual nitrogen were 1.35 g kg^{-1} (HF) and 1.21 g kg^{-1} (LF), those of fungal residual nitrogen were 0.97 g kg^{-1} (HF) and 0.94 g kg^{-1} (LF), and those of bacterial residual nitrogen were 0.37 g kg^{-1} (HF) and 0.27 g kg^{-1} (LF).

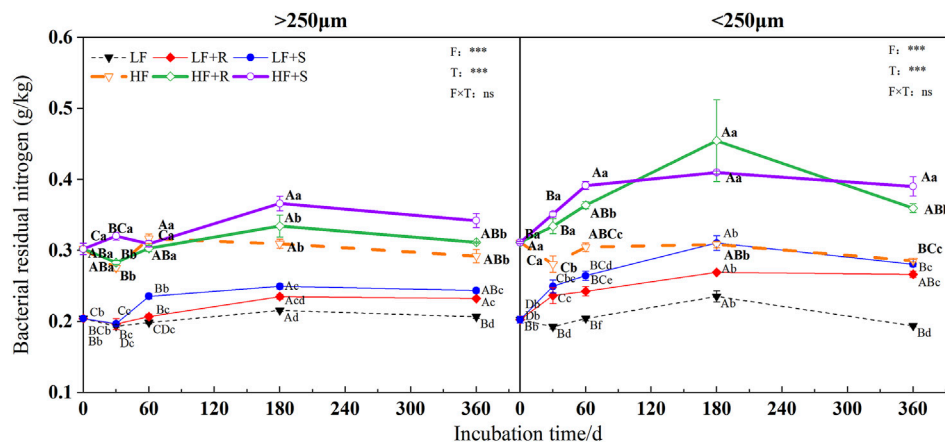


FIGURE 5 | Bacterial residual nitrogen in soil aggregates with different fertility levels after the addition of different parts of maize residues. Note: LF means low fertility, LF + R means low fertility + roots, and LF + S means low fertility + Shoots; HF means high fertility, HF + R means high fertility + roots, and HF + S means high fertility + Shoots. Uppercase letters represent differences between different periods in the same treatment, and lowercase letters represent differences between different treatments at the same period. For the ANOVA, F means fertility level, T means type of maize residues, and F × T means fertility level × type of maize residues. *, **, and *** mean $P < 0.05$, 0.01 and 0.001, respectively. ns means no significance.

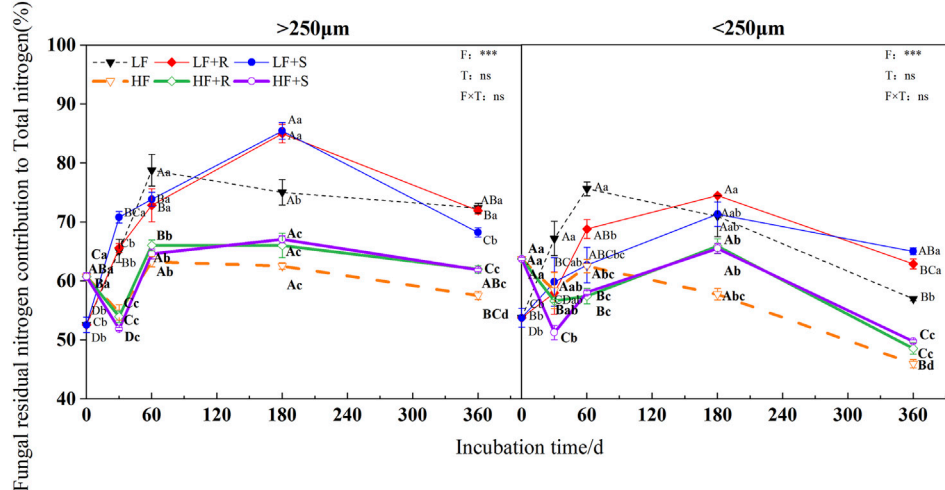


FIGURE 6 | Fungal residual nitrogen contribution to total nitrogen in soil aggregates with different fertility levels after the addition of different parts of maize residues. Note: LF means low fertility, LF + R means low fertility + roots, and LF + S means low fertility + Shoots; HF means high fertility, HF + R means high fertility + roots, and HF + S means high fertility + Shoots. Uppercase letters represent differences between different periods in the same treatment, and lowercase letters represent differences between different treatments at the same period. For the ANOVA, F means fertility level, T means the type of maize residues, and F × T means fertility level × type of maize residues. *, **, and *** mean $p < 0.05$, 0.01, and 0.001, respectively. ns means no significance.

The effects of different types of maize residues on the content of microbial, fungal, and bacterial residual nitrogen in aggregates at all levels were shown by $S > R$ at the end of incubation. In the macroaggregates, the content of microbial residual nitrogen with shoots was 1.02 times more than that with root treatment, and the content of fungal residual nitrogen with shoots was 1.00 times more than that with root treatment. In addition, the content of bacterial residual nitrogen with shoots was 1.08 times more than that with root treatment. In the microaggregates, the content of microbial residual nitrogen with shoots was 1.10 times more than

that with root treatment, and the content of fungal residual nitrogen with shoots was 1.12 times more than that with root treatment. In addition, the content of bacterial residual nitrogen with shoots was 1.07 times more than that with root treatment.

Proportion of Microbial Residual Nitrogen to Total Nitrogen in Soil Aggregates

The fertility level and aggregate level significantly affected the contribution of fungal and bacterial residual nitrogen to total

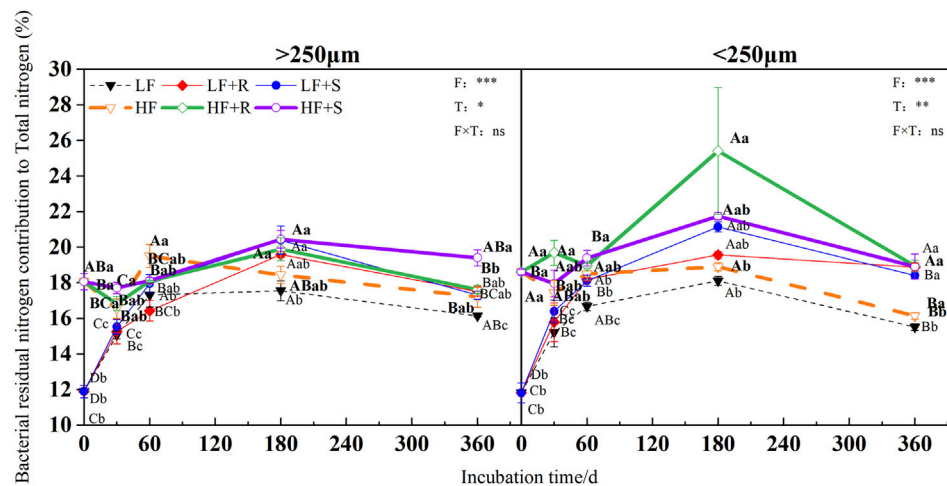


FIGURE 7 | Bacterial residual nitrogen contribution to total nitrogen in soil aggregates with different fertility levels after the addition of different parts of maize residues. Note: LF means low fertility, LF + R means low fertility + roots, and LF + S means low fertility + Shoots; HF means high fertility, HF + R means high fertility + roots, and HF + S means high fertility + Shoots. Uppercase letters represent differences between different periods in the same treatment, and lowercase letters represent differences between different treatments at the same period. For the ANOVA, F means fertility level, T means the type of maize residues, and F × T means fertility level × type of maize residues. *, **, and *** mean $p < 0.05$, 0.01 , and 0.001 , respectively. ns means no significance.

nitrogen ($p < 0.05$), and the contribution of bacterial residual nitrogen to total nitrogen was also significantly affected by the type of maize residues ($p = 0.001$) (Figure 6 and Figure 7). The contributions of fungal nitrogen to total nitrogen in all aggregates were shown by macroaggregates > microaggregates. Nevertheless, the contribution of bacterial residual nitrogen to total nitrogen has shown an opposite trend.

At the end of incubation, compared with control treatment, the addition of maize residues increased the contribution of fungal and bacterial residual nitrogen to total nitrogen in the aggregates of high and low fertility in different degrees. The contribution of fungal residue nitrogen to total nitrogen showed LF > HF, while the contribution of bacterial residual nitrogen to total nitrogen showed inversely. In the macroaggregates, fungal residual nitrogen contributed 61.92% (HF) and 70.10% (LF) to total nitrogen, respectively, while bacterial residual nitrogen contributed 18.51% (HF) and 17.40% (LF) to total nitrogen, respectively. In the microaggregates, fungal residual nitrogen respectively contributed 49.13% (HF) and 63.92% (LF) to total nitrogen, while bacterial residual nitrogen contributed 18.93% (HF) and 18.65% (LF) to total nitrogen, respectively.

In addition, at the end of incubation, the relative contribution of nitrogen from microbial residues to total nitrogen in different aggregates was different due to the different types of maize residues. For the contribution of nitrogen from fungal residues to total nitrogen in macroaggregates, the contribution of nitrogen from roots was 1.03 times more than that from shoots. The microaggregates treated with shoots were 1.03 times more than those treated with roots. The relative contribution of bacterial residual nitrogen to total nitrogen was just the opposite. In macroaggregates, shoot treatment was 1.04 times more than that with root treatment, while in microaggregates, root treatment was 1.01 times more than that with shoot treatment.

In all treatments, the ratio of fungal residual nitrogen to bacterial residual nitrogen was showed by LF > HF (Figure 8). At the end of incubation, different types of maize residues had different effects on the ratio of fungal residual nitrogen to bacterial residual nitrogen in different aggregates, showing R > S in macroaggregates and an opposite trend in microaggregates.

DISCUSSION

Effects of Maize Residues' Parts on Microbial Residual Nitrogen in Soil Aggregates

It had been shown that microbial residues had a longer turnover time in soil than live microorganisms (Liang and Balser, 2008). The contribution of microbial nitrogen to total nitrogen might be higher than that of microbial carbon to soil organic carbon (Simpson et al., 2007; Yang Wang et al., 2020). Therefore, microbial residual nitrogen played an important role in soil nitrogen cycling. At the same time, aggregates could not only regulate the dynamic change of soil nitrogen but also provide a physical barrier to avoid nitrogen loss (Six et al., 2004). Therefore, the process of microbial nitrogen accumulation and distribution in aggregates under the different parts of maize return could be further understood by analyzing the changes of microbial residual nitrogen in aggregates of different parts of maize return.

In general, the addition of different parts of maize residues significantly increased the microbial residual nitrogen, fungal, and bacterial residual nitrogen in different levels of aggregates (Figure 2). At the end of incubation time, the content of fungal residual nitrogen in macroaggregates was higher than that in microaggregates, while the content of bacterial residual nitrogen

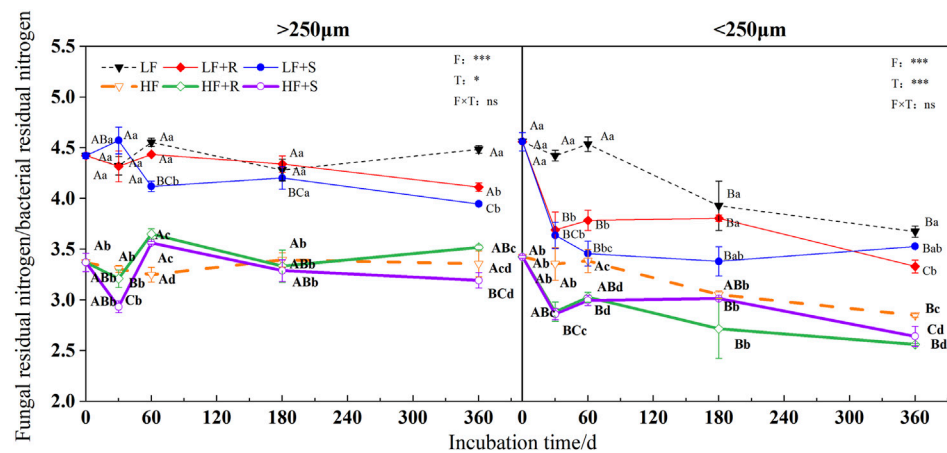


FIGURE 8 | Ratio of fungal to bacterial residual nitrogen in soil aggregates with different fertility levels after the addition of different parts of maize residues. Note: LF means low fertility, LF + R means low fertility + roots, and LF + S means low fertility + Shoots; HF means high fertility, HF + R means high fertility + roots, and HF + S means high fertility + Shoots. Uppercase letters represent differences between different periods in the same treatment, and lowercase letters represent differences between different treatments at the same period. For the ANOVA, F means fertility level, T means the type of maize residues, and F × T means fertility level × type of maize residues. *, **, and *** mean $p < 0.05$, 0.01 , and 0.001 , respectively. ns means no significance.

was the opposite. This might be mainly because the pores in macroaggregates are conducive to the extension of fungal mycelia, while the higher clay content in microaggregates was more conducive to the adsorption and preservation of bacteria (Kandeler et al., 2000), which could be consistent with our hypothesis (1). Among them, the content of microbial residual nitrogen in each aggregate was affected differently by the parts of maize residues. Nevertheless, the content of microbial and fungal residual nitrogen showed a temporary decline in the early incubation time (Figure 2 and Figure 3). The main reason should be the addition of maize provided a large amount of carbon source for microorganisms; most of them were organic nutrients. There were fewer nutrients to be decomposed and utilized easily, such as mineral forms, and the effect of short-term release of nutrients was not evident (Lou et al., 2011; Han and Li, 2018). This caused the microorganisms to be in a state of nitrogen deficiency, which limited the growth and reproduction of microorganisms. At the same time, the C/N of shoots was smaller than that of roots (Table 2), which would provide more nitrogen for microbial growth. Thus, the decrease rate of the nitrogen content of microbial and fungal residues was lower than that of roots. With the gradual decomposition of maize, the nitrogen from maize was gradually released into the soil for microbial utilization. Based on the theory of nitrogen mineralization, when nitrogen is sufficient, soil microbes would propagate rapidly, while the residues could be gradually accumulated in the soil (Jun Di Li et al., 2019). Maize addition could reduce the effectiveness of nitrogen input, accelerating the mineralization of nitrogen in the soil microbial growth (Shahbaz et al., 2018). As an important source of organic matter, microbial residues could supplement the nitrogen reservoir in the soil (Liang and Balser, 2008), so the residual nitrogen content increases. The content of bacterial residual nitrogen in microaggregates did not decrease at the initial stage of incubation time (Figure 4) because the addition of maize could promote the

enrichment of nitrogen in microaggregates (Lidong Li et al., 2019). In the initial stage of maize decomposition, the nutrient released rate was faster, and bacteria could use these nutrients faster than fungi (Marschner et al., 2011). Thus, the content of bacterial residual nitrogen in microaggregates at the initial stage of incubation did not show a downward trend. After 180 days, the content of microbial, fungal, and bacterial residual nitrogen decreased again because the maize entered the slow decomposition stage at the later stage of incubation. There were no other nutrients added in the experiment, resulting in the decrease of available nutrients in the soil. At this time, microbial residues, as an energy source and nitrogen source, would be given priority for decomposition and utilization (Abiven et al., 2005).

During the incubation period, shoots promoted residual nitrogen content, showing it was higher than root treatment. It was that the roots contained more lignin and other substances that were not easy to be decomposed. However, the sugars, cellulose, and hemicellulose that existed in the shoots were easily decomposed, which are easier to be used by microorganisms (Clemente et al., 2013). Therefore, nitrogen in the shoots was more involved in the growth and reproduction of microorganisms than that in the roots to form microbial biomass, even accumulated in the form of residues. These would be consistent with hypothesis (2).

Some studies had shown that the input of plant residues would lead to change the soil nutrient availability, even microbial biomass and community (Blaud et al., 2012; Lemanski and Scheu, 2014; Helfrich et al., 2015). It was reasonable to suggest that the addition of maize residues could affect the composition of microbial residues (Kandeler et al., 2000). However, in this study, the residue type only had a significant effect on bacterial residual nitrogen contribution to total nitrogen. Considering the residue type had a significant effect on the content of fungal residual nitrogen, there should be the addition of residue that could promote the accumulation of bacterial residual nitrogen better than fungal residual nitrogen. At the end of the incubation, the

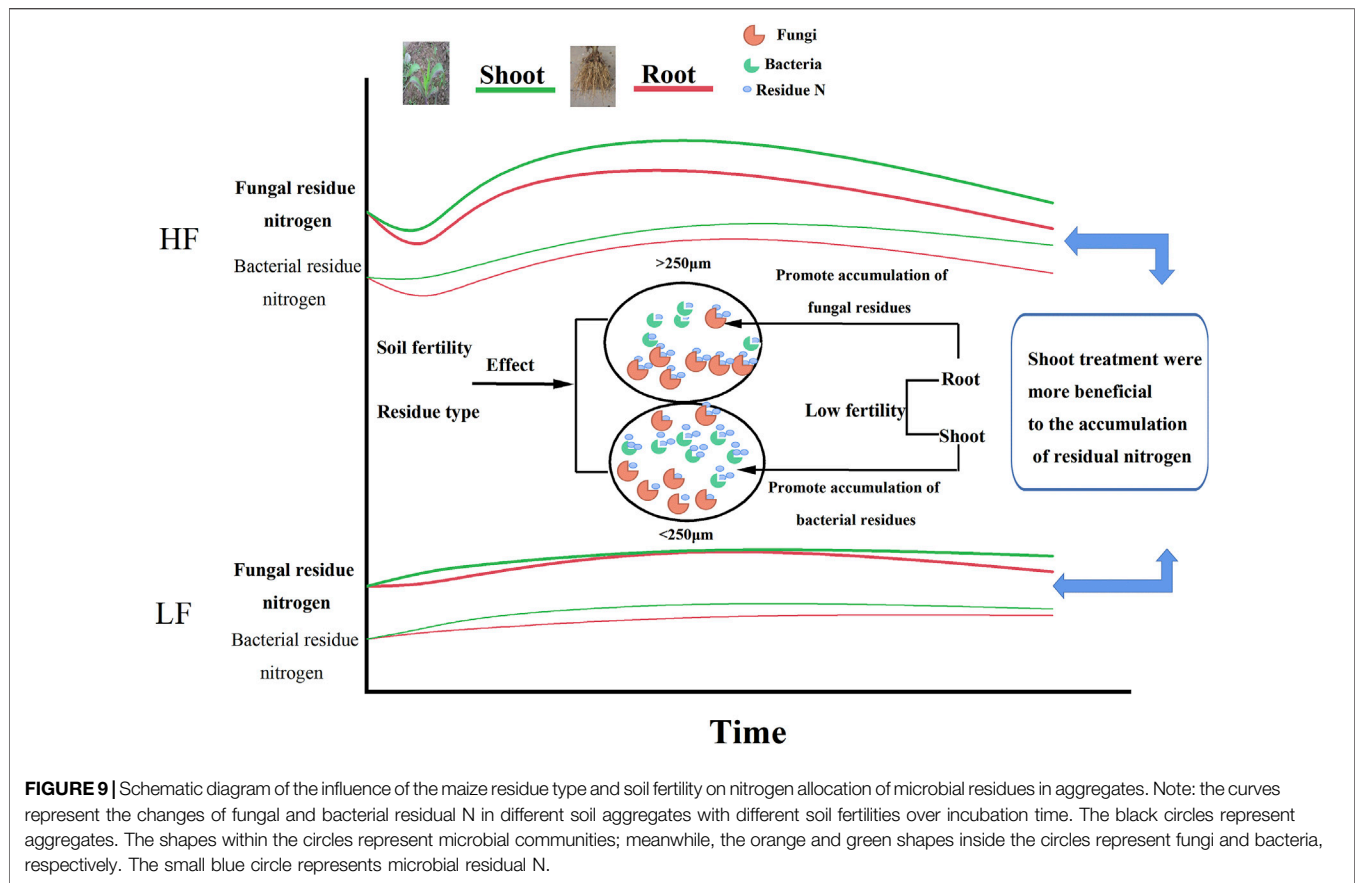


FIGURE 9 | Schematic diagram of the influence of the maize residue type and soil fertility on nitrogen allocation of microbial residues in aggregates. Note: the curves represent the changes of fungal and bacterial residual N in different soil aggregates with different soil fertilities over incubation time. The black circles represent aggregates. The shapes within the circles represent microbial communities; meanwhile, the orange and green shapes inside the circles represent fungi and bacteria, respectively. The small blue circle represents microbial residual N.

results of the ratio of fungal residual nitrogen to total nitrogen in macroaggregates were higher in the root treatment than those in the shoot treatment, while the ratio of bacterial residual nitrogen to total nitrogen was higher in the shoot treatment than that in the root treatment, and the opposite was in the microaggregates. These indicated that the roots were beneficial to the accumulation of fungal residues in the macroaggregates, while the shoots were beneficial to the accumulation of fungal residues in the microaggregates. Similarly, this was also proved by the different ratio of fungal and bacterial nitrogen residues in the aggregates. The results suggested that the input of different parts of maize residues had different effects on the accumulation and distribution of microbial nitrogen in aggregates, which should be consistent with the hypothesis (2). Therefore, studying the distribution of microbial residual nitrogen in aggregates by different types of maize return, understanding the effect of maize types on nitrogen microbial fixation, could provide a basis for modeling the microbial dynamics of nitrogen under the condition of maize return.

Effects of Soil Fertility Levels on Microbial Residual Nitrogen in Soil Aggregates

The soil fertility level also significantly affected the content of microbial, fungal, and bacterial residual nitrogen, showing HF > LF in this study. The low fertility soil due to the lack of nutrients

restricted microbial growth, while the high fertility soil contained more available active nutrients and microbial biomass (Paul et al., 2002), and high microbial biomass would promote the generation and accumulation of microbial residues (Ding et al., 2013; Lidong Li et al., 2019). Thus, high fertility soil could maintain more residual nitrogen, which was consistent with the hypothesis (2). These indicated that high fertility soil could accumulate nitrogen more effectively by the microbial metabolic pathway than that by low fertility soil (Wang et al., 2019). In the early stage of incubation time, the content of bacterial residual nitrogen increased briefly and then decreased in the macroaggregates with high fertility soil treated by shoot addition, but this did not exist in the low fertility soil. The main reason should be high fertility soil contained more available nitrogen; in the meantime, shoots contained more easily decomposed substances and nitrogen (Ding et al., 2019). Compared with roots, shoots could replenish active nitrogen in soil during decomposition, resulting in nitrogen supply that could temporarily meet the demands of bacterial growth and metabolism. Thus, bacterial residues should be temporarily accumulated. With the continuous reproduction of bacteria, nitrogen became a key factor restricting their growth. This is the same reason why the content of microbial and fungal residual nitrogen showed a temporary decline in the early incubation time.

In addition, as a key factor regulating the growth of fungi and bacteria, soil pores provided a basis for their enrichment in

aggregates with different particle sizes. Larger fungi were more likely to live in macroaggregates, while smaller individual bacteria usually lived in microaggregates (Simpson et al., 2004; Mummey et al., 2006; Strickland and Rousk, 2010). In this study, fungal residual nitrogen was more likely to be enriched in macroaggregates than bacterial residual nitrogen, while bacterial residual nitrogen was more likely to be enriched in microaggregates than fungal residual nitrogen. In addition, in this study, there was no interaction between the types of maize residues and fertility levels on microbial residual nitrogen, which was inconsistent with the hypothesis (3).

In this study, the ratio of fungal residual nitrogen to total nitrogen was higher in low fertility soil than that in high fertility, while the ratio of bacterial residual nitrogen to total nitrogen showed an opposite trend. The soil with the lower organic matter was more conducive to the survival of the fungal community than the soil with higher organic matter (Simpson et al., 2004). Compared with the high fertility brown earth, the low fertility brown earth with lower organic matter had less available active nutrients and a higher proportion of refractory substrates, which was difficult to be utilized by bacteria, leading to the dominance of fungi population (Jun Di Li et al., 2019). In addition, compared with fungi, the growth and metabolism of bacteria were more likely to be affected by the available nutrients in the environment (Helfrich et al., 2015), so the lack of phosphorus and potassium content in the low fertility brown earth would affect the proliferation of bacteria. Moreover, after plant residue addition, the soil with low nitrogen was more favorable to the growth of mycorrhizal fungi (Oates et al., 2016), while the high mycorrhizal fungi would lead to the degradation of bacterial residues (He et al., 2011; Ding et al., 2019). Our results indicated that although high fertility could improve the content of microbial residual nitrogen more than low fertility, the effects on the microbial community structure were different due to the difference in the nutrient content, resulting in different promoting effects on the accumulation of microbial residual nitrogen. Regardless of macroaggregates or microaggregates, the high fertility treatment of the microbial source of nitrogen content was higher than low fertility treatment. But because this was in favor of the existence of the fungi in low soil fertility soil, as well as considering the fungi were difficult to degrade, the maize residues returning to the field might be more meaningful for the nutrient enhancement of low fertility soil.

REFERENCES

- Abiven, S., Recous, S., Reyes, V., and Oliver, R. (2005). Mineralisation of C and N from Root, Stem and Leaf Residues in Soil and Role of Their Biochemical Quality. *Biol. Fertil. Soils* 42 (2), 119–128. doi:10.1007/s00374-005-0006-0
- Amelung, W., Miltner, A., Zhang, X., and Zech, W. (2001). Fate of Microbial Residues during Litter Decomposition as Affected by Minerals. *Soil Sci.* 166 (9), 598–606. doi:10.1097/00010694-200109000-00003
- An, T., Schaeffer, S., Zhuang, J., Radosevich, M., Li, S., Li, H., et al. (2015). Dynamics and Distribution of ¹³C-Labeled Straw Carbon by Microorganisms

CONCLUSION

The effects of different maize parts returning to the field on the accumulation of microbial residual nitrogen in brown earth aggregates with different fertility levels were investigated by calculating the contents of amino sugars. **Figure 9** showed the summarized schematic diagram for this study, indicating that the soil with shoot treatments was more likely to accumulate microbial residual nitrogen through microbial metabolic processes. Meanwhile, shoots promoted the accumulation of fungal residual nitrogen in the microaggregates, while roots were more beneficial to the accumulation of fungal residual nitrogen in the macroaggregates. High fertility soil had more microbial residual nitrogen than low fertility, and the soil with low fertility was more conducive to the accumulation of fungal residual nitrogen. Since the fungal residue was difficult to degrade, the maize returning from the soil with low fertility could be more conducive to the increase of soil nitrogen, thereby preventing the loss of nitrogen. Those results were beneficial to the construction of the microbial nitrogen accumulation cycle model on an aggregate scale and would provide a theoretical basis for the rational management of nitrogen nutrients in the dryland of brown earth to prevent soil degradation.

DATA AVAILABILITY STATEMENT

The original contributions presented in the study are included in the article/Supplementary Material, further inquiries can be directed to the corresponding author.

AUTHOR CONTRIBUTIONS

PX wrote the manuscript as the first author. JP revised the manuscript as the corresponding author. JW and NM contributed to the experiment.

FUNDING

The research was supported by the National Key Research and Development Program of China and the National Natural Science Foundation of China. The project number of the National Key Research and Development Program of China is 2021YFD1500204. The project numbers of the National Natural Science Foundation of China are 41977086 and 41807086.

as Affected by Soil Fertility Levels in the Black Soil Region of Northeast China. *Biol. Fertil. Soils* 51 (5), 605–613. doi:10.1007/s00374-015-1006-3

- Blaud, A., Lerch, T. Z., Chevallier, T., Nunan, N., Chenu, C., and Brauman, A. (2012). Dynamics of Bacterial Communities in Relation to Soil Aggregate Formation during the Decomposition of ¹³C-Labeled rice Straw. *Appl. Soil Ecol.* 53, 1–9. doi:10.1016/j.apsoil.2011.11.005
- Bonanomi, G., Cesarano, G., Gaglione, S. A., Ippolito, F., Sarker, T., and Rao, M. A. (2017). Soil Fertility Promotes Decomposition Rate of Nutrient Poor, but Not Nutrient Rich Litter through Nitrogen Transfer. *Plant Soil* 412 (1/2), 397–411. doi:10.1007/s11104-016-3072-1
- Castellano, M. J., Mueller, K. E., Olk, D. C., Sawyer, J. E., and Six, J. (2015). Integrating Plant Litter Quality, Soil Organic Matter Stabilization, and the

- Carbon Saturation Concept. *Glob. Change Biol.* 21 (9), 3200–3209. doi:10.1111/gcb.12982
- Chantigny, M. H., Angers, D. A., Prévost, D., Vézina, L. P., and Chalifour, F. P. (1997). Soil Aggregation and Fungal and Bacterial Biomass under Annual and Perennial Cropping Systems. *Soil Sci. Soc. America J.* 61 (61), 262–267. doi:10.2136/sssaj1997.03615995006100010037x
- Chao Wang, C., Wang, X., Pei, G. T., Xia, Z. W., Peng, B., Sun, L. F., et al. (2020). Stabilization of Microbial Residues in Soil Organic Matter after Two Years of Decomposition. *Soil Biol. Biochem.* 141, 107687. doi:10.1016/j.soilbio.2019.107687
- Clemente, J. S., Simpson, M. J., Simpson, A. J., Yanni, S. F., and Whalen, J. K. (2013). Comparison of Soil Organic Matter Composition after Incubation with maize Leaves, Roots, and Stems. *Geoderma* 192 (1), 86–96. doi:10.1016/j.geoderma.2012.08.007
- Ding, X., He, H., Zhang, B., and Zhang, X. (2011). Plant-N Incorporation into Microbial Amino Sugars as Affected by Inorganic N Addition: A Microcosm Study of ¹⁵N-Labeled maize Residue Decomposition. *Soil Biol. Biochem.* 43 (9), 1968–1974. doi:10.1016/j.soilbio.2011.06.012
- Ding, X., Han, X., Zhang, X., Qiao, Y., and Liang, Y. (2013). Continuous Manuring Combined with Chemical Fertilizer Affects Soil Microbial Residues in a Molliisol. *Biol. Fertil. Soils* 49, 387–393. doi:10.1007/s00374-012-0736-8
- Ding, X., Chen, S., Zhang, B., Liang, C., He, H., and Horwath, W. R. (2019). Warming Increases Microbial Residue Contribution to Soil Organic Carbon in an alpine Meadow. *Soil Biol. Biochem.* 135, 13–19. doi:10.1016/j.soilbio.2019.04.004
- Dorodnikov, M., Blagodatskaya, E., Blagodatsky, S., Marhan, S., Fangmeier, A., and Kuzyakov, Y. (2009). Stimulation of Microbial Extracellular Enzyme Activities by Elevated CO₂ depends on Soil Aggregate Size. *Global Change Biol.* 15 (6), 1603–1614. doi:10.1111/j.1365-2486.2009.01844.x
- Engelking, B., Flessa, H., and Joergensen, R. G. (2007). Shifts in Amino Sugar and Ergosterol Contents after Addition of Sucrose and Cellulose to Soil. *Soil Biol. Biochem.* 39 (8), 2111–2118. doi:10.1016/j.soilbio.2007.03.020
- Fontaine, S., Henault, C., Amor, A., Bdioui, N., Bloor, J. M. G., Maire, V., et al. (2011). Fungi Mediate Long Term Sequestration of Carbon and Nitrogen in Soil through Their Priming Effect. *Soil Biol. Biochem.* 43 (1), 86–96. doi:10.1016/j.soilbio.2010.09.017
- Gunina, A., and Kuzyakov, Y. (2014). Pathways of Litter C by Formation of Aggregates and SOM Density Fractions: Implications from ¹³C Natural Abundance. *Soil Biol. Biochem.* 71, 95–104. doi:10.1016/j.soilbio.2014.01.011
- Han, X. Z., and Li, N. (2018). Research Progress of Black Soil in Northeast China. *Scientia Geographica Sinica* 38 (7), 1032–1041. doi:10.13249/j.cnki.sgs.2018.07.004
- He, H., Zhang, W., Zhang, X., Xie, H., and Zhuang, J. (2011). Temporal Responses of Soil Microorganisms to Substrate Addition as Indicated by Amino Sugar Differentiation. *Soil Biol. Biochem.* 43 (6), 1155–1161. doi:10.1016/j.soilbio.2011.02.002
- Helfrich, M., Ludwig, B., Thoms, C., Gleixner, G., and Flessa, H. (2015). The Role of Soil Fungi and Bacteria in Plant Litter Decomposition and Macroaggregate Formation Determined Using Phospholipid Fatty Acids. *Appl. Soil Ecol.* 96, 261–264. doi:10.1016/j.apsoil.2015.08.023
- Jawson, M. D., Elliott, L. F., Papendick, R. I., and Campbell, G. S. (1989). The Decomposition of ¹⁴C-Labeled Wheat Straw and ¹⁵N-Labeled Microbial Material. *Soil Biol. Biochem.* 21 (3), 417–422. doi:10.1016/0038-0717(89)90153-3
- Joergensen, R. G. (2018). Amino Sugars as Specific Indices for Fungal and Bacterial Residues in Soil. *Biol. Fertil. Soils* 54 (5), 559–568. doi:10.1007/s00374-018-1288-3
- Jun Di Li, J. D., Zhang, Y. M., Zhao, B. H., Hu, C. S., He, H. B., Dong, W., et al. (2019). Effect of Long-Term Addition of Organic Substances on Soil Nitrogen and Amino Sugars in Particle-Size Fractions in the North China Plain. *Chin. J. Eco-Agriculture* 27 (04), 507–518. doi:10.13930/j.cnki.cjea.190084
- Kandeler, E., Tschirko, D., Bruce, K. D., Stemmer, M., Hobbs, P. J., Bardgett, R. D., et al. (2000). Structure and Function of the Soil Microbial Community in Microhabitats of a Heavy Metal Polluted Soil. *Biol. Fertil. Soils* 32, 390–400. doi:10.1007/s003740000268
- Lemanski, K., and Scheu, S. (2014). Incorporation of ¹³C Labelled Glucose into Soil Microorganisms of Grassland: Effects of Fertilizer Addition and Plant Functional Group Composition. *Soil Biol. Biochem.* 69, 38–45. doi:10.1016/j.soilbio.2013.10.034
- Liang, C., Amelung, W., Lehmann, J., and Kästner, M. (2019). Quantitative Assessment of Microbial Necromass Contribution to Soil Organic Matter. *Glob. Change Biol.* 25 (11), 3578–3590. doi:10.1111/gcb.14781
- Liang, C., and Balser, T. C. (2008). Preferential Sequestration of Microbial Carbon in Subsoils of a Glacial-Landscape Toposequence, Dane County, WI, USA. *Geoderma* 148 (1), 113–119. doi:10.1016/j.geoderma.2008.09.012
- Lidong Li, L., Wilson, C. B., He, H., Zhang, X., Zhou, F., and Schaeffer, S. M. (2019). Physical, Biochemical, and Microbial Controls on Amino Sugar Accumulation in Soils under Long-Term Cover Cropping and No-Tillage Farming. *Soil Biol. Biochem.* 135, 369–378. doi:10.1016/j.soilbio.2019.05.017
- Liu, X. B., Zhang, X. Y., Wang, Y. X., Sui, Y. Y., Zhang, S. L., Herbert, S. J., et al. (2010). Soil Degradation: a Problem Threatening the Sustainable Development of Agriculture in Northeast China. *Plant Soil Environ.* 56 (2), 87–97. doi:10.17221/155/2009-PSE
- Lou, Y., Xu, M., Wang, W., Sun, X., and Zhao, K. (2011). Return Rate of Straw Residue Affects Soil Organic C Sequestration by Chemical Fertilization. *Soil Tillage Res.* 113 (1), 70–73. doi:10.1016/j.still.2011.01.007
- Lu, X., Hou, E., Guo, J., Gilliam, F. S., Li, J., Tang, S., et al. (2021). Nitrogen Addition Stimulates Soil Aggregation and Enhances Carbon Storage in Terrestrial Ecosystems of China: A Meta-analysis. *Glob. Change Biol.* 27 (12), 2780–2792. doi:10.1111/gcb.15604
- Marschner, P., Kandeler, E., and Marschner, B. (2003). Structure and Function of the Soil Microbial Community in a Long-Term Fertilizer experiment. *Soil Biol. Biochem.* 35 (3), 453–461. doi:10.1016/s0038-0717(02)00297-3
- Marschner, P., Umar, S., and Baumann, K. (2011). The Microbial Community Composition Changes Rapidly in the Early Stages of Decomposition of Wheat Residue. *Soil Biol. Biochem.* 43 (2), 445–451. doi:10.1016/j.soilbio.2010.11.015
- Mummey, D., Holben, W., Six, J., and Stahl, P. (2006). Spatial Stratification of Soil Bacterial Populations in Aggregates of Diverse Soils. *Microb. Ecol.* 51 (3), 404–411. doi:10.1007/s00248-006-9020-5
- Oates, L. G., Duncan, D. S., Sanford, G. R., Liang, C., and Jackson, R. D. (2016). Bioenergy Cropping Systems that Incorporate Native Grasses Stimulate Growth of Plant-Associated Soil Microbes in the Absence of Nitrogen Fertilization. *Agric. Ecosyst. Environ.* 233, 396–403. doi:10.1016/j.agee.2016.09.008
- Paul, M., Andreas, F., David, D., Lucie, G., Padruot, F., and Urs, N. (2002). Soil Fertility and Biodiversity in Organic Farming. *Science (New York, N.Y.)* 296 (5573), 1694–1697. doi:10.1126/science.1071148
- Roberts, P., Bol, R., and Jones, D. L. (2007). Free Amino Sugar Reactions in Soil in Relation to Soil Carbon and Nitrogen Cycling. *Soil Biol. Biochem.* 39 (12), 3081–3092. doi:10.1016/j.soilbio.2007.07.001
- Ruamps, L. S., Nunan, N., and Chenu, C. (2011). Microbial Biogeography at the Soil Pore Scale. *Soil Biol. Biochem.* 43 (2), 280–286. doi:10.1016/j.soilbio.2010.10.010
- Schlesinger, W. H., Reynolds, J. F., Cunningham, G. L., Huenneke, L. F., Jarrell, W. M., Virginia, R. A., et al. (1990). Biological Feedbacks in Global Desertification. *Science* 247 (4946), 1043–1048. doi:10.1126/science.247.4946.1043
- Schutter, M. E., and Dick, R. P. (2002). Microbial Community Profiles and Activities Among Aggregates of Winter Fallow and Cover-Cropped Soil. *Soil Sci. Soc. America J.* 66 (1), 142–153. doi:10.2136/sssaj2002.0142
- Shahbaz, M., Kumar, A., Kuzyakov, Y., Börjesson, G., and Blagodatskaya, E. (2018). Priming Effects Induced by Glucose and Decaying Plant Residues on SOM Decomposition: A Three-Source ¹³C/¹⁴C Partitioning Study. *Soil Biol. Biochem.* 121, 138–146. doi:10.1016/j.soilbio.2018.03.004
- Simpson, R. T., Frey, S. D., Six, J., and Thiet, R. K. (2004). Preferential Accumulation of Microbial Carbon in Aggregate Structures of No-Tillage Soils. *Soil Sci. Soc. Am. J.* 68 (4), 1249–1255. doi:10.2136/sssaj2004.1249
- Simpson, A. J., Simpson, M. J., Smith, E., and Kelleher, B. P. (2007). Microbially Derived Inputs to Soil Organic Matter: Are Current Estimates Too Low? *Environ. Sci. Technol.* 41 (23), 8070–8076. doi:10.1021/es071217x
- Six, J., Bossuyt, H., Degryze, S., Denef, K., and Denef, K. (2004). A History of Research on the Link between (Micro)aggregates, Soil Biota, and Soil Organic Matter Dynamics. *Soil Tillage Res.* 79 (1), 7–31. doi:10.1016/j.still.2004.03.008

- Strickland, M. S., and Rousk, J. (2010). Considering Fungal:bacterial Dominance in Soils - Methods, Controls, and Ecosystem Implications. *Soil Biol. Biochem.* 42 (9), 1385–1395. doi:10.1016/j.soilbio.2010.05.007
- Tisdall, J. M., and Oades, J. M. (1982). Organic Matter and Water-Stable Aggregates in Soils. *Eur. J. Soil Sci.* 33 (33), 141–163. doi:10.1111/j.1365-2389.1982.tb01755.x
- Wang, X., Butterly, C. R., Baldock, J. A., and Tang, C. (2017). Long-term Stabilization of Crop Residues and Soil Organic Carbon Affected by Residue Quality and Initial Soil pH. *Sci. Total Environ.* 587–588, 502–509. doi:10.1016/j.scitotenv.2017.02.199
- Wang, Y., Li, M., Pei, J., An, T., Saeed, M. F., Shan, T., et al. (2019). Dynamics of maize Straw-Derived Nitrogen in Soil Aggregates as Affected by Fertilization. *J. Soils Sediments* 19 (7), 2882–2890. doi:10.1007/s11368-019-02288-5
- Xu, Y., Ding, F., Gao, X., Wang, Y., Li, M., and Wang, J. (2019). Mineralization of Plant Residues and Native Soil Carbon as Affected by Soil Fertility and Residue Type. *J. Soils Sediments* 19 (3), 1407–1415. doi:10.1007/s11368-018-2152-7
- Xu, Y., Ding, X., Lal, R., Gao, X., Li, S., Sun, L., et al. (2020). Effect of Soil Fertility on the Allocation of Nitrogen Derived from Different maize Residue Parts in the Soil-Plant System. *Geoderma* 379, 114632. doi:10.1016/j.geoderma.2020.114632
- Yang Wang, Y., Xu, Y., Pei, J., Li, M., Shan, T., Zhang, W., et al. (2020). Below Ground Residues Were More Conducive to Soil Organic Carbon Accumulation Than above Ground Ones. *Appl. Soil Ecol.* 148, 103509. doi:10.1016/j.apsoil.2020.103509
- Zhang, X., and Amelung, W. (1996). Gas Chromatographic Determination of Muramic Acid, Glucosamine, Mannosamine, and Galactosamine in Soils. *Soil Biol. Biochem.* 28 (9), 1201–1206. doi:10.1016/0038-0717(96)00117-4
- Conflict of Interest:** The authors declare that the research was conducted in the absence of any commercial or financial relationships that could be construed as a potential conflict of interest.
- Publisher's Note:** All claims expressed in this article are solely those of the authors and do not necessarily represent those of their affiliated organizations, or those of the publisher, the editors, and the reviewers. Any product that may be evaluated in this article, or claim that may be made by its manufacturer, is not guaranteed or endorsed by the publisher.

Copyright © 2022 Xue, Pei, Ma and Wang. This is an open-access article distributed under the terms of the Creative Commons Attribution License (CC BY). The use, distribution or reproduction in other forums is permitted, provided the original author(s) and the copyright owner(s) are credited and that the original publication in this journal is cited, in accordance with accepted academic practice. No use, distribution or reproduction is permitted which does not comply with these terms.



Ectomycorrhizal Fungi Associated With *Pinus sylvestris* var. *mongolica* Were Altered by Soil Environments With Aging Plantation in a Semi-arid Desert

Yue Ren^{1,2,3}, Mishan Guo⁴, Guodong Ding^{1,2,3*} and Yue Wang⁵

¹Key Laboratory of State Forestry and Grassland Administration on Soil and Water Conservation, Beijing Forestry University, Beijing, China, ²Yanchi Research Station, School of Soil and Water Conservation, Beijing Forestry University, Beijing, China, ³Engineering Research Center of Forestry Ecological Engineering, Ministry of Education, Beijing Forestry University, Beijing, China, ⁴China Institute of Water Resource and Hydropower Research, Beijing, China, ⁵College of Resources and Environmental Economics, Inner Mongolia University of Finance and Economics, Hohhot, China

OPEN ACCESS

Edited by:

Shengbo Xie,
Northwest Institute of Eco-
Environment and Resources (CAS),
China

Reviewed by:

Yuling Li,
Agricultural University of Hebei, China
Dang Xiaohong,
Inner Mongolia Agricultural University,
China

*Correspondence:

Guodong Ding
dingguodong@bjfu.edu.cn

Specialty section:

This article was submitted to
Drylands,
a section of the journal
Frontiers in Environmental Science

Received: 20 January 2022

Accepted: 17 March 2022

Published: 27 April 2022

Citation:

Ren Y, Guo M, Ding G and Wang Y
(2022) Ectomycorrhizal Fungi
Associated With *Pinus sylvestris* var.
mongolica Were Altered by Soil
Environments With Aging Plantation in
a Semi-arid Desert.
Front. Environ. Sci. 10:858452.
doi: 10.3389/fenvs.2022.858452

Pinus sylvestris var. *mongolica* (*P. sylvestris*) is a pioneer afforestation species for wind and sand fixation in northern China. However, most plantations have undergone unprecedented degradation since the early 1990s. Ectomycorrhizal (EcM) fungi are expected to be substantially related to the degradation of *P. sylvestris* plantations; however, the direct evidence for this remains unclear. For this purpose, we investigated variation among EcM fungal communities associated with *P. sylvestris* root samples of three age groups (half-mature, near-mature, and mature) in Mu Us Desert. Our results found a total of 72 EcM fungal operational taxonomic unit (OTU) belonging to *Basidiomycota* (63) and *Ascomycota* (9). The EcM fungal community is highly enriched in *Rhizopogon*, *Tuber*, *Tomentella*, and *Inocybe*, and the variations of their abundance mainly contribute to community differences. The diversity index and fungal species richness showed increasing trends toward the mature forest but did not reach a significant level ($p > 0.05$). The main factors that affected the dominant EcM fungal community were URE, INV, and SOC, but for the whole EcM fungal community, the effects of soil environments with plantation aging are not significant ($p > 0.05$). Understanding the effects of environmental factors on the structuring of the EcM fungal communities is critical to sustainable forest management in the future.

Keywords: ectomycorrhizal fungi, *Pinus sylvestris* var. *mongolica*, stand age, edaphic factor, diversity and community composition

1 INTRODUCTION

Ectomycorrhizal (EcM) fungi are well known to form symbiotic associations with many dominant trees in temperate and boreal forest ecosystems (Kolarikova et al., 2017; Koizumi et al., 2018; Sasse et al., 2018). The long-standing coevolution process leads to the mutually beneficial interaction between plants and microorganisms (Lemanceau et al., 2017). EcM fungi obtain carbohydrates from the host plant to meet the needs of their own growth (Zak et al., 2019). As root mutualistic symbionts, EcM fungi assist their host plant by enhancing mineral nutrients and moisture access as well as

protecting against pathogens and environmental stress (Tedersoo et al., 2020). Consequently, EcM fungi play vital roles in host health and stability maintenance of forest systems (Courty et al., 2010; Sebastiana et al., 2018), and various life processes of ecosystem are sustained by them. Soil environments and host features have proven to strongly control soil fungal communities at a local scale (Wang et al., 2021). Various studies have reported that EcM fungal communities are significantly affected by biotic (e.g., plant community) and abiotic (e.g., climate and soil physico-chemical property) factors (Tedersoo et al., 2012; Bachelot et al., 2016; Yang et al., 2019). Climates are crucial in shaping EcM fungal communities, for example, a too high or too low temperature is not suitable for the habit of many EcM fungi (van der Linde et al., 2018). Arnolds (1991) has confirmed that conifers are negatively affected by increasing nitrogen. Further, stand age as a basis feature of the forest ecosystem has a strong impact on the establishment and development of the EcM fungi communities (Spake et al., 2016).

Pinus sylvestris var. *mongolica* (*P. sylvestris*) is the most important tree species for combating desertification in reforestation, Northern China. So far, it was introduced to more than 13 provinces and covered an area of more than 7.0×10^5 ha in semi-arid regions (Song et al., 2019). Unfortunately, *P. sylvestris* plantation has been experiencing dieback since 1990s (Song et al., 2018). To get around this, many hypotheses have been put forward and confirmed (Zhu et al., 2006). The two factors most commonly mentioned in these hypotheses are soil water and nutrients (Liu et al., 2009; Zhao et al., 2020). The water shortage and depletion of nutrients are important factors affecting plant growth in desertification areas in the desertified regions. Water is the major limiting factor for the survival and growth of *P. sylvestris* due to the large water consumption for transpiration and the limitations of natural rainfall conditions in arid and semi-arid ecosystems (Hu et al., 2015; Liu et al., 2021a). In addition, soil nutrient is an essential constraining factor affecting plantation development (Zhang et al., 2021). With the development of forests, soil nutrient depletion is serious, so the nutrients used for the EcM fungal growth are limited. The declined groundwater and erratic precipitation upset the water balance of plants and restrict the growth and development of plants by affecting nutrient absorption (Geml et al., 2017). However, considering these two primary causal factors alone cannot fully explain the phenomenon of plantation degradation. Therefore, it remains a major challenge to reveal why *P. sylvestris* plantations were degraded on such a large scale.

Temperate forest ecosystems of semi-arid deserts are changing as a result of the increased drought (Garcia et al., 2016). Ectomycorrhizal symbionts enhance plant resistance to drought stress and damage compensation and maintain the dynamic balance and structural stability of forest ecosystems. In consequence, the variations of the EcM fungal communities directly affect forest growth and health (Soudzilovskaia et al., 2015). Furthermore, soil microorganisms are sensitive to climate changes; hence, EcM fungi also affect the response of the whole forest ecosystem to environmental change (Tedersoo et al., 2012; van der Linde et al., 2018). *P. sylvestris* is a typical ectomycorrhizal-dependent species, and the existence of it is

almost entirely dependent on the presence of symbiotic fungi (Dean et al., 2015; Guo M.-s. et al., 2020). Consequently, it is becoming increasingly clear that the potential of the EcM fungi in degraded plantations cannot be ignored.

P. sylvestris has been introduced into Mu Us Desert for decades and suffered serious degradation. Here, we hypothesized that the changes in the EcM fungal community are largely a consequence of the variations in the soil system caused by stand aging and lead to the degradation of *P. sylvestris* plantation. For this purpose, we collected the root of *P. sylvestris* plantations with various stand ages in the Mu Us Desert, and the EcM fungi community composition was examined by high-throughput sequencing technology. The objectives of this study were (1) to identify the EcM fungal community composition of *P. sylvestris* plantation among different stand ages and (2) to determine the major drivers of the EcM fungal community compositions of *P. sylvestris* plantation in the Mu Us Desert. This improved information can provide a deep-going implication on efficiently restoring degraded plantations.

2 MATERIALS AND METHODS

2.1 Study Site

The study site was located in the Hongshixia Sandy Botanical Garden of Yulin City, Shaanxi Province (38°26'N, 109°12'E, 1080 m a.s.l.), which is on the southern edge of the Mu Us Desert (**Supplementary Figure S1**). It is characterized by the temperate semi-arid continental monsoon climate with an annual temperature, precipitation, and evaporation of 9.1°C, 385 mm, and 2914 mm, respectively. The frost-free period ranges from 160 to 170 days. The soil is mainly composed of aeolian sandy soil, which is loose and very susceptible to flow and erosion. The dominated arbor plants are *P. sylvestris* and *P. tabuliformis*. The shrub and herb include *Caragana korshinskii*, *Lespedeza bicolor*, *Cares duriuscula*, *Rhamnus parvifolia*, *Salsola collina*, and *Potentilla anserine*.

2.2 Sample Collection and Treatment

Field investigation and sample collection were conducted in August 2017, which is the peak of plant growth season and microbial activity period. We randomly set a 50 m × 50 m plot in *P. sylvestris* plantations across 26, 32, and 43 a, which represent half-mature (MUh), near-mature (MUn), and mature (MUm) forests, respectively (**Table 1**). There were no tending measures and visible disturbance by anthropogenic activities since the establishment of plantations.

At each plot, five healthy and widely spaced standard trees were selected as sampling objects. Loose litters, herbs, and the undergrowth humus layer were gently removed prior to digging out the fine root samples carefully along the base of the trunk. After that, three repeated fine samples were taken from each standard tree; then, the three samples were fully mixed. A total of 15 mixed root samples (3 plots × 5 mixed samples = 15 composite samples) were used for DNA extraction and molecular identification. The ectomycorrhizal infected roots were accompanied with soil placed into plastic bags to keep the

TABLE 1 | General information of sampling plots.

Plot	Stand aGE/a	Slope°	Average height/m	Average DBH/Cm	Canopy density
MUh	26	3	12.48 ± 3.69	11.76 ± 3.72	0.79
MUn	32	4	13.96 ± 2.38	13.58 ± 2.44	0.86
MUm	43	4	14.14 ± 1.84	19.95 ± 3.03	0.73

Values are mean ± standard error (SD), DBH refers to the diameter at breast height, MUh refers to the half-mature forest, MUn refers to the nearly mature forest, and MUm refers to the mature forest. The same is below.

root tips fresh. Root samples were kept cool after sampling and stored at 4°C. Soil samples were collected around the root, with three repeated soil samples collected in each point, and fully mixed into one (3 plots × 5 mixed samples = 15 composite samples). Soil samples from 0 to 20 cm depth were obtained to determine soil physico-chemical properties and enzyme activities. After passing through a 2 mm sieve, the soil samples were divided into two parts; one was stored at 4°C in a refrigerator to determine enzyme activities and the content of available nutrients in soils, and the other was taken straight back to determine soil physical properties, soil organic matter (SOM), and soil total nutrient.

2.3 Soil Property Analysis

Soil water content (SWC) was determined by the gravimetric method after drying the soil sample in an oven at 105°C for 12 h. Soil pH was measured using a pH meter (PHS-3E, INESA, Shanghai, China); the mixture of soil and water is 1:2.5. Soil organic matter (SOM) content was measured by the K₂Cr₂O₇-H₂SO₄ oxidation technique (Walkley and Black, 1934). Soil total nitrogen (TN), total phosphorus (TP), nitrate nitrogen (NO₃⁻-N), and ammonium nitrogen (NH₄⁺-N) were determined using an automated element analyzer (Smartchem 200, Italy). TN used the indophenol-blue spectrophotometric method, and TP used the Mo-Sh anti-colorimetric analysis method (John and Matt, 1970; Mason et al., 1999). Soil invertase (INV) activity, urease (URE) activity, and phosphatase (PHO) activity were assayed as described by Tabatabai (1994).

2.4 Molecular Identification of EcM Fungi

DNA was extracted and purified using the Powersoil® DNA Isolation Kit (Mo Bio Laboratories, Carlsbad, CA, United States), according to the manufacturer's protocol. The genomic DNA concentrations were checked on 1% agarose gels electrophoresis and quantified on a NanoDrop NC2000 spectrophotometer (Thermo Fisher Scientific, Waltham, MA, United States). The fungal internal transcribed spacer (ITS) region was amplified on Eppendorf Mastercycler Gradient Thermocycler (Germany); for the ITS1 regions of fungi, the primers were ITS1F (5'-GGAAGT AAAAGTCGTAACAAGG-3') and ITS2 (5'-TCCTCCGCTTAT TGATATGC-3') (Amend et al., 2010). For each sample, an eight-digit barcode sequence was added to the 5' end of the forward and reverse primers (provided by Allwegene Company, Beijing). The polymerase chain reaction (PCR) mixtures were analyzed on a Mastercycler Gradient (Eppendorf, Germany) using 25 µL reaction volumes, containing 2.5 µL 2 × Taq PCR MasterMix, 3 µL BSA (2 ng/µL), 1 µL Forward Primer (5 µM), 1 µL Reverse

Primer (5 µM), 2 µL template DNA, and 5.5 µL ddH₂O. The cycling parameters were 95°C for 5 min, followed by 28 cycles of 95°C for 45 s, 55°C for 50 s, and 72°C for 45 s with a final extension at 72°C for 10 min. The PCR products were purified using an Agencourt AMPure XP Kit. Deep sequencing was performed on an Illumina Miseq platform at Allwegene Company (China, Beijing). After the run, image analysis, base calling, and error estimation were performed using Illumina Analysis Pipeline Version 2.6.

The raw data were first screened, and then the sequences shorter than 230 bp and with low-quality scores (≤20) were removed. After removing non-fungal sequence reads, the fungal sequences were clustered into operational taxonomic units (OTUs) (Blaxter et al., 2005) at a 97% similarity level using the Uparse algorithm of Vsearch (Version 2.7.1) (Edgar, 2010). The remaining high-quality sequences were queried against the GenBank (<https://academic.oup.com/nar/article/50/D1/D161/6447240>) non-redundant nucleotide database in NCBI using local BLASTn (<https://blast.ncbi.nlm.nih.gov/>). The MEGAN (Version 6.0) program was used to assign BLAST hits to taxa of the NCBI taxonomy. Non-EcM fungal OTUs were filtered out by FUNGuild (Version 1.0, <http://www.stbates.org/guilds/app.php>) (Zhang et al., 2015). The key EcM fungal species were analyzed by using the analysis of modular topological roles (within-module connectivity (Zi) ≥ and among-module connectivity (Pi) ≥ 0.62). All the identified sequences were submitted to the GenBank with the accession numbers of SUB7166485 (from MT229482 to MT229553) (Table 3).

2.5 Data Analysis

Define “dominant species” as the EcM fungi detected in 80% of all samples, “frequent species” as the EcM fungi detected in 30% of all samples, and “rare species” as the EcM fungi detected in less than 30% of all samples. The important value of OTUs is represented by the sum of its relative abundance and relative abundance. α-diversity indices were calculated based on the OTU dates, including the number of identified genera (S), Shannon index (H'), Simpson's index (d), and evenness index of species richness [Pielou (J)]. The differences in community structure of the EcM fungi were analyzed by non-metric multidimensional scaling (NMDS) analysis. Bray-Curtis dissimilarity index was calculated to examine the dissimilarity of the OTU community in different sites. Dissimilarity matrices of environmental data sets were calculated based on Euclidean distance. A redundancy analysis (RDA) was used to determine the correlation between the EcM fungal community (genus level) and soil properties. Subsequently, Spearman rank correlation was used to explain the relationship between the EcM fungal community (genus level)

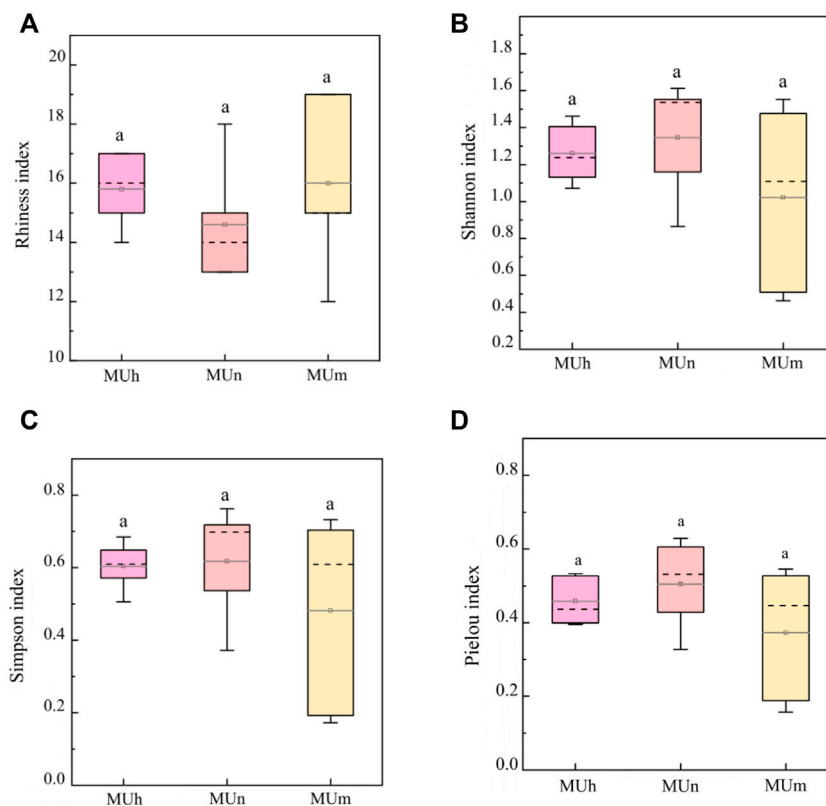


FIGURE 1 | Diversity of the EcM fungi associated with *P. sylvestris* at different age groups. Letters indicate significant differences for each parameter ($p < 0.05$; one-way ANOVA, Tukey test) based on the values determined for each site (5 replicates/site). **(A)** Rhiness index, **(B)** Shannon index, **(C)** Simpson index, **(D)** Pielou index.

TABLE 2 | Bray–Curtis of EM fungi associated with *P. sylvestris* in different age groups.

Bray–Curtis	MUh	MUn	MUm
MUh	—	0.70	0.77
MUn	0.70	—	0.68
MUm	0.77	0.68	—

and soil properties, also based on Bray–Curtis distance. The correction heatmap was a visual correlation between all soil properties and the five most frequently recovered genera. After converting soil properties to a matrix, we performed the Mantel test to determine the significance of each environmental variable. The EcM fungal network was constructed based on random matrix theory using the OTU data, which present in at least eight (>50%) samples (Deng et al., 2012). All network analyses were performed using the MENA platform (<http://ieg4.rccc.ou.edu/mena/main.cgi>).

One-way analysis of variance (ANOVA) with the least-significant difference (LSD) and the Tukey test were performed to determine the significant difference among soil variables and EcM fungal diversity. All statistical analyses were performed in SPSS (Version 20.0), and $p < 0.05$ was considered statistically significant. The α -diversity indices, Bray–Curtis dissimilarity

index, network analysis, correction heatmap, and Mantel test were implemented using the R (Version 3.5.1) program. RDA was performed using CANOCO (Version 4.5). The network diagram was visualized by Cytoscape (Version 3.9.0).

3 RESULTS

3.1 Soil Properties

In *P. sylvestris* plantation, all the soil properties varied by stand age ($p < 0.05$, Table 3). Soil TN, SOM, NO_3^- , INV, and URE were significantly different with stand aging ($p < 0.05$). In general, soil in the MU Us Desert was alkali to neutral. The maximum values of soil nutrient contents (SOM, TN, and TP) were found in half-mature forests. Soil URE and PHO enzymes were the most active in mature forests.

3.2 Diversity and Composition of the EcM Fungal Community

A total of 361,548 high-quality sequences were obtained from roots associated with *P. sylvestris*, assigned to 807 fungal OTUs. A total of 72 of these had an EcM lifestyle and were identified to the genus level and below (Table 2). With stand aging, the numbers of OTUs and rhiness of genus increased first and then decreased; the values of the remaining α -diversity indices gradually decreased. The

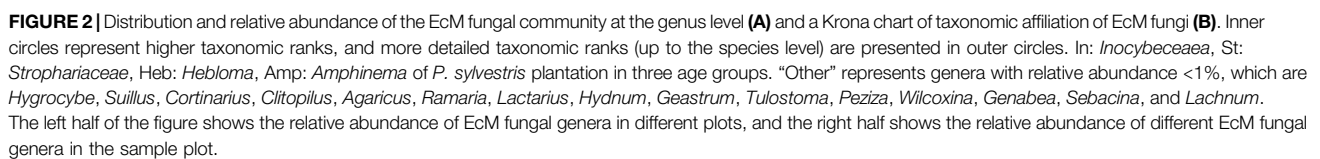


TABLE 3 | Soil properties of *P. sylvestris* with different age groups.

Factors	MUh	MUn	MUm
pH	7.58 ± 0.19 a	7.51 ± 0.04 a	7.27 ± 0.15 b
SWC/%	3.66 ± 0.56 a	2.88 ± 0.17 b	3.46 ± 0.46 a
TN/g·kg	0.12 ± 0.02 b	0.09 ± 0.01 c	0.17 ± 0.02 a
TP/g·kg	0.30 ± 0.02 b	0.37 ± 0.01 a	0.37 ± 0.04 a
SOM/g·kg	1.16 ± 0.21 c	2.38 ± 0.30 b	3.23 ± 0.85 a
NH ₄ ⁺ /mg·kg	1.03 ± 0.06 b	0.94 ± 0.10 b	1.56 ± 0.10 a
NO ₃ ⁻ /mg·kg	2.12 ± 0.02 c	4.06 ± 0.08 b	4.30 ± 0.04 a
INV/U·g	66.88 ± 0.16 a	48.26 ± 1.38 b	17.40 ± 0.24 c
URE/U·g	289.97 ± 16.48 c	319.03 ± 8.44 b	555.66 ± 16.01 a
PHO/U·g	0.59 ± 0.03 b	0.60 ± 0.01 b	0.69 ± 0.03 a

Letters indicate significant differences for each parameter ($p < 0.05$; one-way ANOVA, Tukey test) based on the values determined for each site (5 replicates/site).

impact of stand age on the EcM fungal community has not reached a significant level ($p > 0.05$, **Figure 1**).

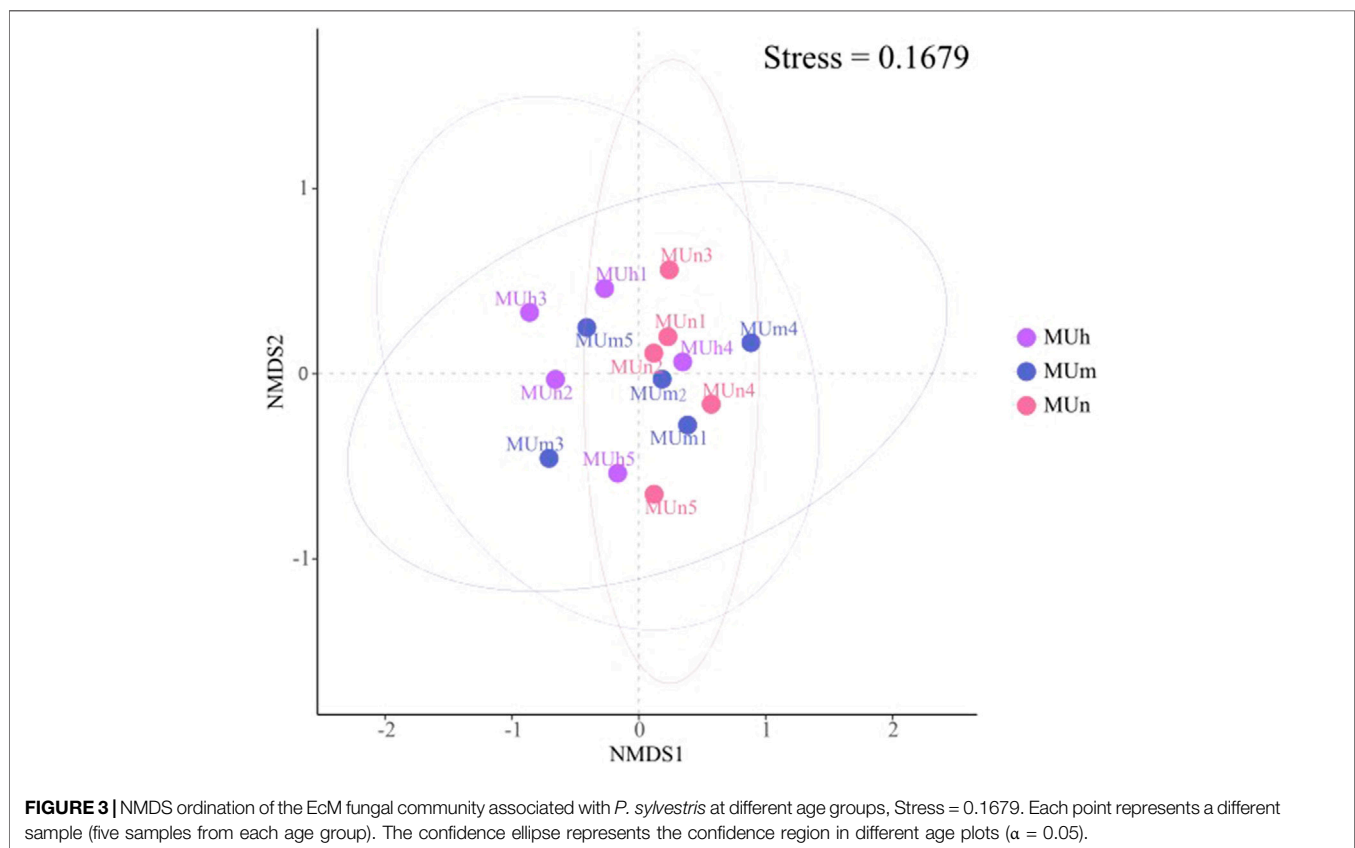
Our studies found that the EcM fungal OTUs of *P. sylvestris* plantations in the Mu Us Desert were assigned to two phyla, four classes, 12 orders, 18 families, and 23 genera (**Figure 2**; **Supplementary Table S1**). Of all 72 EcM OTUs, *Basidiomycota* was the most abundant phylum (83%) with 63 OTUs, following by *Ascomycota* (17%) with nine OTUs. Among them, 13 and 14 species were detected for the dominant and common species, respectively. The rare species was the largest pool (45 species) accounting for 62.50% of the total species. At the

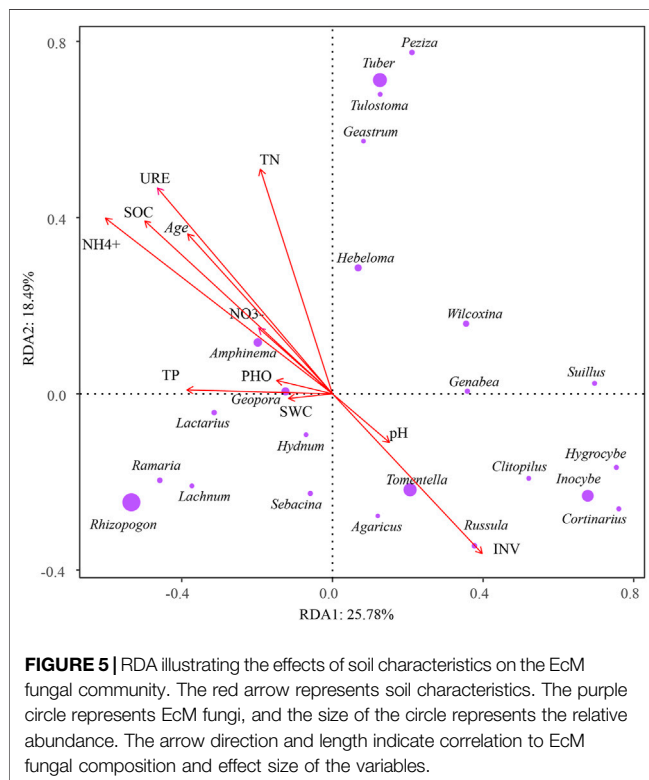
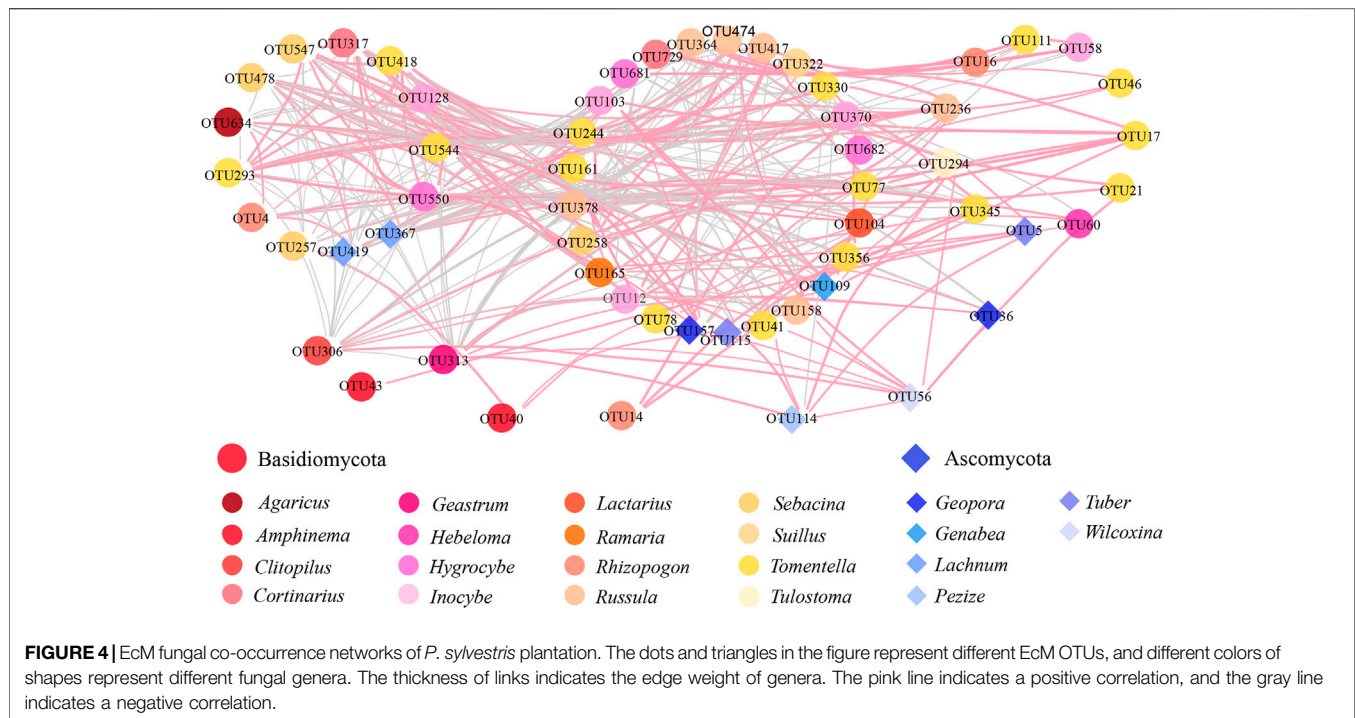
genus level, *Rhizopogon* was the most dominant EcM fungus; it has the highest relative abundance in all age groups, especially in MUn and MUm (more than 50%, **Figure 2**). Besides, the genera of *Tuber*, *Tomentella*, and *Inocybe* were also widely distributed in all plantations. With the aging of stand, *Rhizopogon* increased first and then decreased, while *Tomentella* and *Inocybe* were just the opposite. *Tuber* was accumulated with stand age.

The Bray–Curtis distances of the EcM fungal community composition in three stand ages are shown and ordered by NMDS. The stress value is 0.1679 (< 0.2), so the Bray–Curtis distance can better reflect the difference of community composition (**Table 3**). The coordinates of scatter points indicated that the EcM fungal composition varied in different stand ages (**Figure 3**). ANOSIM results confirmed that the difference of fungal community structure was obvious with stand age ($R = 0.88$, $p > 0.05$). Based on the area of the confidence ellipse and Bray–Curtis distances (**Figure 3**; **Table 3**), the EcM fungal community structures of the near-mature and mature forests were the most similar.

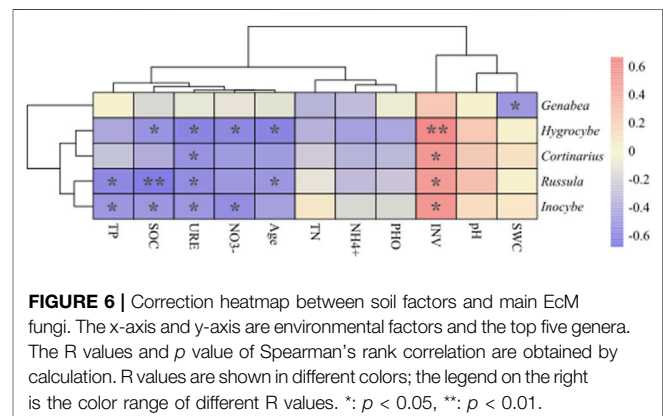
3.3 Corrections Between EcM Fungal Communities

The molecular ecological network of the EcM fungi reflects the coexistence relationship of species in the environment (**Figure 4**). After removing the OTUs with average relative abundances less





than 0.01%, a network that included 57 nodes and 435 edges was constructed. Of all these edges, 206 (47.36%) had shown positive corrections and 229 (52.64%) had shown negative correlations. In the EcM fungal network, the average degree, average clustering



coefficient, and average path distance were 15.263, 0.571, and 1.875, respectively. The modularity calculation of the EcM network divides the whole network into four individual models (**Supplementary Figure S2**). OTU306 (classified as *Rhizopogon mohelnensis*), OTU43 (uncultured *Peziza*, *Peziza* sp.), OTU40 (classified as *Clitopilus* sp.), and OTU14 (classified as *Clitopilus* sp.) of *Basidiomycota* and OTU114 (classified as *Rhizopogon mohelnensis*), OTU56 (classified as *Wilcoxina mikolae*), and OTU36 (classified as *Geopora arenicola*) of *Ascomycota* had weak relationship with other species. We identified key EcM fungal species by using the analysis of modular topological roles. According to within-module connectivity (Z_i) and among-module connectivity (P_i), OTU60 ($Z_i = 2.60 > 2.5$, $P_i = 0.625 > 0.6$, classified as *Hebeloma collariatum*) was the core species of the model (**Supplementary Figure S3**).

3.4 Relationship Between EcM Fungal Communities and Soil Properties

The EcM fungal community composition through stand ages was driven by soil properties (Figures 5, 6; Supplementary Table S3). The redundancy (RDA) analysis revealed the impact of soil characteristics on the EcM fungal community, and the contribution rates of principal components 1 and 2 were 25.78 and 18.49%, respectively. All four axes in total contributed 67.3% of the explanation (Figure 5). Among all soil properties, NO_4^+ content had the highest contribution rate (15.32%). The contributions of SOC, TN, INV, and stand age all exceeded 11%.

The correction heatmap and Mantel test between soil factors and major EcM genera were created by Spearman's rank correlation (Figure 6; Supplementary Tables S2, S3). The INV had a significant positive effect on the EcM fungal community, while SOC, TP, and stand age have a significant negative effect on the major EcM fungi ($p < 0.05$ or $p < 0.01$). URE and NO_3^- had an excellent negative correlation to the EcM fungal community ($p < 0.05$), although their contribution rates were low.

4 DISCUSSION

4.1 Variations in EcM Fungal Diversity and Community Composition

EcM fungi are abundant and diverse in temperate and boreal forests (Steidinger et al., 2020), and the succession and variation of the underground EcM fungal community was a complex ecological process (Bardgett and van der Putten, 2014; Franklin et al., 2014). The diversity indices and community structure of EcM fungi changed with stand aging in the Mu Us Desert, but the effect of forest age was not significant. This was consistent with previous studies that the diversity of the fungal community was not correlated with the aging stand (Wang et al., 2020). As expected, the EcM fungal community was dominated by *Basidiomycota* rather than *Ascomycetes*, which is consistent with previous results (Geml et al., 2017). It is known that most of the known EcM fungi are *Basidiomycota*, which are diverse and adaptive to various environments (Boeraeve et al., 2018). Therefore, *Basidiomycota* considerably contributes to the ecological restoration in deserts.

The endemic genera were found across different stands, and the EcM fungal community structure was significantly different between three age stands. The distribution pattern of the EcM fungi indicates the succession of EcM fungi during forest development and the influence of stand age on it. The variations in plant community and soil characteristics caused by stand age altered the establishment and distribution of the EcM fungal community (Hayward et al., 2015). *Rhizopogon* was the dominant EcM fungal genera of *P. sylvestris* across all stand ages in the Mu Us Desert. Besides, *Tomentella*, *Inocybe*, and *Tuber* were also widely distributed in *P. sylvestris* plantations. These OTU-richest genera are also commonly detected in boreal coniferous forests (van Dorp et al., 2016). They are easily dispersed and widely adapted to the harsh environment (Ryberg et al., 2008; Bahram et al., 2011). Obviously, they are “multistage” fungi with an excellent competitive ability (Taylor and Bruns, 1999).

As the largest genus of hypogeous *Basidiomycota*, *Rhizopogon* were widely distributed and associated with pines; it is also the most common EcM fungi of *P. sylvestris* plantations in the Mu Us Desert. Especially, *Rhizopogon* proliferated in the high-carbon near-mature forest due to the high demand for carbohydrates (Mujic et al., 2014). Further, *R. rubescens* and *R. mohelnensis* contribute to the stress resistance; therefore, they conduce to the improvement in survival of conifer seedlings in a desert environment (Bahram et al., 2011). As saprotrophic EcM fungi, *Tomentella* prospers the nutrient cycling and is widely distributed throughout the Northern hemisphere forests (Han et al., 2017). Besides, *Tomentella* is also of great resistance to environmental stresses, supported by the presence in the degraded oak forest (Mosca et al., 2007). *Inocybe* is ecologically important in the forest succession by providing water and minerals for the host plants (Mason et al., 1983). In the Mu Us Desert, *Inocybe* were clearly decreasing from the half-mature forest to a mature forest. Soil moisture consumption is greatly responsible for this instance due to their preference of an arid environment, which has obvious significance in the desertification region. Furthermore, *Cortinarius*, *Amphinema*, and *Russula* were widely distributed in the mature forest. They are typical “late-stage” fungi, which are usually found associated with older forests and have strong competitive abilities (Hayward et al., 2015; Guo M. et al., 2020). The core fungi of the EcM fungal network are classified as *Hebeloma*, which is a frequent EcM genus, and its species is usually associated with a wide range of *Pinaceae* trees (Gryta et al., 2010).

Suillus is regarded as the most generic EcM fungi associated with pine, but it was diminished in the Mu Us Desert; this result is inconsistent with previous studies (Policelli et al., 2018). *Geopora* is considered to be an important mutual partner for host plants resisting the stress conditions. Notably, *Russula* and *Peziza* are also detected in the *P. sylvestris* plantations, which usually rely on fertile soil and prefer high pH, respectively. *Lactarius*, *Hebeloma*, and *Lachnum* accounted for a very small percentage; this was supported by the previous studies that they were not easily established in desertification regions (Desai et al., 2016). Curiously, some common drought-tolerant and barren-resistant EM fungal species were missed, such as *Lycoperdon* and *Cenococcum* (Jany et al., 2003).

4.2 The Drivers of the EcM Fungal Community

The primary drivers of the EcM fungi community at different scales are not necessarily the same (Peay and Matheny, 2016). EcM fungi were strongly determined by the soil environment, and the edaphic factors are approved to be the major drivers of the EcM fungal community at a local scale (Miyamoto et al., 2015). Forest development is usually accompanied by variations in the soil system (Zhao et al., 2020); EcM fungi are highly sensitive to the environmental changes. Therefore, host-related variables strongly influence the EcM fungal community. The variations of soil properties with stand aging are of great importance to shape fungal communities (Truong et al., 2019). We found that most of the factors we measured in this study were proved to sufficiently affect the community structure of the EcM fungi. Among them, the soil enzyme activities of invertase and urease

were the most major abiotic factors causing EcM fungal communities in cation regions. They were the most important enzymes for soil fertility and nitrogen metabolism. ECM fungi have different preferences and demands for nutrient strategies, and the nutrient competition in fungal communities alters the assembly of the EcM fungal communities (Yang et al., 2021). EcM fungi-induced soil nutrient cycling substantially contributes to the growth and health of host plants. Nitrogen is the foremost limiting nutrient in conifer forest systems (Sebastiana et al., 2018). In our study, N shift was clearly observed, that is, NH_4^+ and NO_3^- concentrations significantly increased with aging stand. Meanwhile, EcM fungi (e.g., *Peziza* and *Russlula*) were negatively correlated with soil N availability. This finding confirms that EM fungal absorption capacity varies in response to the various forms of N, so N availability determines the community composition of EcM fungi (Kjoller et al., 2012). Furthermore, EcM fungi are good decomposers of soil organic matter and play a major role in the turnover and stabilization process of soil nutrients. The sufficient soil nutrients provide a suitable microenvironment for fungi, which is the basis of expanding and prospering the EcM fungal community.

Water shortage was considered to be an important abiotic factor; it was also the strongest abiotic candidate filter (Liu et al., 2021b). This result is consistent with previous studies that soil moisture is a key factor to alter the EcM fungi community composition in arid environments (Dean et al., 2015). Meanwhile, with the specificity of EcM fungi to drought stress, in return, variations in the EcM fungal community have direct impacts on the growth and development of host plants (Kennedy and Peay, 2007). Besides, considerable research studies have been devoted to come to the conclusion that soil pH is another key driver of the EcM fungal community (Kutszegi et al., 2015). The EcM fungal community changes significantly even with a very small variation of pH values. On one hand, soil pH affects the growth of the EcM fungi and mycelial metabolism. On the other hand, soil pH indirectly alters the EcM fungal community by changing nutrient availability (Bennett et al., 2017). Generally, EcM fungi prefer slightly acidic to neutral soils, and the growth of the EcM fungi is inhibited at a higher-pH environment. In the Mu Us Desert, the soil pH ranged from 7.27 to 7.58. The weakly alkaline soil leads to potential variations in the EcM fungal community.

EcM fungi can secrete nutrient-related enzymes to regulate the nutrient cycling. The active soil enzyme contributes to the N and P absorption and slows the decomposition of soil organic matter (Lindahl and Tunlid, 2014). Therefore, the interaction between EcM fungi and the soil system is affected by soil enzyme activity. Generally speaking, urease and phosphatase benefit the mineralization of nitrogen and phosphorus, thus providing available nitrogen and phosphorus for the hosts (Bidartondo et al., 2001). In this study, the urease activity is increasing with stand aging; it is beneficial to available nitrogen supply for host plants. This finding was also confirmed by the soil nitrogen in suit investigation. Invertase is related to the transformation of soil organic carbon, but with the increase in soil organic matter, invertase activities were significantly reduced. This reduction was also reported that only a few EcM fungi

have saprophytic functions and are active in the decomposition of soil organic matter (Jonard et al., 2014).

4.3 Implications of EcM Fungi for *P. sylvestris* Plantation Degradation

EcM fungi and host plants are a community of shared common interests, and they get feedback from each other. The growth of *P. sylvestris* plantation is inseparable from the assistance of EcM fungi, and EcM fungi also benefit from the host plant (Zhu et al., 2006). Therefore, the interaction between EcM fungi and host plants is a potential but crucial indicator for the degradation of *P. sylvestris* plantation. Natural forests with diverse ages and hierarchical structures usually have abundant, diverse, and complex EcM fungal community compositions and structures (Grebenc et al., 2009). Compared to the original forest, artificial plantation is simple in structure and has poor stability, resulting in EcM fungi with low heterogeneity and diversity (Guo M. et al., 2020). Therefore, this simple EcM fungal community composition may be one of the reasons for the degradation of plantation. There is overwhelming evidence corroborating the notion that structure and diversity determine ecosystem function and stability (Huang et al., 2021).

As the most typical EcM fungi, *Suillus* has extreme host specificity of *Pinaceae*, especially *P. sylvestris*. *Suillus* forms symbionts with conifer species and substantially contributes to *P. sylvestris* invasion and seedling establishment by improving soil nutrient absorption (Policelli et al., 2018). Previous studies have demonstrated that *Suillus* is the dominant EcM fungal genus of *P. sylvestris* in nature forests (Truong et al., 2019). However, only one species of *Suillus* associated with *P. sylvestris* was found in the Mu Us Desert. Hence, we deduced that functional EcM fungi *Suillus* (e.g., *Lycoperdon*, *Cenococcum*) commonly found in nature forests contribute to the *P. sylvestris* plantation degradation. This assignment has explained the central importance of EcM fungi in *P. sylvestris* plantation degradation. In a desert environment, there are intensely interspecific and intraspecific competitive interactions for the limiting resources. Therefore, the simplification community structure and the loss of EcM fungal diversity and function eventually lead to the degradation of *P. sylvestris* plantation.

5 CONCLUSION

In Mu Us Desert, the obtained 72 ECM fungal OTUs were identified into two phyla and 23 genera associated with *P. sylvestris* plantation, and the EcM fungal composition was dominated by *Rhizopogon*, *Inocybe*, *Tomentella*, and *Tuber*. Diversity indices and community structures of the EcM fungi had no significant effect by stand age. The major abiotic drivers of the dominant EcM fungal genera were NO_4^+ , SOC, TN, INV, and stand age; thus, the combination of soil physico-chemical properties and soil enzyme activities jointly drives the variations of the major EcM fungal community to a certain extent. We highly suppose that the soil-induced community simplification and assembly variations of the EcM fungi and the loss of some fungal groups (e.g., *Suillus*) with specific functions substantially

contribute to the degradation of *P. sylvestris* plantation. In the future, sustainable forest management requires unremitting efforts on EM fungal community structures and functions at the spatial and temporal multiscale toward a changing world.

DATA AVAILABILITY STATEMENT

The datasets presented in this study can be found in online repositories. The names of the repository/repositories and accession number(s) can be found below: NCBI [accession: MT229482-MT229553].

AUTHOR CONTRIBUTIONS

YR and MG performed the experiments. YR conceived the paper, analyzed the data, and wrote paper. YR and GD led the writing of the

manuscript. All authors performed supervision and finalized the manuscript and agree to be accountable for all aspects of the work.

FUNDING

This work was funded by the Fundamental Research Funds for the Central Universities, the National Key Research and Development Program of China, and the Natural Science Foundation of Inner Mongolia [Grant numbers (2021ZY47), (2018YFC0507100), and (2020BS03001)].

SUPPLEMENTARY MATERIAL

The Supplementary Material for this article can be found online at <https://www.frontiersin.org/articles/10.3389/fenvs.2022.858452/full#supplementary-material>

REFERENCES

- Amend, A. S., Seifert, K. A., Samson, R., and Bruns, T. D. (2010). Indoor Fungal Composition Is Geographically Patterned and More Diverse in Temperate Zones Than in the Tropics. *Proc. Natl. Acad. Sci. U.S.A.* 107 (31), 13748–13753. doi:10.1073/pnas.1000454107
- Arnolds, E. (1991). Decline of Ectomycorrhizal Fungi in Europe. *Agric. Ecosyst. Environ.* 35, 209–244. doi:10.1016/0167-8809(91)90052-Y
- Bachelot, B., Uriarte, M., Zimmerman, J. K., Thompson, J., Leff, J. W., Asaii, A., et al. (2016). Long-lasting Effects of Land Use History on Soil Fungal Communities in Second-Growth Tropical Rain Forests. *Ecol. Appl.* 26, 1881–1895. doi:10.1890/15-1397.1
- Bahram, M., Pölme, S., Kõljalg, U., Zarre, S., and Tedersoo, L. (2011). Regional and Local Patterns of Ectomycorrhizal Fungal Diversity and Community Structure along an Altitudinal Gradient in the Hyrcanian Forests of Northern Iran. *New Phytol.* 193, 465–473. doi:10.1111/j.1469-8137.2011.03927.x
- Bardgett, R. D., and van der Putten, W. H. (2014). Belowground Biodiversity and Ecosystem Functioning. *Nature* 515 (7528), 505–511. doi:10.1038/nature13855
- Bennett, J. A., Maherali, H., Reinhart, K. O., Lekberg, Y., Hart, M. M., and Klironomos, J. (2017). Plant-soil Feedbacks and Mycorrhizal Type Influence Temperate forest Population Dynamics. *Science* 355, 181–184. doi:10.1126/science.aai8212
- Bidartondo, M. I., Ek, H., Wallander, H., and Söderström, B. (2001). Do nutrient Additions Alter Carbon Sink Strength of Ectomycorrhizal Fungi? *New Phytol.* 151, 543–550. doi:10.1046/j.1469-8137.2001.00180.x
- Blaxter, M., Mann, J., Chapman, T., Thomas, F., Whitton, C., Floyd, R., et al. (2005). Defining Operational Taxonomic Units Using Dna Barcode Data. *Phil. Trans. R. Soc. B* 360 (1462), 1935–1943. doi:10.1098/rstb.2005.1725
- Boerave, M., Honnay, O., and Jacquemyn, H. (2018). Effects of Host Species, Environmental Filtering and forest Age on Community Assembly of Ectomycorrhizal Fungi in Fragmented Forests. *Fungal Ecol.* 36, 89–98. doi:10.1016/j.funeco.2018.08.003
- Courty, P.-E., Buée, M., Diedhiou, A. G., Frey-Klett, P., Le Tacon, F., Rineau, F., et al. (2010). The Role of Ectomycorrhizal Communities in forest Ecosystem Processes: New Perspectives and Emerging Concepts. *Soil Biol. Biochem.* 42, 679–698. doi:10.1016/j.soilbio.2009.12.006
- Dean, S. L., Warnock, D. D., Litvak, M. E., Porras-Alfaro, A., and Sinsabaugh, R. (2015). Root-associated Fungal Community Response to Drought-Associated Changes in Vegetation Community. *Mycologia* 107, 1089–1104. doi:10.3852/14-240
- Deng, Y., Jiang, Y.-H., Yang, Y., He, Z., Luo, F., and Zhou, J. (2012). Molecular Ecological Network Analyses. *BMC Bioinformatics* 13, 113. doi:10.1186/1471-2105-13-113
- Desai, N. S., Wilson, A. W., Powers, J. S., Mueller, G. M., Egerton-Warburton, L. M., and Egerton-Warburton, L. M. (2016). Ectomycorrhizal Diversity and Community Structure in Stands of Quercus Oleoides in the Seasonally Dry Tropical Forests of Costa Rica. *Environ. Res. Lett.* 11, 125007. doi:10.1088/1748-9326/11/12/125007
- Edgar, R. C. (2010). Search and Clustering Orders of Magnitude Faster Than BLAST. *Bioinformatics* 26 (19), 2460–2461. doi:10.1093/bioinformatics/btq461
- Franklin, O., Näsholm, T., Högberg, P., Högberg, M. N., and Högberg, M. N. (2014). Forests Trapped in Nitrogen Limitation - an Ecological Market Perspective on Ectomycorrhizal Symbiosis. *New Phytol.* 203, 657–666. doi:10.1111/nph.12840
- Geml, J., Morgado, L. N., Semenova-Nelsen, T. A., and Schilthuizen, M. (2017). Changes in Richness and Community Composition of Ectomycorrhizal Fungi Among Altitudinal Vegetation Types on Mount Kinabalu in Borneo. *New Phytol.* 215, 454–468. doi:10.1111/nph.145610.1111/nph.14566
- Gryta, H., Debaud, J. C., Effosse, A., Gay, G., and Marmeisse, R. (1997). Fine-scale Structure of Populations of the Ectomycorrhizal Fungus Hebeloma Cylindrosporum in Coastal Sand Dune forest Ecosystems. *Mol. Ecol.* 6 (4), 353–364. doi:10.1046/j.1365-294X.1997.00200.x
- Guo, M.-s., Ding, G.-d., Gao, G.-l., Zhang, Y., Cao, H.-y., and Ren, Y. (2020a). Community Composition of Ectomycorrhizal Fungi Associated with *Pinus Sylvestris* Var. *Mongolica* Plantations of Various Ages in the Horqin Sandy Land. *Ecol. Indicators* 110, 105860. doi:10.1016/j.ecolind.2019.105860
- Guo, M., Gao, G., Ding, G., and Zhang, Y. (2020b). Drivers of Ectomycorrhizal Fungal Community Structure Associated with *Pinus Sylvestris* Var. *Mongolica* Differ at Regional vs. Local Spatial Scales in Northern China. *Forests* 11 (3), 323. doi:10.3390/f11030323
- Han, Q., Huang, J., Long, D., Wang, X., and Liu, J. (2017). Diversity and Community Structure of Ectomycorrhizal Fungi Associated with Larix Chinensis across the alpine Treeline Ecotone of Taibai Mountain. *Mycorrhiza* 27, 487–497. doi:10.1007/s00572-017-0766-z
- Hayward, J., Horton, T. R., and Nuñez, M. A. (2015). Ectomycorrhizal fungal communities coinvading with Pinaceae host plants in Argentina: G ringos bajo el bosque. *New Phytol.* 208, 497–506. doi:10.1111/nph.13453
- Hu, Y.-L., Niu, Z.-X., Zeng, D.-H., and Wang, C.-Y. (2015). Soil Amendment Improves Tree Growth and Soil Carbon and Nitrogen Pools in Mongolian pine Plantations on post-mining Land in Northeast China. *Land Degrad. Develop.* 26, 807–812. doi:10.1002/ldr.2386
- Jany, J.-L., Martin, F., and Garbaye, J. (2003). Respiration Activity of Ectomycorrhizas from *Cenococcum Geophilum* and *Lactarius* Sp. In Relation to Soil Water Potential in Five Beech Forests. *Plant Soil* 255, 487–494. doi:10.1023/A:1026092714340

- John, M. K., and Matt, K. J. S. S. (1970). Colorimetric Determination of Phosphorus in Soil and Plant Materials with Ascorbic Acid. *Soil Sci.* 109, 214–220. doi:10.1097/00010694-197004000-00002
- Jonard, M., Fürst, A., Verstraeten, A., Thimonier, A., Timmermann, V., Potočić, N., et al. (2014). Tree mineral Nutrition Is Deteriorating in Europe. *Glob. Change Biol.* 21, 418–430. doi:10.1111/gcb.12657
- Kennedy, P. G., and Peay, K. G. (2007). Different Soil Moisture Conditions Change the Outcome of the Ectomycorrhizal Symbiosis between *Rhizopogon* Species and *Pinus Muricata*. *Plant Soil* 291, 155–165. doi:10.1007/s11104-006-9183-3
- Kjøller, R., Nilsson, L. O., Hansen, K., Schmidt, I. K., Vesterdal, L., and Gundersen, P. (2012). Dramatic Changes in Ectomycorrhizal Community Composition, Root Tip Abundance and Mycelial Production along a Stand-scale Nitrogen Deposition Gradient. *New Phytol.* 194, 278–286. doi:10.1111/j.1469-8137.2011.04041.x
- Koizumi, T., Hattori, M., and Nara, K. (2018). Ectomycorrhizal Fungal Communities in alpine Relict Forests of *Pinus Pumila* on Mt. Norikura, Japan. *Mycorrhiza* 28, 129–145. doi:10.1007/s00572-017-0817-5
- Kolaříková, Z., Kohout, P., Krüger, C., Janoušková, M., Mrnka, L., and Rydlová, J. (2017). Root-associated Fungal Communities along a Primary Succession on a Mine Spoil: Distinct Ecological Guilds Assemble Differently. *Soil Biol. Biochem.* 113, 143–152. doi:10.1016/j.soilbio.2017.06.004
- Kutszegi, G., Siller, I., Dima, B., Takács, K., Merényi, Z., Varga, T., et al. (2015). Drivers of Macrofungal Species Composition in Temperate Forests, West Hungary: Functional Groups Compared. *Fungal Ecol.* 17, 69–83. doi:10.1016/j.funeco.2015.05.009
- Lindahl, B. D., and Tunlid, A. (2014). Ectomycorrhizal Fungi - Potential Organic Matter Decomposers, yet Not Saprotrophs. *New Phytol.* 205, 1443–1447. doi:10.1111/nph.13201
- Liu, Y., Bao, G., Song, H., Cai, Q., and Sun, J. (2009). Precipitation Reconstruction from Hailar pine (*Pinus Sylvestris* Var. *Mongolica*) Tree Rings in the Hailar Region, Inner Mongolia, China Back to 1865 AD. *Palaeogeogr. Palaeoclimatol. Palaeoecol.* 282 (1–4), 81–87. doi:10.1016/j.palaeo.2009.08.012
- Liu, Z., Liu, Q., Wei, Z., Yu, X., Jia, G., and Jiang, J. (2021b). Partitioning Tree Water Usage into Storage and Transpiration in a Mixed forest. *For. Ecosyst.* 8, 72. doi:10.1186/s40663-021-00353-5
- Liu, Z., Zhang, H., Yu, X., Jia, G., and Jiang, J. (2021a). Evidence of Foliar Water Uptake in a conifer Species. *Agric. Water Manage.* 255 (2), 106993. doi:10.1016/j.agwat.2021.106993
- Mason, C. J., Edwards, M., Riby, P. G., and Coe, G. (1999). The Use of Microwaves in the Acceleration of Digestion and Colour Development in the Determination of Total Kjeldahl Nitrogen in Soil. *Analyst* 124 (11), 1719–1726. doi:10.1039/a903623g
- Mason, P. A., Wilson, J., Last, F. T., and Walker, C. (1983). The Concept of Succession in Relation to the Spread of Sheathing Mycorrhizal Fungi on Inoculated Tree Seedlings Growing in Unsterile Soils. *Plant Soil* 71, 247–256. doi:10.1007/BF02182659
- Miyamoto, Y., Sakai, A., Hattori, M., and Nara, K. (2015). Strong Effect of Climate on Ectomycorrhizal Fungal Composition: Evidence from Range Overlap between Two Mountains. *ISME J.* 9, 1870–1879. doi:10.1038/ismej.2015.8
- Mosca, E., Montecchio, L., Sella, L., and Garbaye, J. (2007). Short-term Effect of Removing Tree Competition on the Ectomycorrhizal Status of a Declining Pedunculate oak forest (*Quercus Robur* L.). *For. Ecol. Manage.* 244 (1–3), 129–140. doi:10.1016/j.foreco.2007.04.019
- Mujic, A. B., Hosaka, K., and Spatafora, J. W. (2014). *Rhizopogon Togasawariana* Sp. nov., the First Report of *Rhizopogon* Associated with an Asian Species of *Pseudotsuga*. *Mycologia* 106, 105–112. doi:10.3852/13-055
- Peay, K. G., and Matheny, P. B. (2016). *The Biogeography of Ectomycorrhizal Fungi - A History of Life in the Subterranean*. New York, NY: John Wiley & Sons Ltd, 341–361. doi:10.1002/9781118951446.ch19
- Policelli, N., Bruns, T. D., Vilgalys, R., and Nuñez, M. A. (2019). Suiloid Fungi as Global Drivers of pine Invasions. *New Phytol.* 222, 714–725. doi:10.1111/nph.15660
- Ryberg, M., Nilsson, R. H., Kristiansson, E., Töpel, M., Jacobsson, S., and Larsson, E. (2008). Mining Metadata from Unidentified ITS Sequences in Genbank: a Case Study in *Inocybe* (Basidiomycota). *BMC Evol. Biol.* 8, 50. doi:10.1186/1471-2148-8-50
- Sasse, J., Martinola, E., and Northen, T. (2018). Feed Your Friends: Do Plant Exudates Shape the Root Microbiome? *Trends Plant Sci.* 23, 25–41. doi:10.1016/j.tplants.2017.09.003
- Sebastiana, M., daSilva, A. B., Matos, A. R., Alcántara, A., Silvestre, S., and Malhó, R. (2018). Ectomycorrhizal Inoculation with *Pisolithus Tinctorius* Reduces Stress Induced by Drought in Cork Oak. *Mycorrhiza* 28, 247–258. doi:10.1007/s00572-018-0823-2
- Song, H.-H., Yan, T., and Zeng, D.-H. (2019). Establishment of Mixed Plantations of *Pinus Sylvestris* Var. *Mongolica* and *Populus* × *Xiaozhuanica* May Not Be Appropriate: Evidence from Litter Decomposition. *J. For. Res-Jap.* 12, 857–870. doi:10.1093/jpe/rtz020
- Song, L., Zhu, J., Li, M., Zhang, J., Zheng, X., and Wang, K. (2018). Canopy Transpiration of *Pinus Sylvestris* Var. *Mongolica* in a Sparse wood Grassland in the Semiarid sandy Region of Northeast China. *Agric. For. Meteorology* 250, 192–201. doi:10.1016/j.agrformet.2017.12.260
- Soudzilovskaia, N. A., Douma, J. C., Akhmetzhanova, A. A., van Bodegom, P. M., Cornwell, W. K., Moens, E. J., et al. (2015). Global Patterns of Plant Root Colonization Intensity by Mycorrhizal Fungi Explained by Climate and Soil Chemistry. *Glob. Ecol. Biogeogr.* 24, 371–382. doi:10.1111/geb.12272
- Spake, R., van der Linde, S., Newton, A. C., Suz, L. M., Bidartondo, M. I., and Doncaster, C. P. (2016). Similar Biodiversity of Ectomycorrhizal Fungi in Set-Aside Plantations and Ancient Old-Growth Broadleaved Forests. *Biol. Conservation* 194, 71–79. doi:10.1016/j.biocon.2015.12.003
- Steidinger, B. S., Bhatnagar, J. M., Vilgalys, R., Taylor, J. W., Qin, C., Zhu, K., et al. (2020). Ectomycorrhizal Fungal Diversity Predicted to Substantially Decline Due to Climate Changes in north American Pinaceae Forests. *J. Biogeogr.* 47, 772–782. doi:10.1111/jbi.13802
- Tabatabai, M. A. (1994). *Soil Enzymes*. Madison, Wisconsin: Soil Science Society of America.
- Taylor, D. L., and Bruns, T. D. (1999). Community Structure of Ectomycorrhizal Fungi in a *Pinus Muricata* forest: Minimal Overlap between the Mature forest and Resistant Propagate Communities. *Mol. Ecol.* 8, 1837–1850. doi:10.1046/j.1365-294x.1999.00773.x
- Tedersoo, L., Bahram, M., Toots, M., Diédhiou, A. G., Henkel, T. W., Kjøller, R., et al. (2012). Towards Global Patterns in the Diversity and Community Structure of Ectomycorrhizal Fungi. *Mol. Ecol.* 21, 4160–4170. doi:10.1111/j.1365-294X.2012.05602.x
- Tedersoo, L., Bahram, M., and Zobel, M. (2020). How Mycorrhizal Associations Drive Plant Population and Community Biology. *Science* 367 (6480), eaba1223. doi:10.1126/science.aba1223
- Truong, C., Gabbarini, L. A., Corrales, A., Mujic, A. B., Escobar, J. M., Moretto, A., et al. (2019). Ectomycorrhizal Fungi and Soil Enzymes Exhibit Contrasting Patterns along Elevation Gradients in Southern Patagonia. *New Phytol.* 222, 1936–1950. doi:10.1111/nph.15714
- van der Linde, S., Suz, L. M., Orme, C. D. L., Cox, F., Andreae, H., Asi, E., et al. (2018). Environment and Host as Large-Scale Controls of Ectomycorrhizal Fungi. *Nature* 558, 243–248. doi:10.1038/s41586-018-0189-9
- van Dorp, C. H., Beiler, K. J., and Durall, D. M. (2016). Dominance of a *Rhizopogon* Sister Species Corresponds to forest Age Structure. *Mycorrhiza* 26, 169–175. doi:10.1007/s00572-015-0660-5
- Walkley, A., and Black, I. A. (1934). An Examination of the Degtjareff Method for Determining Soil Organic Matter, and a Proposed Modification of the Chromic Acid Titration Method. *Soil Sci.* 37 (1), 29–38. doi:10.1097/00010694-193401000-00003
- Wang, D. D., Zhao, W., Reyila, M., Huang, K. C., Liu, S., and Cui, B. K. (2020). Diversity of Microbial Communities of *Pinus Sylvestris* Var. *Mongolica* at Spatial Scale. *Microorganisms* 10, 371. doi:10.3390/microorganisms10020371
- Wang, Y.-L., Zhang, X., Xu, Y., Babalola, B. J., Xiang, S.-M., Zhao, Y.-L., et al. (2021). Fungal Diversity and Community Assembly of Ectomycorrhizal Fungi Associated with Five pine Species in Inner mongolia, china. *Front. Microbiol.* 12, 646821. doi:10.3389/fmicb.2021.646821
- Yang, W., Zhang, D., Cai, X., Xia, L., Luo, Y., Cheng, X., et al. (2019). Significant Alterations in Soil Fungal Communities along a Chronosequence of *Spartina Alterniflora* Invasion in a Chinese Yellow Sea Coastal Wetland. *Sci. Total Environ.* 693, 133548. doi:10.1016/j.scitotenv.2019.07.354
- Yang, Y., Zhang, X., Hartley, I. P., Dungait, J. A. J., Wen, X., Li, D., et al. (2021). Contrasting Rhizosphere Soil Nutrient Economy of Plants Associated with Arbuscular Mycorrhizal and Ectomycorrhizal Fungi in Karst Forests. *Plant Soil* 470, 81–93. doi:10.1007/s11104-021-04950-9

- Zak, D. R., Pellitier, P. T., Argiroff, W., Castillo, B., James, T. Y., Nave, L. E., et al. (2019). Exploring the Role of Ectomycorrhizal Fungi in Soil Carbon Dynamics. *New Phytol.* 223, 33–39. doi:10.1111/nph.15679
- Zhang, W., Yuan, Y., Yang, S., Huang, J., and Huang, L. (2015). ITS2 Secondary Structure Improves Discrimination between Medicinal “Mu Tong” Species when Using DNA Barcoding. *PLoS ONE* 10, e0131185. doi:10.1371/journal.pone.0131185
- Zhang, Y., Cao, H., Zhao, P., Wei, X., Ding, G., Gao, G., et al. (2021). Vegetation Restoration Alters Fungal Community Composition and Functional Groups in a Desert Ecosystem. *Front. Environ. Sci.* 9, 589068. doi:10.3389/fenvs.2021.589068
- Zhao, P. s., Guo, M. s., Gao, G. l., Zhang, Y., Ding, G. d., Ren, Y., et al. (2020). Community Structure and Functional Group of Root-associated Fungi of *Pinus Sylvestris* Var. *Mongolica* across Stand Ages in the Mu Us Desert. *Ecol. Evol.* 10 (6), 3032–3042. doi:10.1002/ece3.6119
- Zhu, J., Kang, H., Tan, H., and Xu, M. (2006). Effects of Drought Stresses Induced by Polyethylene Glycol on Germination of *Pinus Sylvestris* Var. *Mongolica* Seeds from Natural and Plantation Forests on sandy Land. *J. For. Res.* 11 (5), 319–328. doi:10.1007/s10310-006-0214-y

Conflict of Interest: The authors declare that the research was conducted in the absence of any commercial or financial relationships that could be construed as a potential conflict of interest.

Publisher’s Note: All claims expressed in this article are solely those of the authors and do not necessarily represent those of their affiliated organizations or those of the publisher, the editors, and the reviewers. Any product that may be evaluated in this article or claim that may be made by its manufacturer is not guaranteed or endorsed by the publisher.

Copyright © 2022 Ren, Guo, Ding and Wang. This is an open-access article distributed under the terms of the Creative Commons Attribution License (CC BY). The use, distribution or reproduction in other forums is permitted, provided the original author(s) and the copyright owner(s) are credited and that the original publication in this journal is cited, in accordance with accepted academic practice. No use, distribution or reproduction is permitted which does not comply with these terms.



Artificial Regulation Effect of Plant Retardants on Leaf Anatomical Characteristics of *Elaeagnus Angustifolia*

Chao Zhang, Wanjiao Li[†], Yong Gao*, Zhengzheng Xu and Xiaoning Tian

College of Desert Control Science and Engineering, Inner Mongolia Agricultural University, Hohhot, China

OPEN ACCESS

Edited by:

Jifeng Deng,
Shenyang Agricultural University,
China

Reviewed by:

Zhi Dong,
Shandong Agricultural University,
China

Metin Turan,

National Eye Institute (NIH),
United States

*Correspondence:

Yong Gao
13948815709@163.com

[†]The author have contributed equally
to this work and share first authorship

Specialty section:

This article was submitted to
Drylands,
a section of the journal
Frontiers in Environmental Science

Received: 21 March 2022

Accepted: 19 April 2022

Published: 06 June 2022

Citation:

Zhang C, Li W, Gao Y, Xu Z and Tian X
(2022) Artificial Regulation Effect of
Plant Retardants on Leaf Anatomical
Characteristics of
Elaeagnus Angustifolia.
Front. Environ. Sci. 10:900960.
doi: 10.3389/fenvs.2022.900960

Aims: In order to explore the adaptation mechanisms of *Elaeagnus angustifolia* to the arid environment in desert areas under the treatment of artificial plant retardants, we used to investigate artificial regulation by using retardants of paclobutrazol (PP₃₃₃), paclobutrazol+adhesive (NPP₃₃₃), and chlormequat (CCC) based on multiple factors and multiple levels.

Methods: Orthogonal experimental design of L₉ (3⁴) was used to design the experimental treatment combinations. Leaf morphological and structural characteristics determined by the paraffin section method were used to explain the effect of different treatments and their combinations.

Results: The leaves of *Elaeagnus angustifolia* were iso-petalous with obvious stellate epidermal fuzzy borders on the upper epidermis. The palisade tissue was well developed and tightly arranged. The T1-T9 treatment significantly increased leaf thickness. Conversely, leaf length and width showed a delayed growth effect, while leaf growth developed as an elongated type after application. After plant retardant control, the upper epidermal, palisade tissue, and spongy tissue thickness of the leaves showed a significant trend to increase, at the same time, the number of xylem rows increased and the number of cells per row increased and were arranged closely. Meanwhile, there was a synergistic evolution phenomenon among the indexes. The best treatment combination of plant retardants to regulate the leaf configuration of plants was selecting the concentration of 600 mg/L of PP₃₃₃, using the root application + leaf application method for two applications.

Conclusions: The study showed that plant retardants improved the ability of plants to resist external environmental stress by reducing leaf area, increasing leaf and epidermal thickness, and promoting the development of mesophyll and vein structures in order to improve water retention capacity and prevent transitional transpiration.

Keywords: plant retardant, *Elaeagnus Angustifolia*, leaf anatomy, environmental adaptability, arid and semi-arid area

1 INTRODUCTION

Under the macro-climate of global warming, land desertification is an ecological challenge facing arid and semi-arid regions (Huang et al., 2020). The ecological environment in arid and semi-arid zones is relatively fragile and human activities have put ecological pressure on the land. Desertification threatens regional human life and economic and ecological security (D'Odorico et al., 2019). Therefore, if regional ecological restoration is to be carried out, the use of economic and ecological plant measures applied to desertification control is the primary choice, as sandy plants will be able to withstand certain wind and sand hazards and resist external influences (Su et al., 2007). However, understanding the drought-resistant mechanisms of plants is of some practical importance in combating land desertification.

At present, there have been many studies on the physiological changes of plants under drought stress and the mechanism of drought tolerance in arid and semi-arid regions (Ramachandra Reddy et al., 2004). When the growing environment changes, plants change their morphological and physiological characteristics to adapt the growing environment (Baquedano and Castillo, 2006). As a consequence, plants growing in different conditions show significant differences in photosynthesis, anatomical characteristics, and physiological characteristics (Dolatabadian et al., 2011; Khandaker et al., 2017; Leon-Sanchez et al., 2020). In arid and semi-arid regions, water deficit and high light exposure are important factors limiting plant growth (Prasad et al., 2008). At the same time, as one of the most important stresses in the environment, drought can cause a series of physiological and biochemical responses in plants.

Identification of plant morphological forms and functions is the first step in improving the resistance of vegetation to harsh growing conditions (Toscano et al., 2018). It is well known that leaves are the main organ for the transpiration and photosynthesis of plants. They have been exposed to the growing environment for a long time, with the largest area of contact with the outside environment. Compared with the branching structure aboveground, leaves are highly sensitive to environments (Xin et al., 2012; Yang et al., 2014). The microscopic anatomical tissue structure of plants, such as epidermal thickness and palisade tissue, affects the intercellular CO₂ concentration and diffusion of gases, with the results of long-term adaptation to harsh environments (He et al., 2008; Galle et al., 2010).

Elaeagnus angustifolia is distributed in arid, semi-arid, and saline areas in China with precipitation less than 150 mm (multi-year average). It is resistant to wind erosion and protects the land surface from erosion, which is usually used to build oasis protection forests in China (Huang et al., 2005; Liu et al., 2014; Yunus et al., 2005). Plant growth retardants delay longitudinal growth, increase aboveground branching structure, and reduce transpiration by reducing leaf area (Karimi et al., 2019). At present, most scholars have studied plant growth retardants to regulate leaf growth characteristics, photosynthesis, and physiological characteristics (Kasele, 1992; Zhou et al., 2019), while fewer scholars have studied the effect on leaf tissue structure. In general, changes in the cellular

organization can efficiently raise mesophyll which is mainly due to the thicker leaf caused by well-developed palisade tissue and spongy tissue. Cells have an excellent capacity to store water and adaptation to drought conditions is enhanced (Chartzoulakis et al., 2002; Gratani and Bombelli, 2000; Hameed et al., 2002). Plant retardants have low toxicity and high efficiency, which are widely used to regulate plant growth and development (Sponsel and Hedden, 2010). They mainly inhibit the division and expansion of the apical meristem of the stem, thereby regulating the distribution of nutrient growth materials to affect the water content of the leaves, the chlorophyll content of the leaves, and the growth of the plant, leaf area, and leaf anatomy (Maienfisch et al., 2001; Zhu and Stafne, 2019). Such plant retardants can alter plant height and leaf size, however, it is not clear whether they can alter the intrinsic anatomy of the leaf to make it drought-tolerant in terms of tissue structure.

This study aimed to select application methods that would modify the morphological characteristics of leaves to enable them to survive successfully in arid and semi-arid environments. In addition, we assessed the relevance of the anatomical and morphological characteristics of leaves after application. We chose *Elaeagnus angustifolia*, a model plant, to evaluate the effects of plant growth retardants regulating leaf characteristics and anatomy. The results will provide a theoretical basis for the subsequent use of *Elaeagnus angustifolia* in desert areas for ecological vegetation restoration and construction of wind and sand-fixing forests.

2 MATERIALS AND METHODS

2.1 Growth Conditions and Plant Material Preparation

The experimental area is located at the southwest edge of Ulanbuhe Desert, in Jilantai, Inner Mongolia Autonomous Region, China (39°46'59"N, 105°37'31"E) which is located in the transition from a semi-arid to an arid region. The climate is a typical temperate continental climate. The mean average precipitation is 109.9 mm, while the average annual evaporation is 2,944 mm. The soil pH is 8.49–9.19, the top soil (0–30 cm) organic matter (SOM) content is 7.15–7.59 g kg⁻¹, the top soil available phosphorus (AP) content is 2.95–4.20 mg kg⁻¹, and the top soil available potassium (AK) content is 571–618 mg kg⁻¹.

Two-year-old *Elaeagnus angustifolia* (from Jilantai local woodland) were used and transplanted in March 2019 and were spaced 1 m × 1 m in the field. Ten plants of each treatment were used as experimental plants and irrigated every 15 days to maintain plant growth. From April to May, watering took place every 10 days to ensure the survival of young plants.

2.2 Experimental Design

The *Elaeagnus angustifolia* were planted in the town of Jilantai. The experiment used an L₉ (3⁴) orthogonal test design with four factors including application method (A), application frequency (B), application type (C), and application concentration (D) with three levels of each factor, as shown in **Table 1**. The experiment

TABLE 1 | The factors and levels of orthogonal design $L_9(3^4)$.

Level	Factors			
	Application Method (A)	Application Frequency (B)	Application Type (C)	Application Concentration (D)
1	Leaf spray 250 ml (Y)	Once (1) Date: 2019.05.10	23% paclobutrazol (PP ₃₃₃)	450 mg/L
2	Irrigate the roots 250 ml (G)	Twice (2) Dates: 2019.05.10 2019.05.20	Cycocel (CCC)	600 mg/L
3	Leaf spray 125 ml and irrigate the roots 125 ml (Y&G)	Three times (3) Dates: 2019.05.10 2019.05.20 2019.06.10	17.5% paclobutrazol and agglutinant (NPP ₃₃₃)	750 mg/L

TABLE 2 | Orthogonal Test Design plan.

Test	Application Method (A)	Application Frequency (B)	Application Type (C)	Application Concentration (D)
T1	Y	1	PP ₃₃₃	450 mg/L
T2	Y	2	CCC	600 mg/L
T3	Y	3	NPP ₃₃₃	750 mg/L
T4	G	1	CCC	750 mg/L
T5	G	2	NPP ₃₃₃	450 mg/L
T6	G	3	PP ₃₃₃	600 mg/L
T7	Y&G	1	NPP ₃₃₃	600 mg/L
T8	Y&G	2	PP ₃₃₃	750 mg/L
T9	Y&G	3	CCC	450 mg/L

was designed with nine treatment combinations as shown in **Table 2** and each treatment was replicated 10 times with a total of 100 plants.

2.3 Method for the Determination of Morphological Characteristics

At the end of plant growth in September 2019, five plants from different treatment methods (T1-T9) were selected from three branches according to East, West, South and North directions. The sampling method was adopted for the random determination of morphological indicators. Ten fresh leaves were collected in each direction and the blade length and width were measured using a cursor caliper (0.01 mm).

2.4 Leaf Anatomical Structure Material Collection

Leaf anatomical measurements were obtained at the end of the experiment in September 2019. The branches selected for the test material were consistent with morphological indexes of mature leaves in the middle of the branches, and two leaves were sampled in each direction. A total of 40 leaves were sampled in each treatment, totaling 360 leaves.

2.5 Paraffin Section Production Method

Mature leaves were taken in different directions (the orthogonal test design plan T1-T9) and properly marked, in 20 ml vials containing FAA fixative (70% alcohol: formaldehyde: glacial

acetic acid = 90:5:5). The vials were pumped (inoculated) using a medical syringe during fixation, and then sealed, sorted, and transported back to the laboratory for leaf dissection tests. The samples were made by the conventional paraffin sectioning method, stained with saffron-solid green, and sealed with neutral resin glue (Galle et al., 2010). A LEICA DM2000 microscope was used to observe leaf anatomy, and LAS V4.12 was used to capture pictures of samples and determine leaf thickness, upper cuticle thickness, upper epidermal thickness, lower epidermal thickness, and fenestrated tissue thickness. The palisade and spongy ratio, tightness of leaf palisade tissue, and tightness of leaf spongy tissue were determined by the formulas below (Karimi et al., 2019).

$$\text{Palisade and spongy ratio} = \text{palisade tissue thickness} / \text{sponge tissue thickness} \quad (1)$$

$$\text{Tightness of leaf palisade tissue} = (\text{palisade tissue thickness} / \text{leaf thickness}) \times 100\% \quad (2)$$

$$\text{Tightness of leaf spongy tissue} = (\text{sponge tissue thickness} / \text{leaf thickness}) \times 100\% \quad (3)$$

2.6 Data Analysis

Data were analyzed by Excel 2010 and SAS software without considering interactions. Effect of changes in the anatomical properties of plant leaves under different treatments (**Table 4**) was determined by one-way analysis of variance (ANOVA). Tukey's HSD (honestly significant difference) test was used to analyze the differences between morphological characteristics. The data presented in the table are the mean value of three replications (mean \pm standard deviation).

TABLE 3 | Variability analysis of the growth of morphological characteristic indexes of *Elaeagnus angustifolia* leaves under different regulation methods.

Test	Relative Leaf Thickness(mm)	Relative Leaf length(mm)	Relative Leaf Width (mm)	Relative Aspect Ratio
T1	5.75 ± 3.83dc	-10.10 ± 3.61cde	-9.93 ± 1.61ed	1.01 ± 0.35a
T2	9.02 ± 1.19abc	-6.45 ± 1.23bcd	-5.99 ± 0.40bc	1.06 ± 0.57a
T3	2.39 ± 1.51d	-8.53 ± 2.73bcd	-8.76 ± 2.47cde	1.05 ± 0.45a
T4	9.40 ± 3.61abc	-4.68 ± 0.31ab	-4.91 ± 1.04ab	1.87 ± 0.15a
T5	5.88 ± 1.15dc	-2.11 ± 0.87a	-1.96 ± 0.22a	3.06 ± 0.86a
T6	9.85 ± 0.79abc	-2.81 ± 0.11a	-3.81 ± 0.32ab	1.34 ± 0.48a
T7	11.90 ± 2.47ab	-13.67 ± 2.31e	-12.34 ± 1.92e	1.14 ± 0.31a
T8	13.03 ± 2.73a	-11.77 ± 2.16ed	-11.10 ± 1.36e	1.07 ± 0.23a
T9	7.63 ± 3.16bc	-7.13 ± 1.54bc	-7.11 ± 2.16bcd	1.13 ± 0.46a

Note: All indicators in the table are the relative growth of the plants, with positive values showing positive (accelerated growth) artificially regulated effects and negative values showing negative (delayed growth) artificially regulated effects, slower than the growth of CK. Values in the table are mean ± standard deviation, different lowercase letters after the data in the same column indicate significant differences ($p < 0.05$).

The data in this study were analyzed using the relative growth of each plant indicator for comparison.

$$Mi = MXi - MYi \quad (4)$$

$$Ki = Mi - CKi \quad (5)$$

Note: Mi is the relative growth amount of the i indicator in the growth period; MXi is the measured value of the i indicator at the end of growth in September 2019 after artificially regulated treatment; MYi is the basal value of the i indicator in May 2019 before application; Ki is the growth amount of the i indicator after application relative to CK; CKi is the control group of the i indicator with the application of clear water.

3 RESULTS

3.1 Morphological Structure of *Elaeagnus Angustifolia* Leaves

The leaf morphological characteristics revealed significant differences among different treatments from T1-T9 (Table 3). The morphological structure of *Elaeagnus angustifolia* leaves changed considerably under the effect of artificial control. Different control methods (T1-T9) had a growth-promoting effect. Plant leaf thickness significantly increased ($p < 0.05$) with maximum growth under T8 treatment (13.03 μm) and the minimum under T3 treatment (2.39 μm). Leaf length growth ranged between 2.11 and 13.67 μm which was smaller compared with control, and leaf width growth ranged between 1.96 and 12.34 μm which was also smaller than control. Relative growth ratio between the leaf length and width was greater than 1, which ranged from 1.01 to 3.06 μm while the changes were not significant.

3.2 Analysis of Anatomical Structure of *Elaeagnus Angustifolia* Leaves

3.2.1 Epidermis

Elaeagnus angustifolia leaves are isobilateral which indicates that the main veins of the leaf blade are raised on the back of the leaf blade in an irregular semi-circular shape. The surface of the leaf blade

showed stellate glandular hairs (Figure 1A), which reduced the damage of strong light and control transpiration of the plant. Both the upper and lower epidermis of the *Elaeagnus angustifolia* leaves consisted of one layer of cells which were small and closely arranged. The upper epidermal cells consisted of a nearly rectangular arrangement of cells while the lower epidermal cells were nearly circular (Figures 1B,C). The upper cells were significantly larger than the lower cells. The upper epidermis showed an accelerated growth trend after each treatment and the maximum growth under T8 treatment reached 1.52 μm in thickness compared with control. The lower epidermis showed a delayed growth trend and the growth of the lower epidermal cells were lower than control (Table 4). The smallest growth was under T8 treatment.

3.2.2 Mesophyll

The leaf mesophyll of *Elaeagnus angustifolia* consists of two parts as fenestrations and spongy tissues. The fenestrations had a double-fenestrated structure and were well developed. The fenestrations were arranged on the inner side of the upper epidermis (Figure 1D). According to the cross-section of the leaf, the fenestrations of *Elaeagnus angustifolia* showed a significant increase in thickness under the nine different treatments used in this experiment ($P < 0.05$).

Table 4 shows that the upper fenestrations consisted of long cylindrical cells arranged closely together and their thickness increased from 1.35 to 4.32 μm. The thickness of the lower fenestrations increased from 0.43 to 2.48 μm indicating that the upper fenestrations were thicker than the lower fenestrations. The spongy tissues also showed a trend of thickening ranging from 0.87 to 4.43 μm while the difference was not significant ($p > 0.05$). The ratio of spongy tissue growth to fenestrated tissue decreased. The spongy tissues gradually fenestrated under T6, T8, and T9 treatment where their relative fenestrated ratio showed an increasing trend. The relative tissue firmness and laxity of the leaf showed an increasing trend and the relative firmness of the leaf tissue structure varied from 77 to 121% with no significant difference among the treatments ($p > 0.05$). Relative laxity of leaf tissue structure varied from 28 to 116% under T3 treatment which was significantly higher than other treatment groups ($p < 0.05$). The relative thickness of the upper and lower fenestrations ranked as T8

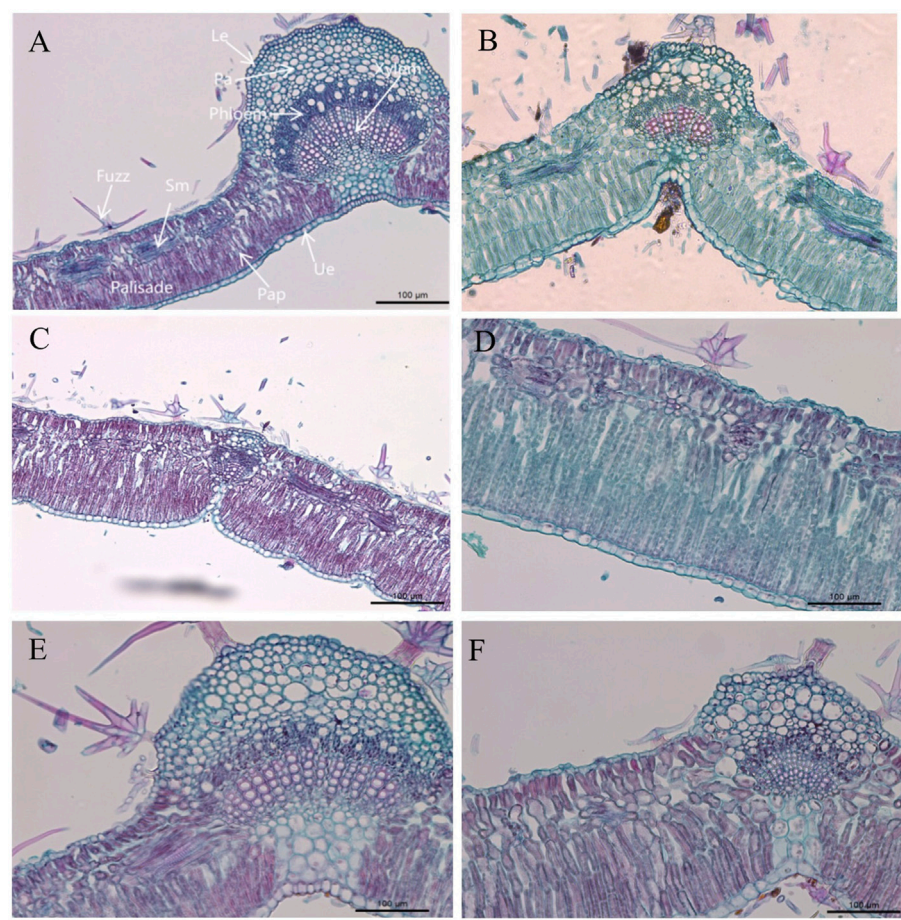


FIGURE 1 | Transverse section of a date palm leaf blade. (A–C) Leaf cross-sections of midrib 10x; (D). Cross-sections of mesophyll 20x; (E,F). Cross-sections of leaf veins 20x; (A) CK, (B) T1 treatment, (C) T5 treatment, (D) T6 treatment showing spongy tissue with obvious fenestration, (E) T8 treatment showing thin-walled tissue development, (F) T9 treatment showing vascular bundle development. Ue. upper epidermis; Le. lower epidermis; Pap. palisade tissue; Sm. spongy tissue.

TABLE 4 | Analysis of variability in the growth of anatomical structural indicators of *Elaeagnus angustifolia* leaves under different regulation methods.

Test	Relative Upper Epidermal Thickness (Um)	Relative Lower Epidermal Thickness (um)	Relative Lower Palisade Cell Thickness (um)	Relative upper Palisade Cell Thickness (um)	Relative Spongy mesophyll Thickness (um)	Palisade Cell and Spongy Cell ratio	Tightness of Leaf Palisade Tissue (%)	Tightness of Leaf Spongy Tissue (%)
T1	0.57 ± 0.04bc	−0.60 ± 0.16ab	0.71 ± 0.27dc	1.35 ± 0.74bc	1.53 ± 0.85a	4.21 ± 1.47a	0.87 ± 0.24a	0.28 ± 0.14b
T2	0.75 ± 0.10bc	−0.99 ± 0.22bc	1.42 ± 0.15bc	2.79 ± 0.49abc	3.87 ± 0.56a	5.83 ± 2.69a	0.90 ± 0.25a	0.30 ± 0.02b
T3	0.38 ± 0.09c	−0.31 ± 0.17a	0.43 ± 0.08d	2.06 ± 1.06c	0.87 ± 0.40a	2.23 ± 1.81a	0.77 ± 0.26a	1.16 ± 0.11a
T4	0.86 ± 0.02bc	−1.13 ± 0.43bc	1.65 ± 0.26bc	3.27 ± 0.39abc	2.56 ± 0.52a	3.36 ± 1.60a	1.11 ± 0.34a	0.41 ± 0.09b
T5	0.40 ± 0.05c	−0.58 ± 0.39ab	0.68 ± 0.19dc	2.57 ± 1.29bc	2.32 ± 0.28a	2.54 ± 1.64a	0.95 ± 0.33a	0.45 ± 0.07b
T6	1.06 ± 0.02ab	−1.25 ± 0.48dc	1.98 ± 0.32bc	3.54 ± 0.18abc	2.06 ± 0.28a	2.67 ± 0.17a	0.97 ± 0.16a	0.36 ± 0.04b
T7	1.16 ± 0.27ab	−1.41 ± 0.58dc	2.04 ± 0.39ab	4.01 ± 0.51ab	2.17 ± 1.10a	3.43 ± 1.88a	0.94 ± 0.29a	0.38 ± 0.06b
T8	1.52 ± 0.23a	−1.84 ± 0.05d	2.87 ± 1.91a	4.32 ± 1.85a	4.43 ± 1.29a	3.69 ± 0.88a	1.21 ± 0.45a	0.37 ± 0.14b
T9	0.60 ± 0.11b	−0.93 ± 0.18abc	1.40 ± 0.18bc	2.89 ± 0.47abc	3.52 ± 0.64a	2.88 ± 0.53a	1.21 ± 0.55a	0.41 ± 0.11b

Note: Values in the table are mean ± standard deviation, different lowercase letters after the data in the same column indicate significant differences (p < 0.05).

TABLE 5 | Orthogonal test analysis of artificially regulated growth of leaf conformation indicators of *Elaeagnus angustifolia*.

Index	k value	September 2019: End of Growth			
		A	B	C	D
Upper epidermis	k1	0.570	0.860	1.050	0.520
	k2	0.770	0.890	0.740	0.990
	k3	1.100	0.680	0.650	0.920
	Range	0.530	0.21	0.40	0.470
	Factor primary → secondary		A D C B		
	Optimum combination		A ₃ B ₂ C ₁ D ₂		
Lower epidermis	k1	−0.632	−1.049	−1.235	−0.704
	k2	−0.989	−1.136	−1.018	−1.220
	k3	−1.396	−0.833	−0.765	−1.094
	Range	−0.764	−0.303	−0.47	−1.094
	Factor primary → secondary		B C A D		
	Optimum combination		A ₃ B ₂ C ₁ D ₂		
Upper palisade tissue	k1	4.005	6.999	7.942	5.268
	k2	6.726	7.765	7.132	7.614
	k3	9.202	5.168	4.859	7.051
	Range	5.197	2.597	3.083	2.346
	Factor primary → secondary		A C B D		
	Optimum combination		A ₃ B ₂ C ₁ D ₂		
Lower palisade tissue	k1	0.853	1.467	1.853	0.927
	k2	1.427	1.657	1.477	1.823
	k3	2.110	1.267	1.060	1.640
	Range	1.257	0.390	0.793	0.896
	Factor primary → secondary		A D C B		
	Optimum combination		A ₃ B ₂ C ₁ D ₂		
Spongy tissue	k1	2.064	2.879	3.073	2.163
	k2	3.02	3.117	2.977	3.443
	k3	3.737	2.825	2.772	3.215
	Range	1.673	0.292	0.301	1.280
	Factor primary → secondary		A D C B		
	Optimum combination		A ₃ B ₂ C ₁ D ₂		
Leaf thickness	k1	5.831	9.125	9.654	6.527
	k2	8.375	9.312	8.684	10.259
	k3	10.853	6.623	6.721	8.273
	Range	5.022	2.689	2.933	3.732
	Factor primary → secondary		A D C B		
	Optimum combination		A ₃ B ₂ C ₁ D ₂		

> T7 > T6 > T4 > T2 > T9 > T1 > T3 > T5. The relative thickness of the spongy tissues ranked as T2 > T8 > T9 > T4 > T5 > T6 > T7 > T1 > T3 which was slightly different from the fenestrations. This showed that drought resistance of *Elaeagnus angustifolia* was improved by plant retardant regulation in terms of leaf mesophyll tissue structure.

3.2.3 Veins

The main veins of leaves were well developed with rounded and prominent structures which consisted of vascular bundles and mechanical tissue. The xylem was composed of 2–8 layers and 9–25 rows of the vessel and the caliber of which increased radially from the upper epidermis to the lower epidermis. The thick-horned tissue and thin-walled cells were well developed under each mode of regulation and showed a good sparing and supporting effect (Figure 1E and Figure 1F).

The k values (Table 5) indicated the strength of the influence under each treatment at different levels on the traits and the best combination was determined according to k1, k2, and k3. The

extreme difference characterized the primary and secondary relationship between the influence of the factors on the measured traits, and the larger the extreme difference R, the greater the influence of the factor on the traits. As can be seen from Table 5, the effects of four treatments on the upper epidermal thickness, lower fenestrated tissue thickness, spongy tissue thickness, and leaf thickness of *Elaeagnus angustifolia* ranked as A > D > C > B, therefore, application method > application concentration > application type > application frequency. In conclusion, all the anatomical structures of *Elaeagnus angustifolia* leaves were positively regulated after artificial control and the optimal combination for the regulation of *Elaeagnus angustifolia* leaf was A₃B₂C₁D₂, (A root application + leaf application B application of two times C PP333 D 600 mg/L).

4 DISCUSSION

As shown in Figure 2, the average temperature in the trial area was high during the plant growth period (March to October).

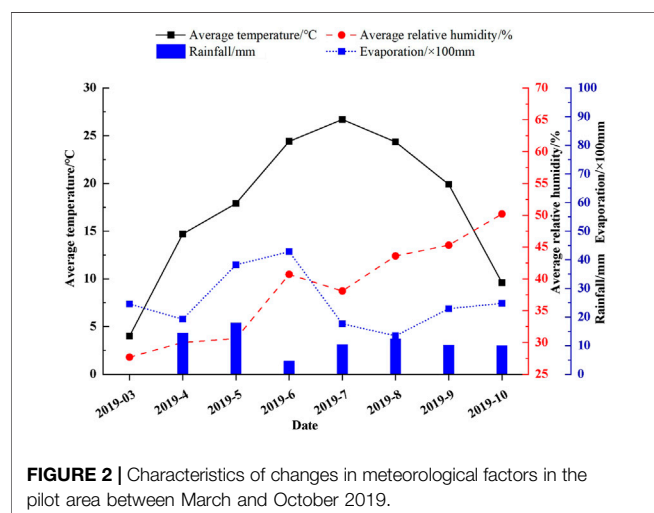


FIGURE 2 | Characteristics of changes in meteorological factors in the pilot area between March and October 2019.

Rainfall was extremely low, but evaporation was high. This makes it difficult for the plants to maintain normal growth. So, applying plant retardants by slowing down the growth rate of the leaves and increasing their transpiration rate is an effective way to increase the growth rate of plants in drought conditions. The leaf is an important organ for plant respiration, photosynthesis, absorption, and secretion, and its morphological characteristics can give feedback on the effect of the ability to adapt to a complex environment (Singh et al., 2005). Photosynthesis is the basis for the synthesis of organic matter and energy storage in plants. It is a decisive factor in the productivity of plants. The leaf is the main organ of photosynthesis and the anatomical structure of the leaf is closely related to the photosynthetic efficiency of the plant. Some studies have shown that photosynthetic rate and leaf epidermal cell thickness, and leaf thickness are positively correlated. On the other hand, the thicker the leaf palisade tissue, the more beneficial the light energy capture. At the same time, it can effectively increase the photosynthetic rate of the leaves (Yang et al., 2017). For example, the thickness of *Nitraria tangutorum* thinned significantly with increasing drought, epidermal and palisade tissue became smaller and more closely packed, and abundant areas of spongy tissue turned into palisade tissue. The leaf size of

Dryas octopetala var. *asiatica* (Nakai) Nakai is increased by air temperature (Zhou et al., 2019). Furthermore, the anatomical structure of the plant leaf is extremely sensitive to changes in external environmental factors and adapts to the growing environment by adjusting its tissue structure to increase photosynthetic rate, reduce transpiration rate, and enhance water storage capacity. Leaf thickness affects the absorption of light by plants, and leaf thickness increase the light energy utilization and water storage capacity of leaves while preventing excessive transpiration and facilitating photosynthesis. The result showed that leaf thickness in desert areas can characterize water use efficiency and the thicker the leaf thickness, the stronger the water use efficiency. The results of this study showed that the application of plant retardant had a thickening effect on plant leaf thickness (compared with the control) which may be caused by other factors, such as our research area located in a high-temperature and low-rainfall area. All these factors may have an effect on the relatively large number of epidermal cells on the leaf surface and further reduce water transpiration to improve plant water storage performance. The results of the present study also demonstrated that the relative leaf length growth and relative leaf width growth of leaves showed inhibition under different regulation methods. The relative leaf length to width ratio increased which indicated that the shape of the plant leaf was long and narrow after the regulation.

Epidermal cells have good water retention and storage properties which help to enhance plant water regulation and prevent excessive water transpiration, thereby resisting external environmental stress (Wyka et al., 2019). The study in this paper showed that the increase in thickness of the upper epidermal cells of the leaves was growth-promoting (positive growth compared to the control) while the increase in the thickness of the lower epidermal cells delayed growth (negative growth compared to the control). Palisade tissues affect the absorption and use of light energy by plants, and well-developed, closely arranged palisade tissues can effectively alleviate the damage to plant leaves from stresses such as strong light and water deficit. The relatively reduced spongy tissue and palisade tissue ratio improves the efficiency of CO_2 conduction from the lower stomatal chamber to the photosynthesis site, while alleviating the phenomenon of reduced CO_2 conduction rate due to changes in leaf flesh tissues

TABLE 6 | Changes in the photosynthetic characteristics of *Elaeagnus angustifolia* Under different regulation methods.

Test	Pn	Gs	Ci	Tr
	$\mu\text{molCO}_2\cdot\text{m}^{-2}\cdot\text{s}^{-1}$	$\mu\text{mol}\cdot\text{m}^{-2}\cdot\text{s}^{-1}$	$\mu\text{mol/mol}$	$\text{g}\cdot\text{dm}^{-2}\cdot\text{h}^{-1}$
CK	$0.22 \pm 0.22\text{f}$	$0.02 \pm 0.02\text{e}$	$0.68 \pm 0.68\text{d}$	$4.64 \pm 4.64\text{e}$
T1	$0.61 \pm 0.61\text{def}$	$0.08 \pm 0.08\text{b}$	$2.86 \pm 2.86\text{b}$	$12.06 \pm 12.06\text{de}$
T2	$0.41 \pm 0.41\text{ef}$	$0.04 \pm 0.04\text{de}$	$1.18 \pm 1.18\text{d}$	$33.00 \pm 33.00\text{b}$
T3	$2.47 \pm 2.47\text{a}$	$0.13 \pm 0.13\text{a}$	$2.54 \pm 2.54\text{bc}$	$53.76 \pm 53.76\text{a}$
T4	$1.05 \pm 1.05\text{bc}$	$0.04 \pm 0.04\text{d}$	$1.50 \pm 1.50\text{cd}$	$20.87 \pm 20.87\text{cd}$
T5	$0.95 \pm 0.95\text{cd}$	$0.04 \pm 0.04\text{d}$	$3.41 \pm 3.41\text{b}$	$27.70 \pm 27.70\text{bc}$
T6	$0.75 \pm 0.75\text{cde}$	$0.06 \pm 0.06\text{bcd}$	$4.94 \pm 4.94\text{a}$	$12.05 \pm 12.05\text{de}$
T7	$0.55 \pm 0.55\text{def}$	$0.06 \pm 0.06\text{bcd}$	$3.74 \pm 3.74\text{ab}$	$6.12 \pm 6.12\text{e}$
T8	$1.41 \pm 1.41\text{b}$	$0.07 \pm 0.07\text{bc}$	$3.84 \pm 3.84\text{ab}$	$12.94 \pm 12.94\text{de}$
T9	$0.86 \pm 0.86\text{cd}$	$0.05 \pm 0.05\text{cd}$	$1.48 \pm 1.48\text{cd}$	$11.60 \pm 11.60\text{de}$

Note: Values in the table are mean \pm standard deviation, different lowercase letters after the data in the same column indicate significant differences ($p < 0.05$).

(Azoz, S. N. et al., 2020), enabling plants to achieve a high conduction rate. The improvement of photosynthesis can make plants adapt to arid environment. The well-developed thick-horn tissue and duct in the main vein can store water and also have protective function. At the same time, developed guard cells can improve the transpiration rate of plants and promote the transport of water by plants (Zaky, I. F. et al., 2019). In this study, several characteristics of the transverse anatomical structure of *Elaeagnus angustifolia* leaves (e.g., thickness of palisade tissue, the thickness of spongy tissue, compactness, laxity, etc.) increased under the treatments of nine plant retardants. The cell volume of palisade tissue was reduced and the number of layers increased while vascular tissue was well developed.

As can be seen from Table 6, photosynthesis in *Elaeagnus angustifolia* leaves was significantly improved by the application of plant retardants. This is consistent with the researchers' conclusion that by altering leaf size, leaf anatomy can improve the photosynthetic capacity of plants.

5 CONCLUSION

In summary, plant retardant treatments T1 to T9 at the early stage of growth affected the morphological structure of plant leaves. These changes reduced transpiration and improved photosynthesis through reducing leaf area and increasing leaf thickness, among which T7 treatment (A root application + leaf application B one application C PP333 + adhesive D 600 mg/L) had the best effect. At the same time, it can changed the surface of the leaf blade, in which T8 treatment (A root application + B leaf application with two applications of C PP333 + 600 mg/L) had the best effect. The optimal combination of leaf regulation was

A₃B₂C₁D₂ (600 mg/L of PP₃₃₃, using the root application + leaf application method twice).

DATA AVAILABILITY STATEMENT

The original contributions presented in the study are included in the article/Supplementary Material, further inquiries can be directed to the corresponding author.

AUTHOR CONTRIBUTIONS

YG, conceptualization: WL and CZ, methodology: ZX and XT, software: CZ, formal analysis and data curation: WL, CZ, and ZX, writing, reviewing, and editing: WL and CZ. All authors have read and agreed to the published version of the manuscript.

FUNDING

This study was funded by the Inner Mongolia Autonomous Region Science and Technology Program (2021GG0073).

ACKNOWLEDGMENTS

We would like to thank Wiley S. Kollar and Yingmei Ma for revising this manuscript.

REFERENCES

- Baquesano, F. J., and Castillo, F. J. (2006). Comparative Ecophysiological Effects of Drought on Seedlings of the Mediterranean Water-Saver *Pinus halepensis* and Water-Spenders *Quercus coccifera* and *Quercus ilex*. *Trees* 20 (6), 689–700. doi:10.1007/s00468-006-0084-0
- Chartzoulakis, K., Patakas, A., Kofidis, G., Bosabalidis, A., and Nastou, A. (2002). Water Stress Affects Leaf Anatomy, Gas Exchange, Water Relations and Growth of Two Avocado Cultivars. *Sci. Hortic.* 95 (1-2), 39–50. doi:10.1016/s0304-4238(02)00016-x
- D'Odorico, P., Rosa, L., Bhattachan, A., and Okin, G. S. (2019). "Desertification and Land Degradation," in *Dryland Ecohydrology*. Editors P. D'Odorico, A. Porporato, and C. Wilkinson Runyan (Cham: Springer International Publishing), 573–602.
- Dolatabadian, A., Sanavy, S. A. M., and Ghanati, F. (2011). Effect of Salinity on Growth, Xylem Structure and Anatomical Characteristics of Soybean. *Not. Sci. Biol.* 3 (1), 41–45. doi:10.15835/nsb315627
- Galle, A., Esper, J., Feller, U., Ribas-Carbo, M., and Fonti, P. (2010). Responses of Wood Anatomy and Carbon Isotope Composition of *Quercus pubescens* Saplings Subjected to Two Consecutive Years of Summer Drought. *Ann. For. Sci.* 67 (8), 1–8. doi:10.1051/forest/2010045
- Gratani, L., and Bombelli, A. (2000). Leaf Anatomy, Inclination, and Gas Exchange Relationships in Evergreen Sclerophyllous and Drought Semideciduous Shrub Species. *Photosynthetica* 37 (4), 573–585. doi:10.1023/A:1007171525298
- Hameed, M., Mansoor, U., Ashraf, M., and Rao, A.-U.-R. (2002). Variation in Leaf Anatomy in Wheat Germplasm from Varying Drought-Hit Habitats. *Int. J. Agric. Biol.* 4, 12–16.
- He, C.-X., Li, J.-Y., Zhou, P., Guo, M., and Zheng, Q.-S. (2008). Changes of Leaf Morphological, Anatomical Structure and Carbon Isotope Ratio with the Height of the Wangtian Tree (*Parashorea chinensis*) in Xishuangbanna, China. *J. Integr. Plant Biol.* 50 (2), 168–173. doi:10.1111/j.1744-7909.2007.00620.x
- Huang, J., MaimaitijiangYang, C., and Wang, C. (2005). Present Situation and Prospect about the Study of *Elaeagnus angustifolia* L. *Chin. Wild Plant Resour.* 2005, 26–28+33
- Huang, J., Zhang, G., Zhang, Y., Guan, X., Wei, Y., and Guo, R. (2020). Global Desertification Vulnerability to Climate Change and Human Activities. *Land Degrad. Dev.* 31 (11), 1380–1391. doi:10.1002/ldr.3556
- Karimi, M., Ahmadi, A., Hashemi, J., Abbasi, A., Tavarini, S., Pompeiano, A., et al. (2019). Plant Growth Retardants (PGRs) Affect Growth and Secondary Metabolite Biosynthesis in *Stevia rebaudiana* Bertoni under Drought Stress. *South Afr. J. Bot.* 121, 394–401. doi:10.1016/j.sajb.2018.11.028
- Kasele, I. N. (1992). *Growth Retardants Promote Drought Resistance in Corn (Zea mays L.)*. Colorado: Colorado State University.
- Khandaker, M., Awang, I., and Ismail, S. Z. (2017). Effects of Naphthalene Acetic Acid and Gibberellic Acid on Plant Physiological Characteristics of Wax Apple (Var. Jambu Madu). *Bulg. J. Agric. Sci.* 23, 396–404.
- Leon-Sanchez, L., Nicolas, E., Prieto, I., Nortes, P., Maestre, F. T., and Ignacio Querejeta, J. (2020). Altered Leaf Elemental Composition with Climate Change Is Linked to Reductions in Photosynthesis, Growth and Survival in a Semi-arid Shrubland. *J. Ecol.* 108 (1), 47–60. doi:10.1111/1365-2745.13259
- Liu, Z., Zhang, H., Sheng, Y., Yang, X., and Di, W. (2014). Effects of NaCl Stress on Growth and Photosynthetic Characteristics of *Elaeagnus angustifolia* Seedlings. *Sci. Silvae Sin.* 50 (1), 32–40. doi:10.11707/j.1001-7488.20140106
- Maiefisch, P., Huerlimann, H., Rindlisbacher, A., Gsell, L., Dettwiler, H., Haettenschwiler, J., et al. (2001). The Discovery of Thiamethoxam: a

- Second-Generation Neonicotinoid. *Pest. Manag. Sci.* 57 (2), 165–176. doi:10.1002/1526-4998(200102)57:2<165::aid-ps289>3.0.co;2-g
- Prasad, P. V. V., Staggenborg, S. A., and Ristic, Z. (2008). *Impacts of Drought And/ or Heat Stress on Physiological, Developmental, Growth, and Yield Processes of Crop Plants*. Response of Crops to Limited Water, 301–355.
- Reddy, A. R., Chaitanya, K. V., and Vivekanandan, M. (2004). Drought-induced Responses of Photosynthesis and Antioxidant Metabolism in Higher Plants. *J. Plant Physiology* 161 (11), 1189–1202. doi:10.1016/j.jplph.2004.01.013
- Singh, S. P., Bargali, K., Joshi, A., and Chaudhry, S. (2005). Nitrogen Resorption in Leaves of Tree and Shrub Seedlings in Response to Increasing Soil Fertility. *Curr. Sci.* 89 (2), 389–396. doi:10.1073/pnas.0505226102
- Sponsel, V. M., and Hedden, P. (2010). *Gibberellin Biosynthesis and inactivation*|| Davies P J. *Plant Hormones*. Dordrecht: Springer, 63–94. doi:10.1007/978-1-4020-2686-7_4
- Su, Y. Z., Zhao, W. Z., Su, P. X., Zhang, Z. H., Wang, T., and Ram, R. (2007). Ecological Effects of Desertification Control and Desertified Land Reclamation in an Oasis-Desert Ecotone in an Arid Region: A Case Study in Hexi Corridor, Northwest China. *Ecol. Eng.* 29 (2), 117–124. doi:10.1016/j.ecoleng.2005.10.015
- Toscano, S., Ferrante, A., Tribulato, A., and Romano, D. (2018). Leaf Physiological and Anatomical Responses of Lantana and Ligustrum Species under Different Water Availability. *Plant Physiology Biochem.* 127, 380–392. doi:10.1016/j.plaphy.2018.04.008
- Wyka, T. P., Bagniewska-Zadworna, A., Kuczynska, A., Mikolajczak, K., Ogradowicz, P., Zytowski, M., et al. (2019). Drought-induced Anatomical Modifications of Barley (*Hordeum Vulgare* L.) Leaves: An Allometric Perspective. *Environ. Exp. Bot.* 166, 103798. doi:10.1016/j.envexpbot.2019.103798
- Xin, C., Zhang, H., and Zhang, Z. (2012). Morphological, Anatomical, Photosynthetic and Physiological Responses of Sorbus Amabilis Seedlings under Different Shade Environments. *J. Northeast For. Univ.* 40, 24–27+33. doi:10.13759/j.cnki.dlxb.2012.10.025
- Yang, S.-J., Sun, M., Zhang, Y.-J., Cochard, H., and Cao, K.-F. (2014). Strong Leaf Morphological, Anatomical, and Physiological Responses of a Subtropical Woody Bamboo (*Sinarundinaria Nitida*) to Contrasting Light Environments. *Plant Ecol.* 215 (1), 97–109. doi:10.1007/s11258-013-0281-z
- Yang, W. L., Zhou, W. Q., and Sun, J. F. (2017). Effects of PP₃₃₃ and Exogenous ABA on Leaf Tissue Structure of *Armeniaca vulgaris* 'Luntaibaixing' [J]. *Agric. Sci. Technol.* 18 (12), 2241–2245. doi:10.16175/j.cnki.1009-4229.2017.12.011
- Yunus, Q., Xiu-Xia, L. I., Yang, L. I., and Jiuguang, G. (2005). Effects of Salt Stress on Membrane Lipid Peroxidation and Protective Enzymes in Leaves of *Elaeagnus Angustifolia* L. *Arid Zone Res.* 2005 (4), 87–91. doi:10.13866/j.azr.2005.04.016
- Zhou, Y., Deng, J., Tai, Z., Jiang, L., Han, J., Meng, G., et al. (2019). Leaf Anatomy, Morphology and Photosynthesis of Three Tundra Shrubs after 7-Year Experimental Warming on Changbai Mountain. *Plants (Basel)* 8 (8), 271. doi:10.3390/plants8080271
- Zhu, H., and Stafne, E. T. (2019). Influence of Paclobutrazol on Shoot Growth and Flowering in a High-Density Pecan Orchard Hort Technology. *Am. Soc. Hortic. Sci.* 29 (2), 201–202. doi:10.21273/HORTTECH04241-18

Conflict of Interest: The authors declare that the research was conducted in the absence of any commercial or financial relationships that could be construed as a potential conflict of interest.

Publisher's Note: All claims expressed in this article are solely those of the authors and do not necessarily represent those of their affiliated organizations, or those of the publisher, the editors and the reviewers. Any product that may be evaluated in this article, or claim that may be made by its manufacturer, is not guaranteed or endorsed by the publisher.

Copyright © 2022 Zhang, Li, Gao, Xu and Tian. This is an open-access article distributed under the terms of the Creative Commons Attribution License (CC BY). The use, distribution or reproduction in other forums is permitted, provided the original author(s) and the copyright owner(s) are credited and that the original publication in this journal is cited, in accordance with accepted academic practice. No use, distribution or reproduction is permitted which does not comply with these terms.



The Optimum Calcium Concentration for Seedling Growth of Mongolian Pine (*Pinus Sylvestris* Var. *Mongolica*) Under Different Soil Types in Northern Semi-Arid Areas of China

Hui Li^{1,2}, Xiangjun Li^{1,2}, Guangqi Zhang^{1,2}, Xiaohang Weng^{1,2}, Shenglan Huang^{1,2}, Yongbin Zhou³, Songzhu Zhang^{1,2}, Liying Liu^{1,2} and Jiubo Pei^{4*}

¹College of Forestry, Shenyang Agricultural University, Shenyang, China, ²Research Station of Liaohe-River Plain Forest Ecosystem, Chinese Forest Ecosystem Research Network (CFERN), Shenyang Agricultural University, Changtu, China, ³Institute of Modern Agricultural Research, Dalian University, Dalian, China, ⁴College of Land and Environment, Shenyang Agricultural University, Shenyang, China

OPEN ACCESS

Edited by:

Guang-Lei GAO,
Beijing Forestry University, China

Reviewed by:

Cao Hongyu,
Beijing Forestry University, China
Jiying Sun,
Inner Mongolia Agricultural University,
China

*Correspondence:

Jiubo Pei
peijiubo@syau.edu.cn

Specialty section:

This article was submitted to
Drylands,
a section of the journal
Frontiers in Environmental Science

Received: 19 April 2022

Accepted: 20 May 2022

Published: 16 June 2022

Citation:

Li H, Li X, Zhang G, Weng X, Huang S, Zhou Y, Zhang S, Liu L and Pei J (2022) The Optimum Calcium Concentration for Seedling Growth of Mongolian Pine (*Pinus Sylvestris* Var. *Mongolica*) Under Different Soil Types in Northern Semi-Arid Areas of China. *Front. Environ. Sci.* 10:923543. doi: 10.3389/fenvs.2022.923543

Mongolian pine, as one of the major tree species of the Three-North Shelterbelt Project in the northern semiarid region of China, is very important for ensuring ecological and environmental security. Ca, as an imperative mineral element for plant development and a second messenger, partakes in photosynthesis and affects the growth of plants. However, the optimal calcium concentration for its growth in different soil types is still unclear. In this study, fifteen treatments with combinations of three different soils (e.g., sandy soil, cinnamon soil, dark brown soil) and five calcium concentration gradients (e.g., 0, 100, 200, 400, and 800 mg·kg⁻¹) were conducted to investigate this effect by measuring the indices of growth, biomass, photosynthetic pigment, gas exchange rate, photosynthates, chlorophyll fluorescence parameters and water use efficiency (WUE) based on a pot experiment. The results showed that the optimal calcium concentration of Mongolian pine seedlings in sandy soil and cinnamon soil was 0–100 mg·kg⁻¹, and the optimal calcium concentration of Mongolian pine seedlings in dark brown soil was 100–200 mg·kg⁻¹. In other words, the results showed that there was an optimal calcium concentration for the growth of Mongolian pine seedlings, and the optimal calcium concentration was different under different soil types. And if the calcium concentration in the soil was too high, it would have an inhibitory effect on Mongolian pine seedlings, low calcium concentration maybe don't work. The addition of an appropriate amount of exogenous calcium could promote the growth of Mongolian pine seedlings in different soil types. The plant height, basal diameter and biomass of Mongolian pine seedlings all increased significantly after applying an appropriate amount of calcium ($p < 0.05$); the addition of an appropriate amount of exogenous calcium could promote the photosynthetic characteristics of Mongolian pine seedlings in different soil types. Under sandy soil and cinnamon soil, the peaks for Pn, Gs, Tr, accumulation of soluble sugar and starch of Mongolian pine seedlings occurred at 0–100 mg·kg⁻¹, and the decreasing trend of the Fv/Fm value was significant in the case of exceeding 200 mg·kg⁻¹ ($p < 0.05$), indicating that the growth of Mongolian pine seedlings was affected when calcium concentrations higher than 200 mg·kg⁻¹ were applied. Moreover, under

dark brown soil, the peaks for Pn, Gs, Tr, and accumulation of soluble sugar and starch of Mongolian pine seedlings occurred at 100–200 mg·kg⁻¹; similarly, the growth of Mongolian pine seedlings was affected when calcium concentrations higher than 200 mg·kg⁻¹ were applied. Compared with the treatment without calcium, after applying an appropriate amount of exogenous calcium, the water use efficiency of Mongolian pine seedlings in different soil types was significantly improved, though it was significantly reduced at 800 mg·kg⁻¹ ($p < 0.05$).

Keywords: calcium, semi-arid regions, soil types, biomass, photosynthetic characteristics, mongolian pine seedlings, chlorophyll fluorescence, water use efficiency

1 INTRODUCTION

The semiarid region has a dry climate, scarce precipitation, uneven distribution and an extremely fragile ecological environment that is very sensitive to human activities and global climate change (Zhang et al., 2020). Artificial forest plays a great role in preventing wind, fixing sand and conserving water and soil in this area. However, under such drought environmental stress, the problems of biological instability and environmental sensitivity and vulnerability of existing plantations are prominent. This can mostly be seen in the inability to resist abnormal environments, vulnerability to fungi and pest attacks, and susceptibility to soil fertility decline (Wang et al., 2021; Wu, 2021), factors that seriously restrict the development and sustainable management of plantations. Ca is an essential nutrient element for plant growth. The main functions of calcium in plant physiology include promoting cell elongation and division, stabilizing cell wall and cell membrane, balancing yin and yang ions, participating in signal transduction as a second messenger, affecting the absorption and utilization of other nutrient elements, participating in multiple physiological metabolic processes in plants, enhancing the ability of plants to resist stress, and playing an important role in protecting and promoting plant growth (Li, 2020; Mulaudzi et al., 2020; Liu, 2021). Therefore, calcium application can be used as a means to alleviate the decline of plantation, so as to realize the healthy development of plantations in semi-arid areas and promote the coordinated development of resources and environment in this area.

Having an appropriate calcium concentration can make plants grow better (Liu et al., 2013; Xu et al., 2013; Muhammad et al., 2015; Aras et al., 2021; Mazumder et al., 2021; Muhammad, 2021). The results showed that spraying calcium on leaves could improve the tolerance of Maize and Sugar Beet to drought stress (Naeem et al., 2018; Hosseini et al., 2019). By measuring the effects of calcium on the growth, photosynthesis and antioxidant response of *Zoysia japonica*, it showed that the application of appropriate calcium concentration improved the drought tolerance of *Zoysia japonica* to a certain extent (Xu et al., 2017). However, In general, Ca-deficiency symptoms in most plants manifest as rot or necrosis at the extremities, the leaf tips or fruits. These symptoms are thought to be due to the important role Ca plays in membrane integrity and in cell wall strengthening (Simon, 1978). For example, when the plant is short of calcium, the normal physiological activities of ginseng roots, stems and

leaves will be disturbed, resulting in the weakening of its resistance to adversity (Yang, 2015). Excessive Ca content may also lead to Ca toxicity. Excessive Ca in plant cells can form precipitation with phosphate, which will inhibit seed germination, interfere with photosynthesis and reduce plant growth rate (Li et al., 2021).

Mongolian pine (*Pinus sylvestris* var. *Mongolica*) is a pioneer tree species in the construction of wind prevention and sand control of the Three-North Shelterbelt. The introduction sites of Mongolian pine are divided according to soil types and mainly include zonal soils such as dark brown soil, brown soil, black soil, chernozem, cinnamon soil, sandy soil, red soil and nonzonal soils such as albic soil, meadow soil and saline alkali soil. Mongolian pine does not have strict requirements for soil. Whether it is the dark brown soil in the fertile Northeast Plain and mountains or geologically barren desert sand dunes in the northwest plain, Mongolian pine can grow normally. Nevertheless, in recent years, Mongolian pine trees in the Three-North Shelterbelt have declined earlier than those of the same age at other sites. Their decline is manifested as early capping, a shortened growth period, inhibition of normal physiological activities, reduced growth, serious pests and diseases, etc. Moreover, the land type with the decline in *Pinus sylvestris* in the Three-North Shelterbelt was mostly sandy soil, while the decline in *Pinus sylvestris* in other land types was not obvious (Zhu et al., 2003; Zhang et al., 2020). In response to the decline of Mongolian pine in semi-arid areas, many researchers put forward the reasons for the decline of Mongolian pine in sandy land from the aspects of climate, nutrients and water, diseases and pests, soil enzyme activity and so on (Yu, 2019; Li et al., 2020; Cao, 2021; Li, 2022). However, there are few studies on how calcium affects the decline of *Pinus sylvestris* var. *mongolica* and the optimal calcium concentration. This study is based on the fact that the absorption of calcium by plants varies according to soil type. After 2 years of planting young avocado trees, their dry weights of shoots and roots were significantly higher in the SL and S soils than in C soil (Bonomelli et al., 2019). Therefore, this study measured and analyzed the effects of exogenous calcium on the growth and photosynthetic characteristics of Mongolian pine seedlings under different soil types in this area, and discussed whether there was the best calcium concentration suitable for the growth of Mongolian pine seedlings. This study will provide a theoretical basis for systematically improving the decline of Mongolian pine seedlings under zonal soil and realizing better management of Mongolian pine forests in the future.

2 MATERIALS AND METHODS

2.1 Cultivation of Mongolian Pine Seedlings

This experiment was carried out at the Beishan experimental station of Shenyang Agricultural University. Three-year-old seedlings of Mongolian pine with uniform growth were selected as tested materials (the average plant height was 22.5 cm, and the average basal diameter was 7.1 mm). They were colonized on 15 June 2018. Different soils were screened to remove stones and impurities, and 3 kg of experimental soil (air-dried soil weight) was accurately weighed and mixed with 2 kg of quartz sand (60 mesh) as pot experimental soil. The substrates used were first mixed thoroughly and then washed with dilute hydrochloric acid before filling the pots to remove the possible Ca^{2+} . The pH of the soil-sand mixture after washing with hydrochloric acid was 6.3. The volume of each pot was 11.36 l, with a lower diameter of 19.4 cm, an upper diameter of 24.3 cm and a height of 26.5 cm (Zhu et al., 2005). One Mongolian pine seedling was colonized in each experimental pot. Plastic trays were set under the basin to prevent water loss. After half a month of recovery, calcium treatment was carried out on July 1, 2018, and the nutrient solution was changed every 7 days until the seedlings were collected on June 17, 2019. The nutrient solution was prepared with ultrapure water according to Xie's (2014) sand culture nutrient solution formula, and the pH value of the nutrient solution was adjusted to five to six with NaOH. The nutrients were 5 ml/L KNO_3 , 5 ml/L MgSO_4 , 5 ml/L KH_2PO_4 , 5 ml/L NaNO_3 and 5 ml/L EATA-Fe.

2.2 Experimental Design

In this experiment, Mongolian pine seedlings in each type of soil were divided into 5 Ca treatments, and each treatment was repeated 6 times. Three soil types: sandy soil, cinnamon soil and dark brown soil. The calcium was applied at five levels: 0, 100, 200, 400 and 800 $\text{mg}\cdot\text{kg}^{-1}$. The CaCl_2 solution was divided into several equal parts, and the soil was then irrigated to ensure a uniform distribution of CaCl_2 in the soil. The test sandy soil was taken from Tieling City, Liaoning Province (123°27'-125°06'E, 41°59'-43°23'N), the test cinnamon soil was taken from Chaoyang City, Liaoning Province (122°25'-123°48'E, 41°12'-42°17'N), and the test dark brown soil was taken from the Daxinganling region (121°12'-127°00'E, 50°10'-53°33'N). This region is located in the semiarid region of China and has an annual average temperature of 5.5–8.4°C and an annual average precipitation of approximately 400 mm. Soil samples between 0–40 cm soil depth were randomly collected from multiple points based on a standard site and then transported to the base of the university. The basic properties of organic matter content, total calcium and water-soluble calcium of mixed sandy soil samples were 5.51%, 1040 $\text{mg}\cdot\text{kg}^{-1}$ and 30 $\text{mg}\cdot\text{kg}^{-1}$, respectively. The basic properties of organic matter content, total calcium and water-soluble calcium of mixed cinnamon soil samples were 8.14%, 1980 $\text{mg}\cdot\text{kg}^{-1}$ and 60 $\text{mg}\cdot\text{kg}^{-1}$, respectively. The basic properties of organic matter content, total calcium and water-soluble calcium of mixed dark brown soil samples were 31.89%, 3580 $\text{mg}\cdot\text{kg}^{-1}$ and 80 $\text{mg}\cdot\text{kg}^{-1}$, respectively.

2.3 Determination of the Growth Indices of Mongolian Pine Seedlings

2.3.1 Growth of Mongolian pine seedlings

The basic plant heights and diameters were measured after planting in June 2018, and the plant heights and diameters of Mongolian pine seedlings were measured again when the seedlings were collected in June 2019. The plant heights were measured with a tape, accurate to 0.10 cm; the basal diameters were measured with a Vernier caliper, accurate to 0.01 mm.

2.3.2 Biomass of Mongolian pine seedlings

After the whole plant was completely removed from the pot, the seedlings with whole roots were carefully washed to remove the substrate. Subsequently, the whole plants were divided into roots, stems and leaves with pruning shears and were placed into envelopes for labelling. The envelopes were then placed in an oven at 105°C for 30 min and dried to a constant weight at 65°C. The dry weights of the roots, stems, leaves and total plant biomass were determined with an analytical balance.

2.4 Determination of the Photosynthetic Characteristics and Water Use Efficiency of Mongolian Pine Seedlings

2.4.1 Gas exchange rates

The net photosynthetic rate (P_n), transpiration rate (T_r) and stomatal conductance (G_s) values of the plants were measured with a LI-COR 6400 system (LI-COR Inc, Lincoln, NE, United States) between 10:00 and 12:00 on each sampling day. The effective light intensity was set at 1000 $\mu\text{mol}\cdot\text{m}^{-2}\cdot\text{s}^{-1}$ and repeated 3 times for each treatment for each soil type.

2.4.2 Photosynthesis

To measure the soluble sugar content, oven-dried samples (50 mg) were macerated in 80% ethanol, and after centrifugation, the supernatant was reacted with anthrone reagent following the method of Shields and Burnett (1960). Calculation was performed from the standard curve of glucose. For starch analysis, 0.5 ml of starch extract and 4.5 ml of distilled water were added to a test tube. The test tube was placed into an ice bath, and then 10 ml of anthrone reagent was slowly added into the test tube. The tubes were placed in a boiling water bath for exactly 7.5 min before being immediately cooled in an ice bath. After cooling, the absorbance at 630 nm in 1 h using a UV-8000 spectrophotometer (Yuanxi, Beijing, China) was measured (Doan et al., 2019).

2.4.3 Chlorophyll fluorescence

To examine the influence of calcium on the minimal fluorescence F_0 , the maximum fluorescence F_m , the variable fluorescence F_v , and the maximal photochemical efficiency of photosynthesis system II, $F_v/F_m = (F_m - F_0)/F_m$, were measured by using a portable pulse modulated chlorophyll fluorescence metre (OS-5P+, United States) between 16:00 and 18:00 on each sampling

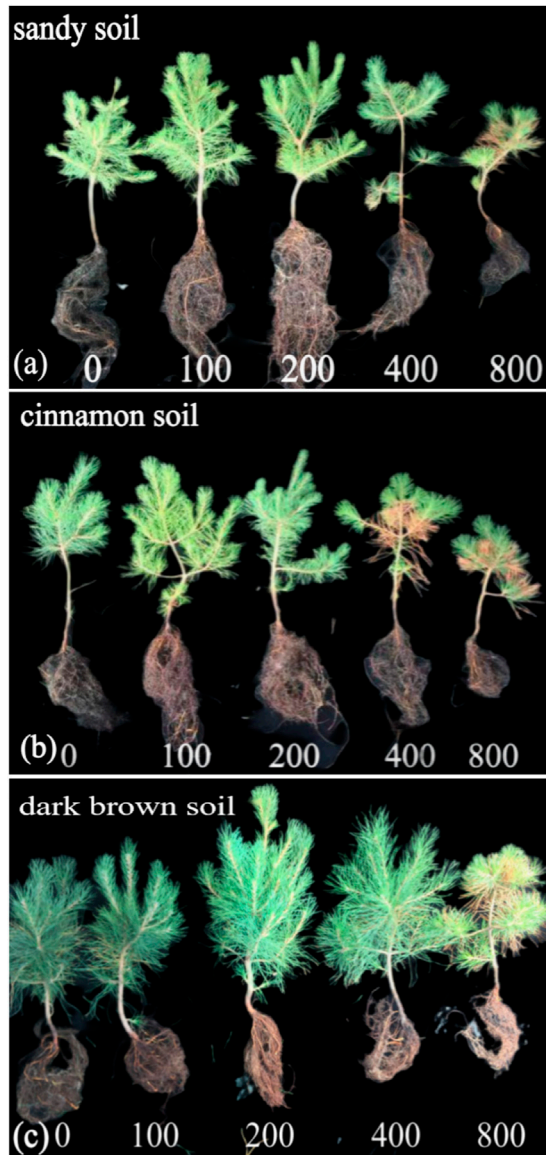


FIGURE 1 | Effects of exogenous calcium on the growth status of Mongolian pine seedlings in different soil types.

day. Before the measurements, the leaves were dark-adapted for 20 min by using light-exclusion clips.

2.4.4 Water use efficiency

The washed plant leaves were put in an oven at 105°C for 30 min, dried at 80°C for 2 h to a constant weight, and then ground through a 100-mesh sieve with a ball mill (Retsch200, Germany). Approximately 0.7 mg of each sample was taken, which was tightly wrapped with a tin boat, and 13°C was then measured using a stable isotope mass spectrometer (DELTA V Advantage Isotope Ratio Mass Spectrometer). Then, the long-term water use efficiency value (WUEL) was calculated from 13°C and used to characterize the overall water use efficiency (WUE) of the Mongolian pine seedlings.

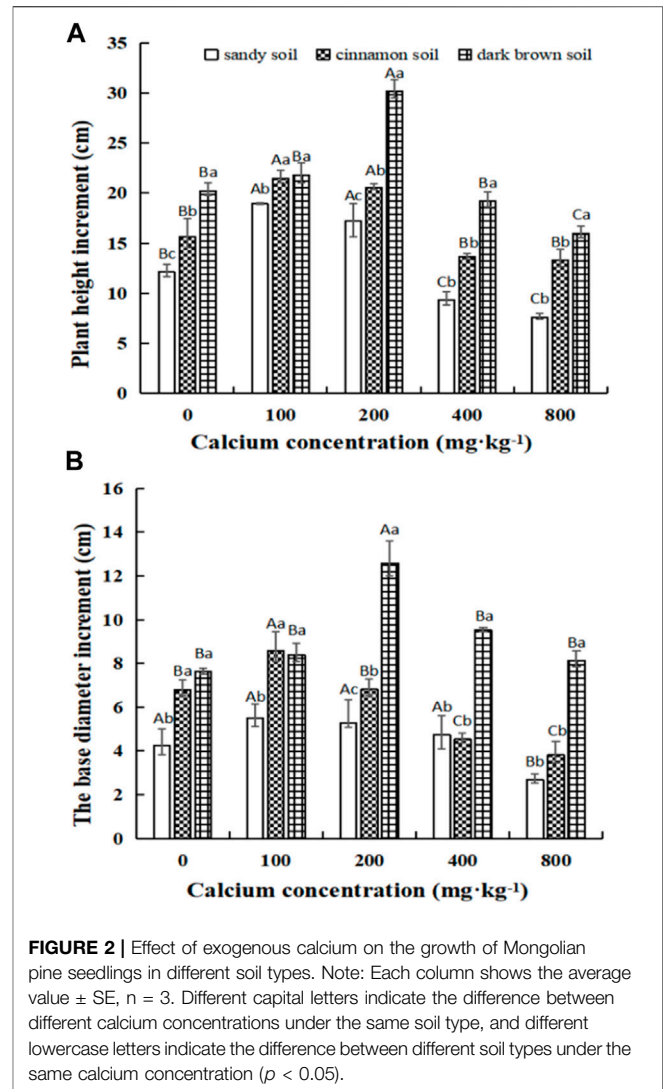


FIGURE 2 | Effect of exogenous calcium on the growth of Mongolian pine seedlings in different soil types. Note: Each column shows the average value \pm SE, $n = 3$. Different capital letters indicate the difference between different calcium concentrations under the same soil type, and different lowercase letters indicate the difference between different soil types under the same calcium concentration ($p < 0.05$).

2.6 Statistical Analysis

All results are expressed as the mean \pm standard error (SE) of three replications. The effects of different calcium treatments on the growth and physiological characteristics of Mongolian pine seedlings were analysed by one-way ANOVA and Duncan's new multiple extreme difference method. Different capital letters indicate the difference between different calcium concentrations under the same soil type, and different lowercase letters indicate the difference between different soil types under the same calcium concentration. The software packages SPSS 19.0 (IBM, Chicago, United States) and Excel 2019 were used to conduct the statistical analyses and to draw charts.

3 RESULTS

3.1 Growth Status of Mongolian Pine Seedlings

The growth status of the Mongolian pine seedlings in different soil types is shown in **Figure 1a–c**. For sandy soil and cinnamon

TABLE 1 | Effects of exogenous calcium on the biomass of Mongolian pine seedlings in different soil types.

Soil Type	Calcium Treatment (mg·kg ⁻¹)	Root Biomass (g)	Longest Root (cm)	Stem Biomass (g)	Leaf Biomass (g)	Total Biomass (g)
Sandy soil	0	26.91 ± 0.03Ab	67.65 ± 0.03Aa	17.867 ± 0.06Cc	24.904 ± 0.03Cb	69.681 ± 0.12Cc
	100	26.845 ± 0.07Ac	50.74 ± 0.03Cb	23.745 ± 0.09Ab	31.14 ± 0.32Ac	81.73 ± 0.16Ac
	200	23.015 ± 0.02Bc	53.59 ± 0.25Bb	23.218 ± 0.01Bb	28.975 ± 0.08Bc	75.208 ± 0.11Bc
	400	18.498 ± 0.01Cb	43.3 ± 0.02Dc	13.618 ± 0.04Db	13.264 ± 0.05Db	45.38 ± 0.08Db
	800	9.666 ± 0.01Dc	42.8 ± 0.64Db	8.561 ± 0.04Ec	9.267 ± 0.24Ec	27.494 ± 0.20Ec
Cinnamon soil	0	29.123 ± 0.08Ba	42.81 ± 0.04Db	22.359 ± 0.06Ba	24.653 ± 0.23Cb	76.1351 ± 0.21Cb
	100	27.809 ± 0.18Cb	37.62 ± 0.02Ec	23.769 ± 0.01Ab	40.455 ± 0.04Ab	92.033 ± 0.16Ab
	200	30.7 ± 0.06Ab	71.15 ± 0.08Aa	20.077 ± 0.01Cc	39.979 ± 0.11Bb	90.756 ± 0.17Bb
	400	16.839 ± 0.01Dc	47.3 ± 0.09Bb	9.058 ± 0.06Ec	10.817 ± 0.09Ec	36.714 ± 0.04Dc
	800	15.522 ± 0.03 Eb	46.21 ± 0.05Ca	10.007 ± 0.06Db	11.454 ± 0.11Db	36.983 ± 0.15Db
Dark brown soil	0	25.94 ± 0.05Cc	40.52 ± 0.10Dc	20.448 ± 0.08Db	46.363 ± 0.04Da	92.751 ± 0.02Da
	100	34.561 ± 0.11Ba	75.92 ± 0.15Aa	28.498 ± 0.01Ba	53.103 ± 0.11Ca	116.162 ± 0.21Ba
	200	44.958 ± 0.08Aa	44.61 ± 0.14Cc	48.287 ± 0.07Aa	72.82 ± 0.08Aa	166.065 ± 0.23Aa
	400	24.585 ± 0.02Da	67.2 ± 0.03Ba	25.846 ± 0.04Ca	63.567 ± 0.07Ba	113.998 ± 0.09Ca
	800	19.391 ± 0.12Ea	31.51 ± 0.18Ec	13.384 ± 0.07Ea	31.67 ± 0.05Ea	64.445 ± 0.00Ea

Each column shows the average value ± SE, n = 3. Different capital letters indicate the difference between different calcium concentrations under the same soil type, and different lowercase letters indicate the difference between different soil types under the same calcium concentration ($p < 0.05$).

soil, the growth status was good at 0–100 mg·kg⁻¹, while for dark brown soil, the growth status of the Mongolian pine seedlings was good at 100–200 mg·kg⁻¹. When the calcium concentration was not appropriate in the different soil types, Mongolian pine seedlings grew poorly or even died.

3.2 Growth and Biomass of Mongolian Pine Seedlings

In general, the growth indicators (plant height and basal diameter) of Mongolian pine seedlings of different soil types increased first and then decreased with increasing calcium concentration (Figure 2A,B). Calcium had different effects on the organs and total biomass of Mongolian pine seedlings in different soil types (Table 1).

The peaks for the average plant height increment and the average basal diameter increment of sandy soil and cinnamon soil occurred at 100 mg·kg⁻¹, while the peaks for the average plant height increment and the average basal diameter increment of dark brown soil occurred at 200 mg·kg⁻¹ (Figure 2).

Regarding the biomass of Mongolian pine seedlings (Table 1), the influence of calcium on the stems, leaves and total biomass of the three soils was consistent. The peaks for sandy soil and cinnamon soil occurred at 100 mg·kg⁻¹, and the peak for dark brown soil occurred at 200 mg·kg⁻¹. Subsequently, the downwards trends for the stem, leaf and total biomass of the three soils were shown with the increase in calcium concentration ($p < 0.05$). The three lowest values of stem, leaf and total biomass in sandy soil and dark brown soil occurred at 800 mg·kg⁻¹, while the three lowest values of stem, leaf and total biomass in cinnamon soil occurred at 400 mg·kg⁻¹. The peaks for root biomass in cinnamon soil and dark brown soil occurred at 200 mg·kg⁻¹, while the peak in sandy soil occurred at 0–100 mg·kg⁻¹, and the three lowest values for the three soils occurred at 800 mg·kg⁻¹. The peak for the longest root biomass in sandy soil occurred at 0, that in cinnamon soil was at 200 mg·kg⁻¹, and that in dark brown soil was at 100 mg·kg⁻¹, while the three lowest values also appeared at different calcium gradients.

3.3 Gas Exchange Rates of Mongolian Pine Seedlings

In general, the gas exchange rates (Pn, Gs, Tr) showed a trend of first increasing and then decreasing with increasing calcium concentration in different soil types (Figure 3A–C).

First, the peaks for the gas exchange rates (Pn, Gs, Tr) of sandy soil all occurred at 100 mg·kg⁻¹, which were 12.55 μmol·m⁻²·s⁻¹, 0.12 molH₂O·m⁻²·s⁻¹, and 2.74 mmolH₂O·m⁻²·s⁻¹ and were 89.01%, 50.01% and 168.62% higher, respectively, than when external calcium was not applied ($p < 0.05$); the peak (17.21 μmol·m⁻²·s⁻¹) for the Pn of cinnamon soil occurred at 100 mg·kg⁻¹, which was 72.44% higher than that without external calcium ($p < 0.05$). Nevertheless, the peaks for the Gs and Tr of cinnamon soil occurred at 200 mg·kg⁻¹, which were 0.23 molH₂O·m⁻²·s⁻¹ and 8.01 mmolH₂O·m⁻²·s⁻¹ and were 187.5% and 125.63% higher, respectively, than when external calcium was not applied ($p < 0.05$); dark brown soil was similar to cinnamon soil, and the peak (22.71 μmol·m⁻²·s⁻¹) for the Pn occurred at 100 mg·kg⁻¹. The peaks for Gs and Tr occurred at 200 mg·kg⁻¹, which were 0.28 molH₂O·m⁻²·s⁻¹ and 8.59 mmolH₂O·m⁻²·s⁻¹ and were 154.54% and 112.1% higher, respectively, than those without exogenous calcium ($p < 0.05$).

In addition, the downwards trends of Pn, Gs and Tr of sandy soil were shown in the case of reaching and exceeding 100 mg·kg⁻¹, and the downwards trends of Pn, Gs and Tr of cinnamon soil and dark brown soil were shown in the case of reaching and exceeding 200 mg·kg⁻¹.

3.4 Photosynthesis of Mongolian Pine Seedlings

In general, the photosynthates (soluble sugar, starch) showed a trend of first increasing and then decreasing with increasing calcium concentration in different soil types (Figure 4A,B).

First, the peaks for the soluble sugar and starch contents of sandy soil occurred at 100 mg·kg⁻¹, which were 55.65 μg/g and

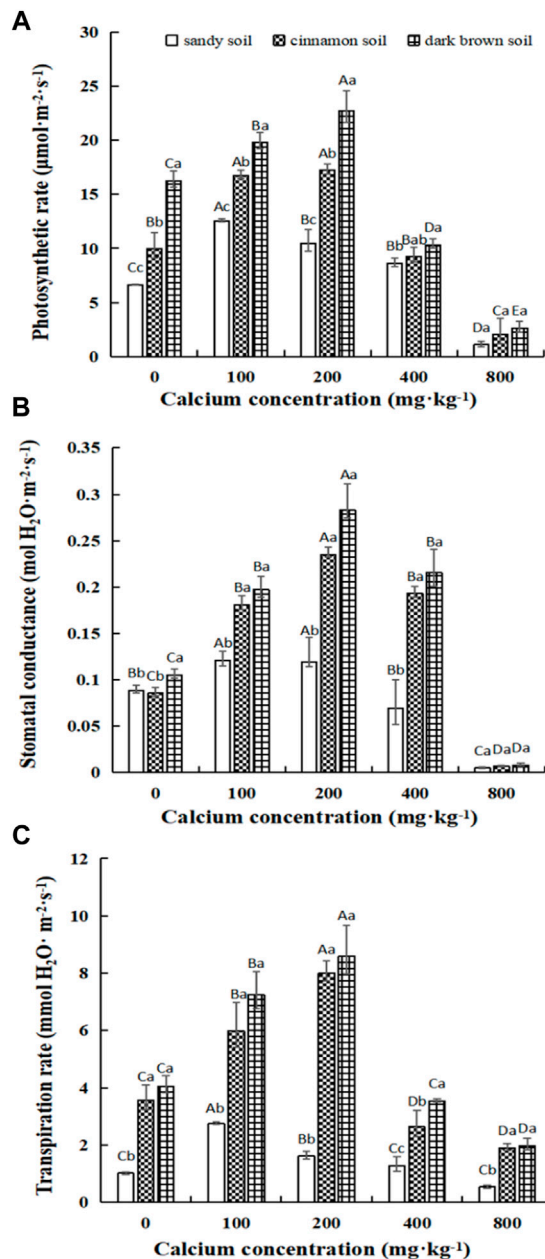


FIGURE 3 | Effects of exogenous calcium on gas exchange rates of Mongolian pine seedlings in different soil types. Note: Each column shows the average value \pm SE, $n = 3$. Different capital letters indicate the difference between different calcium concentrations under the same soil type, and different lowercase letters indicate the difference between different soil types under the same calcium concentration ($p < 0.05$).

7.35 $\mu\text{g/g}$ and were 4.51% and 35.35% higher, respectively, than those without external calcium. Cinnamon soil is similar to sandy soil. The peaks for the soluble sugar content and starch content of cinnamon soil occurred at 100 $\text{mg}\cdot\text{kg}^{-1}$, which were 52.39 $\mu\text{g/g}$ and 8.37 $\mu\text{g/g}$ and were 55.18% and 33.92% higher, respectively, than those without exogenous calcium. Unexpectedly, the peaks for the soluble sugar content and starch content of dark brown

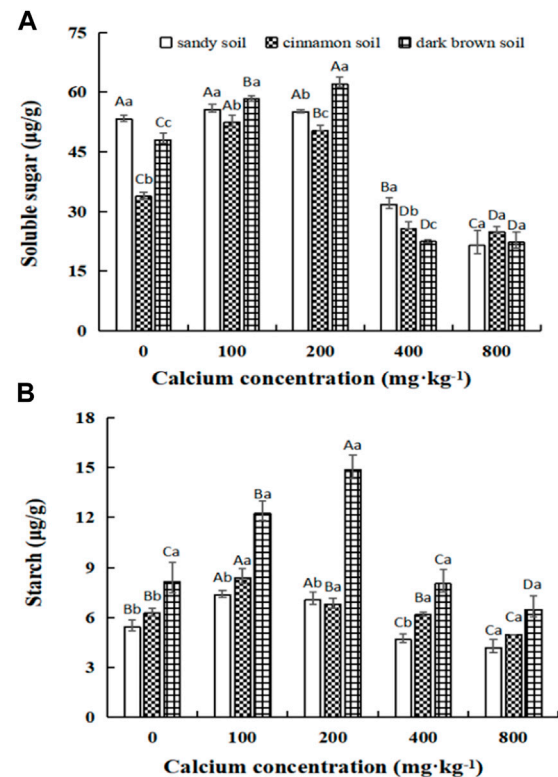


FIGURE 4 | Effect of exogenous calcium on photosynthates of Mongolian pine seedlings in different soil types. Note: Each column shows the average value \pm SE, $n = 3$. Different capital letters indicate the difference between different calcium concentrations under the same soil type, and different lowercase letters indicate the difference between different soil types under the same calcium concentration ($p < 0.05$).

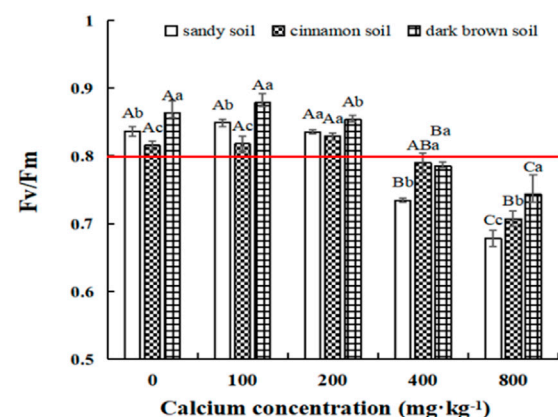


FIGURE 5 | Effects of exogenous calcium on chlorophyll fluorescence of Mongolian pine seedlings in different soil types. Note: Each column shows the average value \pm SE, $n = 3$. Different capital letters indicate the difference between different calcium concentrations under the same soil type, and different lowercase letters indicate the difference between different soil types under the same calcium concentration ($p < 0.05$).

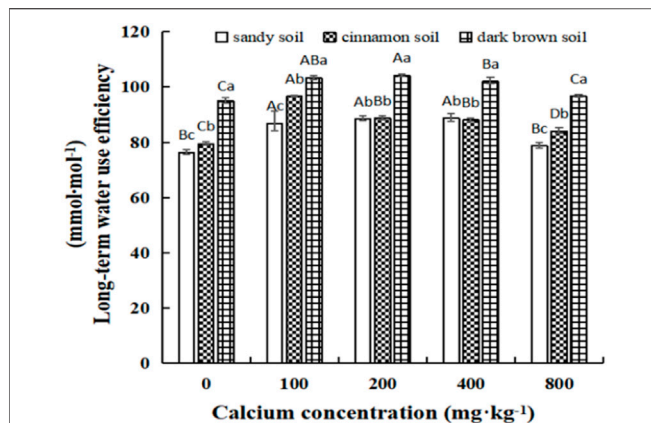


FIGURE 6 | Effects of exogenous calcium on the long-term water use efficiency of Mongolian pine seedlings in different soil types. Note: Each column shows the average value \pm SE, $n = 3$. Different capital letters indicate the difference between different calcium concentrations under the same soil type, and different lowercase letters indicate the difference between different soil types under the same calcium concentration ($p < 0.05$).

soil occurred at 200 mg·kg⁻¹, which were 62.09 μ g/g and 14.86 μ g/g and were 29.3% and 82.33% higher, respectively, than those without exogenous calcium.

In addition, under sandy soil and cinnamon soil, the downwards trends of the soluble sugar content were shown in the case of reaching and exceeding 400 mg·kg⁻¹, and the downwards trends of the starch content were shown in the case of reaching and exceeding 200 mg·kg⁻¹; under dark brown soil, the downwards trends of the soluble sugar content and starch content were shown in the case of reaching and exceeding 400 mg·kg⁻¹.

3.5 Chlorophyll Fluorescence of Mongolian Pine Seedlings

In general, the Fv/Fm values showed a decreasing trend with increasing calcium concentration in the different soil types (Figure 5).

First, the Fv/Fm values of sandy soil, cinnamon soil and dark brown soil were close to those of exogenous calcium at 0, 100 and 200 mg·kg⁻¹, and the changes were relatively gradual. Second, for the three soils, when the exogenous calcium content was greater than or equal to 400 mg·kg⁻¹, the Fv/Fm values were all lower than 0.8, indicating that the seedling growth of Mongolian pine was in a stressed state. The differences were that the Fv/Fm values of sandy soil were reduced by 12.04% and 19.27% at 400 and 800 mg·kg⁻¹, respectively, compared with no exogenous calcium and showed significant differences ($p < 0.05$). The Fv/Fm value of cinnamon soil was reduced by 13.58% at 800 mg·kg⁻¹ compared with no exogenous calcium and showed a significant difference ($p < 0.05$). The Fv/Fm values of dark brown soil were reduced by 10.46% and 13.95% at 400 and 800 mg·kg⁻¹, respectively, compared with no exogenous calcium and showed significant differences ($p < 0.05$).

3.6 Water Use Efficiency of Mongolian Pine Seedlings

In general, the long-term water use efficiency (WUEL) showed a trend of first increasing and then decreasing with increasing calcium concentration in the different soil types (Figure 6).

First, the peak (88.66 mmol·mol⁻¹) for the WUEL of sandy soil occurred at 400 mg·kg⁻¹, which was 16.32% higher than that without exogenous calcium ($p < 0.05$); the peak (96.56 mmol·mol⁻¹) for the WUEL of cinnamon soil occurred at 100 mg·kg⁻¹, which was 21.75% higher than that without exogenous calcium ($p < 0.05$); and the peak (104.14 mmol·mol⁻¹) for the WUEL of dark brown soil occurred at 200 mg·kg⁻¹, which was 9.75% higher than that without exogenous calcium ($p < 0.05$).

In addition, downwards trends of the WUEL of sandy soil, cinnamon soil and dark brown soil were shown in the case of reaching and exceeding 800, 200 and 400 mg·kg⁻¹, respectively.

4 DISCUSSION

4.1 An Optimal Calcium Concentration for the Growth of Mongolian Pine Seedlings

Calcium is essential not only for maintaining membrane integrity and improving cell structure, but it is also a signal for protecting plant cell walls and a second messenger for membrane stabilizers. At the same time, according to changes in the external environment, calcium can also provide timely feedback to the plants. (Singh and Pandey, 2020; Martins et al., 2021; Raina et al., 2021; Zhao et al., 2021). Our results showed that the appropriate amount of exogenous calcium promotes the plant height, base diameter and biomass of Mongolian pine seedlings in different soil types. Studies have shown that when plants are deficient in calcium, they often show the characteristics of blocked growth, short internodes, short and soft plant heights, yellow leaves, necrotic growth points, and little or no fruit (Liu et al., 2019; Hagagg et al., 2020; Aras et al., 2021). However, our results are slightly different from this, showing that the leaves of Mongolian pine seedlings are more likely to turn yellow at high calcium, while the performance of Mongolian pine seedlings is not obvious at low. Our results showed that an appropriate amount of exogenous calcium could improve the photosynthetic characteristics of Mongolian pine seedlings, and improve their adaptability to the environment. This is consistent with previous research results. Salinity radically slowed down growth of rice seedlings and Ca²⁺ noticeably improved growth performances. Exogenous application of Ca²⁺ (10 mM CaCl₂) increased the total chlorophyll content, while the 15 mM CaCl₂ sometimes showed negative effect on the aspect of mitigating effect of salinity in rice (Rani et al., 2019). It may be that when the calcium content in the external environment is too high, the excessive calcium in the plant inhibits the absorption and utilization of other elements, which causes the plant to receive calcium stress, which leads to slow growth and development (Madani et al., 2013; Peng et al., 2020; Feng et al., 2021; Wang, 2021). Foliar application of calcium reduces the effects of low night temperature (LNT) stress on the growth and photosynthetic characteristics of *Arachis hypogaea* and significantly improves its cold resistance (Wu et al., 2020). Supplementation with Ca²⁺ helps to

alleviate the effect of Cd stress on the photosynthetic light response of rice (Sebastian and Prasad, 2019). In the study of exogenous calcium on plant chlorophyll fluorescence, it has been found that supplementation with 20 or 25 mM Ca^{2+} can increase the maximum quantum yield (Fv/Fm) of PSII to greater than 0.8, thereby enhancing the freezing resistance of spinach (Min et al., 2021). A concentration of 5 mM Ca^{2+} can significantly increase the Fv/Fm value and most effectively alleviate the damage of drought stress to Tung tree seedlings (Li et al., 2017). Our results showed that applying an appropriate amount of exogenous calcium significantly increased the photosynthates of Mongolian pine seedlings. This is consistent with previous research results. Calcium can increase the activity levels of various enzymes under cadmium stress by inducing the biosynthesis of nitric oxide (NO) and hydrogen sulfide (H_2S), thereby increasing carbohydrate accumulation (Khan et al., 2020). Similarly, in terms of water use efficiency, our results were consistent with the previous research results. It was considered that exogenous calcium could significantly improve the water use efficiency of Mongolian pine seedlings (Ren et al., 2020). In summary, the seedlings of Mongolian pine in our experiment had the most suitable calcium concentration for growth. The optimal calcium concentration can promote the growth of Mongolian pine seedlings under different soil types and enable them to improve their own gas exchange rates, increase the accumulation of their own photosynthates, improve their own water use efficiency, and enhance their own drought resistance.

4.2 The Optimal Calcium Concentration Varies Among Different Soils

Our results showed that the surface of the sandy soil layer dries faster under the same temperature and light conditions, the water in the soil flows into the tray set at the bottom faster, and the water storage capacity of dark brown soil is significantly stronger than that of cinnamon soil and stronger than that of sandy soil. Although the three soil types of Mongolian pine seedlings were uniformly watered and irrigated in our experiment, due to the different soil aggregate structures of sandy soil, cinnamon soil and dark brown soil, their soil water retention capacities were also different. Studies have revealed that soil water content plays a vital role in plant growth (Reich et al., 2018; Zhou et al., 2019; Sutinen and Middleton, 2020). Studies have emphasized that the observed soil moisture conditions are responsible for the degradation of Mongolian pine (Dang et al., 2021). Therefore, the phenomenon that Mongolian pine seedlings is more prone to decline in sandy soil can be explained to a certain extent.

Our research finds that there is an optimal calcium concentration for seedling growth of Mongolian pine, the optimal calcium concentration of Mongolian pine seedlings is different under different soil types, and the optimal calcium concentration required by Mongolian pine seedlings in dark brown soil is higher than those of sandy soil and cinnamon soil. The author speculates that the occurrence of this phenomenon is related to the structural properties of the soil itself (Cristina et al., 2020; Zhao et al., 2021; Bonomelli et al., 2019); the reason may be that during the cultivation of Mongolian pine seedlings, the seedlings grown in dark brown soil show stronger water retention capacity. In the experiment, exogenous calcium was added to the soil by dissolving it in water, which caused

more calcium to be stored in the soil in the dark. This is in line with the experimental results: Mongolian pine seedlings have the longest root system in the dark brown soil environment. The root system is an important nutrient organ of the plant and plays important roles in the absorption of water and nutrients in the plant body and in improving the soil structure (Griffiths et al., 2021; Suzdaleva et al., 2021; Xiao et al., 2021; Xiao et al., 2020). The soil water retention capacity of Mongolian pine seedlings on sandy soil is weak, which results in less calcium content in the soil compared with dark brown soil. From the data point of view, its root system growth is not as developed as that of dark brown soil, and ultimately, the growth status is not as strong as that of dark brown soil. Therefore, the tests show that the optimal calcium concentration of Mongolian pine seedlings in sandy soil is lower than that in dark brown soil. Many research results are similar to our results, that is, plants need calcium within a certain concentration range, and there is an optimal calcium concentration to make plants grow better. For example, 80 mmol·L⁻¹ is the optimal calcium concentration to increase the germination rate of corn under low-temperature stress, which is conducive to the development of cold-tolerant corn varieties, and 20 mmol·L⁻¹ is an appropriate calcium concentration to increase corn yield in coal mining areas under the synergistic effect of AMF (Li et al., 2013; Zhang et al., 2020). In summary, during the cultivation of Mongolian pine seedlings in semiarid areas, according to the physical and chemical properties and structure of the soil itself, different concentrations of exogenous calcium should be applied to the soil to achieve the optimal growth effect.

5 CONCLUSION

Exogenous calcium promoted plant growth in semiarid regions. Adding an appropriate amount of exogenous calcium could enhance the plant height, basal diameter, biomass, photosynthetic characteristics, photosynthates and water use efficiency of Mongolian pine seedlings in different soil types. However, excessive exogenous calcium inhibited the growth of Mongolian pine seedlings and an insufficient concentration of exogenous calcium may not work. The results showed that there was an optimal calcium concentration for the growth of Mongolian pine seedlings, and the optimal calcium concentration was different under different soil types. The optimal calcium concentration of Mongolian pine seedlings in sandy soil and cinnamon soil was 0–100 mg·kg⁻¹, and the optimal calcium concentration of Mongolian pine seedlings in dark brown soil was 100–200 mg·kg⁻¹.

DATA AVAILABILITY STATEMENT

The raw data supporting the conclusion of this article will be made available by the authors, without undue reservation.

AUTHOR CONTRIBUTIONS

HL: Conceptualization, investigation, methodology, visual-ization, Writing—review and editing. XL: Data analysis and sorting.

testing, writing—original draft, cultivating seedlings. GZ: Cultivating seedlings, Writing—review and editing. XW, Cultivating seedlings, Writing—review and editing. SH, Cultivating seedlings, testing. YZ, Conceptualization, Methodology. SZ: Methodology. LL: Methodology. JP: Methodology, Writing—review and editing; Conceptualization.

REFERENCES

- Aras, S., Keles, H., and Bozkurt, E. (2021). Physiological and Histological Responses of Peach Plants Grafted onto Different Rootstocks under Calcium Deficiency Conditions. *Sci. Hortic.* 281, 109967–109968. doi:10.1016/j.scienta.2021.109967
- Bonomelli, C., Gil, P. M., and Schaffer, B. (2019). Effect of Soil Type on Calcium Absorption and Partitioning in Young Avocado (*Persea Americana* Mill.) Trees. *Agronomy* 9 (12), 837. doi:10.3390/agronomy9120837
- Cao, Y. L. (2021). Reasons for the Decline of *Pinus Sylvestris* Var. *Mongolica* Plantation in Zhanggutai Sandy Land and Sustainable Management Measures. *Agric. Technol.* 41 (03), 75–77. doi:10.19754/j.nyyjs.20210215023
- Cristina, G., Camelin, E., Tommasi, T., Fino, D., and Pugliese, M. (2020). Anaerobic Digestates from Sewage Sludge Used as Fertilizer on a Poor Alkaline Sandy Soil and on a Peat Substrate: Effects on Tomato Plants Growth and on Soil Properties. *J. Environ. Manag.* 269, 1–12. doi:10.1016/j.jenvman.2020.110767
- Dang, H., Han, H., Chen, S., and Li, M. (2021). A Fragile Soil Moisture Environment Exacerbates the Climate Change-Related Impacts on the Water Use by Mongolian Scots Pine (*Pinus Sylvestris* Var. *Mongolica*) in Northern China: Long-Term Observations. *Agric. Water Manag.* 251, 1–12. doi:10.1016/j.agwat.2021.106857
- Dien, D. C., Mochizuki, T., and Yamakawa, T. (2019). Effect of Various Drought Stresses and Subsequent Recovery on Proline, Total Soluble Sugar and Starch Metabolisms in Rice (*Oryza Sativa* L.) Varieties. *Plant Prod. Sci.* 22 (4), 530–545. doi:10.1080/1343943X.2019.1647787
- Feng, X. W., Huang, Y., Wu, G. L., Peng, J. Y., and Peng, Y. L. (2021). Effects of Different Calcium Concentrations on Growth and Magnesium Absorption of Flue-Cured Tobacco. *J. crops* 2021 (03), 190–194. doi:10.16035/j.issn.1001-7283.2021.03.029
- Griffiths, M., Wang, X., Dhakal, K., Guo, H., Seethepalli, A., Kang, Y., et al. (2021). Interactions Among Rooting Traits for Deep Water and Nitrogen Uptake in Upland and Lowland Ecotypes of Switchgrass (*Panicum Virgatum* L.). *J. Exp. Bot.* 73, 967–979. doi:10.1093/jxb/erab437
- Hagagg, L. F., Merwad, M. A., Shahin, M. M. F., and El-Hady, E. S. (2020). Ameliorative Effect of Foliar Application of Calcium on Vegetative Growth and Mineral Contents of Olive Trees Kalmata and Manzanillo Cultivars Irrigated with Saline Water. *Bull. Natl. Res. Cent.* 44 (1), 35–41. doi:10.1186/s42269-020-00374-0
- Hosseini, S. A., Réthoré, E., Pluchon, S., Ali, N., Billiot, B., and Yvin, J.-C. (2019). Calcium Application Enhances Drought Stress Tolerance in Sugar Beet and Promotes Plant Biomass and Beetroot Sucrose Concentration. *Ijms* 20 (15), 3777. doi:10.3390/ijms20153777
- Kamran, M., Wang, D., Xie, K., Lu, Y., Shi, C., EL Sabagh, A., et al. (2021). Pre-sowing Seed Treatment with Kinetin and Calcium Mitigates Salt Induced Inhibition of Seed Germination and Seedling Growth of Choysum (*Brassica Rapa* Var. *Parachinensis*). *Ecotoxicol. Environ. Saf.* 227, 112921. doi:10.1016/j.ecoenv.2021.112921
- Khan, M. N., Siddiqui, M. H., AlSolami, M. A., Alamri, S., Hu, Y., Ali, H. M., et al. (2020). Crosstalk of Hydrogen Sulfide and Nitric Oxide Requires Calcium to Mitigate Impaired Photosynthesis under Cadmium Stress by Activating Defense Mechanisms in *Vigna Radiata*. *Plant Physiology Biochem.* 156, 278–290. doi:10.1016/j.plaphy.2020.09.017
- Li, F., Zhang, Q., Tang, M., and Yi, Y. (2021). Effects of High Calcium Stress on Gene Expression in Roots of *Arabidopsis thaliana*. *J. Genomics Appl. Biol.* 40 (04), 1793–1800. doi:10.13417/j.gab.040.001793
- Li, M.-Y., Fang, L.-D., Duan, C.-Y., Cao, Y., Yin, H., Ning, Q.-R., et al. (2020). Greater Risk of Hydraulic Failure Due to Increased Drought Threatens Pine Plantations in Horqin Sandy Land of Northern China. *For. Ecol. Manag.* 461 (C), 117980. doi:10.1016/j.foreco.2020.117980
- Li, S. P., Bi, Y. L., Chen, P. Z., Yrryschan, Z., and Liu, S. (2013). “Effects of AMF Cooperating with Exogenous Calcium on Maize Growth and Soil Improvement,” in *Editorial Office of Transactions of the Chinese Society of Agricultural Engineering* 29 (1), 109–116.
- Li, S. U. (2022). Reasons for the Decline of *Pinus Sylvestris* Var. *Mongolica* Plantation and its Transformation Measures. *Anhui Agron. Bull.* 28 (03), 79–80. + 83. doi:10.16377/j.cnki.issn1007-7731.2022.03.040
- Li, Z.-G. (2020). Regulative Role of Calcium Signaling on Methylglyoxal-Improved Heat Tolerance in Maize (*Zea mays* L.) Seedlings. *Plant Signal. Behav.* 15 (9), 1788303. doi:10.1080/15592324.2020.1788303
- Li, Z., Tan, X. F., Lu, K., Liu, Z. M., and Wu, L. L. (2017). The Effect of CaCl_2 on Calcium Content, Photosynthesis, and Chlorophyll Fluorescence of Tung Tree Seedlings under Drought Conditions. *Photosynth.* 55 (3), 553–560. doi:10.1007/s11099-016-0676-x
- Liu, J. (2021). Research Overview of Calcium Ion on Plant Growth and Development. *J. Mod. salt Chem. Ind.* 48 (05), 137–138. + 145. doi:10.19465/j.cnki.2095-9710.2021.05.062
- Liu, Y.-f., Han, X.-r., Zhan, X.-m., Yang, J.-f., Wang, Y.-z., Song, Q.-b., et al. (2013). Regulation of Calcium on Peanut Photosynthesis under Low Night Temperature Stress. *J. Integr. Agric.* 12 (12), 2172–2178. doi:10.1016/S2095-3119(13)60411-6
- Liu, Y., Riaz, M., Yan, L., Zeng, Y., and Cuncang, J. (2019). Boron and Calcium Deficiency Disturbing the Growth of Trifoliate Rootstock Seedlings (*Poncirus Trifoliate* L.) by Changing Root Architecture and Cell Wall. *Plant Physiology Biochem.* 144, 345–354. doi:10.1016/j.plaphy.2019.10.007
- Madani, B., Mohamed, M. T. M., Awang, Y., and Kadir, J. (2013). Effect of Foliar Calcium Application on Nutrient Concentration and Morphological Characteristics of Papaya Seedlings (*Carica Papaya* L. “Eksotika Ii”). *Acta Horticulturae*, 131–137. doi:10.17660/actahortic.2013.984.12
- Martins, V., Unlubayir, M., Teixeira, A., Lanoue, A., and Gerós, H. (2021). Exogenous Calcium Delays Grape Berry Maturation in the White Cv. Loureiro while Increasing Fruit Firmness and Flavonol Content. *Front. Plant Sci.* 12, 1–10. doi:10.3389/fpls.2021.742887
- Mazumder, M. N. N., Misran, A., Ding, P., Wahab, P. E. M., and Mohamad, A. (2021). Preharvest Foliar Spray of Calcium Chloride on Growth, Yield, Quality, and Shelf Life Extension of Different Lowland Tomato Varieties in Malaysia. *Horticulturae* 7 (11), 466. doi:10.3390/HORTICULTURAE7110466
- Min, K., Liu, B., Lee, S.-R., and Arora, R. (2021). Supplemental Calcium Improves Freezing Tolerance of Spinach (*Spinacia Oleracea* L.) by Mitigating Membrane and Photosynthetic Damage, and Bolstering Anti-oxidant and Cell-Wall Status. *Sci. Hortic.* 288, 110212–12. doi:10.1016/j.scienta.2021.110212
- Muhammad, B. K., Mubshar, H., Abid, R., Shahid, F., and Khawar, J. (2015). Seed Priming with CaCl_2 and Ridge Planting for Improved Drought Resistance in Maize. *Turkish J. Agric. For.* 39, 193–203. doi:10.1007/s10457-014-9784-4
- Mulauzdi, T., Hendricks, K., Mabiya, T., Muthevhuli, M., Ajayi, R. F., Mayedwa, N., et al. (2020). Calcium Improves Germination and Growth of Sorghum Bicolor Seedlings under Salt Stress. *Plants* 9 (6), 730. doi:10.3390/plants9060730
- Naeem, M., Naeem, M. S., Ahmad, R., and Ihsan, M. Z. (2018). Foliar Calcium Spray Confers Drought Stress Tolerance in Maize via Modulation of Plant Growth, Water Relations, Proline Content and Hydrogen Peroxide Activity. *Archives Agron. Soil Sci.* 64 (1), 116–131. doi:10.1080/03650340.2017.1327713
- Peng, B., Xu, M. Z., Wang, Y., and Liu, Y. G. (2020). Effects of Calcium Stress on Growth and Stress Physiological Indexes of *Typha Latifolia*. *West. For. Sci.* 49 (04), 163–170. doi:10.16473/j.cnki.xbykx1972.2020.04.025
- Raina, M., Kumar, A., Yadav, N., Kumari, S., Yusuf, M. A., Mustafiz, A., et al. (2021). StCaM2, a Calcium Binding Protein, Alleviates Negative Effects of

- Salinity and Drought Stress in Tobacco. *Plant Mol. Biol.* 106 (1–2), 185–108. doi:10.1007/s11103-021-01131-1
- Rani, R. P., Md, T. U. A., Sadik, P. M. A., Zakir, H. M., and Afzal, H. M. (2019). Physiological Mechanisms of Exogenous Calcium on Alleviating Salinity-Induced Stress in Rice (*Oryza Sativa* L.). *Physiology Mol. Biol. plants Int. J. Funct. plant Biol.* 25 (3), 611–624. doi:10.1007/s12298-019-00654-8
- Reich, P. B., Sendall, K. M., Stefanski, A., Rich, R. L., Hobbie, S. E., and Montgomery, R. A. (2018). Effects of Climate Warming on Photosynthesis in Boreal Tree Species Depend on Soil Moisture. *Nat. Int. Wkly. J. Sci.* 562 (7726), 263–267. doi:10.1038/s41586-018-0582-4
- Ren, C. S., Li, H., Weng, X. H., Shi-fei, Y., Juan, M., Wen-ting, L., et al. (2020). Effects of Exogenous Calcium on the Growth, Photosynthetic Characteristics and Water Use Efficiency of *Fraxinus Mandshurica*. *J. Shenyang Agric. Univ.* 2020 (6). doi:10.3969/j.issn.1000-1700.2020.06.004
- Sebastian, A., and Prasad, M. N. V. (2019). Photosynthetic Light Reactions in *Oryza Sativa* L. Under Cd Stress: Influence of Iron, Calcium, and Zinc Supplements. *EuroBiotech J.* 3 (4), 175–181. doi:10.2478/ebtj-2019-0021
- Shields, R., and Burnett, W. (1960). Determination of Protein-Bound Carbohydrate in Serum by Modified Anthrone Method. *Anal. Chem.* 32 (7), 885–886. doi:10.1021/ac60163a053
- Simon, E. W. (1978). The Symptoms of Calcium Deficiency in Plants. *New Phytol.* 80, 1–15. doi:10.1111/j.1469-8137.1978.tb02259.x
- Singh, N., and Pandey, G. K. (2020). Calcium Signatures and Signal Transduction Schemes during Microbe Interactions in *Arabidopsis thaliana*. *J. Plant Biochem. Biotechnol.* 29, 675–686. doi:10.1007/s13562-020-00604-6
- Sutinen, R., and Middleton, M. (2020). Soil Water Drives Distribution of Northern Boreal Conifers *Picea Abies* and *Pinus Sylvestris*. *J. Hydrology* 588. doi:10.1016/j.jhydrol.2020.125048
- Suzdaleva, A. V., Verkhovtseva, N. V., Shein, E. V., Dembovetsky, A. V., and Abrosimov, K. N. (2021). Structure of the Soil Pore Space in the Seedling Bed before the Seedling Stage: Studies Using the Microtomography Method. *IOP Conf. Ser. Earth Environ. Sci.* 862 (1), 1–7. doi:10.1088/1755-1315/862/1/012047
- Wang, L. X., Li, C. C., Luo, Y. Q., Ren, L. L., Lv, N., Zhou, J. J., et al. (2021). Mongolian Pine Forest Decline by the Combinatory Effect of European Woodwasp and Plant Pathogenic Fungi. *Sci. Rep.* 11 (1), 19643. doi:10.1038/S41598-021-98795-Y
- Wang, W. J. (2021). *Study on the Mechanism of Calcium Inhibition in Litchi Pulp*. Hainan University.
- Wu, D., Liu, Y. F., Pang, J. Y., Yong, J. W. H., Chen, Y. L., Bai, C. M., et al. (2020). Exogenous Calcium Alleviates Nocturnal Chilling-Induced Feedback Inhibition of Photosynthesis by Improving Sink Demand in Peanut (*Arachis hypogaea*). *Front. Plant Sci.* 11, 1–14. doi:10.3389/fpls.2020.607029
- Wu, X. (2021). Reasons for the Decline of *Pinus Sylvestris* Var. *Mongolica* and its Control Techniques. *Seed Technol.* 39 (23), 115–116. doi:10.19904/j.cnki.cn14-1160/s.2021.23.053
- Xiao, L. D., Li, C., Cai, Y., Zhou, T., Zhou, M. X., Gao, X. Y., et al. (2021). Interactions between Soil Properties and the Rhizome-Root Distribution in a 12-year Moso Bamboo Reforested Region: Combining Ground-Penetrating Radar and Soil Coring in the Field. *Sci. Total Environ.* 800, 1–11. doi:10.1016/j.scitotenv.2021.149467
- Xiao, L., Yao, K. H., Li, P., Liu, Y., Chang, E. H., Zhang, Y., et al. (2020). Increased Soil Aggregate Stability Is Strongly Correlated with Root and Soil Properties along a Gradient of Secondary Succession on the Loess Plateau. *Ecol. Eng.* 143. doi:10.1016/j.ecoleng.2019.105671
- Xie, X. M. (2014). *Soil and Plant Nutrition Experiments*. Hangzhou: Zhejiang University Press.
- Xu, C. B., Li, X. M., and Zhang, L. H. (2013). The Effect of Calcium Chloride on Growth, Photosynthesis, and Antioxidant Responses of *Zoysia Japonica* under Drought Conditions. *PLoS One* 8 (7), e68214. doi:10.1371/journal.pone.0068214
- Xu, C. B., Li, X. M., and Zhang, L. H. (2017). The Effect of Calcium Chloride on Growth, Photosynthesis, and Antioxidant Responses of *Zoysia Japonica* under Drought Conditions. *J. PLoS ONE* 8 (7), e68214. doi:10.1371/journal.pone.0068214
- Yang, Z. (2015). “Effects of Calcium on the Growth and Development of Ginseng [D],” in *Chinese Academy of Agricultural Sciences*. 2015.
- Yu, D. L., Lei, Z. Y., Zhao, G. J., Zhou, Y. P., Yu, D. W., Lu, H., et al. (2019). Response of Soil Enzyme Activity to the Decline of *Pinus Sylvestris* Var. *Mongolica* Plantation in Sandy Land. *Environ. Chem.* 38 (01), 97–105. doi:10.7524/j.issn.0254-6108.2018020901
- Zhang, Q., Liu, Y. X., Yu, Q. Q., Ma, Y., Gu, W. R., and Yang, D. G. (2020). Physiological Changes Associated with Enhanced Cold Resistance during Maize (*Zea mays*) Germination and Seedling Growth in Response to Exogenous Calcium. *Crop Pasture Sci.* 71 (6), 529–538. doi:10.1071/CP19510
- Zhang, T., Song, L. N., Zhu, J. J., Wang, G. C., Li, M. C., Zheng, X., et al. (2020). Spatial Distribution of Root Systems of *Pinus Sylvestris* Var. *Mongolica* Trees with Different Ages in a Semi-arid Sandy Region of Northeast China. *For. Ecol. Manag.* 2020. doi:10.1016/J.FORECO.2020.118776
- Zhang, X. D., Li, Z. M., Siddique, K. H. M., Shayakhmetova, A., Jia, Z. K., and Han, Q. F. (2020). Increasing Maize Production and Preventing Water Deficits in Semi-arid Areas: A Study Matching Fertilization with Regional Precipitation under Mulch Planting. *Agric. Water Manag.* 2020, 241. doi:10.1016/j.agwat.2020.106347
- Zhao, C. H., Tang, Y. H., Wang, J. L., Zeng, Y. H., Sun, H. Q., Zheng, Z. C., et al. (2021). A Mis-regulated Cyclic Nucleotide-gated Channel Mediates Cytosolic Calcium Elevation and Activates Immunity in *Arabidopsis*. *New Phytol.* 230 (3), 1078–1094. doi:10.1111/nph.17218
- Zhao, T., Tang, X. C., Wang, G. L., Wan, L., Wang, X. S., and Zhang, X. X. (2021). A Study on Characteristics of Unsaturated Sandy Soils Based on the CT Scanning Method. *Chem. Technol. Fuels Oils* 57, 160–172. doi:10.1007/s10553-021-01235-w
- Zhou, H., Zhao, W. Z., He, Z. B., Yan, J. L., and Zhang, G. F. (2019). Variation in Depth of Water Uptake for *Pinus Sylvestris* Var. *Mongolica* along a Precipitation Gradient in Sandy Regions. *J. Hydrology* 577. doi:10.1016/j.jhydrol.2019.123921
- Zhu, J. J., Fan, Z. P., Zeng, D. H., Jiang, F. Q., and Takeshi, M. (2003). Comparison of Stand Structure and Growth between Artificial and Natural Forests of *Pinus Sylvestris* Var. *Mongolica* on Sandy Land. *J. For. Res.* 14 (2), 103–111. doi:10.1007/BF02856774
- Zhu, J. J., Kang, H. Z., Li, Z. H., Wang, G. C., and Zhang, R. S. (2005). Impact of Water Stress on Survival and Photosynthesis of Mongolian Pine Seedlings on Sandy Land. *Acta Ecol. Sin.* 2005 (10), 2527–2533. doi:10.3321/j.issn:1000-0933.2005.10.010

Conflict of Interest: The authors declare that the research was conducted in the absence of any commercial or financial relationships that could be construed as a potential conflict of interest.

Publisher's Note: All claims expressed in this article are solely those of the authors and do not necessarily represent those of their affiliated organizations, or those of the publisher, the editors and the reviewers. Any product that may be evaluated in this article, or claim that may be made by its manufacturer, is not guaranteed or endorsed by the publisher.

Copyright © 2022 Li, Li, Zhang, Weng, Huang, Zhou, Zhang, Liu and Pei. This is an open-access article distributed under the terms of the Creative Commons Attribution License (CC BY). The use, distribution or reproduction in other forums is permitted, provided the original author(s) and the copyright owner(s) are credited and that the original publication in this journal is cited, in accordance with accepted academic practice. No use, distribution or reproduction is permitted which does not comply with these terms.



Spatio-Temporal Evolution of Sandy Land and its Impact on Soil Wind Erosion in the Kubuqi Desert in Recent 30 Years

Xiaohong Dang^{1,2}, Ya Na^{1,3*}, Wenfeng Chi^{4,5*}, Jiangjia Zhao⁶, Yuanyuan Zhao⁶, Yue Wang^{4,5}, Xiaoguang Wu^{1,7} and Yuetian Wang^{4,5}

¹Inner Mongolia Agricultural University, Hohhot, China, ²Inner Mongolia Hangjin Desert Ecological Position Research Station, Ordos, China, ³Key Laboratory of Grassland Resources of the Ministry of Education, Key Laboratory of Forage Cultivation, Processing and High Efficient Utilization of the Ministry of Agriculture and Rural Affairs, Inner Mongolia Key Laboratory of Grassland Management and Utilization, Inner Mongolia Agricultural University, Hohhot, China, ⁴College of Resources and Environmental Economics, Inner Mongolia University of Finance and Economics, Hohhot, China, ⁵Resource Utilization and Environmental Protection Coordinated Development Academician Expert Workstation in the North of China, Inner Mongolia University of Finance and Economics, Hohhot, China, ⁶Key Laboratory of Soil and Water Conservation and Desertification Combating, Ministry of Education, School of Soil and Water Conservation, Beijing Forestry University, Beijing, China, ⁷Inner Mongolia Autonomous Region Land and Space Planning Institute, Hohhot, China

OPEN ACCESS

Edited by:

Shengbo Xie,
Northwest Institute of Eco-
Environment and Resources (CAS),
China

Reviewed by:

Bojie Wang,
Inner Mongolia University, China
Yongfang Wang,
Inner Mongolia Normal University,
China

*Correspondence:

Ya Na
naya@imau.edu.cn
Wenfeng Chi
cwf@imufe.edu.cn

Specialty section:

This article was submitted to
Drylands,
a section of the journal
Frontiers in Environmental Science

Received: 22 May 2022

Accepted: 10 June 2022

Published: 11 July 2022

Citation:

Dang X, Na Y, Chi W, Zhao J, Zhao Y,
Wang Y, Wu X and Wang Y (2022)
Spatio-Temporal Evolution of Sandy
Land and its Impact on Soil Wind
Erosion in the Kubuqi Desert in
Recent 30 Years.
Front. Environ. Sci. 10:950196.
doi: 10.3389/fenvs.2022.950196

Continuous remote-sensing monitoring of sand in desert areas and the exploration of the spatio-temporal evolution characteristics of soil-wind erosion has an important scientific value for desertification prevention and ecological restoration. In this study, the Kubuqi Desert was selected as the study area, and the Landsat series satellite remote sensing data, supplemented by satellite remote sensing data such as GE images, SPOT-5, ZY-3, GF-1/2/6, etc., integrated object-oriented, decision tree, and auxiliary human-computer interaction interpretation methods, developed the Kubuqi Desert area dataset from 1990 to 2020, and established a soil erosion intensity database of the past 30 years based on the soil-wind erosion correction equation. The results show that the application of the training samples obtained by a high-score collaborative ground sampling to land use/cover classification in desert areas can effectively improve the efficiency of remote-sensing mapping of sand changes and the accuracy of change information identification, and the overall accuracy of the classification results is 95%. In general, the sandy area of the Kubuqi Desert area has decreased year by year, during which the mobile sand in the hinterland of the desert has expanded in a scattered distribution. The overall soil-wind erosion intensity showed a downward trend, especially since 2000; the ecological improvement trend after the implementation of desertification control projects is obvious. Changes in the sand type contributed the most to the reduction of soil-wind erosion intensity (contribution 81.14%), ecological restoration played a key role in reducing the soil-wind erosion intensity (contribution 14.42%), and the increase of forest and grass vegetation covers and agricultural oases played a positive role in solidifying the soil- and wind-proof sand fixation. The pattern of sandy land changes in desert areas is closely related to the national ecological civilization construction policy and the impact of climate change.

Keywords: sandy land change, soil wind erosion, spatio-temporal evolution, remote sensing, Kubuqi Desert

1 INTRODUCTION

Desertification is one of the most critical problems in the global ecological environment. The problems such as the reduction of land resources, the decline of soil quality, and the frequent dust storms seriously restrict the socio-economic development and sustainable land use (Wang, 2003; Sachs, 2004; Schimel, 2010; Pravalie, 2016). Desertified land is also affected severely by soil-wind erosion. The area of wind erosion desertification in China reaches $160.74 \times 10^4 \text{ km}^2$, accounting for 16.7% of the total land area (Ci and Wu, 1997), which hinders the development of regional resources and sustainable ecological development (Zhang et al., 2018). Sandy lands and deserts are widely distributed in northern China. The climate changes and human activities have led to the aggravation of desertification in arid regions and have increased the intensity of soil-wind erosion (Wang et al., 2008; Uno et al., 2006; Liang et al., 2021). As the area of drylands in the world is expanding (Koutroulis, 2019), improving the desertification combating and adaption in northern China is one of the effective ways to mitigate the risks of climate change in the future (World Economic Forum, 2020). The development of the new era emphasizes the vision of “beautiful China” in 2035 and 2050. The desertification combating and ecological restoration project plays a vital role

in building a beautiful China. “Greening” and ecological restoration in deserts can be realized through ecological environment protection and ecological engineering construction (Chen et al., 2019; Ge et al., 2020; Ma et al., 2020). Over the past 30 years, the intensity of soil-wind erosion in China has decreased, but the inter-annual wind erosion intensity fluctuates greatly. The desertification caused by soil-wind erosion cannot be ignored (Chi et al., 2019). Desertification monitoring and assessment is an important indicator to understand the impact of climate changes and human activities on the ecological environment. Dynamic monitoring is a significant way to combat desertification scientifically. Therefore, to carry out desertification monitoring, accurately grasping the scope and spatio-temporal dynamics of desertification, and determining the evolution process of soil-wind erosion intensity are critical prerequisites for desertification land prevention (Hamed and Rao, 1998; Chen et al., 2019).

The analysis of the land desertification pattern in evolution and its influence on soil-wind erosion is not only an important basis for exploring the simulation and prediction of ecological environmental change, ecological protection and desertification combating in northern China, but also one of the contents of the current ecological environmental protection (Ouyang et al.,

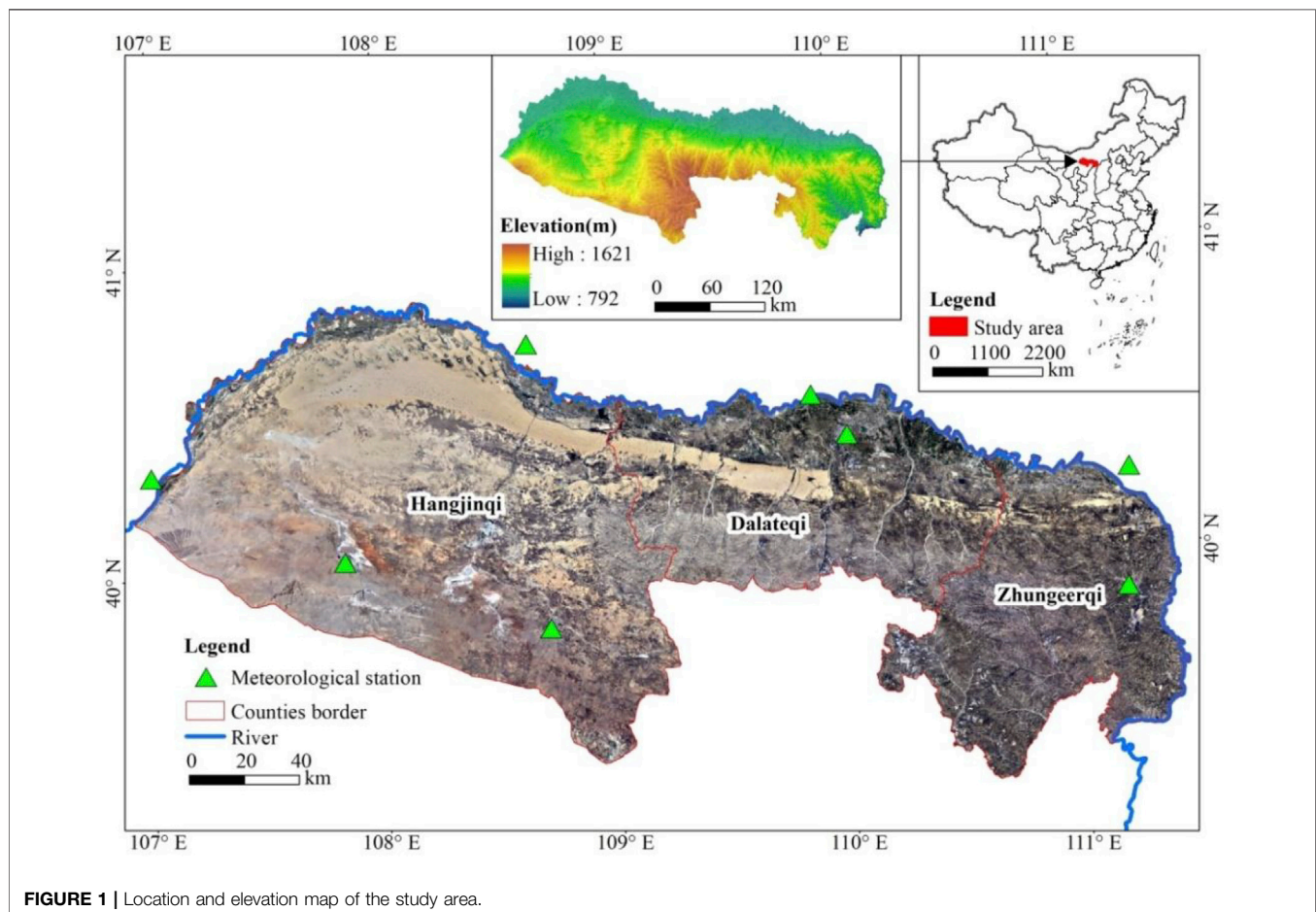


TABLE 1 | Detailed information of the selected images.

Year	Sensor	Path/row	Acquired time
1990, 1995, 2000, 2005, 2010, 2015, and 2020	Landsat 5 TM	126/32, 126/33, 127/32, 127/33, 128/32, 128/33, and 129/32	199,006-199,010, 199,506-199,510, 200,006-200,010, 200,506-200,510, 201,006-201,010, 201,506-201,510, 202,006-202,010

2016). Relevant research mainly focuses on remote sensing monitoring and analysis, soil-wind erosion simulation, and driving force analysis. In terms of desertification monitoring, remote sensing technology has become an important means to monitor land surface (Liu et al., 2020). With its comprehensiveness, timeliness, and operability, remote sensing technology has become one of the main and efficient means to obtain desertification and ecological restoration data (Liu and Deng, 2009; Jia et al., 2014), promoting desertification combating and ecological environmental comprehensive management. Based on remotely sensed monitoring data, about a quarter of the global green area from 2000 to 2017 came from China, ranking first in terms of contribution, 42% of which comes from afforestation together with agricultural oasis as an important manifestation (Chen et al., 2019). Meanwhile, with the development of other new information technologies including cloud computing, big data, and artificial intelligence, remote sensing information extraction has become more efficient and accurate (Liu et al., 2019). In terms of monitoring and evaluating soil-wind erosion, the methods adopted in China mainly include wind erosion profile and relic observation, cutting method, wind tunnel experiment, particle size analysis, mapping and remote sensing analysis, sediment transport rate observation, ^{137}Cs tracing method, wind erosion model, etc. Among them, the combination of ground investigation, experiment, and GIS simulation has become widely used on a regional scale. Modified Wind Erosion Equation (RWEQ) (Fryrear et al., 1996; Fryrear et al., 2001) can provide a more reliable spatio-temporal pattern of soil erosion, then explore the impact of a large-scale ecological construction on the wind erosion process (Chi et al., 2019; Zhao et al., 2020).

Kubuqi Desert is the seventh largest desert in China, the nearest desert to the capital Beijing, and a crucial part of the ecological barrier in northern China. Since the beginning of the 21st century, Kubuqi Desert has vigorously implemented the ecological protection and restoration policy, and has successively conducted a series of major ecological protection and restoration projects, such as the “Three North” shelter forest, conversion of croplands to forests and grasslands, Beijing-Tianjin Sandstorm Sources Control, grassland protection and construction, and the national closed reservation of desertification land, and achieved satisfactory results. As the only desert that has been treated in the world, the “Kubuqi Model” is a textbook-level world miracle. Kubuqi Desert has been identified as an “eco-economic demonstration zone in a global desert” by the United Nations Environment Program, and has gradually become a research hotspot concerned by scholars at home and abroad (Wang, 2017;

Lin et al., 2020). Some domestic scholars have studied the macroscopic pattern evolution and the scale of soil-wind erosion sample points of the Kubuqi Desert ecosystem. However, there is still a lack of research on desertification process monitoring and spatiotemporal evolution of soil-wind erosion based on the regional scale (Meng et al., 2014; Zhao et al., 2017; Dong et al., 2019). Based on this study, a new research method is proposed to carry out sand classification in the Kubuqi Desert. The proposed method presents good accuracy to extract sandy land distribution. Then, exploring climate change and ecological engineering play an important role in the change of sandy land area. Therefore, quantitatively analyzing the spatio-temporal variation of the sandy land in the Kubuqi Desert, determining the evolution of soil wind erosion, and understanding the driving factors as well as the influence of the evolution of sandy land patterns are beneficial to better evaluate the implementation of existing ecological protection and restoration policies, finding out problems and putting forward-targeted countermeasures, which is of great significance for building an ecological security barrier in northern China. In addition, it also plays a positive role in promoting ecological protection and high-quality development in the Yellow River Basin, and can also be used as a reference for global desertification combating.

2 MATERIALS AND METHODS

2.1 Study Area

Kubuqi Desert is the seventh largest desert in China, which is located in the Ordos Plateau. It is characterized by a zonal distribution, extending from east to west. The length is about 40 km and its area is about $1.45 \times 10^6 \text{ km}^2$, with geographical coordinates of $107^\circ\text{--}112^\circ \text{ E}$ and $39^\circ\text{--}41^\circ \text{ N}$. It spans parts of the Hangjin Banner, Dalat Banner, and Jungar Banner in Inner Mongolia, among which, the Hangjin Banner has the most serious desertification (Figure 1). The study area is composed of quicksand and semi-fixed dunes, dominated by crescent mobile sand dunes with strong mobility. This area is a typical continental climate area, which is located in the transition zone between the temperate arid steppe and the desert steppe, belonging to the semi-arid continental monsoon climate zone. The area is characterized by strong arid winds and annual gale days of 25–35 days. There is less precipitation in this area, and the moisture conditions in the east are quite different from the west. The average annual precipitation is 240–360 mm, and the average annual evaporation is 2,160 mm, which is more than 8 times of the rainfall. The main vegetation types are semi-arid steppe vegetation, meadow steppe

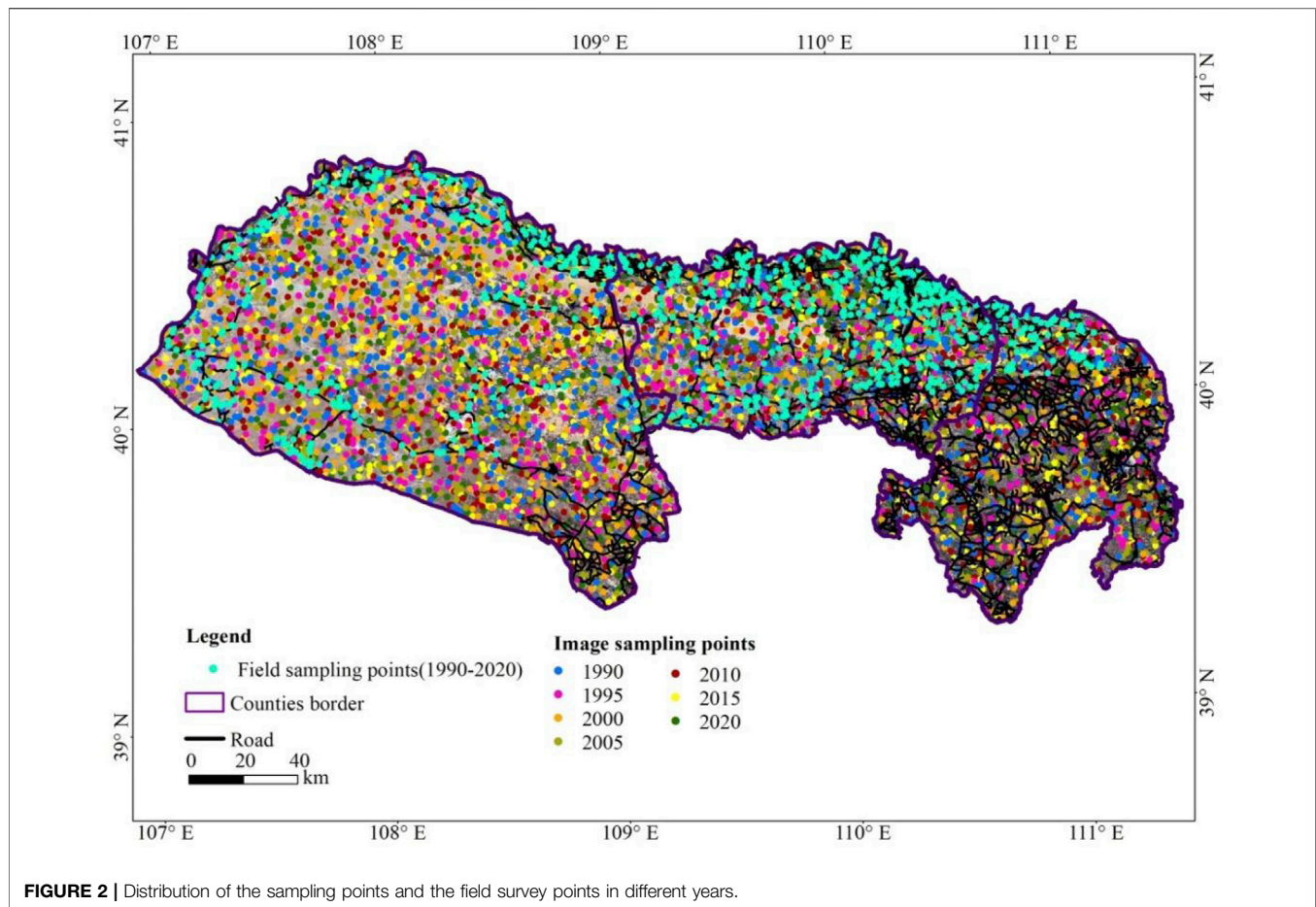


FIGURE 2 | Distribution of the sampling points and the field survey points in different years.

vegetation, and dry steppe sandy vegetation. The forest vegetation is mainly plantations.

2.2 Data

2.2.1 Landsat Data

Landsat satellite images are widely used in spatio-temporal dynamic monitoring of desertification because of their wide coverage, long time-series, and easy acquisition. In this study, remote sensing image data were obtained every 5 years (1990, 1995, 2000, 2005, 2010, 2015, and 2020) since 1990, and at least seven scenes were collected every 5 years (orbital parameters are 126/32, 126/33, 127/32, 127/33, 128/32, 128/33, and 129/32). In order to obtain the information of desert control and vegetation restoration, the data of the growing season (from June to October) were selected from remote sensing images taken by Landsat 5 (Table 1).

2.2.2 Soil-Wind Erosion Model Parameters

Remote sensing monitoring of soil-wind erosion mainly collects data like vegetation cover, meteorology, soil, snow cover, and a basic geographical background for model inversion. Among them, the maximum synthetic normalized vegetation index (NDVI) time-series data of GIMMS and MODIS from 1990 to 2020 were obtained through the NASA website (<https://www.nasa.gov/>),

using the general “dimidiate pixel model” (Shen et al., 2014) to obtain the annual and monthly vegetation coverage datasets. The meteorological data came from the National Meteorological Science Data Center (<http://data.cma.cn/>), and the daily average temperature, precipitation, average wind speed, wind direction, sandstorm, and sunshine duration of the meteorological stations in and around the study area were selected. The time scale of the meteorological data was from 1990 to 2020. The station-based data, interpolated based on the ANUSPLIN method, were subject to quality inspection and control to obtain the spatial data with a long time-series covering the entire study area. Snow cover factor was obtained through NASA website. The topography, digital elevation, soil type, vegetation type, basic geographic data, and other environmental background data involved in this study were obtained through the application from Resource and Environment Science and Data Center of Chinese Academy of Sciences (<https://www.resdc.cn/>).

2.2.3 Sampling Data

In order to construct the land use/cover classification method, set training samples, and evaluate the classification accuracy, this study adopted a human-computer interaction and field investigation to sample the land use/cover types in different years from Landsat TM, Google Earth historical image, SPOT-

TABLE 2 | Validation of the classification results in 1990–2020.

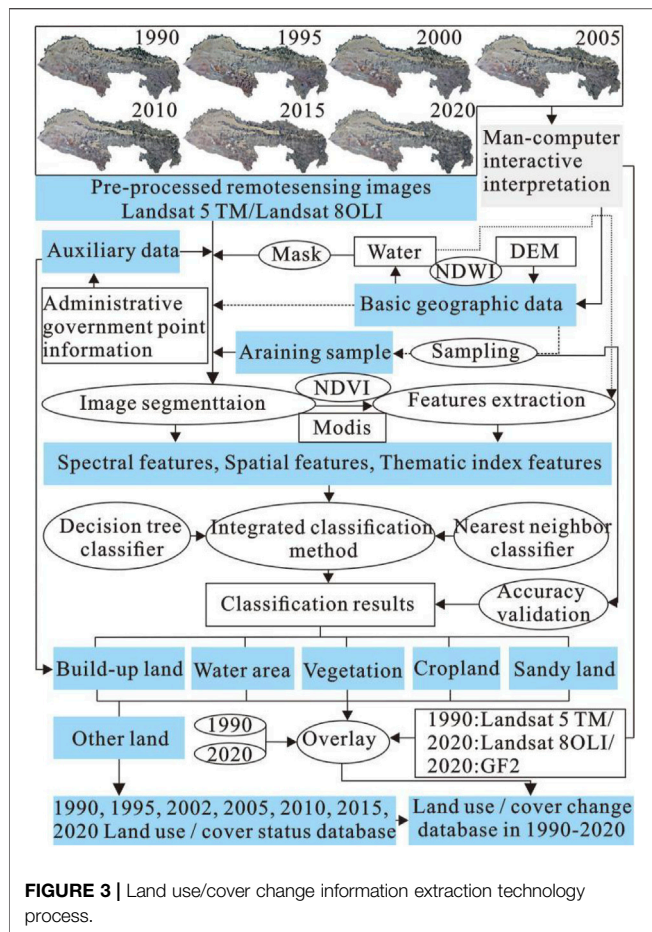
Year	Type		Classified class		Total
			Sandy land	Non-sandy land	
1990	Actual class	Sandy land	633	14	647
		Non-sandy land	13	101	114
		Total number	646	115	761
		Producer's accuracy	97.84%	88.60%	-
		User's accuracy	97.99%	87.83%	-
		Overall accuracy		96.45%	-
		Kappa coefficient		0.86	-
					-
1995	Actual class	Sandy land	612	20	632
		Non-sandy land	15	142	157
		Total number	627	162	789
		Producer's accuracy	96.84%	90.45%	-
		User's accuracy	97.61%	87.65%	-
		Overall accuracy		95.56%	-
		Kappa coefficient		0.86	-
					-
2000	Actual class	Sandy land	647	12	659
		Non-sandy land	8	81	89
		Total number	655	93	748
		Producer's accuracy	98.18%	91.01%	-
		User's accuracy	98.78%	87.10%	-
		Overall accuracy		97.33%	-
		Kappa coefficient		0.87	-
					-
2005	Actual Class	Sandy land	676	26	702
		Non-sandy land	14	129	143
		Total number	690	155	845
		Producer's accuracy	96.30%	90.21%	-
		User's accuracy	97.97%	83.23%	-
		Overall accuracy		95.27%	-
		Kappa coefficient		0.84	-
					-
2010	Actual Class	Sandy land	691	22	713
		Non-sandy land	17	101	118
		Total number	708	123	831
		Producer's accuracy	96.91%	85.59%	-
		User's accuracy	97.60%	82.11%	-
		Overall accuracy		95.31%	-
		Kappa coefficient		0.81	-
					-
2015	Actual class	Sandy land	708	23	731
		Non-sandy land	13	114	127
		Total number	721	137	858
		Producer's accuracy	96.85%	89.76%	-
		User's accuracy	98.20%	83.21%	-
		Overall accuracy		95.80%	-
		Kappa coefficient		0.84	-
					-
2020	Actual Class	Sandy land	697	25	722
		Non-sandy land	16	162	178
		Total number	713	187	900
		Producer's accuracy	96.54%	91.01%	-
		User's accuracy	97.76%	86.63%	-
		Overall accuracy		95.44%	-
		Kappa coefficient		0.86	-
					-

5 image, ZY-3 satellite image, and GF-1/2/6 image. Based on geostatistical methods, 5,732 samples were selected in total, which belonged to sandy land (4,806 samples) and non-sandy land (926 samples). The field survey data involved 737 sampling points and 36 field verification points of soil–wind erosion (**Figure 2**).

2.3 Classification Method and the Wind Erosion Model

2.3.1 Land Use/Cover Classification

The main features of sandy land are high-surface reflectance, low soil moisture, and low vegetation coverage. In order to effectively identify sandy land and other types of land use



(water body, cropland, forestland, and grassland, constructive land and other types), spectral features, spatial features, and thematic index features were selected to construct classification methods (Zhan et al., 2021). The spectral features adopted the average reflectance index (Takemura et al., 2002), the spatial features adopted the area, shape, and other indices (Zhan et al., 2021), and the thematic index features adopted the normalized vegetation index (NDVI) (Wang et al., 2013) and normalized water index (NDWI) (Li et al., 2011). This study used the combination of the decision tree and nearest neighbor classifier, together with human-machine interactive interpretation to obtain land use/cover change information (**Figure 3**): 1) pre-processing of the remote sensing images and basic data, including radiometric correction, geometric correction, atmospheric correction etc., to obtain surface reflectance. 2) Using NDWI and human-computer interactive interpretation (Liu et al., 2009) to extract the water bodies in the Kubuqi Desert from 1990 to 2020. Referring to auxiliary data like urban annotation data and traffic distribution data, constructive land is extracted by human-computer interaction. Select the threshold with NDVI less than 0.2 to determine sandy land and vegetation-free areas (Zhan et al., 2021). 3) Using the data of sampling points, the object-oriented classification of

image segmentation and feature extraction (Camara et al., 1996) was used to in each ground feature. 4) Selecting typical land use/cover samples that are widely distributed in the image to build and test the classification tree (Quinlan, 1986). Based on the feature information of the thematic index, the heterogeneity of separated plots was analyzed; then, the vegetation and unclassified information were divided. Masking the unclassified information of the extracted water bodies and constructive land, the remaining unclassified objects were inputted into the nearest neighbor classification process (Kuncheva and Jain, 1999), and finally obtained sand, water body, cropland, forestland and grassland, constructive land, and other types. 5) The human-computer interactive interpretation method was adopted to verify and correct the land use/cover information in each period, and integrate the database of the current land use/cover situation and dynamic change information from 1990 to 2020.

2.3.2 Soil-Wind Erosion Model

The combination of ground investigation and the RWEQ model was used to evaluate the annual soil wind erosion intensity from 1990 to 2020. The model measured soil-wind erosion by considering factors such as climate, soil erodibility, soil crust, surface roughness, and vegetation residue cover. Its basic expression was as follows (Fryrear et al., 1996; Fryrear, 2001):

$$Q_{wind} = \frac{2x}{s^2} Q_{max} e^{-\left(\frac{x}{s}\right)^2},$$

$$Q_{max} = 109.8 (WF \times EF \times SCF \times K' \times COG),$$

$$s = 150.71 (WF \times EF \times SCF \times K' \times COG)^{-0.3711},$$

where Q_{wind} is the soil-wind erosion modulus used to characterize the soil-wind erosion intensity; x is the actual plot length; s is the critical field length; WF is the weather factor calculated using data on wind velocity, precipitation, temperature, and snow cover; EF is the soil erodibility factor; SCF is the soil crust factor, and they depend on the contents of organic matter content, sand, and clay; K' is the soil roughness; and COG is the combined vegetation factor including growing vegetation canopy, flat cover, and standing residuals. We localized the parameters based on land use/cover data and field survey. The surface roughness on different land covers was obtained by using the ruler measurement method with the corresponding parameters corrected. Meanwhile, we conducted a quadrat survey in different seasons to establish the relationship between field-withered vegetation, standing residual, growing vegetation and NDVI inversion coverage, and correct vegetation factors (Chi et al., 2018).

2.4 Accuracy Evaluation

Accuracy verification is a quantitative analysis of land use/cover data products obtained by computer classification and human-computer interactive interpretation on the basis of a qualitative evaluation. It is a process of evaluating the quality

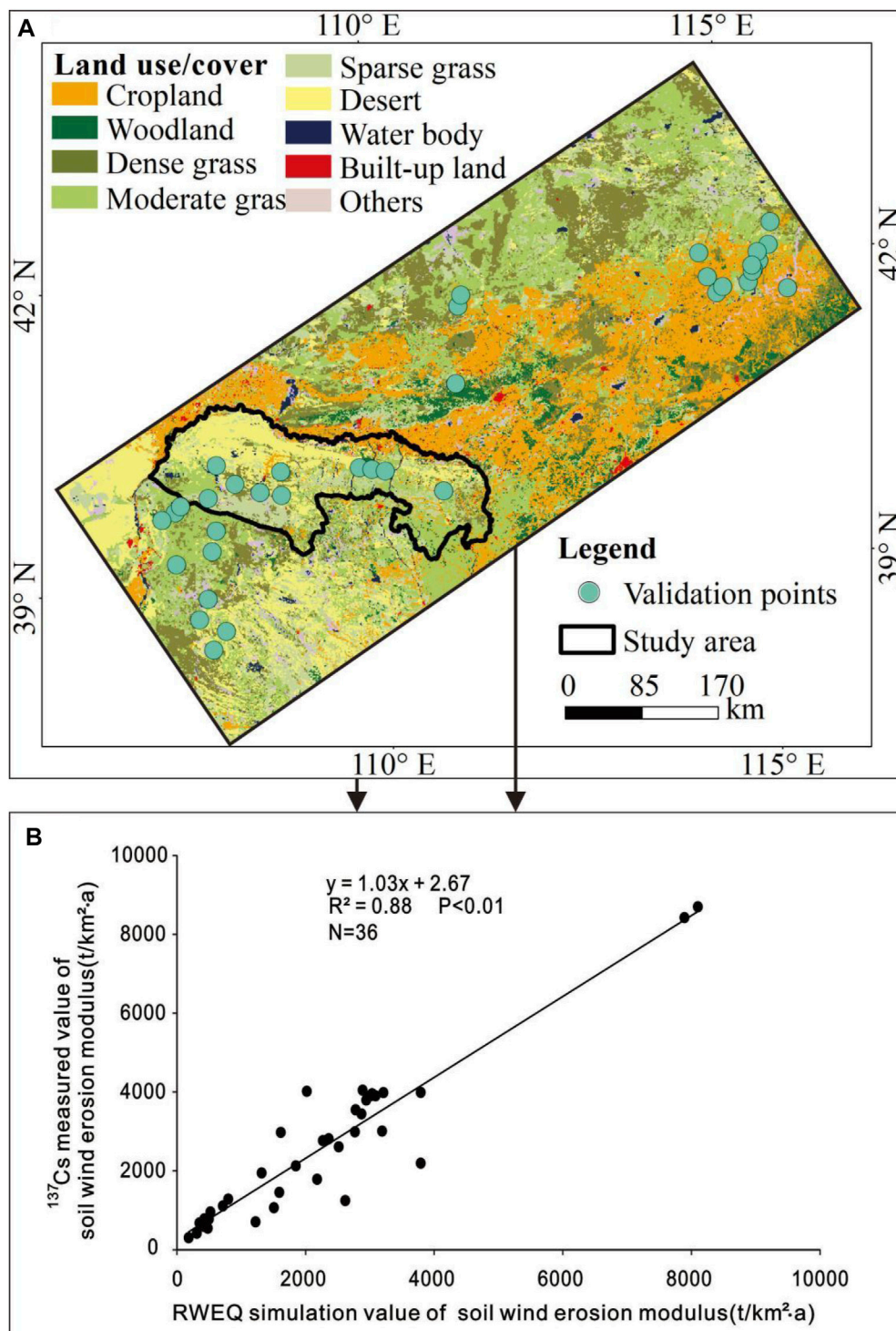
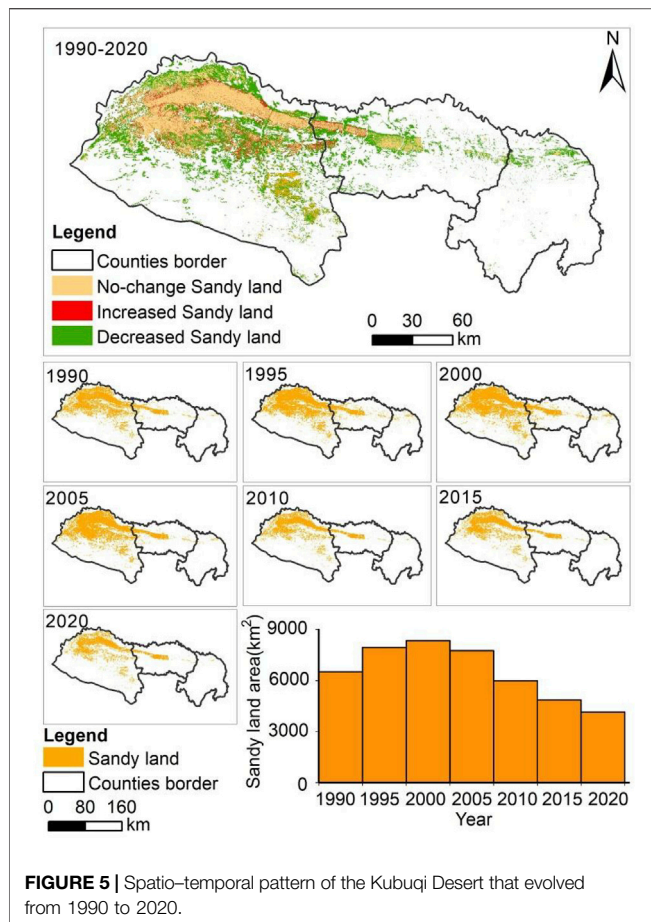


FIGURE 4 | Field sampling verification of the soil-wind erosion modulus. **(A):** Distribution of field sampling verification points, **(B):** RWEQ simulation value of the soil-wind erosion modulus.

of land use/cover products using sampling data (Figure 2) as well as remote sensing data with high-precision and high-resolution. The method to quantitatively measure the classification quality

of land use/cover data adopted the confusion matrix method (Stehman, 2009), which was counting the number of land-use categories corresponding to the location of reference and



verification points, and forming a $n \times n$ matrix, in which the number of statistics on the diagonal was the number of samples correctly classified after verification. Relevant indicators for evaluating the accuracy of the whole and each category based on the confusion matrix method included overall accuracy (OA), producer accuracy (PA), user accuracy (UA) and kappa coefficient (Congalton and Green, 2009).

3 RESULTS

3.1 Validation of the Classification Results

The confusion matrix of land use/cover classification accuracy based on high-resolution remote sensing images/field sampling data is showed in Table 2. A total of 5,732 sample points were randomly sampled from high-resolution remote sensing images during 1990–2020, including 4,806 in sandy areas and 926 in non-sandy areas. In 2020, there were 737 sampling points in the field survey, including 59 in sandy areas and 678 in non-sandy areas. Through the object-oriented classification method, the spectral features, spatial features, and thematic index features were integrated to extract various types of ground features hierarchically, and the human-machine interactive

TABLE 3 | Areas and changes in sandy land area between 1990 and 2020.

Year	Area (km ²)	Period	Change area (km ²)
1990	6,504.74	1990–1995	1,442.20
1995	7,946.95	1995–2000	391.57
2000	8,338.51	2000–2005	–582.97
2005	7,755.54	2005–2010	–1770.62
2010	5,984.92	2010–2015	–1,124.17
2015	4,860.75	2015–2020	–710.49
2020	4,150.26	-	-

interpretation was fully sampled for modification. The classification of sandy land and non-sandy land (water body, cropland, forestland and grassland, constructive land, and other types) had achieved good results. The overall accuracy of the seven classification results was over 95%, and the Kappa coefficient was more than 0.80. Therefore, the results could be used for a spatiotemporal pattern analysis as well (Zhan et al., 2021).

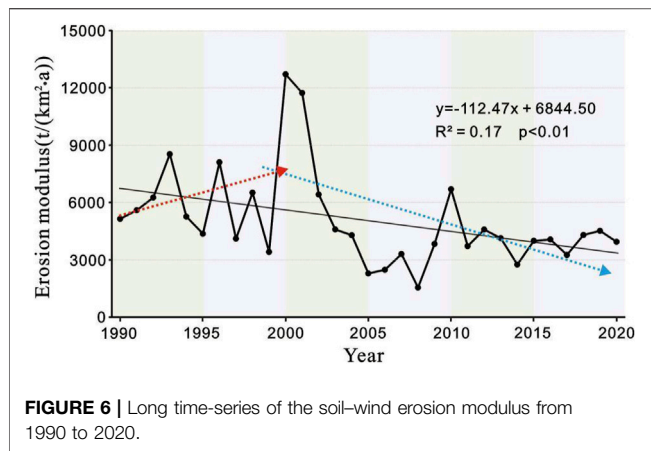
¹³⁷Cs tracer technology was used to verify the soil-wind erosion modulus (Chi et al., 2019). This study involved the data of 36 sampling points. By comparing the verification points with the model inversion data, the value of R^2 reached 0.88 (Figure 4).

3.2 Spatial Distribution and Evolution of Sandy Land

Figure 5 and Table 3 indicate the regional mapping and area statistics of the Kubuqi Desert from 1990 to 2020, respectively. According to the remote sensing monitoring, the area of the Kubuqi Desert increased from 6,504.74 km² in 1990–4,150.26 km² in 2020, accounting for 11.99% of the total study area. The sandy land was distributed as a belt along the Yellow River, which in Hangjin Banner, was widely distributed, followed by Dalat Banner, and Jungar Banner in the East was less distributed. In terms of time, the area of the Kubuqi Desert first increased and then decreased, with the largest sandy area in 2000. In terms of space, the area around the Kubuqi Desert was constantly decreasing, and the expansion of mobile sand was scattered in the hinterland of the desert.

3.3 Spatio-temporal Characteristics of Soil-Wind Erosion

In the past 30 years, the soil-wind erosion modulus in the Kubuqi Desert has shown a downward trend as a whole. Especially since 2000, the ecological environment improvement has improved significantly after the implementation of the desertification control project ($p < 0.01$) (Figure 6). From 1990 to 2020, the average value of the soil-wind erosion modulus was 4,542 T/(km²·a) (Moderate). In general, the change of soil-wind erosion from 1990 to 2010 fluctuated greatly, and had been relatively stable since 2010. In 2000, the soil-wind erosion reached the peak, and the soil-wind erosion modulus was 12,703 T/(km²·a) (Very severe). The intensity of the soil-wind erosion reached the second peak in 2001 (11,728 T/(km²·a)). Figure 7 reflects the spatial



distribution of soil-wind erosion in the Kubuqi Desert during the study period. Overall, the wind erosion intensity of Hangjin Banner located in the eastern hinterland of the Kubuqi Desert was the largest, Dalat Banner in the middle was the second, and Jungar Banner in the west was the lowest. Although the soil-wind erosion intensity in the Kubuqi Desert showed a

decreasing trend as a whole, there were regional differences and a large spatial heterogeneity after the implementation of desertification control and ecological engineering construction, contributing to the improvement in vegetation coverage and the significant decrease in the soil-wind erosion modulus.

3.4 Influence of Spatio-temporal Evolution of Sandy Land on Soil-Wind Erosion Intensity

Land use/cover change is an important factor for the formation and intensity of soil-wind erosion. In order to study the influence of different land use/cover types on soil-wind erosion intensity and analyze the differences of soil-wind erosion intensity (Zhang et al., 2018), this study counted the soil-wind erosion intensity of different land use/cover types in the Kubuqi Desert from 1990 to 2020 (Table 4). The results showed that the changes of sandy land contributed the most to the reduction of soil-wind erosion intensity (81.14%), the restoration of vegetation played a key role (14.42%), and the transformation of sandy lands into an agricultural oasis led to the reduction of soil-wind erosion (2.79%). The human-computer interactive interpretation (Liu

TABLE 4 | Land use/cover changes in the Kubuqi Desert from 1990 to 2020.

Land use/cover types	1990 (thousand km ²)	2020 (thousand km ²)	Land use/cover changes		Soil wind erosion changes (%)		
			Area (thousand km ²)	Change rate (%)	Amount (million ton)	Contribution rate (%)	
Sandy land	6,504.74	4,150.26	−2,354.48	−36.20%	−57.13	81.14%	
Vegetation	22,232.46	24,097.52	1865.06	8.39%	−10.15	14.42%	
Build-up land	801.2219	1,216.14	414.92	51.79%	−0.03	0.05%	
Water area	1,058.49	952.23	−106.26	−10.04%	−0.71	1.00%	
Cropland	3,378.154	3,663.13	284.97	8.44%	−1.97	2.79%	
Other land	633.2496	529.04	−104.21	−16.46%	−0.42	0.60%	
2020	Vegetation	Build-up land	Water area	Cropland	Other land	-	
1990	Area (thousand km ²)						
Sandy land	2099.13	85.64	12.10	148.57	9.01	-	
	Soil wind erosion changes (million ton)						
	−18.66	−0.85	−0.12	−1.22	−0.09	-	
	Contribution rate (%)						
	89.08%	4.05%	0.59%	5.83%	0.45	-	
Typical area of Kubuqi Desert	VFC(%)		Soil wind erosion modulus (T/km ² ·a)				
	1990	2020	Change	1990	2020	Change	Level change
a	7.07	16.88	9.81	15,490	13,428	−2062	Destructive- > Very severe
b	5.96	15.12	9.16	14,539	8,153	−6,386	Destructive- > severe
c	9.15	40.89	31.74	18,449	5,138	−13811	Destructive- > severe
d	10.04	34.31	24.27	10,311	3,323	−6,988	Severe- > moderate
e	8.68	25.05	16.37	14,902	4,929	−9,373	Very severe- > moderate

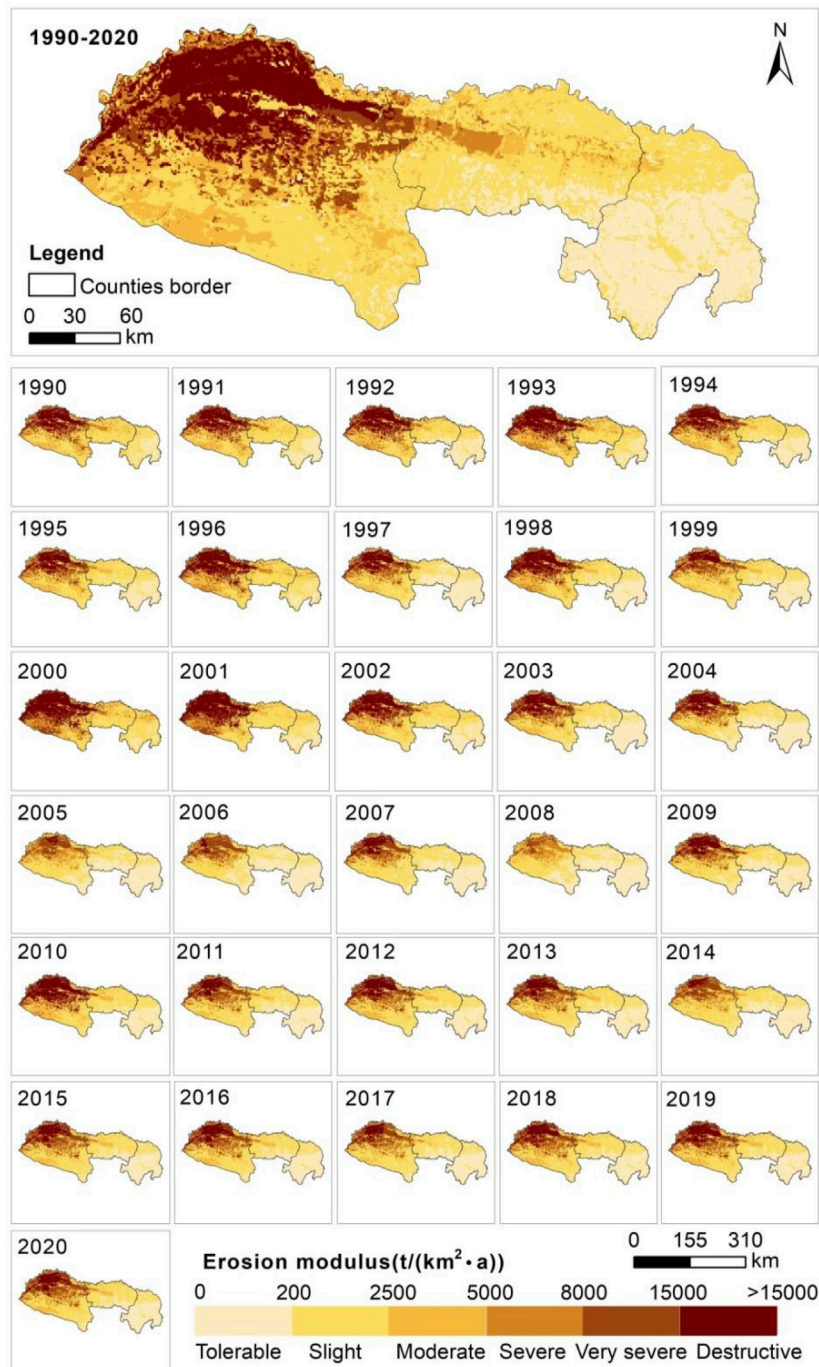


FIGURE 7 | Spatial distributions of soil-wind erosion in the Kubuqi Desert region during 1990–2020.

et al., 2019) was used to extract the changes of sandy lands from 1990 to 2020 (**Figure 3; Table 4**). The area of sandy lands decreased by 2,354.48 km². Among them, the area converted from sandy lands to vegetation (forestlands and grasslands) was the largest (2099.13 km²), accounting for 89.16% in the reduced area. The area converted from sandy lands to croplands was 148.57 km², and from sandy lands to

constructive lands was 85.64 km². The conversion from sandy lands to forestlands and grasslands could effectively inhibit soil-wind erosion (contribution for 89.08%), and the increase of vegetation coverage could reduce soil-wind erosion as well. The conversion from sandy lands to croplands slowed down the soil-wind erosion by 0.85 million tons. According to the research on the typical area in the Kubuqi Desert (**Table 4**;

Figure 8), the desertification control project effectively improved the vegetation coverage in the desert area, solidified the soil, and played a positive role in wind prevention and sand fixation.

4 DISCUSSION

4.1 Accuracy of Remote Sensing Classification

Desertification restricts regional sustainable development, so the quantitative study on sandy land is particularly important for desertification control and ecological construction and restoration (Liu and Dong, 1999). Based on Landsat satellite data, we sampled

the sandy land classification and dynamic change mapping with object-oriented and human-machine interactive interpretation, and analyzed the spatio-temporal evolution of the Kubuqi Desert's sandy lands from 1990 to 2020. Compared with previous studies (Lei et al., 2021; Lin et al., 2021), the collaboration of object-oriented classification (Zhan et al., 2021) and human-computer interactive interpretation (Zhang et al., 2014; Liu et al., 2009) effectively overcomes the problem of spectral similarity between sparse vegetation areas and sandy areas, and comprehensively extracts land use/cover information by using the spectral, spatial, and thematic features of remote sensing images. On the other hand, MODIS data sources with medium and low resolution are used in the monitoring of vegetation cover changes in desert areas (Piao et al., 2004; Feng et al., 2016; Zolch et al., 2018); however, the

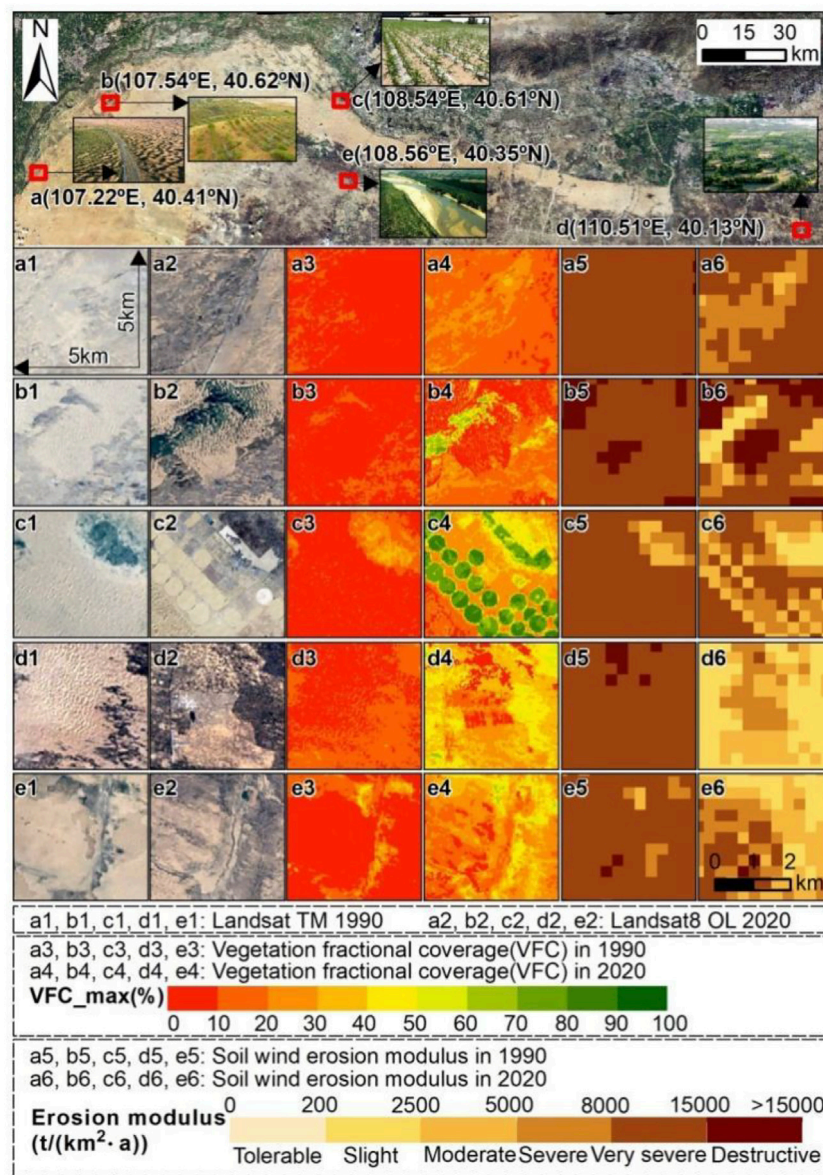
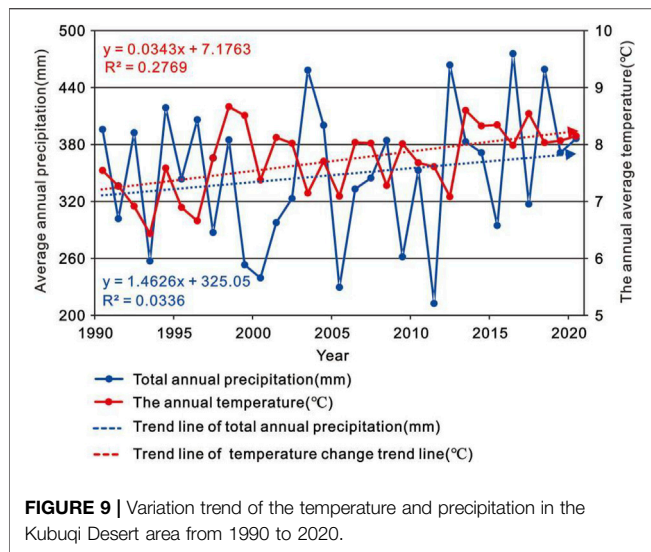


FIGURE 8 | Schematic diagram of the vegetation cover and soil-wind erosion intensity in typical areas of sandy land change.



problem of regional scale-mixed pixels directly affects the accuracy of sandy land and vegetation cover monitoring. With the development of remote sensing technology, the adoption of medium- and high-resolution satellite data such as Landsat, Sentinel 1/2, GF1/2 series is becoming more and more mature in achieving high-precision and long time-series land use/cover information. Meanwhile, with the development of new information technology such as cloud computing, big data, and artificial intelligence, remote sensing information extraction technology is more efficient and accurate (Liu et al., 2019).

In the current study, sufficient sampling data and field survey data can effectively improve the accuracy in extracting sandy land changes. We have collected a large number of ground surveys and field quadrat data of different seasonal phases, which can effectively correct the heterogeneity of remote sensing spectra and thematic parameters in the classification (Chi et al., 2019). In addition, a lot of manpower is invested to deal with the position error caused by the sawtooth effect of the grating vector transformation, and the classification results are corrected by human-computer interaction. The overall accuracy of the method involved is more than 90%.

4.2 Sustainability of the Ecological Project

Desertification leads to ecological degradation, and land resources show a trend from structural damage to functional disorder. Ecological restoration and reconstruction has become a challenge for human survival and sustainable development (Li et al., 2011; Fu et al., 2017). In recent decades, a series of measures have been carried out in northern China to improve the ecological environment. The ecological engineering construction has played an important role in regional desertification control, vegetation restoration, and soil erosion control (Chi et al., 2019; Wang et al., 2019; Li et al., 2021), and has improved the main ecosystem services (Lv et al., 2012; Fu et al., 2017; Zhao et al., 2020). However, unreasonable ecological construction layout may threaten regional water resources (Feng et al., 2016), food security (Chen et al., 2015), and ecological sustainable development (Zastrow, 2019). Some scholars have found

that changes in precipitation are not the driving force of vegetation greening in northern China, but rather, the construction of a national large-scale ecological engineering is the key factor in promoting the greening of desert lands. However, unreasonable vegetation restoration in arid regions may lead to catastrophic consequences (Chen et al., 2019; Wang et al., 2019).

According to the observational data of 8 meteorological stations in the Kubuqi Desert area (Figure 1), we found that the climate showed a warm and humid trend from 1990 to 2020 (Figure 9). Ecological engineering and climate conditions have contributed to the vegetation restoration in the Kubuqi Desert. Nevertheless, large-scale afforestation may lead to a dry layer on local soil and aggravate local water resource stress, especially in semi-arid areas sensitive to climate change (Li et al., 2021). As a result, it is necessary to further reveal the relationship between main ecological services and vegetation restoration, and to analyze the safety threshold of afforestation to satisfy vegetation growth and sustainable water use under the influence of climate changes and human activities (Wang et al., 2019; Li et al., 2021), especially the research on the non-linear response of an arid ecosystem to climate change and driving mechanism, in order to provide support for ecological restoration and sustainable development of resources and the environment.

5 CONCLUSION

Based on Landsat remote sensing data and the RWEQ model, we obtained the information of land use cover change and soil-wind erosion intensity in the Kubuqi Desert from 1990 to 2020, and further analyzed the evolution of the Kubuqi Desert sand and its impact on soil-wind erosion intensity in the recent 30 years. According to the analysis of the spatio-temporal dynamic pattern of sandy land and soil-wind erosion intensity, the change of the Kubuqi Desert area was consistent with soil-wind erosion intensity, showing a trend of first increasing and then decreasing. Meanwhile, before 2000, the process of soil-wind erosion was more intense than that of ecological restoration. From 1990 to 2020, the area of sandy lands decreased by 2,354.48 km², and since 2000, a series of desert control and ecological restoration projects have been implemented, and the area of sandy lands have decrease continuously. In addition, the transformation of sandy lands and the ecological restoration and improvement of vegetation coverage can effectively inhibit and slow down the intensity of soil-wind erosion. Among them, the transformation of sandy lands contributes the most (81.14%), and the reduction of forestlands, grasslands, and agricultural oases can effectively reduce soil-wind erosion. Overall, this study provides important information for understanding the desertification control and “Greening” process of sandy lands in this region. These findings will help improve the cognition of decision-makers, support the strategic decision-making of sustainable development of the ecosystem in the Kubuqi Desert, scientifically implement ecological protection and restoration projects, promote the comprehensive treatment projects of mountains, rivers, forests, fields, lakes, grass, and sand, build the virtuous cycle of the ecosystem, and promote the sustainable development of land resource utilization.

DATA AVAILABILITY STATEMENT

The original contributions presented in the study are included in the article/Supplementary Material; further inquiries can be directed to the corresponding authors.

AUTHOR CONTRIBUTIONS

XD: data curation and writing—original draft preparation. YN: supervision, investigation, and reviewing and editing. WC: supervision, investigation, and data curation, editing, and funding acquisition. JZ: reviewing and editing. YZ: conceptualization and validation. YW: software and methodology. XW: software and methodology. YW: data curation. All authors contributed to the article and approved the submitted version.

REFERENCES

- Camara, G., Souza, R. C. M., Freitas, U. M., and Garrido, J. (1996). SPRING: Integrating Remote Sensing and GIS with Object-Oriented Data Modelling. *Comput. Graph.* 15, 13–22. doi:10.1016/0097-8493(96)00008-8
- Chen, C., Park, T., Wang, X., Piao, S., Xu, B., Chaturvedi, R. K., et al. (2019). China and India Lead in Greening of the World through Land-Use Management. *Nat. Sustain.* 2, 122–129. doi:10.1038/s41893-019-0220-7
- Chen, Y., Wang, K., Lin, Y., Shi, W., Song, Y., and He, X. (2015). Balancing Green and Grain Trade. *Nat. Geosci.* 8, 739–741. doi:10.1038/ngeo2544
- Chi, W. F., Kuang, W. H., Jia, J., and Liu, Z. J. (2018). Study on Dynamic Remote Sensing Monitoring of LUCC and Soil Wind Erosion Intensity in the Beijing-Tianjin Sandstorm Source Control Project Region. *Remote Sens. Technol. Appl.* 33, 965–974. doi:10.11873/j.issn.1004-0323.2018.5.0965
- Chi, W., Zhao, Y., Kuang, W., and He, H. (2019). Impacts of Anthropogenic Land Use/Cover Changes on Soil Wind Erosion in China. *Sci. Total Environ.* 668, 204–215. doi:10.1016/j.scitotenv.2019.03.015
- Ci, L. J., and Wu, B. (1997). Classification of Climate Types and Determination of Potential Occurrence Range of Desertification in China. *J. Desert Res.* 17, 107–112.
- Congalton, R. G., and Green, K. (2009). *Assessing the Accuracy of Remotely Sensed Data: Principles and Practices*. Boca Raton: CRC Press.
- Dong, T., Xiao, Y., Zhang, L., Xiao, Y., Zheng, H., and Ouyang, Z. Y. (2019). Analysis of Driving Factors that Influence the Pattern and Quality of the Ecosystem in Ordos. *Acta Ecol. Sin.* 39, 660–671. doi:10.5846/stxb201804080788
- Feng, X., Fu, B., Piao, S., Wang, S., Ciais, P., Zeng, Z., et al. (2016). Revegetation in China's Loess Plateau Is Approaching Sustainable Water Resource Limits. *Nat. Clim. Change* 6, 1019–1022. doi:10.1038/nclimate3092
- Fryrear, D. W., Chen, W., and Lester, C. (2001). Revised Wind Erosion Equation. *Ann. Arid. Zone.* 40, 265–279.
- Fryrear, D. W., Saleh, A., Bilbro, J. D., Zobeck, T. M., and Stout, J. E. (1996). "Field Tested Wind Erosion Model," in *The Proceedings of the International Symposium "Wind Erosion in West Africa: The Problem and its Control"*. Editors B. Buerkert, B. E. Allison, and M. V. Oppen (Hohenheim, Germany: Margraf Verlag Press), 343–355.
- Fu, B., Wang, S., Liu, Y., Liu, J., Liang, W., and Miao, C. (2017). Hydrogeomorphic Ecosystem Responses to Natural and Anthropogenic Changes in the Loess Plateau of China. *Annu. Rev. Earth Planet. Sci.* 45, 223–243. doi:10.1146/annurev-earth-063016-020552
- Ge, Q. S., Fang, C. L., and Jiang, D. (2020). Geographical Missions and Coupling Ways between Human and Nature for the Beautiful China Initiative. *Acta Geogr. Sin.* 75, 1109–1119. doi:10.11821/dlxb202006001
- Hamed, K. H., and Ramachandra Rao, A. (1998). A Modified Mann-Kendall Trend Test for Autocorrelated Data. *J. Hydrology* 204, 182–196. doi:10.1016/S0022-1694(97)00125-X
- Jia, K., Wei, X., Gu, X., Yao, Y., Xie, X., and Li, B. (2014). Land Cover Classification Using Landsat 8 Operational Land Imager Data in Beijing, China. *Geocarto Int.* 29, 941–951. doi:10.1080/10106049.2014.894586
- Koutroulis, A. G. (2019). Dryland Changes under Different Levels of Global Warming. *Sci. Total Environ.* 655, 482–511. doi:10.1016/j.scitotenv.2018.11.215
- Kuncheva, L. I., and Jain, L. C. (1999). Nearest Neighbor Classifier: Simultaneous Editing and Feature Selection. *Pattern Recognit. Lett.* 20, 1149–1156. doi:10.1016/S0167-8655(99)00082-3
- Lei, Y. H., Ding, G. D., Li, Z. M., Chi, W. F., Gao, G. L., and Zhao, Y. Y. (2021). Land Use/Cover Change and its Ecosystem Service Value Response in the Beijing-Tianjin Sandstorm Source Control Project Area. *J. Desert Res.* 41, 29–40. doi:10.7522/j.issn.1000-694X.2021.00085
- Li, C., Fu, B., Wang, S., Stringer, L. C., Wang, Y., Li, Z., et al. (2021). Drivers and Impacts of Changes in China's Drylands. *Nat. Rev. Earth Environ.* 2, 858–873. doi:10.1038/s43017-021-00226-z
- Li, H., Kondoh, A., and Shen, Y. (2011). Interannual Changes in the Distribution of Paddy Field in Sanjiang Plain, Northeast China by Satellite Remote Sensing. *J. Jpn. Soc. Hydrology Water Resour.* 24, 328–336. doi:10.3178/jjshwr.24.328
- Liang, P., Chen, B., Yang, X., Liu, Q., Li, A., Mackenzie, L., et al. (2022). Revealing the Dust Transport Processes of the 2021 Mega Dust Storm Event in Northern China. *Sci. Bull.* 67, 21–24. doi:10.1016/j.scib.2021.08.014
- Lin, L. Z., Chen, Y. S., Ma, W. Z., Lin, Z., and Yu, Q. (2021). Evolution and Driving Forces of Ecosystem Pattern in Kubuqi Desert of Northern China. *J. B. For. Univ.* 43, 108–123. doi:10.12171/j.1000-1522.20200242
- Lin, L. Z., Li, D., and Lin, Z. (2020). Evaluation of Water Resources Carrying Capacity in Kubuqi Desert Area Based on Entropy Weight and TOPSIS Model. *J. Cent. Chin. Norm. Univ. Nat. Sci. Ed.* 54, 640–648. doi:10.19603/j.cnki.1000-1190.2020.04.015
- Liu, J., and Deng, X. (2010). Progress of the Research Methodologies on the Temporal and Spatial Process of LUCC. *Chin. Sci. Bull.* 55, 1354–1362. doi:10.1007/s11434-009-0733-y
- Liu, J. Y., Zhang, Z. X., and Zhang, S. W. (2020). Innovation and Development of Remote Sensing-Based Land Use Change Studies Based on Shupeng Chen's Academic Thoughts. *J. Geo-inf. Sci.* 22, 680–687. doi:10.12082/dqxkx.2020.200052
- Liu, X., Pei, F., Wen, Y., Li, X., Wang, S., Wu, C., et al. (2019). Global Urban Expansion Offsets Climate-Driven Increases in Terrestrial Net Primary Productivity. *Nat. Commun.* 10, 5558. doi:10.1038/s41467-019-13462-1
- Liu, Y. H., and Dong, Y. X. (1999). Tentative Study on Desertification and Sustainable Development in China. *J. Desert Res.* 19, 17–22.
- Lü, Y., Fu, B., Feng, X., Zeng, Y., Liu, Y., Chang, R., et al. (2012). A Policy-Driven Large Scale Ecological Restoration: Quantifying Ecosystem Services Changes in the Loess Plateau of China. *PLoS One* 7, e31782. doi:10.1371/journal.pone.0031782
- Ma, Y. J., Wang, Z. M., Wang, J. H., Zuo, X. A., Duan, H. T., Liu, G., et al. (2020). Construction of Evaluation Index System on Beautiful China in Typical Areas.

FUNDING

This research was supported by the National Natural Science Foundation of China "Research on the Greening process and its mechanism of regional ecosystem services in the Kubuqi Desert" (42061069), the science and technology innovation project of the department of natural resources of Inner Mongolia Autonomous Region "Research on the sustainable utilization and development of natural resources with the integration of space and space in Inner Mongolia Autonomous Region," the key technology and application of ecological quality diagnosis and integrated management of "Beautiful Inner Mongolia" (2019GG010), the Research Foundation of Education Bureau of Inner Mongolia, China (NJYT-19-B29) and Inner Mongolia Autonomous Region talent development fund project in 2021.

- Remote Sens. Technol. Appl.* 35, 287–294. doi:10.11873/j.issn.1004-0323.2020.2.0287
- Meng, J. J., Yan, Q., and Xiang, Y. Y. (2014). The Optimization of Ecological Security Pattern Based on Land Use and Assessment of Schemes in Ordos, Inner Mongolia, China. *J. Desert Res.* 34, 590–596. doi:10.7522/j.issn.1000-694X.2013.00352
- Ouyang, Z. Y., Xu, W. H., and Xiao, Y. (2016). *Ecosystem Patterns, Quality, Services, and Evolution in China*. Beijing: Science Press.
- Piao, S., Fang, J., Ji, W., Guo, Q., Ke, J., and Tao, S. (2004). Variation in a Satellite-Based Vegetation Index in Relation to Climate in China. *J. Veg. Sci.* 15, 219. doi:10.1658/1100-9233(2004)015[0219:viasvi]2.0.co;2
- Právělie, R. (2016). Drylands Extent and Environmental Issues. A Global Approach. *Earth-Science Rev.* 161, 259–278. doi:10.1016/j.earscirev.2016.08.003
- Quinlan, J. R. (1986). Induction of Decision Trees. *Mach. Learn.* 1, 81–106. doi:10.1007/BF00116251
- Sachs, J. D. (2004). Sustainable Development. *Science* 304, 649. doi:10.1126/science.304.5671.649
- Schimel, D. S. (2010). Drylands in the Earth System. *Science* 327, 418–419. doi:10.1126/science.1184946
- Shen, B., Fang, S., and Li, G. (2014). Vegetation Coverage Changes and Their Response to Meteorological Variables from 2000 to 2009 in Naqu, Tibet, China. *Can. J. Remote Sens.* 40, 67–74. doi:10.1080/07038992.2014.917580
- Takemura, T., Nakajima, T., Dubovik, O., Holben, B. N., and Kinne, S. (2002). Single-Scattering Albedo and Radiative Forcing of Various Aerosol Species with a Global Three-Dimensional Model. *J. Clim.* 15, 333–352. doi:10.1175/1520-0442(2002)015<0333:ssaarf>2.0.co;2
- Uno, I., Wang, Z., Chiba, M., Chun, Y. S., Gong, S. L., Hara, Y., et al. (2006). Dust Model Intercomparison (DMIP) Study over Asia: Overview. *J. Geophys. Res.* 111, 212–213. doi:10.1029/2005JD006575
- Wang, F., Pan, X. B., Gerlein-Safdi, C., Cao, X., Wang, S., Gu, L., et al. (2019). Vegetation Restoration in Northern China: A Contrasted Picture. *Land Degrad. Dev.* 4, 15. doi:10.1002/ldr.3314
- Wang, L., Huang, J., Du, Y., Hu, Y., and Han, P. (2013). Dynamic Assessment of Soil Erosion Risk Using Landsat TM and HJ Satellite Data in Danjiangkou Reservoir Area, China. *Remote Sens.* 5, 3826–3848. doi:10.3390/rs083826
- Wang, T. (2003). *Desert and Desertification in China*. Shijiazhuang: Hebei Science and Technology Press.
- Wang, X., Chen, F., Hasi, E., and Li, J. (2008). Desertification in China: An Assessment. *Earth-Science Rev.* 88, 188–206. doi:10.1016/j.earscirev.2008.02.001
- Wang, Z. Y. (2017). China Plan " for Combating Desertification in the World: Analysis of Kubuqi Model (I). *North. Econ.* 12, 4–7.
- World Economic Forum (2020). *The Global Risks Report 2020*. Available at: https://www3.weforum.org/docs/WEF_Global_Risk_Report_2020.pdf January 15, 2020).
- Zastrow, M. (2019). China's Tree-Planting Drive Could Falter in a Warming World. *Nature* 573, 474–475. doi:10.1038/d41586-019-02789-w
- Zhan, Q., Zhao, W., Yang, M., and Xiong, D. (2021). A Long-Term Record (1995–2019) of the Dynamics of Land Desertification in the Middle Reaches of Yarlung Zangbo River Basin Derived from Landsat Data. *Geogr. Sustain.* 2, 12–21. doi:10.1016/j.geosus.2021.01.002
- Zhang, H., Fan, J., Cao, W., Harris, W., Li, Y., Chi, W., et al. (2018). Response of Wind Erosion Dynamics to Climate Change and Human Activity in Inner Mongolia, China during 1990 to 2015. *Sci. Total Environ.* 639, 1038–1050. doi:10.1016/j.scitotenv.2018.05.082
- Zhang, Z., Wang, X., Zhao, X., Liu, B., Yi, L., Zuo, L., et al. (2014). A 2010 Update of National Land Use/Cover Database of China at 1:100000 Scale Using Medium Spatial Resolution Satellite Images. *Remote Sens. Environ.* 149, 142–154. doi:10.1016/j.rse.2014.04.004
- Zhao, M. M., Zhou, L. H., and Wang, S. Y. (2017). Effects of Ecological Policies on Land Use Types and Ecosystem Service Values in Hobq Desert. *Res. Soil Water Conserv.* 24, 252–258. doi:10.13869/j.cnki.rswc.2017.02.041
- Zhao, Y., Chi, W., Kuang, W., Bao, Y., and Ding, G. (2020). Ecological and Environmental Consequences of Ecological Projects in the Beijing-Tianjin Sand Source Region. *Ecol. Indic.* 112, 106111. doi:10.1016/j.ecolind.2020.106111
- Zölch, T., Wamsler, C., and Pauleit, S. (2018). Integrating the Ecosystem-Based Approach into Municipal Climate Adaptation Strategies: the Case of Germany. *J. Clean. Prod.* 170, 966–977. doi:10.1016/j.jclepro.2017.09.146

Conflict of Interest: The authors declare that the research was conducted in the absence of any commercial or financial relationships that could be construed as a potential conflict of interest.

Publisher's Note: All claims expressed in this article are solely those of the authors and do not necessarily represent those of their affiliated organizations, or those of the publisher, the editors, and the reviewers. Any product that may be evaluated in this article, or claim that may be made by its manufacturer, is not guaranteed or endorsed by the publisher.

Copyright © 2022 Dang, Na, Chi, Zhao, Zhao, Wang, Wu and Wang. This is an open-access article distributed under the terms of the Creative Commons Attribution License (CC BY). The use, distribution or reproduction in other forums is permitted, provided the original author(s) and the copyright owner(s) are credited and that the original publication in this journal is cited, in accordance with accepted academic practice. No use, distribution or reproduction is permitted which does not comply with these terms.



Characteristics of Canopy Conductance and Environmental Driving Mechanism in Three Monsoon Climate Regions of China

Rui-Qiao Wu^{1,2,3}, Jian-Bo Jia^{1,2,3*}, Wen-De Yan^{1,2,3*}, Lei Hu^{1,2,3}, Yi-Fan Wang^{1,2,3} and Yu Chen¹

¹Central South University of Forestry and Technology, Changsha, China, ²Hunan Lutou Forest Ecosystem National Positioning Observation and Research Station, Yueyang, China, ³National Engineering Laboratory of Forestry Ecological Application Technology in Southern China, Changsha, China

OPEN ACCESS

Edited by:

Jifeng Deng,
Shenyang Agricultural University,
China

Reviewed by:

Wenping Deng,
Jiangxi Agricultural University, China
Guodong Jia,
Beijing Forestry University, China

*Correspondence:

Jian-Bo Jia
jjiajianbo@csuft.edu.cn
Wen-De Yan
csfuywd@hotmail.com

Specialty section:

This article was submitted to
Drylands,
a section of the journal
Frontiers in Environmental Science

Received: 04 May 2022

Accepted: 30 May 2022

Published: 11 July 2022

Citation:

Wu R-Q, Jia J-B, Yan W-D, Hu L,
Wang Y-F and Chen Y (2022)
Characteristics of Canopy
Conductance and Environmental
Driving Mechanism in Three Monsoon
Climate Regions of China.
Front. Environ. Sci. 10:935926.
doi: 10.3389/fenvs.2022.935926

Canopy conductance was an important index to measure the process of water exchange between canopy and atmosphere interface of forest ecosystem, as well as to judge the status of water use or the degree of drought stress. Therefore, the accurate estimation of forest canopy conductance was of great significance for the research of water-use efficiency. In the past, canopy conductance was measured on vegetation types in a single-point region, but there were few studies on systematic comparison in different climate zones. Based on the data sets of EC flux and conventional meteorological elements from the eddy covariance (EC) flux observation station during 2003–2010 in three typical climate zones (temperate continental monsoon climate zone, south subtropical monsoon climate zone, and mid-subtropical monsoon climate zone), Penman-Monteith model was used to calculate forest canopy conductance in different climate regions and analyze the dynamic changes of canopy conductance in different time scales. At the same time, combined with environmental factors including temperature, net radiation, soil water content, and vapor pressure deficit to explore their driving ability on the canopy conductivity of forest ecosystem in different climate regions, we finally explored the mechanism driving the canopy conductivity of forest ecosystem under different climates. The results showed that: 1) the driving ability of environmental factors in different climate regions to the canopy conductance was different, and the contribution rate of soil water content to the canopy conductance in subtropical monsoon climate zone was the largest. It was 36.01%, and the contribution rate of vapor pressure deficit to the canopy conductance in mid-subtropical monsoon climate region was the largest. It was 29.4% and the contribution rate of temperature to the canopy conductance in temperate monsoon climate region was the largest; it was 28.14%. 2). Temperature was an important factor limiting and driving canopy conductance, and there was a synergistic effect between water and temperature, which jointly drove the change in canopy conductance. 3) Environmental factors in different climate regions had threshold for the synergistic driving effect of canopy conductance. When the factors were within the appropriate threshold, the factors had a strong promoting effect on canopy conductance.

Keywords: canopy conductivity, Penman-Monteith model, driving mechanism, environmental factors, monsoon climate zones

1 INTRODUCTION

1.1 Overview of Canopy Conductance

Canopy was the core place of water vapor exchange between plant and atmosphere in soil-plant-atmosphere continuum (SPAC) (Evaristo et al., 2015), and the canopy-atmospheric water vapor output process could be divided into canopy water vapor export process and near-leaf turbulent water vapor output process. In the process of canopy water vapor output, the resistance of water vapor inside the canopy when it diffused outward through the stomatal layer and boundary layer is called canopy resistance, which was usually quantified by canopy conductivity (Wang et al., 2021). Canopy conductance as an indicator of stomatal regulation at ecosystem scale had been widely concerned (De Boer et al., 2011; Deng and Ding, 2015; Bai et al., 2017), and dynamic changes reflected stomatal behavior and water regulation mode of plants, which was the overall index of material and energy exchange in the plant canopy (Hu et al., 2019), and had been widely used in the study of plant stomatal behavior regulation (Chen et al., 2021).

1.2 Effects of Environmental Factors on Canopy Conductance at Different Scales

Canopy conductance was easily affected by different environmental conditions which was an important biological factor indicating the response of ecosystem to environmental factors (Igarashi et al., 2015). Changes in canopy conductance and control mechanisms had been applied to different ecosystems, such as poplar plantations (Song et al., 2021), tropical rainforest (Yoshifuji et al., 2020), farmland shelterbelt (Fu et al., 2016), and temperate deciduous forests (Wehr et al., 2017) conduct research. In addition to tree species, the reason for the difference in canopy conductance was that the regional environment also played a particularly important role in driving the change in canopy conductance (Saito et al., 2017). It was found that canopy conductance had different responses to the changes of vapor pressure deficit (VPD), net radiation (Rn), air temperature (T), and soil water content (SWC) at different scales (Komatsu et al., 2012). In addition to tree species, the cause may be related to regional environment (Saito et al., 2017). On long time scales, soil moisture was an important factor affecting canopy conductance. Soil water content was the controller of canopy conductance on both seasonal and interannual scales (Harris et al., 2004). When soil moisture was higher, stomatal sensitivity to various environmental factors was relatively small, and canopy stomatal conductance was high (Kumagai et al., 2008). When soil water was subjected to drought stress, with the increase of stress degree, stomatal sensitivity to vapor pressure deficit and solar radiation increases, and canopy conductance was inhibited (Mo et al., 2014). Therefore, by exploring the change in canopy conductance, we can judge the soil water status or the degree of drought stress, which played an important role in the forest ecosystem to better adapt to the changing environmental conditions under global climate change (Richardson et al., 2013). On the daily scale, vapor pressure deficit was the main dominant factor in environmental variables (Pataki et al., 1998.) As an important factor affecting canopy conductance, vapor pressure deficit can significantly affect the sensitivity of stomatal conductance to transpiration, photosynthesis, and other physiological processes,

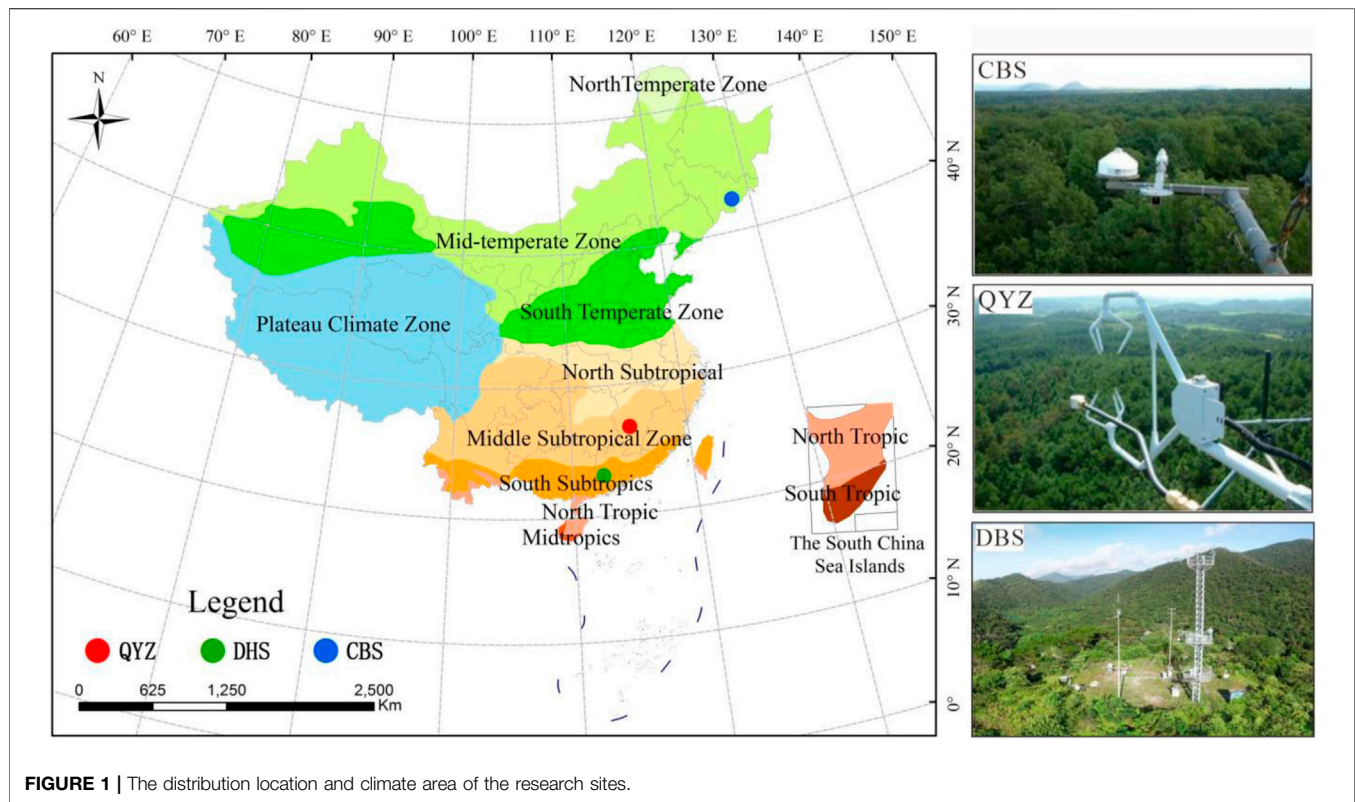
and had an important impact on evapotranspiration and water-use efficiency of forest ecosystems (Wang et al., 2016; Rodriguez-Dominguez et al., 2019). At high vapor pressure deficit, stomatal conductance decreased and transpiration increased in most species (Grossiord et al., 2020). Radiation was another important factor that regulates the canopy conductance. Increasing solar radiation could induce pore opening to some extent, resulting in increased tree transpiration, while under high solar radiation, pores were partially closed, causing reduced stomatal conductance (Martin et al., 1997; She et al., 2013). In addition, studies have found that high temperatures can lead to lower stomatal conductivity in the tree canopy (Gillner et al., 2017). It was found that temperature more often regulates canopy conductance on seasonal and interannual scales (Yoshida et al., 2010). Therefore, it is crucial to explore the response of canopy conductance to environmental factors at different time scales to better understand the adaptation of ecosystems to climate change. Although there were many studies on canopy conductance of different vegetation types, there were few studies on the characteristics of canopy conductance in the macro perspective, such as the climate areas where different vegetation types were located, and there were few studies on the relative contribution rate of various environmental factors driving the change in canopy stomatal conductance and the impact on the change process of canopy stomatal conductance in different thresholds.

1.3 Study Area Selection

Exploring the changes of canopy stomatal conductivity and its response to environmental variables under different environmental conditions not only could deepen the understanding of the environmental control mechanism of plant stomatal behavior but also be of great significance to judge the water-use relationship of plants and select the stomatal regulation mode of tree species. To achieve this goal, long-term observations were indispensable. The National Changbai Mountain temperate mixed forest (CBS), Qianyanzhou subtropical plantation conifer (QYZ), and Dinghushan subtropical mixed forest (DHS) Critical Zone Observatory were distributed in the main forest areas and climate zones in China; the three sites located in different climate zones were all located in eastern China and belong to the monsoon climate zone, and the hydrothermal conditions had obvious latitudinal gradient characteristics from north to south. Therefore, the selection of these three climate stations could form a fully representative long-term forest flux observation network in the monsoon climate region of eastern China.

1.4 Aims and Objectives

This study was based on the carbon water flux and conventional meteorological element observation dataset of flux observation station from 2003 to 2010 (Wu et al., 2021; Li et al., 2021; Dai et al., 2021). Combined with environmental factors such as temperature (T), net radiation (Rn), soil water content (SWC), and vapor pressure deficit (VPD), we explored the variation characteristics of canopy conductance in different climate regions on different time scales and correlation with various environmental factors, and quantitatively analyzed the contribution of



environmental factors in different climate regions to canopy conductance variation and forest water vapor exchange.

The aim of this study was to explore the main controlling factors of canopy conductance change in forest ecosystem in different climate areas, and reveal the environmental driving mechanism of canopy conductance change of forest ecosystem in different climate areas.

The results of our study will hopefully provide a theoretical basis for the study of water and heat exchange in forest ecosystems in different monsoon climate regions in eastern part of China.

2 MATERIALS AND METHODS

2.1 Study Area

The distribution, location, and climate area of the research sites are shown in **Figure 1**. The data of China's climate zoning came from the resource and environmental science and data center of the Chinese Academy of Sciences. Dinghushan National Nature Reserve (23°09'21"N–23°11'30"N, 112°30'39"E–112°33'41"E) was located in Dinghu District, Zhaoqing City, Guangdong Province, with an altitude of 100–700 m. The region has south subtropical monsoon climate (Li et al., 2021). The vegetation was mainly subtropical zonal vegetation, which was abundant on the Tropic of Cancer, mainly composed of *Castanopsis chinensis*, *Schinus molle*, *Cryptocarya chinensis*, and other communities (Li et al., 2021). The eddy covariance (EC) flux observation system of Qianyanzhou (115°04'E, 26°43'N) is located at Qianyanzhou Station, Guanxi Town, Taihe County, Jiangxi Province, with an average altitude of

110.8 m. The station area has subtropical monsoon climate (Xu et al., 2021). The station area belongs to the subtropical evergreen broad-leaved forest area. The existing forests were mainly artificial forests built around 1985, and the main tree species were *Pinus Massoniana*, *P. elliottii*, and *Cunninghamia Lanceolata* (Wen et al., 2005). Changbai Mountain Nature Reserve is located in the southeast of Jilin Province (41°41'49"N–42°25'18"N, 127°42'5"E–128°16'48"E). It belongs to temperate continental monsoon climate, with distinct seasonal alternations (Wang et al., 2016). The temperate broad-leaved Korean pine forest in Changbai Mountain is the main part of mountain forest system in northeast China (Wang et al., 2016).

2.2 Data Observation and Processing

2.2.1 Observation of Eddy Covariance Flux and Micrometeorological Elements

Each platform was equipped with micro meteorological observation tower and open eddy covariance (EC) flux observation system (OPEC). A set of microclimate gradient observation system was installed on the observation tower to simultaneously observe conventional meteorological elements such as wind speed, temperature, humidity, precipitation, light, and effective radiation, as well as CO₂ and water and heat flux at the canopy–atmosphere interface. The main observation devices were vorticity correlation system by ultrasonic anemometer and OPEC system by ultrasonic anemometer (CAST3, Campbell Scientific Inc., Logan, Utah, United States), and open-loop CO₂/H₂O infrared gas analyzer (Li7500, Licor Inc., Lincoln, Nebraska) was used to measure three-dimensional wind speed and CO₂/H₂O concentration pulse

TABLE 1 | Basic information of site.

Site	Dinghushan	Qianyanzhou	Changbai Mountain
Geographical coordinates	23°09'21"–23°11'30"N, 112°30'39"–112°33'41"E	115°04'E, 26°43'N	41°41'49"–42°25'18"N, 127°42'5"–128°16'48"E
Altitude/m	100	110.8	738
Climate type	South subtropical monsoon climate	Mid-subtropical monsoon climate	Temperate continental monsoon climate
Annual average temperature/°C	22.5	17.9	3.6
Average annual precipitation/mm	1714	1489	695
Vegetation types	Coniferous and broad-leaved mixed forest	Artificial coniferous forest	Temperate primitive coniferous broad-leaved mixed forest
Soil type	Latosolic red	Red earth	Mountain dark brown soil
Dominant species	<i>Schima superba</i> , <i>Castanopsis chinensis</i> , <i>Pinus Massoniana</i>	<i>Pinus Massoniana</i> , <i>P. Elliottii</i> , and <i>Cunninghamia Lanceolata</i>	<i>Tiliaamurensis</i> , <i>Pinus koraiensis</i> , <i>Fraxinus mandshurica</i> , <i>Quercus mongolica</i>

(Alistair et al., 2017), sensible/latent heat flux (Li-7500A, Li-COR), air temperature, relative humidity (HMP45C, VAISALA, Finlang), and wind speed WS (A100R, Campbell, United States), effective radiation (Li-190SB, Licor), soil water content (CS615-L, Campbell Scientific Inc., Logan, Utah, United States), and air temperature/humidity (HMP45C, CR23X, Campbell) (Wu et al., 2021; Li et al., 2021; Dai et al., 2021).

2.2.2 The Data Collection

The flux observation data used in this paper were from the continuous flux observation data of three EC flux observation stations (DHS, QYZ, CBS) in recent 8 years (2003–2010) of China terrestrial ecosystem flux observation network (ChinaFLUX). The flux station adopts a unified open circuit vorticity correlation system and observation technology to observe the fluxes of CO₂, water and energy between vegetation and atmosphere for a long time. In order to ensure better comparability between ecosystem carbon exchange data obtained by different observation stations, instruments, data collectors, and data storage formats of vorticity-related systems at all flux observation stations of ChinaFLUX adopt unified standards (Yu et al., 2006). The dataset was downloaded from the National Science and Technology Basic Conditions Platform - National Ecological Science Data Center (<http://www.nesdc.org.cn>), and for a small number of missing records, linear interpolation or the correlation between meteorological elements and the internal relationship of physical quantities were used for interpolation. **Table 1** provides the basic information of each research and observation station.

2.3 Calculation of Vapor Pressure Deficit

Vapor pressure deficit (VPD/kPa) refers to the difference between the saturated vapor pressure and the actual vapor pressure at a certain air temperature (Yu et al., 2006). It is one of the important driving factors of evapotranspiration and one of the most important climatic factors for simulating plant water and carbon fluxes in ecological models. VPD could be estimated from atmospheric relative humidity (RH/%) temperature (T/°C) (Endler et al., 1999).

Calculation formula:

$$VPD = 0.611 \times e^{\frac{17.27 \times T_a}{T_a + 237.3}} \times \left(1 - \frac{RH}{100}\right) \quad (1)$$

2.4 Calculation of the Aerodynamic Resistance

Aerodynamic resistance was caused by the turbulent motion in the turbulent layer above the canopy, which was regarded as the irregular fluctuation motion of an independent vortex. The aerodynamic conductivity could be calculated according to Monin–Obukov formula (Granier et al., 2000).

$$g_a = \frac{k^2 \cdot u}{\left[\frac{\ln(z-d)}{z_0}\right]^2} \quad (2)$$

Z₀ is the surface roughness (about 0.1 h, h was forest average tree height), d is the zero plane displacement (about 0.75 h); K is the von Karman's constant (0.4) and u (m/s) is the wind speed at height Z (m).

2.5 Calculation of Canopy Conductance

In the flux tower, vorticity correlation technology was used to measure latent and sensible heat fluxes of the two stands, and instruments were installed for meteorological observation, including air temperature (Ta/°C), relative humidity (RH/%). H is the sensible heat flux (W/M²), and λE is the latent heat flux (W/M²).

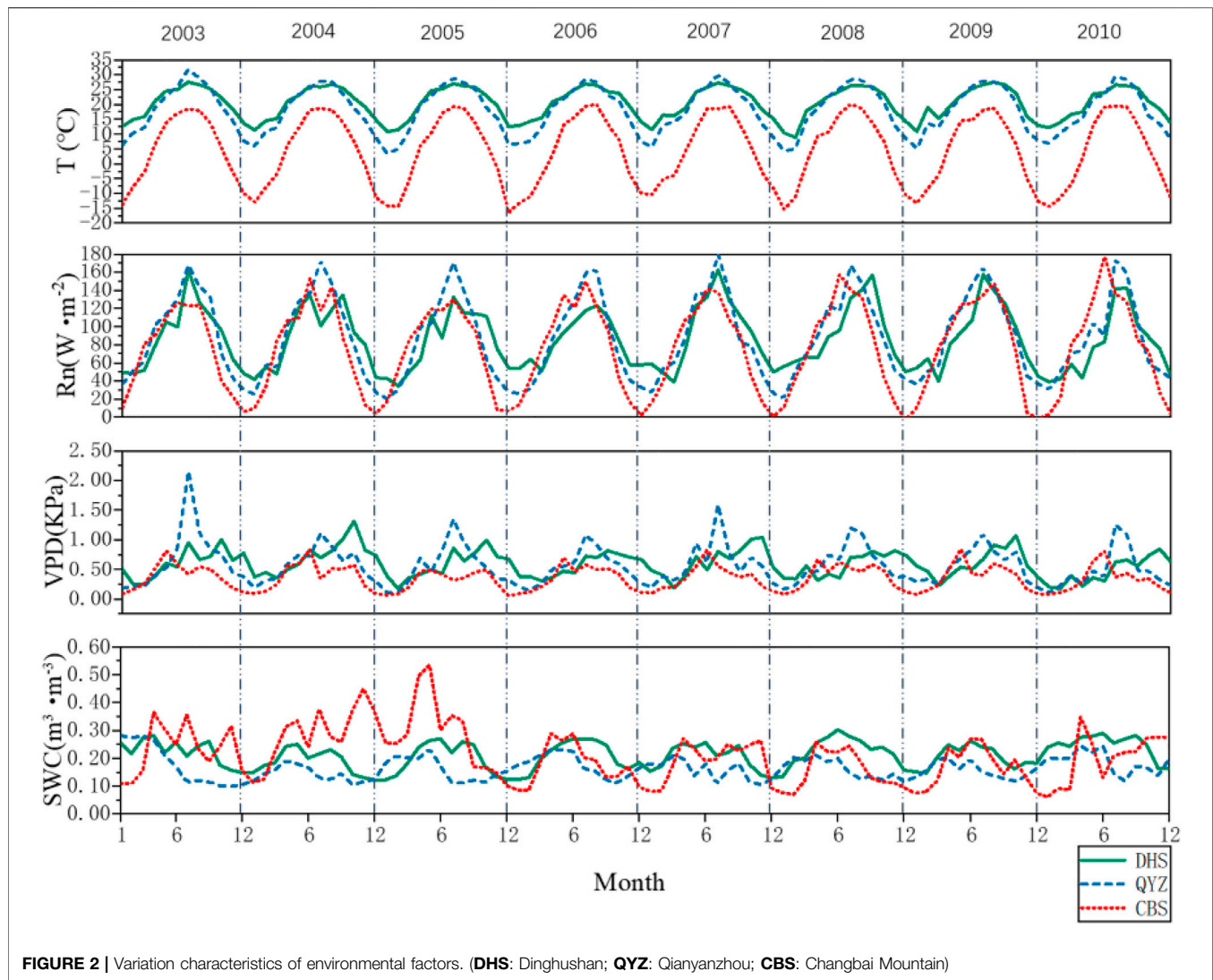
The canopy conductivity g_s (mm/s) was calculated using Penman–Monteith equations (Xu et al., 2018):

$$g_s = \left(\frac{\Delta}{\gamma} \cdot \frac{H}{\lambda E} - 1\right) g_a + \frac{\rho C_p}{\gamma} \cdot \frac{VPD}{\lambda E} \quad (3)$$

Δ is the function slope of saturated vapor pressure and temperature (Pa/K); C_p is the specific heat of dry air at constant pressure (J/(kgK)) and the value in this study was 1,005; γ is the dry and wet gauge constant (Pa/K); and the value in this study was 0.067; VPD is the vapor pressure deficit (kPa); ρ is the air density (kg/m³); H and λE are sensible heat flux and latent heat flux (W/m²) calculated by vorticity covariance method; g_a is the aerodynamic resistance (m/s).

2.6 The Data Analysis

Based on the calculated canopy conductance, this study analyzes the changes in canopy conductance in different

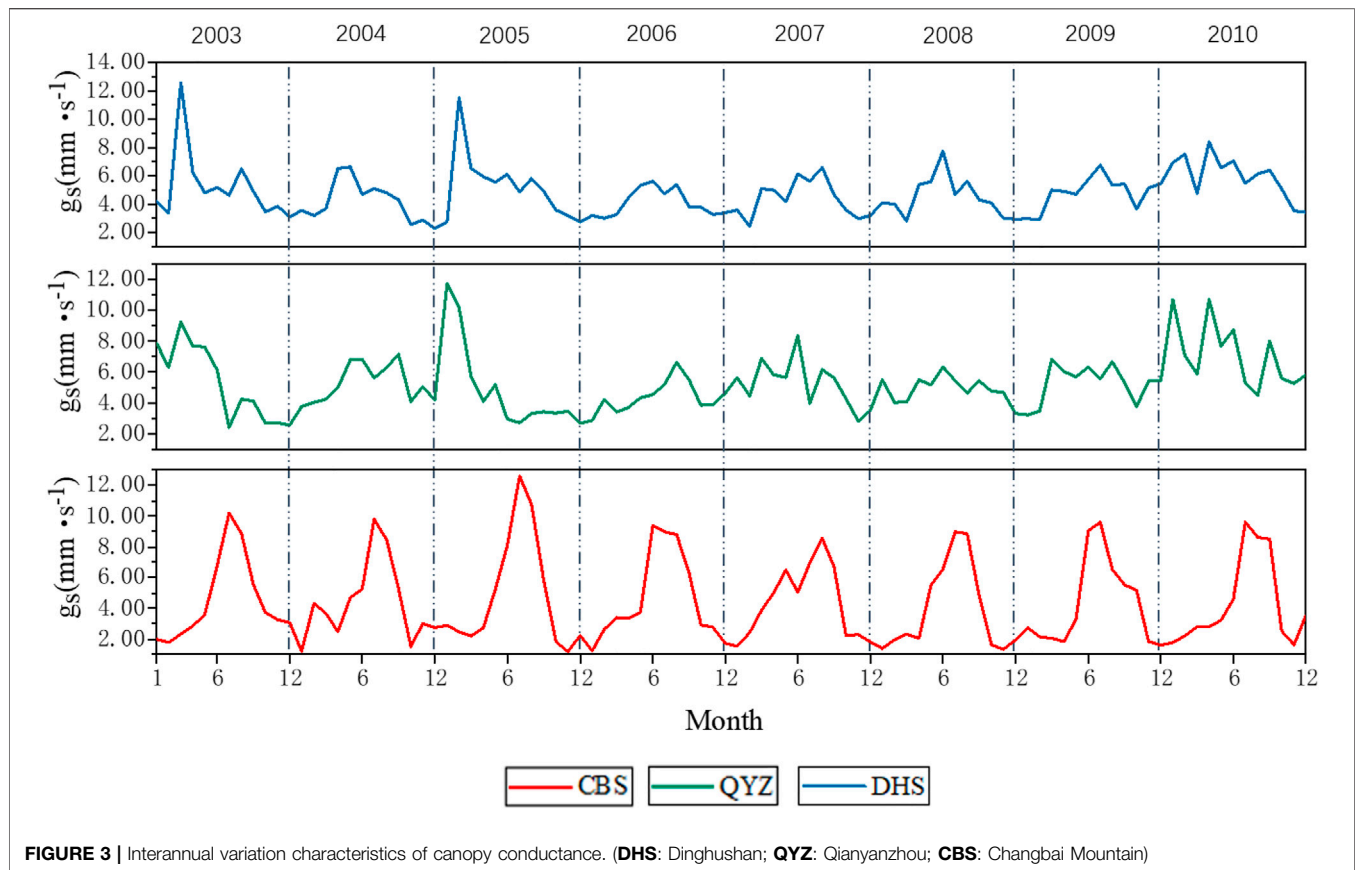


climate regions on different time scales, combined with environmental factors such as temperature, net radiation, soil water content, and vapor pressure deficit. SPSS Statistics 23 was used to analyze the correlation between canopy conductance change and environmental factors in different climate regions. OriginPro2018 software (OriginLab, Northampton, MA, United States) was used to fit the generalized linear regression, logarithm, and logical model of canopy conductance to each factor. Finally, the well-fitting function with higher value and lower *p*-value was selected, and the contribution rate of each factor to driving canopy conductance was calculated. In this study, we used the factor contribution rate to clarify the driving ability of environmental factors on canopy conductance, and quantitatively analyzed the contribution of environmental factors in different climate regions to the change of forest ecosystem canopy conductance and forest carbon and water exchange.

3 RESULTS

3.1 Characteristics of Meteorological Factors

The interannual variation characteristics of environmental factors in different climate zones are shown in **Figure 2**. As can be seen from the figure, canopy temperature has a parabolic seasonal characteristics with an obvious peak value. The temperature rises gradually from growing season every year, reaches the maximum in June to July, and then in non-growing season begins to decline. The temperature of Dinghushan was higher than Qianyanzhou and Changbai Mountain. The temperature of Changbai Mountain was lower. The highest temperature appeared in July 2008, and the temperature was 20.1°C, and the temperature fluctuates greatly. Net radiation had a similar trend with temperature, and net radiation in temperate climate zone was significantly lower than that in Subtropical climate zone, which accorded



with the law of latitudinal gradient hydrothermal change. In the non-growing season, the change and the value were small, and reached the maximum value in summer, but Dinghushan had a lag response to this, and the variation of soil bulk water content also had obvious seasonality, which varies with the change of precipitation with a small range. However, there were also seasonal droughts with mismatched rainfall and temperature, resulting in low soil water content.

3.2 Characteristics of Canopy Conductance in Different Climate Zones

3.2.1 Variation Characteristics of Canopy Conductance

There were significant differences in the interannual variation characteristics of canopy conductance in different climate types, which reflected the response of canopy conductance to environmental factors in different climate regions. As shown in **Figure 3**, on the whole, the seasonal variation of subtropical canopy conductance was obvious, reaching the peak in spring and the minimum in winter. In 2003 and 2007, the seasonal variation pattern of canopy conductance in Qianyanzhou did not follow the general law, and decreased in July. The vegetation phenology and climate conditions with four distinct seasons of Changbai Mountain area made the canopy conductance of temperate coniferous and broad-leaved mixed forest ecosystem in Changbai Mountain and showed

obvious seasonal changes. The peak value of canopy conductance in Changbai Mountain was from July to August, and the change in canopy conductance was more active in summer, followed by spring and autumn, and the weakest in winter.

3.2.2 Characteristics of Monthly Canopy Conductance

The variation in average monthly canopy conductance in different climatic regions is shown in **Figure 4**, which shows that the canopy conductance value increased gradually from May to September, while it decreased gradually from October to next April. However, in the subtropical climate area, the canopy conductance did not reach the peak in July, and the value of canopy conductance was small. The variation dynamics of canopy conductance in Changbai Mountain was consistent with the seasonal variation and the variation trend of meteorological factors. Specifically, the canopy conductance began to increase gradually in spring, and it showed that the canopy conductance gradually increases in spring, fluctuates, and then decreases after reaching the maximum in summer, and returns to a lower level in winter. The mean variance of monthly canopy conductance was small and the change was stable, that is, the coupling degree between the change of canopy conductance and the change of environmental factors was high in temperate monsoon climate area. However, the subtropical monsoon climate region showed an obvious changing trend similar to but not

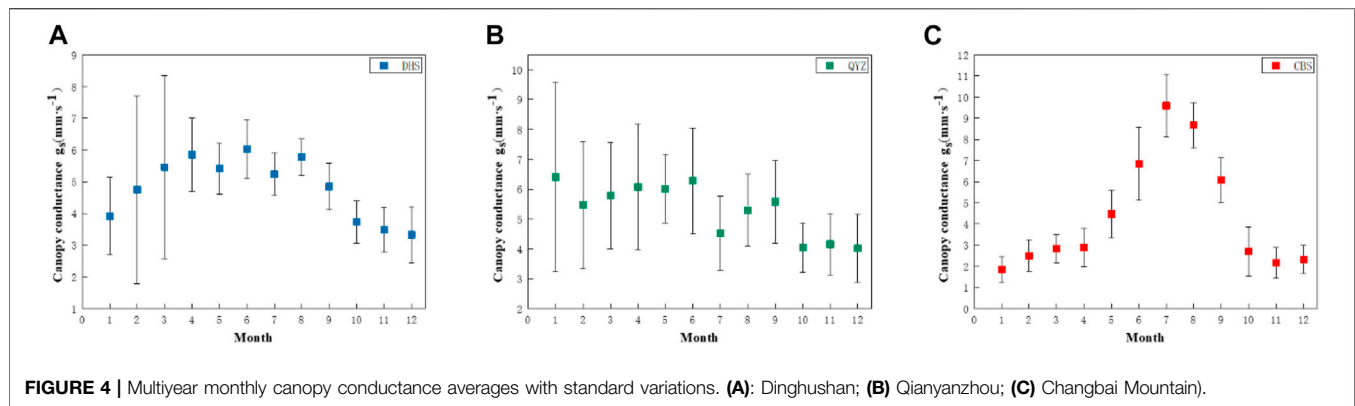


FIGURE 4 | Multiyear monthly canopy conductance averages with standard variations. **(A):** Dinghushan; **(B)** Qianyanzhou; **(C)** Changbai Mountain.

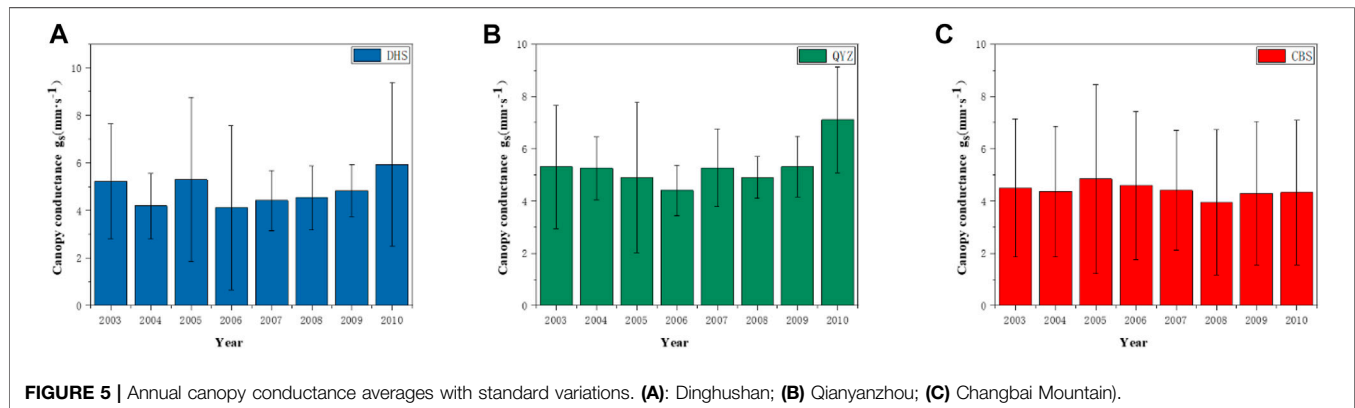


FIGURE 5 | Annual canopy conductance averages with standard variations. **(A):** Dinghushan; **(B)** Qianyanzhou; **(C)** Changbai Mountain.

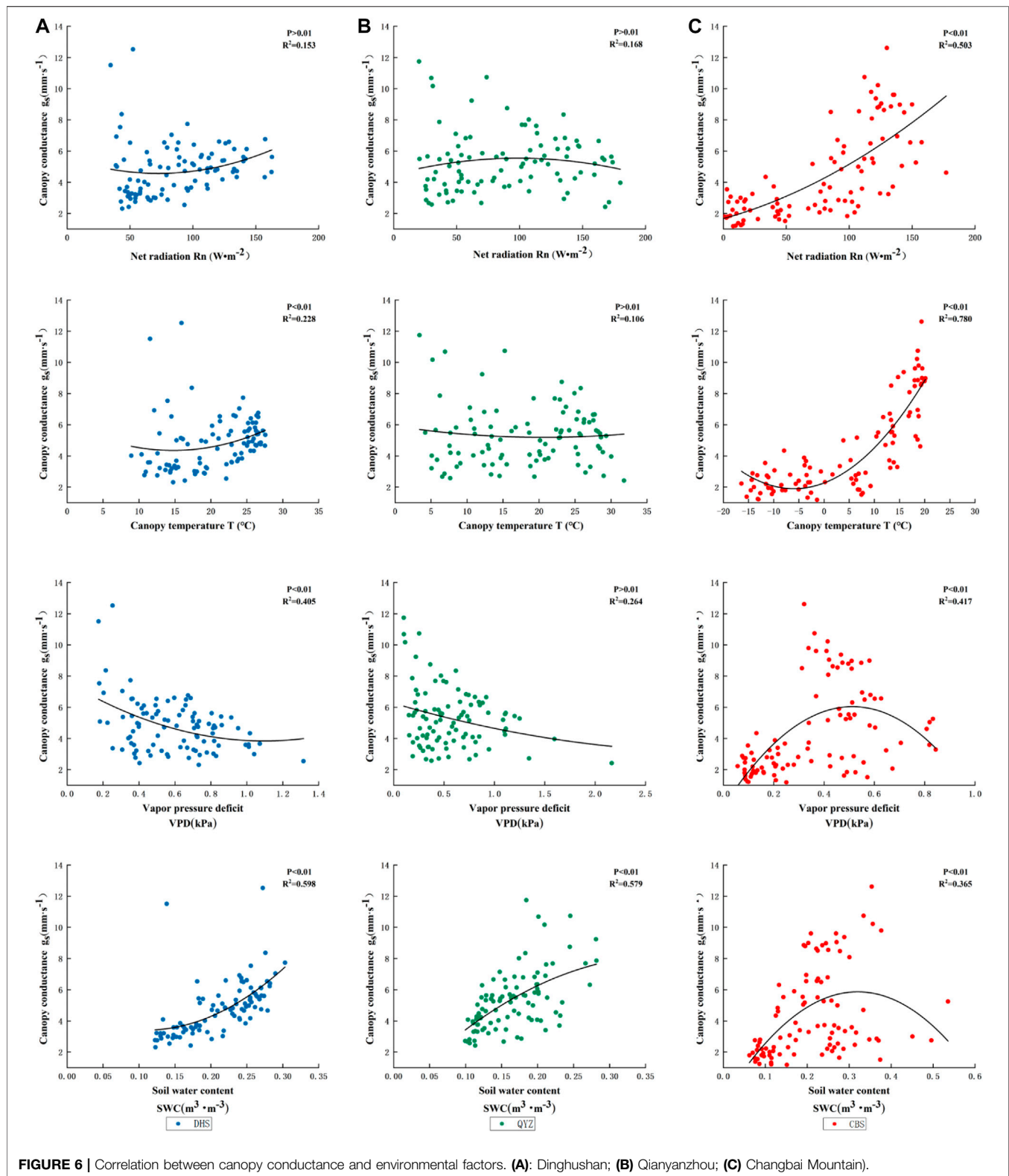
completely corresponding to the seasonal change, which was also related to the seasonal growth change of leaves and the influence of forest's underlying surface. The variation degree of the average value of monthly canopy conductance in the subtropical monsoon climate region was also high, especially in Qianyanzhou, and the trend showed a fluctuating decline.

3.2.3 Characteristics of Annual Canopy Conductance

In the variation of annual average canopy conductance (Figure 5), the annual average canopy conductance in subtropical monsoon climate area was higher than that in the temperate monsoon climate area. The average canopy conductance of Dinghushan was 4.82 mm/s^{-1} , that of Qianyanzhou was 5.3 mm/s^{-1} , and that of Changbai Mountain was 4.41 mm/s^{-1} . The variation rate of interannual canopy conductance in subtropical zone was also higher than that in temperate monsoon zone, and the interannual variability of canopy conductance in Dinghushan, Qianyanzhou, and Changbai Mountain was 12.24, 13.94, and 5.51%, respectively. The average annual variation of canopy conductance increases with passing years on the whole. Global warming may lead to an overall trend of temperature rise. Climate change will affect forest canopy transpiration and increase the transpiration rate of forest ecosystem.

3.3 Correlation Analysis Between Canopy Conductance and Environmental Factors

Correlation analysis was conducted between canopy conductance values and environmental factors such as temperature (T_a), net radiation (R_n), vapor pressure deficit (VPD), and soil water content (SWC) (as shown in Figure 6) in different climate zones. The results showed that net radiation and temperature had different responses to canopy conductance in different climate regions. Although the change of canopy conductance in subtropical monsoon climate region had a positive correlation with the response of net radiation and temperature, the correlation coefficient was small. The response of a single factor to canopy conductance was weakened, and in 2003, 2004, and 2006, the change in canopy conductance was inconsistent with the changing trend of net radiation and temperature. They decreased with the increase in net radiation. Similarly, the temperature also had such a changing trend. In the temperate monsoon climate area, the canopy conductance increased with the increase of net radiation and temperature, and there was a significant correlation between it and the change of canopy conductance, R^2 was 0.715 and 0.780. Therefore, the change of canopy conductance in the temperate monsoon climate was sensitive to the change of temperature and net radiation, that is, net radiation and temperature play an important role in the change of forest canopy conductance in the temperate monsoon climate area.



The canopy conductance also had a strong correlation with the vapor pressure deficit, and the canopy conductance of subtropical forest also decreased with the increase in vapor pressure deficit.

Therefore, the vapor pressure deficit was an important factor affecting the change in subtropical canopy conductance. R^2 of Dinghushan, Qianyanzhou, and Changbai Mountain were 0.405,

0.264, and 0.417, respectively, $p < 0.01$, while in Changbai Mountain, under the obvious climate conditions of hydrothermal synchronization, when the vapor pressure deficit was low, with the increase in temperature and the increase in vapor pressure in the substomatal cavity, water escaped from the plant leaves, strengthened the transpiration rate, and increased the canopy conductance. When the vapor pressure deficit was higher than 0.5 kPa, the canopy conductance decreased gradually.

Soil water content was a physical quantity indicating the degree of soil dryness and wetness in a certain depth of soil layer, and soil humidity determines the water supply of vegetation. Canopy conductance in different climatic areas was more sensitive to soil water content, R^2 was 0.598, 0.579, and 0.365, $p < 0.01$. With the increase of soil water content, the canopy conductance in subtropical monsoon climate area obviously increased in logarithmic function. The influence of the change of soil water content in Changbai Mountain on canopy conductance was different from that in subtropical monsoon area. The change of soil water content in Changbai Mountain had a certain threshold. When the soil water content was lower than 0.3, the canopy conductance increased with the increase in water content, but when the soil water content was higher than 0.3, the canopy conductance decreased gradually with the increase in water content.

3.4 Driving Ability of Environmental Factors to Canopy Conductance Change

3.4.1 Estimation of Contribution Rate of Environmental Factors to Canopy Conductance Change

In order to deeply study the driving force of various environmental factors on canopy conductance under different climate types, this study used the factor contribution rate to clarify the driving ability of environmental factors on canopy conductance. The contribution rate of various environmental factors of different climate types to driving the change of canopy conductance is shown in **Figure 7**. The factor with the strongest driving force of Dinghushan environmental factors on canopy conductance was soil water content, with a contribution rate of 36.01%, followed by temperature. In terms of net radiation and vapor pressure deficit, the strongest driving force of Qianyanzhou environmental factors on canopy conductance was vapor pressure deficit, with a contribution rate of 29.4%, followed by temperature, net radiation, and soil water content. The strongest driving factor of environmental factors on canopy conductance in Changbai Mountain was temperature, with a contribution rate of 28.14%, followed by net radiation, vapor pressure deficit, and soil water content, that is, soil water content was the first driving factor of canopy conductance change in subtropical monsoon climate area, and vapor pressure deficit was the first driving factor of canopy conductance change in subtropical monsoon climate area, The first driving factor of canopy conductance change in temperate monsoon climate area was temperature.

3.4.2 Synergistic Driving Effect Among Environmental Factors

The driving effect of various factors on canopy conductance was not invariable, and the change in canopy conductance was not only driven by a single factor but also driven by other factors. Therefore, we selected the environmental factors with the highest and second highest contribution rate to the change in canopy conductance in different climate regions, and conducted a three-dimensional two-factor analysis (as shown in **Figure 8**) to explore the synergistic driving ability of factors in different climate regions on the change in canopy conductance. In this study, when the canopy conductance value in the climate area was greater than 4 mm s^{-1} , it indicated that the canopy conductance was high.

Soil water content was the factor driving the change in canopy conductance in the South subtropical monsoon climate zone, and temperature was the factor contributing the second; when soil water content was $0.12\text{--}0.3 \text{ m}^3 \text{ m}^{-3}$, and the temperature was $13\text{--}24^\circ\text{C}$, it had a strong synergistic driving effect on the canopy conductance in the south subtropical monsoon climate zone. However, with the increase in water content and temperature, the canopy conductance increased. When the temperature was too low, plants would be subjected to low-temperature stress and the canopy conductance decreased.

Vapor pressure deficit is the environmental factor with the largest driving contribution to the change in canopy conductance in the mid-subtropical monsoon climate area, and there was a significant negative correlation between it and the change of canopy conductance. The vapor pressure deficit will affect the opening of stomata and the change of canopy conductance. Compared with the south subtropical climate area, the suitable threshold of tree species for temperature was wide in the mid-subtropical climate area, and the suitable temperature threshold was $5\text{--}28^\circ\text{C}$. With the increase in temperature, the canopy conductance increased, but when the temperature exceeded the threshold range, it had a strong inhibitory effect on the canopy conductance, and the canopy conductance value was low. Therefore, when the vapor pressure deficit was $0.2\text{--}1.5 \text{ kPa}$ and the temperature was $5\text{--}28^\circ\text{C}$, it had a strong synergistic driving effect on the canopy conductance in the mid-subtropical monsoon climate area.

Temperature contributed greatly to driving changes of canopy conductance in monsoon climate region. Changbai Mountain belongs to the temperate monsoon climate zone, and the heat conditions on the canopy conductance change driving effect was greater than the water condition, and the optimum temperature range was narrow and for $5\text{--}20^\circ\text{C}$, the suitable threshold of net radiation was $80\text{--}180 \text{ W m}^{-2}$. To the temperate monsoon climate zone, canopy conductance synergy drive effect was stronger, as with the increase in temperature and net radiation, canopy conductance exponential function to increase, but the different climate zones environmental factors driving action had a certain threshold, when factor in climate zones outside environmental factors suitable threshold value, lower canopy conductance instead. Therefore, temperature in different climatic regions was an important factor limiting and driving canopy conductance, and there was a strong

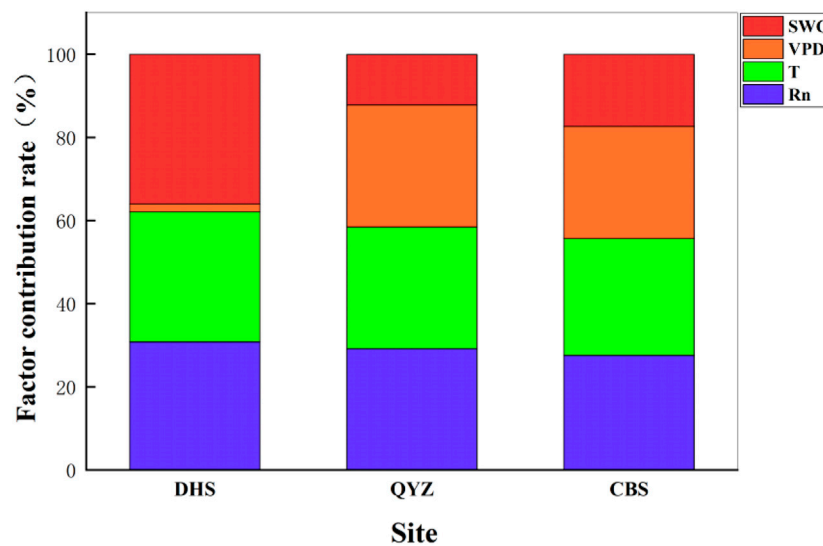


FIGURE 7 | Contribution of different forest environmental factors to canopy conductance change. (DHS: Dinghushan; QYZ: Qianyanzhou; CBS: Changbai Mountain).

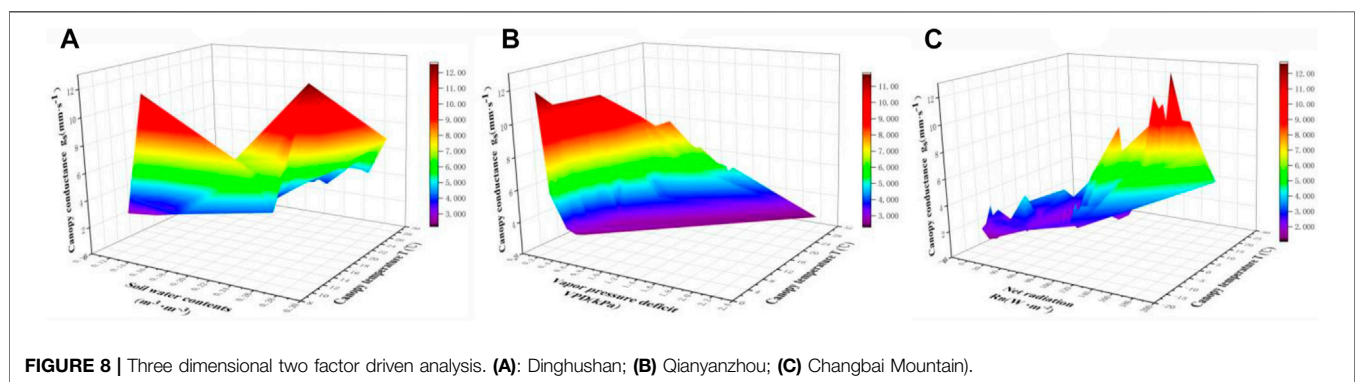


FIGURE 8 | Three dimensional two factor driven analysis. (A): Dinghushan; (B) Qianyanzhou; (C) Changbai Mountain).

synergistic driving effect among the factors, thus jointly affecting the change in canopy conductance.

4 DISCUSSION

4.1 Differences of Canopy Conductance in Different Climatic Regions

There were significant differences in canopy conductance at different time scales in different climatic regions. On the whole, canopy conductance increased gradually in rainy season and decreased gradually in dry season. In the temperate monsoon climate zone, the seasonal variation is obvious, so the change of canopy conductance also conforms to the trend of gradually increasing from spring, fluctuating and decreasing after reaching the maximum in summer, and finally recovering to a lower level in winter. However, the subtropical regions of China had abundant annual rainfall but frequent seasonal droughts (Xu et al., 2021). In summer,

high temperature and insufficient precipitation result in mismatch between rainfall and temperature, and seasonal droughts often occur. If drought stress occurs, for example, when Qianyanzhou drought occurred in summer (2003 and 2007), the seasonal pattern of canopy conductance did not follow the general law and decreased in July, which is consistent with the results obtained by M. Xu et al. (Xu et al., 2021). If the seasonal rainfall decreases, the leaf stomata will close, and the transpiration rate will show a downward trend, that is, the stomata tended to close under water stress, resulting in the decrease of canopy conductance. The peak value of canopy conductance in Changbai Mountain was generally from July to August, which is consistent with the research results of Xiaofei Lu's study (Lu, 2018). When the temperature increased, the increase of the vapor pressure in the lower stomatal cavity was greater than that of the air vapor pressure, so the increase of the vapor pressure deficit marked the water escape in the leaves of plants and strengthened the transpiration rate.

The canopy conductance in different climatic regions had an overall trend of increasing with the passing of the year on the annual scale, which was related to the overall rising trend of global warming temperature. Climate change will affect the canopy transpiration of forest ecosystem and increase the plant transpiration rate. Compared with the temperate monsoon climate area, the growth trend of annual average canopy conductance in the subtropical monsoon climate area was more obvious. The three stations in different climate areas were located in the east of China and belong to the monsoon affected area. The hydrothermal conditions had obvious latitudinal gradient characteristics from north to south. Therefore, with the decrease in latitude, the temperature increased and the forest structure was complex, which would affect the plant transpiration rate.

The difference of canopy conductance was also related to the structural characteristics of leaves and xyloids of tree species. The annual canopy conductance of Dinghushan was lower than that of Qianyanzhou, which was also related to the main vegetation of Dinghushan, this being evergreen broad-leaved forest, and the increase in canopy leaf area will hinder air flow, so the canopy conductance will be affected. In Qianyanzhou, coniferous species such as *Masson pine* and *Cunninghamia lanceolata* were the main species, and their stomata were round and large in diameter, while in Dinghushan, there were more broad-leaved species such as *Schima superba* and *Castanea*, and the broad-leaved stomata were slender and small (Zhang et al., 2017). During the day, coniferous forest showed a stronger stomatal sensitivity, and stomatal conductance fluctuated greatly. In addition, the xylem structure of coniferous forest was non-porous wood, which could maintain higher water transport efficiency under high vapor pressure deficit conditions (Peters et al., 2010).

4.2 Correlation Between Canopy Conductance and Environmental Factors

Canopy conductance had a corresponding response to the changes in various environmental factors, and the main driving factors of canopy conductance were different with different vegetation types. For example, in the subtropical monsoon climate zone, the response of canopy conductance to net radiation and temperature was weak, and the change of canopy conductance in 2003, 2004, and 2006 was inconsistent with the changed trend of net radiation and temperature. In case of high-temperature stress, the high-temperature stress will cause photoinhibition, and the transpiration between canopy will be weakened, thus affecting canopy conductance. Or when the net radiation is too strong, leaves lose more water, trees will adjust stomata to maintain their own water, so stomata opening threshold become smaller, the canopy conductance decreases. However, temperature and net radiation were the important factors affecting the change of canopy conductance in the temperate monsoon climate zone, which showed that with the increase in temperature and net radiation, the stomata of vegetation opened to exchange matter and energy, and the canopy conductance increased.

The canopy conductance in subtropical climate area increased significantly as the soil water content increased. In the dry season, less rainfall and low soil humidity will lead to soil drought, less vegetation

water content, weak forest transpiration, and low canopy conductance. However, with the change of seasons and the advent of rainy season, the rainfall increased, the temperature increased, the transpiration became stronger, and the canopy conductance also increased. The temperate monsoon climate region had different response to canopy conductance. Although the rainfall in the subtropical monsoon region was more than temperate monsoon region, the higher temperature in the subtropical region promotes the increase of evaporation. Therefore, the soil water content promoted the increase of canopy conductivity within an appropriate threshold. When the soil water content was more than 0.3, the temperate monsoon climate region will have the phenomenon of soil overwetting due to thermal conditions, and the soil overwetting will reduce the soil aeration, affect the activities of soil microorganisms, inhibit the respiration, growth, and other life activities of vegetation roots, and weaken the transpiration of plants, thus affecting the change of canopy conductance, that is, higher soil water content cannot promote the maintenance of large opening or infinite increase of plant stomatal conductance.

The same was true for the vapor pressure deficit. Vapor pressure deficit was easily affected by hydrothermal conditions. When the vapor pressure deficit was low, with its increases, the vapor pressure in the lower stomatal cavity increased, which made the water escape from the plant leaves, strengthened the transpiration rate, increased the transpiration rate of the forest ecosystem, and the canopy conductance gradually increased. When high temperature stress occurred in summer, the vapor pressure deficit increased, resulting in the closure of some stomata and the decrease of canopy conductance. When high-temperature stress was easy to occur in summer, the vapor pressure deficit increased, resulting in the closure of some stomata, and when the vapor pressure deficit was higher than 0.5, the canopy conductance no longer increased with the increase of the vapor pressure deficit. The vapor pressure deficit was the key factor limiting the opening and closing of pores. Therefore, an appropriate vapor pressure deficit ensured the appropriate threshold of pore opening and maintained a large degree of pore opening to ensure the efficient flow of water vapor.

4.3 Synergistic Driving Effect Among Environmental Factors

In this study, the factor contribution rate was used to clarify the driving ability of environmental factors on canopy conductance in different monsoon climate regions. The results showed that in different climate regions, the driving ability of environmental factors on canopy conductance change was different, but temperature was an important factor limiting and driving canopy conductance, and there was a synergistic effect between water and temperature factors to jointly drive the change of canopy conductance. The driving ability of heat factor on the change of canopy conductance in temperate climate area was greater than that of water factor. There was a synergistic driving effect between temperature and net radiation, which jointly affected the change of canopy conductance. The first factor driving the change of canopy conductance in the South subtropical monsoon climate area was soil water content. There was a significant correlation between the change of canopy conductance and the change of soil water content, and the

synergistic driving effect was obvious. When the value of temperature or soil water content was not within the threshold that was conducive to driving the increase of canopy conductance, as the factor changed, its driving effect on canopy conductance would be inhibited. During the study period, Qianyanzhou was subjected to more drought stress, resulting in increased evapotranspiration and increased vapor pressure deficit. In order to reduce water dissipation, plants will close some stomata and reduce canopy conductance. Therefore, the first factor driving the change of canopy conductance in the mid-subtropical monsoon climate area was vapor pressure deficit; temperature was still a synergistic factor, which drove the change of canopy conductance together. When the temperature was at a threshold favorable to drive the change in canopy conductance, the canopy conductance also increased with increasing temperature. But when the temperature was above or below this threshold, the driving effect of temperature on canopy conductance was suppressed. Therefore, the change of the canopy conductance in each climate area did not depend on only one main factor, but there are significant synergistic driving phenomena among all factors, which jointly affect the change of canopy conductance.

5 CONCLUSIONS

- 1) The driving ability of environmental factors in different climate regions to the canopy conductance was different. The contribution rate of soil water content to the canopy conductance in South subtropical monsoon climate region was the largest, it was 36.01%, and the contribution rate of vapor pressure deficit to the canopy conductance in mid-subtropical monsoon climate region was the largest, and it was 29.4%, and the contribution rate of temperature to the canopy conductance in temperate monsoon climate region was the largest, it being 28.14%.
- 2) For different climate regions, temperature was an important factor limiting and driving canopy conductance, and there was a synergistic effect between moisture and temperature factors to jointly drive the change of canopy conductance. In the south tropical monsoon climate region, the synergistic effect of soil water content and temperature on canopy conductance was stronger. In the mid-subtropical monsoon climate region, vapor pressure deficit and temperature played a synergistic role in driving canopy conductance. In the temperate monsoon climate region, the net radiation and temperature synergistically drove the change of canopy conductance.
- 3) The synergistic driving effects of environmental factors in different climatic regions all had a certain threshold. When the soil water content was $0.12\text{--}0.3\text{ m}^3\text{ m}^{-3}$ and the temperature was $13\text{--}24^\circ\text{C}$, there was a strong positive synergistic driving effect on the canopy conductance in the subtropical monsoon climate zone. In the mid-subtropical monsoon climate zone, when the water vapor pressure deficit was $0.2\text{--}1.5\text{ kPa}$ and the temperature was $5\text{--}28^\circ\text{C}$, there was a strong synergistic driving effect on the canopy conductance,

which showed that the canopy conductance increased with the increase of temperature. When the temperature was $5\text{--}20^\circ\text{C}$ and the net radiation was $80\text{--}180\text{ W}\cdot\text{m}^{-2}$, the temperature and net radiation had a stronger effect on the canopy conductance in the temperate monsoon climate zone.

5.1 Permission to Reuse and Copyright

The author agreed that figures, tables, and images will be published under a Creative Commons CC-BY license and permission must be obtained for use of copyrighted material from other sources (including re-published/adapted/modified/partial figures and images from the internet). It was the responsibility of the authors to acquire the licenses, to follow any citation instructions requested by third-party rights holders, and cover any supplementary charges.

DATA AVAILABILITY STATEMENT

Publicly available datasets were analyzed in this study. These data can be found here: <http://www.cnern.org.cn/>.

AUTHOR CONTRIBUTIONS

R-QW (First Author) contributed to writing the whole manuscript, count the final data and analyze the results, and complete the first draft. J-BJ (Corresponding Author) contributed to conception and design of the study, provided funding support, and supervised project schedule. W-DY (corresponding author) contributed to comment on article structure and content revisions, provided funding support, and supervised the progress of the manuscript. LH contributed to the manuscript and performed the data collation and calculation. Y-FW validated the results of the paper and revised the article. YC performed the statistical analysis and used software to present more intuitive results. All authors agree to be accountable for the content of the work.

FUNDING

This research was funded by the key research and development program in Hunan province (2020NK2022) and Three Gorges Follow-up Project of Ministry of Water Resources (HY110161A0012022).

ACKNOWLEDGMENTS

The authors gratefully acknowledge all the grants for this research and the teachers and colleague who helped them to finalize the study.

REFERENCES

- Bai, Y., Li, X., Liu, S., and Wang, P. (2017). Modelling Diurnal and Seasonal Hysteresis Phenomena of Canopy Conductance in an Oasis Forest Ecosystem. *Agric. For. Meteorology* 246, 98–110. doi:10.1016/j.agrformet.2017.06.006
- Bai, Y. J., Zhu, Y. J., Ma, J. Y., Liu, P., Yang, R. Z., Li, C., et al. (2020). Seasonal Variation in Canopy Conductance of Urban Green Land and its Environmental Control. *Chin. J. Ecol.* 39 (1), 120–129. doi:10.13292/j.1000-4890.202001.028
- Chen, S.-N., Chen, Z.-S. -N., and Zhang, Z.-Q. (2021). Canopy Stomatal Conductance Characteristics of *Pinus Tabulaeformis* and *Acer Truncatum* and Their Responses to Environmental Factors in the Mountain Area of Beijing. *Chin. J. Plant Ecol.* 45 (12), 1329–1340. doi:10.17521/cjpe.2021.0198
- Dai, X. Q., Wang, H. M., Xu, M. J., Yang, F., Wen, X., Chen, Z., et al. (2021). An Observation Dataset of Carbon and Water Fluxes of Artificial Coniferous Forests in Qianyanzhou (2003–2010). *Chin. Sci. data* 6 (01), 36. Online edition in English and Chinese. doi:10.11922/csdata.2020.0036.zh
- De Boer, H. J., Lammertsma, E. I., Wagner-Cremer, F., Dilcher, D. L., Wassen, M. J., and Dekker, S. C. (2011). Climate Forcing Due to Optimization of Maximal Leaf Conductance in Subtropical Vegetation under Rising CO₂. *Proc. Natl. Acad. Sci. U.S.A.* 108 (10), 4041–4046. doi:10.1073/pnas.1100555108
- Deng, J., Yao, J., Zheng, X., and Gao, G. (2021). Transpiration and Canopy Stomatal Conductance Dynamics of Mongolian Pine Plantations in Semiarid Deserts, Northern China. *Agric. Water Manag.* 249 (11b), 106806–113938. doi:10.1016/j.agwat.2021.106806
- Endler, J. A., Campbell, A. G. S., and Norman, J. M. (1999). An Introduction to Environmental Biophysics. Gaylon S. Campbell, John M. Norman. *Q. Rev. Biol.* 74, 488–489. doi:10.1086/394187
- Evaristo, J., Jasechko, S., and McDonnell, J. J. (2015). Global Separation of Plant Transpiration from Groundwater and Streamflow. *Nature* 525 (7567), 91–94. doi:10.1038/nature14983
- Fu, S., Sun, L., and Luo, Y. (2016). Canopy Conductance and Stand Transpiration of *Populus Simonii* Carr in Response to Soil and Atmospheric Water Deficits in Farmland Shelterbelt, Northwest China. *Agroforest Syst.* 91 (6), 1165–1180. doi:10.1007/s10457-016-0002-4
- Gillner, S., Korn, S., Hofmann, M., and Roloff, A. (2017). Contrasting Strategies for Tree Species to Cope with Heat and Dry Conditions at Urban Sites. *Urban Ecosyst.* 20, 853–865. doi:10.1007/s11252-016-0636-z
- Granier, A., Biron, P., and Lemoine, D. (2000). Water Balance, Transpiration and Canopy Conductance in Two Beech Stands. *Agric. For. Meteorology* 100 (4), 291–308. doi:10.1016/S0168-1923(99)00151-3
- Grossiord, C., Buckley, T. N., Cernusak, L. A., Novick, K. A., Poulter, B., Siegwolf, R. T. W., et al. (2020). Plant Responses to Rising Vapor Pressure Deficit. *New Phytol.* 226, 1550–1566. doi:10.1111/nph.16485
- Harris, P. P., Huntingford, C., Cox, P. M., Gash, J. H. C., and Malhi, Y. (2004). Effect of Soil Moisture on Canopy Conductance of Amazonian Rainforest. *Agric. For. Meteorology* 122 (3–4), 215–227. doi:10.1016/j.agrformet.2003.09.006
- Hu, Y., Duman, T., Vanderklein, D., Zhao, P., and Schäfer, K. V. (2019). A Stomatal Optimization Approach Improves the Estimation of Carbon Assimilation from Sap Flow Measurements. *Agric. For. Meteorology* 279, 107735. doi:10.1016/j.agrformet.2019.107735
- Igarashi, Y., Kumagai, T. o., Yoshifuji, N., Sato, T., Tanaka, N., Tanaka, K., et al. (2015). Environmental Control of Canopy Stomatal Conductance in a Tropical Deciduous Forest in Northern Thailand. *Agric. For. Meteorology* 202, 1–10. doi:10.1016/j.agrformet.2014.11.013
- Komatsu, H., Onozawa, Y., Kume, T., Tsuruta, K., Shinohara, Y., and Otsuki, K. (2012). Canopy Conductance for a Moso Bamboo (*Phyllostachys Pubescens*) Forest in Western Japan. *Agric. For. Meteorology* 156, 111–120. doi:10.1016/j.agrformet.2012.01.004
- Kumagai, T. o., Tateishi, M., Shimizu, T., and Otsuki, K. (2008). Transpiration and Canopy Conductance at Two Slope Positions in a Japanese Cedar Forest Watershed. *Agric. For. Meteorology* 148, 1444–1455. doi:10.1016/j.agrformet.2008.04.010
- Li, Y. L., Yan, J. H., Meng, Z., Huang, J. Q., Zhang, L. M., Chen, Z., et al. (2021). An Observation Dataset of Carbon and Water Fluxes in a Mixed Coniferous Broad-Leaved Forest at Dinghushan, Southern China (2003–2010). *Chinese Sci. Data* 6 (01). doi:10.11922/csdata.2020.0046.zh
- Lu, X. F. (2018). *Response of Carbon-Water Flux to Climate Change in Temperateconiferous and Broad-Leaved Mixed Forests in Changbai Mountain*. Shenyang City, China: Shenyang Agricultural University.
- Martin, T. A., Brown, K. J., Cermák, J., Ceulemans, R., Kucera, J., Meinzer, F. C., et al. (1997). Crown Conductance and Tree and Stand Transpiration in a Second-Growth *Abies Amabilis* Forest. *Can. J. For. Res.* 27, 797–808. doi:10.1139/x97-006
- Mo Kangle, 莫., Chen Lixin, 陈., Zhou Jie, 周., Fang Xianrui, 方., Kang Manchun, 康., and Zhang Zhiqiang, 张. (2014). Transpiration Responses of a Poplar Plantation to the Environmental Conditions on a Floodplain in Northern China. *Acta Eco Sin.* 34 (20), 5812–5822. doi:10.5846/stxb201301280172
- Pataki, D. E., Oren, R., Katul, G., and Sigmon, J. (1998). Canopy Conductance of *Pinus Taeda*, Liquidambar *Styraciflua* and *Quercus Phellos* under Varying Atmospheric and Soil Water Conditions. *Tree Physiol.* 18 (5), 307–315. doi:10.1093/treephys/18.5.307
- Peters, E. B., Mcfadden, J. P., and Montgomery, R. A. (2010). Biological and Environmental Controls on Tree Transpiration in a Suburban Landscape. *J. Geophys. Res.* 115 (G4), 1266. doi:10.1029/2009jg001266
- Richardson, A. D., Keenan, T. F., Migliavacca, M., Ryu, Y., Sonnentag, O., and Toomey, M. (2013). Climate Change, Phenology, and Phenological Control of Vegetation Feedbacks to the Climate System. *Agric. For. Meteorology* 169, 156–173. doi:10.1016/j.agrformet.2012.09.012
- Rodriguez-Dominguez, C. M., Hernandez-Santana, V., Buckley, T. N., Fernández, J. E., and Diaz-Espejo, A. (2019). Sensitivity of Olive Leaf Turgor to Air Vapour Pressure Deficit Correlates with Diurnal Maximum Stomatal Conductance. *Agric. For. Meteorology* 272–273, 156–165. doi:10.1016/j.agrformet.2019.04.006
- Rogers, A., Medlyn, B. E., Dukes, J. S., Bonan, G., Caemmerer, S., Dietze, M. C., et al. (2017). A Roadmap for Improving the Representation of Photosynthesis in Earth System Models. *New Phytol.* 213, 22–42. doi:10.1111/nph.14283
- Saito, T., Kumagai, T. o., Tateishi, M., Kobayashi, N., Otsuki, K., and Giambelluca, T. W. (2017). Differences in Seasonality and Temperature Dependency of Stand Transpiration and Canopy Conductance between Japanese Cypress (*Hinoki*) and Japanese Cedar (*Sugi*) in a Plantation. *Hydrol. Process.* 31 (10), 1952–1965. doi:10.1002/hyp.11162
- She, D., Xia, Y., Shao, M., Peng, S., and Yu, S. (2013). Transpiration and Canopy Conductance of Caragana *Korsinskii* Trees in Response to Soil Moisture in Sand Land of China. *Agroforest Syst.* 87, 667–678. doi:10.1007/s10457-012-9587-4
- Song, L., Zhu, J., Zhang, T., Wang, K., Wang, G., and Liu, J. (2021). Higher Canopy Transpiration Rates Induced Dieback in Poplar (*Populus × Xiaozhuanica*) Plantations in a Semiarid Sandy Region of Northeast China. *Agric. Water Manag.* 243, 106414. doi:10.1016/j.agwat.2020.106414
- Wang, S. Y., Zhang, X. X., Zhu, T., Yang, W., and Zhao, J. Y. (2016). Assessment of Ecological Environment Quality in the Changbai Mountain Nature Reserve Based on Remote Sensing Technology. *Prog. Geogr.* 35 (10), 1269–1278. doi:10.18306/dlkxjz.2016.10.010
- Wang, Z. Y., Yan, W. D., Yan, C. Z., Luo, Z., and Jia, J. (2021). Simulation and Environmental Response of Canopy-Atmospheric transpiration. Conductance of *Platycladus Orientalis* Forests in the Beijing Mountain Area. *Acta Ecol. Sin.* 41 (6), 11. doi:10.5846/stxb201910202197
- Wehr, R., Commene, R., Munger, J. W., McManus, J. B., Nelson, D. D., Zahniser, M. S., et al. (2017). Dynamics of Canopy Stomatal Conductance, Transpiration, and Evaporation in a Temperate Deciduous Forest, Validated by Carbonyl Sulfide Uptake. *Biogeosciences* 14 (2), 389–401. doi:10.5194/bg-14-389-2017
- Wen, X. F., Yu, G. R., Sun, X. M., and Liu, Y. F. (2005). Turbulence Flux Measurement above the Overstory of a Subtropical *Pinus* Plantation over the Hilly Region in Southeastern China. *Sci. China (Series D: Earth Sci.)* 48 (S1), 63–73. doi:10.1360/05zd0006
- Wu, J. B., Guan, D. X., Wang, A. Z., Yuan, F. H., Diao, H. Y., Yu, G. R., et al. (2021). A Dataset of Carbon and Water Flux Observation in a Broad-Leaved Red Pine Forest in Changbai Mountain (2003–2010). *Sci. Data Bank.* 6 (01), 41. Chinese science data: Online edition in English and Chinese. doi:10.11922/csdata.2020.0041.zh
- Xu, S., Yu, Z., Zhang, K., Ji, X., Yang, C., and Sudicky, E. A. (2018). Simulating Canopy Conductance of the *Haloxylon Ammodendron* Shrubland in an Arid Inland River Basin of Northwest China. *Agric. For. Meteorology* 249, 22–34. doi:10.1016/j.agrformet.2017.11.015
- Xu, M., Hu, J., Zhang, T., Wang, H., Zhu, X., Wang, J., et al. (2021). Specific Responses of Canopy Conductance to Environmental Factors in a Coniferous

- Plantation in Subtropical China. *Ecol. Indic.* 131, 108168. doi:10.1016/j.ecolind.2021.108168
- Yoshida, M., Ohta, T., Kotani, A., and Maximov, T. (2010). Environmental Factors Controlling Forest Evapotranspiration and Surface Conductance on a Multi-Temporal Scale in Growing Seasons of a Siberian Larch Forest. *J. Hydrology* 395 (3-4), 180–189. doi:10.1016/j.jhydrol.2010.10.023
- Yoshifuji, N., Kumagai, T. o., Ichie, T., Kume, T., Tateishi, M., Inoue, Y., et al. (2020). Limited Stomatal Regulation of the Largest-Size Class of *Dryobalanops Aromatica* in a Bornean Tropical Rainforest in Response to Artificial Soil Moisture Reduction. *J. Plant Res.* 133 (2), 175–191. doi:10.1007/s10265-019-01161-3
- Yu, G.-R., Wen, X.-F., Sun, X.-M., Tanner, B. D., Lee, X., and Chen, J.-Y. (2006). Overview of ChinaFLUX and Evaluation of its Eddy Covariance Measurement. *Agric. For. Meteorology* 137 (3-4), 125–137. doi:10.1016/j.agrformet.2006.02.011
- Zhang, T., Hong, X. L., Sun, L. W., and Liu, Y. J. (2017). Particle-Retaining Characteristics of Six Tree Species and their Relations with Micro-Configurations of Leaf Epidermis. *J. Beijing For.* 39 (6), 70–77. doi:10.13332/j.1000-1522.20170012

Conflict of Interest: The authors declare that the research was conducted in the absence of any commercial or financial relationships that could be construed as a potential conflict of interest.

Publisher's Note: All claims expressed in this article are solely those of the authors and do not necessarily represent those of their affiliated organizations, or those of the publisher, the editors, and the reviewers. Any product that may be evaluated in this article, or claim that may be made by its manufacturer, is not guaranteed or endorsed by the publisher.

Copyright © 2022 Wu, Jia, Yan, Hu, Wang and Chen. This is an open-access article distributed under the terms of the Creative Commons Attribution License (CC BY). The use, distribution or reproduction in other forums is permitted, provided the original author(s) and the copyright owner(s) are credited and that the original publication in this journal is cited, in accordance with accepted academic practice. No use, distribution or reproduction is permitted which does not comply with these terms.



Characteristics of Energy Distribution in a Desert Ecosystem in Inner Mongolia, Northern China

Yumeng Pan¹, Huijie Xiao^{1*}, Zhiming Xin², Junran Li³, Abbas Miri⁴ and Qiqi Cao⁵

¹School of Soil and Water Conservation, Beijing Forestry University, Beijing, China, ²Inner Mongolia Dengkou Desert Ecosystem National Observation Research Station, Experimental Center of Desert Forestry, Chinese Academy of Forestry, Dengkou, China, ³Department of Geosciences, The University of Tulsa, Tulsa, OK, United States, ⁴Department of Watershed and Range Management, Faculty of Water and Soil, University of Zabol, Zabol, Iran, ⁵Shandong Key Laboratory of Eco-Environmental Science for the Yellow River Delta, Binzhou University, Binzhou, China

OPEN ACCESS

Edited by:

Jifeng Deng,
Shenyang Agricultural University,
China

Reviewed by:

Jiabing Wu,
University of Chinese Academy of
Sciences, China
Xiaohui Yang,
Chinese Academy of Forestry, China

*Correspondence:

Huijie Xiao
soilandwater2006@hotmail.com

Specialty section:

This article was submitted to
Drylands,
a section of the journal
Frontiers in Environmental Science

Received: 09 May 2022

Accepted: 01 June 2022

Published: 19 July 2022

Citation:

Pan Y, Xiao H, Xin Z, Li J, Miri A and
Cao Q (2022) Characteristics of Energy
Distribution in a Desert Ecosystem in
Inner Mongolia, Northern China.
Front. Environ. Sci. 10:939782.
doi: 10.3389/fenvs.2022.939782

Desert ecosystems are vulnerable to climate change because of their fragile environment and poor self-regulation ability. Exploring the land–surface energy balance and the water/heat transfer processes of such regions for water resource management purposes is critical. The processes of surface water and heat transfer throughout the desert ecosystems and the effects of environmental factors on the energy distribution remain poorly studied. In this study, we used an eddy covariance system and surface meteorological data (2019–2021) to investigate the characteristics of the energy balance of Dengkou Desert ecosystem located in Inner Mongolia, northern China. Also, we evaluated the effects of different environmental factors on the energy distribution in this desert ecosystem. We found that the temporal patterns of both sensible heat flux (H) and latent heat flux (LE) with time are consistent with that of net radiation (R_n), and R_n is dominated by H . The sum of the daily average soil heat flux during the observation period was positive, indicating that soil was a heat sink and that the atmosphere transfers heat to the soil. During the observation period, the energy distribution of H/R_n fluctuated greatly, presenting a general U-shaped trend, while LE/R_n presented an inverted V-shaped trend. The main factor affecting H was R_n , followed by saturated vapor pressure, air temperature (T_a), and relative humidity. For LE , the main influencing factors were T_a , and R_n . The energy closure of the half-hour flux in the Inner Mongolian desert ecosystem during the observation period was 48%–68%, and the energy balance ratio was 0.54–0.74. The energy closure at the daily scale was higher than that at the half-hour scale, and the energy closure during daytime was higher than that at night.

Keywords: desert ecosystem, eddy covariance method, energy balance, environmental factors, energy closure

1 INTRODUCTION

As the main energy source in an ecosystem, solar radiation is mostly returned to the atmosphere in the form of latent heat and sensible heat (except for the small part used for plant photosynthesis, internal heat reserves of crops, and heating of soil) (Brown and Rosenberg, 1973). Surface radiation and the energy balance, which are the core components of land–surface processes and land–air interactions, are used to describe the exchange process of matter and energy between the ground and

the atmosphere (Yue et al., 2013). In recent years, many studies investigated the characteristics, distribution, and closure of the energy flux using flux towers in different ecosystems in China (Ma et al., 2014; Yuan et al., 2015; Li et al., 2018; Niu et al., 2018; Zhou et al., 2019). Energy distribution can promote material exchange, and the influence of water exchange is particularly important because it is manifested in the promotion of the water cycle by increasing sensible heat flux (H). A clear understanding of the transport processes of water vapor and energy in the boundary layer is very important for understanding the regional climate and water cycle.

The eddy covariance (EC) method is considered as a reasonable standard for measuring evapotranspiration, because it can directly measure water, heat, and CO_2 fluxes between various underlying surfaces and atmosphere and achieve long-term continuous observations. The obtained results can represent the overall average exchange rate between the surface and the atmosphere over a certain area (Zhao et al., 2011). In recent years, EC technology has been widely applied to the study of material and energy transmission and exchange in the field of ecology (Wu et al., 2018; Reddy et al., 2020; Wang et al., 2020), and many studies focused on the energy distribution within different ecosystems (Li et al., 2014; Jiao et al., 2018; Zhou et al., 2019). These studies found notable differences in the energy distribution within different ecosystems of different regions. Even for the same ecosystem, the characteristics of the energy distribution will vary on different temporal and spatial scales. Many studies conducted in-depth analyses on various factors affecting water and heat transport between ecosystems and the atmosphere (Majozi et al., 2017; Yue et al., 2018; Huang et al., 2019), and the results indicate that differences in the energy distribution are mainly affected by environmental factors and vegetation growth factors. Energy closure refers to the balance between the turbulent flux and the effective energy measured by an EC system. According to the basic assumption of EC system observations and the law of energy conservation, energy closure can be used as an effective method to evaluate the performance and data quality of an observation system. In a study of forest in the Amazon, Renata et al. (2019) found that an increase of the energy balance closure residual indicates that the EC technique underestimates the energy flux.

Desert ecosystems exhibit special geographical, climatological, hydrological, and geological conditions. Owing to the lack of water, vegetation in desert areas is generally sparse, plant species are monotonous, biological production is low, energy flow and material circulation are slow, and environmental regulation and adaptability are poor. Because of the unique geographical environment and special characteristics of the surface albedo, the underlying surface of a desert is unique in terms of the energy, water, and material circulation rules, and its response to solar radiation is also distinct from that of other ecosystems. The exploration of both land-surface processes and land-air interactions in desert regions has long been the focus of climate research in arid regions (Qi et al., 2020). The radiation balance, energy balance, and their distributions represent the basis of the formation of a microclimate (Tan et al., 2015). However, in arid desert regions, because of the special climate and the underlying surface conditions, the microclimatic

characteristics are different to those of other ecosystems. Few studies investigated the energy balance in desert ecosystems. Therefore, to comprehensively understand the energy and water vapor cycles and the effects of climate change in arid regions, exploring the radiation budget and the energy distribution of desert ecosystems is important.

The objectives of this study were to analyze the characteristics of energy and energy closure in desert ecosystems over different time scales and to preliminarily explore the causes and influencing mechanisms of the imbalance of surface energy budget and expenditure. The findings of the present study deepen the understanding of the energy imbalance in the near strata, unify the influence of flow characteristics on energy non-closure in desert areas, contribute to the understanding of the energy cycle mechanism in desert ecosystems, and lay a foundation for the evaluation of the regional water and energy balance.

2 MATERIAL AND METHODS

2.1 Site Description

The experimental area is located in the northeast of the Ulan Buh Desert in Dengkou County, Bayannaoer City, Inner Mongolia, China (Figure 1A). The field measurements were conducted at a desert comprehensive observation station (40°24'N, 106°43'E, 1,050 m above sea level, Figure 1B) in the second experimental field at the Desert Forestry Experimental Center of the Chinese Academy of Forestry. The area exhibits a temperate continental arid climate, with an annual average temperature of 7.8°C and annual average rainfall of approximately 145 mm. Precipitation falls mainly during June–September, accounting for 70%–80% of the annual total. Annual evaporation in the study area is approximately 2,327 mm, and the soil type is wind-sand soil. *Nitraria Tangutorum* is the dominant plant within the study site. The *Nitraria* population exists in the form of *Nitraria nebkhas*, which are approximately 1–3 m high and 6–10 m in diameter. The main associated dominant plants are *Artemisia sphaerocephala*, *Artemisia ordosica*, *Psammochloa villosa*, and *Agriophyllum squarrosum*, and the overall community coverage is 10%–20%.

2.2 Energy Flux and Meteorological Measurements

The fluxes and meteorological data of the desert oasis transition zone were measured simultaneously using an EC system and an auxiliary meteorological element gradient monitoring system. The EC system installed at the center of the desert comprehensive observation station (Figure 1C) composed a closed-path $\text{CO}_2/\text{H}_2\text{O}$ analyzer (EC155, Campbell, United States), 3D ultrasonic anemometer (CSAT-3, Campbell scientific Inc., United States) and data logger (CR3000, Campbell scientific Inc., United States). The predominant wind direction in this region is from the northwest, and the fetch length is considered adequate for EC measurements. The observations consisted of both mean and high-frequency turbulent measurements. The gradient monitoring system comprised a soil temperature sensor (CS616, Campbell Scientific Inc., United States), four-component radiation sensor (NR-LITE, Kipp & Zonen,

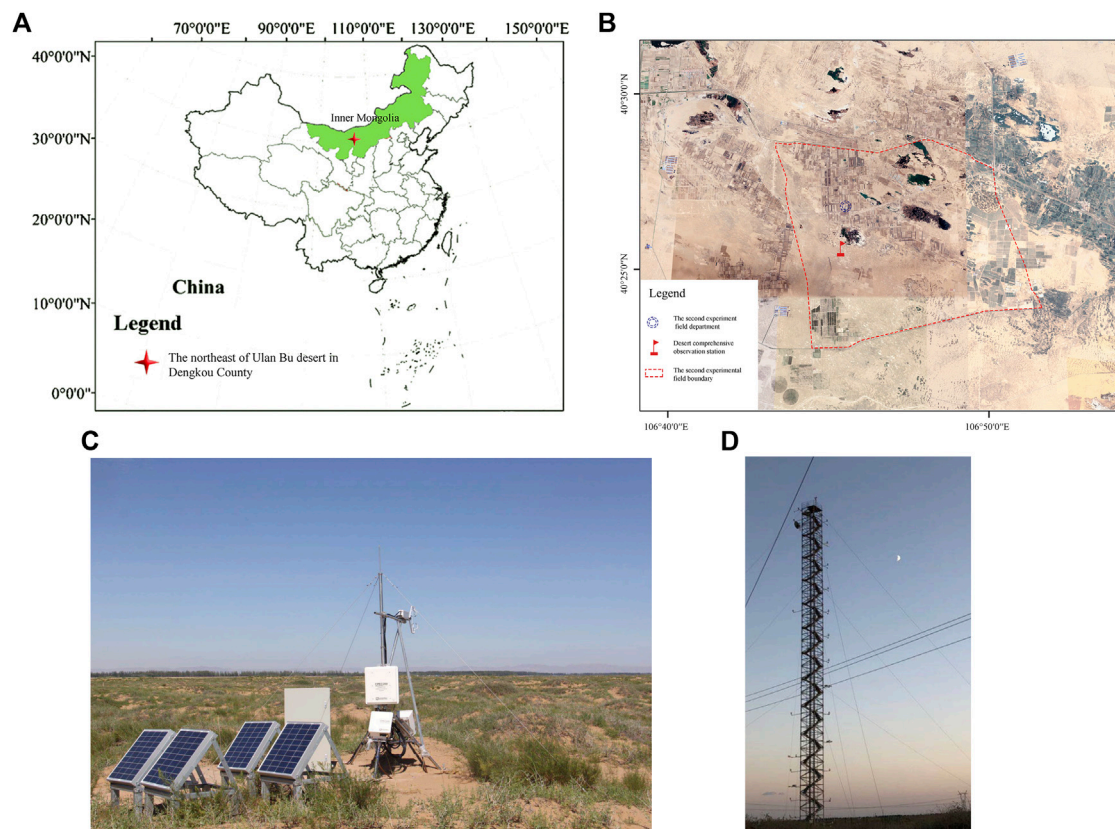


FIGURE 1 | (A) Overview of the study area; **(B)** The experimental site; **(C)** Eddy covariance (EC) system; **(D)** The meteorological station.

TABLE 1 | Summary of the specifications of the instruments integrated on the eddy covariance flux tower. All measurements are averaged over 30-min interval.

Name	Instrument model	Observation elements	Depth/height (m)
Close-path H ₂ O/CO ₂ analyzer	EC155, Campbell Scientific Inc., United States	Water vapor content; latent heat flux	2
3D ultrasonic anemometer	CSAT-3, Campbell Scientific Inc., United States	Wind speed and direction	2
Four component radiation sensor	NR-LITE, Kipp & Zonen, Netherlands	Surface radiation fluxes	2
Temperature and humidity sensor	HMP45C, Vaisala Inc., Finland	Air temperature and relative humidity	2.0, 1.5
Soil heat flux plate	4xHFP01, Hukseflux, Netherlands	Soil heat flux	−0.1
Soil temperature sensor	CS616, Campbell Scientific Inc., United States	Soil temperature and humidity	0.02, 0.05, 0.1, 0.15, and 0.2
Data logger	CR3000, Campbell Scientific Inc., United States	—	—

Netherlands), and a temperature and humidity sensor (HMP45C, Vaisala Inc., Finland). Four soil heat flux plates (HFP01, Hukseflux, Netherlands) were installed at the depth of 0.1 m. Flux measurements were taken at a sampling frequency of 10 Hz. Further details including the specifications of the instruments are presented in **Table 1**. Also, all sensors used were previously subjected to calibration at the factory, and their performance was thoroughly evaluated. Measurements collected during 2019–2021 were used in the present study. Owing to failure of observation instruments and the influence of certain weather conditions, some data were recognized as abnormal, and some data were missing.

Meteorological parameters were observed simultaneously on the daily scale by using the meteorological station located

in the study area (**Figure 1D**). The main observation elements included average temperature, maximum temperature, minimum temperature, relative humidity (*RH*), and precipitation. Next, daily averages of the recorded data were calculated for the period from January 2019 to October 2021.

2.3 Parameter Calculation and Data Analysis

2.3.1 Data Processing

The formulas for the calculation of *H* and latent heat flux (*LE*) are as follows (Swinbank, 1951):

$$H = \rho C_p \overline{w' T'}, LE = \rho \lambda \overline{w' q'}, \quad (1)$$

where ρ is air density ($\text{kg}\cdot\text{m}^{-3}$), C_p is the heat capacity of air ($\text{J}\cdot\text{kg}^{-1}\cdot\text{C}^{-1}$), λ is the latent heat of evaporation ($\text{J}\cdot\text{kg}^{-1}$), w' is vertical wind speed ($\text{m}\cdot\text{s}^{-1}$), T' is air temperature ($^{\circ}\text{C}$), and q' is specific humidity.

The original turbulent data with sampling frequency of 10 Hz were preprocessed using the EddyPro software developed by the LI-COR company. First, the original observational data of the EC system were rotated twice for 30 min, an ultrasonic virtual temperature correction was performed for H , and a WPL correction was performed for LE (Webb et al., 1980). On this basis, the outliers were eliminated. Through data correction and noise elimination, valid data accounted for 75% of the total. To understand the dynamic changes of water and heat fluxes over time, continuous water and heat flux data are needed. Deleted data and missing data were replaced using either of the following two interpolation methods: missing data over a period of less than 2 h were interpolated using the linear interpolation method, and missing data over a period of greater than 2 h were interpolated by means of the diurnal variation method (Falge et al., 2001).

2.3.2 Evaluation of Surface Energy Budget

The weather–climate system is a dynamic system driven by the absorption of sunlight and emission of longwave radiation. These two fluxes are an integral part of the surface energy balance (SEB) from which the ground temperature is estimated in weather prediction models (Mihalakakou et al., 1997; Curry and Webster, 1999). In general terms, the SEB can be expressed as follows:

$$R_n - G = LE + H, \quad (2)$$

where R_n is net radiation flux ($\text{W}\cdot\text{m}^{-2}$), G is ground heat flux ($\text{W}\cdot\text{m}^{-2}$), and H and LE are sensible heat and latent heat fluxes, respectively ($\text{W}\cdot\text{m}^{-2}$). The convention used here is that all radiative fluxes (non-radiative fluxes) directed toward the surface are positive (negative).

Lack of closure of SEB fluxes measured by EC systems is a known issue that remains unresolved (Wilson et al., 2002), and it appears in terms of discrepancies between the turbulent heat fluxes ($H + LE$) and available energy ($R_n - G$). In this paper, the energy balance ratio (EBR) and ordinary least squares (OLS) were used to analyze the closure degree of the energy balance.

EBR, which refers to the ratio of turbulent energy and effective energy measured directly by the EC system, can be expressed as follows:

$$EBR = \frac{\sum (LE + H)}{\sum (R_n - G)} \quad (3)$$

A value of $EBR = 1$ indicates perfect closure of the SEB. Although using 30-min averaged measurements demonstrates the advantage of smoothing out random errors and higher-frequency fluctuations, it can also lead to overestimation of upward (downward) fluxes during the day (night) (Mahrt, 1998).

The OLS method calculates the regression slope (S) and intercept (b) of the turbulent flux and the effective energy to

analyze the closure degree of the energy balance, in which S can reflect the balance of instantaneous energy. The basic assumption of OLS regression is to minimize E_{OLS} , and the OLS regression equation can be expressed as follows:

$$LE + H = S (R_n - G) + b \quad (4)$$

where $(LE + H)$ is the turbulent flux, $(R_n - G)$ is the effective energy, S is the slope of the linear regression, and b is the intercept. Under ideal conditions, the value of S of the linear regression of the effective energy ($R_n - G$), the turbulent flux ($LE + H$) is 1, and the value of b is 0.

2.3.3 Data Analysis

All the monitoring data were sorted using Excel 2013, and the parameters were calculated and analyzed with R software and MATLAB software. Curve fitting and the comparisons of different subsets of the data were performed using Origin 2019b (Origin Lab Corporation, Northampton, MA, United States).

3 RESULTS

3.1 Variations in Environmental Factors

The observational data obtained by the gradient meteorological system and the conventional meteorological station showed that the variations of all the daily meteorological factors demonstrated obvious seasonal patterns (Figure 2). Both air temperature (T_a) and vapor pressure deficit (VPD) showed a single-peaked trend of change. In contrast to the above meteorological variables, RH fluctuated with a jagged pattern. During the observation period, the maximum value of daily T_a was 29.6°C (13 July 2021), the minimum value of daily T_a was -20.6°C (6 January 2021), and the values of VPD and T_a were similar. Although the daily average VPD showed significant seasonal variation, it did not show significant interannual variation, with the annual average VPD of 0.58, 0.58, and 0.71 kPa in 2019, 2020, and 2021, respectively. Compared with 2019, 2020, and 2021, the annual average RH was 43.3%, 44.6%, and 38.1%, respectively, and the daily average relative humidity in 2021 was slightly lower. Next, the study area is arid and demonstrates little rainfall, and the average precipitation in the three studied years was 101 mm. Precipitation is usually concentrated in May–September, and May–September precipitation in 2019 and 2020 accounted for 71.6% and 97.2% of the total annual precipitation, respectively. Additionally, precipitation is distributed extremely unevenly in terms of quantity and time.

3.2 Dynamic Characteristics of Energy Component and Energy Partitioning

3.2.1 Seasonal Variations of Energy Flux and Energy Partitioning

In the process of surface energy exchange, net radiation (R_n), H , and LE are the main variables, and their characteristics and variation rules are affected by many local factors. Figure 3

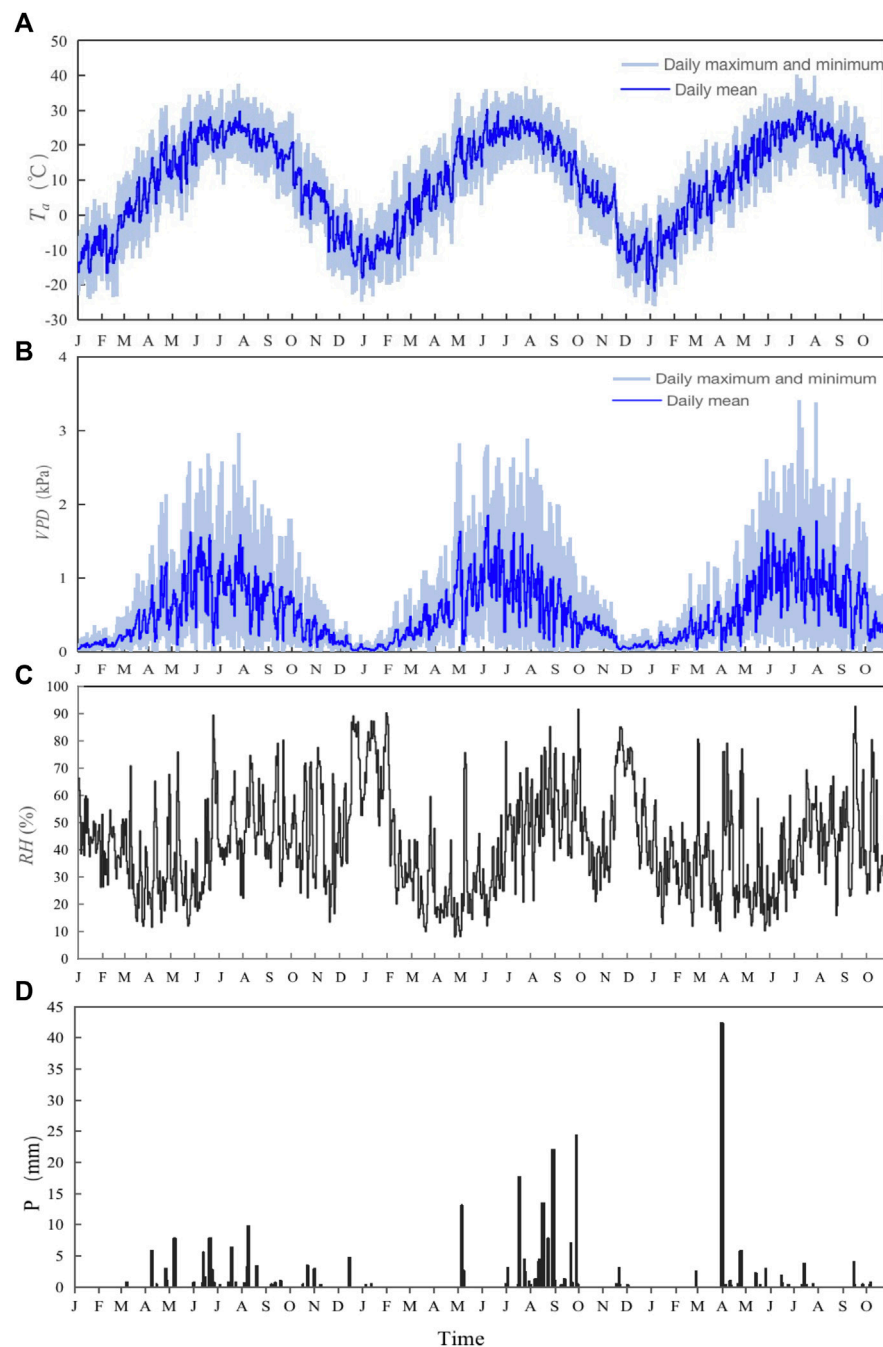


FIGURE 2 | Seasonal dynamics of (A) daily average relative air temperature (T_a), (B) vapor pressure deficit (VPD), (C) humidity (RH) and (D) interannual distribution of total daily precipitation (P) in the study area.

shows the seasonal variation characteristics of the daily average of half-hour energy flux in the Inner Mongolian desert ecosystem during the observation period. The seasonal variation of R_n is obvious, and the annual average daily R_n approximates single-peak variation. Owing to the change of mesoscale climatic conditions, R_n presents a serrated fluctuation, especially in the case of rainfall, and a large diurnal difference is found in R_n . The

sum of the daily average soil heat flux (G) in the observation period of 2019, 2020, and 2021 was positive, indicating that the soil was a heat sink and that heat was transferred from the atmosphere to the soil. In 2019, 2020, and 2021, the mean values were 5.93, 2.84, and 1.07 $\text{W}\cdot\text{m}^{-2}$, respectively.

The seasonal variation trend of H in the study area was broadly consistent with that of R_n . The fluctuation range of daily average

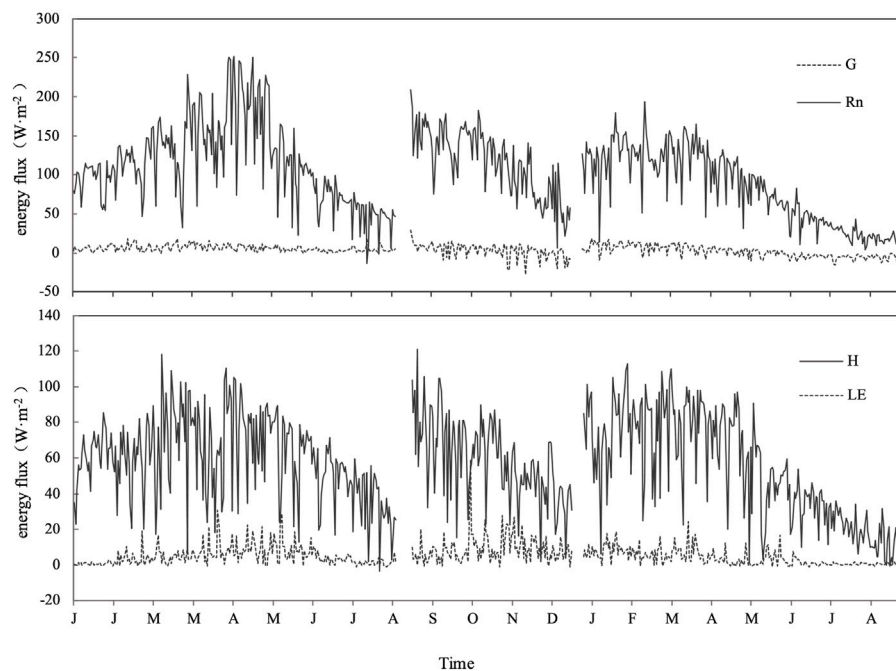


FIGURE 3 | Seasonal and interannual variation of energy flux of the desert ecosystem in Dengkou County, Inner Mongolia.

TABLE 2 | Monthly total amount of daily average energy components (W m^{-2}) and energy distribution in a desert ecosystem in Dengkou County (Inner Mongolia) during the observation period.

Time		G	H	LE	R_n	H/R_n	G/R_n	LE/R_n
2019	March	118.03	1520.84	11.97	2304.51	0.72	0.05	0.01
	April	219.59	1726.36	89.58	3223.97	0.54	0.07	0.03
	May	222.55	2233.87	146.15	3982.57	0.58	0.06	0.04
	June	264.29	2008.80	212.52	4638.34	0.47	0.06	0.05
	July	214.89	2343.77	265.21	6037.54	0.39	0.03	0.05
	August	148.26	2023.25	273.83	3557.19	0.59	0.06	0.08
	September	85.42	1546.72	122.13	2245.25	0.69	0.04	0.05
	October	152.70	1099.54	32.62	1471.24	0.75	0.15	0.02
2020	June	231.65	2131.77	158.52	4106.24	0.53	0.05	0.04
	July	147.93	1918.07	327.64	4330.67	0.45	0.03	0.08
	August	33.11	1741.98	337.79	3452.25	0.51	0.00	0.10
	September	-52.93	1251.23	239.69	2044.61	0.64	-0.06	0.13
2021	May	248.67	2255.72	258.66	3722.04	0.61	0.05	0.08
	June	249.85	2365.83	184.50	3787.70	0.62	0.06	0.05
	July	202.32	2544.29	223.39	4045.86	0.63	0.04	0.06
	August	75.40	2223.05	288.61	3173.12	0.72	0.01	0.03
	September	-2.98	1383.75	100.12	2299.31	0.61	0.00	0.05
	October	-144.83	1089.53	34.53	1414.75	0.80	-0.13	0.02
	November	-179.55	682.88	13.78	788.28	0.90	-0.24	0.02
	December	-187.10	404.09	8.62	546.98	0.74	-0.37	0.02

H during the observation period was $-3.64 \text{ W} \cdot \text{m}^{-2}$ (23 October 2019) to $120.98 \text{ W} \cdot \text{m}^{-2}$ (8 June 2020), and the average value was $57.22 \text{ W} \cdot \text{m}^{-2}$. In conditions of underlying surface drought and sparse vegetation, the magnitude of the values of LE in the study area was small, but there was notable seasonal variation for which the main trend was similar to that of R_n . LE fluctuated markedly

in the rainy season during the growing period, which is consistent with the fluctuation of the time of precipitation and R_n . In 2019, 2020, and 2021, the mean values of LE were 4.89, 8.84, and $3.73 \text{ W} \cdot \text{m}^{-2}$, respectively.

Table 2 shows the calculation results of the annual monthly total value of the energy flux components in the Inner Mongolian

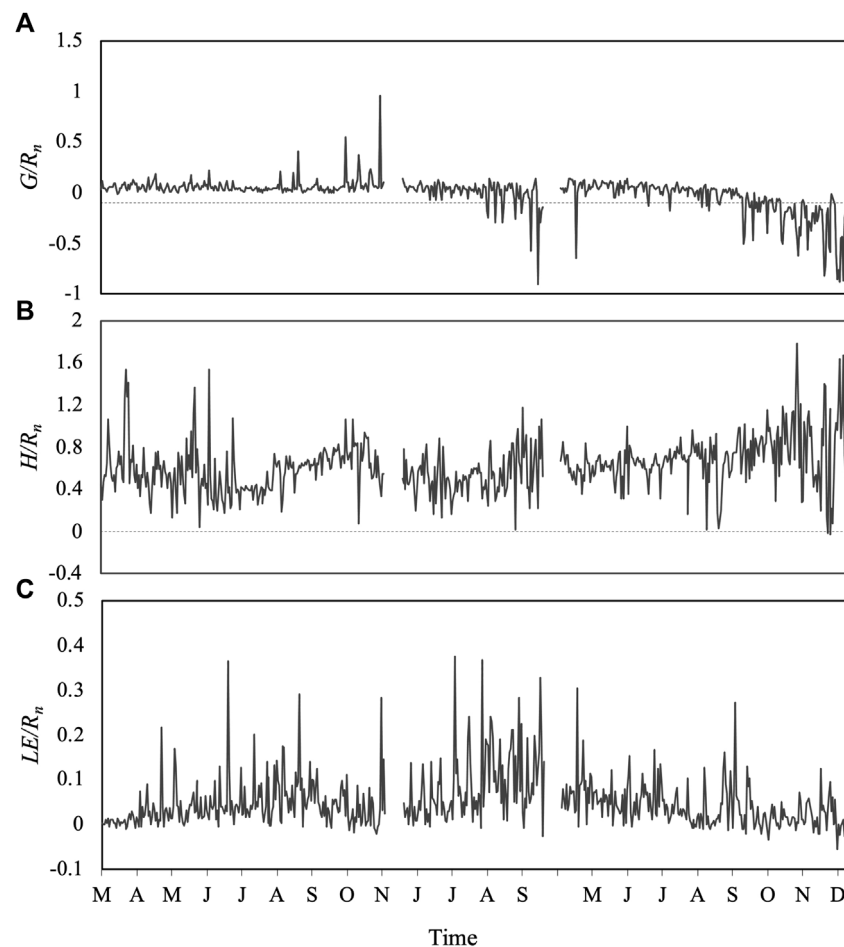


FIGURE 4 | Seasonal and interannual variation of energy distribution of the desert ecosystem in Dengkou County, Inner Mongolia.

desert ecosystem during 2019–2021. Overall, R_n , H , and LE all show a monthly trend of initial increase and then decrease during the year. The maximum values appeared in the growing season, and the fluctuation of the monthly total was slightly different from the month in which the maximum value occurred. Also, the monthly total amount of G increased with the increase of R_n , but marked positive and negative changes were found in different months. In 2019, the monthly total amount of G was positive, whereas in 2020 and 2021, the monthly total amount of G was negative during September–December, indicating that the direction of heat transfer in the Inner Mongolian desert ecosystem was from the soil to the atmosphere.

The seasonal variation of the distribution of H and LE can be used to determine the dry/wet conditions of the underlying surface. The R_n allocation of the Inner Mongolian desert ecosystem is mainly dominated by H (Figure 4). During the observation period, the energy allocation of H/R_n fluctuated greatly, and the change curve presents a U-shaped trend. The value in the non-growing season was larger than that in growing season. In 2019, 2020, and 2021, the mean values were 0.58, 0.52, and 0.70, respectively. Next, according to comparative analysis of

H/R_n in different months (Table 2), H/R_n reached the peak value of 0.72 at the initial stage of vegetation growth (March) in 2019. Subsequently, with further vegetation growth, part of R_n was absorbed and reflected by the canopy, and the H/R_n value began to decrease gradually. At the end of vegetation growth, the H/R_n value began to increase and then decreased after November. The monthly average H/R_n value ranged from 0.39 (July) to 0.75 (October) in 2019, and the H/R_n values in 2020 and 2021 remained high (> 0.5). During the observation period, LE/R_n exhibited obvious seasonal variation, and the overall change curve presents an inverted V-shaped distribution. The average daily LE/R_n values in 2019, 2020, and 2021 were 0.04, 0.09, and 0.04, respectively. Next, the ratio of G to R_n fluctuated by less than 0.1 in the growing season, and the daily average G/R_n values varied from -0.01 to 0.96 , -0.29 to 0.14 and -0.91 to 0.14 in 2019, 2020, and 2021, respectively.

3.2.2 Diurnal Variations of Energy Flux and Energy Partitioning

According to soil temperature and the phenological period of *N. tangutorum*, the observation time was divided into four periods:

TABLE 3 | Daily mean values of energy components in different periods.

	Pre-growth period	Growth period			Declining period		Freezing period
	2019	2019	2020	2021	2019	2021	2021
R_n ($W \cdot m^{-2}$)	98.04	129.93	97.55	102.04	44.79	42.14	20.53
G ($W \cdot m^{-2}$)	5.55	4.23	2.32	4.67	-4.51	-4.93	-6.18
H ($W \cdot m^{-2}$)	57.57	63.98	56.17	67.97	32.56	34.21	16.56
LE ($W \cdot m^{-2}$)	1.52	14.32	15.14	10.41	0.77	0.58	0.29

pre-growth period (March–April), growth period (May–September), declining period (October), and freezing period (November–February). In this study, H , LE , R_n , and G data at 30-min intervals during 2019–2021 were analyzed, and the mean and standard deviation of the energy flux were extracted for the same time for all days in each period. The daily average value of the diurnal variation of the energy components in different years in the same period demonstrated little variation (Table 3). The obtained average daily variation of the energy flux of the Inner Mongolian desert ecosystem in each of the different periods is shown in Figure 5.

In each period, R_n showed a single peak in the daily trend with low values in the morning and evening and high values at noon. The peak value of R_n appeared during 12:00–12:30 local time, and no notable difference was found between different years and periods. The maximum value of daily variation of R_n in each period was as follows: growth period > pre-growth period > declining period > freezing period. The daily dynamic change of G was consistent with that of R_n , although its peak time lagged R_n , i.e., it usually occurred during 15:00–15:30 local time. The diurnal variation of G in each period was obvious, being mostly positive during the day and negative at night. The changes of H were highly consistent with that of R_n , but the trend was gentler, and the daily change trend of each period was similar. Except for the fluctuation of LE in the vigorous growth period, it changed little in other periods, and it was approximately zero. LE was mostly positive during the day but negative at night when the temperature was $<0^\circ C$, indicating frost or condensation.

The daily dynamics of the energy distribution in the different periods showed that H played a dominant role in energy consumption (Figure 6). Moreover, the energy distribution during the day and at night was different. The energy distribution during the day was $H/R_n > G/R_n > LE/R_n$, and the energy distribution at night was $G/R_n > H/R_n > LE/R_n$. The dominant factor was G . Both H/R_n and G/R_n showed a gradual increasing trend during the day and fluctuated greatly at night, while LE/R_n changed slightly at night, fluctuated violently before and after sunrise and sunset, and was relatively stable during the day, when the value was higher than that at night. Also, the diurnal variation trend of LE/R_n in the early growth period, declining period, and freezing period was very stable, when it fluctuated above and below zero. However, it fluctuated greatly in the vigorous growth period, and obvious positive and negative changes occurred before and after sunset.

3.3 Influencing Factors of Energy Flux and Energy Distribution

To analyze the relationship between LE , H , the energy distribution, and environmental factors, correlation analysis was performed between the daily average flux data from March–October 2019 and the data of environmental factors (R_n , VPD , T_a , RH , T_{s-10cm} : soil temperature at 10 cm depth, and SWC_{10cm} : soil water content at 10 cm depth) in the same period (Table 4). The results revealed that H demonstrated a very significant positive correlation with R_n , VPD , T_a , and SWC_{10cm} and a very significant negative correlation with RH ; LE demonstrated a very significant positive correlation with R_n , VPD , RH , T_a , T_{s-10cm} , and SWC_{10cm} ; LE/R_n demonstrated a very significant positive correlation with T_a , RH , T_{s-10cm} , and SWC_{10cm} ; H/R_n was negatively correlated with T_a , VPD , RH , T_{s-10cm} , and SWC_{10cm} .

3.4 Energy Closure

3.4.1 Half-hour Scale Energy Closure

According to the linear regression analysis of effective energy and turbulent flux and the analysis results of the energy balance ratio (Figure 7; Table 5), the energy closure rate of the half-hour flux of the Inner Mongolian desert ecosystem in different periods was different, with a variation range of 48%–68%. Generally, the intercept of the obtained linear regression line cannot pass through the origin. Therefore, in the analysis process, this paper gave linear regression S_1 , intercept b , determination coefficient R_1^2 , linear regression S_2 , and determination coefficient R_2^2 forced through the origin. In the different periods, the variation range on the half-hour scale of regression slope S_1 was 0.48–0.68, S_2 was 0.50–0.77, b was 2.72–27.95 $W \cdot m^{-2}$, and R^2 was 0.56–0.78, which can better explain the results of the linear regression between effective capacity and turbulent flow. Additionally, S_2 was greater than S_1 in each period, indicating that the energy closure is improved slightly by forced linear fitting across the origin.

According to the half-hour flux data, the EBR range in the different periods was 0.54–0.74. The EBR value in the vigorous growth period was the largest, followed by that in the early growth period, while the EBR value in both the declining period and the freezing period was small. The number of observation samples in 2019 and 2021 was broadly the same. Next, the comparative analysis showed no significant difference in energy closure between the 2 years. The EBR value calculated from all observation data in 2019 was 0.67, i.e., the annual average energy closure was 67%, and the EBR in 2021 was 0.69. In

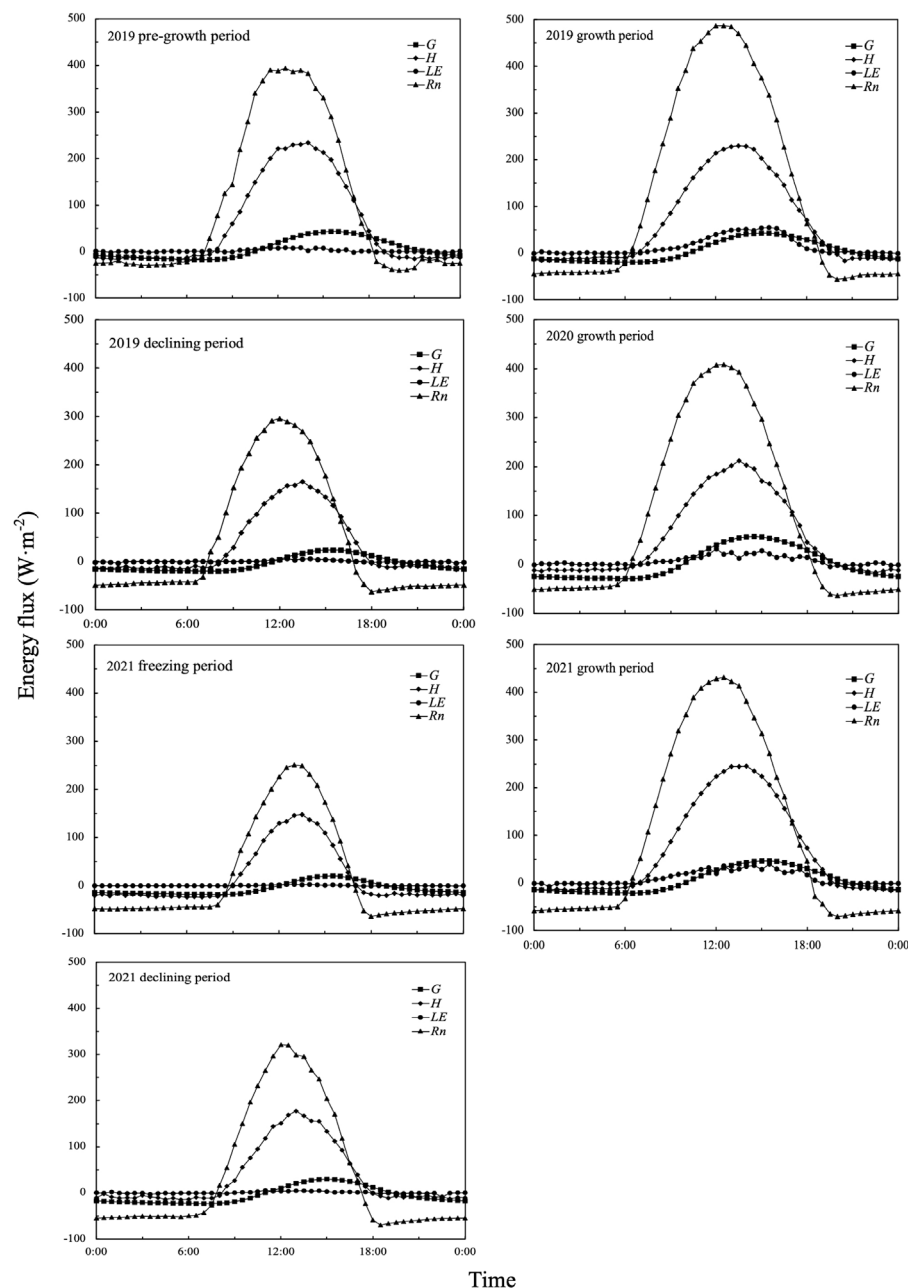


FIGURE 5 | Diurnal variation of energy flux in the Inner Mongolian desert ecosystem in different periods.

2019, the energy closure during the day and at night was 65% and 20%, respectively, and in 2021, the energy closure during the day was also higher than that at night (76% and 37% respectively). Additionally, it can be seen from **Table 5** that the energy closure obtained using the EBR method was greater than that calculated using the correlation method.

3.4.2 Daily Scale Energy Closure

If the observation time is short and the energy balance component and distribution are not synchronized, a lag

effect will occur that results in energy non-closure. If the time scale is properly extended, the energy closure can be improved. Therefore, the energy closure calculated from the half-hour scale flux data was lower than that on the daily scale. To study the influence of different time scales on energy closure and reduce the error of a large number of nighttime flux data on the half-hour scale, two methods were also used to analyze the energy closure under the calculation of daily average flux data. The slopes of the linear regression of the 3-year effective energy and turbulent flow were slightly higher

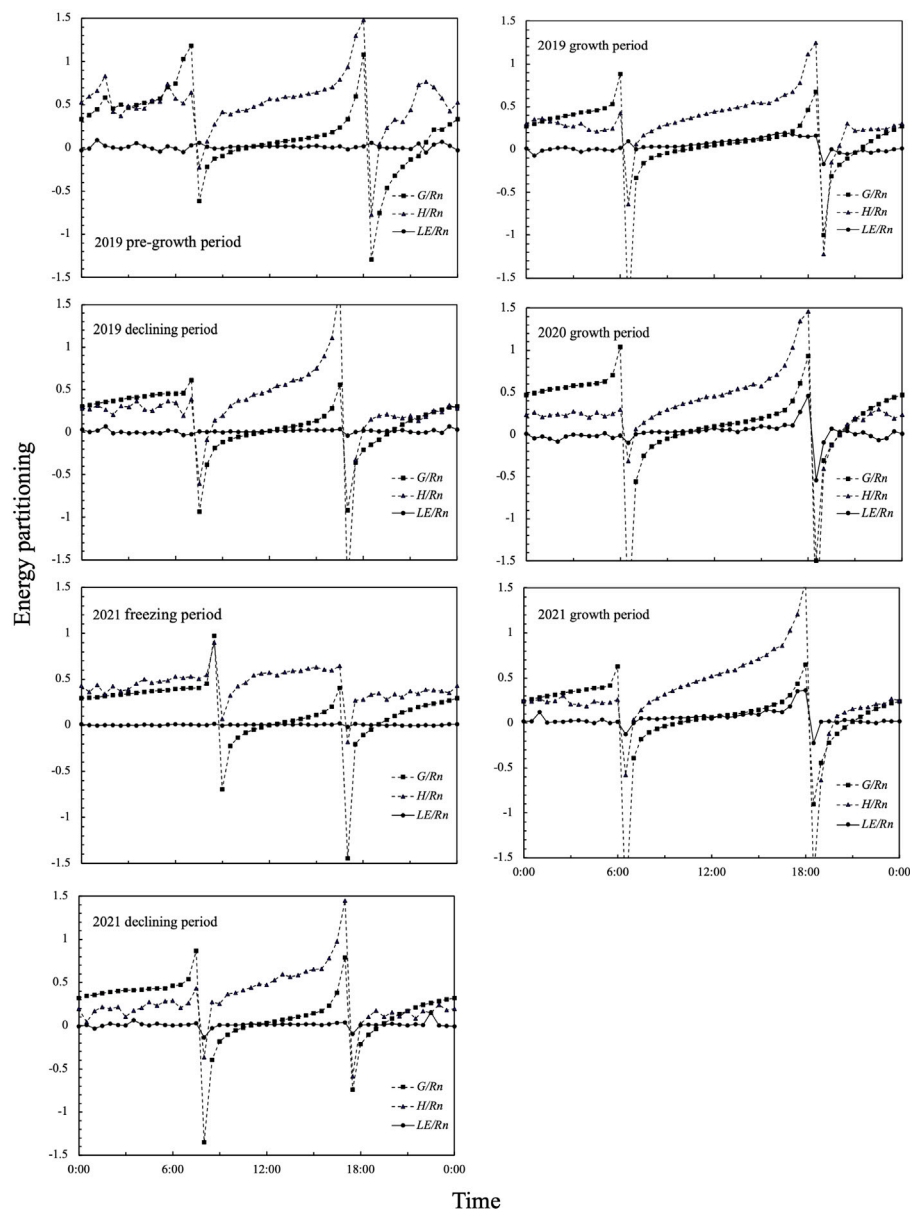


FIGURE 6 | Diurnal variation of energy distribution in the Inner Mongolian desert ecosystem during different observation periods.

than those calculated for the half-hour scale in the same period. The energy closure of the daily average flux in 2019, 2020, and 2021 was 67%, 66%, and 67%, respectively (energy closure on the half-hour scale was 64%, 66%, and 63%, respectively). The energy closure on the daily scale in 2021 increased by 3%, and the R^2 of the linear regression equation also increased significantly (i.e., 0.96). On the daily scale, the EBR values in 2019, 2020, and 2021 were 0.77, 0.80, and 0.70, respectively. In comparison with the half-hour data (0.67, 0.74, and 0.69 in 2019, 2020, and 2021 respectively), the average energy closure increased by approximately 6% (**Figure 8; Table 6**).

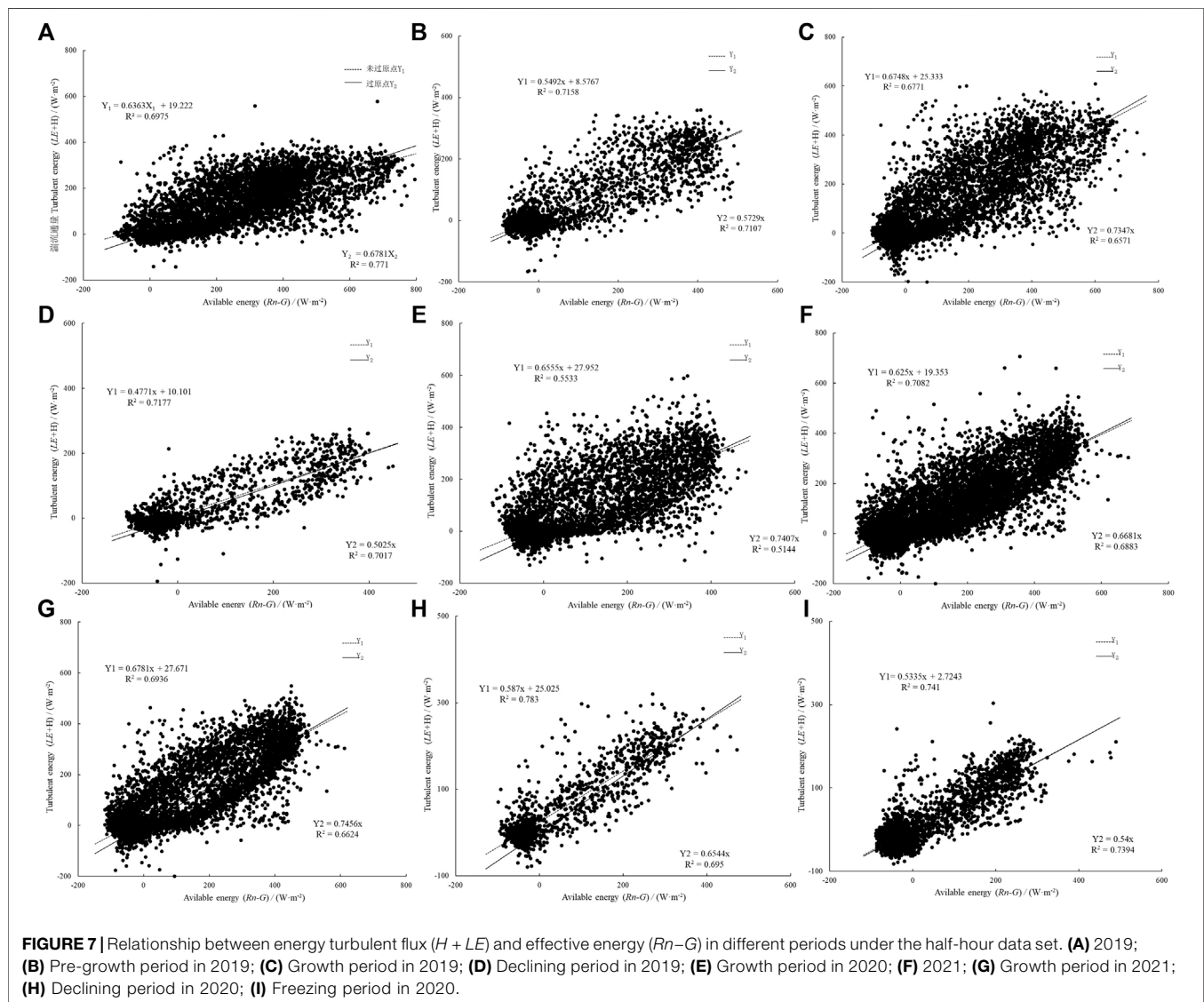
4 DISCUSSIONS

4.1 Energy Distribution Characteristics

Sensible heat exchange depends on the turbulent heat exchange coefficient and the T_a gradient difference. The greater the gradient difference, the rougher the ground, the stronger the surface heat exchange, and the greater the sensible heat. This study found that the sensible heat was greater than the latent heat, which was similar to the energy balance characteristics reported for the growing season of the Inner Mongolian Desert Grassland (Yang and Zhou, 2010) and the hinterland of the Taklimakan Desert (Qi et al., 2020) all year round. Next, the variation trend of

TABLE 4 | Correlation between energy flux and environmental factors in the same periods.

	T_a	VPD	RH	T_{s-10cm}	SWC_{10cm}	R_n	H	LE	LE/R_n	H/R_n
T_a	1	0.804**	0.068	0.970**	0.272**	0.549**	0.311**	0.470**	0.259**	-0.309**
VPD		1	-0.466**	0.745**	0.097	0.573**	0.456**	0.185**	-0.026	-0.200**
RH			1	0.132*	0.166**	-0.159*	-0.363**	0.341**	0.422**	-0.167**
T_{s-10cm}				1	0.258**	0.560**	0.369**	0.477**	0.259**	-0.254**
SWC_{10cm}					1	0.214**	0.155*	0.352**	0.265**	-0.152*
R_n						1	0.618**	0.370**	-0.082	-0.527**
H							1	0.116	-0.173**	0.250**
LE								1	0.768**	-0.297**
LE/R_n									1	-0.083
H/R_n										1

**FIGURE 7** | Relationship between energy turbulent flux ($H + LE$) and effective energy ($Rn - G$) in different periods under the half-hour data set. **(A)** 2019; **(B)** Pre-growth period in 2019; **(C)** Growth period in 2019; **(D)** Declining period in 2019; **(E)** Growth period in 2020; **(F)** 2021; **(G)** Growth period in 2021; **(H)** Declining period in 2020; **(I)** Freezing period in 2020.

both H and G was consistent with that of R_n in three periods, i.e., a single-peaked diurnal variation, but with a curve that was not as smooth as that of R_n , which might reflect indirect turbulent

transmission (Zhang et al., 2002). Because the specific heat of soil is much greater than that of air and because the change of soil temperature occurs later than that of T_a , the time for G to reach its

TABLE 5 | Characteristics of energy closure of the Inner Mongolian desert ecosystem at the half-hour scale.

Data set		Number of samples	S_1	S_2	b	R_1^2	R_2^2	EBR
2019	Pre-growth period	2,641	0.57	0.60	11.35	0.71	0.76	0.60
	Growth period	7,345	0.66	0.71	24.06	0.68	0.76	0.73
	Declining period	1,682	0.48	0.50	10.01	0.72	0.76	0.54
	Daytime	5,829	0.61	0.68	28.53	0.53	0.83	0.65
	Night	5,829	0.40	0.36	8.93	0.58	0.55	0.20
	Whole year	1,1661	0.64	0.67	19.22	0.70	0.77	0.67
2020	Growth period	5,793	0.66	0.74	27.95	0.56	0.68	0.74
2021	Growth period	7,345	0.68	0.75	27.67	0.69	0.76	0.67
	Declining period	1,489	0.59	0.65	25.03	0.78	0.78	0.63
	Freezing period	2,929	0.53	0.54	2.72	0.74	0.76	0.58
	Daytime	5,881	0.65	0.68	39.45	0.65	0.79	0.76
	Night	5,881	0.23	0.26	16.14	0.53	0.58	0.37
	Whole year	11,761	0.63	0.67	19.35	0.71	0.76	0.69

peak lags behind R_n , and the time lag is affected by the sunrise time. Although the ratio of G to R_n is very small, the characteristics of G absorbing energy during the day and releasing energy at night and storing energy in summer and releasing energy in winter play a role of an “energy buffer” in the surface energy budget. Therefore, when studying the energy balance of desert ecosystems in Inner Mongolia, the influence of G cannot be ignored.

During the observation period in the study area, LE/R_n was always very small, i.e., < 0.1 most of the time. This is because in the Ulan Buh desert area, soil water is scarce, vegetation transpiration is slow, LE is less than H , and the soil type is

sandy soil, which is conducive to rapid vertical drainage, thereby reducing the potential impact of soil water on LE . The differences in the energy distribution of desert ecosystems are determined by climatic characteristics, soil moisture status, and the underlying vegetation (Liu and Feng, 2012; Majozi et al., 2017; Yue et al., 2018; Ren et al., 2022). The results of this study showed that water resource status is the key factor affecting energy distribution in extremely arid desert areas. If the water supply of the ecosystem is sufficient, the energy consumption is mainly LE . If the water supply of the ecosystem is insufficient, the energy consumption is mainly H .

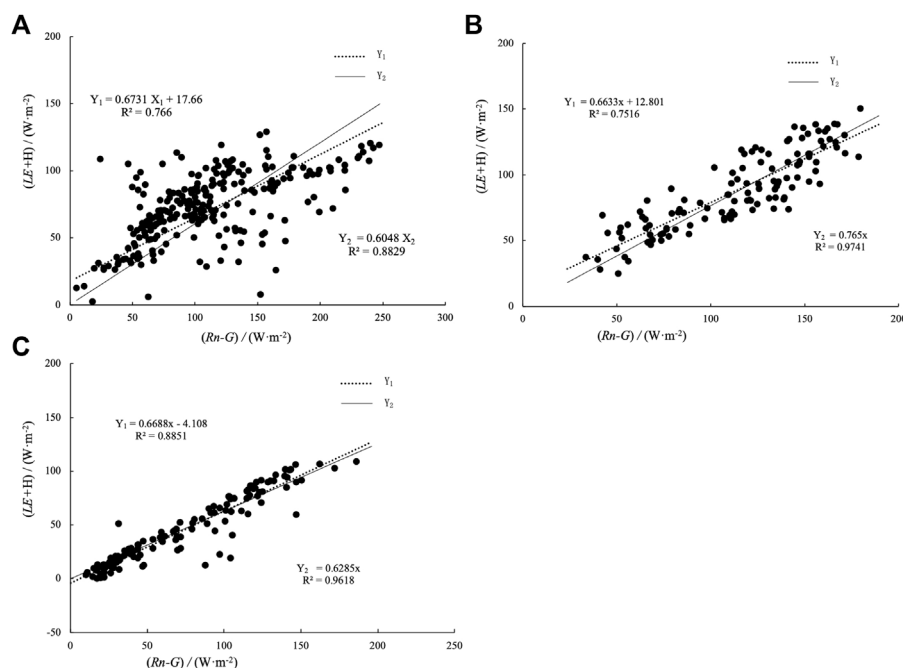
**FIGURE 8** | Relationship between energy turbulent flux ($H + LE$) and effective energy ($R_n - G$) in different periods under the daily average data set. **(A)** 2019; **(B)** 2020; **(C)** 2021.

TABLE 6 | Characteristics of energy closure of the Inner Mongolian desert ecosystem at the daily scale.

Data set		Number of samples	S_1	S_2	b	R_1^2	R_2^2	EBR
Year	Month							
2019	3–10	244	0.67	0.61	17.66	0.77	0.88	0.77
2020	6–9	122	0.66	0.77	12.80	0.75	0.97	0.80
2021	5–12	246	0.67	0.63	-4.11	0.89	0.96	0.70

4.2 Influence of Environmental Factors on the Energy Distribution

The correlation analysis revealed that the main factor affecting sensible heat is R_n . The previous analysis established that H increases with increasing R_n and that it shows similar dynamic changes with R_n on daily and seasonal scales, followed by VPD , soil temperature, T_a , and RH . Soil water content exhibits little effect on latent heat. For latent heat, T_a , soil temperature and R_n are the main influencing factors, followed by VPD , RH , and wind speed. Many earlier studies showed that climatic factors (e.g., precipitation, radiation, temperature, and VPD) and biological factors (e.g., leaf area index) affect the energy distribution (Matsumoto et al., 2008; Launiainen, 2010; Jia et al., 2016; Launiainen et al., 2016). For the desert ecosystem of Inner Mongolia with its arid climate, sparse vegetation, and fragile ecological environment, the key factors affecting the energy distribution are water conditions and the underlying surface conditions (Yue et al., 2019).

4.3 Energy Closure

In the process of observing the carbon, water, and heat fluxes using an EC system, the closure of energy balance is an important index with which to measure the data quality (Mahrt, 1998; Li et al., 2004), but energy non-closure is a common phenomenon in EC observation. In terms of data processing, different time scales and energy balance evaluation methods obtain different energy closure results. At the FLUXNET site, the slope range is 0.53–0.99, the average value is 0.79, the intercept range is -32.9 to 36.9 $W\ m^{-2}$, and the average value is 3.7 $W\ m^{-2}$, including grassland, farmland, and forest (Wilson et al., 2002). At the ChinaFLUX stations, the slope variation range is 0.49–0.81, the average value is 0.67, the intercept value range is 10.8–79.9 $W\ m^{-2}$, and the average value is 28.9 $W\ m^{-2}$ (Li et al., 2005). The EBR of FLUXNET sites is between 0.34 and 1.69, with an average value of 0.84; the EBR range of ChinaFLUX sites is 0.58–1.00, with an average value of 0.83 (Li et al., 2005). The water and heat fluxes of different underlying surfaces are very different. Next, depending on the characteristics of the underlying surface, the degree of surface energy closure varies. The closure rate of desert and the desert underlying surface is 63%–96% (Beyrich, et al., 2002).

In the observation period of 2019 (2021), the energy closure of the Inner Mongolian desert ecosystem was 64% (63%). However, the phenomenon of energy non-closure in the study area always existed, and the range of energy loss is 30%–40%. According to the half-hour flux data, the EBR range in different periods was 0.54–0.74. The EBR value in the growth period was the largest, followed by the pre-

growth period, and the EBR value in both the declining period and the freezing period was small. By comparing the results of the two methods, it was found that the slope of the OLS method can reflect the closure of the energy balance only when the correlation coefficient of the regression equation is effective. The EBR method needs to average the random error of the measured half-hour values to analyze the equilibrium ratio of all energy over a certain period of time.

5 CONCLUSION

The maximum value of the daily average of R_n during 2019–2021 was 251.73, 208.17, and 193.65 $W\ m^{-2}$, respectively. The energy distribution showed obvious seasonal and diurnal changes. The distribution of R_n in the Inner Mongolian desert ecosystem is mainly dominated by H . The energy distribution of H/R_n fluctuated greatly, showing a U-shaped change trend, while LE/R_n generally presents an inverted V-shaped distribution, and LE/R_n was low in winter, fluctuating above and below zero. Next, G/R_n fluctuated slightly in the growing season and was < 0.1 . The energy component and energy distribution showed reasonable correlation with various environmental factors. The main factor affecting sensible heat was R_n , followed by VPD , soil temperature, T_a , and RH . For latent heat, the main influencing factors were T_a , soil temperature, and R_n .

The energy closure rate of half-hour flux data in the Inner Mongolian desert ecosystem in different periods was different, with a variation range of 48%–68%. In different years, little difference occurred in the degree of energy closure. According to the half-hour flux data, the EBR range in the different periods was 0.54–0.74. The EBR value in the vigorous growth period was largest, followed by that in the early growth period, and the EBR value in both the declining period and the freezing period was small. The energy closure during the day was higher than that at night. Comparison and analysis of the energy closure at the half-hour and daily average scales revealed that the energy closure of the daily average flux in 2019, 2020, and 2021 was 67%, 66%, and 67%, respectively, i.e., higher than that at the half-hour scale (64%, 66%, and 63%, respectively).

The special location of the desert ecosystem in Inner Mongolia increases the complexity of the spatial distribution and temporal variation of the physical quantities on the surface. Additionally, this study did not consider the energy closure caused by the loss of energy flux, heat storage in the vegetation canopy and air, measurement errors, and other issues. Furthermore, the

continuity and integrity of the data need to be improved. Analysis of the energy balance during other weather conditions and seasons or on longer time scales is lacking for this region. Therefore, the heat and water transfer in the Dengkou Desert ecosystem in Inner Mongolia needs further study.

DATA AVAILABILITY STATEMENT

The original contributions presented in the study are included in the article/Supplementary Material. Further inquiries can be directed to the corresponding author.

AUTHOR CONTRIBUTIONS

YP and ZX contributed to conception and design of the study. YP wrote the original draft. HX contributed to the revision of the

manuscript. All authors contributed to manuscript revision, read, and approved the submitted version.

FUNDING

This study was funded by the Project of Intergovernmental International Cooperation in Science and Technology Innovation (NO. 2019YFE0116500).

ACKNOWLEDGMENTS

We are grateful for the support from the Inner Mongolia Dengkou Desert Ecosystem National Observation Research Station, Dengkou, China. We also thank the journal editors and reviewers for their comments and efforts on this article. Also, we thank James Buxton, MSc, from Liwen Bianji (Edanz) (www.liwenbianji.cn/), for editing the English text of a draft of this manuscript.

REFERENCES

- Beyrich, F., De Bruin, H. A. R., Schipper, J. W., Meijninger, W. M. L., Lohse, H., and Lohse, H. (2002). Results from One-Year Continuous Operation of a Large Aperture Scintillometer Over a Heterogeneous Land Surface. *Boundary-Lay. Meteorol.* 105 (1), 85–97. doi:10.1023/a:1019640014027
- Brown, K. W., and Rosenberg, N. J. (1973). A Resistance Model to Predict Evapotranspiration and its Application to a Sugar Beet Field¹. *Agron. J.* 65 (3), 341–347. doi:10.2134/agronj1973.00021962006500030001x
- Curry, J., and Webster, P. (1999). *Thermodynamics of Atmospheres and Oceans*. San Diego, CA: Academic Press, 65, 1–471.
- Falge, E., Baldocchi, D., Olson, R., Anthoni, P., Aubinet, M., Bernhofer, C., et al. (2001). Gap Filling Strategies for Defensible Annual Sums of Net Ecosystem Exchange. *Agric. For. Meteorol.* 107 (1), 43–69. doi:10.1016/s0168-1923(00)00225-2
- Huang, T. Y., Liu, X. T., Wang, G. L., Duan, L. M., and Chen, X. P. (2019). Dynamic Changes of Water and Heat Fluxes and Responses to Environmental Factors in Cascade Ecological Zone. *J. Soil Water Conserv.* 26 (03), 122–127+134. doi:10.13869/j.cnki.rswc.2019.03.018
- Jia, X., Zha, T. S., Gong, J. N., Zhang, Y. Q., Qin, S. G., Chen, G. P., et al. (2016). Energy Partitioning Over a Semi-Arid Shrubland in Northern China. *Hydrol. Process.* 30 (6), 972–985. doi:10.1002/hyp.10685
- Jiao, L., Ding, R., Kang, S., Du, T., Tong, L., and Li, S. (2018). A Comparison of Energy Partitioning and Evapotranspiration Over Closed Maize and Sparse Grapevine Canopies in Northwest China. *Agric. Water Manage.* 203, 251–260. doi:10.1016/j.agwat.2018.03.019
- Launiainen, S., Katul, G. G., Lindroth, A., Lohila, A., Aurela, M., Varlagin, A., et al. (2016). Do the Energy Fluxes and Surface Conductance of Boreal Coniferous Forests in Europe Scale with Leaf Area? *Glob. Change Biol.* 22 (12), 4096–4113. doi:10.1111/gcb.13497
- Launiainen, S. (2010). Seasonal and Inter-Annual Variability of Energy Exchange above a Boreal Scots Pine Forest. *Biogeosciences* 7 (12), 3921–3940. doi:10.5194/bg-7-3921-2010
- Li, H. D., Guan, D. X., Yuan, F. H., Ren, Y., Wang, A. Z., Jin, C. J., et al. (2014). Diurnal and Seasonal Variations of Energy Balance Over Horqin Meadow. *Chin. J. Appl. Ecol.* 25 (01), 69–76. doi:10.13287/j.1001-9332.2014.01.010
- Li, T., Yan, C. H., Wang, B., Zhao, W., L., Zhang, Y., and Qiu, G. Y. (2018). Characteristics of Energy Balance in a Mixed Forest in Jiuzhaigou Valley. *Acta Ecol. Sin.* 38 (22), 8098–8106. doi:10.5846/stxb201712182270
- Li, Z. Q., Yu, G. R., Wen, X. F., Zhang, L. M., Ren, C. Y., and Fu, Y. L. (2004). Evaluation of Energy Balance Closure of ChinaFLUX Network. *Sci. China Earth Sci.* 34 (S2), 46. doi:10.1360/zd2004-34-S2-46
- Li, Z. Q., Yu, G. R., Wen, X. F., Zhang, L. M., Ren, C. Y., and Fu, Y. L. (2005). Energy Balance Closure at ChinaFLUX Sites. *Sci. China (Ser. D)*. 48 (S1), 51–62. doi:10.1360/05zd0005
- Liu, H., and Feng, J. W. (2012). Seasonal and Interannual Variations of Evapotranspiration and Energy Exchange over Different Land Surfaces in a Semiarid Area of China. *J. Appl. Meteor. Clim.* 51 (10), 1875–1888. doi:10.1175/JAMC-D-11-0229.1
- Ma, H., Chen, Y. N., and Li, W. H. (2014). Characteristics of Energy Balance of Riparian *Tamarix* Shrubs in Desert. *J. Desert Res.* 34 (01), 108–117. (In Chinese). doi:10.7522/j.issn.1000-694X.2013.00134
- Mahrt, L. (1998). Flux Sampling Errors for Aircraft and Towers. *J. Atmos. Ocean. Technol.* 15 (2), 416–429. doi:10.1175/1520-0426(1998)015<0416:fsefaa>2.0.co;2
- Majozi, N. P., Mannaerts, C. M., Ramoelo, A., Mathieu, R., Nickless, A., and Verhoef, W. (2017). Analysing Surface Energy Balance Closure and Partitioning over a Semi-arid Savanna FLUXNET Site in Skukuza, Kruger National Park, South Africa. *Hydrol. Earth Syst. Sci.* 21 (7), 3401–3415. doi:10.5194/hess-21-3401-2017
- Matsumoto, K., Ohta, T., Nakai, T., Kuwada, T., Daikoku, K. I., Iida, S. I., et al. (2008). Energy Consumption and Evapotranspiration at Several Boreal and Temperate Forests in the Far East. *Agric. For. Meteorol.* 148 (12), 1978–1989. doi:10.1016/j.agrformet.2008.09.008
- Mihalakakou, G., Santamouris, M., Lewis, J. O., and Asimakopoulos, D., N. (1997). On the Application of the Energy Balance Equation to Predict Ground Temperature Profiles. *Sol. Energy* 60 (3–4), 181–190. doi:10.1016/s0038-092x(97)00012-1
- Niu, X. D., Liu, X. J., Liu, S. R., and Sun, P. S. (2018). Energy Balance Characteristics of a Natural Oak Forest (*Quercus Aliena*) at a Transitional Area from a Subtropical to Warm Temperate Climate, China. *Acta Ecol. Sin.* 38 (18), 6701–6711. (In Chinese). doi:10.5846/stxb201803290650
- Qi, F. F., Ali, M., Huo, W., He, Q., and Liu, Y. Q. (2020). Characteristics of Surface Radiation and Energy Balance and Microclimate in the Hinterland of Taklimakan Desert. *Arid. Meteorol.* 38 (1), 32–39. (In Chinese). doi:10.11755/j.issn.1006-7639(2020)-01-0032
- Reddy, N. N., Temimi, M., Fonseca, R. M., Weston, M. J., Wehbe, Y., Thota, M. S., et al. (2020). Micrometeorological Measurements in an Arid Environment: Diurnal Characteristics and Surface Energy Balance Closure. *Atmo. Res.* 234, 104745. doi:10.1016/j.atmosres.2019.104745
- Ren, X. Y., Zhang, Q., Yue, P., Yan, X., and Yang, Y. (2022). Energy Distribution Characteristics and Environmental Impact Factors in Different Regions of the Summer Monsoon Transition Zone. *Front. Environ. Sci.* 10 (4), 1–14. doi:10.3389/fenvs.2022.847725
- Renata, G. A., Carlo, R. D. M., Leonardo, J. G. A., Mariano, M. E., and Graciela, R. F. (2019). Energy Balance Closure in the Southwest Amazon Forest Site: Astatistical Approach. *Theor. Appl. Climatol.* 136 (3–4), 1209–1219. doi:10.1007/s00704-018-2548-8

- Swinbank, W. C. (1951). The Measurement of Vertical Transfer of Heat and Water Vapor by Eddies in the Lower Atmosphere. *J. Meteor.* 8 (3), 135–145. doi:10.1175/1520-0469(1951)008<0135:tmovto>2.0.co;2
- Tan, Z. H., Yu, G. R., Zhou, G. Y., Liao, Z. Y., Zhao, J. F., Yang, L. Y., et al. (2015). Microclimate of Forests across East Asia Biomes: 1. Radiation and Energy Balance. *Chin. J. Plant Ecol.* 39 (06), 541–553. doi:10.17521/cjpe.2015.0052
- Wang, X., Huo, Z., Shukla, M. K., Wang, X., Guo, P., Xu, X., et al. (2020). Energy Fluxes and Evapotranspiration Over Irrigated Maize Field in an Arid Area with Shallow Groundwater. *Agric. Water Manage.* 228, 105922. doi:10.1016/j.agwat.2019.105922
- Webb, E. K., Pearman, G. I., and Leuning, R. (1980). Correction of Flux Measurements for Density Effects Due to Heat and Water Vapour Transfer. *Q. J. Roy. Meteor. Soc.* 106 (447), 85–100. doi:10.1002/qj.49710644707
- Wilson, K. B., Goldstein, A. H., Falge, E., Tenhunen, J., Valentini, R., and Verma, S. (2002). Energy Balance Closure at FLUXNET Sites. *Agric. For. Meteorol.* 113 (1–4), 223–243. doi:10.1016/s0168-1923(02)00109-0
- Wu, F. T., Cao, S. K., Cao, G. C., Han, G. Z., Lin, Y. Y., and Chen, S. Y. (2018). Variation of CO₂ Flux of Alpine Wetland Ecosystem of *Kobresia Tibetica* Wet Meadow in Lake Qinghai. *J. Ecol. Rural. Environ.* 34 (02), 124–131. (In Chinese). doi:10.11934/j.issn.1673-4831.2018.02.004
- Yang, F., and Zhou, G. (2010). Characteristics and Driving Factors of Energy Budget Over a Temperate Desert Steppe in Inner Mongolia. *Acta Ecol. Sin.* 30 (21), 5769–5780.
- Yuan, W. W., Tong, X. J., Zhang, J. S., Meng, P., Li, J., and Zheng, N. (2015). Characteristics of Energy Balance of a Mixed Plantation in the Xiaolangdi Area in the Growing Season. *Acta Ecol. Sin.* 35 (13), 4492–4499. (In Chinese). doi:10.5846/stxb201411062195
- Yue, P., Zhang, Q., Yang, Y., Zhang, L., Zhang, H., Hao, X. C., et al. (2018). Seasonal and Inter-Annual Variability of the Bowen Smith Ratio over a Semi-Arid Grassland in the Chinese Loess Plateau. *Agric. For. Meteorol.* 252, 99–108. doi:10.1016/j.agrformet.2018.01.006
- Yue, P., Zhang, Q., Zhang, L., Li, H. Y., Yang, Y., Zeng, J., et al. (2019). Long-Term Variations in Energy Partitioning and Evapotranspiration in a Semiarid Grassland in the Loess Plateau of China. *Agric. For. Meteorol.* 278, 107671. doi:10.1016/j.agrformet.2019.107671
- Yue, P., Zhang, Q., Zhao, W., Wang, J. S., Wang, R., Y., Yao, Y. B., et al. (2013). Effects of Clouds and Precipitation Disturbance on the Surface Radiation Budget and Energy Balance over Loess Plateau Semi-Arid Grassland in China. *Acta Phys. Sin.* 62 (20), 1–14. (In Chinese). doi:10.7498/aps.62.209201
- Zhang, J. H., Ding, Z. H., Han, S. J., Zou, C.-J., and Zhou, Y.-M. (2002). Turbulence Regime Near the Forest Floor of a Mixed Broad Leaved Korean Pine Forest in Changbai Mountains. *J. For. Res.* 13 (2), 119–122. doi:10.1007/BF02857234
- Zhao, W., Z., Ji, X. B., and Liu, H. (2011). Progresses in Evapotranspiration Research and Prospect in Desert Oasis Evapotranspiration Research. *Arid. Zone Res.* 28 (03), 463–470. (In Chinese). doi:10.13866/j.azr.2011.03.029
- Zhou, G. L., Li, Y. H., Sun, X. Y., Zhang, T. J., and Zhao, C. L. (2019). Characteristics of Surface Energy Fluxes Over Different Types of Underlying Surfaces in North China. *Arid. Meteorol.* 37 (4), 577–585. (In Chinese).

Conflict of Interest: The authors declare that the research was conducted in the absence of any commercial or financial relationships that could be construed as a potential conflict of interest.

Publisher's Note: All claims expressed in this article are solely those of the authors and do not necessarily represent those of their affiliated organizations or those of the publisher, the editors, and the reviewers. Any product that may be evaluated in this article, or claim that may be made by its manufacturer, is not guaranteed or endorsed by the publisher.

Copyright © 2022 Pan, Xiao, Xin, Li, Miri and Cao. This is an open-access article distributed under the terms of the Creative Commons Attribution License (CC BY). The use, distribution or reproduction in other forums is permitted, provided the original author(s) and the copyright owner(s) are credited and that the original publication in this journal is cited, in accordance with accepted academic practice. No use, distribution or reproduction is permitted which does not comply with these terms.



Microclimate and Wind Regime of Three Typical Landscapes in the Northeastern Ulan Buh Desert

Fengmin Luo¹, Huijie Xiao², Junliang Gao¹, Yuan Ma¹, Xing Li¹, Junran Li³, Abbas Miri⁴, Qiqi Cao⁵ and Zhiming Xin^{1*}

¹Inner Mongolia Dengkou Desert Ecosystem National Observation Research Station/Experimental Center of Desert Forestry, Chinese Academy of Forestry, Dengkou, China, ²School of Soil and Water Conservation, Beijing Forestry University, Beijing, China, ³Department of Geosciences, The University of Tulsa, Tulsa, OK, United States, ⁴Department of Watershed and Range Management, Faculty of Water and Soil, University of Zabol, Zabol, Iran, ⁵Shandong Key Laboratory of Eco-Environmental Science for the Yellow River Delta, Binzhou University, Binzhou, China

OPEN ACCESS

Edited by:

Jifeng Deng,
Shenyang Agricultural University,
China

Reviewed by:

Liang Ning,
Nanjing Normal University, China
Guoming Zhang,
Beijing Normal University, China
Zhengcai Zhang,
Northwest Institute of Eco-
Environment and Resources (CAS),
China

*Correspondence:

Zhiming Xin
xzmlkn@163.com

Specialty section:

This article was submitted to
Drylands,
a section of the journal
Frontiers in Environmental Science

Received: 09 May 2022

Accepted: 14 June 2022

Published: 25 July 2022

Citation:

Luo F, Xiao H, Gao J, Ma Y, Li X, Li J,
Miri A, Cao Q and Xin Z (2022)
Microclimate and Wind Regime of
Three Typical Landscapes in the
Northeastern Ulan Buh Desert.
Front. Environ. Sci. 10:939739.
doi: 10.3389/fenvs.2022.939739

Knowledge of the microclimate and wind regimes of different land landscapes can be used to support natural resource development and agricultural productivity in desert areas. The aim of this study is to provide a theoretical basis and technical support for the management of Ulan Buh Desert Oasis and the comprehensive prevention and control of sandstorms from the surrounding desert in northern China. We examined the microclimate and wind regime of three landscapes—desert, desert–oasis ecotone, and oasis—and discussed the factors underlying the observed variations. Similar patterns were found in annual temperature, annual relative humidity, and wind speed between the desert, desert–oasis, and the oasis. Compared with the desert and the desert–oasis ecotone, the average annual temperature and wind speed in the oasis were lower by 2.56%–5.38% and 32.99%–37.05%, respectively. Average annual relative humidity in the oasis was higher than in other areas by 1.31%–2.57%. The desert, desert–oasis ecotone, and the oasis were dominated by westerly winds. Wind direction was relatively stable in the oasis and variable in the desert and desert–oasis ecotone. There were intermediate wind energy fields in the desert and the desert–oasis ecotone and a low wind energy field in the oasis. In the desert–oasis ecotone, drift potential (DP), resultant drift potential (RDP), and resultant drift direction (RDD) were 231.87 VU, 97.21 VU, and 104.33°, respectively. In the desert, DP was 228.45 VU, RDP was 92.65 VU, and RDD was 76.05°. In the oasis, the DP was 61.85 VU, RDP was 38.04 VU, and RDD was 92.97°. In the desert and the desert–oasis ecotone, sediment transport potential was the highest in spring, second highest in autumn, third highest in winter, and lowest in summer. In the oasis, it was the highest in winter, second highest in autumn, third highest in spring, and lowest in summer. There are complex variations in the dominant sediment transport directions in the desert and desert–oasis ecotone in the study area. Variations in the dominant sediment transport direction in the oasis are less complicated and are associated with the seasons. The oasis is primarily threatened by sandstorms from the south-southeast in spring.

Keywords: Ulan Buh desert, oasis, desert–oasis ecotone, meteorological data, wind and sand activity, drift potential

1 INTRODUCTION

Oasis exists in the desert but is different from the desert. Under certain conditions, matter and energy are exchanged between oases and deserts (Zhang and Hu, 2002). The desert–oasis ecotone is an important part of the ecological barrier between an oasis and the surrounding arid areas. There is a complex relationship between landscapes and microclimate (Feng et al., 2006). Sandstorm intensity plays a crucial role in oasis evolution (Wang, 2009). The microclimate serves as a quantitative indicator of the degree of desertification and the intensity of the feedback mechanisms in the desertification process (Shen et al., 1993). Wind is an important factor that affects landforms and causes the movement of sand in the arid regions of Northwest China (Skidmore, 1986). Sandstorms can cause a series of problems, including continued expansion of deserts, which constantly threatens the survival of oases (Lal, 2001). Desert and desert–oasis ecotone are distributed around the oasis with a fragile ecological environment. It is the main source of sandstorms in the oasis, which directly affects the stability and sustainable development of the oasis. In oases, humans have been conducting land development projects on unreasonable scales. Around oases, there have been frequent occurrences of sandstorms in recent years. As a result, the carrying capacities of oases have been declining year to year. Therefore, sand control and the protection of the oasis environment are becoming increasingly urgent priorities (Wen et al., 1996). Therefore, it is very important to study the synchronous wind conditions of the desert, desert–oasis ecotone, and oasis.

Most studies on desert wind and sand activity have mainly focused on evolution mechanisms, particle size, intensity of sand activity, and aeolian sand environments (Zu et al., 2005; He et al., 2009). An increasing number of studies are starting to examine oasis evolution, mechanisms, and wind field characteristics (Li et al., 2004; Yang et al., 2012; Mao et al., 2019). These studies provide important reference information for the control of sand activity and the protection of the oasis environment. In China, Ulan Buh Desert is an important source of sand. There has been a series of severe winds and sand activity events, and the desert is expanding eastward and southward (Du et al., 2012). The normal function of the transportation network and water conservation facilities of the adjacent oasis is affected. In the oasis, agriculture, animal husbandry, human health, and environmental security are being threatened (Du et al., 2012; Liu, 2013; Wang et al., 2015). The Ulan Buh Desert Oasis comprises mainly farmland and planted forests that act as shelterbelts. As an important part of the Three-North Shelter Forest Program, the Ulan Buh Desert Oasis plays an important role in promoting the economic development of the Hetao region as well as reducing the frequency and intensity of disasters associated with severe wind and sand activity events. Over the years, many studies have been carried out on the ecological effects of the shelterbelt (Hao, 2007; Luo et al., 2019) and the microclimate (Aussenac, 2000; Jin et al., 2017). However, there have been few systematic studies on the annual characteristics of the microclimate and wind regime of the different landscapes in the same region. There have been no comparison studies because of lack of synchronous data from different sites.

In this study, we collected meteorological data, including temperature, relative humidity, and wind speed and direction from Ulan Buh Desert, the oasis in the northeastern part of the desert, and the desert–oasis transition zone. We conducted a preliminary quantitative analysis of the differences between the three landscapes in terms of microclimate and wind regime.

2 MATERIALS AND METHODS

2.1 Study Area

Ulan Buh Desert is a transition zone between the arid and semiarid regions in northern China (Figure 1). It covers a total area of about $1.0 \times 10^4 \text{ km}^2$. It has an elevation of 1,028–1,054 m and an elevation decrease in the direction of Hetao Plain (Du et al., 2012). The region has a temperate continental monsoon climate, which is under the effects of the southeastern monsoon in summer and autumn and the control of the Siberian–Mongolian cold anticyclone in winter and spring. The main natural disasters in the study area are associated with severe wind and sand activity events (Luo et al., 2019). The tower in the desert has a distance of 14.55 km from that in the desert–oasis, and the tower in the desert–oasis has a distance of 2.85 km from that in the oasis. The desert mainly comprises mobile and semi-fixed dunes. The desert–oasis ecotone comprises fixed and semi-fixed dunes, which are dominated by *Nitraria tangutorum* at a height of 1.2–3.6 m. The oasis area is protected by a shelterbelt, which covers an area of 1,487.3 ha. The shelterbelt is 32 m wide and comprises eight rows of trees. Spacing of auxiliary and miniature forest belts is 98 and 398 m, respectively (Figure 2).

2.2 Data Acquisition

Meteorological data were simultaneously collected using Windsonic two-dimensional ultrasonic wind speed and direction sensors (1590-PK-020, Campbell, USA) and temperature and humidity sensors (1590-PK-020, Campbell, USA). The anemometer has a minimum detectable wind speed of 0.01 m/s. Accuracy, operating range, and output resolution are $\pm 3^\circ$, 0–359°, and 1° for wind direction and $\pm 2\%$, 0–60 m/s, and 0.01 m/s for wind speed, respectively.

The instruments were installed on three towers located in the desert, desert–oasis, and oasis. The tower in the desert has a distance of 14.55 km from that in the desert–oasis, and the tower in the desert–oasis has a distance of 2.85 km from that in the oasis. Measurements of temperature and relative humidity were made at a height of 8 m. Wind speed and direction were monitored at a height of 12 m. To ensure data quality, we calibrated the instruments on the three towers simultaneously, examined extreme data values, and verified the time consistency of the non-conforming data. In this study, following the conventional definition of seasons used by the meteorology community in China (Zhu et al., 2005), March to May was defined as spring, June to August as summer, September to November as autumn, and December to February as winter. The data were collected between January 1 and 31 December 2018.

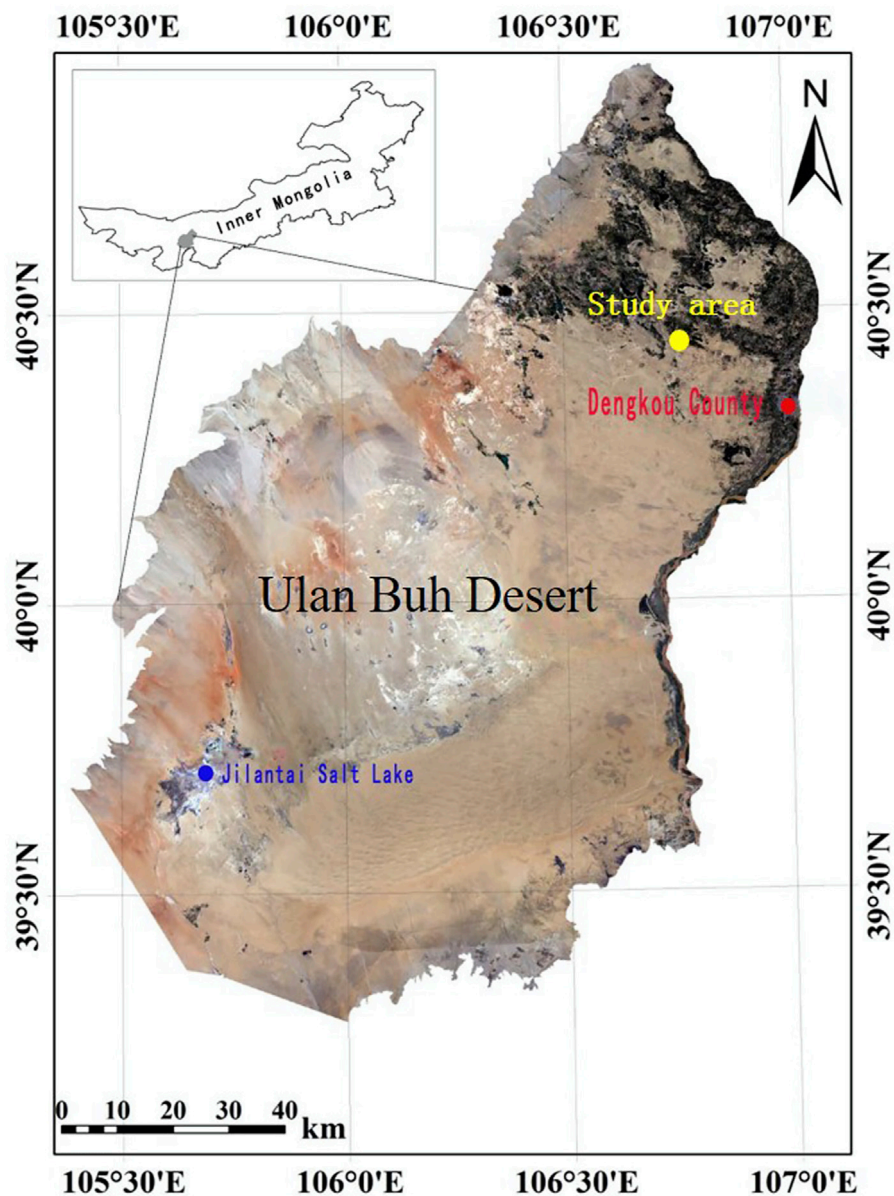


FIGURE 1 | Location of the study area.



FIGURE 2 | Map of three landscapes in the northeastern Ulan Buh Desert. (A) Desert area, (B) Desert-oasis ecotone, and (C) Oasis.

2.3 Data Analysis

We used wind speed and direction and sandstorm frequency data, which were available in 10-min units. Following Du et al. (2015), months with the sand-driving wind (≥ 5 m/s) were identified, and the average and maximum wind speeds were calculated for these months. It is calculated as follows:

$$u_t = \frac{u_{*t}}{k} \ln \frac{z}{z_0}, \quad (1)$$

where u_t is critical friction speed, k is Karman constant (0.4), z is the height (2.0 m), and z_0 is the dynamic roughness (3.265×10^{-3} m).

We calculated the frequency and speed of sand-moving wind from each of the 16 cardinal, intercardinal, and secondary intercardinal directions (N, NNE, NE, ENE, E, ESE, SE, SSE, S, SW, SSW, W, WNW, NW and NNW), and wind speed (V) was classified into four categories including $5 \text{ m/s} \leq V < 7 \text{ m/s}$, $7 \text{ m/s} \leq V < 9 \text{ m/s}$, $9 \text{ m/s} \leq V < 11 \text{ m/s}$, and $V \geq 11 \text{ m/s}$. The results were represented on sandstorm rose diagrams (Fan et al., 2006).

The sand drift potential (DP) is an important parameter that reflects the potential sand transport capacity of a region (An et al., 2018). It represents yearly total wind power and therefore describes the potential maximum amount of sand transport for each wind direction that includes values above the threshold velocity, and it is in a vector unit (VU). According to the calculation of the DP equation proposed by Fryberger and Dean (1979), the DP in different periods can be obtained. It is calculated as follows:

$$DP = V^2 (V - V_t)t, \quad (2)$$

where DP is the sand transport potential or drift potential, expressed in vector unit VU; V is the sand-driving wind speed in knots ($1 \text{ knot} \approx 0.5 \text{ m/s}$); V_t is the critical sand-driving wind speed in knots; t is the sand-driving wind time, which is the duration of sand-driving wind observed during the observation period as a percentage of the duration of the observation period.

Resultant drift potential (RDP) represents the net DP (magnitude and direction) based on a summation of the DP values in each compass direction. It is calculated as follows (Al-Awadhi et al., 2005):

$$RDP = (C^2 - D^2)^{0.5}, \quad (3)$$

$$C = \sum (VV) \sin(\theta), \quad (4)$$

$$D = \sum (VV) \cos(\theta), \quad (5)$$

where VV represents the DP in each wind direction (in this article, we grouped winds into 16 sand transport directions), in vector units, and θ is the angle measured clockwise from 0 (north) for the midpoint of each wind direction class.

The resultant drift direction (RDD) represents the direction in which sand will be transported. It is calculated as follows (Al-Awadhi et al., 2005):

$$RDD = \arctan(C/D). \quad (6)$$

Directional variability (RDP/DP) is the ratio of the resultant drift potential (RDP) to the drift potential (DP). RDP/DP values

close to 1 indicate a narrowly unidirectional wind regime, with a single dominant drift direction, whereas values close to 0 indicate a multidirectional wind regime with multiple significant drift directions.

According to DP values, the regional wind energy field was classified as high (>400 VU), intermediate (200–400 VU), or low (<200 VU). The directional variability index was also classified as high (≥ 0.8), intermediate (0.3–0.8), or low (≤ 0.3) (Zhang et al., 2011).

3 RESULTS

3.1 Annual Variations

For the desert, desert–oasis ecotone, and the oasis, the annual average temperatures were 9.66, 9.38, and 9.14°C, respectively. The annual average relative humidity was 40.07, 40.58, and 41.11%, respectively. The annual average wind speeds were 4.13, 3.88, and 2.60 m/s, respectively (Figure 3). The oasis reduced the average annual temperature by 2.56%–5.38%, increased the average relative humidity by 1.31%–2.57%, and reduced the average annual wind speed by 32.99%–37.05%. The annual temperature curves were similar in the desert, desert–oasis, and oasis (Figure 3A). In July, the temperature in the oasis was 0.38°C lower than that in the desert and 1.17°C lower than that in the desert–oasis ecotone. In January, the temperature in the oasis was 1.00°C higher than that in the desert and 0.31°C higher than that in the desert–oasis ecotone. The annual relative humidity curves were similar in the three areas (Figure 3B). The relative humidity was the highest in August and the lowest in March. The three annual wind speed curves were similar in the three areas (Figure 3C). The wind speed was the highest in the desert (the annual average wind speed was 4.13 m/s) and the lowest in the oasis (the annual average wind speed was 2.60 m/s). The differences between the three landscapes were considerable in terms of wind speed but were small in terms of air temperature and relative humidity. Monthly distributions of air temperature and relative humidity are highly similar for the three ecosystems monitored. However, wind speed in the oasis is notably lower than in both desert–oasis and desert systems.

The desert, desert–oasis ecotone, and the oasis were dominated by westerly winds (W, WSW, SW, and SSW) (Figure 4). In the desert, the main wind directions were SW and SSW. In the desert–oasis ecotone, the main wind direction was SW. The frequency of winds from NE was also relatively high, but speeds were low (5–7 m/s). In the oasis, the main wind directions were W and WNW. Wind direction was relatively stable in the oasis and was variable in the desert and in the desert–oasis ecotone.

Among the three landscapes, the drift potential (DP) was the highest (231.87 VU) in the desert–oasis ecotone. This indicates the presence of a low wind energy field (Figure 5). The resultant drift potential (RDP) and resultant drift direction (RDD) were 97.21 VU and 104.33°, respectively. The directional variability index (RDP/DP) was medium (0.40). Northwest and northeast

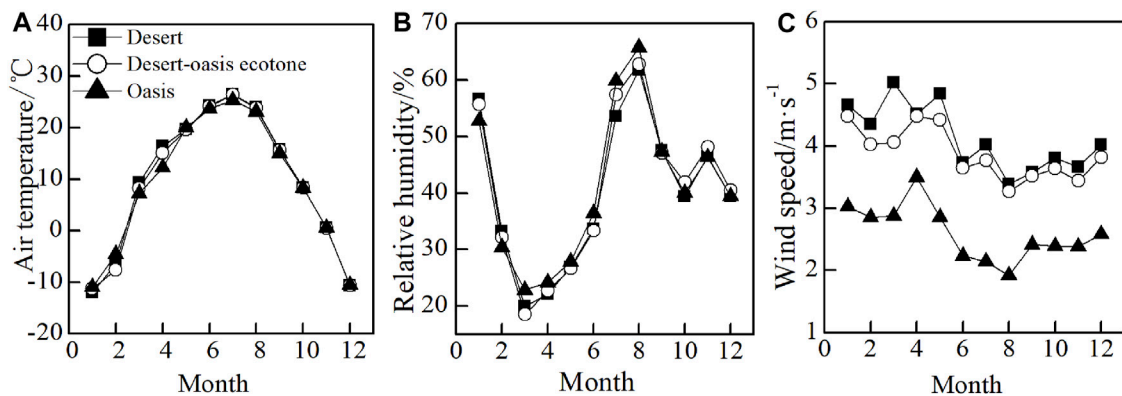


FIGURE 3 | Monthly variations of (A) air temperature, (B) relative humidity, and (C) wind speed.

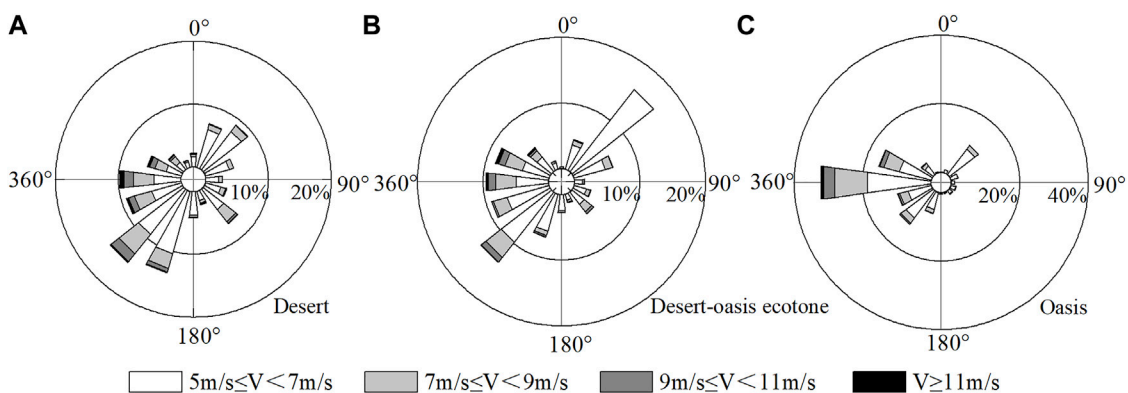


FIGURE 4 | Wind speed and direction rose chart for the (A) desert, (B) desert-oasis ecotone, and (C) oasis during the experimental period of time. The different parts of wind rose represent the proportion of different wind speed segments in different directions.

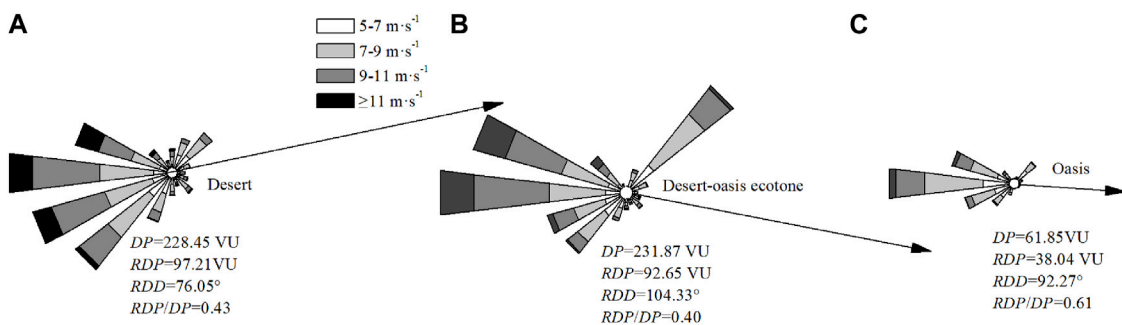


FIGURE 5 | Sand drift potential for the (A) desert, (B) desert-oasis ecotone, and (C) oasis during the experimental period of time. The calculated resultant drift potential (RDP) and resultant drift direction (RDD) are shown in black arrow.

were the dominant DP directions. DP in the NW was the highest, with a value of 115.74 VU, accounting for 49.92% of the annual DP. The DP was the second highest in the desert, with a value of 228.45 VU, indicating the presence of a low wind energy field. In the desert, the RDP was 92.65 VU, and RDD was 76.05°. The

RDP/DP was medium (0.43). There was more variability in the direction of sediment transport in the desert than that in the desert-oasis ecotone. In the desert, SW, WSW, W, and WNW were the dominant DP directions. DP values were 35.15, 41.61, 47.18, and 28.52 VU, respectively, and collectively accounted for

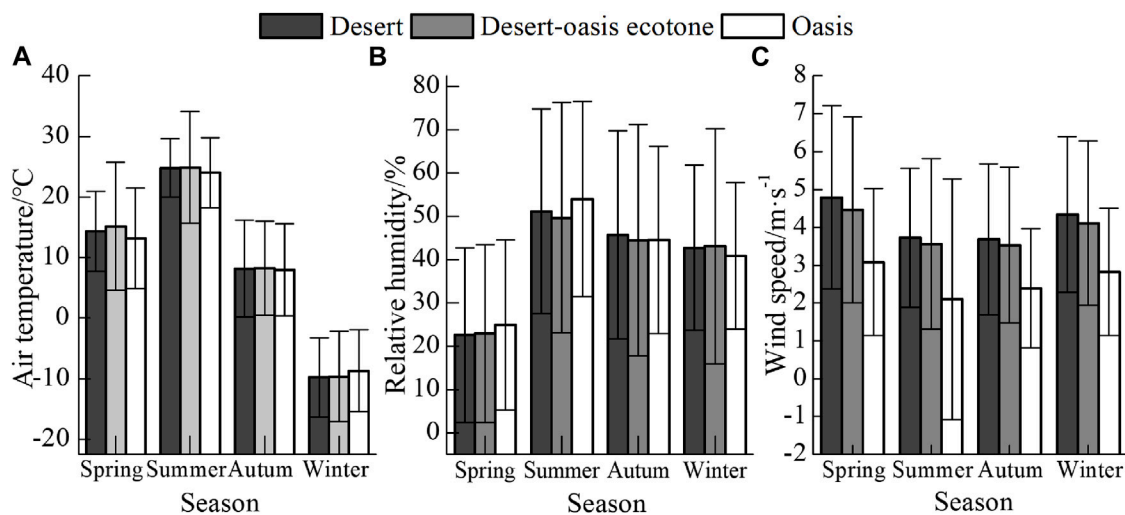


FIGURE 6 | Seasonal variations of (A) air temperature, (B) relative humidity, and (C) wind speed.

66.74% of the annual DP. The DP was the lowest in the oasis, with a value of 61.85 VU, indicating the presence of a low wind energy field. In the oasis, the RDP was 38.04 VU and RDD was 92.97°. The RDP/DP was medium (0.61). There was little variability in the direction of sediment transport; W and WNW were the dominant DP directions.

3.2 Seasonal Variations

For all three landscapes, average temperatures were the highest in summer, second highest in spring, and the third highest in autumn. The lowest average temperature was in winter. The average temperature was the highest in the desert–oasis ecotone and the second highest in the desert. The lowest average temperature was in the oasis. The difference between the average temperature in the desert–oasis ecotone and that in the desert was small (Figure 6). For all three landscapes, average relative humidity was the highest in summer, second highest in autumn, and third highest in winter. The lowest average relative humidity was in spring. The average relative humidity was the highest in the oasis and second highest in the desert. The lowest average relative humidity was in the desert–oasis ecotone. The difference between the relative humidity in the desert–oasis ecotone and that of the desert was small. There were large differences between the average wind speeds associated with the three landscapes. For each season, the average wind speed was the highest in the desert, the second highest in the desert–oasis ecotone, and the lowest in the oasis. For the three landscapes, average wind speeds were the highest in spring. In the desert and the desert–oasis ecotone, average wind speeds were the second highest in winter, the third highest in summer, and the lowest in autumn. In the oasis, the average wind speed was the second highest in winter, the third highest in autumn, and the lowest in summer. The summer lush vegetation weakens the wind. As a result, the average wind speed in summer is lower than that in autumn.

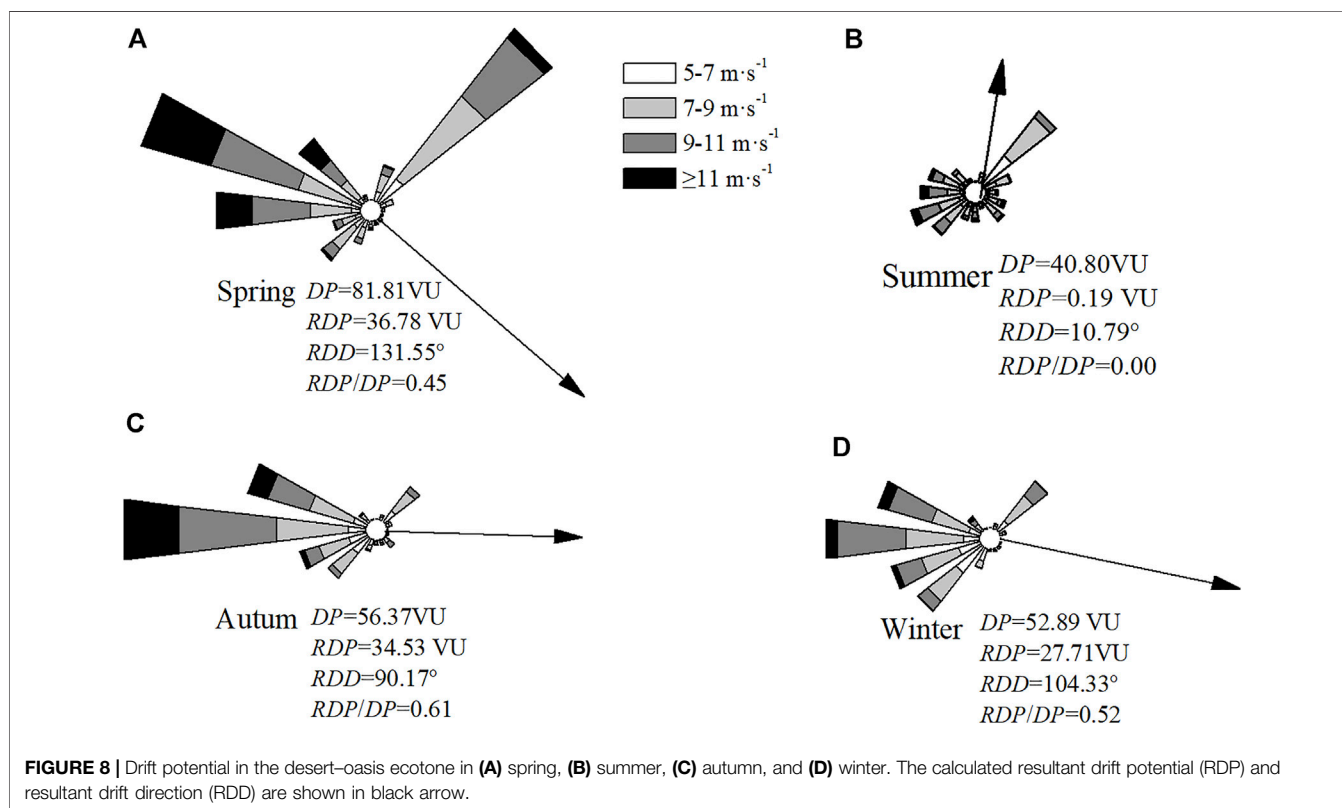
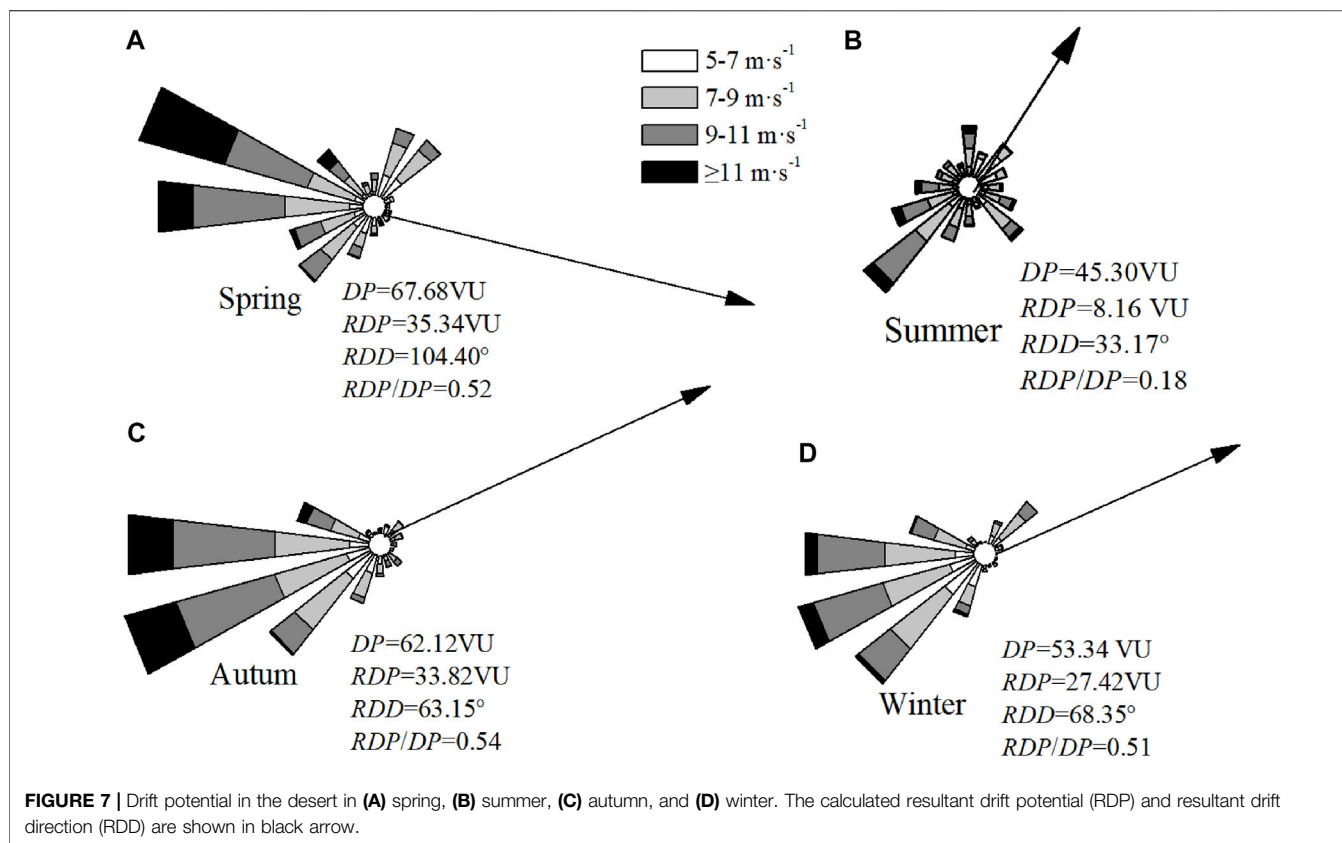
In the desert, seasonal variations were observed in DP. The DP and RDP in spring were considerably higher (67.68 VU and 35.34 VU, respectively) than those in other seasons (Figure 7). In

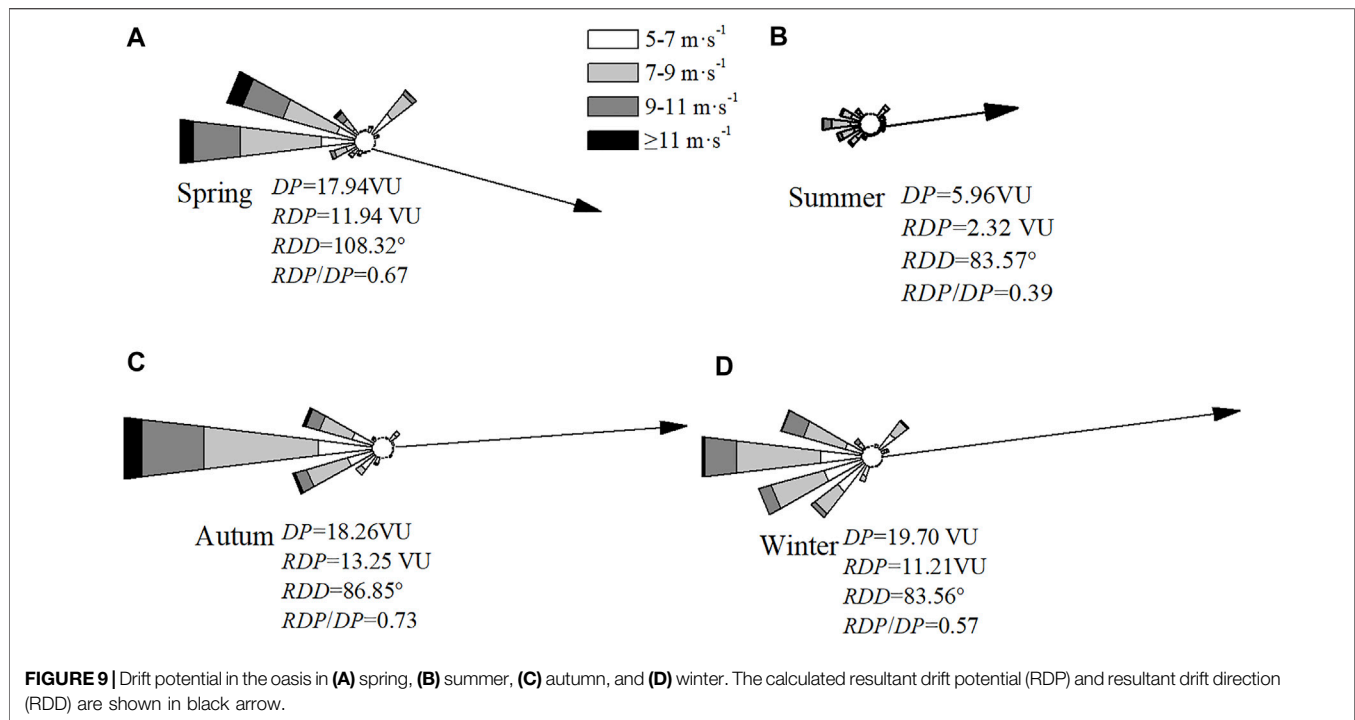
spring, the RDD was 104.40° (ESE) and the RDP/DP was medium (0.52). In autumn, the DP and RDP were the second highest (62.12 VU and 33.82 VU, respectively), the RDD was 63.15° (ENE), and the RDP/DP was medium (0.54). In winter, DP and RDP were 53.34 VU and 27.42 VU, respectively, the RDD was 68.35° (ENE), and the RDP/DP was medium (0.51). In summer, the DP and RDP were the lowest (45.30 VU and 8.16 VU, respectively), the RDD is 33.17° (NNE), and the RDP/DP was low (0.18).

In the study area, the average wind speed is relatively high in spring (Figure 5). Relatively high wind speed, low precipitation, melting of frozen surface soil, surface exposure, and the combined action of multiple factors create favorable dynamic conditions and abundant sand sources for surface sand migration in spring. As a result, sandstorm activity in the study area is the highest in spring.

In the desert–oasis, seasonal variations were observed in DP. In the desert–oasis ecotone, the DP and RDP in spring were considerably higher (81.81 VU and 36.78 VU, respectively) than those in other seasons (Figure 8). In spring, the RDD was 131.55° (SE) and the RDP/DP was medium (0.45) and the DP and RDP in the autumn (56.37 VU and 34.53 VU, respectively) were the second highest. In autumn, the RDD was 90.17° (E) and the RDP/DP was medium (0.61). In winter, DP and RDP were 52.89 VU and 27.71 VU, respectively, the RDD was 104.33° (ESE), and the RDP/DP was medium (0.52). In summer, the DP and RDP were the lowest (40.80 VU and 0.19 VU, respectively), the RDD was 10.79° (NNE), and the RDP/DP was low (0.00).

In the oasis, DP was the highest in winter, second highest in autumn, third highest in spring, and lowest in summer (Figure 9). In winter, the DP and RDP were 19.70 VU and 11.12 VU, respectively, the RDD was 83.56° (E), and the RDP/DP was medium (0.57). In autumn, the DP and RDP were 18.26 VU and 13.25 VU, respectively, the RDD was 86.85° (E), and the RDP/DP was medium (0.73). In spring, the DP and RDP were 17.94 VU and 11.94 VU, respectively, the RDD was 108.32° (ESE) and the RDP/DP was medium (0.67). In summer, the DP and





RDP were 5.96 VU and 2.32 VU, respectively, the RDD was 83.57° (E) and the RDP/DP was medium (0.39).

In the desert and desert–oasis ecotone, DP was the highest in spring, second highest in autumn, third highest in winter, and lowest in summer. In the oasis, DP was the highest in winter, second highest in autumn, third highest in spring, and lowest in summer. In the desert, the dominant DP direction shifted over the seasons. It was ESE in spring, NNE in summer, ENE in autumn, and ENE in winter. In the desert–oasis ecotone, the dominant DP direction also shifted over the seasons. It was SE in spring, NNE in summer, E in autumn, and ESE in winter. In the oasis, the dominant DP direction was ESE in spring and remained E throughout summer, autumn, and winter. Our results indicate complex variations in the dominant sediment transport directions in the desert and desert–oasis ecotone. Variations in the dominant sediment transport direction in the oasis are less complex and are associated with the seasons. The oasis is primarily threatened by sandstorms from the south-southeast in spring.

4 DISCUSSION

In this study, we analyzed meteorological data obtained simultaneously at three observation sites located in the desert, the desert–oasis ecotone, and the oasis to improve our understanding of atmospheric circulation. The three sites differ in terms of terrain and thermal characteristics. Therefore, we also found differences in terms of local meteorological elements, including wind speed and direction. Our results show that microclimate and wind regime vary with landscapes.

The sand drift potential reflected the ability of sand transport by wind in a certain period. It is an important measure of the

intensity of regional sand activity and aeolian landform evolution (Fryberger and Dean, 1979). There are complex interactions and feedback mechanisms between sand activity and landscapes (Mao et al., 2017). Factors such as atmospheric circulation, landscape, and topography result in considerable variations between wind regimes of different regions. The wind regime is an important determinant of the characteristics of aeolian landforms (Zu et al., 2005). Knowledge of the wind regime is essential for estimating the intensity and regularity of sand activity and formulating measures to prevent and control sandstorm damage. Because wind speed is greatly reduced by the blocking effect of the tall trees and crops in the oasis, the average monthly wind speed in the oasis is much lower than that in the desert and desert–oasis ecotone (Mao et al., 2017). Differences in wind speed in the three landscapes result in considerable differences in the drift potential. Wind frequency and drift potential are the highest in the desert and desert–oasis ecotone, where there are medium wind energy fields. Drift potential is the lowest in the oasis, where there is a low wind energy field. Similar characteristics were found in the wind dynamic environment between the typical surface in the Dunhuang. Due to the difference of wind speed, the sand transport potential of desert, oasis, and Gobi is significantly different. Gobi has the highest sand-driving wind frequency and sand transport potential and belongs to the high wind energy field. The desert and oasis have lower sand transport potential than the Gobi and belong to the low wind energy field.

In the desert and desert–oasis ecotone, wind and drift potential are higher in spring and autumn. In the oasis, wind and drift potential are higher in spring, autumn, and winter. In the desert and the desert–oasis ecotone, the drift potential is the highest in spring. In the oasis, the drift potential is the highest in

winter; the difference between the drift potential in winter and that in spring is small. Therefore, it is necessary to implement measures to prevent and control sandstorms in spring in the study area.

Differences in surface vegetation types, vegetation coverage, topography, water distribution, surface soil composition, and seasonal variations result in considerable differences between the climate in the desert and the climate in the oasis (Zhu et al., 2005; Yu et al., 2020). Vegetation improves the local microclimate in deserts and has a positive impact on regional climate regulation (Pan et al., 2004; Shi et al., 2015). The effects of desert plant species on microclimate vary and can include cooling, humidification, and windbreaking (Pang et al., 2011). The oasis in northeastern Ulan Buh Desert reduced the average annual temperature and wind speed by 2.56%–5.38% and 32.99%–37.05%, respectively, and increased the average annual relative humidity by 1.31%–2.57%. The shelterbelt clearly improved the local microclimate by reducing the temperature and increasing the humidity in the oasis (Hu et al., 1992; Zhang et al., 1996). Our results show the positive effects of oasis shelterbelts in regulating microclimate include cooling, humidifying, and reducing wind speed. Oasis shelterbelts support the sustainable development of oases. Heat is transferred from the ground to the atmospheric boundary layer *via* radiation, turbulence, convection, and latent heat transfer. Vegetation absorbs and reflects solar radiation and reduces atmospheric heating and air temperature. Transpiration and the shading effect of plants result in lower temperature and higher humidity in the oasis and contribute toward the cold island effect of oases (Du et al., 2015). The tall shelterbelt blocks airflow and leads to lower wind speed in the oasis.

The difference in landscape between the desert and the oasis results in strong local atmospheric circulations and interactions (Zuo and Hu 1994). In northeastern Ulan Buh Desert, there are also local exchanges of water and heat between the desert and the oasis. Vegetation cover and soil moisture are the main factors affecting the difference in microclimate between the oasis and the desert (Lv et al., 2005). Therefore, to improve the microclimate, ensure agricultural productivity, and protect human health, vegetation coverage should be increased, in both natural and planted vegetation. If conditions permit, measures to reduce the amount of water used in agricultural irrigation can be strengthened to improve the microclimate and ensure agricultural productivity in the oasis.

Studies of the characteristics of sand activity in different regions in northern China and their relationships with aeolian landform formation can provide a theoretical basis for the evaluation of future sand activity intensity. The findings contribute to the field of aeolian landform research and provide reference information that can be used to design measures to control sandstorm hazards in different areas. To evaluate the intensity of regional surface sand activity, we need to analyze field observations of wind and sand activity in addition to wind speed and direction data.

5 CONCLUSION

- 1) The annual temperature curves were similar between the desert, desert–oasis, and oasis. Similarity in the annual relative humidity and wind speed curves was also found

between the three sites. The oasis reduced average annual temperature and wind speed by 2.56%–5.38% and 32.99%–37.05%, respectively, and increased the average annual relative humidity by 1.31%–2.57%.

- 2) The desert, desert–oasis ecotone, and oasis were dominated by westerly winds. Wind direction was relatively stable in the oasis and was variable in the desert and in the desert–oasis ecotone.
- 3) There were large differences between the annual drift potential of the three landscapes. There were intermediate wind energy fields in the desert and the desert–oasis ecotone and a low wind energy field in the oasis. In the desert–oasis ecotone, drift potential (DP), resultant drift potential (RDP), and resultant drift direction (RDD) were 231.87 VU, 97.21 VU, and 104.33°, respectively. In the desert, DP was 228.45 VU, RDP was 92.65 VU, and RDD was 76.05°. In the oasis, the DP was 61.85 VU, RDP was 38.04 VU, and RDD was 92.97°.
- 4) In the desert and the desert–oasis ecotone, sand transport potential was the highest in spring, second highest in autumn, third highest in winter, and lowest in summer. In the oasis, it was the highest in winter, second highest in autumn, third highest in spring, and lowest in summer. There are complex variations in the dominant sediment transport directions in the desert and desert–oasis ecotone in the study area. Variations in the dominant sediment transport direction in the oasis are less complex and are associated with the seasons. The oasis is primarily threatened by sandstorms from the south-southeast in spring.

DATA AVAILABILITY STATEMENT

The original contributions presented in the study are included in the article/Supplementary Material. Further inquiries can be directed to the corresponding author.

AUTHOR CONTRIBUTIONS

FL, HX, JG, YM, XL, and ZX contributed to the conception and design of the study. FL organized the database. HX performed the statistical analysis. FL wrote the first draft of the manuscript. HX, JG, YM, XL, JL, AM, QC, and ZX wrote sections of the manuscript. All authors contributed to manuscript revision and read and approved the submitted version.

FUNDING

This study was funded by the Project of Intergovernmental International Cooperation in Science and Technology Innovation (NO.2019YFE0116500) and the Science and Technology Planning Project of Inner Mongolia Autonomous Region (2020GG0125).

REFERENCES

- Al-Awadhi, J. M., Al-Helal, A., and Al-Enezi, A. (2005). Sand Drift Potential in the Desert of Kuwait. *J. Arid Environ.* 63, 425–438. doi:10.1016/j.jaridenv.2005.03.011
- An, Z.-s., Zhang, K.-c., Tan, L.-h., Zhang, H., and Niu, B.-c. (2018). Dune Dynamics in the Southern Edge of Dunhuang Oasis and Implications for the Oasis Protection. *J. Mt. Sci.* 15 (10), 2172–2181. doi:10.1007/s11629-017-4723-2
- Aussenac, G. (2000). Interactions Between Forest Stands and Microclimate: Ecophysiological Aspects and Consequences for Silviculture. *Ann. For. Sci.* 57 (3), 287–301. doi:10.1051/forest:2000119
- Du, H. Q., Xue, X., and Sun, J. H. (2012). Underlying Surface Characteristics and Observation of Blown-Sand Movement in Ulan Buh Desert Along Bank of Yellow River. *Trans. Chin. Soc. Agric. Eng.* 28 (22), 156–165. doi:10.3969/j.issn.1002-6819.2012.22.023
- Du, M. X., Zhang, M. J., and Wang, S. J. (2015). The Cold Island and Wet Island Effects of Typical Oases in Xinjiang. *Chin. J. Ecol.* 34 (6), 1523–1531. doi:10.13292/j.1000-4890.2015.0132
- Fan, L. H., Ge, L. M., He, Q., and Pan, X. L. (2006). Analysis On Daily Change of Climate Characteristics About Oasis-Intermediate Belt-Desert. *J. Xinjiang Agric. Univ.* 29 (1), 5–9.
- Feng, Q., Si, J., Zhang, Y., Yao, J., Liu, W., and Su, Y. (2006). Microclimatic Characteristics of The Heihe Oasis in The Hyperarid Zone of China. *J. Geogr. Sci.* 16 (1), 34–44. doi:10.1007/s11442-006-0104-4
- Fryberger, S. G., and Dean, G. (1979). “Dune Forms and Wind Regime,” in *A Study of Global Sand Seas*. Editor E. D. McKee (Washington D.C.: U.S. Government Printing Office), 137–169.
- Hao, Y. G. (2007). *Study on Ecological Effects of Oasis-Making Process in The Northeast Part of Ulan Buh Desert*. Beijing: Beijing Forestry University.
- He, Q., Yang, X. H., Huo, W., Wang, S. G., Shang, K. Z., and Liu, H. Y. (2009). Characteristics of Sand Granularity from Kumtag Desert and its Environmental Significance. *J. Desert Res.* 29 (1), 18–22.
- Hu, Y. Q., Yang, X. L., and Zhang, Q. (1992). The Characters of Energy Budget on The Gobi and Desert Surface in Hexi Region. *Acta Meteorol. Sin.* 26 (1), 86–95. CNKI: SUN:QXXW.0.1992-01-007.
- Jin, L. L., Li, Z. J., He, Q., Huo, W., Yang, F., and Yang, X. H. (2017). Microclimate Over the Center and Edge Areas of The Artificial Shelter Forest Land in Taklimakan Desert. *J. Desert Res.* 37 (5), 986–996. doi:10.7522/j.issn.1000-694X.2016.00068
- Lal, R. (2001). Soil Degradation by Erosion. *Land Degrad. Dev.* 12, 519–539. doi:10.1002/ldr.472
- Li, S., Li, F., Sun, W., and Li, B. S. (2004). Modern Desertification Process in Ejina Oasis and its Dynamic Mechanism. *Sci. Geogr. Sin.* 24 (1), 61–67. doi:10.13249/j.cnki.sgs.2004.01.61
- Liu, Y. (2013). *Research on Dynamic Change of Land Use in Ulan Buh Desert in Recent 40 Years*. Hohhot: Inner Mongolia Normal University.
- Luo, F. M., Gao, J. L., Xin, Z. M., Hao, Y. G., Ge, G. B. T., Li, X. L., et al. (2019). Low-altitude Structure of Sandstorms for inside and Outside the Shelterbelt in The Northeast Marginal Zone of the Ulan Buh Desert. *Arid Zone Res.* 36 (4), 1032–1040. doi:10.13866/j.azr.2019.04.29
- Lv, S. H., Shang, L. Y., Liang, L., and Luo, S. Q. (2005). Numerical Simulation of Microclimate Effect in Jinta Oasis. *Plateau Meteorol.* 24 (5), 649–655.
- Mao, D. L., Cai, F. Y., Lei, J. Q., Yang, X. F., Yang, Y. H., and Xuan, J. (2017). Spatial Analysis on Changes of Microclimate in Typical Landscapes in Desert-Wilderness-Oasis in Cele, Xinjiang. *Sci. Geogr. Sin.* 37 (4), 630–640. doi:10.13249/j.cnki.sgs.2017.04.017
- Mao, D. L., Cai, F. Y., Yang, X. F., Wang, X. M., Lai, F. B., and Xue, J. (2019). Characteristics of Wind Filed Over Different Underlying Surfaces in The Oasis-Desert Ecotone in Qira, Xinjiang. *Arid Zone Res.* 36 (5), 1117–1126. doi:10.13866/j.azr.2019.05.08
- Pan, X. L., Zeng, X. B., Zhang, J., Shi, Q. D., Chao, Q. C., and Chao, J. P. (2004). Interaction of Evolution of Ecological Landscape Pattern and Climate Change in Xinjiang. *J. Xinjiang Univ. Sci. Ed.* 21 (1), 1–7.
- Pang, Y. J., Lei, J. Q., Zeng, F. J., Li, S. Y., Mao, D. L., and He, Z. H. (2011). Microclimatic Characteristics of Oasis-Desert Transitional Zone in Qira County of Xinjiang Wei Autonomous Region. *Bull. Soil Water Conservation* 31 (5), 240–245. doi:10.13961/j.cnki.stbctb.2011.05.013
- Shen, J. Y., He, Z. Y., Li, S. G., Wang, T. L., and Harazono, Yoshinobu. (1993). Study on Microclimate of Desertified Land in Naiman Area. *J. Desert Res.* 13 (2), 44–50. CNKI: SUN: ZGSS.0.1993-02-007.
- Shi, X., Li, W., Yang, W. B., Ding, G. D., and Feng, W. (2015). Microclimatic Characteristics and the Effects of Low Coverage Sand Fixing Forest Belts. *J. Arid Land Resour. Environ.* 29 (10), 117–121. doi:10.13448/j.cnki.jalre.2015.338
- Skidmore, E. L. (1986). *Soil Erosion by Wind: An Overview*. Netherlands: Springer, 261–273. doi:10.1007/978-94-009-4388-9_18
- Wang, H., Jia, X., Li, Y., and Peng, W. (2015). Selective Deposition Response to Aeolian-Fluvial Sediment Supply in The Desert Braided Channel of The Upper Yellow River, China. *Nat. Hazards Earth Syst. Sci.* 15 (2), 1955–1962. doi:10.5194/nhess-15-1955-2015
- Wang, T. (2009). Review And Prospect of Research on Oasisification and Desertification in Arid Regions. *J. Desert Res.* 29 (1), 1–9.
- Wen, Z. X., Dong, G. R., and Qu, J. J. (1996). Paying Emphasis on The Study of Desert Oasis in China. *Adv. Earth Sci.* 11 (3), 270–274. CNKI: SUN: DXJZ.0.1996-03-006.
- Yang, X. H., He, Q., Huo, W., and Cheng, Y. J. (2012). Study on Wind-Blown Sand Characteristics at Different Directions Near the Surface in The Frontier of An Oasis-Desert Ecotone in Qira County, Xinjiang. *Arid Zone Res.* 29 (6), 1100–1104. doi:10.13866/j.azr.2012.06.023
- Yu, Y. P., Zhang, K. C., An, Z. S., and Zhang, Y. (2020). Dynamic Environment of Wind Along the Dunhuang-Golmud Railway. *J. Desert Res.* 40 (1), 41–48. doi:10.7522/j.issn.1000-694X.2019.00042
- Zhang, Q., and Hu, Y. Q. (2002). The Geographical Features and Climatic Effects of Oasis. *Adv. Earth Sci.* 17 (4), 477–486. doi:10.11867/j.issn.1001-8166.2002.04.0477
- Zhang, Q., Hu, Y. Q., Yang, Y. F., and Zhao, H. Y. (1996). The Variability Process of Atmosphere Over Heterogeneous Underlying Surface in Hexi Region. *Plateau Meteorol.* 15 (3), 282–292. CNKI: SUN: GYQX.0.1996-03-003.
- Zhang, Z. C., Dong, Z. B., Zhao, A. G., and Qian, G. Q. (2011). Relationship Between Sand Transport and Sand Drift Potential. *J. Desert Res.* 31 (4), 824–827.
- Zhu, R. Z., Tan, G. R., and Wang, S. L. (2005). *Introduction to Applied Climatology*. Beijing: Meteorological Press, 2–3.
- Zu, R. P., Zhang, K. C., and Qu, J. J. (2005). The Intensity of Sand-Drift Activities in Taklimakan Desert. *Geogr. Res.* 24 (5), 699–707. doi:10.11821/yj2005050006
- Zuo, H. C., and Hu, Y. Q. (1994). Seasonal Variation of Microclimatic Characteristics for Oasis and Gobi in Heihe and Their Comparative Analysis. *Plateau Meteorol.* 13 (3), 246–255. CNKI: SUN: GYQX.0.1994-03-002.

Conflict of Interest: The authors declare that the research was conducted in the absence of any commercial or financial relationships that could be construed as a potential conflict of interest.

Publisher’s Note: All claims expressed in this article are solely those of the authors and do not necessarily represent those of their affiliated organizations or those of the publisher, the editors, and the reviewers. Any product that may be evaluated in this article, or claim that may be made by its manufacturer, is not guaranteed or endorsed by the publisher.

Copyright © 2022 Luo, Xiao, Gao, Ma, Li, Li, Miri, Cao and Xin. This is an open-access article distributed under the terms of the Creative Commons Attribution License (CC BY). The use, distribution or reproduction in other forums is permitted, provided the original author(s) and the copyright owner(s) are credited and that the original publication in this journal is cited, in accordance with accepted academic practice. No use, distribution or reproduction is permitted which does not comply with these terms.



Soil Seed Bank Characteristics of *Nitraria tangutorum* Nebkhas in a Desert–Oasis Ecotone

Min Li¹, Huijie Xiao^{1*}, Zhiming Xin², Xing Li², Junran Li³, Abbas Miri⁴ and Qiqi Cao⁵

¹School of Soil and Water Conservation, Beijing Forestry University, Beijing, China, ²Inner Mongolia Dengkou Desert Ecosystem National Observation Research Station, Experimental Center of Desert Forestry, Chinese Academy of Forestry, Dengkou, China, ³Department of Geosciences, The University of Tulsa, Tulsa, OK, United States, ⁴Department of Watershed and Range Management, Faculty of Water and Soil, University of Zabol, Zabol, Iran, ⁵Shandong Key Laboratory of Eco-Environmental Science for the Yellow River Delta, Binzhou University, Binzhou, China

OPEN ACCESS

Edited by:

Shengbo Xie,
Northwest Institute of Eco-
Environment and Resources (CAS),
China

Reviewed by:

Jiabing Wu,
University of Chinese Academy of
Sciences, China
Zhongjie Shi,
Chinese Academy of Forestry, China

*Correspondence:

Huijie Xiao
soilandwater2006@hotmail.com

Specialty section:

This article was submitted to
Drylands,
a section of the journal
Frontiers in Environmental Science

Received: 06 May 2022

Accepted: 13 June 2022

Published: 04 August 2022

Citation:

Li M, Xiao H, Xin Z, Li X, Li J, Miri A and
Cao Q (2022) Soil Seed Bank
Characteristics of *Nitraria tangutorum*
Nebkhas in a Desert–Oasis Ecotone.
Front. Environ. Sci. 10:937257.
doi: 10.3389/fenvs.2022.937257

Understanding soil seed banks (SSBs) of *Nitraria tangutorum* nebkhas is critical for vegetation restoration and ecological management in desert–oasis ecotones. In this study, we conducted a survey in the field and a seed germination experiment in the laboratory to investigate the characteristics of SSB in different sizes and parts of nebkhas and to examine their relationship with aboveground vegetation. The results showed that there were 17 species of plants in six families in the SSB of *Nitraria tangutorum* nebkhas in a desert–oasis ecotone, dominated by Chenopodiaceae. The life forms were mainly annual herbs, accounting for 58.82%–71.43%. The number of species in the SSB were in the order of large nebkha > medium nebkha > small nebkha, and there was no significant difference in SSB density. However, SSB densities in different parts of each nebkha were in the order bottom > middle > top. The densities were significantly different and showed a decreasing trend as soil depth increased. Most of the plant seeds were distributed in the 0–5 cm soil layer. The similarity coefficient between the SSB of each nebkha and the aboveground vegetation was high. From the bottom to the top, the number of common species and similarity coefficient between the aboveground vegetation and the SSB decreased, and the number of species in the SSB was greater than that of the aboveground vegetation. Vegetation plays a decisive role in the initial development of a nebkha. When the nebkha develops to a certain extent, it reacts to the vegetation, thereby intensifying the differences in the composition of vegetation species in different parts of the nebkha and further affecting the SSB.

Keywords: *Nitraria tangutorum* nebkhas, soil seed bank, spatial distribution, aboveground vegetation, desert–oasis ecotone

1 INTRODUCTION

The term soil seed bank (SSB) refers to the sum of all viable seeds present on and in the soil (Roberts, 1981). As a potential population, it provides provenance for plant species renewal, community succession, and dispersal processes (Bakker et al., 1996; Zhang et al., 2021b). SSBs are fundamental to the process of plant population settlement, survival, reproduction, and diffusion. They play an important role in reshaping and maintaining biodiversity and can indicate the vegetation on the ground (Bakker et al., 1996; Peterson and Baldwin, 2004; Schwenbacher et al., 2010; He et al., 2018).

For this reason, analyzing the regularity and succession of vegetation growth and development in SSBs is a critical component of vegetation reconstruction and restoration studies (Yang et al., 2010).

Nebkhas are aeolian landforms produced by sand deposited near to and obstructed by shrubs, and their development is mainly affected by plants, aeolian sand deposition, and hydrogeological conditions (Li and Ravi, 2018). In China, nebkhas are widely distributed in desert–oasis ecotones, desert steppe marginal zones, interlaced agricultural–pastoral zones, and other regions (Wang et al., 2006). Natural factors and human activities interfere with their formation and development to a large extent, and their appearance has a great impact on the ecological environment (Tengberg and Chen, 1998; Langford, 2000; Li and Ravi, 2018). A large number of *Nitraria tangutorum* thickets grow in the transition zone between the desert oases in the northeastern part of the Ulan Buh Desert, and nebkhas of different sizes are formed by the annual accumulation of sand. These form a natural “sand prevention wall” around the desert oasis, effectively preventing quicksand from invading the ecological environment of the oasis and playing a positive role in the stability of its environment (Dang et al., 2019). As important sand-fixing vegetation in the transition zone of desert oases, *N. tangutorum* shrub communities, however, have gradually declined, and some parts have even been activated and disintegrated (Xu et al., 2008a). This has greatly weakened the ecological function of the community, increased the vulnerability of the oasis, and jeopardized associated industrial and agricultural production of the oasis (Jia et al., 2002).

There has been considerable research into the development and evolution of nebkhas: morphological changes, soil physicochemical properties, vegetation biomass predictions, reasons for vegetation degradation, restoration techniques, conservation measures, and wind erosion (Zhang et al., 2021a; Abdurimithi and Yusuf, 2016; Du et al., 2010; Li et al., 2010). However, a majority of these studies have ignored the ecological function of nebkhas. Additionally, studies of species composition and size, species diversity characteristics, spatial distribution characteristics, and plant succession of the underground SSB of potential plant provenance on the horizontal scale of *N. tangutorum* nebkhas are also limited. Here, we examined a suite of *N. tangutorum* nebkhas with different sizes in the field and conducted seed germination experiments in the laboratory to analyze the characteristics of SSB and their relationship with aboveground vegetation. The goal of this study is to reveal the relationship between SSBs and the establishment, evolution, and degradation of nebkhas in a desert–oasis ecotone, which is critical for vegetation restoration and land degradation prevention in desert areas.

2 MATERIALS AND METHODS

2.1 Study Area

The study area was located in the northeastern part of the Ulan Buh Desert (40°18′–40°30′, 106°34′–106°58′ E), Inner Mongolia,

northern China, which is a transition zone from steppe desert to desert steppe. It has a temperate continental monsoon climate, with an annual average temperature of 7.6°C and annual precipitation of 100–145 mm. About 80% of the annual precipitation occurs from July to September. Strong northwestern winds are common in spring and winter seasons. In the study area, brown calcium and gray desert soils with quicksand are common. Native vegetation in the study area is dominated by communities of *N. tangutorum*, which exist in the form of nebkhas. The height of nebkhas ranges from approximately 1 to 3 m. The nebkhas are moderately dynamic and advance from west to east at a speed of 3–5 m every year. The nebkhas are characterized by mixed species with three to eight species per 1 m². The plant communities have a height of 34–74 cm and cover 25–80% of the dune surface. A total of 22 species of plants were identified in the study area, belonging to six families and 18 genera. More information about vegetation species composition in the study area is listed in **Table 1**.

2.2 Methods

2.2.1 Experimental Setup and Vegetation Survey

In April 2021, a continuous distribution of *N. tangutorum* in the northeastern part of the Ulan Buh Desert, covering an area of 1 km², was selected as the experimental quadrat. We randomly surveyed 100 *N. tangutorum* nebkhas in the quadrat. The nebkhas selected were classified based on the height of the nebkhas into large (height >1.5 m), medium (1 m < height <1.5 m), and small (height <1 m). We also selected nine similar typical nebkhas from each of the three types for a vegetation survey and SSB sampling, which yielded a total of 27 nebkhas surveyed (**Table 2**).

The height, volume, long axis, short axis, slope, vegetation coverage, and vegetation height of these nebkhas were measured. Nine 50 cm × 50 cm sampling points were set up at the bottom, middle, and top of each nebkha in the four directions (east, west, south, and north), and the composition and quantity of aboveground plant species were investigated. Among them, vegetation survey was not carried out in the middle of the small nebkha (**Figure 1**; **Table 2**).

2.2.2 Soil Sampling and Greenhouse Experiment

A metal soil sampler (8 cm in diameter) was used to collect soil samples at depths of 0–10 cm (divided into two layers: 0–5 cm, 5–10 cm) in the center of the bottom, middle, and top of each nebkha. A total of 486 soil samples were collected and brought to the laboratory for further analysis.

The seed bank density and species composition were determined by the indoor seed germination method. The germination test was carried out at the Inner Mongolia Dengkou Desert Ecosystem National Observation Research Station in May 2021. Soil samples for the seed bank determination were placed on 30 cm × 20 cm sample trays at room temperature. Non-soil components were removed (e.g., residual roots and animal and plant debris), and sufficient water was added to keep the soil moisture. The types and number of seeds germinating in each soil sample were recorded daily. After the species were identified, we moved the germinated but unidentified seedlings to pots

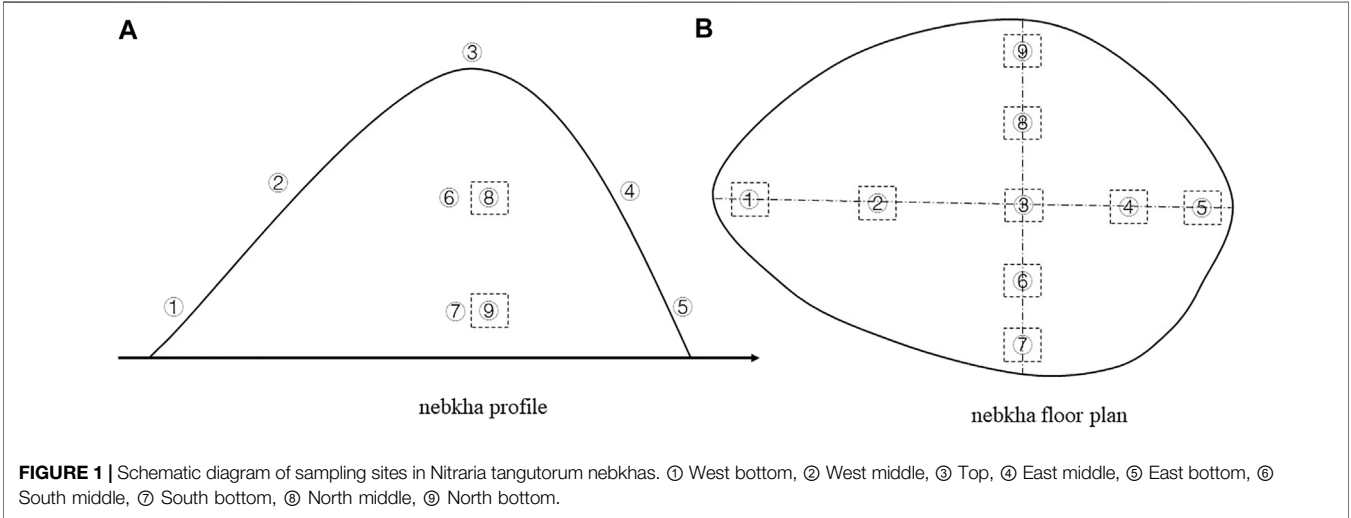
TABLE 1 | Vegetation species composition in the study area.

Life form	Species	Genus	Family
Annual herb	<i>Bassia dasyphylla</i>	<i>Bassia</i>	Chenopodiaceae
	<i>Salsola collina</i>	<i>Salsola</i>	Chenopodiaceae
	<i>Agriophyllum squarrosum</i>	<i>Agriophyllum</i>	Chenopodiaceae
	<i>Corispermum patelliforme</i>	<i>Corispermum</i>	Chenopodiaceae
	<i>Corispermum candelabrum</i>	<i>Corispermum</i>	Chenopodiaceae
	<i>Corispermum stauntonii</i>	<i>Corispermum</i>	Chenopodiaceae
	<i>Corispermum declinatum</i>	<i>Corispermum</i>	Chenopodiaceae
	<i>Halogeton glomeratus</i>	<i>Halogeton</i>	Chenopodiaceae
	<i>Aristida adscensionis</i>	<i>Aristida</i>	Poaceae
	<i>Setaria viridis</i>	<i>Setaria</i>	Poaceae
	<i>Eragrostis pilosa</i>	<i>Eragrostis</i>	Poaceae
	<i>Echinops gmelinii</i>	<i>Echinops</i>	Compositae
Perennial herb	<i>Psammochloa villosa</i>	<i>Psammochloa</i>	Poaceae
	<i>Pugionium comutum</i>	<i>Pugionium</i>	Cruciferae
	<i>Scorzonera divaricata</i>	<i>Scorzonera</i>	Compositae
	<i>Inula salsoloides</i>	<i>Inula</i>	Compositae
	<i>Phragmites australis</i>	<i>Phragmites</i>	Poaceae
Shrub	<i>Artemisia ordosica</i>	<i>Artemisia</i>	Compositae
	<i>Artemisia sphaerocephala</i>	<i>Artemisia</i>	Compositae
	<i>Nitraria tangutorum</i>	<i>Nitraria</i>	Zygophyllaceae
	<i>Haloxyton ammodendron</i>	<i>Haloxyton</i>	Chenopodiaceae
	<i>Reaumuria soongorica</i>	<i>Reaumuria</i>	Tamaricaceae

TABLE 2 | Characteristics of the nebkhas measured in this studya.

Nebkha classification	Volume (m ³)	Height (m)	Major axis (m)	Minor axis (m)	Plant height (cm)	Number of vegetation survey samples	Number of soil samples
Large (n = 9)	1.75 (0.4)	0.44 (0.4)	3.35 (1.1)	3.08 (1.1)	50.64 (0.3)	81	162
Medium (n = 9)	17.45 (0.2)	1.18 (0.5)	7.41 (0.8)	5.94 (0.9)	52.34 (0.3)	81	162
Small (n = 9)	48.25 (0.3)	1.95 (0.6)	9.32 (1.2)	7.95 (1.2)	62.74 (0.4)	45	162

^aValues are means and standard deviations in parentheses.



and placed them at a certain depth until they were identified and removed, as their root systems were too long to fit in the sample tray. This avoided distortion of the accuracy of the experimental results compared with the seedlings of desert vegetation. The germination culture continued for 2 months (Table 2).

2.3 Data Analysis

In this study, the density of an SSB was expressed by the number of viable seeds per unit area of soil, obtained by converting the seeds in the sampling area into the number of 1 m². The counted plants were divided into four types: annual herbs, perennial herbs, shrubs, and trees, and the percentage of each type of species in the total number of species was calculated separately. The Margalef richness index, Simpson diversity index, Shannon–Wiener diversity index, and Pielou evenness index were used to describe the characteristics of species diversity (Jia et al., 2017), and the Jaccard similarity coefficient was used to characterize the similarity of species (Jaccard, 1908) as follows:

Margalef richness index:

$$R = (S - 1)/\ln N.$$

Simpson diversity index:

$$H = 1 - \sum_{i=1}^S P_i^2.$$

Shannon–Wiener diversity index:

$$D = -\sum_{i=1}^S (P_i) \ln P_i.$$

Pielou evenness index:

$$E = D/\ln S.$$

Jaccard similarity coefficient:

$$C_j = \frac{j}{a + b - j}.$$

Here, S is the total number of species in the aboveground vegetation or SSB; N is the number of plants or SSBs of the total species; P_i is the ratio of the number of SSBs or plants of the i th species to the total number of all species; a is the total number of species in SSB; b is the total number of species in aboveground vegetation; and j is the number of species common to SSB and aboveground vegetation.

Soil seed bank density at different locations of the nebkhas was analyzed using the one-way analysis of variance (ANOVA) with a significant level at 0.05. Finally, correlation analyses were performed to reveal the relationship between the characteristics of nebkha, plant species, and SSB.

3 RESULTS

3.1 Species Composition and Floristic Compositions of Soil Seed Banks

A total of 17 plant species in six families were identified through the seed germination test. Among them, the family of Chenopodiaceae comprised the largest proportion, with seven species accounting for 41.18% of the total species. There were five species in the family of Compositae, accounting for 29.14% of the total species. Species in the families of Poaceae and Cruciferae account for 11.77% and 5.88% of the total species, respectively. It

should be noted that the study area is not suitable for trees. *Ulmus pumila* seeds are likely carried by the wind in a farm shelter 3 km away from the study area.

There were 17, 16, and 12 species of plants at the bottom, middle, and top of the large nebkhas, respectively. There were 16, 16, and 13 species of plants at the bottom, middle, and top of the medium nebkhas, respectively. For small nebkhas, we found 14, 14, and 15 species of plants at the bottom, middle, and top, respectively. It was clear that the larger the nebkha, the fewer the SSB species at the top. The SSB density of companion species such as *Bassia dasyphylla*, *Salsola collina*, and *Agriophyllum squarrosum* was relatively large. In addition, the seeds of *Halogeton glomeratus*, *Pugionium cornutum*, *Psammochloa villosa*, and *Scorzonera divaricata* were only present at the bottom and in the middle of the nebkhas.

We did not find notable difference of life forms in the SSBs of different nebkhas (Figure 2). Irrespective of the nebkha size, the proportion of annual herbs was the highest (58.82%–71.43%), followed by shrubs (17.65%–23.08%), perennial herbs (0%–17.65%), and trees (0%–5.88%). Similar to nebkhas with different sizes, SSBs in nebkhas with the same size category but different location are also dominated by annual herbs, and the proportion generally increased from the bottom to the top of the dunes, except for the small nebkhas.

3.2 Spatial Distribution of Soil Seed Bank

3.2.1 Horizontal Distribution Characteristics

The SSB density at the bottom of large and medium nebkha sites was higher than that at the top ($p < 0.05$). The SSB density between the middle and top locations of the nebkhas was not statistically significant, regardless the size of the nebkhas. We did not observe consistent patterns of SSB density for the same relative locations of the nebkhas with various sizes (Figure 3).

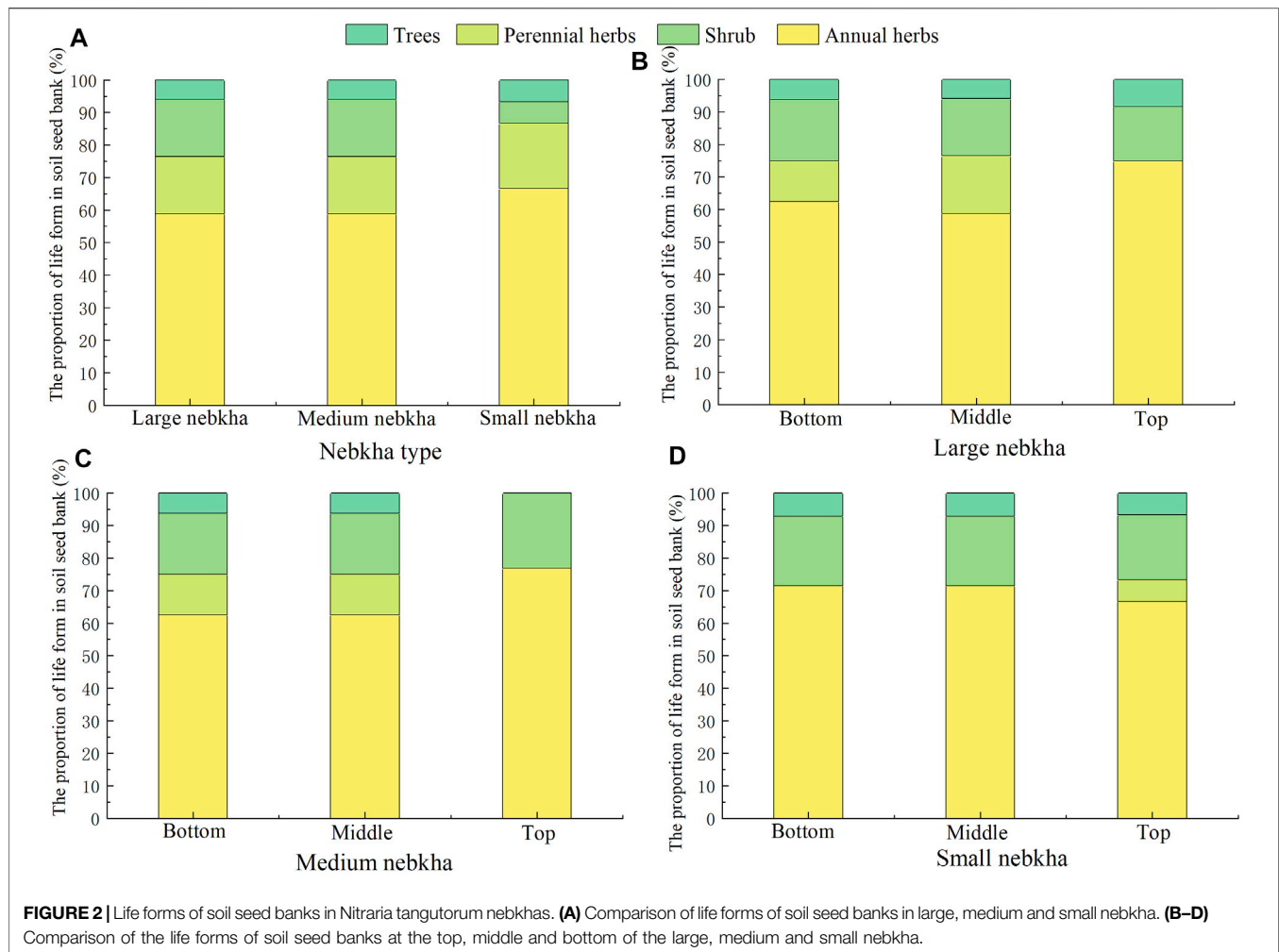
3.2.2 Vertical Distribution Characteristics

The number of species in the top 5 cm of the soil profile fell in the range of 6–14, with a general trend that bottom parts of the nebkhas have a higher number of species than those of the top ones (Table 3). A similar pattern was found for the SSB at a deeper soil profile (5–10 cm), with the largest number of species of 16 found at the bottom of the large nebkhas and the smallest number of species of seven found at the top of both large and small nebkhas.

Most plant seeds were distributed in the 0–5 cm soil layer (Figure 4). The average SSB density in the 0–5 cm and 5–10 cm soil layers was medium nebkha > large nebkha > small nebkha, and the difference between the three types of nebkha was not significant ($p > 0.05$). In the range of 0–10 cm soil layer, the SSB density at the bottom of large, medium, and small nebkha sites was higher than that at the top ($p < 0.05$). We did not detect a consistent pattern of SSB density between the top 5 cm and 5–10 cm of the soil profiles, regardless of the size of the nebkhas.

3.3 Relationship Between Soil Seed Bank and Aboveground Vegetation

The survey found 14 species of aboveground vegetation in *N. tangutorum* nebkhas, belonging to 5 families and 12 genera.



Among them, Chenopodiaceae accounted for the largest proportion with six species, accounting for 42.86% of the total species. In addition, Compositae (four species), Poaceae (two species), Cruciferae (one species), and Tribulus (one species) accounted for 28.57%, 14.29%, 7.14%, and 7.14% of the total species, respectively. In general, SSBs in nebkhas are similar to the number of aboveground vegetation species (Table 4).

The vegetation survey also showed that at the bottom of the nebkhas, the number of aboveground vegetation species is the highest, followed by middle and then top, regardless of the size of the nebkhas (Table 5). A similar pattern was found for the commonly owned species at different locations of the nebkhas. Overall, we found some strong similarities for the bottom of the nebkhas for all the nebkhas we measured.

In all parts of the nebkhas, the number of species in the SSB was more than that of the aboveground vegetation. *N. tangutorum*, *Bassia dasyphylla*, and *Salsola collina* appeared both on the ground and in the soil. Some species appeared only in the SSB and did not appear in the aboveground vegetation, such as *Corispermum patelliforme*, *C. candelabrum*, *C. stauntonii*, *Aristida adscensionis*, *Pugionium cornutum*, *Psammochloa villosa*, *Scorzonera divaricate*, and *Artemisia*

ordosica (Table 5). The Jaccard similarity coefficients between the SSB and the aboveground vegetation species of different types of nebkha were 0.82 (large nebkha) > 0.56 (medium nebkha) > 0.50 (small nebkha) (Table 4). In addition, the difference of the Jaccard similarity coefficient between different parts of large nebkha and medium nebkha was obvious (range: 0.23–0.52), while the difference between the top and bottom of small nebkha was only 0.038. From the bottom to the top of the nebkhas, the number of common species and similarity between the aboveground vegetation and the SSB showed a decreasing trend (Table 5).

3.4 Influence of Morphological Characteristics of *N. tangutorum* Nebkhas on Vegetation and Soil Seed Bank

This study used the Pearson method to analyze the morphological parameters, vegetation, and SSB parameters of 27 *N. tangutorum* nebkhas (Table 6). There were significant differences in the volume, height, long axis, and short axis of different nebkhas ($p < 0.05$). There were different degrees of correlation between the morphological parameters of *N. tangutorum* nebkhas and

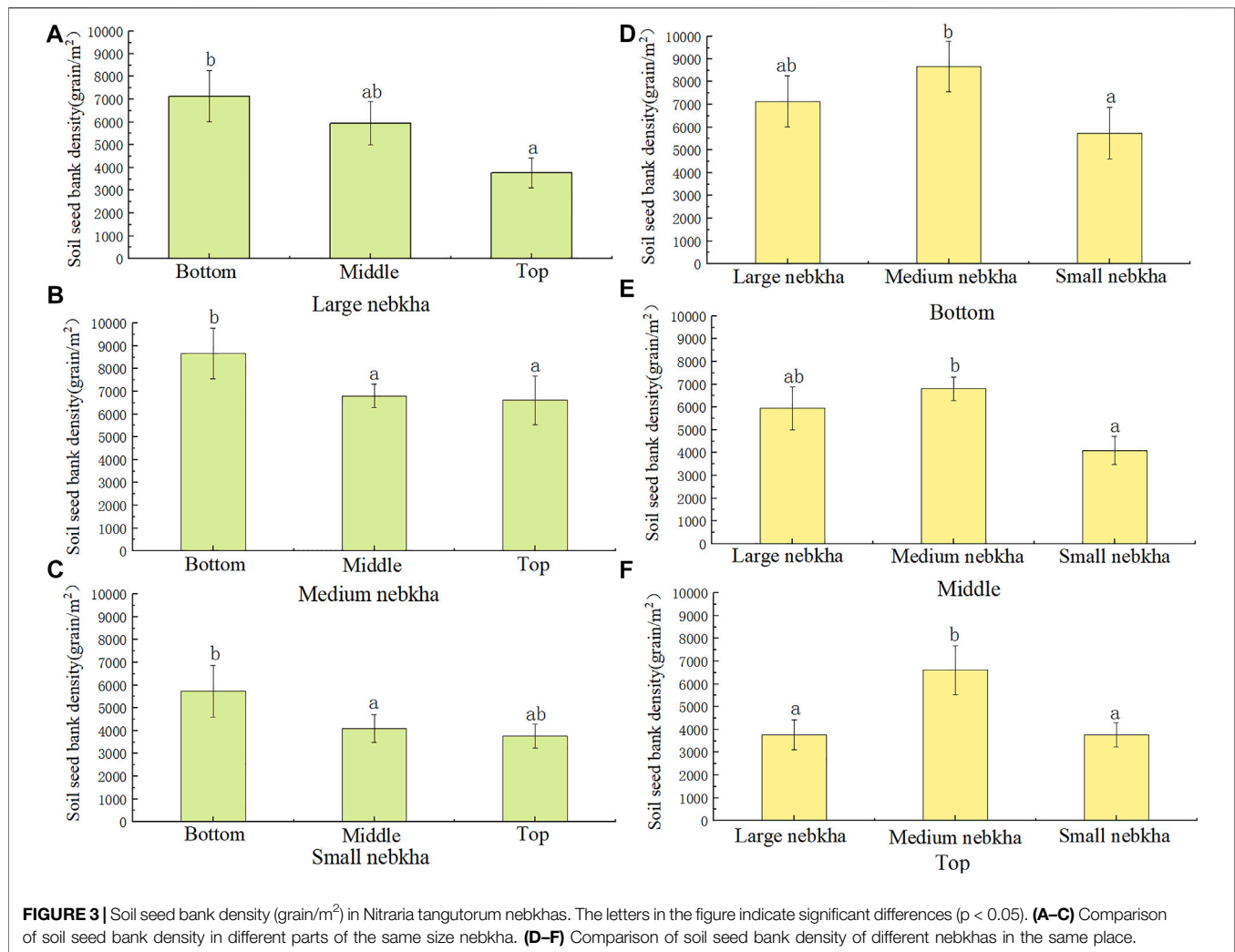


TABLE 3 | Vertical distribution of soil seed banks (number of species) in *Nitraria tangutorum* nebkhas.

Nebkha type	Soil depth	Bottom	Middle	Top
Large	0–5 cm	14	14	6
	5–10 cm	16	14	7
Medium	0–5 cm	14	15	13
	5–10 cm	12	14	11
Small	0–5 cm	13	14	12
	5–10 cm	12	11	7

vegetation parameters. The species number in the SSB at the top of the nebkhas was significantly negatively correlated with the volume, height, long axis, short axis, and slope of the nebkhas ($p < 0.01$). There was a significant positive correlation between the vegetation coverage of a nebkha and its volume, long-axis slope, and short-axis slope ($p < 0.05$). The number of vegetation species of a nebkha had a strong and significant positive correlation with the nebkha volume, height, long axis, short axis, long-axis slope, and plant height ($p < 0.05$). It was shown that the morphological

parameters of *N. tangutorum* nebkhas affected the plant height, the number of species in the nebkha vegetation, and the number of species in the SSB at the top of a nebkha. Vegetation plays a decisive role in the initial development of a nebkha. When the nebkha develops to a certain extent, it will react to the vegetation, thereby intensifying the differences in the composition of vegetation species in its different parts and further affecting the SSB.

4 DISCUSSION

We found that annual herbaceous plants, primarily *Bassia dasyphylla*, *Salsola collina*, *Agriophyllum squarrosum*, and *Aristida adscensionis*, accounted for the largest proportion of species on nebkhas in a desert–oasis ecotone in northwestern China. This finding was consistent with the studies of SSBs in the Alxa Desert region (Zeng et al., 2003), the central desert of the Hexi Corridor (Lu et al., 2019), and the Gurbantunggut Desert (Zhang and Li, 2018), which also reported that the species life

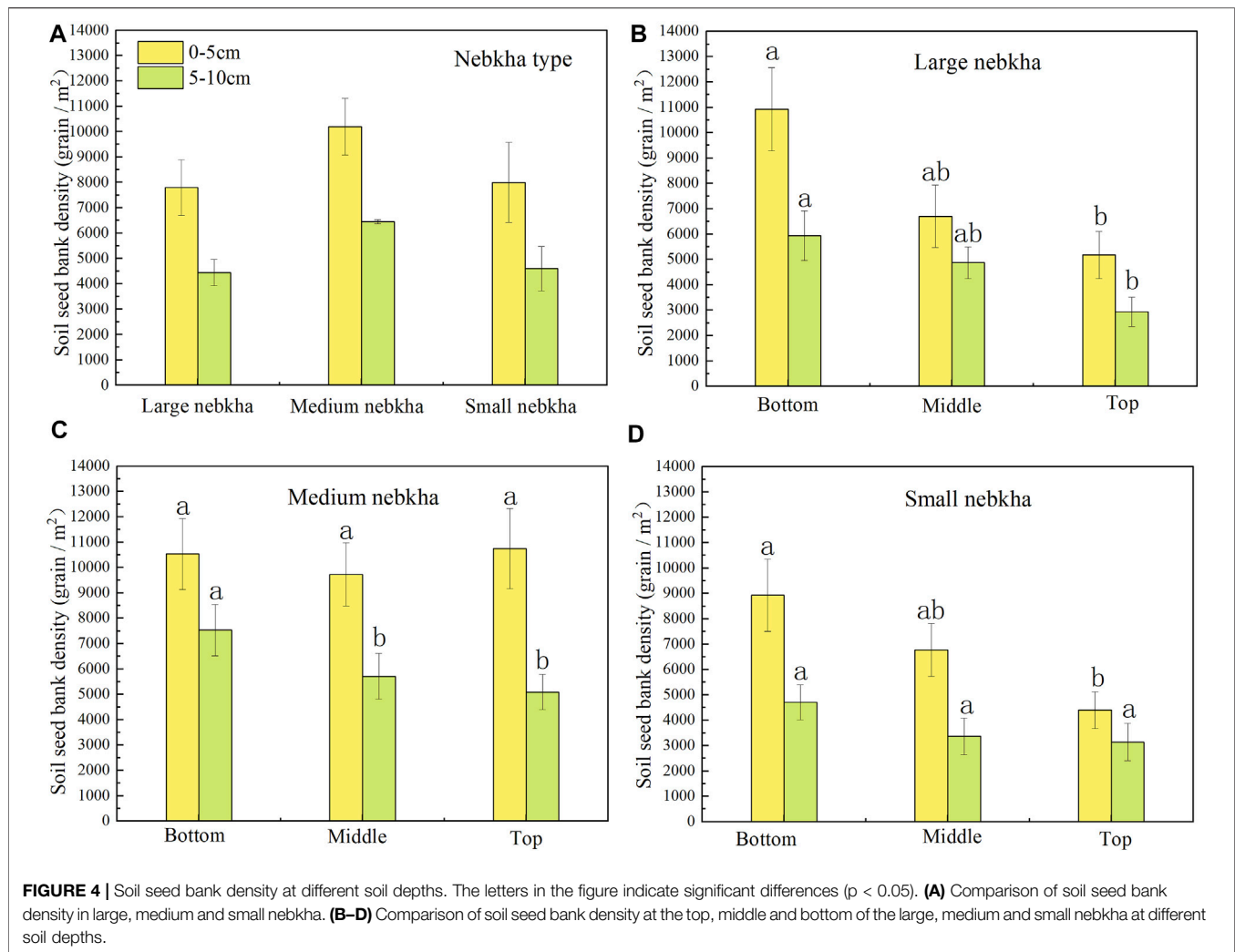


TABLE 4 | Similarity of soil seed bank (SSB) and aboveground vegetation in *Nitraria tangutorum* nebkh.

Nebkhas type	Number of aboveground vegetation species	Number of SSB species	Commonly owned species	Jaccard similarity coefficient
Large	8	17	14	0.82
Medium	9	16	9	0.56
Small	9	15	8	0.50

TABLE 5 | Similarity between soil seed bank (SSB) and aboveground vegetation in different parts of nebkh.

Nebkha type	Position	Number of aboveground vegetation species	Number of SSB species	Commonly owned species	Jaccard similarity coefficient
large	Bottom	14	16	13	0.88
	Middle	11	17	11	0.65
	Top	5	12	5	0.42
Medium	Bottom	12	16	12	0.75
	Middle	9	16	8	0.47
	Top	3	13	3	0.23
Small	Bottom	9	14	8	0.53
	Top	7	15	8	0.57

TABLE 6 | Correlation analysis of nebkha, vegetation, and soil seed bank (SSB) parameters in *Nitraria tangutorum* nebkhas.

	Volume	Height	Major axis	Minor axis	Horizontal scale	Long-axis slope	Short-axis slope	Vegetation cover	Plant height	Species number of sandpile	Species number of SSB
Height	0.77**	1									
Long axis	0.65**	0.86**	1								
Stub axle	0.65**	0.90**	0.95**	1							
Horizontal scale	0.66**	0.89**	0.99**	0.98**	1						
Long-axis slope	0.59**	0.80**	0.42*	0.52**	0.47*	1					
Short-axis slope	0.62**	0.77**	0.51**	0.47*	0.50**	0.89**	1				
Vegetation cover	0.42*	0.22	−0.10	−0.09	−0.10	0.47*	0.51**	1			
Plant height	0.44*	0.54**	0.49**	0.63**	0.57**	0.31	0.17	−0.04	1		
Species number of sandpile	0.44*	0.60**	0.58**	0.65**	0.62**	0.40*	0.30	−0.11	0.54**	1	
Species number of SSB	0.20	0.30	0.35	0.32	0.34	0.25	0.30	0.21	0.14	0.14	1
Species number of SSB at the top of nebkhas	−0.60**	−0.66**	−0.50**	−0.57**	−0.54**	−0.57**	−0.49*	−0.19	−0.34	−0.36	−0.39*

** indicates a significant correlation at the 0.01 level and * indicates a significant correlation at the 0.05 level.

forms were mainly annual herbs. This is not surprising as annuals have strong drought tolerance and larger niche breadth (Jia et al., 2017). Additionally, the rainfall in our study area was low and mostly concentrated in July–September, allowing most annual herbs to complete their entire life cycle during this period and to produce a large number of seeds.

In this study, the SSB density is relatively high and is consistent with studies conducted in a South American warm desert (Luis et al., 1998) and a desert–oasis marginal zone in middle reaches of Heihe River, China (Li and Fang, 2008). The density of SSB plants is different from the SSB density observed in other arid and extremely arid deserts (Yu et al., 2015; Zhang and Li, 2018; Hadinezhad, et al., 2021). This difference may be caused by the fact that nebkhas, with various shrub species, increase buried seeds in soil by directly trapping seeds or by indirect mechanisms through an intermediary animal or plant species (Giladi et al., 2013). More importantly, abiotic factors such as wind regime, landform, and soil condition also affected SSB density (Chambers and MacMahon, 1994). There were also significant differences in the spatial distribution patterns of SSB in different nebkha sites because of the strong habitat heterogeneity in the study area. Previous studies have shown that at the bottom of nebkhas, the light intensity is relatively weak, the soil water storage capacity is relatively strong, and thus soil moisture and nutrient conditions are better, which favor seed germination, survival, and establishment of plants (Xu et al., 2008b; Liu et al., 2011; Wang, 2021). However, compared with the middle and bottom of nebkhas, the light intensity is higher at the top, and the plants cannot obtain the soil moisture and nutrients needed for their growth, so there are relatively few species. Likewise, in the southern margin of the Gurbantunggut Desert, the density of each dune slope was found to decrease in sequence at the bottom, lower middle, upper middle, and top (Jia et al., 2017). Plant seeds generally fall on the soil surface or enter the surface layer after they mature, and only a small proportion enter deeper soil layers as a result of wind erosion and sand burial (Yang et al., 2016; Liu et al., 2021).

The study area is located in a windy desert area, and a majority of the windy conditions occur in spring (Cui et al., 2010; Gao

et al., 2014). When the wind passes through the nebkhas, areas of low wind speed form in the lower-middle parts of the nebkhas because of the influence of the shrubs on the wind–sand flow. When the wind speed decreases, the ability of the wind–sand flow to carry seeds decreases, so that more seeds will accumulate in the lower-middle parts (Qian et al., 2016; Ma et al., 2021). Consequently, at the bottom of nebkhas, the SSB density in the surface layer is relatively high. Due to the fluctuation of nebkha height, soil moisture, light radiation, soil nutrients, and sand buried by wind erosion would change slightly in small local areas (Jia et al., 2021); at the bottom of nebkhas, wind erosion was not too severe. More plant litter accumulates, which reduces the loss of soil water and nutrients (Shao et al., 2001; Haas, 2004), and the increase in soil fertility improves vegetation growth, resulting in an increase in the number of species in aboveground vegetation (Zhang et al., 2006; Hadinezhad et al., 2021).

Previous studies have shown that in desert regions, more than one-half of all species were found in SSB as well as in the aboveground vegetation (Ma, et al., 2015; Teng et al., 2020; Lv et al., 2021). In this study, 14 species appeared both in the aboveground vegetation and in the SSB, three species appeared only in the SSB, and no species appeared only in the aboveground vegetation. These observations were similar to those reported in a previous study (Teng et al., 2020). The main reason for this was that the study area was located in the transition zone of desert and oasis and there were few plant species, which increased the probability of the same species appearing both in SSB and in aboveground vegetation in the different parts of the nebkhas. *Bassia dasyphylla*, *Salsola collina*, and *N. tangutorum* appeared in the aboveground vegetation and SSB. Thus, *B. dasyphylla* and *S. collina* could be the dominant species on nebkhas because their reproductive ability was very strong. In addition to seed germination, the main propagation method of *N. tangutorum*, as a constructive species in this area, is to bury its own branches by intercepting sand by itself and carrying out clonal propagation with branches or root tillers under suitable water and heat conditions.

The succession process of *N. tangutorum* nebkhas is strongly related to the process of plant growth, development, and change.

With sufficient sand supply under the same wind conditions, vegetation with different ecological characteristics creates different wind speed and wind flow fields, thus developing different forms of nebkha (Yin et al., 2017). Plant morphology, quantity, structure, and litter affect the development of nebkhas through their impact on the environment and ability to block sandstorms (Miao et al., 2020; Han et al., 2021). Some studies have found that the changes in nebkha morphology are determined by the coverage, distribution, abundance, and height of plants (Hesp and McLachlan, 2000; Hesp, 2002). A study of nebkha morphology in Ulan Buh Desert by Gao et al. (2015) found that crown size and plant height affected the development of nebkhas. The nebkha slope may also affect the distribution of nebkha SSB. Seeds on a steep slope are more likely to slide to the bottom of the slope under the action of wind and rainfall (Pa et al., 2016; Li et al., 2018). Our results showed that the morphological characteristics of *N. tangutorum* nebkhas can affect the number of aboveground vegetation and SSB species and the vegetation height. During the development of *N. tangutorum* nebkhas, the growth and development of vegetation can inversely affect nebkha morphology. This reflects the decisive role that vegetation plays in the initial development of nebkhas. When they develop to a certain extent they react to the vegetation, thus intensifying the difference in the vegetation species composition in different parts of the nebkhas and further affecting the SSB.

5 CONCLUSION

We recorded 17 species of plants in six families in the SSB of *N. tangutorum* nebkhas in a desert–oasis ecotone, dominated by Chenopodiaceae. The life forms were mainly annual herbs, accounting for 58.82%–71.43%. The number of species in the SSB followed the sequence large nebkha > medium nebkha > small nebkha, and there was no significant difference in SSB density. However, the SSB densities in different parts of each nebkha were in the sequence bottom > middle > top. The SSB densities were significantly different and showed a decreasing trend with the increase in soil depth. In the range of 0–10 cm soil layer, most of the plant seeds were distributed in the 0–5 cm layer, which

decreased with the increase of soil depth. The similarity coefficient between the SSB of each nebkha and the aboveground vegetation was high. From the bottom to the top, the number of common species and similarity coefficient between the aboveground vegetation and the SSB decreased, and the number of species in the SSB was more than that of the aboveground vegetation. Vegetation plays a decisive role in the initial development of a nebkha. When a nebkha develops to a certain extent, it reacts to the vegetation, thereby intensifying the differences in the composition of vegetation species in its different parts and further affecting the SSB.

DATA AVAILABILITY STATEMENT

The original contributions presented in the study are included in the article/supplementary material; further inquiries can be directed to the corresponding author.

AUTHOR CONTRIBUTIONS

ML, HX, and ZX contributed to conception and design of the study. ML wrote the original draft. HX wrote sections of the manuscript. ML, HX, JL, AM, XL, and QC contributed to the revision of the manuscript. All authors contributed to manuscript revision and read and approved the submitted version.

FUNDING

This study was funded by the Project of Intergovernmental International Cooperation in Science and Technology Innovation (No. 2019YFE0116500).

ACKNOWLEDGMENTS

We are grateful for the support from the Inner Mongolia Dengkou Desert Ecosystem National Observation Research Station, Dengkou, China. We also thank the journal editors and reviewers for their comments and efforts on this article.

REFERENCES

- Abdurimithi, A., and Yusuf, B. (2016). Morphological Characteristics of White Thorn Scrub Sandpiles in Different Habitats in the Yanqi Basin. *Chin. Agric. Sci. Bull.* 32 (32), 117–123. doi:10.11924/j.issn.1000-6850.casb16030228
- Bakker, J. P., Bakker, E. S., Rosén, E., Verweij, G. L., and Bekker, R. M. (1996). Soil Seed Bank Composition along a Gradient from Dry Alvar Grassland to Juniperus shrubland. *J. Veg. Sci.* 7, 165–176. doi:10.2307/3236316
- Chambers, J. C., and MacMahon, J. A. (1994). A Day in the Life of a Seed: Movements and Fates of Seeds and Their Implications for Natural and Managed Systems. *Annu. Rev. Ecol. Syst.* 25 (1), 263–292. doi:10.1146/annurev.es.25.110194.001403
- Cui, Y., Wang, X., Pan, Y. X., Wang, Z., and Qi, P. (2010). Differences in Soil Seed Bank in Different Microhabitats of Natural Fixed Sandy Areas. *Acta Ecol. Sin.* 30 (08), 1981–1989.
- Dang, X., Xia, P., Yong, G., Yang, L., Zhenyi, W., and Zhongju, M. (2019). Spatial Heterogeneity of Wind-Eroded Soil Particles Around *Nitraria Tangutorum* Nebkhas in the Ulan Buh Desert. *Écoscience* 26 (4), 347–358. doi:10.1080/11956860.2019.1646064
- Du, J., Yan, P., and Dong, Y. (2010). Current Status and Perspectives of Research on Scrub Sandpiles in Arid Regions. *Acta Geogr. Sin.* 65 (03), 339–350. doi:10.11821/xb201003009
- Gao, J., Xin, Z., Liu, F., Yuan, W. J., Feng, W., Xu, J., et al. (2014). Analysis of Atmospheric Dust Fall Characteristics and Influencing Factors in Northeastern Ulaanbaatar Desert. *J. Arid. Land Res. Environ.* 28 (08), 145–150. doi:10.13448/j.cnki.jalre.2014.08.014
- Gao, Y., Dang, X., Yu, Y., Wang, J., Wang, S., Yuan, W., et al. (2015). Nabkha Morphological Characteristics and Sand Fixing Capacity of *Artemisia sphaerocphala* in the Southeastern Edge of the Ulan Buh Desert. *J. Desert Res.* 35 (01), 1–7. doi:10.7522/j.issn.1000-694X.2014.00080
- Giladi, I., Segoli, M., and Ungar, E. D. (2013). Shrubs and Herbaceous Seed Flow in a Semi-arid Landscape: Dual Functioning of Shrubs as Trap and Barrier. *J. Ecol.* 101 (1), 97–106. doi:10.1111/1365-2745.12019

- Ha, S. (2004). Preliminary Study on the Structural Variation of Wind and Sand Flow on the Surface of Sand Dunes at the Southeast Edge of Tengger Desert. *Chin. Sci. Bull.* 49 (11), 1099–1104. doi:10.3321/j.issn:0023-074X.2004.11.015
- Hadinezhad, M., Erfanzadeh, R., and Ghelichnia, H. (2021). Soil Seed Bank Characteristics in Relation to Different Shrub Species in Semiarid Regions. *Land Degrad. Dev.* 32 (5), 2025–2036. doi:10.1002/ldr.3856
- Han, D., Zhang, W., Nurmati, Y., and Yang, Y. (2021). Complementary Constraints on the Renewal of Plant Populations. *Chin. J. Plant Ecol.* 45 (01), 1–12. doi:10.17521/cjpe.2020.0246
- He, F. L., Guo, C., Ma, J. M., Wu, H., and Jin, H. X. (2018). Dynamic Changes in Soil Seed Banks and Their Relationships with Aboveground Vegetation during the Decaying of *Haloxylon Ammodendron* Plantations at the Edge of the Minqin Oasis. *Acta Ecol. Sin.* 38 (13), 4657–4667. doi:10.5846/stxb201706141084
- Hesp, P. (2002). Foredunes and Blowouts: Initiation, Geomorphology and Dynamics. *Geomorphology* 48, 245–268. doi:10.1016/s0169-555x(02)00184-8
- Hesp, P., and McLachlan, A. (2000). Morphology, Dynamics, Ecology and Fauna of *Arctotheca Populifolia* and *Gazania Rigens* Nabkha Dunes. *J. Arid Environ.* 44, 155–172. doi:10.1006/jare.1999.0590
- Jaccard, P. (1908). Nouvelles recherches sur la distribution florale. *Bull. Soc. Vaud. Sci. Nat.* 44, 223–270. doi:10.5169/seals-268384
- Jia, B., Ci, L., Cai, T., Gao, Z., and Ding, F. (2002). Preliminary Study on the Characteristics of Soil Moisture Changes in the Oasis-Desert Interlacing Zone. *Chin. J. Plant Ecol.* 26 (02), 203–208. doi:10.3321/j.issn:1005-264X.2002.02.011
- Jia, F., Tiyp, T., Wu, N., Tian, C., and Zhang, Y. (2017). Characteristics of Soil Seed Banks at Different Geomorphic Positions within the Longitudinal Sand Dunes of the Gurbantunggut Desert, China. *J. Arid. Land* 9 (3), 355–367. doi:10.1007/s40333-017-0055-x
- Jia, F., Bai, Y., and Ren, J. (2021). A Review of Studies on the Seed Bank of Sand Dune Soils and its Relationship with Above-Ground Vegetation. *J. Ili Agric. Univ. Nat. Sci.* 15 (01), 37–44. doi:10.3969/j.issn.1673-999X.2021.01.008
- Langford, R. P. (2000). Nabkha (Coppice Dune) Fields of South-Central New Mexico, U.S.A. *J. Arid Environ.* 46 (9), 25–41. doi:10.1006/jare.2000.0650
- Li, H. R., Wang, J., Jiang, Z., and Ji, Y. F. (2010). Piercing White Sandbags Development Process of Soil Water and the Relationship Between Root Biomass. *J. Gansu Agri. Univ.* 45 (6), 133–138. doi:10.13432/j.cnki.jgsau.2010.06.002
- Li, J., and Ravi, S. (2018). Interactions Among Hydrological-Aeolian Processes and Vegetation Determine Grain-Size Distribution of Sediments in a Semi-arid Coppice Dune (Nabkha) System. *J. Arid Environ.* 154, 24–33. doi:10.1016/j.jaridenv.2018.03.011
- Li, Q., and Fang, H. Y. (2008). Study on Soil Seed Bank of *Nitraria Sphaerocarpa* Coppice Dune in a Desert Oasis Marginal Zone. *Arid. Zone Res.* 4, 502–506. doi:10.13866/j.azr.2008.04.019
- Li, L., Fang, Z., Aiqbayr, M., Zhou, L., and Lu, B. (2018). Study on Soil Seed Bank and Seedling Regeneration of Different Populations of *Phellodendron Chinense* in Wild Fruit Forests in the Western Tianshan Mountains. *Plant Sci. J.* 36 (04), 534–540. doi:10.11913/PSJ.2095-0837.2018.40534
- Liu, H.-L., Shi, X., Wang, J.-C., Yin, L.-K., Huang, Z.-Y., and Zhang, D.-Y. (2011). Effects of Sand Burial, Soil Water Content and Distribution Pattern of Seeds in Sand on Seed Germination and Seedling Survival of *Eremosparton Songoricum* (Fabaceae), a Rare Species Inhabiting the Moving Sand Dunes of the Gurbantunggut Desert of China. *Plant Soil* 345 (1–2), 69–87. doi:10.1007/s11104-011-0761-7
- Liu, S. Q., Du, X., Li, Q., Zhang, Z., Wei, Y. C., and Ai, F. (2021). Characterization of the Seed Bank of *Salix* Community in the Southeastern Margin of Mu Us Sandy Land. *J. Northwest Fore. Univ.* 36 (06), 140–144. doi:10.3969/j.issn.1001-7461.2021.06.20
- Lu, Y. F., Ma, L., Zhan, Y. F., Qian, W. J., Zhen, W. L., and Teng, Y. F. (2019). A Review of the Soil Seed Bank of Artificial Desert Vegetation in the Hexi Corridor. *Fore. Sci. Technol.* 60 (11), 64–66. doi:10.13456/j.cnki.lykt.2018.08.08.0001
- Luis, M., Bertilde, E. R., and Manuel, E. H. (1998). Timing and Spatial Patterning of Seed Dispersal and Redistribution in a South American Warm Desert. *Plant Ecol.* 137 (2), 143–150. doi:10.2307/20050657
- Lv, Y., Shen, M., Meng, B., Zhang, H., Sun, Y., Zhang, J., et al. (2021). The Similarity between Species Composition of Vegetation and Soil Seed Bank of Grasslands in Inner Mongolia, China: Implications for the Asymmetric Response to Precipitation. *Plants* 10 (9), 1890. doi:10.3390/PLANTS10091890
- Ma, Q., Lu, Q., Wei, L., and Jin, H. (2015). Varying Characteristics of Soil Seed Banks during the Succession Process of *Nitraria Tangutorum* Vegetation in an Arid Desert Area. *Acta Eco Sin.* 35 (7), 326. doi:10.5846/stxb201306041326
- Ma, R., Zhao, J. M., Ma, Y., and Lu, J. (2021). Morphological Characteristics and Spatial Distribution of *Nitraria Tangutorum* Nabkhas Near Shifting Sand of Southern Margin of Badain Jaran Desert. *J. Soil Water Conserv.* 35 (04), 217–221+236. doi:10.13870/j.cnki.stbcb.2021.04.030
- Miao, B. L., Pei, H., Jiang, Y. F., Jia, C. Z., and Wu, H. (2020). Classification of Sand Cover Surface Morphology and Morphological Characteristics and Developmental Processes. *Meteor. J. Inn. Mong.* 29 (05), 37–42. doi:10.14174/j.cnki.nmqx.2020.05.008
- Pa, R., Dong, X. L., Zhang, Y. L., and Mou, C. (2016). Characteristics of Soil Seed Bank and its Effect on Seed Germination in *Staphylinia Variegata* in Xinjiang. *J. Xinjiang Agric. Univ.* 39 (06), 458–462. doi:10.3969/j.issn.1007-8614.2016.06.006
- Peterson, J. E., and Baldwin, A. H. (2004). Seedling Emergence from Seed Banks of Tidal Freshwater Wetlands: Response to Inundation and Sedimentation. *Aquat. Bot.* 78 (3), 243–254. doi:10.1016/j.aquabot.2003.10.005
- Qian, J., Liu, Z., Hatier, J.-H. B., and Liu, B. (2016). The Vertical Distribution of Soil Seed Bank and its Restoration Implication in an Active Sand Dune of Northeastern Inner Mongolia, China. *Land Degrad. Dev.* 27 (2), 305–315. doi:10.1002/ldr.2428
- Roberts, H. A. (1981). Seed Banks in Soils. *Adv. Appl. Biol.* 6, 1–55. doi:10.2307/1937400
- Schwiebacher, E., Marcante, S., and Erschbamer, B. (2010). Alpine Species Seed Longevity in the Soil in Relation to Seed Size and Shape - A 5-year Burial Experiment in the Central Alps. *Flora - Morphol. Distribution, Funct. Ecol. Plants* 205 (1), 19–25. doi:10.1016/j.flora.2008.10.007
- Shao, Y. Q., Zhao, J., and Bao, Q. H. (2001). Study on the Vertical Distribution of Microbial Biomass in Soil of Kubuqi Fixed Dune. *J. Desert Res.* 21 (01), 91–95. doi:10.3321/j.issn:1000-694X.2001.01.018
- Teng, Y. F., Zhan, Y. F., Ma, L., Lu, Y. F., Qian, W. J., and Tian, X. P. (2020). Characteristics of Soil Seed Bank of Different Artificial Vegetation Types in Jinta Desert. *Bull. Soil Water Conserv.* 40 (03), 163–169. doi:10.13961/j.cnki.stbctb.2020.03.023
- Tengberg, A., and Chen, D. (1998). A Comparative Analysis of Nabkhas in Central Tunisia and Northern Burkina Faso. *Geomorphology* 22 (2), 181–192. doi:10.1016/s0169-555x(97)00068-8
- Wang, W. (2021). F. Effects of Sand Dune Microtopography on Soil, Vegetation and Arthropod Community Distribution in a Desert Sand-Fixing Vegetation Zone. *Ningxia University*. doi:10.27257/d.cnki.gnxhc.2021.001172
- Wang, X., Wang, T., Dong, Z., Liu, X., and Qian, G. (2006). Nabkha Development and its Significance to Wind Erosion and Land Degradation in Semi-arid Northern China. *J. Arid Environ.* 65, 129–141. doi:10.1016/j.jaridenv.2005.06.030
- Xu, H., Ye, M., Li, J. M., and Zhang, Q. Q. (2008a). Effect of Different Water Availability on Seed Germination in the Seed Bank of the Lower Tarim River Soil. *Arid. Land Geogr.* 31 (05), 650–658. doi:10.13826/j.cnki.cn65-1103/x.2008.05.003
- Xu, L. H., Wang, J. H., Li, Y., Ma, Q. L., Zhang, D. K., Liu, Y. J., et al. (2008b). Characteristics of Soil Physical Property Changes during the Reversal of Desertification in the Southern Edge of Tengger Desert. *J. Desert Res.* 28 (04), 690–695.
- Yang, L., Wang, Y. R., and Yu, J. D. (2010). Progress of Research on Soil Seed Bank in Arid Desert Areas. *Acta pratac. Sin.* 19 (02), 227–234. doi:10.3724/SP.J.1077.2010.01263
- Yang, C. B., Li, Y., Shan, L. S., and Duan, Y. N. (2016). Assessment of the Seed Bank of Red Sand Scrub Soils and Their Natural Regeneration Potential in Loess Hilly Gully Areas. *Bull. Soil Water Conserv.* 36 (02), 105–109+114. doi:10.13961/j.cnki.stbctb.2016.02.020
- Yin, R. P., Guo, J. Y., Dong, Z., He, J. L., Li, J. R., Tian, S. M., et al. (2017). Wind and Sand Characteristics of Typical Sand Dunes of Different Heights along the Ulaanbaatar Desert Section of the Yellow River. *Res. Soil Water Conserv.* 24 (05), 157–161. doi:10.13869/j.cnki.rswc.2017.05.024
- Yu, J., Gao, L., Yan, Z., and Wang, Z. (2015). Characteristics of Soil Seed Bank of Sand Dune in Different Succession Stages in the Eastern Kubuqi Desert. *Chin. J. Grass.* 37 (04), 80–85. doi:10.3969/j.issn.1673-5021.2015.04.013

- Zeng, Y., Wang, Y., and Nan, Z. (2003). Study on the Soil Seed Bank of Different Vegetation Types in the Alashan Arid Desert Region. *Chin. J. Appl. Ecol.* 14 (9), 1457–1463. doi:10.3321/j.issn:1001-9332.2003.09.011
- Zhang, Y., and Li, J. (2018). Spatial Pattern of Seed Bank and Seedlings in Gurbantunggut Desert Soils the "protection Effect" of Scrub. *Arid. Zone Res.* 35 (05), 1138–1145. doi:10.13866/j.azr.2018.05.17
- Zhang, T., Tian, C. G., Sun, Y., and Feng, G. (2006). Study on the Soil Seed Bank of Short-Lived Plants in the Gurbantunggut Desert Region. *Arid. Land Geogr.* 33 (05), 675–681. doi:10.13826/j.cnki.cn65-1103/x.2006.05.010
- Zhang, Y. N., Li, C. L., Zhao, P., Duan, X. F., and Qiu, X. N. (2021a). Progress of Research on Soil Seed Bank in Arid Desert Areas. *Seed Sci. Te.* 39 (17), 9–11. doi:10.19904/j.cnki.cn14-1160/s.2021.17.004
- Zhang, Z. G., Dong, X., Xin, Z. M., Zhang, J. B., Wang, X. Q., Kan, K. M., et al. (2021b). Biomass Allocation and Prediction in *Nitraria* Nabkhas. *Pratac. Sci.* 38 (06), 1069–1077. doi:10.11829/j.issn.1001-0629.2020-0727

Conflict of Interest: The authors declare that the research was conducted in the absence of any commercial or financial relationships that could be construed as a potential conflict of interest.

Publisher's Note: All claims expressed in this article are solely those of the authors and do not necessarily represent those of their affiliated organizations or those of the publisher, the editors, and the reviewers. Any product that may be evaluated in this article, or claim that may be made by its manufacturer, is not guaranteed or endorsed by the publisher.

Copyright © 2022 Li, Xiao, Xin, Li, Li, Miri and Cao. This is an open-access article distributed under the terms of the Creative Commons Attribution License (CC BY). The use, distribution or reproduction in other forums is permitted, provided the original author(s) and the copyright owner(s) are credited and that the original publication in this journal is cited, in accordance with accepted academic practice. No use, distribution or reproduction is permitted which does not comply with these terms.



OPEN ACCESS

EDITED BY
Jifeng Deng,
Shenyang Agricultural University, China

REVIEWED BY
Jing Qin,
China Institute of Water Resources and
Hydropower Research, China
Wenyi Dong,
Chinese Academy of Agricultural
Sciences (CAAS), China

*CORRESPONDENCE
Yong Niu,
niu Yong1988@126.com
Chuanjie Zhang,
Zhangchuanjie1983@126.com

[†]These authors have contributed equally
to this work and share first authorship

SPECIALTY SECTION
This article was submitted to Drylands,
a section of the journal
Frontiers in Environmental Science

RECEIVED 24 June 2022
ACCEPTED 28 July 2022
PUBLISHED 24 August 2022

CITATION
Li X, Li Y, Di S, Niu Y and Zhang C (2022),
Evapotranspiration and land surface
temperature of typical urban green
spaces in a semi-humid region:
Implications for green management.
Front. Environ. Sci. 10:977084.
doi: 10.3389/fenvs.2022.977084

COPYRIGHT
© 2022 Li, Li, Di, Niu and Zhang. This is
an open-access article distributed
under the terms of the [Creative
Commons Attribution License \(CC BY\)](#).
The use, distribution or reproduction in
other forums is permitted, provided the
original author(s) and the copyright
owner(s) are credited and that the
original publication in this journal is
cited, in accordance with accepted
academic practice. No use, distribution
or reproduction is permitted which does
not comply with these terms.

Evapotranspiration and land surface temperature of typical urban green spaces in a semi-humid region: Implications for green management

Xinhao Li^{1†}, Yiran Li^{2†}, Suchuang Di³, Yong Niu^{1*} and
Chuanjie Zhang^{4*}

¹College of Forestry, Shandong Agricultural University, Taian, China, ²School of Soil and Water Conservation, Beijing Forestry University, Beijing, China, ³Beijing Water Science and Technology Research Institute, Beijing, China, ⁴College of Water Conservancy and Civil Engineering, Shandong Agricultural University, Taian, China

Ecological deterioration and water scarcity motivate people to seek a balance between ecological reserves and water consumption in cities located in Semi-humid regions. This study is designed to develop a method for evaluating cooling water-saving characteristics of green space structures. Land surface temperature (T_s), vegetation quantity (VQ) and evapotranspiration (ET) of typical green vegetation structures in 50 plots with an average area of 10,000 m² were studied. Parameters were obtained based on data from three temporal remote sensing images; the surface energy balance algorithm for land (SEBAL) model, single-channel algorithm, and normalized difference vegetation index (NDVI) were utilized in the calculation. The relationships between the T_s , VQ, and ET of green land were explored using regression analysis. A comprehensive index (EWI) was proposed to evaluate the cooling and water-saving abilities of different green space structures. Based on assessment results, species were classified into three: good ($EWI \geq 0.795$), common ($0.795 > EWI \geq 0.419$), and weak ($EWI < 0.419$). The characteristics of 17 species or species compositions with good cooling and water-saving abilities were summarized as: 1) a mix of the arbor, shrub, and herb, and 2) complete cover of green space by shrub.

KEYWORDS

urban green space, vegetation structure, remote sensing inversion, heat island effect, water-saving

Introduction

Water is the source of life; efficient water use has significant implications for people who live in regions with little precipitation. Approximately 53% of China's territory is made up of arid and Semi-humid regions. Ranked 121th in the world, China has annual per capita water resources of only 2,200 m³, and with over 400 cities, there is a serious water deficiency especially in the north. Currently, deficits existing between the water

demand and supply are becoming the principal bottleneck to sustainable development. To alleviate the pressure on water resources, the Chinese government has implemented several significant water transfer and water-saving projects (Cai, 2008). However, with rapid urbanization, people have to cope with the problems brought about by the deterioration of the ecological environment in cities, such as water pollution, hazy weather, and heat island effect etc. This has resulted in economic losses.

As an important part of the urban ecosystem, urban green spaces can provide vital services to humans (World Resources Institute, 2005), and make both the ecosystem and society sustainable (Katherine et al., 2010). Although urban green spaces might be smaller in size compared to other land uses, the value of its ecosystem services is likely to be disproportionately higher depending on their locations (Perino et al., 2014). Maximizing the ecological value of green spaces partly depends on a reasonable mix of landscape plants (Katherine et al., 2010). In 2011, the green coverage rate reached 38.62% in the cities of China (The National Afforestation Committee, 2019), but there are still problems such as unreasonable green space structure and inefficient use of water. Take Beijing as an example; in 2009, the green space area was 617 km², urban green coverage rate was 43.5%, and annual irrigation water requirement was $2.2 \text{ m}^3 \times 10^8 \text{ m}^3$, nearly 10% of the gross city water consumption (Beijing Municipal Bureau of Statistics, 2019). The great water requirement of green space irrigation further aggravates the pressure on water supply in the cities, especially in the arid and Semi-humid regions. It is critical to understand the potential tradeoffs between service functional values of ecology and city water usage. In this regard, it is necessary to conduct a study on water consumption and ecological functions of vegetation structures. We also hope that our work can bridge the gap between ecological environmental quality and water resources in the arid and Semi-humid regions.

Hydrology is regarded as an important technological path in the study of water utilization and vegetation management (Masoud et al., 2007; Cheng et al., 2009; Yan et al., 2010; Zhao et al., 2010). This method laid the foundation for understanding plant water consumption. However, only a few studies focused on different green space structures with monoculture species. Also, the hydrology method is difficult when comparing large quantities of objects because of the unbearable cost (Li et al., 2009). Analogously, existing studies on service function of vegetation are mostly single case studies that focused on carbon sequestration, dust-retention, and oxygen releasing abilities, etc. (Katri et al., 2011; Yen and Lee, 2011; Liu et al., 2013; Zhao et al., 2013). Thus, there is a lack of comparative analysis. Meanwhile, spatial gradient analysis was widely used in landscape ecology studies, but it was not suitable for a plot scale (Kong et al., 2005; Tohru et al., 2011). The vegetation evapotranspiration, leaf quantity, and temperature of

50 different green space communities in the Beijing urban area can reflect the regional ecological carrying capacity to a certain extent. Above all, there would be some disadvantages of the above research methodology in a comparative study of ecological functions and water consumption of various urban green space structures.

The capacity and efficiency of environmental information collection for the Earth's surface have been greatly improved by the development of remote sensing (RS) technology. Many algorithms have been applied to estimate vegetation evapotranspiration, structure, and land surface temperature at multiple spatial scales (Liu et al., 2007). Historically, there are three methods applied in the estimation of evapotranspiration: statistical methods (Jackson et al., 1977), energy residual methods (Granger and Gray, 1989; Hobbins et al., 1999), and numerical models. Recently, many quantitative RS studies have been conducted with *SEBAL* (Surface Energy Balance Algorithm for Land), *SEBS* (Surface Energy Balance System), and *S-SEBI* (Simplified-Surface Energy Balance Index) models (*SEBS* model and *S-SEBI* model were generated based on *SEBAL* model) (Idso et al., 1975; Bastiaanssen et al., 1998a; Roerink et al., 2000; Su, 2002), and good results were obtained. Since 1960, several algorithms including single-channel, split-window, multi-view single-channel, and multi-channel and multi-angle algorithms, have been proposed for the calculation of surface temperature with different RS data. (Becker, 1987; Roerink et al., 2000; Dash et al., 2002; Su, 2002; Jiménez Muñoz and Sobrino, 2003; Qin et al., 2010) used different algorithms to estimate the temperature of underlying surfaces.

This study investigated the vegetation evapotranspiration, leaf quantity, and temperature of 50 different green space communities in the Beijing urban area. The study sought to explore a method for evaluating the cooling and water-saving abilities of typical green space structures using RS and GIS and to provide a reasonable focus on green space structure and information in the management of urban green space, and research results are of significance in improving the ecological carrying capacity of the Semi-humid Region.

Materials and methods

Study site

The study sites were located in Beijing, northern China (Figure 1). Beijing, an ancient city with over 1,000 years of history, is a rapidly developing city, with more than eight million urban residents. The city consists of 14 administrative districts and four counties. In downtown, there are approximately 40 main parks.

The main study area, located in the northwest of the city (116°14'38.6"E–116°24'29.34"E, 39°57'7.36"N–40°2'51.3"N), includes parts of Haidian, Chaoyang, Changping, Dongcheng, and Xicheng district, with a gross area of 147.5 km²; the annual total

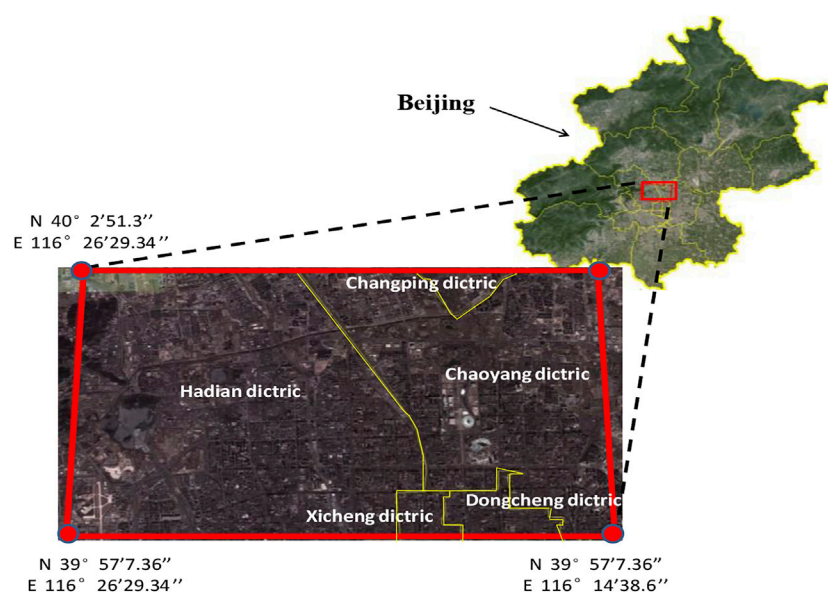


FIGURE 1
Study area (bold-red bordered line).

rainfall ranges from 544.7 to 575.6 mm (Figure 1). The green space is mainly located in the National Olympic Park, Old summer Palace Park, summer Palace Park, Bajia Park, Haidian Park, Beitucheng Park, etc. Buildings, roads, water, green land, and bare land are the main land cover types present. Monoculture and mix-species arbor forests, shrubbery, grass and multi vegetation structures of tree-shrub-grass typically make up the green vegetation types.

Remote sensing data

Three temporal remote sensing Landsat-8 images, which were generated on 12 May 2013, 13 June 2013, 1 Sep 2013, respectively, were used. The standard Landsat eight data products provided by the USGS EROS Center (<http://landsat.usgs.gov/index.php>) consist of multispectral image data acquired by both the Operational Land Imager (OLI) and Thermal Infrared Sensor (TIRS). One image scene consists of nine spectral bands with a spatial resolution of 30 m for bands one to seven and 9. Thermal bands 10 and 11 are useful in providing more accurate surface temperatures and are collected at 100 m.

Meteorological data

The meteorological data were collected on 12 May 2013, 13 June 2013, 1 Sep 2013, respectively, and the hourly meteorological data involved in this study were collected from

the Beijing Weather Observatory website (<http://cdc.bjmb.gov.cn/shuju.asp>), and this included solar radiation, rainfall, wind speed, temperature, and relative humidity. The collected meteorological data were used to evaluate the cooling and water-saving abilities of typical green space structures.

Sample plots

50 plots with different vegetation communities were selected in the study area; their areas ranged from 6,400 to 12,100 m² (average size, 100 m × 100 m), and away from buildings and water. Vegetation structure can be classified into pure arbor type, arbor-grass type, arbor-shrub type, arbor-shrub-grass type, shrub-grass type, and grass type. The vegetation structure information was collected by field survey, and it included: dominant plant species, species coverage, and sand density (as shown in Table 1).

Vegetation quantity

There is a reasonable relationship between vegetation quantity and NDVI in pixel scale (Di et al., 2012) for the study area, and this was expressed as:

$$VQ_i = \frac{1}{\left(\frac{1}{30000} + 0.0002 \times 0.03^{NDVI_i}\right)} \quad (1)$$

TABLE 1 Sample plot status.

Serial number	Arbor layer			Shrub layer		Herb layer	
	Dominant species	Coverage (%)	Sand density (Stem/ha)	Dominant species	Coverage (%)	Dominant species	Coverage (%)
1	<i>Sophora japonica, pinus tabuliformis</i>	81	404	<i>Deutzia parviflora Bunge</i>	61	<i>Liriope graminifolia</i>	40
2	<i>Populus, sophora japonica</i>	69	631	<i>Weigela florida</i>	53	<i>Liriope graminifolia, Bambuseae</i>	51
3	<i>Populus</i>	32	326	<i>Lonicera maackii</i>	44	<i>Buchloe dactyloides</i>	63
4	<i>Salix babylonica</i>	29	531	<i>Ligustrum lucidum</i>	23	<i>Buchloe dactyloides</i>	41
5	<i>Populus</i>	50	632	<i>Sabina vulgaris, Lonicera maackii</i>	59	<i>Liriope graminifolia</i>	46
6	<i>Sophora japonica</i>	86	615	<i>Syngia reticulata</i>	23	<i>Buchloe dactyloides</i>	82
7	<i>Platanus orientalis</i>	23	319	<i>Sabina vulgaris</i>	27	<i>Buchloe dactyloides</i>	55
8	<i>Platycladus orientalis</i>	75	1,501	<i>Lonicera maackii</i>	43	<i>Commelina communis</i>	53
9	<i>Ailanthus altissima, Sophora japonica</i>	51	817	<i>Lonicera maackii, Amygdalus triloba</i>	39	<i>Viola pekinensis</i>	60
10	<i>Pinus tabuliformis</i>	22	401	<i>Syngia reticulata</i>	57	<i>Poa annua, Viola pekinensis</i>	40
11	<i>Salix babylonica</i>	59	322	<i>Prunus cerasifera</i>	54	<i>Viola pekinensis</i>	82
12	<i>Acer truncatum bunge</i>	47	336	<i>Magnolia denudata</i>	41	<i>Poa annua</i>	77
13	<i>Acer truncatum bunge</i>	92	636	<i>Rosa xanthina</i>	53	<i>none</i>	0
14	<i>Pinus tabuliformis</i>	12	229	<i>Rosa chinensis</i>	0	<i>none</i>	100
15	<i>Fraxinus sogdiana Bunge</i>	53	435	<i>none</i>	0	<i>Buchloe dactyloides</i>	100
16	<i>Populus</i>	49	863	<i>none</i>	0	<i>Setaria viridis</i>	100
17	<i>Populus</i>	65	1,006	<i>none</i>	0	<i>Liriope graminifolia</i>	100
18	<i>Salix babylonica</i>	44	869	<i>none</i>	0	<i>Poa annua</i>	24
19	<i>Pinus tabuliformis</i>	55	1,193	<i>none</i>	0	<i>Poa annua</i>	50
20	<i>Populus, metasequoia glyptostroboides</i>	51	1,229	<i>none</i>	0	<i>Viola pekinensis</i>	100
21	<i>Pinus bungeana</i>	4	645	<i>none</i>	61	<i>Trifolium repens</i>	21
22	<i>Ulmus pumila, sabina chinensis</i>	62	1,021	<i>none</i>	0	<i>Viola pekinensis</i>	40
23	<i>Koeleruteria paniculate, pinus bungeana</i>	78	996	<i>none</i>	0	<i>Liriope graminifolia</i>	39
24	<i>Pinus tabuliformis, Pinus bungeana</i>	82	1,100	<i>none</i>	0	<i>Viola pekinensis</i>	61
25	<i>Populus</i>	70	638	<i>none</i>	0	<i>Viola pekinensis</i>	55
26	<i>Sophora japonica, salix babylonica</i>	87	656	<i>none</i>	0	<i>Viola pekinensis</i>	31
27	<i>Sophora japonica</i>	93	673	<i>none</i>	0	<i>Humulus japonicus</i>	71
28	<i>Sophora japonica</i>	83	687	<i>none</i>	0	<i>Poa annua</i>	61
29	<i>Populus</i>	61	913	<i>none</i>	0	<i>Liriope graminifolia</i>	19
30	<i>Salix babylonica</i>	72	1,006	<i>none</i>	0	<i>Potentilla chinensis, Viola pekinensis</i>	37
31	<i>Populus</i>	70	961	<i>none</i>	0	<i>Poa annua</i>	95
32	<i>Sophora japonica</i>	68	811	<i>none</i>	0	<i>Poa annua</i>	79
33	<i>Populus</i>	82	863	<i>none</i>	0	<i>Poa annua</i>	66
34	<i>Sabina chinensis</i>	49	1,139	<i>none</i>	0	<i>Poa annua</i>	77

(Continued on following page)

TABLE 1 (Continued) Sample plot status.

Serial number	Arbor layer			Shrub layer		Herb layer	
	Dominant species	Coverage (%)	Sand density (Stem/ha)	Dominant species	Coverage (%)	Dominant species	Coverage (%)
35	<i>Koelreuteria paniculata</i> , <i>salix babylonica</i>	78	996	none	0	<i>Poa annua</i>	91
36	<i>Pinus tabuliformis</i>	67	937	none	0	<i>Poa annua</i>	89
37	<i>Ginkgo biloba</i>	49	233	none	0	none	0
38	<i>Sophora japonica</i>	78	921	none	0	none	0
39	<i>Koelreuteria</i>	91	833	none	0	none	0
40	<i>Sophora japonica</i> , <i>Fraxinus chinensis</i>	83	563	none	0	none	0
41	<i>Sophora japonica</i>	95	1,114	none	0	none	0
42	<i>Sabina chinensis</i>	73	1,661	none	0	none	0
43	<i>Cedrus deodara</i>	55	812	none	0	none	0
44	none	0	0	<i>Malus spectabilis</i> , <i>F. atropu tpurea</i>	21	<i>Poa annua</i>	81
45	none	0	0	<i>Prunus persica</i> , <i>Chrysanthemoides</i>	78	<i>Poa annua</i>	43
46	none	0	0	<i>Amygdalus triloba</i>	77	<i>Poa annua</i>	60
47	none	0	0	<i>Magnolia denudata</i>	23	<i>Poa annua</i>	95
48	none	0	0	none	0	<i>Buchloe dactyloides</i>	100
49	none	0	0	none	0	<i>Poa annua</i>	100
50	none	0	0	none	0	<i>Poa annua</i> , <i>buchloe dactyloides</i>	91

Note: "none" in the table means there is none or few of this type of plant (arbor or shrub or herb) in a sample plot.

Where VQ_i ($m^2/900 m^2$) is the vegetation quantity in pixels, which were covered by sample plots, and $NDVI_i$ is the normalized difference vegetation index in pixels; the $NDVI_i$ estimation model was obtained from Eq. 2 (Di et al., 2012).

$$NDVI_i = \frac{\rho_5 - \rho_4}{\rho_5 + \rho_4} \quad (2)$$

Where ρ_5 is reflectivity in OLS-5 band, and ρ_4 is reflectivity in OLS-4 band.

Mean VQ per-plot was calculated as follows:

$$VQ_{RS} = \frac{1}{n} \sum_{i=1}^n VQ_i \quad (3)$$

Where n is the number of pixels covered by a sample plot.

On 12 May 2013, 13 June 2013, and 1 Sep 2013, the VQ of 10 plots were measured with a LAI-2200 canopy analyzer (LI-COR, United States) to verify the accuracy of calculation of VQ_{RS} .

Land surface temperature

In this paper, The land surface temperature (T_s) of different land-use types was calculated with a single-channel algorithm (Di et al., 2012), including road, urban water body, residential area, high vegetation quantity area and low vegetation quantity area, as shown in Eqs 4,5. The mean T_s of a sample plot was expressed as an average of the temperature values of all the pixels covered by the sample plot in 3 days, which corresponded to days when the three remote sensing images were taken. These were defined by the equations below.

$$T_{10} = \frac{K_2}{\ln\left(\frac{K_1}{L_{10}} + 1\right)} \quad (4)$$

$$T_s = \frac{T_{10}}{\epsilon^{0.25}} \quad (5)$$

Where T_{10} is radiant brightness temperature (K) in TIRS-10 band, °C, T_s (K) is land surface temperature, °C, K_1 ($m^2 sr \mu m$) and K_2 (K) are constants, ϵ is thermal emissivity, and L_{10} is radiant brightness ($m^2 sr \mu m$) in TIRS-10 band.

Evapotranspiration

The calculation of evapotranspiration (ET) was based on *SEBAL*, which was established by (Bastiaanssen et al., 1998b) and widely used in the retrieval of ET by RS (Mohammad and Samaneh, 2012). The processes involved in *SEBAL* utilization can be summarized as the instantaneous latent heat fluxes of every pixel that can be gotten by surface energy balance, as expressed in equation Eq. 6. The instantaneous evaporative fraction is shown in the literature to be similar to the 24-h evaporative fraction (Shuttleworth et al., 1989), and thus daily average value of ET can be calculated through time scale transformation (Brutsaert and Sugita, 1992; Crago, 1996), as expressed in Eqs 7,8. The mean ET of a sample plot was expressed as an average of the ET values of all the pixels that were covered by the sample plot in 3 days, and this corresponded to days when the three RS images were taken. In Bajia Park, the actual ET s were measured in seven plots based on the principle of water balance to verify its accuracy.

$$ET_{ins} = \frac{R_n - G - H}{\lambda} \quad (6)$$

$$A_{ins} = \frac{R_n - G - H}{R_n - G} = \frac{\lambda ET}{R_n - G} = A_{24} \quad (7)$$

$$ET_{24} = \frac{R_{n24} \times A_{24} \times 86400}{[2.501 - 0.002361 \times (T - 273.15_s)] \times 10^6} \quad (8)$$

where R_n is the instantaneous net radiation (Wm^{-2}); G is the instantaneous soil heat fluxes (Wm^{-2}); H is the instantaneous sensible heat exchange between air and land surface (Wm^{-2}); λ is the latent heat of vaporization of water ($Wm^{-2} mm^{-1}$), and A_{ins} and A_{24} are the instantaneous and 24-h evaporative fractions. The algorithms of the above parameters are similar to those established by (Du et al., 2013).

Model evaluation criteria

Using satellite data and meteorological data, the coefficient of determination (R^2), mean absolute relative error ($MARE$) and average relative error (\bar{Re}) were used to measure the performance of the estimates of ET and VQ . In general, the R^2 value, which was calculated by linear regression analysis, is an indicator of the strength of relationship between the observed and simulated values. If the R^2 values are less than or very close to zero, the prediction of the modeling system is considered unacceptable or poor. The $MARE$ and (\bar{Re}) indicate the model's ability to predict the values of a given prediction. They were defined as follows:

$$MARE = \frac{\sum_{i=1}^n |x_i^*/x_i - 1|}{n} \quad (9)$$

$$\bar{Re} = \frac{\sum_{i=1}^n (x_i^* - x_i)}{n} \times 100\% \quad (10)$$

where x_i is the i th observation, x_i^* is the i th simulation value, and n denotes the total number of data points (observations) in the record. Lower values of $MARE$ and (\bar{Re}) are preferred.

Evaluation of vegetation eco-water-saving ability

A comprehensive eco-water-saving ability index of vegetation (EWI) was proposed to evaluate vegetation cooling and water-saving abilities of different vegetation structures. EWI can be defined as:

$$EWI_i = 1 - \frac{T_i}{\bar{T}} \times \frac{ET_i/LAI_i}{ET/\bar{LAI}} \quad (11)$$

Where EWI_i is the comprehensive eco-water-saving ability index value of the i th vegetation structure, and it is dimensionless value greater than 0; T_i is the land temperature of the i th vegetation structure, $^{\circ}C$; \bar{T} is the mean land temperature of all 50 sample plots in $^{\circ}C$; LAI is leaf area index, and both LAI and VQ can reflect the leaf volume of plants. ET_i/LAI_i is the i th daily evapotranspiration per unit LAI of the i th vegetation structure in mm/d ; and ET/\bar{LAI} is the mean daily evapotranspiration per unit LAI of all 50 sample plots in mm/d . A high EWI indicates that the comprehensive eco-water-saving ability of the vegetation is preferred.

Result

Surface temperature of the study area

The results showed that temperature between different land use types in the growing season varies (Figure 2). The T_s of the road was the highest, followed by those of the residential area, low vegetation quantity area, high vegetation quantity area, and urban water body, respectively. Compared with other land use types, the temperatures of the urban water body and high vegetation quantity area are 9–18 degrees lower. This indicates that vegetation can help to relieve the urban heat island effect, and vegetation index appears to be an indicator of environmental temperature (Gallo et al., 1993).

Evapotranspiration of study area

After an evaluation of the ET results calculated using the *SEBAL* model and that measured based on the water balance principle of four sample plots on May-12-2013, June-13-2013, and Sep-1-2013, a linear relationship was observed between the calculated ET and measured ET ; R^2 was 0.445, $MARE$ was 0.16, and (\bar{Re}) was -21.3%. This indicated that the accuracy of the model calculation is acceptable. Errors may arise due to interference in the pixel data of sample plots by land objects in the surroundings of these sample plots, such as buildings and roads.

The distribution of ET on May-12-2013 and June-13-2013 is shown in Figure 3; the highest ET was observed in water bodies such as the Kunming Lake, Fuhai, Jing-Mi water diversion canal, and Olympic lake ($7.2 \pm 1.6 mm$). The second highest ET value was

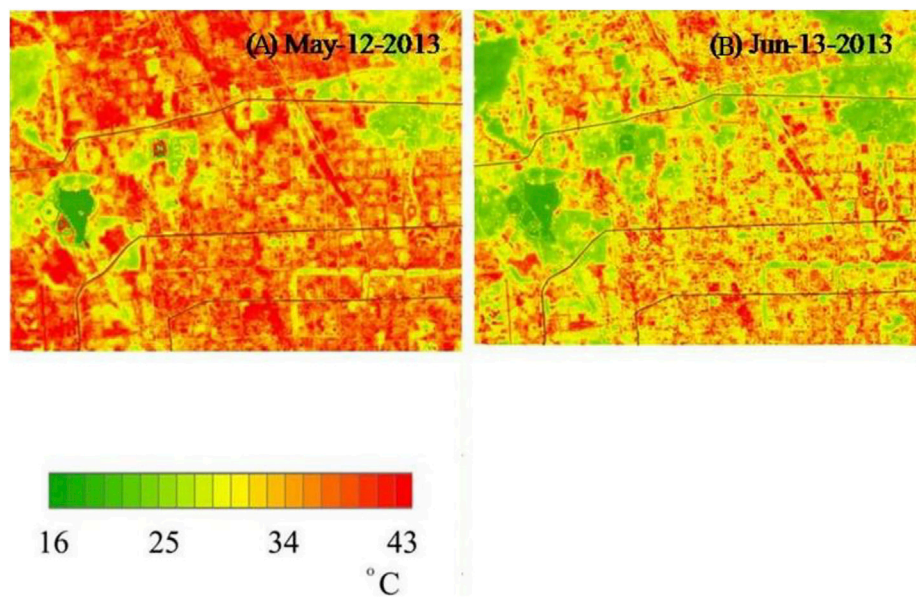


FIGURE 2

Dynamics of T_s patterns in the study area in (A) May and (B) June 2013 based on the surface energy balance method using Landsat-8 satellite data. Each date had different ranges.

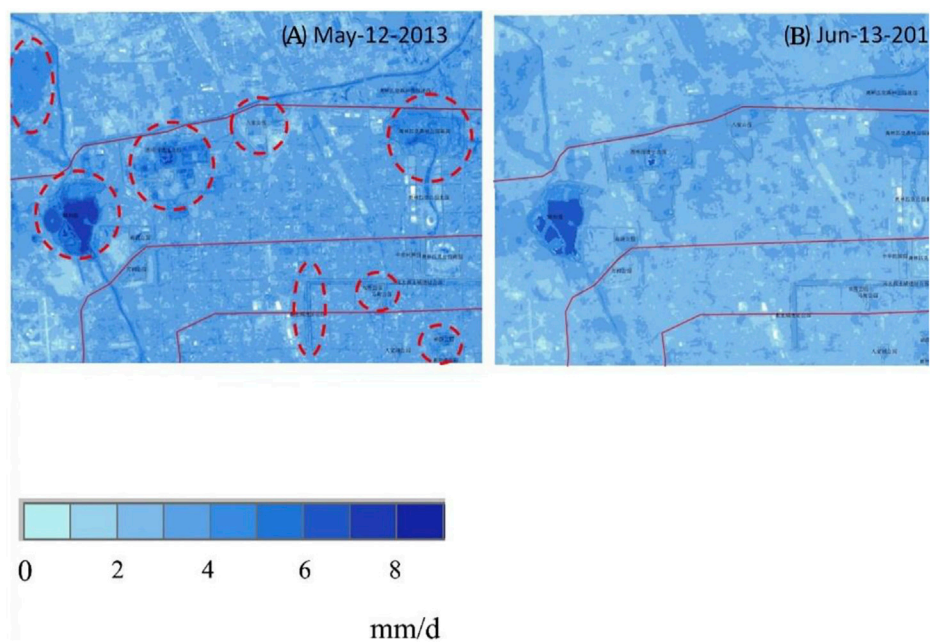


FIGURE 3

Dynamics of evapotranspiration patterns in the study area during (A) May and (B) June, 2013 based on surface energy balance method using Landsat-8 satellite data. Each date had different ranges.

observed in places with greater vegetation coverage. For instance, the Olympic Forest Park, the summer Palace, and Dongsheng country parks were in the area bounded by the dotted line (4.3 ± 2.1 mm).

The third-highest ET regions were the residential areas and greenbelts along the city roads with lower vegetation coverage (3.3 ± 1.7 mm). Dense human settlements and commercial

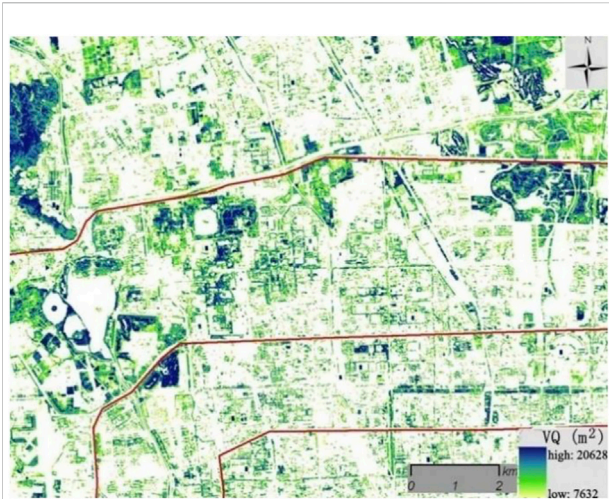


FIGURE 4
Distribution of vegetation quality per pixel; the area of a single pixel is 900 m².

districts had the lowest *ET* value which shows that vegetation played a significant role in the water consumption of the soil-plant-atmosphere system. In different months, *ET* in June is lower than that in May, because May is the dry season, with less rainfall and less air humidity, while June is the rainy season, with more rainfall and higher air humidity, resulting in smaller *ET*.

Vegetation quantity of study area

Based on an evaluation of *VQ* results calculated using the *NDVI* and actual *VQ* observation of 12 sample plots on May-12-2013, June-13-2013, and Sep-1-2013, a linear relationship was detected between the calculated *VQ* and observed *VQ*; R^2 was 0.66, *MARE* was 0.21, and (\bar{Re}) was 13.5%, which indicated that the accuracy of the model calculation is acceptable. The main sources of error resource may be similar to that of the *ET* inversion. The mean vegetation quality of the study area is presented in Figure 4; the green land area is 56.87 km², which is 38.6% of the total study area. Vegetation quality area is 822.1 km².

Relationships between surface temperature, evapotranspiration, and *LAI*

The mean T_s , *ET*, and *LAI* of 50 sample plots were presented in a scatter plot (Figure 5). A negative correlation was observed between mean T_s and mean *LAI*; an increase in mean *LAI* by 1, can reduce T_s by 0.62-degree centigrade. However, a positive correlation was observed between mean *ET* and mean *LAI*; an increase in mean *LAI* increase by 1 mm/d can increase mean *ET* by 0.073 mm/d.

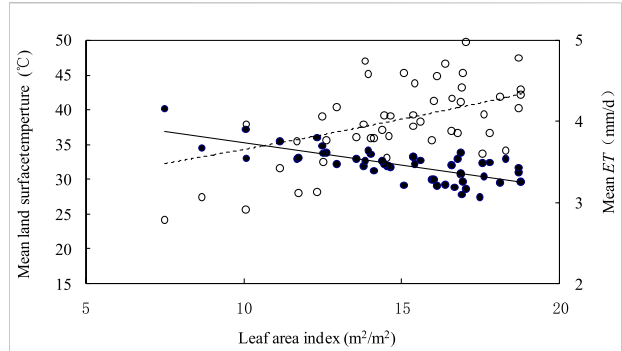


FIGURE 5
Relationships between mean T_s , mean *ET* and mean *LAI*. Regression line for mean *ET* and mean *LAI* can be expressed as: $ET = 3e^{0.019LAI}$, $R^2 = 0.127$; $p < 0.01$ (unfilled circles, unbroken line). Regression line for mean T_s and mean *LAI* can be expressed as: $ET = -0.62LAI + 41.42$, $R^2 = 0.49$; $p < 0.01$ (filled circles, broken line).

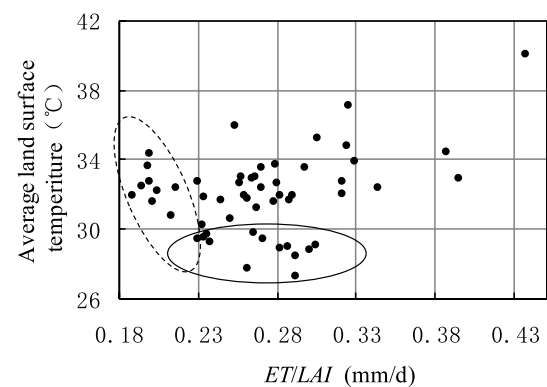


FIGURE 6
Relationships between T_s and *ET/LAI*.

To analyze the effect of species, the mean *ET* of sample plots were expressed as *ET* per *LAI* (*ET/LAI*), and the relationship between mean T_s and *ET/LAI* was determined as Figure 6. There were 11 species (indicated by the points in a solid line ellipse) with a mean $T_s < 30^\circ\text{C}$. Their corresponding serial numbers are 8, 9, 10, 16, 22, 23, 24, 25, 29, 45, and 48 (Table 1), respectively, accounting for 22% of the total. Eleven species (indicated by points in a dashed ellipse) had *ET/LAI* < 0.23 mm/d, accounting for 22% of the total. Their corresponding serial numbers are 1, 2, 11, 12, 13, 16, 32, 39, 40, 44, and 47, respectively (Table 1).

As shown in Table 2, the *EWI*s of species or species compositions in 50 sample plots were divided into three categories based on the natural breakpoint method by their *EWI* value: Good ($EWI \geq 0.795$), Common ($0.795 >$

TABLE 2 *EWI* of species or species compositions of 50 example plots.

Good	Serial number	39	24	9	47	2	16	8	40	29	12	11	48	38	22	10
	<i>EWI</i>	0.99	0.985	0.984	0.975	0.957	0.956	0.956	0.955	0.955	0.951	0.946	0.943	0.942	0.936	0.934
Good	Serial number	44	45	17	13	23	32	25	19	1	46	5	49	18	26	
	<i>EWI</i>	0.924	0.918	0.917	0.912	0.899	0.899	0.885	0.88	0.86	0.856	0.825	0.824	0.803	0.795	
Common	Serial number	27	4	20	30	50	14	21	43	33	15	31	7	36	41	
	<i>EWI</i>	0.762	0.734	0.734	0.688	0.683	0.674	0.65	0.64	0.61	0.603	0.553	0.496	0.443	0.419	
Weak	Serial number	6	3	42	37	28	34	35								
	<i>EWI</i>	0.376	0.21	0.192	0.172	0.118	0.098	0								

Note: Serial numbers here corresponds to the serial numbers in Table 1 of 50 sample plots.

$EWI \geq 0.419$) and Weak ($EWI < 0.419$). Each category included 5–29 species or species compositions. The species or species compositions were classified as Good, it means that the species or species need less water for per unit *LAI*.

Discussion

Two characters of vegetation structures with lower *T_s* can be found: 1) those with higher arbor density, 2) warm-season turf grasses. This because the arbor has higher vegetation quantity and more water is used in cooling air by transpiration compared to that used by shrubs and herbs. Furthermore, the evapotranspiration of warm-season grasses is higher than that of cool-season grasses (Aronson et al., 1987; Xiao et al., 2006). The vegetation structures with lower *ET* can be summarized as 1) thin native trees with greater species composition, such as *Sophora japonica* and *Pinus tabulaeformis*, 2) cool-season turf grasses. Since the average water consumption of native vegetation is lower than that of extrinsic vegetation in arid areas, it is difficult to have optimal cooling and water-saving abilities for green spaces. However, because of water shortages, green space managers in Semi-humid areas have to compromise with ecological benefit for less irrigation. In that case, species or species compositions which can balance ecological benefit and water-saving for urban green space should be used.

In this study, 50 typical vegetation structures were divided into three categories according to *EWI*; the main difference can be found by a comparison of the different categories: the proportion of vegetation structures which include the arbor, shrub, and herb is 28% in the category with good comprehensive eco-water-saving ability; and the proportion is 21% and 29%, respectively, for the remaining

two categories. In addition, the proportion of vegetation structures without shrub is 79% and 71% in the categories with common and weak eco-water-saving ability, respectively, and these are significantly higher than that of the category Good. It is indicated that, generally, the arbor-shrub-herb mix and complete coverage by shrubs gave vegetation structures a better comprehensive eco-water-saving ability. This ability can be explained by the features of their vegetation structures such as great heat capacity and high reflectivity, and relatively low water consumption (Zhou et al., 2005; Song et al., 2007).

Conclusion

Urban ecological environment and water resources are key issues of concern. In this study, *RS* inversion methods were utilized to calculate the land temperature, evapotranspiration and vegetation quantity of 50 typical green space vegetation structures. According to verification tests, the accuracy of calculation is acceptable. The relationships between *T_s*, *VQ*, and *ET* of green land were determined with regression analysis. An eco-water-saving abilities index (*EWI*) was proposed to evaluate different green space structures. Fifty species or species compositions were classified into good ($EWI \geq 0.795$), common ($0.795 > EWI \geq 0.419$) and weak ($EWI < 0.419$) categories, respectively, based on the assessment results. The characteristics of 17 species or species compositions with good cooling and water-saving abilities were summarized as 1) a mix of arbor, shrub and herb, 2) complete coverage of green space by shrub. The method and eco-water-saving species or species composition can be utilized in developing possible models of urban green space management, and were of significance in improving the ecological carrying capacity of the Semi-humid Region.

Data availability statement

The original contributions presented in the study are included in the article/supplementary material, further inquiries can be directed to the corresponding authors.

Author contributions

XL: Conceptualization, Methodology, Formal analysis, Writing—Original Draft, Writing—Review and Editing, Visualization. YL: Methodology, Formal analysis, Writing—Original Draft, Software, Visualization. SD: Resources, Data Curation, Writing—Review and Editing, Supervision, Project administration, Funding acquisition. YN: Conceptualization, Methodology, Writing—Review and Editing. CZ: Conceptualization, Methodology, Visualization.

Funding

This study was financially supported by the Natural Science Foundation of Shandong Province (Grant No. ZR2016DB12).

References

- Aronson, L. J., Gold, A. J., Hull, R. J., and Cisar, J. L. (1987). Evapotranspiration of cool-season turfgrasses in the humid northeast ¹. *Agron. J.* 79, 901–905. doi:10.2134/agronj1987.00021962007900050029x
- Bastiaanssen, W. G. M., Menenti, M., Feddes, R. A., and Holtslag, A. A. M. (1998). A remote sensing surface energy balance algorithm for land (SEBAL). 1. Formulation. *J. Hydrol. X.* 212, 198–212. doi:10.1016/s0022-1694(98)00253-4
- Bastiaanssen, W. G. M., Pelgrum, H., Wang, J., Ma, Y., Wal, T. V. D., Roerink, G., et al. (1998). A remote sensing surface energy balance algorithm for land (SEBAL). *J. Hydrol. X.* 212–213, 213–229. doi:10.1016/s0022-1694(98)00254-6
- Becker, F. (1987). The impact of spectral emissivity on the measurement of land surface temperature from a satellite. *Int. J. Remote Sens.* 8, 1509–1522. doi:10.1080/01431168708954793
- Beijing Municipal Bureau of Statistics (2019). *Beijing statistical yearbook*. Available at: <http://www.bjstats.gov.cn/tjnj> (accessed June, 26)
- Brutsaert, W., and Sugita, M. (1992). Application of self-preservation in the diurnal evolution of the surface energy budget to determine daily evaporation. *J. Geophys. Res.* 97, 18377–18382. doi:10.1029/92jd00255
- Cai, X. (2008). Water stress, water transfer and social equity in northern China—implications for policy reforms. *J. Environ. Manage.* 87, 14–25. doi:10.1016/j.jenvman.2006.12.046
- Cheng, X., Huang, M., Shao, M., and Warrington, D. N. (2009). A comparison of fine root distribution and water consumption of mature Caragana korshinskii Kom grown in two soils in a semiarid region, China. *Plant Soil* 315, 149–161. doi:10.1007/s11104-008-9739-5
- Crago, R. D. (1996). Conservation and variability of the evaporative fraction during the daytime. *J. Hydrol. X.* 180, 173–194. doi:10.1016/0022-1694(95)02903-6
- Dash, P., Göttsche, F. M., Olesen, F. S., and Fischer, H. (2002). Land surface temperature and emissivity estimation from passive sensor data: Theory and practice-current trends. *Int. J. Remote Sens.* 23, 2563–2594. doi:10.1080/01431160110115041
- Di, S. C., Wu, W. Y., Liu, H. L., and Pan, X. Y. (2012). Water consumption estimation and evapotranspiration inversion based on remote sensing technology. *Trans. Chin. Soc. Agric. Eng.* 28, 98–104.
- Du, J., Song, K., Wang, Z., Zhang, B., and Liu, D. (2013). Evapotranspiration estimation based on MODIS products and surface energy balance algorithms for

Acknowledgments

The insightful comments by editors and reviewers are greatly acknowledged. These comments helped us improve our original manuscript greatly.

Conflict of interest

The authors declare that the research was conducted in the absence of any commercial or financial relationships that could be construed as a potential conflict of interest.

Publisher's note

All claims expressed in this article are solely those of the authors and do not necessarily represent those of their affiliated organizations, or those of the publisher, the editors and the reviewers. Any product that may be evaluated in this article, or claim that may be made by its manufacturer, is not guaranteed or endorsed by the publisher.

- land (SEBAL) model in Sanjiang Plain, Northeast China. *Chin. Geogr. Sci.* 23, 73–91. doi:10.1007/s11769-013-0587-8
- Gallo, K. P., McNab, A. L., Karl, T. R., Brown, J. F., Hood, J. J., and Tarpley, J. D. (1993). The use of a vegetation index for assessment of the urban heat island effect. *Int. J. Remote Sens.* 14, 2223–2230. doi:10.1080/01431169308954031
- Granger, R. J., and Gray, D. M. (1989). Evaporation from natural nonsaturated surfaces. *J. Hydrol. X.* 111, 21–29. doi:10.1016/0022-1694(89)90249-7
- Hobbins, M. T., Ramírez, J. A., and Brown, T. C. (1999). The complementary relationship in regional evapotranspiration: The CRAE model and the advection-aridity approach. *Proc. Ninet. Annu. A. G. U. Hydrol. Days*, 199–212.
- Idso, S. B., Jackson, R. D., and Reginato, R. J. (1975). Estimating evaporation: A technique adaptable to remote sensing. *Science* 189, 991–992. doi:10.1126/science.189.4207.991
- Jackson, R. D., Reginato, R. J., and Idso, S. B. (1977). Wheat canopy temperature: A practical tool for evaluating water requirements. *Water Resour. Res.* 13, 651–656. doi:10.1029/wr013i003p00651
- Jiménez Muñoz, J. C., and Sobrino, J. A. (2003). A generalized single-channel method for retrieving land surface temperature from remote sensing data. *J. Geophys. Res.* 108 (D22), 2003JD003480. doi:10.1029/2003jd003480
- Katherine, N. I., Richard, A. F., Patrick, D. W., Jamie, T., Sarah, R. P., Philip, H. W., et al. (2010). Ecological and psychological value of urban green space. *Dimensions Sustain. City Future City* 2, 215–237.
- Katri, O., Aigars, I., Iveta, V. K., Malle, M., Tatjana, K., Jaan, K., et al. (2011). Changes in the canopies of Pinus sylvestris and Picea abies under alkaline dust impact in the industrial region of Northeast Estonia. *For. Ecol. Manage.* 262, 82–87. doi:10.1016/j.foreco.2010.07.031
- Kong, F., Nakagoshi, N., Yin, H., and Kikuchi, A. (2005). Spatial gradient analysis of urban green spaces combined with landscape metrics in Jinan City of China. *Chin. Geogr. Sci.* 15, 254–261. doi:10.1007/s11769-005-0038-2
- Li, Z. Z., Li, G. H., Zhao, B. X., Lai, N. N., and Jing, L. J. (2009). Water consumption of green space and gardens in the Summer Palace of Beijing. *J. Beijing For. Univ.* 31, 66–72.
- Liu, C. S., Gao, Z. Q., and Gao, W. (2007). Retrieval evapotranspiration and land surface temperature in response to land use/cover change based on remote sensing data. *Trans. Chin. Soc. Agric. Eng.* 23, 1–8.

- Liu, L., Guan, D., Peart, M. R., Wang, G., Zhang, H., and Li, Z. (2013). The dust retention capacities of urban vegetation—A case study of Guangzhou, south China. *Environ. Sci. Pollut. Res.* 20, 6601–6610. doi:10.1007/s11356-013-1648-3
- Masoud, E., Sayyed, A. K., Ali, A. M., and Ali, B. (2007). Water consumption of a six-year-old river red gum plantation in the Southern Zagros Mountains, Iran. *J. Mt. Sci.* 4, 136–145. doi:10.1007/s11629-007-0136-y
- Mohammad, T. D., and Samaneh, P. (2012). Evaluation of water balance in a mountainous upland catchment using SEBAL approach. *Water Resour. Manage.* 26, 2069–2080. doi:10.1007/s11269-012-9999-y
- Perino, G., Andrews, B., Kontoleon, A., and Bateman, I. (2014). The value of urban green space in Britain: A methodological framework for spatially referenced benefit transfer. *Environ. Resour. Econ. (Dordr.)* 57, 251–272. doi:10.1007/s10640-013-9665-8
- Qin, Z., Karnieli, A., and Berliner, P. (2010). A mono-window algorithm for retrieving land surface temperature from Landsat TM data and its application to the Israel-Egypt border region. *Int. J. Remote Sens.* 22, 3719–3746. doi:10.1080/01431160010006971
- Roerink, G. J., Su, Z., and Menenti, M. (2000). S-SEBI: A simple remote sensing algorithm to estimate the surface energy balance. *Phys. Chem. Earth Part B Hydrology Oceans Atmos.* 25, 147–157. doi:10.1016/s1464-1909(99)00128-8
- Shuttleworth, W. J., Gurney, R. J., Hsu, A. Y., and Ormsby, J. P. (1989). *The variation in energy partitioning at surface flux sites, remote sensing and large scale global processes*. Wallingford, UK: IAHS.
- Song, Y. T., Yu, S. X., and Li, N. (2007). Spatial structure of the surface temperature in Shenzhen. *Acta Ecol. Sin.* 27, 1489–1498.
- Su, Z. (2002). The Surface Energy Balance System (SEBS) for estimation of turbulent heat fluxes. *Hydrol. Earth Syst. Sci.* 6, 85–100. doi:10.5194/hess-6-85-2002
- The National Afforestation Committee (2019). *China greening bulletin*. Available at: http://www.forestry.gov.cn/portal/main/s/195/content_531395.html (accessed July, 12).
- Tohru, M., Keitaro, I., Daisuke, H., Dai, I., Takashi, U., and Shuji, I. (2011). *Landscape ecology in Asian cultures*. Japan: Springer.
- World Resources Institute (2005). *Millennium ecosystem Assessment: Ecosystems and human well-being: Biodiversity synthesis*. Washington DC: Island Press.
- Xiao, J., Sun, X. H., and Li, G. Y. (2006). The water consumption regularity and irrigation system of Turfgrass under the condition of spray irrigation. *Sci-Tech Inf. Dev. Econ.*, 152–153.
- Yan, M., Yamanaka, N., Yamamoto, F., and Du, S. (2010). Responses of leaf gas exchange, water relations, and water consumption in seedlings of four semiarid tree species to soil drying. *Acta Physiol. Plant.* 32, 183–189. doi:10.1007/s11738-009-0397-x
- Yen, T., and Lee, J. (2011). Comparing aboveground carbon sequestration between moso bamboo (*Phyllostachys heterocycla*) and China fir (*Cunninghamia lanceolata*) forests based on the allometric model. *For. Ecol. Manage.* 261, 995–1002. doi:10.1016/j.foreco.2010.12.015
- Zhao, K. L., Fu, W. J., Jiang, P. K., and Zhou, G. M. (2013). *Functions of natural organic matter in changing environment*. Zhejiang (China): Zhejiang University Press.
- Zhao, W., Niu, Z., Chang, X., and Li, S. (2010). Water consumption in artificial desert oasis based on net primary productivity. *Sci. China Earth Sci.* 53, 1358–1364. doi:10.1007/s11430-010-4028-6
- Zhou, L. C., Shi, W. Y., Xue, W. J., Wang, T. Z., Ge, Z. M., Zhou, H., et al. (2005). Relationship between vegetation structure and the temperature and moisture in urban green spaces of Shanghai. *Chin. J. Ecol.* 24, 1102–1105.



OPEN ACCESS

EDITED BY

Jifeng Deng,
Shenyang Agricultural University, China

REVIEWED BY

Jagdish Chander Dagar,
Indian Council of Agricultural Research
(ICAR), India
Hossein Bashari,
Isfahan University of Technology, Iran

*CORRESPONDENCE

Haroun Chenchouni,
chenchouni@gmail.com

SPECIALTY SECTION

This article was submitted to Drylands,
a section of the journal
Frontiers in Environmental Science

RECEIVED 30 December 2021

ACCEPTED 28 July 2022

PUBLISHED 07 September 2022

CITATION

Macheroum A and Chenchouni H
(2022), Short-term land degradation
driven by livestock grazing does not
affect soil properties in semiarid
steppe rangelands.
Front. Environ. Sci. 10:846045.
doi: 10.3389/fenvs.2022.846045

COPYRIGHT

© 2022 Macheroum and Chenchouni.
This is an open-access article
distributed under the terms of the
Creative Commons Attribution License
(CC BY). The use, distribution or
reproduction in other forums is
permitted, provided the original
author(s) and the copyright owner(s) are
credited and that the original
publication in this journal is cited, in
accordance with accepted academic
practice. No use, distribution or
reproduction is permitted which does
not comply with these terms.

Short-term land degradation driven by livestock grazing does not affect soil properties in semiarid steppe rangelands

Amale Macheroum ^{1,2} and Haroun Chenchouni ^{3,4*}

¹Department of Nature and Life Sciences, Faculty of Exact Sciences and Nature and Life Sciences, University of Tebessa, Tebessa, Algeria, ²Laboratory of Plant Ecology and Environment, Faculty of Biological Sciences, Houari Boumediene University of Sciences and Technology (USTHB), Algiers, Algeria, ³Department of Forest Management, Higher National School of Forests, Khenchela, Algeria, ⁴Laboratory of Natural Resources and Management of Sensitive Environments "RNAMS", University of Oum-El-Bouaghi, Oum-El-Bouaghi, Algeria

The soil–vegetation relationships are reciprocal and fundamental for terrestrial ecosystem integrity. However, the long-term degradation of vegetation cover alters edaphic conditions, which can lead to degradation of habitats, and obstructs proper ecosystem functioning. This study aimed to assess the effects of the degradation of perennial steppe vegetation due to overgrazing (i.e., continuous and free grazing) on the physicochemical characteristics and soil fertility in the steppe rangelands of Halfa (*Macrochloa tenacissima* syn. *Stipa tenacissima*) of semi-arid areas in Algeria. The edaphic parameters of the superficial horizons of degraded steppes and other undegraded steppes were compared in order to suggest adequate strategies for rangeland management and remedy the degradation of vegetation and thereby ensure the sustainability of these agro-pastoral systems. The soil, collected from the surface horizons (A1 and A2) of pedological profiles, was analyzed according to standard methods of soil physicochemical analyses to determine the particle size fractions (clay, silt, and sands), pH, electrical conductivity (EC), total and active CaCO₃, organic matter (SOM), organic carbon, total nitrogen, and the C: N ratio. The distribution and variation of soil parameters between horizons and the two types of steppes were examined using generalized linear mixed models and redundancy analysis. Findings of this study revealed that the degradation of steppe vegetation cover by short-term overgrazing did not cause a significant variability in soil physicochemical parameters between degraded and undegraded steppes and the horizons A1 and A2. The sites studied have clayey–silty textures in non-degraded steppes and coarse textures dominated by sands in degraded steppes. The edaphic environment of the Halfa grass steppes was characterized by a calcareous substratum with high carbonate content (total CaCO₃ = 36.8–41%, active CaCO₃ = 17.5–18.5%), with an alkaline pH (8.09–8.19) and EC averaging 0.99 ± 1.24 dS/m. Soils had low SOM contents (1.42–2.93%), organic carbon (0.82–1.64%), and nitrogen (0.1–0.15%). The strong positive correlations recorded between the fine-size fractions, SOM, total CaCO₃, nitrogen, and EC indicated good soil structural stability in undegraded steppes, while the negative correlations between these same variables with sand and pH substantiate the structural degradation of the

soil. The negative correlation between C:N ratio and SOM indicated that the rate of SOM mineralization was rapid in semiarid steppes, with a higher fertility state in the undegraded steppe. Our findings suggest and urge to implement a restoration plan against the degradation of semi-arid Halfa steppes in order to avoid the irreversible state of soil and habitat destruction in the future because even the degradation of rangeland plant cover due to livestock overgrazing—in the short term—has not affected the edaphic characteristics of steppe rangelands.

KEYWORDS

land degradation, Mediterranean steppes, rangeland soil, soil fertility, soil organic matter, livestock grazing, haplic calcisols, drylands

Introduction

Soil degradation results from the combination of factors which drive the soil to an evolution different from the natural evolution linked to the local climate and vegetation (Osman, 2018; Dragović and Vulević, 2020; Smith et al., 2020). Land degradation is generally directly linked to the action of human activities *via*, for example, 1) the replacement of the native diversified vegetation (known as climax) by a secondary vegetation, a monoculture in the worst case, which modifies the humus and soil formation processes (Fialho and Zinn, 2014); 2) decrease in the soil organic carbon pool induced by overexploitation of the organic matter in the soil (non-return or insufficient return of the exported matter) and/or its leaching (Joosten, 2015; Garcia et al., 2018); 3) destruction of humus and insoluble clay–humic complexes of the soil due to inappropriate agricultural practices such as plowing which buries and destroys the living upper layers of the soil, or by excessive tillage, i.e., too intensive or too frequent (Baranian Kabir et al., 2017; Garcia et al., 2018); 4) acidification, salinization, and desertification which can be induced or exacerbated not only by climate change but also by irrigation and drainage (Dragović and Vulević, 2020; Smith et al., 2020); 5) water and wind erosions, which are facilitated by plowing, vegetation clearing, and overgrazing, which leaves the soils bare for too long; therefore, they become prone to deconstruction and degradation by the impact of droughts and/or rains which trigger surface runoff and sheet erosion instead of infiltration (Benabderramane and Chenchouni, 2010; Arar and Chenchouni, 2014; Belala et al., 2018); 6) pollution by heavy metals or biocidal substances which harm soil essential organisms (fungi and earthworms) and thus disrupt the cohesion and capillarity of the soil (Singh et al., 2020); and 7) soil compaction, which is one of the most serious and common forms of soil degradation; it induces a sharp drop in the natural porosity of the soil and causes soil asphyxiation. Soil compaction is most often related to agricultural and forestry machinery, but overgrazing and over-frequentation of an environment by humans can contribute locally to vegetation trampling (Osman, 2018). The degradation of a given soil can ideally be assessed by

comparisons of physicochemical and biological parameters with identical undegraded soil (Yong-Zhong et al., 2005; Neffar et al., 2013; Fialho and Zinn, 2014; Bouaroudj et al., 2019; Chenchouni et al., 2019).

The arid and semi-arid regions of North Africa are currently experiencing a severe degradation of natural resources (Le Houérou, 2009; Slimani et al., 2010). The region comprises various plant formations including forests, shrublands, matorrals, and steppes, which are experiencing a regression under climatic and anthropogenic influences (Aidoud and Touffet, 1996; Chenchouni, 2010; Kouba et al., 2021). This dual action induced physiognomic and landscape changes which are at the origin of long-term dynamics and major changes in the region's resources (Le Houérou, 2009; Negm et al., 2020).

With about tenth of the Algerian territory, the steppe rangelands sustain the livelihood of the agro-pastoral population (~12% of the total population), which depends essentially on the proper functioning and integrity of these ecosystems (Hadeid, 2006; Nedjraoui and Bedrani, 2008; Hamel, 2018). The degradation state of the Algerian steppe rangelands is translated *via* the decline in natural resources observed in several regions throughout the country (Nedjraoui and Bédrani, 2008; Moulay et al., 2012). Climate changes combined with overgrazing and an increase in the number of livestock are the main sources of steppe vegetation degradation, causing land desertification and serious decline in steppe areas of *Macrochloa tenacissima* (L.) Kunth (syn. *Stipa tenacissima* L.) named in Arabic Alfa or Halfa (Macheroum and Kadik, 2015; Merdas et al., 2021). Free grazing with a high number of animals adversely affects the natural resources of these rangelands already weakened by climatic hazards, including severe droughts and intense heatwave events (Nedjraoui and Bédrani, 2008; Belala et al., 2018; Kouba et al., 2021). Already, the productivity and regeneration of the Algerian steppes have reached a critical state of degradation (Martínez-Valderrama et al., 2018), where the degradation islands constantly expand across the considerable diffuse surfaces, whereas in the past, these localized patches of degradation were spatially limited (Kadi-Hanifi, 1998; Macheroum and Kadik, 2015). Steppe degradation was

amplified and aggravated by the anarchic clearing and plowing combined with inadequate development of steppe areas and poor grazing management by farmers and pastoralists in the context of aids granted by the state for exploitation of the steppes (Hadeid, 2006). These degradation conditions favor the establishment of plants of low forage value that do not meet the needs of the animal load, but rather this accentuates the pressure of overgrazing on non-degraded areas (Hasnaoui and Bouazza, 2015; Merdas et al., 2021).

In steppe ecosystems, soil physicochemical properties play a key role in soil–vegetation relationships because the distribution of the vegetation is closely linked to the characteristics of the abiotic environment, especially the edaphic and climatic parameters (Chenchouni, 2017; Bezzalla et al., 2019) and also biotic interactions (Bansal and Sheley, 2016; Merdas et al., 2021) including livestock grazing (Liu et al., 2020), which also has various feedback influences on the soil itself (Haynes and Williams, 1992; Dormaar and Willms, 1998; Yong-Zhong et al., 2005; Cheng et al., 2016; Ye et al., 2016). Several studies have extensively investigated environmental-related problems of North African steppes in terms of soil erosion, desertification, droughts, plant community diversity, and vegetation cover dynamics in relation to livestock grazing and various land managements (Aidoud and Touffet, 1996; Benabderramane and Chenchouni, 2010; Belala et al., 2018). However, the situation of the soils of North African steppe ecosystems, and in particular those of Algeria, is poorly understood and very little studied in the context of different temporal scales of land degradation due to grazing pressures inducing plant cover changes, which are constantly increasing in order to meet growing socioeconomic needs. In North Africa, studies that have investigated the fate of soil properties in degraded steppes are very rare (Aidoud et al., 1999; Jeddi and Chaieb, 2010; Amghar et al., 2012; Neffar et al., 2013; Hasnaoui and Bouazza, 2015; Neffar et al., 2022). The scientific questions addressed in this study are as follows: 1) does the degradation of steppe vegetation induce degradation or significant change in soil characteristics? 2) Is this change dependent on the time during which the steppe was subjected to degradation? 3) In response to land degradation, will steppe soil parameters react in the same way at the different horizons? 4) How do soil parameters interact with each other for different degradation conditions of semi-arid steppes (degraded vs. undegraded)? Thus, this study aimed to determine and compare the variations in edaphic properties in different soil horizons and between degraded and undegraded steppes of Halfa (*M. tenacissima*) in semi-arid areas of Algeria. Under degradation conditions of the steppe plant cover, it is expected that a decrease in soil fertility is observed and a depletion of soil organic matter (SOM), which determines the amount of soil organic carbon (SOC), phosphorus and nitrogen and therefore the C:N:P ratio that was taken as a reliable indicator of soil fertility (Boudjabi and Chenchouni, 2021; (Boudjabi and Chenchouni, 2022).

Nevertheless, while the above-ground biomass and litterfall are expected to experience a significant and rapid decrease in degraded rangelands (Snyman, 2005), the effect of vegetation degradation on soil carbon and nitrogen stock dynamics is a slow process where tangible changes are expected to be observed at long-term (Chapin et al., 2009; Chenchouni and Neffar, 2022). Therefore, the current study seeks to first determine whether short-term degradation could induce significant deterioration of soil conditions, and subsequently, it aims to suggest recommendations for restoring the habitat to a state with balanced and well-functional soil.

Materials and methods

Study area and sampling sites

The study area “Region of Tebessa” is located in the highlands of northeast Algeria (Figure 1). Included between 35°29′N and 35°40′N latitudes and 07°35′E and 08°23′E longitudes, the region involves agro-sylvo-pastoral systems where agricultural lands occupy 56%, forests and shrubs 26%, and steppe rangelands 11% of the studied area (Macheroum and Kadik, 2015). The rainfall data for the period 1972–2016 (Tebessa weather station) showed that the rainiest month was September (40.9 mm) and the driest month was July (14.9 mm). The seasonal regime showed a maximum in spring (112.96 mm) and a minimum in summer (43.21 mm). Annual precipitation was highly variable (mean = 372 mm/year), with a coefficient of variation of 27.62%. This interannual variation is a characteristic of arid climates, but it is here slightly below the level given for the arid zones of North Africa (Le Houérou, 2001, 2009). The mean of minimum temperature of the coldest month (January) was 1.7°C, and the maximum temperature of the hottest month was 35°C, recorded in July. The study area has a Mediterranean semi-arid bioclimate with cool winter. The Emberger’s pluviothermal aridity index (Q2) was estimated to be 38.85. According to the Köppen climate classification (Supplementary Appendix S1), the region falls under a cold semi-arid (steppe) climate (Köppen code: BSk). Two seasons marked the climate each year, a cold and humid season (November–April) and the second is hot and dry (May–October). The impact of drought is accentuated by frequent events of the sirocco (southerly hot and dry wind) which occur in late spring and summer. With haplic calcisols (Boudjabi and Chenchouni, 2022), three different steppe regions dominated by Halfa grass were studied in the Tebessa region. Within each of these regions, the soil of two types of steppes, i.e., degraded recently (< 2,3 years) and undegraded (Figure 2) was sampled. The various characteristics of degraded and undegraded steppes studied and sampling sites are listed in Table 1.

Site 1: El-Houdjbet (35°17′50″N, 08°17′36″E, altitude: 1,000–1,200 m a.s.l.) is located 23 km south-east of Tebessa

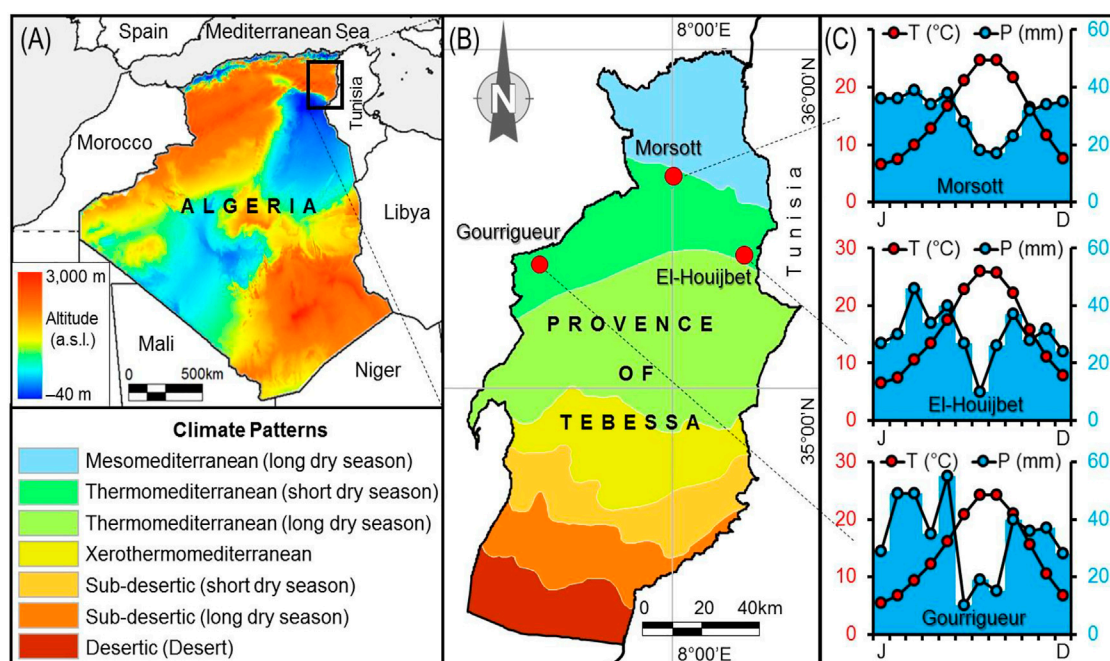


FIGURE 1

(A) Altitude map of Algeria in North Africa, (B) map of climate zones of the Province of Tebessa, northeastern Algeria, displaying the geographic locations of the steppe rangelands studied, (C) ombrothermic diagrams of Gaussen and Bagnouls of the three study sites in Tebessa, where mean temperature (T in °C) and precipitation (P in mm) are monthly averages.

City. The relief has a moderate topography with varied slopes (0–12%), and is characterized by limestone and hard dolomitic geological substrates (74.1% of the total surface), alluvium and sands (24%), and marls (1.9%) (HCDS-BNEDER, 2007). Climatically, the average annual precipitation rate was 342 mm with 54 days of rain, where March was the rainiest month (43 mm) and June was the driest (10 mm). The minimum temperature ($6.5 \pm 0.8^\circ\text{C}$) was recorded in January, while July was the hottest month with a mean maximum temperature of $35 \pm 3.5^\circ\text{C}$ (Supplementary Appendix S2). The climate was cool (lower zone) semi-arid, according to the Emberger classification ($Q_2 = 35.2$) with De Martonne aridity index = 14 and a continentality index = 36.9 (Supplementary Appendix S1).

Site 2: Gourrigueur ($35^\circ 25' 22''\text{N}$, $07^\circ 35' 36''\text{E}$, altitude: 863–1456 m a.s.l.) is located 47 km north-west of Tebessa. Geomorphologically, the site includes gullied slopes (average slope ~10–25%), glacia dominated by limestone and hard dolomite substrates (54.5% of the surface), alluvium, sands, and limestone crust (22.12%), and marl (11.05%) (HCDS-BNEDER, 2007). The average annual rainfall was 377 mm (63 rainy days), the large amount of rainfall was recorded during May (50 mm), and the lowest was recorded in June (10 mm); the lowest temperature was recorded in January ($5.5 \pm 2^\circ\text{C}$), and it reached a maximum of $35 \pm 2^\circ\text{C}$ in July (Supplementary Appendix S2). This region is located at the upper zone of cool semi-arid bioclimate ($Q_2 = 38.85$), with De Martonne

aridity index = 16 and a continentality index = 34.7 (Supplementary Appendix S1). At the landscape scale, a homogeneous structure characterized the steppe surface (4,520 ha); however, it presented locally a discontinuity due to the presence of scattered patches of cultivated and/or degraded areas.

Site 3: Morsott ($35^\circ 40' 06''\text{N}$, $08^\circ 00' 26''\text{E}$, altitude: 600–1,000 m a.s.l.) is located 38 km north of Tebessa. The geomorphological forms corresponded to low to medium slopes (5–20%), glacia (0–4% of the surface), and marl–limestone geological substratum (63.24%) (HCDS-BNEDER, 2007). Climatically, annual precipitation averaged 351 mm recorded on 59 days of rain. The highest amount of rain was recorded in March (37 mm) and the lowest in July and August (17 mm). The mean minimum temperature was recorded in January ($6.5 \pm 2.2^\circ\text{C}$), while the maximum was measured in July ($35 \pm 3.1^\circ\text{C}$). This sampling site falls within the lower zone of the cool semi-arid bioclimate ($Q_2 = 36.17$), with De Martonne aridity index = 15 and a continentality index = 32.6 (Supplementary Appendix S1 and Supplementary Appendix S2).

Soil sampling

In this study, the analysis of soil characteristics in the sampling sites aimed at demonstrating whether the

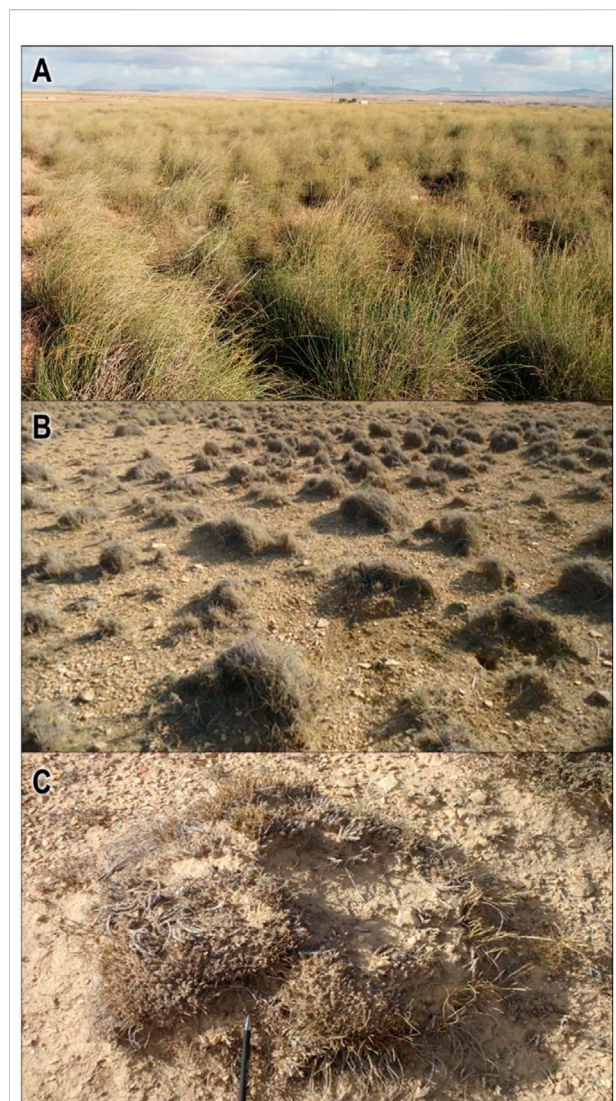


FIGURE 2

Photographs of semi-arid steppes rangelands of *Macrochloa tenacissima* syn. *Stipa tenacissima* in northeastern Algeria. (A) Undegraded steppe with healthy and dense Halfa vegetation, (B) degraded steppe rangeland due to overgrazing by sheep and goats, (C) a close-up view showing the morphological aspect of a tuft of Halfa containing necromass of roots and small-size living leaves lasting after livestock overgrazing.

degradation of the Halfa vegetation cover in the short term is accompanied by serious modifications in soil essential components. According to the study by Kadi-Hanifi (1998), each phytoecological study should be completed by the analysis of edaphic variables and vice versa. Therefore, this study focused on the comparison of soil physicochemical characteristics between degraded and undegraded Halfa steppes in each of the three sampling sites. The soil sampling was carried out during the fall of 2016. Using a pickaxe, three soil profiles in each type of steppe (degraded vs. undegraded,

Figure 2) were dug vertically to a maximum depth of 1 m, and six soil samples with three replicates were recovered from each sampling site. The thickness of the surficial soft layers of each profile was determined, and then a soil sample was taken from each of the horizons A1 and A2 of each type of steppe. The distinction between the A1 and A2 horizons was mainly based on color, layer thickness, and morphological appearance. The soil samples were collected in a paper bag labeled with the sample information. The samples were dried in open air for a week. After desiccation, the soil was sieved using a sieve with a 2-mm mesh to separate the coarse elements from the fine earth, which was used for soil analyses following standard soil analysis techniques (Mathieu and Pielain, 2003; Baize, 2018).

Soil physicochemical analyses

All soil physicochemical analyses were performed using fine earth ($\phi < 2$ mm). For each soil sample, the particle size distribution was determined after the destruction of soil organic matter (SOM) using an energetic oxidant (oxygen water), and then the mineral particles were dispersed using an alkaline dispersant (sodium hexametaphosphate). Coarse-size particles larger than 0.05 mm in diameter were separated by sieving, and medium-size and fine-size particles were measured by sedimentation rate. The type of soil texture was determined following the USDA textural soil classification (Duchaufour, 1997). Soil pH (pH_w) was measured in a soil/solution suspension prepared with distilled water with a ratio of 1/5 (s/w) by the electrometric method using a pH meter (Mathieu and Pielain, 2003). The electrical conductivity (EC) was estimated with a conductivity meter in the soil extract prepared by stirring a mixture of sol/water (ratio s/w = 1/5) for 15 min (Mathieu and Pielain, 2003). Total carbonate calcium equivalent (TCCE) was calculated using the Bernard calcimeter method (Baize, 2018). The Drouineau–Galet’s method (Mathieu and Pielain, 2003) was used to determine the active carbonate calcium equivalent (ACCE), which was neutralized with oxalates. Organic matter was quantified from SOC content (i.e., $\text{SOM} = \text{SOC} \times 1.724$), which was evaluated using the method of Anne (Duchaufour, 1997). Total nitrogen was determined following the Kjeldahl method (Mathieu and Pielain, 2003; Baize, 2018). The C:N stoichiometry of soil was appraised, using the ratio of SOC to nitrogen content as a good indicator of nitrogen and humus richness (Duchaufour, 1997; Mehalaine and Chenchouni, 2022).

Statistical analyses

Soil physicochemical parameters were expressed as means and standard deviations, whereas descriptive statistics of the data were plotted for soil horizons A1 and A2 for both degraded and undegraded steppe rangelands. The coefficient of variation (CV)

TABLE 1 Characteristics of degraded and undegraded steppes in sampling sites of Halfa grass (*Macrochloa tenacissima* syn. *Stipa tenacissima*) rangelands in northeastern Algeria.

Characteristics	Study sites		
	El-Houidjbet	Gourrigueur	Morsott
Undegraded steppe rangelands			
Dominant plant species	<i>M. tenacissima</i> , <i>Ampelodesma mauritanicum</i> , and <i>Artemisia herba-alba</i>	<i>M. tenacissima</i> (pure steppe, Figure 2A)	<i>M. tenacissima</i> , <i>Rosmarinus officinalis</i> , and <i>Genista microcephala</i>
Total vegetation cover (%)	45–80	45–75	40–70
Vegetation cover of Halfa (%)	30–60	30–55	20–35
Plant litter cover (%)	5–15	5–10	1–5
Sand deposit sheets (%)	25–10	—	—
Bare ground cover (%)	—	20–05	20–10
Coarse-grained materials (%)	0–5	5–30	15–35
Bedrock outcrop (%)	0–5	—	0–5
Maximum height of Halfa (cm)	40–100	35–70	30–55
Animal load (ha/sheep unit)	2.0–3.0	2.73–1.69	2.32–1.91
Degraded steppe rangelands			
Dominant plant species	<i>Artemisia campestris</i> , <i>Thymelaea hirsuta</i> , <i>Carthamus pinnatus</i> , <i>M. tenacissima</i> (present as necromass, Figure 2C)	<i>M. tenacissima</i> (degraded, Figure 2B) <i>Atractylis humilis</i> <i>Thymus algeriensis</i>	<i>M. tenacissima</i> (degraded, Figure 2B) <i>Pituranthos scoparius</i>
Total vegetation cover (%)	20–35	10–35	10–30
Vegetation cover of Halfa (%)	5–10	5–20	5–15
Plant litter cover (%)	5–25	10–15	5–10
Sand deposit sheets (%)	40–50	—	—
Bare ground cover (%)	—	20–55	25–45
Coarse-grained materials (%)	5–10	40–50	45–50
Bedrock outcrop (%)	0–10	1–5	5–15
Maximum height of Halfa (cm)	10–25	10–30	10–25
Animal load (ha/sheep unit)	3.43–4.17	3.41–3.87	3.94–6.57
Grazing pressure (heads)	36,612	59,356	36,098
Total agricultural land area (ha)	15,400	39,684	21,923

was computed to measure the dispersion of the frequency distribution for soil grain fractions (clay, silt, and sand). The variation of each soil parameter between soil horizons and rangeland steppe conditions (degraded and undegraded) was tested using generalized linear mixed models (GLMMs). In each model, steppe conditions, soil horizons, and their interaction were the fixed effects, whereas the three sampling sites ([Figure 1](#)) were considered random effects. Linear interrelationships between all soil physicochemical parameters were examined separately for degraded and undegraded steppes using Pearson's correlation tests. The results of correlations (Pearson coefficients and p -values) were mapped in the form of a correlation matrix. The Mantel test was applied between the two correlation matrices in order

to demonstrate how the pattern of soil parameter interactions was similar between degraded and undegraded steppes. The distribution of the Pearson coefficient between two matrices and p -value were estimated from 10,000 permutations. Statistical significance of all tests was set at $p < 0.05$. In order to visualize the correlative relations between soil fertility indicators (i.e., organic carbon, total nitrogen, and C:N ratio) and the rest of soil physicochemical parameters (i.e., clay, silt, sand, pH, EC, ACCE, and TCCE) at each soil horizon and for degraded and undegraded steppes, a redundancy analysis (RDA) was implemented. All statistical analyses and graphic plotting of the current study were carried out using the packages {nlme}, {ggplot2}, {vegan}, and {corrplot} of the free statistical software R ([Core Team, 2020](#)).

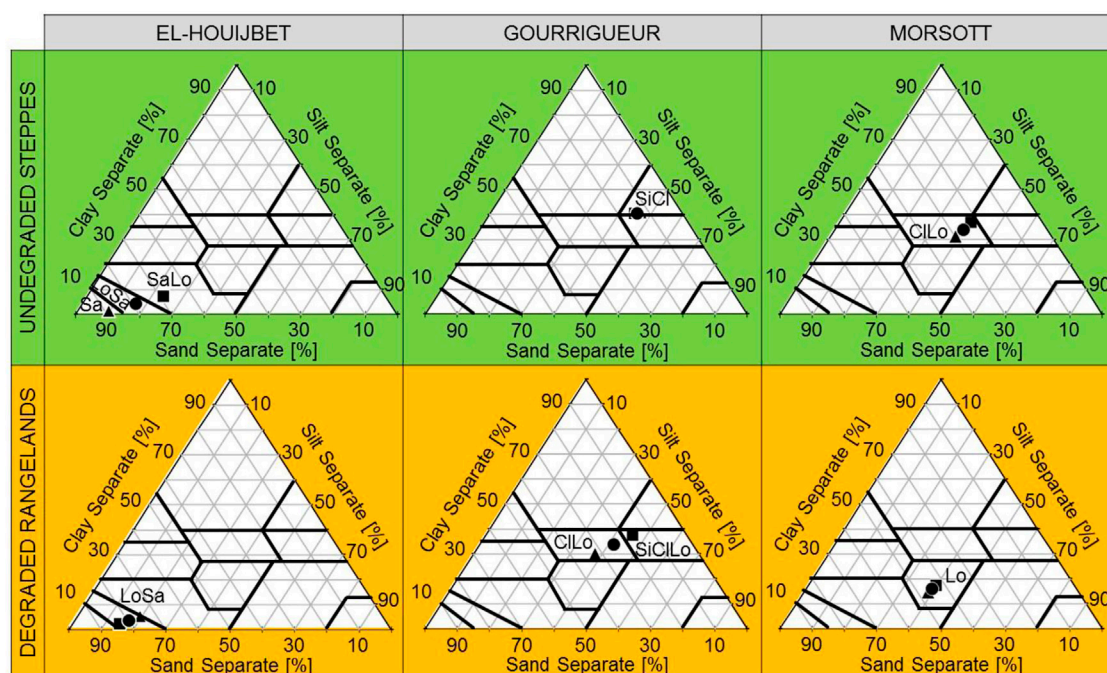


FIGURE 3

Soil textural triangles (following the USDA classification) of study sites for degraded and undegraded steppe rangelands in northeastern Algeria. Symbols plotted within each triangle represent soil samples of horizon A1 (▲), horizon A2 (■), and the average (●). (CiLo: clay loam, Lo: loam, LoSa: loamy sand, Sa: sand, SaLo: sandy loam, SiCl: silty clay, and SiCiLo: silty clay loam).

Results

Classification of soil texture

The texture of soil samples in degraded steppes ranged from medium-size types (silty clay loam, clay loam, and loam) to coarse-grain type (i.e., loamy sand) compared with the soil texture observed in undegraded steppes, where the soils in the north of the study area at Morsott and north-west at Gourrigueur had medium-size (i.e., clay loam) and moderately fine textures (i.e., silty clay), respectively. The soils in the southeast of the study area at El-Houidjbet were coarse and included sand, loamy sand, and sandy loam (Figure 3). For the same sampling site and the same steppe type (degraded vs. undegraded), there was no vertical variation in the distribution of grain size between the horizons (degraded or undegraded).

Distribution of particle size fractions

The content of the clay fraction was higher in the undegraded steppes for both A1 and A2 horizons with $24.5 \pm 20.5\%$ (mean \pm standard deviation) and $28.1 \pm 18.2\%$, respectively, than in the degraded steppes where clay averaged $16.7 \pm 12.5\%$ and $19.1 \pm$

17.6% , respectively (Figure 4). The level of the silt fraction was relatively unvarying between the soil horizons of the two types of steppes; it ranged from $31.8 \pm 10.9\%$ to $36.5 \pm 11.2\%$. Sand levels in degraded steppes ($51.5 \pm 22\%$) were significantly higher than those of undegraded ranges ($43.9 \pm 40\%$), especially at the A1 horizon compared with A2 ($47.6 \pm 33.5\%$). The large values of the coefficients of variation (CVs) indicated a high heterogeneity in the spatial distribution of the particle size fractions of the texture of the studied soils. According to CV, the distribution of particle fractions was more unbalanced in the A1 horizon of undegraded steppes than in the A2 horizon of degraded steppes.

Soil physicochemical characteristics

Figure 5 illustrates the variation of the soil physicochemical parameters of the A1 and A2 horizons for degraded and undegraded steppes. The pH values measured at the two types of steppes (degraded vs. undegraded) showed some stability and indicated that the soils where Halfa exists were alkaline, with pH ranging from 8.09 ± 0.21 to 8.19 ± 0.4 (mean \pm standard deviation). Soil EC indicates that the study area had—generally—low saline soil in all the steppes studied, while the highest values were recorded in the undegraded sites on the

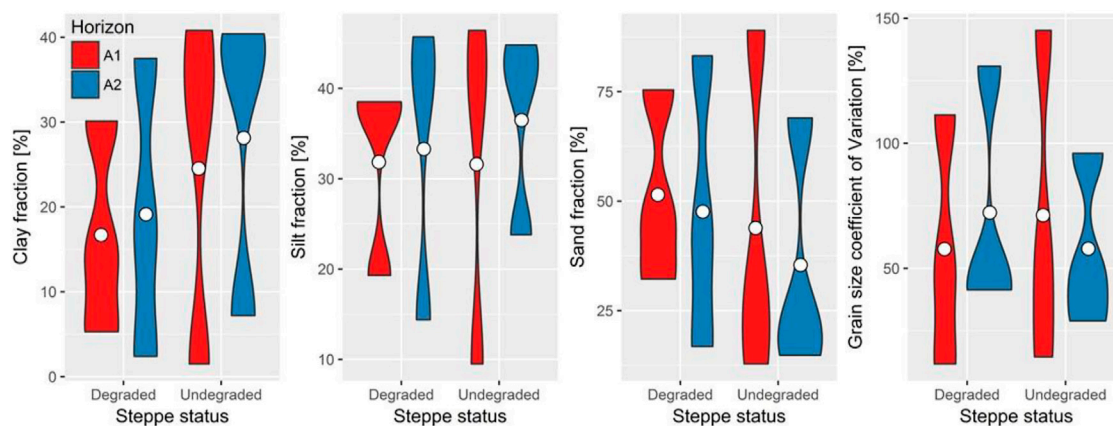


FIGURE 4

Violin plots displaying the range of soil grain fractions (clay, silt, and sand) and the coefficient of variation measured at soil horizons A1 and A2 for degraded and undegraded steppe rangelands of the Halfa grass (*Macrochloa tenacissima*) in northeastern Algeria. Solid white circles represent the mean of observed data.

A2 horizon ($EC = 0.99 \pm 1.24$ dS/m). Regardless of steppe degradation status, the levels of TCCE, ranging from $36.8 \pm 30.2\%$ to $41 \pm 33\%$, revealed that the analyzed soils were moderately rich in $CaCO_3$. The content of active $CaCO_3$ was almost stable in all soil samples. It fluctuated between $17.5 \pm 2.1\%$ and $18.5 \pm 0.3\%$. The analyzed soils were considered rich in ACCE. Because of the vegetation heterogeneity between the degraded and undegraded steppes, the content of SOC was moderately low throughout the study area, where the lowest ($0.82 \pm 0.13\%$) and highest ($1.64 \pm 1.14\%$) values were observed in the A2 and A1 horizons, respectively, of the undegraded steppes. Overall, the nitrogen content was very low in the steppe rangelands sampled as it varied between $0.1 \pm 0.01\%$ and $0.15 \pm 0.06\%$. However, the highest values were recorded in the A1 horizon for both degraded ($0.15 \pm 0.06\%$) and undegraded ($0.13 \pm 0.07\%$) steppes. The C:N ratio revealed that the SOM decomposition was slower in the A2 horizon of undegraded steppes ($12 \pm 3\%$) and the A1 horizon of degraded steppes ($10 \pm 4\%$) when compared to the moderately fast SOM decomposition in the rest of soil horizons of sampled steppes.

Variations of soil parameters

The GLMMs testing the variation of soil parameters between degraded and undegraded steppes at the soil horizons A1 and A2 revealed significant differences in the clay fraction ($p = 0.011$) and sand fraction ($p = 0.042$) between degraded and undegraded steppes (Table 2). However, there was no significant variation ($p = 0.093$ – 0.972) in the rest of the soil parameters between the different soil horizons, steppe degradation status, and for horizons in interaction with steppe degradation conditions.

Relationships between soil parameters for degraded and undegraded steppes

In general, the soil parameters were poorly correlated with each other throughout the study area (Table 3). The significant positive correlations found in the two steppe cases included the following: clay–silt, silt–TCCE, and SOM–SOC, whereas significant negative correlations were observed between sand (clay, silt, and TCCE) and pH–EC. Soil parameters that showed strong positive correlations in degraded steppes were clay–EC ($r = 0.93$, $p = 0.006$), sand–pH ($r = 0.82$, $p = 0.046$), and N–TCCE ($r = 0.83$, $p = 0.039$), while the strong negative correlations included clay–pH ($r = -0.93$, $p = 0.008$) and sand–EC ($r = -0.84$, $p = 0.037$). In steppe rangelands with undegraded vegetation, strong significant correlations were observed between clay–TCCE ($r = 0.94$, $p = 0.005$), SOM–N ($r = 0.95$, $p = 0.003$), and N–SOC ($r = 0.96$, $p = 0.003$). However, the C:N ratio was negatively correlated with SOC and SOM ($r = -0.87$, $p = 0.023$). Mantel's test showed that soil correlation matrices of degraded and undegraded steppes were significantly correlated (two-tailed test: $r = 0.704$, $p < 0.001$), which specified that the patterns of interrelations observed between soil variables for each steppe were very close.

Influence of soil properties in degraded and undegraded steppes on soil fertility

The redundancy analysis (RDA) investigating the relationships between soil fertility indicators (i.e., organic carbon, total nitrogen, and C:N ratio) and the rest of soil physicochemical parameters in degraded and undegraded

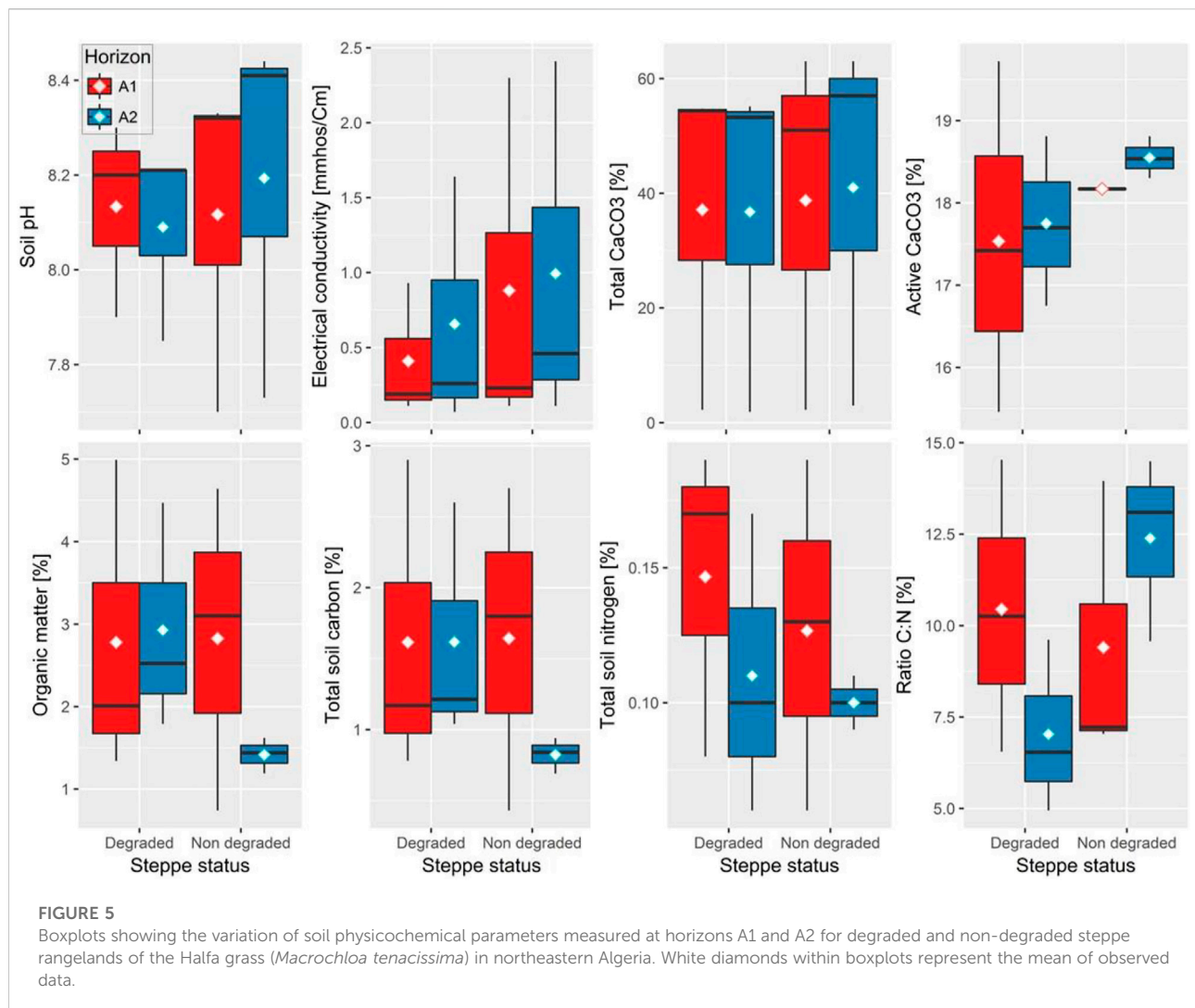


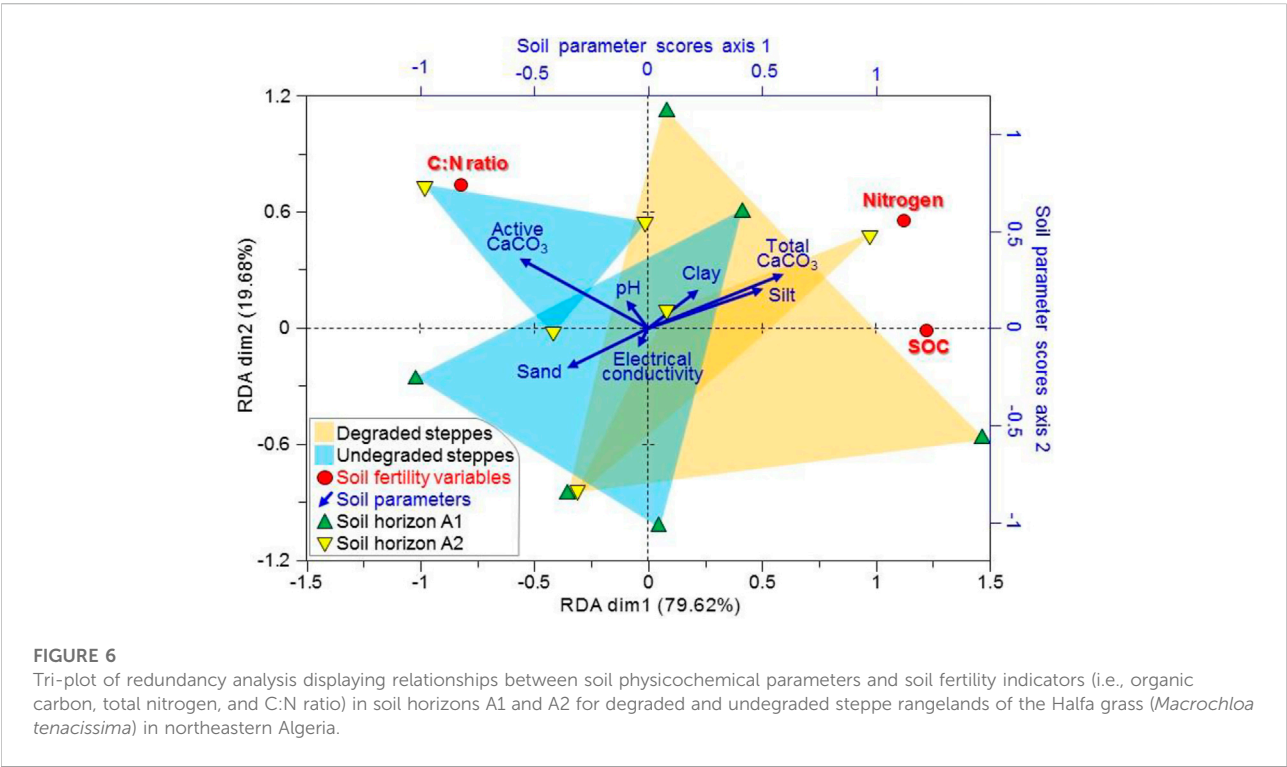
TABLE 2 Generalized linear mixed-effect models (GLMMs) testing the variation of soil physicochemical parameters between soil horizons (A1 and A2) and habitat conditions “degraded and undegraded” of steppe rangelands of Halfa grass (*Macrochloa tenacissima*) in northeastern Algeria.

Variables	<i>Df</i>	χ^2	<i>p</i>	χ^2	<i>p</i>	χ^2	<i>p</i>	χ^2	<i>P</i>	χ^2	<i>p</i>	χ^2	<i>p</i>	χ^2	<i>P</i>
		Clay		Silt		Sand		CV grain		pH		EC			
Steppe conditions	1	6.55	0.011	0.33	0.567	4.13	0.042	0.001	0.972		0.51	0.477		3.45	0.063
Soil horizons	1	0.84	0.359	1.48	0.224	1.60	0.205	0.003	0.960		0.07	0.784		0.69	0.407
Condition \times horizon	1	0.03	0.859	0.44	0.507	0.22	0.637	1.353	0.245		0.97	0.324		0.09	0.759
		TCCE		ACCE		SOM		SOC		N		C:N ratio			
Steppe conditions	1	3.06	0.080	1.68	0.195	1.47	0.225	1.29	0.255		0.73	0.392		1.28	0.258
Soil horizons	1	0.31	0.576	0.29	0.589	1.09	0.296	1.47	0.225		3.27	0.070		0.01	0.910
Condition \times horizon	1	0.61	0.435	0.02	0.886	1.67	0.197	1.48	0.224		0.08	0.775		2.82	0.093

(CV: coefficient of variation of soil grain fractions (clay, silt, and sand), EC: electrical conductivity, TCCE: total CaCO_3 , ACCE: active CaCO_3 , SOM: soil organic matter, SOC: soil organic carbon; and N: total nitrogen).

TABLE 3 Matrices of Pearson's correlations between soil physicochemical parameters measured in degraded (above diagonal) and non-degraded (below diagonal) steppe rangelands in northeastern Algeria (see the subsection "2.3. Soil physicochemical analyses" for abbreviations of soil properties). Pearson's correlation coefficients shown in boldface text are significant at $p < 0.05$.

Soil physicochemical parameters of degraded steppe rangelands											
Soil physicochemical parameters of non-degraded steppe rangelands	Clay	0.87	−0.97	−0.93	0.93	0.78	0.56	−0.14	−0.07	0.37	0.57
	0.98	Silt	−0.96	−0.64	0.67	0.96	0.09	0.34	0.41	0.69	0.28
	−0.99	−0.99	Sand	0.82	−0.84	−0.90	−0.35	−0.09	−0.16	−0.54	−0.44
	−0.63	−0.60	0.62	pH	−0.95	−0.58	−0.75	0.34	0.31	−0.15	−0.60
	0.71	0.69	−0.70	−0.98	EC	0.53	0.67	−0.40	−0.35	0.03	0.53
	0.94	0.90	−0.93	−0.39	0.46	TCCE	0.03	0.49	0.55	0.83	0.25
	0.15	0.21	−0.18	−0.30	0.40	0.01	ACCE	−0.77	−0.76	−0.27	0.74
	0.50	0.54	−0.53	−0.20	0.13	0.61	−0.39	SOM	0.99	0.70	−0.57
	0.50	0.54	−0.53	−0.20	0.13	0.61	−0.39	1.00	SOC	0.76	−0.50
	0.48	0.55	−0.51	0.01	−0.04	0.62	−0.35	0.95	0.96	N	0.18
	−0.72	−0.72	0.72	0.64	−0.58	−0.71	0.17	−0.87	−0.87	−0.73	C:N



steppe rangelands totaled 75.11% of explained variance in the first two axes of the RDA triplot that accounted for 79.62 and 19.68% of the constrained inertia, respectively (Figure 6). Both total and active CaCO_3 were the main edaphic variables explaining the change in soil fertility of degraded and undegraded steppes (Table 4). Total CaCO_3 was positively correlated ($r = 0.660$, $p = 0.019$) on the first axis of RDA and influenced both organic carbon and total nitrogen in degraded steppes, whereas the active CaCO_3 was negatively correlated

($r = -0.627$, $p = 0.029$) of the same axis and significantly affected the C:N ratio in undegraded steppes, especially is soil samples collected from the A2 horizon. Total nitrogen and SOC were associated with soil samples collected from the A1 horizon, mainly in degraded steppes (Figure 6). The contribution of the second axis of RDA (19.68%) was marginal as soil variables were not significantly correlated (Table 4), and there was no clear scheme in the distribution of these variables between soil horizons nor steppe degradation status (Figure 6).

TABLE 4 Intraset correlation coefficients (r) and probability values (p) of soil physicochemical variables with the first three axes of RDA ordination. Percentages between brackets are constrained inertia of each axis. Significant correlations ($p < 0.05$) are indicated in boldface font.

Soil variables	RDA axis 1 (79.62%)		RDA axis 2 (19.68%)		RDA axis 3 (0.70%)	
	r	p	R	p	R	p
Clay fraction	0.248	0.437	0.262	0.410	-0.618	0.032
Silt fraction	0.561	0.058	0.269	0.398	-0.469	0.124
Sand fraction	-0.399	0.198	-0.272	0.393	0.563	0.056
pH	-0.110	0.734	0.189	0.557	0.726	0.008
Electrical conductivity	-0.048	0.882	-0.128	0.693	-0.638	0.026
Total CaCO ₃	0.660	0.019	0.371	0.236	-0.328	0.299
Active CaCO ₃	-0.627	0.029	0.471	0.122	-0.589	0.044
Organic carbon	0.887	< 0.001	-0.011	0.972	0.094	0.771
Total nitrogen	0.812	0.001	0.400	0.198	-0.066	0.840
C:N ratio	-0.590	0.043	0.533	0.075	0.051	0.874

Discussion

This study investigated the influence of the short-term degradation of the steppe vegetation on some edaphic parameters in the Halfa (*M. tenacissima*) rangelands where grazing is practiced freely throughout the year. The results suggest that this land degradation can be corrected if appropriate management measures are implemented because the comparisons of edaphic parameters between degraded and undegraded rangelands of the three sampled steppes revealed a state of non-deterioration in soil conditions. Therefore, in the short term, the soil has been able to maintain its good state of fertility and functioning, which indicates that the restoration of the vegetation cover will allow the recovery of the initial state of the Halfa steppe. In the steppes of the high plains of Algeria, the Halfa, a Mediterranean perennial species, represents an iconic and emblematic species that stretches over vast areas. It plays the role of “keystone” within the steppe ecosystem in semi-arid and arid zones (Kadi-Hanifi, 1998; Jeddi and Chaieb, 2010; Merdas et al., 2021). Acting as a biological barrier against the advance of the desert through its highly developed root system, the species provides better soil fixation and protection against erosion (Moulay et al., 2012). In recent decades, the Halfa has undergone an advanced degradation triggered mainly by human activities, in particular overgrazing, which is the first driver for the disappearance of very large areas of Halfa and the extension of rainfed crops that further aggravated the effects of desertification (Aidoud and Touffet, 1996; Belala et al., 2018; Martínez-Valderrama et al., 2018). However, the decline in the vegetation cover of Halfa steppes in the short term, especially by grazing, does not seem to induce significant and immediate edaphic changes. According to the study by Aronson et al. (1995), the degradation of vital soil attributes, such as SOM or soil nutrients and fertility, can only be effectively detected after

a period of about 10 years. But according to the study by Albaladejo et al. (1998), soil degradation was found to be somewhat faster; in fact, they estimated that after about 5 years, the reduction in plant cover can have a significant impact on soil characteristics through the decrease in SOM and soil fertility and even the deterioration of soil physical properties.

The results relating to the percentage of clay from sampling sites confirm that in degraded steppes, the level of clay was low compared to the dominance of coarse elements, i.e., sand. This particular state is due to the soil structure degradation at the level of clay–humic complexes and especially resulted from the sand encroachment and accumulation of coarse grains transported by the wind following the destitution of the soil and the reduction of vegetation cover, which represent the most efficient shield against wind and water erosions. Therefore, we can deduce that the presence of a good cover of Halfa favors the conservation of steppe soils by maintaining a balanced soil with high resilience to various forms of land degradation. The climatic conditions of the last decades, characterized by long periods of intense drought (Belala et al., 2018; Kouba et al., 2021), have been at the origin of the degradation of the vegetation cover of steppe formations dominated by *M. tenacissima*, *Atriplex halimus*, and *Artemisia herba-alba*, where large areas have been covered with thorny plants and/or species of low forage quality. With regard to soil productivity, the degradation of pastoral areas in Algeria from the 1980s to date shows a decrease in the indices of the productive value of pastures. In fact, plant cover represents 40% of the total pastoral area, while 3–4% of this area has been invaded by grazing areas; hence, the plant area declined to 20%, while the density of grazing livestock reached 12 heads per hectare which exceeds the carrying capacity (Macheroum and Kadik, 2015; Macheroum and Kadik, 2018). Moreover, among the most common and frequent forms of degradation that threaten the steppe



FIGURE 7

Photographs showing different forms of degradation and threat of Halfa (*Macrochloa tenacissima* syn. *Stipa tenacissima*) steppe rangelands in NE Algeria. **(A)** Plowing within extensive undegraded Halfa steppe, **(B)** uncontrolled discharge of solid wastes, **(C)** cultivation of rainfed cereal crops (*Hordeum vulgare*, *Triticum durum*, and *Triticum aestivum*), **(D)** overgrazing due to free grazing with an animal load exceeding the livestock carrying capacity, **(E)** rangeland fires, often associated with forest fire, **(F)** clearing of natural vegetation and water erosion, **(G)** sand encroachment and sand dune movement, and **(H)** Aeolian and water erosion.

rangelands of Algeria are desertification, invasion of sand dunes, plowing of steppe lands and creation of new agricultural perimeters, clearing of natural vegetation, depletion of surface and underground water, land salinization, soil fertility loss, fires, water, and wind erosion, and uncontrolled discharge of solid waste and wastewater (Figure 7).

Overall, our findings suggest that land degradation driven by short-term heavy grazing of vegetation did not cause a significant variation of soil physicochemical parameters between degraded and undegraded steppes and between the soil horizons A1 and

A2. The particle size classification of soil textures shows a fairly contrasting composition. In degraded steppes, the level of clay was low compared to undegraded steppes. The comparison of soil textures shows an overall decrease in the fine grain fraction, and at the same time, the texture becomes coarser and sandy due to degradation of the plant cover by overgrazing and trampling, which promotes soil erosion, destruction of soil aggregates, transport particles, and sand encroachment (Aidoud et al., 1999; Slimani et al., 2010; Schmalz et al., 2013). The negative correlations observed between sands and fine grain particles (clay

and silt) confirmed this, as is the case in degraded habitats (Douaoui et al., 2001; Aliat et al., 2016). Therefore, the presence of dense Halfa tufts in undegraded steppes (Figure 2A) promotes soil fixation against erosion (Hasnaoui and Bouazza, 2015). This kind of plant constitutes a real “nebka-trap” in windy open environments (Slimani, 1998; Bradai et al., 2015; Chenchouni et al., 2019; Chenchouni et al., 2022). The abundance of the fine grain fraction in the Halfa steppes of North Africa results from its origin, which belongs to the marl-limestone geological substratum (Kadi-Hanifi, 1998). It is noteworthy mentioning that the superficial horizons A1 and A2 of the same soil profile have high physicochemical homogeneity despite their morphological heterogeneity.

All soil samples studied had an alkaline pH according to the study by Baize (2018). In semi-arid lands, this parameter is considered among the most important indicators of soil changes (Li and Shao, 2006). In rangelands, it is strongly influenced by parental material (Rezaei and Gilkes, 2005) than the low biological activities of hot arid soils. Indeed, the studied soils are classified as strongly calcareous (Baize, 2018) because of the limestone origin of the region (Djebaili, 1984; Halitim, 1988), where the active fraction of CaCO_3 varied between 17.5 ± 2.1 and $18.5 \pm 0.3\%$. This high level of CaCO_3 explains the soil alkalinity (Neffar et al., 2013); indeed the sampled soils were rich in active CaCO_3 ($> 10\%$). Soil pH generally encompasses the synthesis of several chemical interactions between edaphic variables (Douaoui et al., 2001). The alkalinity of the pH is also attributed to animal trampling and the alkalinizing effect of sheep urine, which has a high pH of about 8.7 (Haynes and Williams, 1992). During the hydrolysis of urea of urine into NH_4^+ in the soil, the release of OH^- causes an increase in pH and also enrichment of inorganic nitrogen in the soil (Ma et al., 2007). This explains the level of nitrogen in degraded steppes which was quite equal to N levels in undegraded steppes (mainly generated from SOM) and thus specifies the origin of nitrogen in each type of steppe. Indeed, there is a strong positive correlation between N and SOM ($r = 0.95$, $p = 0.003$) and C ($r = 0.96$, $p = 0.003$) in undegraded steppes (i.e., nitrogen has mainly an organic origin) and between N and total CaCO_3 ($r = 0.83$, $p = 0.039$) in degraded steppes (i.e., nitrogen has mainly an inorganic origin). More generally, however, the measured concentrations of mineral nitrogen in all soil samples studied were low (Cortina and Maestre, 2005). These low levels of mineral nitrogen are attributed to competition for nitrogen consumption between microorganisms active in the rhizosphere of pastures and the roots of steppe plant species (Huntjens, 1971). Indeed, the contents of all the nutrients in the soil solution are generally low in steppes and, therefore, the ionic strength is low as reported in the study by Edmeades et al. (1985) in prairies. These observations between CaCO_3 and SOC, N, and C:N ratio were confirmed by the RDA where the rate of mineralization (i.e., C:N ratio) was associated with alkalization (i.e., active CaCO_3), whereas the low contents of SOC and nitrogen are considered

a typical characteristic of the calcareous soils (i.e., rich in total CaCO_3) in semiarid steppes of N Africa where the haplic calcisols dominate. According to the study by Duchaufour (1997), the soil is considered rich in SOM when its level is higher than 2%, and according to the assessments of Djebaili (1984) this rate does not exceed 3% in steppe soils. Accordingly, the studied soils are moderately rich in SOM, except for the A2 horizon of undegraded Halfa steppes which was the poorest in SOM ($1.42 \pm 0.22\%$). However, according to the study by Kadi-Hanifi (1998), the studied soils can be classified as low in SOM. The statistical analyses showed that there is no significant difference in SOM and SOC content when changing from an undegraded steppe to a degraded steppe. The relatively high levels of SOM and SOC in the undegraded steppes are due to Halfa tufts, which form small mounds and contribute actively in improving soil properties by providing SOM and intercepting and then fixing soil fine grain elements (Aidoud et al., 1999). This explains the richness with SOM of the surface horizon of the soil. While the traces of SOM in the degraded steppes are justified by the importance of the necromass (Figure 2C) released from Halfa tufts after trampling and/or grazing by livestock in the form of plant litter and animal excreta.

Often an alkaline soil pH indicates the presence of salinity and correlates with electrical conductivity (Mehalaine and Chenchouni, 2020). But in our case, the EC correlates negatively with pH and sand and positively with clay, while the increase in pH value and level of sand is accompanied by a proportional decrease in salinity and clay fraction. This may be related to the nature of the salts (Chenchouni, 2017) and the moisture level of the land (Mihi et al., 2019). The comparison of the electrical conductivity of sampled soils in this study with the classification proposed in the study by Mathieu and Pieltain (2003) shows that the surface horizon (A1) of the soil in degraded steppes is non-saline, whereas the rest of the soil samples were slightly salty. The low EC of the A1 horizon is due to the coarse grain texture which induces an influence that makes grains unable to retain cations because of its permeability and favors it to accumulate in the A2 horizon, which was more saline than in A1. Although the EC was low, the presence of slight salinity in the undegraded steppes can be explained by the high level of clay which makes the soil less or impermeable and favors the stagnation of water laden with cations (Chenchouni, 2009, 2017), which slightly increases the salinity once the salts accumulate on the surface after water evaporation or by the capillary rise of saline solution to the surface (Osman, 2018). This indicates that EC does not always imply structural degradation of the edaphic environment (Douaoui et al., 2001).

This study revealed strong positive correlations between the fine fraction (clay and silt) and SOM (Slimani, 1998), total limestone (Mbagwu and Bazzoffi, 1998), nitrogen, and low salinity (electrical conductivity), which seem to be indicators of the improvement of the structural stability of the soil (Douaoui

et al., 2001). The negative correlations observed between these same variables with the coarse fractions (Slimani, 1998) and the alkaline pH can be considered indicators of processes favoring the structural degradation of the soil (Douaoui et al., 2001). The strong negative correlation between the level of SOM and the C:N ratio indicates the rapidity of SOM mineralization, which is a characteristic of arid and semiarid North African steppes (Djebaili, 1984; Boudjabi and Chenchouni, 2022).

The results of this study showed that the short-term degradation of the steppe vegetation cover by grazing did not lead to a large significant difference in the soil chemical parameters between the degraded and undegraded Halfa steppes because short-term grazing has impact on the biotic order, which causes the destruction of perennial species (Aidoud and Touffet, 1996). Therefore, significant changes in the soil are considered the final stage in the degradation of the ecosystem and a threshold of irreversibility in the long-term decline of natural habitats (Slimani, 1998). In this sense, several studies have shown that long-term grazing negatively affects the vegetation, soil physicochemical properties, and ecosystem services of grasslands and steppes (Zeng et al., 2015; Dlamini et al., 2016; Pulido et al., 2017; Zhang et al., 2017; Gao et al., 2018). But, on the other hand, the implementation of appropriate enclosure land management systems, such as grazing exclusion, drives significant improvements in both soil and vegetation properties in degraded rangelands (Jeddi and Chaieb, 2010; Linstädter and Baumann, 2013; Mekuria and Aynekulu, 2013; Kouba et al., 2021). In addition, the rehabilitation of arid and semiarid steppe rangelands using plantations “plant nurses” has proven to efficiently trigger increases in soil fertility, plant diversity, and vegetation cover (Neffar et al., 2013, 2015, 2018). Also, Cheng et al. (2016) showed that the exclusion of pastures significantly increased biodiversity, litter, and soil fertility (total nitrogen and SOC). But, they also found that long-term grazing exclusion had a negative effect on the diversity and abundance of soil bacteria. The comparison of soil physicochemical parameters and the floristic richness between grazed and short-term grazing exclusion in arid degraded steppes showed significant variations in coarse elements, sand, and biodiversity (Amghar et al., 2012; Kouba et al., 2021). But, there was no variation in soil chemical characteristics. The results of the study by Ye et al. (2016) showed that the effects of grazing during 18 months were not important on the functioning (i.e., chemical and biological parameters) of the soil. Shrestha and Stahl (2008) also observed no change in SOC. Moreover, by studying the effect of grazing on the soil, Dormaar and Willms (1998) observed similar results to our study, in which SOC contents did not vary significantly between grazed meadows and non-grazed lands, with very little change in the C:N ratio associated with light grazing. But, long-term heavy grazing pressures induced a significant decrease in SOC levels, while increasing pH, CaCl_2 , and total nitrogen. High grazing pressure reduces soil fertility by

significantly inhibiting soil respiration rates (Chen et al., 2017). Therefore, long-term grazing causes slow and continuous changes in both vegetation and soil, inducing persistent land degradation of the ecosystem (Porensky et al., 2016). In the steppes of West Algeria, Aidoud et al. (2011) observed a decrease in the level of clay of 57% and in SOM of 61% in steppes grazed for 30 years, while the decrease was not significant for the two soil variables in steppes with grazing exclusion. The long-term degradation of the Halfa steppe was accompanied by severe deterioration of edaphic properties.

Conclusion and recommendations

The degradation of vegetation by livestock grazing in the short term (up to 2 years) did not cause significant variations in soil physicochemical properties in the different soil horizons of the semi-arid steppes of Halfa. This demonstrated that the degradation of vegetation by grazing has not affected the edaphic environment, and thus this short-term degradation can be corrected by urgent land restoration actions. The soils analyzed in the Halfa steppes of NE Algeria are characterized by moderately fine textures in the undegraded steppes and coarse textures in the degraded steppes. The high accumulations of CaCO_3 in the soils in these areas are linked to the type of substrate. The low contents of SOM, carbon, and nitrogen resulted from the rate of mineralization, which is faster in alkaline and slightly salty habitats, especially under hot semi-arid conditions. North African steppe rangelands are prone to land degradation because of their high sensitivity to desertification, severe drought events, erosion, and livestock overgrazing. Given the current ecological situation of steppe ecosystems in semi-arid zones, it is necessary to promote a homogeneous steppe management program with the participation of local populations in the long and medium term. In order to solve the problems of land and steppe vegetation degradation and accordingly avoid soil degradation in the future, the actions of land management to be implemented in the near future in degraded and/or vulnerable steppes are, in particular, 1) rehabilitation by planting degraded areas and enclosure of rangelands that are too affected, sensitive, and/or very degraded in order to stimulate natural regeneration, 2) adoption of a rotational grazing system that considers short periods of free grazing alternated with grazing exclusion in order to sustain the productivity of the rangeland, and 3) consideration of livestock carrying capacity of the grazed rangeland in the grazing management in order to prevent overgrazing and soil trampling (Chenchouni and Neffar, 2022).

Data availability statement

The datasets used and/or analyzed in this study are available from the corresponding author upon reasonable request.

Author contributions

AM: conceptualization, methodology, investigation, and writing—original draft. HC: conceptualization, formal analysis, visualization, validation, writing—original draft, and writing—review and editing.

Conflict of interest

The authors declare that the research was conducted in the absence of any commercial or financial relationships that could be construed as a potential conflict of interest.

References

- Aidoud, A., Slimani, H., Aidoud-Lounis, F., and Touffet, J. (1999). Changements édaphiques le long d'un gradient d'intensité de pâturage dans une steppe d'Algérie. *Ecol. Mediterr.* 25 (2), 163–171. doi:10.3406/ecmed.1999.1881
- Aidoud, A., Slimani, H., and Rozé, F. (2011). La surveillance à long terme des écosystèmes arides méditerranéens : Quels enseignements pour la restauration ? Cas d'une steppe d'Alfa (*Stipa tenacissima* L.) en Algérie. *Ecol. Mediterr.* 37 (2), 17–32. doi:10.3406/ecmed.2011.1335
- Aidoud, A., and Touffet, J. (1996). La régression de l'Alfa (*Stipa tenacissima* L.), graminée pérenne, un indicateur de désertification des steppes algériennes. *Sécheresse* 7 (3), 187–193.
- Albaladejo, J., Martinez-Mena, M., Roldan, A., and Castillo, V. (1998). Soil degradation and desertification induced by vegetation removal in a semiarid environment. *Soil Use Manag.* 14, 1–5. doi:10.1111/j.1475-2743.1998.tb00602.x
- Aliat, T., Kaabeche, M., Khomri, H., Nouri, L., Neffar, S., and Chenchouni, H. (2016). A pedological characterisation of some inland wetlands and Ramsar sites in Algeria. *Land Degrad. Dev.* 27 (3), 693–705. doi:10.1002/ldr.2467
- Amghar, F., Forey, E., Margerie, P., Langlois, E., Brouri, L., and Kadi-Hanifi, H. (2012). Grazing enclosure and plantation: A synchronic study of two restoration techniques improving plant community and soil properties in arid degraded steppes (Algeria). *Rev. Écol. (Terre Vie)* 67, 257–269.
- Arar, A., and Chenchouni, H. (2014). A "simple" geomatics-based approach for assessing water erosion hazard at montane areas. *Arab. J. Geosci.* 7 (1), 1–12. doi:10.1007/s12517-012-0782-4
- Aronson, J., Floret, C., Le Floch, E., Ovalle, C., and Pontanier, R. (1995). "Restauration et réhabilitation des écosystèmes dégradés en zones arides et semi-arides. Le vocabulaire et les concepts," in *L'homme peut-il refaire ce qu'il a défilé ?* Editors R. Pontanier, A. M'hiri, J. Aronson, N. Akrimi, and E. Le Floch (Paris: J. Libbey Eurotext), 11–29.
- Baize, D. (2018). *Guide des analyses en pédologie: 3e édition revue et augmentée*. Paris: Editions Quae.
- Bansal, S., and Sheley, R. L. (2016). Annual grass invasion in sagebrush steppe: The relative importance of climate, soil properties and biotic interactions. *Oecologia* 181 (2), 543–557. doi:10.1007/s00442-016-3583-8
- Baranian Kabir, E., Bashari, H., Mosaddeghi, M. R., and Bassiri, M. (2017). Soil aggregate stability and organic matter as affected by land-use change in central Iran. *Archives Agron. Soil Sci.* 63 (13), 1823–1837. doi:10.1080/03650340.2017.1308492
- Belala, F., Hirche, A., Muller, S. D., Tourki, M., Salamani, M., Grandi, M., et al. (2018). Rainfall patterns of Algerian steppes and the impacts on natural vegetation in the 20th century. *J. Arid. Land* 10 (4), 561–573. doi:10.1007/s40333-018-0095-x
- Benabderrahmane, M. C., and Chenchouni, H. (2010). Assessing environmental sensitivity areas to desertification in Eastern Algeria using Mediterranean desertification and land use "MEDALUS" model. *Swes* 1 (1), 5–10. doi:10.5383/swes.01.01.002.5
- Bezzalla, A., Houhamdi, M., and Chenchouni, H. (2019). "Vegetation analysis of Chott Tinsilt and Sebkhet Ezzemoul (two Ramsar sites in Algeria) in relation to soil properties," in *Exploring the nexus of geoeology, geography, geoarcheology and geotourism*. Editors H. Chenchouni, E. Errami, F. Rocha, and L. Sabato (Cham: Springer), 39–42. doi:10.1007/978-3-030-01683-8_8
- Bouaroudj, S., Menad, A., Bounamous, A., Ali-Khodja, H., Gherib, A., Weigel, D. E., et al. (2019). Assessment of water quality at the largest dam in Algeria (Beni

Publisher's note

All claims expressed in this article are solely those of the authors and do not necessarily represent those of their affiliated organizations, or those of the publisher, the editors, and the reviewers. Any product that may be evaluated in this article, or claim that may be made by its manufacturer, is not guaranteed or endorsed by the publisher.

Supplementary material

The Supplementary Material for this article can be found online at: <https://www.frontiersin.org/articles/10.3389/fenvs.2022.846045/full#supplementary-material>

- Haroun Dam) and effects of irrigation on soil characteristics of agricultural lands. *Chemosphere* 219, 76–88. doi:10.1016/j.chemosphere.2018.11.193
- Boudjabi, S., and Chenchouni, H. (2021). On the sustainability of land applications of sewage sludge: how to apply the sewage biosolid in order to improve soil fertility and increase crop yield?. *Chemosphere* 282, 131122. doi:10.1016/j.chemosphere.2021.131122
- Boudjabi, S., and Chenchouni, H. (2022). Soil fertility indicators and soil stoichiometry in semi-arid steppe rangelands. *CATENA* 210 (3), 105910. doi:10.1016/j.catena.2021.105910
- Bradai, L., Bouallala, M. H., Bouziane, N. F., Zaoui, S., Neffar, S., and Chenchouni, H. (2015). An appraisal of eremophyte diversity and plant traits in a rocky desert of the Sahara. *Folia Geobot.* 50 (3), 239–252. doi:10.1007/s12224-015-9218-8
- Chen, W., Zheng, X., Wolf, B., Yao, Z., Liu, C., Butterbach-Bahl, K., et al. (2019). Long-term grazing effects on soil-atmosphere exchanges of CO₂, CH₄ and N₂O at different grasslands in inner Mongolia: A soil core study. *Ecol. Indic.* 105, 316–328. doi:10.1016/j.ecolind.2017.09.035
- Chenchouni, H. (2009). "Place des argiles dans la caractérisation écopédologique du Chott de Djendli (Batna, Algérie) et mise en évidence de la relation salinité-répartition des halophytes," in *Proceedings of the 3rd Maghrebin Symposium on Clays "SMA", Algérie, November 2009*, 23–25.
- Chenchouni, H. (2010). "Drought-induced mass mortality of Atlas Cedar forest (*Cedrus atlantica*) in Algeria," in *The international forestry Review, 33th IUFORO world congress*. Editors J. A. Parrota and M. A. Carr (Seoul, Korea. 23–28 August 2010).
- Chenchouni, H. (2017). Edaphic factors controlling the distribution of inland halophytes in an ephemeral salt lake "Sabbkha ecosystem" at North African semi-arid lands. *Sci. Total Environ.* 575, 660–671. doi:10.1016/j.scitotenv.2016.09.071
- Chenchouni, H., Errami, E., Rocha, F., and Sabato, L. (2019). *Exploring the nexus of geoeology, geography, geoarcheology and geotourism: Advances and applications for sustainable development in environmental sciences and agroforestry research*. Cham: Springer. doi:10.1007/978-3-030-01683-8
- Chenchouni, H., Chaminé, H. I., Khan, M. F., Merkel, B. J., Zhang, Z., Li, P., et al. (Editors) (2022). *New prospects in environmental geosciences and hydrogeosciences* (Cham: Springer). doi:10.1007/978-3-030-72543-3
- Chenchouni, H., and Neffar, S. (2022). Soil organic carbon stock in arid and semi-arid steppe rangelands of North Africa. *CATENA* 212 (1), 106004. doi:10.1016/j.catena.2021.106004
- Cheng, J., Jing, G., Wei, L., and Jing, Z. (2016). Long-term grazing exclusion effects on vegetation characteristics, soil properties and bacterial communities in the semi-arid grasslands of China. *Ecol. Eng.* 97, 170–178. doi:10.1016/j.ecoleng.2016.09.003
- Cortina, J., and Maestre, F. T. (2005). "Plant effects on soils in drylands: Implications for community dynamics and ecosystem restoration," in *Tree species effects on soils: Implications for global change*. Editors D. Binkley and O. Menyailo (Dordrecht: Springer), 85–118. doi:10.1007/1-4020-3447-4_6
- Dalila, D., and Slimane, S. (2008). La désertification dans les steppes algériennes : Causes, impacts et actions de lutte. *Vertigo* 8 (1), 15. doi:10.4000/vertigo.5375
- Djebaili, S. (1984). *Steppe algérienne, phytosociologie et écologie. Recherche phytosociologique et écologique sur la végétation des hautes plaines steppiques et de l'Atlas saharien*. Algiers: Office des publications universitaires.

- Dlamini, P., Chivenge, P., and Chaplot, V. (2016). Overgrazing decreases soil organic carbon stocks the most under dry climates and low soil pH: A meta-analysis shows. *Agric. Ecosyst. Environ.* 221, 258–269. doi:10.1016/j.agee.2016.01.026
- Dormaar, J. F., and Willms, W. D. (1998). Effect of forty-four years of grazing on fescue grassland soils. *J. Range Manag.* 51 (1), 122–126. doi:10.2307/4003574
- Douaoui, A., Benboual, E. H., and Gaouar, A. (2001). Les facteurs intrinsèques de dégradation de la structure de surface des sols du bas Chelif. *Ann. Inst. Natl. Agron. – El-Harrach* 22 (1–2), 27–47.
- Dragović, N., and Vulević, T. (2020). “Soil degradation processes, causes, and assessment approaches,” in *Life on land. Encyclopedia of the UN sustainable development goals*. Editors W. Leal Filho, A. Azul, L. Brandli, A. Lange Salvia, and T. Wall (Cham: Springer). doi:10.1007/978-3-319-71065-5_86-1
- Duchauffour, P. (1997). *Sol, végétation, environnement*. 5th Edition. Paris: Masson, 291. Abrégé de pédologie
- Edmeades, D. C., Wheeler, D. M., and Clinton, O. E. (1985). The chemical composition and ionic strength of soil solutions from New Zealand topsoils. *Soil Res.* 23 (2), 151–165. doi:10.1071/sr9850151
- Fialho, R. C., and Zinn, Y. L. (2014). Changes in soil organic carbon under eucalyptus plantations in Brazil: A comparative analysis. *Land Degrad. Dev.* 25 (5), 428–437. doi:10.1002/ldr.2158
- Gao, X., Thomas, B. W., Beck, R., Thompson, D. J., Zhao, M., Willms, W. D., et al. (2018). Long-term grazing alters soil trace gas fluxes from grasslands in the foothills of the rocky mountains, Canada. *Land Degrad. Dev.* 29 (2), 292–302. doi:10.1002/ldr.2664
- Garcia, C., Nannipieri, P., and Hernandez, T. (2018). “The future of soil carbon,” in *The future of soil carbon: Its conservation and formation*. Editors C. Garcia, P. Nannipieri, and T. Hernandez (Academic Press), 239–267. doi:10.1016/b978-0-12-811687-6.00009-2
- Hadeid, M. (2006). *Les mutations spatiales et sociales d'un espace à caractère steppique. Le cas des hautes plaines sud-oranaises (Algérie)*. Doctoral thesis. Besançon, France: Univ. Franche-Comté.
- Halitim, A. (1988). *Sols des régions arides*. Algiers: Office des publications universitaires.
- Hamel, M. (2018). *The Impact of climate change on erosion and food security in the extreme west of Algeria (Tafna Basin)*. Master dissertation. Tlemcen, Algeria: Pan African university.
- Hasnaoui, O., and Bouazza, M. (2015). Indicateurs de Dégradation des Bio-Ressources Naturelles de l'Algérie Occidentale : Cas de la Steppe de la Wilaya de Saïda = Indicators of Degradation of Natural Bio-Resources of Western Algeria : Case of Steppe of Saïda Province. *Algerian J. Arid Environ.* 5 (1), 63–75. doi:10.12816/0045908
- Haynes, R. J., and Williams, P. H. (1992). Changes in soil solution composition and pH in urine-affected areas of pasture. *J. Soil Sci.* 43 (2), 323–334. doi:10.1111/j.1365-2389.1992.tb00140.x
- HCDS-BNEDER (2007). *Fiche d'identification des potentialités culturelles de la commune d'El Houidjbet*. Algiers: Bureau National d'Études pour le Développement Rural & High Commission for the Development of Steppe (HCDS).
- Huntjens, J. L. M. (1971). The influence of living plants on mineralization and immobilization of nitrogen. *Plant Soil* 35 (1–3), 77–94. doi:10.1007/bf01372634
- Jeddi, K., and Chaieb, M. (2010). Changes in soil properties and vegetation following livestock grazing exclusion in degraded arid environments of South Tunisia. *Flora - Morphol. Distribution, Funct. Ecol. Plants* 205 (3), 184–189. doi:10.1016/j.flora.2009.03.002
- Joosten, H. (2015). “Current soil carbon loss and land degradation globally: Where are the hotspots and why there?,” *Soil carbon: Science, management and policy for multiple benefits*. Editors S. A. Banwart, E. Noellemeier, and E. Milne (UK: CAB International), 71, 224–234. doi:10.1079/9781780645322.0224
- Kadi-Hanifi, H. (1998). *L'Alfa en algérie: Syntaxonomie, relations milieu-végétation, dynamique et perspectives d'avenir*. Algeria: Doctoral thesis, Univ. USTHB.
- Kouba, Y., Merdas, S., Mostephaoui, T., Saadali, B., and Chenchouni, H. (2021). Plant community composition and structure under short-term grazing exclusion in steppic arid rangelands. *Ecol. Indic.* 120, 106910. doi:10.1016/j.ecolind.2020.106910
- Le Houérou, H. N. (2001). Biogeography of the arid steppeland north of the Sahara. *J. Arid Environ.* 48 (2), 103–128. doi:10.1006/jare.2000.0679
- Le Houérou, H. N. (2009). “Long-term dynamics in arid-land vegetation and ecosystems of North Africa,” in *Arid land ecosystems: Volume 2, structure, functioning and management*. Editors D. W. Goodall, R. A. Perry, and K. M. W. Howes (Cambridge University Press), 357–384.
- Li, Y. Y., and Shao, M. A. (2006). Change of soil physical properties under long-term natural vegetation restoration in the Loess Plateau of China. *J. Arid Environ.* 64 (1), 77–96. doi:10.1016/j.jaridenv.2005.04.005
- Linstädter, A., and Baumann, G. (2013). Abiotic and biotic recovery pathways of arid rangelands: Lessons from the high atlas mountains, Morocco. *Catena* 103, 3–15. doi:10.1016/j.catena.2012.02.002
- Liu, W., Sun, S., Zhang, C., Lv, S., and Dong, Q. (2020). Linking plant spatial aggregation with reproductive traits and near-source seed dispersal: Ecological adaptation to heavy grazing. *J. Plant Ecol.* 13 (4), 489–498. doi:10.1093/jpe/rtaa036
- Ma, X., Wang, S., Jiang, G., Haneklaus, S., Schnug, E., and Nyren, P. (2007). Short-term effect of targeted placements of sheep excrement on grassland in inner Mongolia on soil and plant parameters. *Commun. Soil Sci. Plant Analysis* 38 (11–12), 1589–1604. doi:10.1080/00103620701378516
- Macheroum, A., and Kadik, L. (2015). *Étude de l'étude actuel de la végétation du Nord de la wilaya de Tébessa sur le plan phytocologie et pastoral*. France: Éditions, Saint-Denis.
- Macheroum, A., and Kadik, L. (2018). Évaluation des ressources pastorales et de la biodiversité floristique du nord de Tébessa. *Biocénoses* 9 (1), 42–63.
- Martínez-Valderrama, J., Ibáñez, J., Del Barrio, G., Alcalá, F. J., Sanjuán, M. E., Ruiz, A., et al. (2018). Doomed to collapse: Why Algerian steppe rangelands are overgrazed and some lessons to help land-use transitions. *Sci. Total Environ.* 613–614, 1489–1497. doi:10.1016/j.scitotenv.2017.07.058
- Mathieu, C., and Peltain, F. (2003). *Analyse chimique des sols: Méthodes choisies*. Paris: Tec & Doc.
- Mbagwu, J. S. C., and Bazzoffi, P. (1998). Soil characteristics related to resistance of breakdown of dry soil aggregates by water-drops. *Soil Tillage Res.* 45 (1–2), 133–145. doi:10.1016/S0933-3630(96)00133-X
- Mehalaine, S., and Chenchouni, H. (2020). Plants of the same place do not have the same metabolic pace: Soil properties affect differently essential oil yields of plants growing wild in semiarid mediterranean lands. *Arab. J. Geosci.* 13 (23), 1263. doi:10.1007/s12517-020-06219-4
- Mehalaine, S., and Chenchouni, H. (2022). “Effect of edaphic factors on essential oil production in wild plants growing under semiarid Mediterranean conditions,” in *New prospects in environmental geosciences and hydrogeosciences*. Editors H. Chenchouni, H. I. Chaminé, M. F. Khan, B. J. Merkel, Z. Zhang, P. Li, et al. (Cham: Springer), 151–156. doi:10.1007/978-3-030-72543-3_34
- Mekuria, W., and Aynekulu, E. (2013). Exclosure land management for restoration of the soils in degraded communal grazing lands in northern Ethiopia. *Land Degrad. Dev.* 24 (6), 528–538. doi:10.1002/ldr.1146
- Merdas, S., Kouba, Y., Mostephaoui, T., Farhi, Y., and Chenchouni, H. (2021). Livestock grazing-induced large-scale biotic homogenization in arid Mediterranean steppe rangelands. *Land Degrad. Development/Anthos* 32, 5099–5107. doi:10.22541/au.161494226.60674414
- Mihi, A., Tarai, N., and Chenchouni, H. (2019). Can palm date plantations and oasisification be used as a proxy to fight sustainably against desertification and sand encroachment in hot drylands? *Ecol. Indic.* 105, 365–375. doi:10.1016/j.ecolind.2017.11.027
- Moulay, A., Benabdeli, K., and Morsli, A. (2012). Quel avenir pour la steppe à Alfa dans le sud-ouest Algérien. *Forêt Méditerranéenne* 33, 277–286. Available at: <https://www.foret-mediterranee.org/fr/catalogue/id-1723>.
- Neffar, S., Chenchouni, H., Beddiar, A., and Redjel, N. (2013). Rehabilitation of degraded rangeland in drylands by prickly pear (*Opuntia ficus-indica* L.) plantations: Effect on soil and spontaneous vegetation. *Ecol. Balk.* 5 (2), 63–83.
- Neffar, S., Beddiar, A., and Chenchouni, H. (2015). Effects of soil chemical properties and seasonality on mycorrhizal status of prickly pear (*Opuntia ficus-indica*) planted in hot arid steppe rangelands. *Sains Malays.* 44, 671–680. doi:10.17576/jsm-2015-4405-05
- Neffar, S., Beddiar, A., Menasria, T., and Chenchouni, H. (2022). Planting prickly pears as a sustainable alternative and restoration tool for rehabilitating degraded soils in dry steppe rangelands. *Arab. J. Geosci.* 15 (3), 287. doi:10.1007/s12517-022-09579-1
- Neffar, S., Menasria, T., and Chenchouni, H. (2018). Diversity and functional traits of spontaneous plant species in Algerian rangelands rehabilitated with prickly pear (*Opuntia ficus-indica* L.) plantations. *Turk. J. Bot.* 42, 448–461. doi:10.3906/bot-1801-39
- Negm, A., Bouderbala, A., Chenchouni, H., and Barcelo, D. (2020). *Water resources in Algeria - Part I: Assessment of surface and groundwater*. Switzerland: Springer Nature. doi:10.1007/978-3-030-57895-4
- Osman, K. T. (2018). *Management of soil problems*. Cham: Springer. doi:10.1007/978-3-319-75527-4
- Porensky, L. M., Mueller, K. E., Augustine, D. J., and Derner, J. D. (2016). Thresholds and gradients in a semi-arid grassland: Long-term grazing treatments induce slow, continuous and reversible vegetation change. *J. Appl. Ecol.* 53 (4), 1013–1022. doi:10.1111/1365-2664.12630
- Pulido, M., Schnabel, S., Lavado Contador, J. F. L., Lozano-Parra, J., Gómez-Gutiérrez, Á., Brevik, E. C., et al. (2017). Reduction of the frequency of herbaceous roots as an effect of soil compaction induced by heavy grazing in rangelands of SW Spain. *Catena* 158, 381–389. doi:10.1016/j.catena.2017.07.019

- R Core Team (2020). *R: A language and environment for statistical computing*. Vienna, Austria: R Foundation for Statistical Computing. Available at: www.R-project.org.
- Rezaei, S. A., and Gilkes, R. J. (2005). The effects of landscape attributes and plant community on soil chemical properties in rangelands. *Geoderma* 125 (1–2), 167–176. doi:10.1016/j.geoderma.2004.07.010
- Schmalz, H. J., Taylor, R. V., Johnson, T. N., Kennedy, P. L., DeBano, S. J., Newingham, B. A., et al. (2013). Soil morphologic properties and cattle stocking rate affect dynamic soil properties. *Rangel. Ecol. Manag.* 66 (4), 445–453. doi:10.2111/rem-d-12-00040.1
- Shrestha, G., and Stahl, P. D. (2008). Carbon accumulation and storage in semi-arid sagebrush steppe: Effects of long-term grazing exclusion. *Agric. Ecosyst. Environ.* 125 (1–4), 173–181. doi:10.1016/j.agee.2007.12.007
- Singh, A. K., Zhu, X., Chen, C., Wu, J., Yang, B., Zakari, S., et al. (2020). The role of glomalin in mitigation of multiple soil degradation problems. *Crit. Rev. Environ. Sci. Technol.* 52, 1604–1638. doi:10.1080/10643389.2020.1862561
- Slimani, H., Aidoud, A., and Rozé, F. (2010). 30 Years of protection and monitoring of a steppic rangeland undergoing desertification. *J. Arid Environ.* 74 (6), 685–691. doi:10.1016/j.jaridenv.2009.10.015
- Slimani, H. (1998). *Effet du pâturage sur la végétation et le sol et désertification. Cas de la steppe d'Alfa (Stipa tenacissima L.) de Rogassa des Hautes Plaines occidentales algériennes*. Algiers: Magister dissertation, USTHB.
- Smith, P., Calvin, K., Nkem, J., Campbell, D., Cherubini, F., Grassi, G., et al. (2020). Which practices co-deliver food security, climate change mitigation and adaptation, and combat land degradation and desertification? *Glob. Change Biol.* 26 (3), 1532–1575. doi:10.1111/gcb.14878
- Snyman, H. A. (2005). Rangeland degradation in a semi-arid south Africa-I: Influence on seasonal root distribution, root/shoot ratios and water-use efficiency. *J. Arid Environ.* 60 (3), 457–481. doi:10.1016/j.jaridenv.2004.06.006
- Stuart Chapin III, F. S., McFarland, J., David McGuire, A. D., Euskirchen, E. S., Ruess, R. W., and Kielland, K. (2009). The changing global carbon cycle: Linking plant-soil carbon dynamics to global consequences. *J. Ecol.* 97 (5), 840–850. doi:10.1111/j.1365-2745.2009.01529.x
- Ye, L., Lata, J. C., Masse, D., Nacro, H. B., and Barot, S. (2016). Effets du pâturage sur la biomasse herbacée et sur des paramètres chimiques et biologiques des sols dans une savane arbustive au Burkina Faso. *Int. J. Bio. Chem. Sci.* 10 (6), 2539–2554. doi:10.4314/ijbcs.v10i6.11
- Yong-Zhong, S., Yu-Lin, L., Jian-Yuan, C., and Wen-Zhi, Z. (2005). Influences of continuous grazing and livestock exclusion on soil properties in a degraded sandy grassland, Inner Mongolia, northern China. *CATENA* 59 (3), 267–278. doi:10.1016/j.catena.2004.09.001
- Zeng, C., Wu, J., and Zhang, X. (2015). Effects of grazing on above- vs. below-ground biomass allocation of alpine grasslands on the Northern Tibetan Plateau. *PloS One* 10 (8), e0135173. doi:10.1371/journal.pone.0135173
- Zhang, J., Zuo, X., Zhou, X., Lv, P., Lian, J., and Yue, X. (2017). Long-term grazing effects on vegetation characteristics and soil properties in a semiarid grassland, northern China. *Environ. Monit. Assess.* 189 (5), 216. doi:10.1007/s10661-017-5947-x



OPEN ACCESS

EDITED BY

Guang-Lei Gao,
Beijing Forestry University, China

REVIEWED BY

Rende Wang,
Hebei Academy of sciences, China
Ki Hyung Park,
National Institute of Forest Science
(NIFoS), South Korea

*CORRESPONDENCE

Lianyou Liu,
Lianyou.Liu@bnu.edu.cn

SPECIALTY SECTION

This article was submitted to Drylands,
a section of the journal
Frontiers in Environmental Science

RECEIVED 03 June 2022

ACCEPTED 02 September 2022

PUBLISHED 29 September 2022

CITATION

Qu Z, Li Z, Hu L, Liu L, Hu X, Zhang G,
Lv Y, Guo L, Yang Y, Yang Z and Han G
(2022), The branching architecture of
artemisia ordosica and its resistance to
wind erosion.
Front. Environ. Sci. 10:960969.
doi: 10.3389/fenvs.2022.960969

COPYRIGHT

© 2022 Qu, Li, Hu, Liu, Hu, Zhang, Lv,
Guo, Yang, Yang and Han. This is an
open-access article distributed under
the terms of the [Creative Commons
Attribution License \(CC BY\)](#). The use,
distribution or reproduction in other
forums is permitted, provided the
original author(s) and the copyright
owner(s) are credited and that the
original publication in this journal is
cited, in accordance with accepted
academic practice. No use, distribution
or reproduction is permitted which does
not comply with these terms.

The branching architecture of *artemisia ordosica* and its resistance to wind erosion

Zhiqiang Qu^{1,2}, Zhiguo Li^{1,2}, Linxi Hu^{1,2}, Lianyou Liu*, Xia Hu³,
Guoming Zhang³, Yanli Lv³, Lanlan Guo³, Yanyan Yang⁴,
Ziqiong Yang^{1,2} and Guodong Han^{1,2}

¹College of Grassland, Resources and Environment, Inner Mongolia Agricultural University, Hohhot, China, ²Key Laboratory of Grassland Resources, Ministry of Education P.R. of China, Inner Mongolia Agricultural University, Hohhot, China, ³Academy of Disaster Reduction and Emergency Management, Ministry of Civil Affairs and Ministry of Education, Beijing Normal University, Beijing, China, ⁴Institute of Ecological Protection and Restoration, Chinese Academy of Forestry, Beijing, China

Different branching architectures reflect the adaptation strategies of different plants and affect their resistance to wind erosion. This study presents field-based observations that demonstrate the relationship between the branching architecture of *Artemisia ordosica* and its resistance to wind erosion. This species is the dominant plant species in the semi-fixed and fixed dunes of the Mu Us Sandy land. The overall bifurcation ratio (OBR) of semi-fixed sandy land is higher than the fixed sandy land 0.27; Similarly, the total stepwise bifurcation ratio (SBR) is higher than the fixed sandy land about 0.74; The length of first levels of total branches is also higher than 8.07. The aerodynamic roughness was greater than the *A. ordosica* community in the fixed and semi-fixed sandy land than in the bare sandy land. The airflow fields in the cross-wind direction were strongly affected by the windward shape of the plants, which became gradually narrower from the base to the top, while in the leeward direction, the wind speed at different heights behind the plant returned to the incoming airflow velocity. The result confirms that the influence of the windward shape of the plant on the surrounding airflow field is much larger than the influence of plant thickness, porosity or other factors.

KEYWORDS

branching architecture, wind erosion, growing locations, psammophyte, Mu Us sandland

1 Introduction

Psammophytes are adapted to growing in special habitat conditions. Their adaptation characteristics include resistance to wind erosion, sand burial, aridity and soil infertility, and these adaptations play an important role in maintaining the stability of the fragile ecosystem and in reconstructing damaged ecosystems (Zhou, 2001). Psammophytes influence the protection of surface soil in complex ways. Previous research has focused on the effect of plant groups rather than individual plants. However, the morphological characteristics of single plants have a great influence on sand resistance and fixation.

A plant can be regarded as a collection of modules. There are variety modules having different architecture characteristics due to their arrangement in space, so a plant presents diverse morphological structures (Harper, 1977; White, 1979; Barlow, 1989). The concept of the architecture characteristics of the plant, which in a narrow sense mainly refers to branching architecture, was advanced by Halle and others in 1978. Different branching architectures not only reflect the utilization of space, light and other resources by plants, but also indicate different adaptation strategies of plants at different growth stages. At the same time, branching architectures affects a plant's resistance to wind erosion.

With respect to the branching architecture of plants, woody plants and herbs growing in tropical or humid areas have been relatively well studied. Research both in China and abroad has mainly focused on the morphological characteristics of plant branches and the quantitative study of the meristem dynamic relationship (Sprugel et al., 1991; Ohsawa and Nitta, 1997; Nitta and Ohsawa, 1998; Sun and Chen, 1999). For woody plants, studies have often focused on the crown and trunk studying the development, morphology and growth dynamics of branching, and dynamic changes and mutual relations among other components of the branches. Studies of herbs have mainly addressed the adaptation strategies of clonal ramets as reflected in their placement mode in different habitats. However, studies of the branching architecture of psammophytes have been much less common. Existing research has primarily focused on the quantitative study of plant populations at the component level, as well as adaption strategies to different environments as reflected in different branching architectures (Anwar and Yin, 1997; Sun et al., 1997; He et al., 2005; He et al., 2006; Zhang et al., 2009). Few studies have concentrated on the influence of psammophyte branching architecture on resistance to wind erosion.

The Mu Us Sandy land is located in the transition zone between arid or semi-arid areas and sub-humid areas of northern China. The region is a typical multi-level ecotone in terms of geography and geology and is one of the areas most seriously affected by desertification in China (Wu and Ci, 1998). Due to these special features, the Mu Us Sandy land has a variety plant types, and shrubs are the dominant species. The psammophytic semi-shrub community, dominated by the species *Artemisia ordosica*, is the most developed type, playing a significant role in desert ecosystem reconstruction and rehabilitation. *A. ordosica*, which commonly appears at the southern edge of the Mu Us Sandy land, was selected as the subject of this study. This study investigates the resistance of *A. ordosica* to wind erosion through its architecture characteristics. The result of this study has important scientific and practical significance: quantitative determination of the mechanisms used by psammophytes

to resist wind erosion, and the exploration of plant variety in the semi-fixed and fixed dunes of the Mu Us Sandy land.

2 Materials and methods

2.1 Experimental site

The study was conducted during the 2016 windy season, in the site of an *A. ordosica* community for windbreak and sand-fixation at the southern edge of the Mu Us Sandy land in northern China (37°38'42"~37°47'54"N, 108°50'54"~108°58'00"E) (Figure 1). This location is in a semi-arid region with a temperate monsoon climate characterized by hot summers and mild winters. Desert shrubs and herbs comprise the primary plant communities in the research area. *A. ordosica* is the most developed type, and its communities occupy most of the sand dunes and sand ridges. The site receives approximately 400 mm annual average rainfall, mostly during the summer (www.cdc.cma.gov.cn). Annual pan evaporation exceeds 2,400 mm, which is over 6 times greater than annual average precipitation (www.cdc.cma.gov.cn). Thirty-year average annual wind speed is 3.2 m s^{-1} . Aeolian sand activity occurs mainly between March to May, when wind speeds are greater than 4.0 m s^{-1} (the threshold velocity of sand), and this period accounts for 50.2% of total annual aeolian activity. Vegetation recovery began in the 1970s. Most drifting dune activity ceased after afforestation, and semi-fixed dunes and fixed dunes are now the prevailing landforms.

2.2 Experimental design

2.2.1 Plot design and determination of branching architecture

Two areas were chosen on the semi-fixed and fixed dunes, where *A. ordosica* is concentrated within the research area. Ten mature plants were selected as the research samples in each site. The plant selection criteria included similar size, good growth, no pest or man-made damage, and a distance far enough from other plants to reduce the impact on plant modules of intraspecific and interspecific competition for space resources. A steel tape (with a precision of 0.1 cm) was used to measure the height, diameter at chest height, branch lengths at all levels, the interval between branches and other parameters of each plant. A protractor was used to measure the inclination of the branches and a caliper was used to measure the base diameter of the branches at all levels. The branch sequence was defined on the basis of the Strahler method (Sun and Chen, 1999), which is used to determine the branch sequence from the outside to the inside of the canopy layer. The first external branch is the first level, the branch formed by intersection of the two first levels is

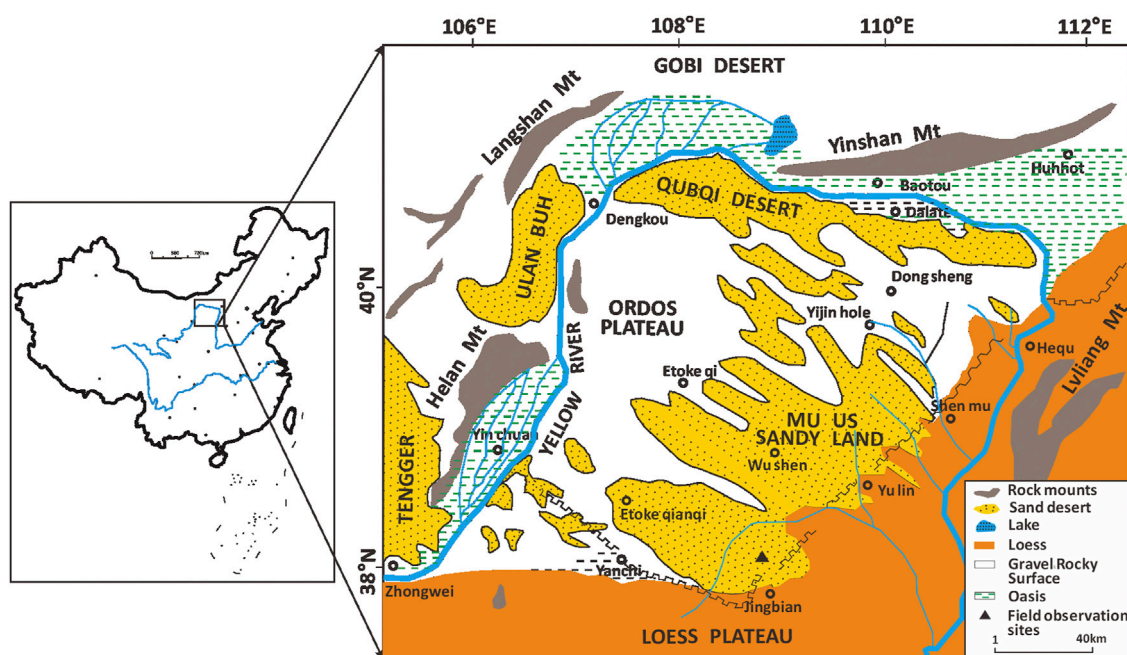


FIGURE 1

Location of the study area on the southern fringe of the Mu Us Sandy land, China (37°38'42"~37°47'54"N, 108°50'54"~108°58'00"E).

the second level, and so forth. If different branch levels intersect, then the one that is higher is regarded as the branch level.

2.2.2 Determination of flow field characteristics

Wind profile observation was conducted in the two study areas mentioned above. At the same time, one bare sandy area with no vegetation cover, was selected within the study site as a control plot. Wind speed was measured continuously at 9 different heights in the center of the communities using anemometers connected to a data logging system. The wind cup heights of the measuring points were 5 cm, 25 cm, 50 cm, 75 cm, 100 cm, 150 cm, 200 cm, 300 cm and 400 cm. Wind speed was recorded with a 30 s frequency, and each group of data was recorded for 5 min, making a total of 10 measurements in each data group. We ensured that the atmosphere was relatively stable while the test was being conducted. Data collected below the threshold velocity of sand (4 m s^{-1}) were selected for regression analysis (Wu, 2003). Wind profiles were drawn, and wind roughness was calculated.

An individual shrub on a gentle slope in the semi-fixed sandy terrain was selected for airflow visualization. There were 67 total measuring points located at the windward side, leeward side and crosswind side of the plant. Three-cup wind speed sensors for each measuring point were located at the base, the mean height, the top of the plant and at a height of 200 cm. Simultaneously, one control site was set at

an open location on the windward side, and the wind velocity at a height of 200 cm was used as a control. Each point was continuously measured for 5 min. After taking the average, the data were standardized according to the values obtained during the corresponding period at the control site, so that the data from all of the measuring points were converted to the average wind speed during the same 5 min period. The airflow fields at the other three heights were then obtained.

2.3 Statistical analysis

2.3.1 Statistical method of branching architecture

Branching architecture was analyzed using the following indicators: bifurcation ratio, the ratio of branch diameters, and the fractal dimensions of branching. The ratio of branch diameter (RBD) is given by

$$RBD = D_{i+1}/D_i \quad (1)$$

where D_{i+1} and D_i are the diameter (in cm) of the $i+1$ and i branch levels, respectively. The bifurcation ratio describes the branching capability of the branches and the quantitative configuration of each branch. It can be measured by the overall bifurcation ratio (OBR) and the stepwise bifurcation ratio (SBR), which were proposed by Whitney, (1976) and modified by Steingraeber and Waller, (1986). OBR is expressed by

$$OBR = (N_T - N_S) / (N_T - N_1) \quad (2)$$

where N_T is the total number of branches at all branch levels (i.e., $N_T = \sum N_i$), N_S is the number of branches at the highest level and N_1 is the number of branches at the first level. SBR is expressed by

$$SBR_{i:i+1} = N_i / N_{i+1} \quad (3)$$

where N_{i+1} and N_i are the total number of $i+1$ and i level branches, respectively. The relationship between the number of branches (SB), branch length (LB), and the fractal dimension of branching (D) of each level of branches of different psammophytes can be described by

$$SB = C \times LB^D \quad (4)$$

where C is a constant proportionality coefficient. After transformation, the above equation can be written as follows:

$$\ln SB = \ln C + D \ln LB \quad (5)$$

There is a good visible linear relationship between SB and LB when plotted on double logarithm coordinates, and D , the fractal dimension, is the slope of the resulting line.

2.3.2 Standardization of wind speed

The collected wind speed data was analyzed by converting data to the average wind speed within 5 min from the beginning of observations. The standardized method adapted from Zhang et al., (2006) is as follows:

$$\hat{U}_Z = \frac{U_{(t=5, z=2.0)}}{U_{(t, z=2.0)}} \times U_{(t, z)} \quad (6)$$

where \hat{U}_Z is the standardized wind speed of an arbitrary measuring point at the height z , $U_{(t=5, z=2.0)}$ is the average wind speed of the control point between t and $t+5$ min at a height of 2.0 m, $U_{(t, z=2.0)}$ is the average wind speed of the control point from the beginning of the observation to 5 min at a height of 2.0 m and $U_{(t, z)}$ is the wind speed of the measuring point from t to $t+5$ min at a height of z . To ensure that no sand airflow was generated during the test, data showing a wind speed below the threshold velocity of sand were selected. A graph of the airflow field near the surface was drawn using the standardized wind speed data.

3 Results and discussion

3.1 Analysis of branching architecture characteristics

The average plant height of the sampled *A. ordosica* on the semi-fixed sandy land was 55 ± 0.4 cm with a porosity of 48%, and an average crown size of 150 ± 2 cm \times 140 ± 2 cm. However, the average plant height on the fixed sandy land was 50 ± 0.3 cm with a porosity of 49%, and an average crown size of 130 ± 2 cm \times $120 \pm$

2 cm. *A. ordosica* grows better on semi-fixed dunes, sandy land and soil covered with sand and grows particularly well on loose sand dunes. However, on fixed dunes, due to enhanced soil compaction, *A. ordosica* is less suited to the environmental conditions. Although the number of plants can be large, the plant sizes are generally small. The number of dry branches increases and growth declines gradually. The seeds are small and light, and it is difficult for seeds to be retained in sand dunes, thus *A. ordosica* has a relatively smaller distribution in mobile sandy environments.

3.1.1 Branching angle of branches

Branching angles are not only important indicators of plant spatial distribution, but are also a factor in the plants' erosion resistance. *A. ordosica* has a wide base and a gradually narrowing middle-upper part and is visualized as a hemisphere based on this morphology. The outside branches of the plant are weak branching angles, with branching angles between 35° and 50° . Partial branches may grow nearly horizontally in a creeping manner. This structure is beneficial for forming adventitious roots for clonal growth, generating new plants, and enhancing vegetation coverage of the covered sandy land. The interior branches of the plant are mostly middle branching angles, with branching angles between 50° and 70° , along with some strong branching angles between 70° and 85° . This structure means that the growth of each branch does not disturb the growth of the other branches, thereby maximizing the use of space. There was little difference in the inclinations of the highest level of branches on the windward, leeward and crosswind sides, which demonstrates that they were not influenced by the force of the wind. However, the angles of the penultimate levels of branches had different values (Table 1).

The branching angles of the penultimate levels of branches on the windward side were between 30° and 80° , with a relatively large range, and included weak branching angle types and middle branching angle types. Due to the more direct exposure to wind on the windward side, branching angles of the outside penultimate levels of branches gradually increased. However, the angles on branches on the internal penultimate levels were closer to the angles at the highest level, and the branching angles decreased. Branching angles of the branches on the leeward side, were weak branching angles. The branching angles on the crosswind side, which was less affected by the wind, were in between the angles on the windward and leeward sides.

3.1.2 Bifurcation ratio and ratio of branch diameter

The branch diameter ratio (RBD) is an indicator of the bearing capacity of different levels of branch. The larger the branch diameter, the greater the loading on branches at the next level. In general, if the plant has a large branch diameter, the bifurcation ratio is relatively large. The bifurcation ratio

TABLE 1 The branching angle of samples of *Artemisia ordosica*.

Sequence number		The inclination of the highest level of branches			The angles of the penultimate levels of branches		
		Windward side	Leeward side	Crosswind side	Windward side	Leeward side	Crosswind side
1	Outside	22	33	8	81	56	34
2		19	46	17	79	23	39
3		23	35	30	78	26	47
4		31	30	36	59	31	35
5		41	26	33	72	36	50
6	Inside	70	83	85	41	39	56
7		51	70	60	44	54	36
8		65	72	66	32	35	64
9		76	67	73	30	31	59
10		79	65	82	36	55	40

TABLE 2 Analysis of the branching architecture of *Artemisia ordosica*.

		Windward side	Leeward side	Crosswind side	Total
Semi-fixed sandy land	OBR	2	1.68	2.46	2.05
	SBR _{1:2}	2.11	1.08	3.07	2.09
	SBR _{2:3}	4.5	4.17	1.88	3.52
	RBD _{2:1}	1.47	1.51	2.35	1.78
	RBD _{3:2}	2.65	3.08	2.28	2.67
	Length of first levels of branches (cm)	16.10	25.60	23.70	21.80
Fixed sandy land	OBR	2.21	1.26	1.86	1.78
	SBR _{1:2}	1.78	0.51	1.77	1.35
	SBR _{2:3}	3.08	1.68	1.41	2.06
	SBR _{3:4}	4.17	5	3.36	4.18
	SBR _{4:5}		2.67	3.67	3.17
	RBD _{2:1}	1.55	1.34	1.81	1.57
	RBD _{3:2}	2.30	1.94	1.91	2.05
	RBD _{4:3}	3.43	2.04	1.94	2.47
	RBD _{5:4}		2.19	1.88	2.04
	Length of first levels of branches (cm)	16.10	13.30	11.80	13.73

describes the branching capability of the branches, as well as the number of configurations among all branch levels. The value of the bifurcation ratio is closely related to the branching angle and the branch diameter ratio. A higher bifurcation ratio shows a higher level of a plant's utilization of its spatial resources.

The average number of the highest level of branches of *A. ordosica* on the windward side was equal to the number on the leeward side, and both were less than that of the crosswind side. The branches on the windward and the leeward sides accounted for 27% of the total number of branches on each side, while the branches on the crosswind side accounted for 46% of the total

number. The distribution of the branches in all four directions was similar, leading each individual plant to resemble a symmetrical semicircle. Wind had no significant effect on the distribution of the branches of *A. ordosica*.

The branches of *A. ordosica* were divided into 4-5 levels in the fixed sandy land and 3 levels in the semi-fixed sandy land. The index statistics for the branching architecture on the windward, leeward and crosswind sides, and for branches divided according to the azimuth of the highest levels of branches, are given in Table 2.

The overall branching ratio of *A. ordosica* on the semi-fixed sandy land was greater than that of plants on the fixed

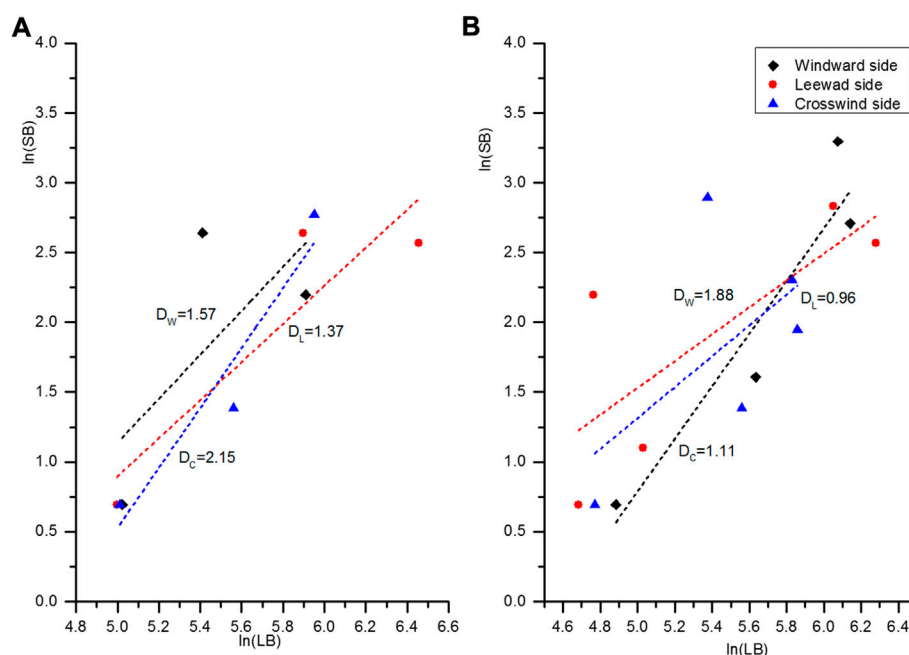


FIGURE 2

Linear fitting of the fractal dimension of branching of *Artemisia ordosica* in sandy land [(A) Semi-fixed sandy land; (B) Fixed sandy land].

sandy land, but both were less than 5 and had low branching rates. The overall branching ratio on the leeward side was less than that on the windward and crosswind sides. The branching number of the highest level of branches was the greatest at each azimuth on the semi-fixed sandy land. However, in the fixed sandy land, the number of the highest level of branches was greatest on the windward and crosswind sides, while the number of second level branches was the greatest on the leeward side. The ratio of branch diameter in the semi-fixed sandy land was larger than that in the fixed sandy land, and the base diameter of the highest level of branches on the crosswind side was the largest. The branch diameter ratio of branches in all directions in the semi-fixed sandy land showed little difference, while in the fixed sandy land the ratio in the windward direction was larger than that on the leeward and crosswind sides. These characteristics of *A. ordosica* not only reflect the impact of blown sand activities, but also indicate a type of adaptive strategy that simultaneously plays an effective role in controlling wind erosion and desertification.

3.1.3 Fractal dimension of branching

The fractal dimension of branching (D) is an important parameter for measuring the spatial distribution pattern of plant branches. If D is less than 1.4000, the plant has a weak fractal dimension (WD), indicating that the branching pattern of the plant is simple. If D is larger than 1.8000, the plant would have a strong

fractal dimension (SD), showing that the branching pattern of the plant is complex. If D is between 1.4000 and 1.8000, the plant has a moderate fractal dimension (MD). After fitting each level of branch numbers (SB) and branch lengths (LB) of the sampled *A. ordosica* plants in the semi-fixed and fixed sandy lands, the straight lines and fractal dimensions are shown in Figure 2.

A. ordosica exhibited different D values in the three directions. On fixed sandy land, *A. ordosica* was WD on the leeward and crosswind sides, and SD on the windward side. In semi-fixed sandy land, they were MD on the windward and the leeward side, and SD on the crosswind side. Because growth of *A. ordosica* was poor in the fixed sandy land, D was smaller than in the semi-fixed sandy land and the branching pattern was relatively simple. Because blown sand activities in the semi-fixed sandy land is stronger than in fixed sandy land, branches on the windward side were more strongly affected by in the fixed sandy land. However, in the semi-fixed sandy land, the branches on the windward and the crosswind side developed a more complex branching pattern, which enlarged the upwind projected area of the plant, so as to adapt to the blown sand.

3.2 Wind speed profile and aerodynamic roughness of the *Artemisia ordosica* community

When air flows over a surface covered by vegetation, the projected upwind shape of the plants plays a key role in

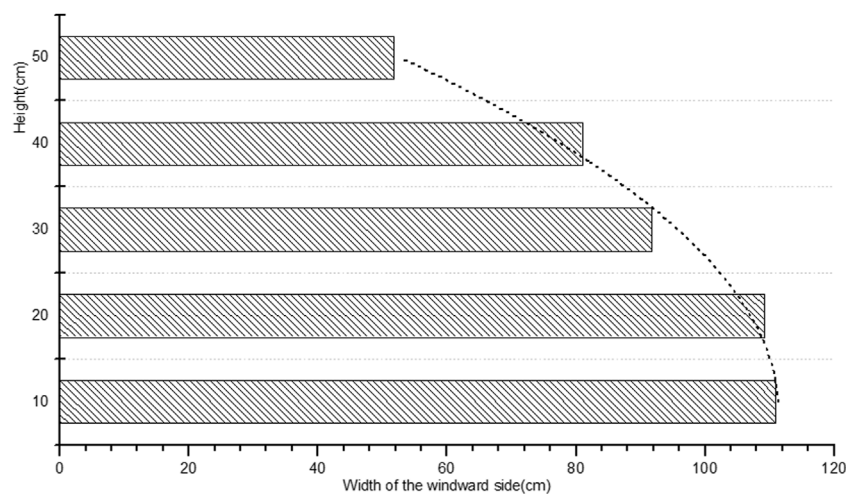


FIGURE 3
The width of *Artemisia ordosica* on the windward side at different heights.

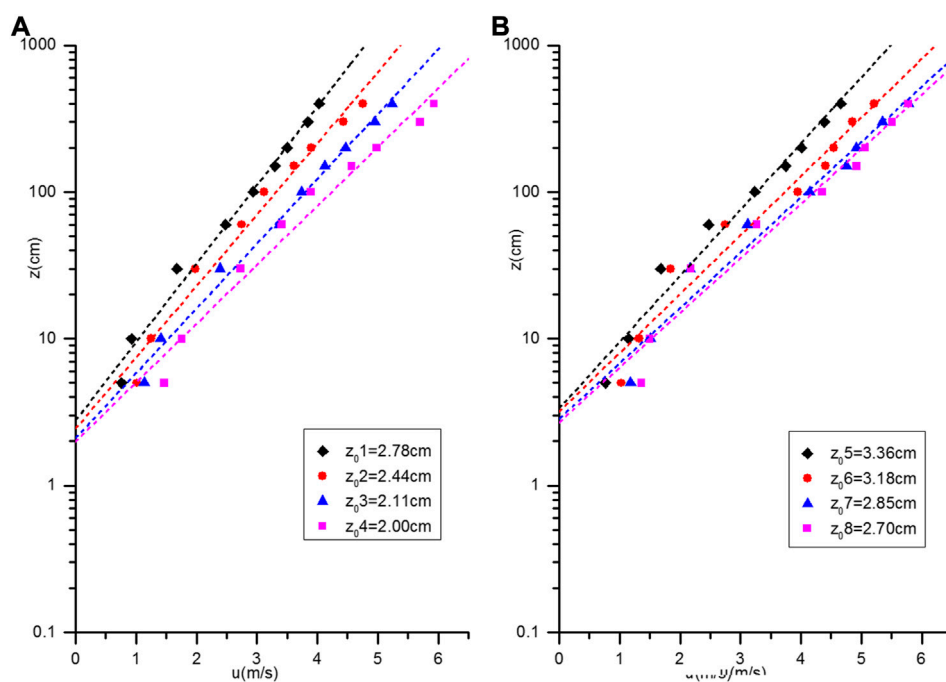


FIGURE 4
Wind profiles of the *Artemisia ordosica* community on sandy land under non-sand-driving wind [(A) Semi-fixed sandy land; (B) Fixed sandy land].

their resistances to wind-blown sand. The shape of the plants can be expressed by differences in their morphological structures, including their height, width, and porosity. The width of the windward side at different heights of the plants under investigation is shown in Figure 3.

The average height of the plants was 0.53 m, and the average width on the windward side was 0.90 m. The widest part of the windward side was located within 0–20 cm of the base and gradually decreased with height. This hemispherical shape is conducive to sand accumulation at the base of the plant.

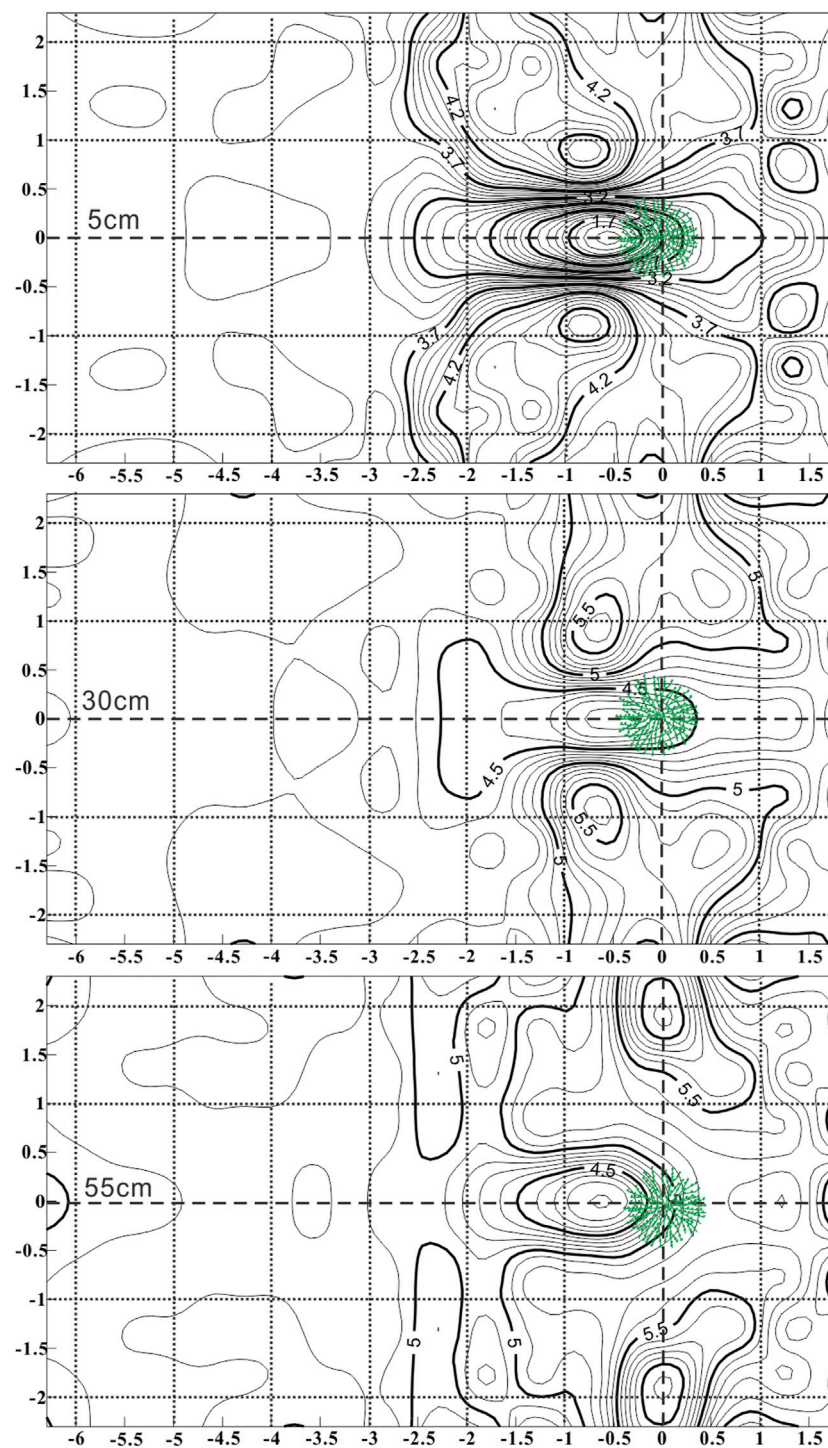


FIGURE 5
Airflow fields at three heights around an individual *Artemisia ordosica*.

Aerodynamic roughness (z_0) is defined as the height where surface wind velocity decreases to zero. It represents the aerodynamic characteristics of the surface and reflects the

decreasing effects of wind speed on the ground surface and the influence of ground surface on wind airflow (Liu and Dong, 2003). The most common method for calculating

aerodynamic roughness is using a least squares method with a logarithmic profile equation for the measured wind profile (Dong et al., 2001). Given stable and neutral atmospheric stratification, the velocity profile has a logarithmic relationship as follows:

$$u_z = a + b \ln z \quad (7)$$

where u_z is the velocity at height z ($\text{m}\cdot\text{s}^{-1}$), and a and b are fitted constants. If $u_z = 0$, then:

$$z_0 = \exp(-a/b) \quad (8)$$

A. ordosica communities with similar plant heights, numbers and uniform distributions were selected on the fixed sandy land and semi-fixed sandy land. Coverage of the fixed sandy land with generated crusts was 35%, while coverage of the semi-fixed sandy land was 20%. According to wind velocity observations, four groups of wind speed, at a height of 2 m, were lower than the threshold velocity of the surface that was used to fit the wind profiles (Figure 4), and these wind speeds were then used to calculate the aerodynamic roughness (z_0).

The logarithmic curve fitting result of wind profile is relatively accurate, and the fitting coefficient (R^2) is close to 0.9. z_0 of the *A. ordosica* community in the fixed sandy land was between 2.70 and 3.36 cm, and that in the semi-fixed sandy land was between 2 and 2.78 cm. Both were larger than the value in the bare sandy land, which was 0.04 cm (Qiu et al., 2004). Roughness of the fixed sandy land was enhanced, which supports positive succession of plants and soils.

3.3 Airflow field characteristics of individual *Artemisia ordosica*

An individual shrub, that was 55 cm high and located on a gentle slope in semi-fixed sandy land, was selected for airflow visualization. Three-cup wind speed sensors at each measuring point were located at heights of 5 cm, 30 cm and 55 cm, respectively. The results from the airflow fields at each of the three heights are shown in Figure 5. From the figure, it can be observed that the airflow fields change drastically because wind velocity in the cross-wind direction was affected by the windward shape of the plant, which became gradually narrower from the base to the top. Two wind acceleration regions formed on both sides of the plants. Those at the base were larger and affected a range of 2.50 m behind the plant, while at the mean of the range, 1.50 m behind the plant was affected, and at the top only a range of 0.50 m behind the plant was affected. The wind acceleration regions at the base and the mean were located at the post-lateral side of the plant and 1 m away from the center of the plant. However, the wind

acceleration regions at the top were located at both sides of the plant and 2 m away from the center of the plant. Although the plant widths became gradually narrower from bottom to top, the wind speed in the windward direction at different heights behind the plants returned to the incoming airflow velocity approximately 2 m from the plant. This result confirms that the influence of the windward shape of a plant on the surrounding airflow field is much larger than the influence of plant thickness, porosity or other factors.

4 Summary and conclusion

Research on the impact of the branching architecture of psammophytes on the prevention of wind erosion is still in its early stages. Although this study has presented a number of results, there are many issues that require further research.

The architecture of psammophytes is not only the result of their growth, development and adaptation, but is also a restrictive condition that affects their further development at certain architectural growth stages. Not only does the difference in architecture influence resistances to wind erosion, but sand airflow also plays a role in formation of the architecture. Elimination of other environmental factors is the key to analyzing the effect on wind erosion control of the architecture under field conditions. However, a good method has still not been developed to achieve this goal. Pot experiments can simulate environmental conditions to a certain extent, but there are still significant shortcomings with this method. One limitation is that cultivation requires an extended period of time. Also, differences have been reported between pot experiments and field studies because the experiments do not entirely represent the field conditions. Therefore, better methods to overcome this problem need to be developed through future studies.

The classification of psammophyte architecture is the basis for researching the mechanisms of resistance to wind erosion. He et al., 2005 divided desert plants into four types according to their architecture index, based on statistics relating to branching architecture, including all levels of branching angles, branch length, branch diameter ratios and other indicators. However, they did not consider the effects of environmental conditions on the differences in architecture. To describe the architecture characteristics fully, one needs to describe, for instance, the change in psammophyte architecture with growth stage, the external space-time difference, the climate characteristics and the geographical differences in soils to establish a psammophyte architecture index system to enable comprehensive classification of psammophytes.

Data availability statement

The original contributions presented in the study are included in the article/Supplementary Material, further inquiries can be directed to the corresponding author.

Author contributions

ZQ: Writing - original draft, Data curation, Methodology, Conceptualization. ZL: Co-first Author, Writing - review & editing. LH: Writing - review & editing. LL: corresponding author, Writing - review & editing, Conceptualization, Methodology. XH: Methodology. GZ: Writing - review. YL: Writing - review, Data curation. LG: Methodology. YY: Methodology. YZ: Writing - review & editing. GH: Methodology. All authors contributed to the article and approved the submitted version.

Funding

This research was supported by a grant from the National Natural Science Foundation of China (No. 31960361) and Natural Science Foundation of Inner Mongolia Autonomous Region (No. 2022MS04010). The authors express their sincere

appreciation to their supporters. All errors and omissions are the responsibility of the authors.

Conflict of interest

The authors declare that the research was conducted in the absence of any commercial or financial relationships that could be construed as a potential conflict of interest.

Publisher's note

All claims expressed in this article are solely those of the authors and do not necessarily represent those of their affiliated organizations, or those of the publisher, the editors and the reviewers. Any product that may be evaluated in this article, or claim that may be made by its manufacturer, is not guaranteed or endorsed by the publisher.

Supplementary material

The Supplementary Material for this article can be found online at: <https://www.frontiersin.org/articles/10.3389/fenvs.2022.960969/full#supplementary-material>

References

- Anwar, M., and Yin, L. K. (1997). The study on biomass of tamarix. *Environ. Prot. Xinjiang* 1, 46–50.
- Barlow, P. W. (1989). Meristems, metamers and modules and the development of shoot and root systems. *Botanical J. Linn. Soc.* 100, 255–279. doi:10.1111/j.1095-8339.1989.tb01721.x
- Dong, Z. B., Wang, X. M., Zhao, A. G., Liu, L. Y., and Liu, X. W. (2001). Aerodynamic roughness of fixed sandy beds. *J. Geophys. Res.* 6, 11001–11011. doi:10.1029/2001jb900009
- Harper, J. L. (1977). *Population biology of plants*. London: Academic Press.
- He, M. Z., Wang, H., and Zhang, J. G. (2005). Classification of the branching architectures of the desert plants in minqin county. *Acta Bot. boreal.-occident. Sin.* 9, 1827–1832. doi:10.1360/biodiv.050022
- He, M. Z., Zhang, J. G., and Wang, H. (2006). Analysis of branching architecture factors of desert plants. *J. desert Res.* 4, 625–630. doi:10.3321/j.issn:1000-694X.2006.04.023
- Liu, X. P., and Dong, Z. B. (2003). Review of aerodynamic roughness length. *J. desert Res.* 4, 337–346.
- Nitta, I., and Ohsawa, M. (1998). Bud structure and shoot architecture of canopy and understorey evergreen broad-leaved trees at their northern limit in east asia. *Ann. Bot.* 81, 115–129. doi:10.1006/anbo.1997.0545
- Ohsawa, M. M., and Nitta, I. (1997). Patterning of subtropical / warm-temperate evergreen broad-leaved forests in east asian mountains with special reference to shoot phenology. *Tropics* 6, 317–334. doi:10.3759/tropics.6.317
- Qiu, G. Y., In-Bok, L., Shimizu, H., Gao, Y., and Ding, G. D. (2004). Principles of sand dune fixation with straw checkerboard technology and its effects on the environment. *J. Arid Environ.* 56, 449–464. doi:10.1016/s0140-1963(03)00066-1
- Sprugel, D. G., Hinckley, T. M., and Schaap, W. (1991). The theory and practice of branch autonomy. *Annu. Rev. Ecol. Syst.* 22, 309–334. doi:10.1146/annurev.es.22.110191.001521
- Steingraeber, D. A., and Waller, D. M. (1986). Non-stationarity of tree branching patterns and bifurcation ratios. *Proc. R. Soc. Lond. B* 228, 187–194. doi:10.1098/rspb.1986.0050
- Sun, J. M., Li, G. T., Qin, F. C., Sun, F., Zhang, D. Y., Jia, S. Y., et al. (1997). The prediction research of aboveground biomass of artificial *Haloxylon ammodendron* forestry. *Inn. Mong. For. Sci. Technol.* 3, 9–11.
- Sun, S. C., and Chen, L. Z. (1999). The architectural variation of *Quercus liaotungensis* in different habitats. *Acta Ecol. Sin.* 3, 359–364. doi:10.3321/j.issn:1000-0933.1999.03.012
- White, J. (1979). The plant as a metapopulation. *Annu. Rev. Ecol. Syst.* 10, 109–145. doi:10.1146/annurev.es.10.110179.000545
- Whitney, G. G. (1976). The bifurcation ratio as an indicator of adaptive strategy in woody plant species. *Bull. Torrey Botanical Club* 103, 67–72. doi:10.2307/2484833
- Wu, B., and Ci, L. J. (1998). The developing situation and expanding causes of desertification in Mu Us Sandy Land since the 1950s. *Quat. Sci.* 2, 165–172.
- Wu, Z. (2003). *Aeolian geomorphology and sand control engineering*. Beijing: Science Press.
- Zhang, C. L., Zou, X. Y., Cheng, H., Yang, S., Pan, X. H., and Wang, H. T. (2006). Near surface air flow field across the shelterbelt of shapotou section, Baotou-Lanzhou line. *J. Basic Sci. Eng.* 3, 353–360. doi:10.3969/j.issn.1005-0930.2006.03.006
- Zhang, D. K., Wang, J. H., Ma, Q. L., Liu, H. J., and Liu, Y. J. (2009). Study on branch module characteristics of *Artemisia ordosica* and *Artemisia arenaria*. *Grassl. Turf* 1, 43–46. doi:10.13817/j.cnki.cycyp.2009.01.001
- Zhou, H. Y. (2001). Current status and perspective of eco-physiological researches in psammophytes. *Chin. Bull. Bot.* 6, 643–648. doi:10.3969/j.issn.1674-3466.2001.06.002



OPEN ACCESS

EDITED BY
Jifeng Deng,
Shenyang Agricultural University, China

REVIEWED BY
Jun Li,
Beijing Forestry University, China
Yanli Jing,
Mianyang Normal University, China

*CORRESPONDENCE
Xiaoming Cao,
caoxm@caf.ac.cn

SPECIALTY SECTION
This article was submitted to Drylands,
a section of the journal
Frontiers in Environmental Science

RECEIVED 28 April 2022
ACCEPTED 20 July 2022
PUBLISHED 04 October 2022

CITATION
Wang L, Gao Y, Cao X and Lu W (2022),
Carbon dioxide fluxes of cyanobacterial
crusts and underlying soil under
different precipitation patterns in the
Ulan Buh Desert, China.
Front. Environ. Sci. 10:930961.
doi: 10.3389/fenvs.2022.930961

COPYRIGHT
© 2022 Wang, Gao, Cao and Lu. This is
an open-access article distributed
under the terms of the [Creative
Commons Attribution License \(CC BY\)](#).
The use, distribution or reproduction in
other forums is permitted, provided the
original author(s) and the copyright
owner(s) are credited and that the
original publication in this journal is
cited, in accordance with accepted
academic practice. No use, distribution
or reproduction is permitted which does
not comply with these terms.

Carbon dioxide fluxes of cyanobacterial crusts and underlying soil under different precipitation patterns in the Ulan Buh Desert, China

Lili Wang, Ying Gao, Xiaoming Cao* and Weiwei Lu

Institute of Ecological Conservation and Restoration, Chinese Academy of Forestry, Beijing, China

Cyanobacterial crusts, sensitive to changes in the moisture content, are widely distributed in the Ulan Buh Desert. Changes in precipitation patterns due to global climate change are expected to influence the carbon emission and photosynthetic carbon fixation of soil in areas covered with cyanobacterial crusts. We assessed how changes in precipitation amount and frequency affect carbon processes of Cyanobacterial Crusts. Taking average precipitation amount and frequency in August during the past 30 years as control, we established nine precipitation patterns (three amounts × three frequencies). The net carbon flux (NCF) and dark respiration rate (DRR) of cyanobacterial crusts and underlying soil were investigated. Precipitation could stimulate NCF and DRR immediately. With increasing water application times, the peak values of NCF, DRR and 12 h cumulative carbon emissions gradually decreased. Both precipitation amount and frequency significantly affected cumulative carbon emissions but without an interactive effect. Under the same frequency, cumulative carbon emissions increased with increasing precipitation amounts. Under the same total precipitation amount, cumulative carbon emissions caused by high-frequency events were the highest, followed by those of low-frequency precipitation and the control. However, such changes, against the background of a changing global climate, will result in increased carbon emissions of cyanobacterial crusts and underlying Soil, suggesting that cyanobacteria should be considered in projections of the future carbon budget.

KEYWORDS

cyanobacterial crusts, carbon dioxide fluxes, precipitation amount, precipitation frequency, biological soil crusts

Introduction

According to various climate models, global and local precipitation patterns will change in the context of climate change (Feng and Fu, 2013; Stocker et al., 2014). Precipitation will increase in high-latitude areas and the tropical Pacific areas, similar to the average precipitation in many mid-latitude humid areas; in contrast, average

precipitation will decrease in mid-latitude and subtropical dry areas (Stocker et al., 2014; Yongping and Guoya, 2013); in many areas, changes in precipitation intensity and time distribution (rainfall frequency and interval time) will further be aggravated, and more extreme precipitation events will occur (Solomon et al., 2007; Stocker et al., 2014). Precipitation determines the soil moisture, thus further regulating carbon cycling in terrestrial ecosystems (Huxman et al., 2004; Reed et al., 2012; Zelikova et al., 2012; Maestre et al., 2013; Peng et al., 2013; De Guevara et al., 2014; Escolar et al., 2015). In turn, such changes may feed back to the climate system, exacerbating or slowing down climate changes.

Precipitation drives resource availability and productivity. In arid and semi-arid regions, which account for 41% of the total land area (Reynolds et al., 2007), the soil carbon reserves account for 27% of the global total reserves (Roy and Saugier, 2001). Though not the highest, the carbon flux rate of arid and semi-arid ecosystems contributes significantly to the global carbon budget (Wohlfahrt et al., 2008; Piao et al., 2009; Xie et al., 2009; Peng et al., 2013). Moisture-limited arid and semi-arid ecosystems are, however, unable to support uniform and continuously distributed vegetation with high coverage, while they show a wide distribution of biological soil crusts (BSCs) (Belnap and Lange, 2003). Such crusts, which are the main components of desert ecosystems, are heterogeneous complexes formed by cryptogams (such as cyanobacteria, desert algae, lichens, and mosses) and soil microorganisms, as well as other related organisms, which are cemented with soil surface particles through mycelium, rhizoid, and secretions (Belnap and Lange, 2003; Xinrong et al., 2009; Yuanming and Xueqin, 2010). On the surface of desert areas, BSCs cover approximately 40% of the total area, reaching 70% or more in some regions. They are sensitive to changes in the external environment, especially moisture levels, and their weak source or sink characteristics are prone to directional reversal under the disturbance of rainfall, resulting in great uncertainty in carbon source and sink functions.

Several studies have focused on the effects of precipitation pattern changes (e.g., amount, intensity) on net primary productivity of BSCs, soil respiration and carbon process in arid and semi-arid regions. However, the impact of precipitation time distribution (rainfall frequency and interval time) on carbon processes was largely neglected, and there is a lack of field observations of fixed stations to support studies about carbon processes of BSCs caused by precipitation pattern changes.

The cyanobacterial crust is the primary development stage of BSCs, which is composed of pioneer species in desert areas. The cyanobacterial crust is characterized by high tolerance to extreme environmental conditions, such as drought, strong radiation and low in nutrients. It is widely distributed in harsh environments in arid regions and is one of the important surface cover landscape features of the Ulan Buh Desert, western Inner Mongolia Plateau. In this study, we used the cyanobacterial crust of the Ulan Buh

Desert as the research object to explore the carbon flux process of cyanobacterial crust-covered soil under nine precipitation patterns, involving three frequencies at three amounts, with the aim to provide a scientific basis for the accurate estimation of carbon emission and sequestration by ecosystems in arid regions.

Materials and methods

Site description

The study site was located in Dengkou County (40°9'N~40°57'N, 106°9'E~107°10'E), at the source of the Hetao Plain in western Inner Mongolia, China, and on the eastern edge of the Ulan Buh Desert. The prevailing climate is a temperate continental monsoon climate, with an annual average temperature, precipitation, and evaporation of 7.6°C, 144.5 mm, and 2,397.6 mm, respectively. The soils in the study region are mainly gray-brown desert soil and sandy soil [Cambic Arenosols and Luvic Gypsisols in FAO (Food and Agriculture Organization of the United Nations) taxonomy]. The area is a transitional belt between a desert and steppe, covered with psammophytic vegetation of desert areas.

The BSCs covered above 80% of desert land. The types of BSCs in this region includes cyanobacterial crusts, lichen crusts, and moss crusts. Cyanobacterial crusts account for the largest proportion in the vast majority of sandy land without plant cover. The dominant species in the cyanobacterial crusts are *Microcoleus vaginatus*.

Research methods

Experimental design

According to the assessment report (Stocker et al., 2014), it is estimated that by the end of the 21st century, the annual precipitation in Northwest China will increase by 10–60%, and the changes in precipitation intensity and time distribution in many places will be further aggravated. Therefore, three precipitation amounts were tested: an increase by 30% (6.84 mm), an increase by 60% (8.12 mm), and the average precipitation (5.26 mm) in August during the 30 years from 1986 to 2015 (control). For each of the aforementioned three precipitation amounts, three frequencies were established: a frequency increase by 50% (12 times), a frequency reduction by 50% (3 times), and the average frequency (6 times) in August during the 30 years from 1986 to 2015 (control). A total of nine precipitation patterns (three sizes × three frequencies) were studied (Table 1), with three repetitions for each treatment. On an average, a frequency increase by 50% divided a single precipitation into two, while a frequency reduction by 50% superimposed two adjacent precipitations. The total precipitation amount was the same under

TABLE 1 Factors of the experimental design.

Pattern	30-year average amount	Amount increase by 30%	Amount increase by 60%
Frequency reduction by 50%	A0F-	A30F-	A60F-
30-year average frequency	A0F0	A30F0	A60F0
Frequency increase by 50%	A0F+	A30F+	A60F+

different frequency treatments at the same amount. To avoid interference of natural precipitation, the samples were covered with transparent plastic cloth.

Sample collection

Flat areas, far away from vegetated areas and with well-developed cyanobacterial crusts, were sampled in July 2018. For this, 27 undisturbed soil cores covered with cyanobacterial crusts were collected using a self-made PVC sampler with a diameter of 20.3 cm (area: 0.032 m²) and a height of 20 cm. Prior to sample collection, the crust surface was moistened with distilled water to ensure sample integrity.

Monitoring of NCF and DRR

From the end of July 2018 to the end of August 2018, simulated precipitation experiments were conducted, and the net carbon flux (NCF) and dark respiration rate (DRR) were determined. Six water application experiments were conducted under patterns A0F0, A30F0, and A60F0, with NCF and DRR being determined for each experiment. Three water application experiments were conducted under patterns A0F-, A30F-, and A60F-, with NCF and DRR being determined for each experiment. Twelve water application experiments were conducted under patterns A0F+, A30F+, and A60F+, with NCF and DRR being determined for nine of them (the other three experiments were conducted with water only, and NCF and DRR were not determined).

At 6:00 a.m. on the day of water application, the soil respiration measurement system LI-8150 (LI-COR) was connected to the transparent air chamber to determine NCF prior to water application, and subsequently, the transparent air chamber was covered with opaque cloth to determine DRR. Starting from 7:00 a.m., the calculated amount of water was sprayed slowly and evenly into the soil cores using a watering can to largely avoid runoff. Immediately after watering and after 0, 1, 2, 4, 8, 12, and 24 h, NCF and DRR were determined. For each sample, light and dark measurements were paired, and the paired measurements were taken as simultaneously as possible to avoid a shift in the environmental conditions.

Statistical analysis

The time-weighted method was adopted to calculate the 12-h cumulative net carbon flux (12-h NCF) and the total net

carbon flux (TNCF), as well as the 12-h cumulative carbon release flux (12-h DRR) and the total carbon release flux (TDRR) under nine precipitation patterns. A one-way ANOVA was adopted for variance analysis of 12-h NCF and 12-h DRR. A two-way ANOVA was adopted for variance analysis of TNCF, TDRR, and total photosynthetic carbon sequestration (TPCS). For statistical analysis and mapping, we used the software packages SPSS 20.0, Excel 2010, and R statistical software.

The photosynthetic rate (PR) is calculated based on NCF and DRR:

$$PR = DRR - NCF, \quad (1)$$

where PR is the photosynthetic rate value; the greater the value, the greater the photosynthetic rate and the stronger the carbon sequestration capacity.

Results

Effects of different precipitation patterns on NCF

After water application, the NCF values of all precipitation patterns increased rapidly and peaked at 1 h, followed by a gradual decrease and a return to background levels after 12 h. Among the NCF values before and 24 h after water application, some values were negative, indicating that the cyanobacterial crust sequestered carbon and functioned as a carbon sink (Figure 1).

After the first time of water application, the peak values of NCF under the nine precipitation patterns were 5.09 (A0F-), 5.46 (A30F-), 7.26 (A60F-), 5.31 (A0F0), 5.61 (A30F0), 5.87 (A60F0), 3.83 (A0F+), 3.62 (A30F+), and 3.93 (A60F+) $\mu\text{mol m}^{-2} \text{ s}^{-1}$, respectively. Nevertheless, after the last time of water application, the peak values were 2.19 (A0F-), 2.1 (A30F-), 1.75 (A60F-), 2.28 (A0F0), 1.75 (A30F0), 2.9 (A60F0), 0.71 (A0F+), 1.15 (A30F+), and 1.48 (A60F+) $\mu\text{mol m}^{-2} \text{ s}^{-1}$, respectively, showing a large reduction (50–80%) compared to the first time.

For clearly comparing the changes of net carbon flux among different precipitation patterns, we calculated the 12-NCF after every water application and took the average. We found the 12-h

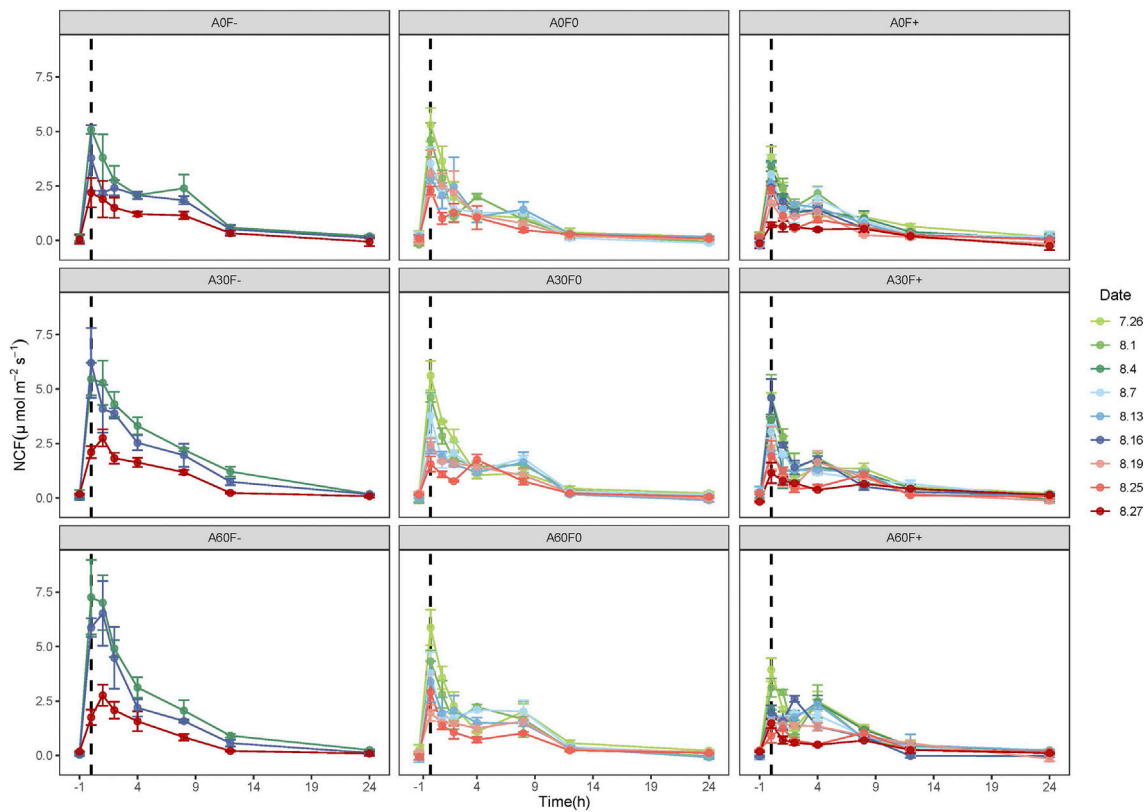


FIGURE 1 Dynamics of NCF in soil covered with cyanobacterial crust. -1 is the value determined before water application, and 7.26, and 8.1, etc., are the experimental dates. NCF: net carbon flux.

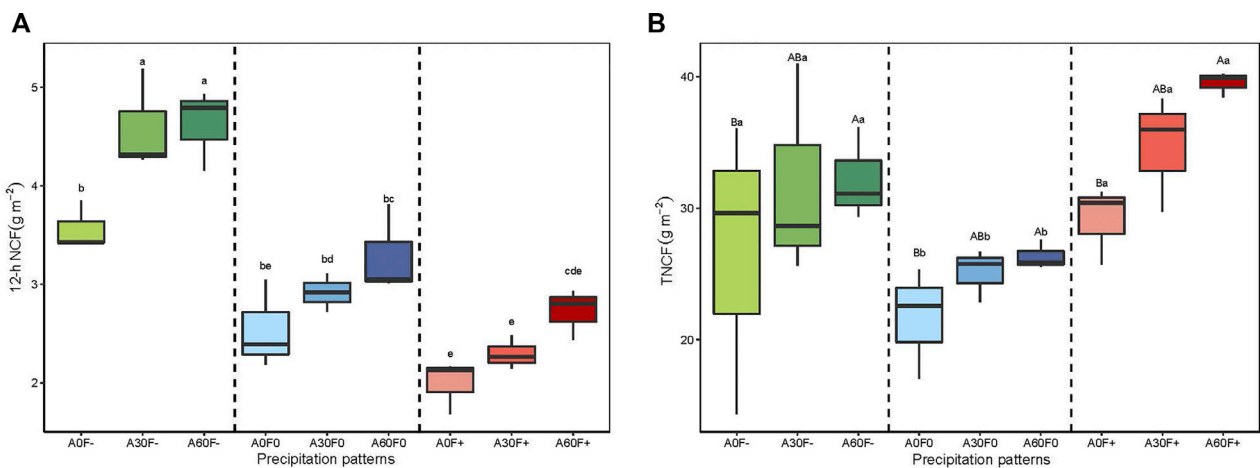


FIGURE 2 (a) 12-h NCF of soil covered with cyanobacterial crust; (b) TNCF of soil covered with cyanobacterial crust; statistically significant differences in precipitation amount are denoted with capital letters whereas statistically significant differences of precipitation frequency are denoted with lowercase letters. 12-h NCF: 12-h cumulative net carbon flux; TNCF: total net carbon flux.

TABLE 2 Variance analysis of effects of precipitation amount and frequency on TNCF, TDRR, and TPCS.

Source	TNCF			TDRR			TPCS		
	df	F	P	df	F	P	df	F	P
Frequency	2	8.090	0.003	2	13.78	0.00	2	0.144	0.867
Amount	2	3.915	0.039	2	6.60	0.01	2	0.109	0.897
Frequency * amount	4	0.285	0.884	4	0.74	0.58	4	0.070	0.990

Note: TNCF: total net carbon flux; TDRR: total carbon release flux; TPCS: total photosynthetic carbon sequestration.

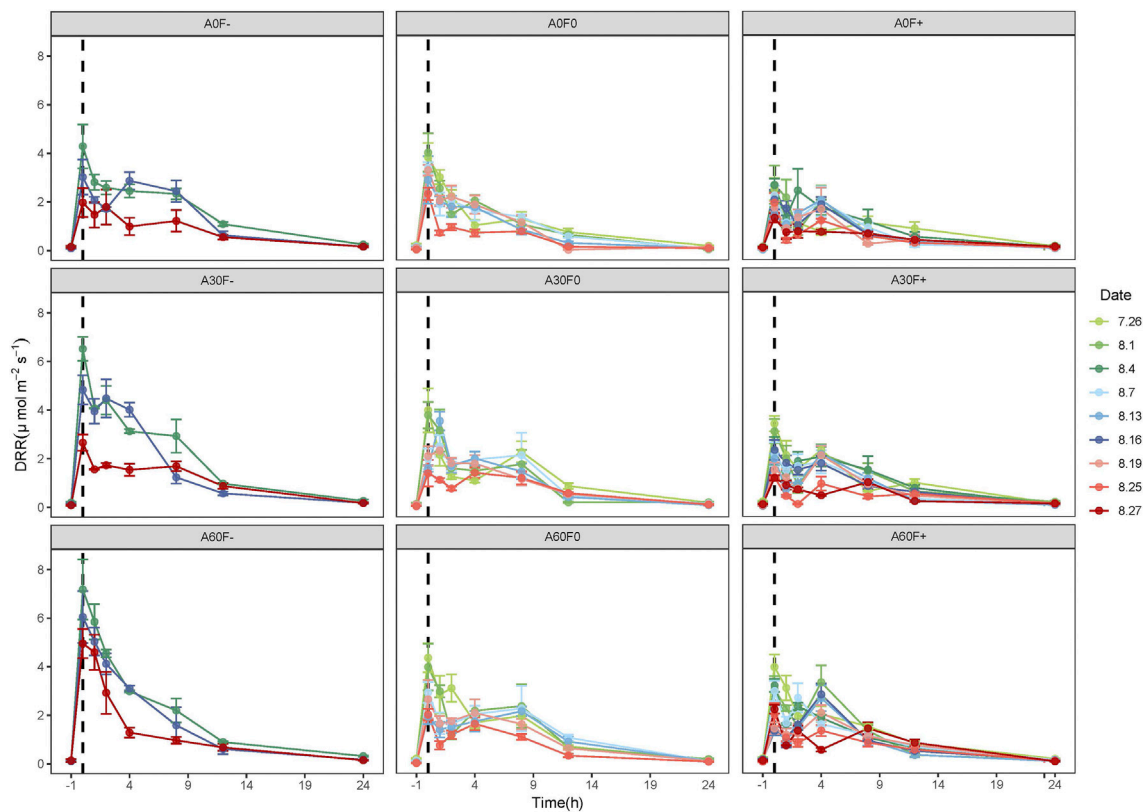
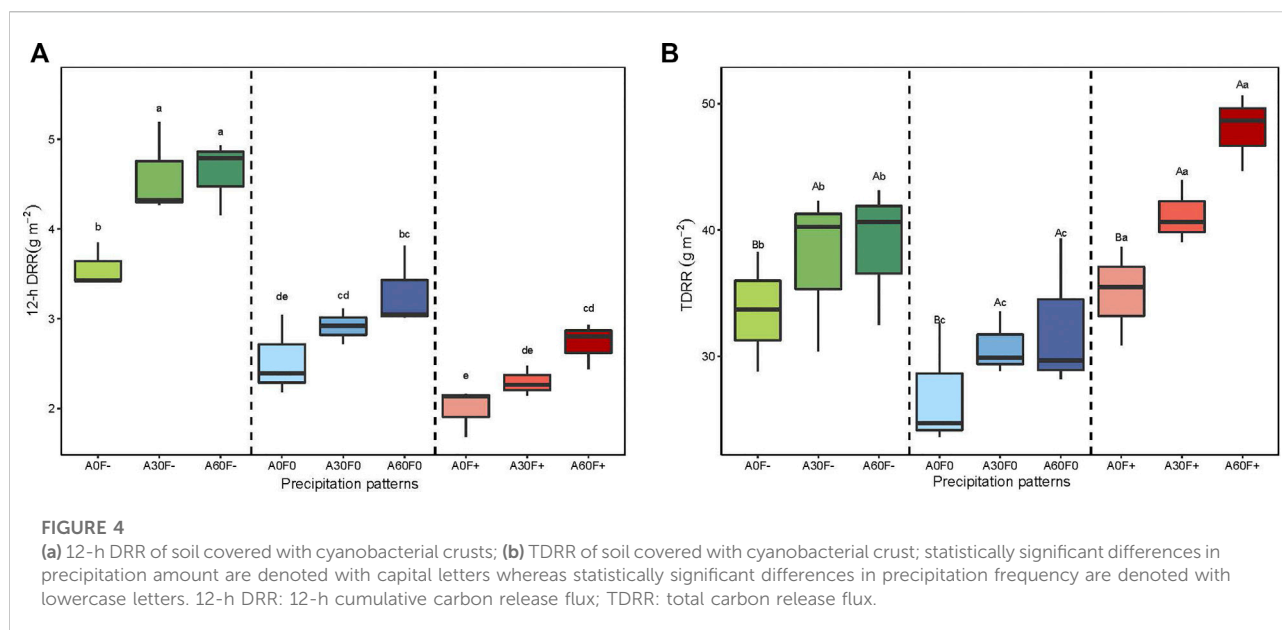


FIGURE 3 Dynamics of DRR in soil covered with cyanobacterial crust. -1 is the value determined before water application; 7.26, and 8.1, etc., are the experimental dates. DRR: dark respiration rate.

NCF had a negative relationship with precipitation frequency (−50% > normal > +50%) (Figure 2). Under −50% frequency treatment, the 12-h NCF of +30% and +60% amount were significantly higher than normal ($p < 0.05$). However, under +50% frequency and normal frequency treatments, the 12-h NCF were not significantly different ($p > 0.05$). With the increase of water application times, the 12-h NCF showed a decreasing trend under all precipitation patterns. Compared with the first time, the

12-h NCF after the last time water application was decreased by 38–63%.

To compare the carbon flux across the whole experiment period, we use the weighted average method to calculate TNCF. We found that the TNCF values of +50% frequency and −50% frequency treatments were significantly higher than that in normal frequency ($p < 0.05$) whereas there is no significant difference between +50% frequency and −50% frequency



($p > 0.05$). At the same frequency, the TNCF in treatments of +60% amount was significantly higher than normal amount ($p < 0.05$) (Figure 2). However, two-way anova analysis showed that individual precipitation amount and frequency has significant effects on TNCF ($p < 0.05$), but they did not show significant interactive effects (Table 2, $p > 0.05$).

Effects of different precipitation patterns on DRR

Precipitation can significantly stimulate soil respiration. Under the nine different precipitation patterns, DRR significantly increased after water application, reaching a peak value within 1 h and then gradually decreased, reaching background levels about 12 h after water application (Figure 3).

With the increase of water application times, peak values of DRR under the nine patterns had a similar decreasing trend to that of NCF. After first time water application, the peak values of DRR were 4.29 (A0F-), 6.52 (A30F-), 7.18 (A60F-), 3.82 (A0F0), 3.98 (A30F0), 4.38 (A60F0), 2.51 (A0F+), 3.42 (A30F+), and 4.20 (A60F+) $\mu\text{mol m}^{-2} \text{s}^{-1}$, respectively. After last time water application, the peak values of DRR were 2.17 (A0F-), 2.66 (A30F-), 5.66 (A60F-), 2.32 (A0F0), 1.89 (A30F0), 2.08 (A60F0), 1.40 (A0F+), 1.27 (A30F+), and 2.23 (A60F+) $\mu\text{mol m}^{-2} \text{s}^{-1}$, with a reduction of 40–60% compared to the first time (Figure 3).

Similar to NCF, the 12-h DRR also had a negative relationship with precipitation frequency ($-50\% > \text{normal} > +50\%$). Under normal and +50% frequency treatment, the 12-h DRR increased along with increasing amount, and the 12-h DRR of amount +60% was significantly greater than that +30% and

normal ($p < 0.05$). Under -50% frequency treatment, the following order was observed: +60% amount $>$ +30% amount $>$ normal amount, and the difference between the amounts was statistically significant ($p < 0.05$) (Figure 4). With the increase of water application times, the 12-h DRR showed a decreasing trend under all precipitation patterns. Compared with the first time, the 12-h DRR after the last time water application was decreased by 33–52%.

At the same amount, the TDRR at the three frequencies showed the following order: +50% frequency $>$ -50% frequency $>$ normal frequency; the levels significantly differed among the different frequencies. At the same frequency, The TDRR increased with increasing amount, the TDRR in treatments of +30 and +60% amount were significantly greater than normal amount ($p < 0.05$) (Figure 4). However, two-way anova analysis showed that individual precipitation amount and frequency significantly affected TDRR ($p < 0.05$), but without an interactive effect ($p > 0.05$) (Table 2).

Effects of different precipitation patterns on carbon sequestration

As shown in Figure 5, PR generally showed an upward trend after water application, reaching the maximum value about 4 h after water application and gradually falling to background levels after 12 h. Among them, the values of PR at 0 h after water application were positive under A30F-, A60F-, and A60F+, with the carbon sequestration rate first decreasing and reaching the minimum value at the first hour, followed by a gradual increase. There was no significant difference in the effects of amount,

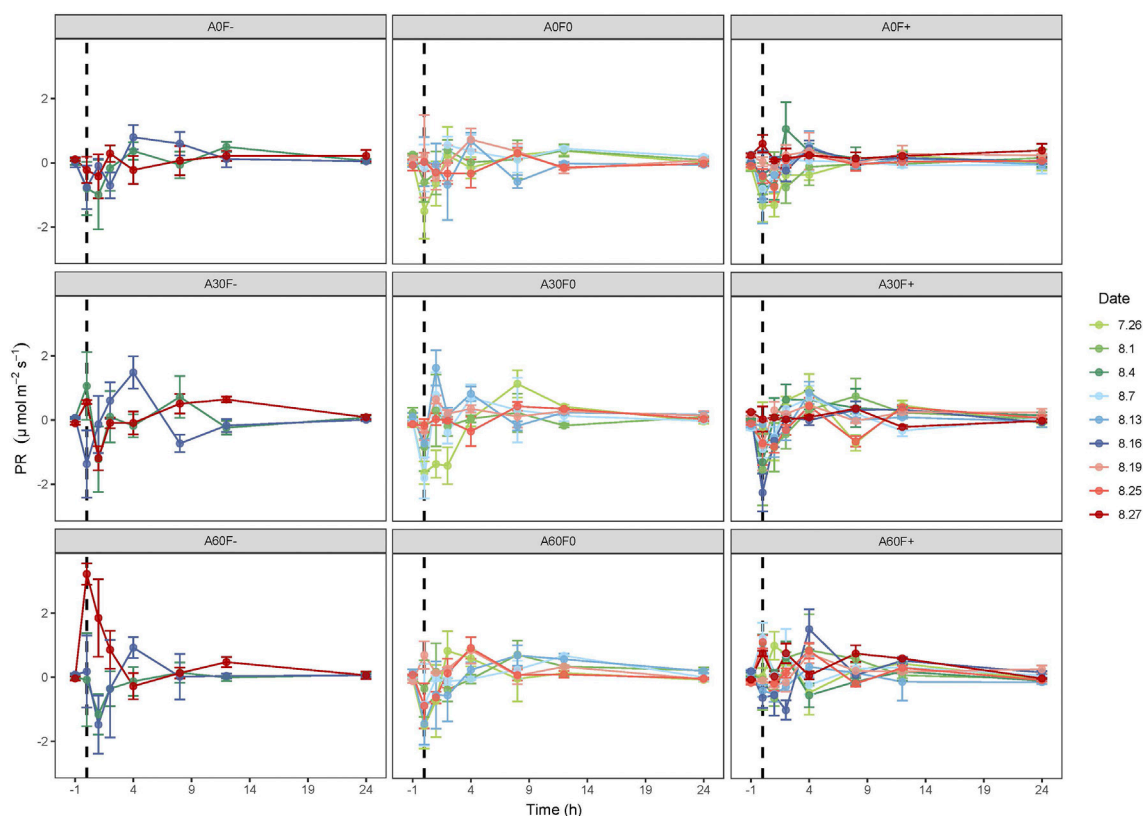


FIGURE 5

Dynamics of PR of the cyanobacterial crust. -1 is the value determined before water application; 7.26, and 8.1, etc., are the experimental dates. PR: photosynthetic rate.

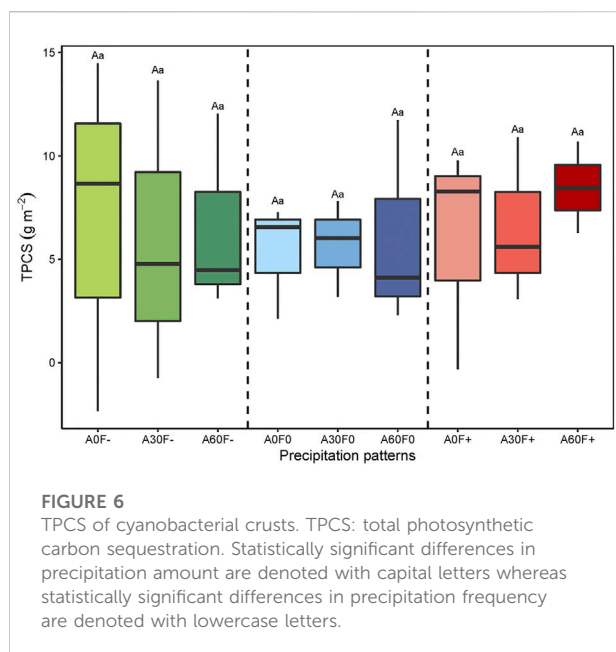
frequency, and their interaction on TPCS ($p > 0.05$) (Figure 6, Table 2).

Discussion

In arid regions, moisture is the main limiting factor for biological activities. Precipitation can directly alternating soil moisture, which will affect the soil carbon cycling and cause the changes of soil carbon stock. In this study, the results showed that precipitation could stimulate NCF and DRR and then they gradually decreased to background level. This finding is consistent with previous observations (Sponseller, 2007; Xiaohong et al., 2016). This could be attributed to two main reasons: first, organisms in cyanobacterial crust were very sensitive to water. Under the dry condition, cyanobacterial crust will enter to a dormant state, but after water application, physiological activities and respirations of it could quickly recover. Secondly, arid region has the loose soil, so amount of CO_2 might potentially accumulate in soil gaps, which would be discharged when rainwater infiltrated.

Previous studies have found that the carbon emissions of biological crust areas increased with increasing precipitation amounts (Housman et al., 2007; Thomas et al., 2008; Thomas and Hoon, 2010; Castillo-Monroy et al., 2011; Feng et al., 2013). Consistently, in our study, 12-h NCF and 12-h DRR, TNCF and TDRR of cyanobacterial crust and underlying soil also showed increased with the increase of individual water application amount at the same frequency. However, when the amount increased to a certain extent, it no longer had an obvious acceleration effect on soil carbon emissions. In our experiment, for 12-h NCF and 12-h DRR under -50% frequency treatment and TDRR, +30% (A30F-) and +60% (A60F-) amount were significantly greater than normal amount (A0F-) ($p < 0.05$), but the difference between A30F- and A60F- was not significant ($p > 0.05$). There is an optimal level of hydration for biocrust organisms (NASH III, 1996; Lange, 2001), high precipitation amounts increase diffusional resistance and decrease CO_2 availability to crust (Grote et al., 2010).

In addition to precipitation amount, precipitation frequency also had significant effects on the carbon processes of BSCs. Precipitation frequency disturbs carbon exchange modes by



affecting the dry-wet alternation of the soil (Reed et al., 2012). In this study, we observed that 12-h NCF and 12-h DRR decreased with increased water application frequency, which was mainly due to the large evaporation in arid regions. In this region, lower water application amount in high water application frequency can only moisten the soil surface and the water from water application will be evaporated in a short time, so soil and cyanobacterial crust could not utilize it, causing the decrease of carbon emission. However, for the entire experiment period, under the same precipitation amount, TNCF and TDRR did not showed a decreased trend with increased water application frequency. Specifically, TNCF and TDRR in high-frequency treatments were highest, followed by low-frequency and then normal-frequency treatments. This may be due to a synergetic effect between the individual precipitation amount, the precipitation frequency, and other environmental factors such as antecedent moisture, temperature (Baldauf et al., 2018).

Precipitation significantly promoted the soil carbon emission rate and increased cumulative carbon emissions, but with the increase in precipitation times, that is, with more dry-wet alternations, this effect was gradually weakened. Our results has found that most of the increased water application amount treatments significantly promoted soil carbon emission rate (represented by NCF and DRR), and cumulative carbon emissions (represented by 12-NCF, TNCF, 12-DRR and TDRR). However, with the increase of water application time, the peak values of NCF, DRR, 12-h NCF, and 12-h DRR decreased along with the increase in dry-wet alternation times. This significant increased effect was gradually weakened. This may be due to the changes in available organic matter, microbial biomass, and

microbial community structure in the soil through continuous dry-wet alternations. On the one hand, after repeated dry-wet alternations, the stability of soil aggregates was improved, and the amount of organic matter released therefrom was reduced (Denef et al., 2001). On the other hand, with further dry-wet alternations, the composition of the microbial community reestablished in the soil changed as a response to changes in the soil water potential (Mikha et al., 2005), reducing its sensitivity to changes in water potential. As a consequence, the mortality of microorganisms was reduced, thus reducing the active organic matter available to microorganisms.

Previous studies have found that BSCs responded quickly to precipitation. The photosynthetic process of BSCs could start within 10 min even under a small amount of precipitation and could maintain photosynthetic capacity. In addition, the photosynthetic rate is very likely to show an increased trend first and then decrease (Lange et al., 1994; Brostoff et al., 2005; Grote et al., 2010; Feng et al., 2014). Consistently, in our study, the photosynthetic rate of cyanobacterial crusts also peaked about 4 h after water application and then gradually decreased to background levels. This is likely because cyanobacterial crusts are generally in a dormant state under water limitation condition and metabolism of photosynthetic process would start rapidly once the environment becomes wet. However, photosynthetic carbon sequestration capacity is weak and discontinuous. In addition, the crusts also respire while photosynthesizing, and its respiration rate is greater than its photosynthetic rate at the early stage after water application.

With regard to NCF between soil and the atmosphere, our result showed that NCF value was positive, indicating that CO_2 which was fixed from atmosphere could not offset its emission. However, we also found NCF values of some crusted areas were negative, indicating that carbon fixation process existed in these areas. In addition, we found this phenomenon always occurred in the morning. Previous research has found that BSCs can rapidly restore their metabolism with 0.1 mm of water (Lange et al., 1994). In dry region, dew, fog, and even greater air humidity could be main water sources for photosynthetic process (Lange et al., 1997). Thus, this is probably due to condensed water and lower temperatures in the morning. Specifically, condensed water facilitated photosynthetic process, while the lower temperatures inhibited soil respiration in the morning. Consequently, carbon could be sequestered in the morning.

Furthermore, with the increase in annual precipitation, the annual carbon sequestration of BSCs showed an increasing trend (Yoshitake et al., 2010; Coe and Sparks, 2014; Feng et al., 2014). Similarly, the TPCS which represented annual carbon sequestrations in our study also increased with increasing precipitation amounts, but the individual effects of precipitation and frequency, and interaction effects of these two factors were all not significant on TPCS. This may be due to the low carbon sequestration capacity of cyanobacterial crusts, as well as the experimental period.

Conclusion

Precipitation had a significant stimulating effect on soil carbon emission. Both precipitation amount and frequency significantly affected cumulative carbon emissions, but without an interactive effect. Under the same precipitation frequency, cumulative carbon emissions increased with increasing precipitation amount. However, when precipitation amount increased to a certain extent, it no longer accelerated soil carbon emission. Under the same precipitation amount, cumulative carbon emissions caused by high-frequency events were highest, followed by those of low-frequency precipitation and the control. For individual water application, the carbon emissions caused by low-frequency heavy events were significantly greater than those caused by high-frequency light events. Another important finding was that the stimulating effect of precipitation to soil carbon emissions decreased with the increase of water application times. Changes in precipitation amount and frequency caused by global climate change will increase carbon emissions of cyanobacterial crusts and underlying Soil, suggesting that cyanobacteria should be considered in projections of the future carbon budget.

Data Availability Statement

The raw data supporting the conclusion of this article will be made available by the authors, without undue reservation.

Author contributions

LW wrote the main manuscript. YG prepared figures, and reviewed the manuscript. XC and WL reviewed the manuscript.

References

- Baldauf, S., de Guevara, M. L., Maestre, F. T., and Tietjen, B. (2018). Soil moisture dynamics under two rainfall frequency treatments drive early spring CO₂ gas exchange of lichen-dominated biocrusts in central Spain. *PeerJ* 6, e5904. doi:10.7717/peerj.5904
- Belnap, J., and Lange, D. H. C. O. L. (2003). *Biological soil crusts: Structure, function, and management*. Berlin Heidelberg: Springer.
- Brostoff, W. N., Sharifi, M. R., and Rundel, P. W. (2005). Photosynthesis of cryptobiotic soil crusts in a seasonally inundated system of pans and dunes in the Western Mojave Desert, CA: Field studies. *Flora-Morphology Distribution Funct. Ecol. Plants* 200, 592–600. doi:10.1016/j.flora.2005.06.008
- Castillo-Monroy, A. P., Maestre, F. T., Rey, A., Soliveres, S., and García-Palacios, P. (2011). Biological soil crust microsites are the main contributor to soil respiration in a semiarid ecosystem. *Ecosystems* 14, 835–847. doi:10.1007/s10021-011-9449-3
- Coe, K. K., and Sparks, J. P. (2014). Physiology-based prognostic modeling of the influence of changes in precipitation on a keystone dryland plant species. *Oecologia* 176, 933–942. doi:10.1007/s00442-014-3067-7
- De Guevara, M. L., Lazaro, R., Quero, J. L., Ochoa, V., Gozalo, B., Berdugo, M., et al. (2014). Simulated climate change reduced the capacity of lichen-dominated biocrusts to act as carbon sinks in two semi-arid Mediterranean ecosystems. *Biodivers. Conserv.* 23, 1787–1807. doi:10.1007/s10531-014-0681-y
- Denef, K., Six, J., Bossuyt, H., Frey, S. D., Elliott, E. T., Merckx, R., et al. (2001). Influence of dry-wet cycles on the interrelationship between aggregate, particulate organic matter, and microbial community dynamics. *Soil Biol. Biochem.* 33, 1599–1611. doi:10.1016/S0038-0717(01)00076-1
- Escolar, C., Maestre, F. T., and Rey, A. (2015). Biocrusts modulate warming and rainfall exclusion effects on soil respiration in a semi-arid grassland. *Soil Biol. Biochem.* 80, 9–17. doi:10.1016/j.soilbio.2014.09.019
- Feng, S., and Fu, Q. (2013). Expansion of global drylands under a warming climate. *Atmos. Chem. Phys.* 13, 10081–10094. doi:10.5194/acp-13-10081-2013
- Feng, W., Zhang, Y. Q., Wu, B., Zha, T. S., Jia, X., Qin, S. G., et al. (2013). Influence of disturbance on soil respiration in biologically crusted soil during the dry season. *Sci. World J.* 2013, 1–6. doi:10.1155/2013/408560

Funding

This research was funded by the general fund from the National Natural Science Foundation of China (NO. 41971398), the central public welfare scientific research institutes Special fund for basic scientific research business expenses (No. CAFYBB2020ZB007), the special program for basic resources of the Ministry of science and technology (NO. 2019FY102002), Fundamental Research Funds for the Central Nonprofit Research Institution of Chinese Academy of Forestry (CAFYBB2017QA038).

Acknowledgments

The authors thank the Experimental Center of Desert Forestry, Chinese Academy of Forestry, for providing the 30-year precipitation and frequency data of the region of interest from 1986 to 2015.

Conflict of Interest

The authors declare that the research was conducted in the absence of any commercial or financial relationships that could be construed as a potential conflict of interest.

Publisher's Note

All claims expressed in this article are solely those of the authors and do not necessarily represent those of their affiliated organizations, or those of the publisher, the editors, and the reviewers. Any product that may be evaluated in this article, or claim that may be made by its manufacturer, is not guaranteed or endorsed by the publisher.

- Feng, W., Zhang, Y., Wu, B., Qin, S., and Lai, Z. (2014). Influence of environmental factors on carbon dioxide exchange in biological soil crusts in desert areas. *Arid Land Res. Manag.* 28, 186–196. doi:10.1080/15324982.2013.835006
- Grote, E. E., Belnap, J., Housman, D. C., and Sparks, J. P. (2010). Carbon exchange in biological soil crust communities under differential temperatures and soil water contents: Implications for global change. *Glob. Change Biol.* 16, 2763–2774. doi:10.1111/j.1365-2486.2010.02201.x
- Housman, D., Grote, E., and Belnap, J. (2007). “Annual CO₂ flux from a biological soil crust system on the Colorado Plateau: effects of increased temperature and summer precipitation,” in *Ecological society of America annual meeting abstracts* (Washington: Ecological Society of America).
- Huxman, T. E., Snyder, K. A., Tissue, D., Leffler, A. J., Ogle, K., Pockman, W. T., et al. (2004). Precipitation pulses and carbon fluxes in semiarid and arid ecosystems. *Oecologia* 141, 254–268. doi:10.1007/s00442-004-1682-4
- Lange, O. L. (2001). “Photosynthesis of soil-crust biota as dependent on environmental factors,” in *Biological soil crusts: structure, function, and management* (Springer), 217–240. doi:10.1007/978-3-642-56475-8_18
- Lange, O. L., Belnap, J., Reichenberger, H., and Meyer, A. (1997). Photosynthesis of green algal soil crust lichens from arid lands in southern Utah, USA: Role of water content on light and temperature responses of CO₂ exchange. *Flora* 192, 1–15. doi:10.1016/s0367-2530(17)30749-1
- Lange, O., Meyer, A., Zellner, H., and Heber, U. (1994). Photosynthesis and water relations of lichen soil crusts: Field measurements in the coastal fog zone of the namib desert. *Funct. Ecol.* 8, 253–264. doi:10.2307/2389909
- Maestre, F. T., Escobar, C., Guevara, M. L., Quero, J. L., Lazaro, R., Delgado-Baquerizo, M., et al. (2013). Changes in biocrust cover drive carbon cycle responses to climate change in drylands. *Glob. Chang. Biol.* 19, 2697–2698. doi:10.1111/gcb.12659
- Mikha, M. M., Rice, C. W., and Milliken, G. A. (2005). Carbon and nitrogen mineralization as affected by drying and wetting cycles. *Soil Biol. Biochem.* 37, 339–347. doi:10.1016/j.soilbio.2004.08.003
- NASH III, T. (1996). *Photosynthesis, respiration, productivity and Lichen biology*, 88–120.
- Peng, S., Piao, S., Shen, Z., Ciais, P., Sun, Z., Chen, S., et al. (2013). Precipitation amount, seasonality and frequency regulate carbon cycling of a semi-arid grassland ecosystem in inner Mongolia, China: A modeling analysis. *Agric. For. Meteorology* 178–179, 46–55. doi:10.1016/j.agrformet.2013.02.002
- Piao, S., Yin, L., Wang, X., Ciais, P., Peng, S., Shen, Z., et al. (2009). Summer soil moisture regulated by precipitation frequency in China. *Environ. Res. Lett.* 4, 044012. doi:10.1088/1748-9326/4/4/044012
- Reed, S. C., Coe, K. K., Sparks, J. P., Housman, D. C., Zelikova, T. J., and Belnap, J. (2012). Changes to dryland rainfall result in rapid moss mortality and altered soil fertility. *Nat. Clim. Chang.* 2, 752–755. doi:10.1038/nclimate1596
- Reynolds, J. F., Smith, D. M. S., Lambin, E. F., Turner, B. L., Mortimore, M., Batterbury, S. P. J., et al. (2007). Global desertification: Building a science for dryland development. *Science* 316, 847–851. doi:10.1126/science.1131634
- Roy, J., and Saugier, B. (2001). *Terrestrial global productivity*. Amsterdam, Netherlands: Elsevier, 122–598.
- Solomon, S., Manning, M., Marquis, M., and Qin, D. (2007). *Climate change 2007-the physical science basis: Working group I contribution to the fourth assessment report of the IPCC*, 4. Cambridge University Press, Cambridge, United Kingdom.
- Sponseller, R. A. (2007). Precipitation pulses and soil CO₂ flux in a Sonoran Desert ecosystem. *Glob. Chang. Biol.* 13, 426–436. doi:10.1111/j.1365-2486.2006.01307.x
- Stocker, T. F., Qin, D., Plattner, G. K., Tignor, M. M. B., Allen, S. K., Boschung, J., et al. IPCC (2014). *Climate change 2013: the physical science basis. Contribution of working group I to the fifth assessment report of the intergovernmental panel on climate change*. Cambridge University Press, Cambridge, United Kingdom. doi:10.1017/CBO9781107415324
- Thomas, A. D., and Holon, S. R. (2010). Carbon dioxide fluxes from biologically-crusted Kalahari Sands after simulated wetting. *J. arid Environ.* 74, 131–139. doi:10.1016/j.jaridenv.2009.07.005
- Thomas, A. D., Hoon, S. R., and Linton, P. E. (2008). Carbon dioxide fluxes from cyanobacteria crusted soils in the Kalahari. *Appl. Soil Ecol.* 39, 254–263. doi:10.1016/j.apsoil.2007.12.015
- Wohlfahrt, G., Fenstermaker, L., and Arnone, J., Iii (2008). Large annual net ecosystem CO₂ uptake of a Mojave Desert ecosystem. *Glob. Change Biol.* 14, 1475–1487. doi:10.1111/j.1365-2486.2008.01593.x
- Xiaohong, J., Chen, G., Bo, W., Yuanshou, L., Long, C., and Xinrong, L. (2016). Responses of carbon dioxide fluxes from biological soil crusted soils to pulse rain in arid desert ecosystem. *J. desert Res.* 036, 423–432. doi:10.7522/j.issn.1000-694X.2015.00199
- Xie, J., Li, Y., Zhai, C., Li, C., and Lan, Z. (2009). CO₂ absorption by alkaline soils and its implication to the global carbon cycle. *Environ. Geol.* 56, 953–961. doi:10.1007/s00254-008-1197-0
- Xinrong, L., Yuanming, Z., and Yunge, Z. (2009). A study of biological soil crusts: Recent development, trend and prospect. *Adv. nearth science* 24, 11–24. doi:10.11867/j.issn.1001-8166.2009.01.0011.
- Yongping, S., and Guoya, W. (2013). Key findings and assessment results of IPCC WGI fifth assessment Report. *J. Glaciol. Geocryol.* 35, 1068–1076. doi:10.7522/j.issn.1000-0240.2013.0120
- Yoshitake, S., Uchida, M., Koizumi, H., Kanda, H., and Nakatsubo, T. (2010). Production of biological soil crusts in the early stage of primary succession on a High Arctic glacier foreland. *New Phytol.* 186, 451–460. doi:10.1111/j.1469-8137.2010.03180.x
- Yuanming, Z., and Xueqin, W. (2010). Summary on formation and developmental characteristics of biological soil crusts in desert areas. *Acta Ecol. Sin.* 30, 4484–4492. doi:10.1016/S1872-5813(11)60001-7
- Zelikova, T. J., Housman, D. C., Grote, E. E., Neher, D. A., and Belnap, J. (2012). Warming and increased precipitation frequency on the Colorado plateau: Implications for biological soil crusts and soil processes. *Plant Soil* 355, 265–282. doi:10.1007/s11104-011-1097-z



OPEN ACCESS

EDITED BY
Hamid Gholami,
University of Hormozgan, Iran

REVIEWED BY
Shengbo Xie,
Northwest Institute of Eco-
Environment and Resources (CAS),
China
Xiaojing Qin,
Henan Polytechnic University, China

*CORRESPONDENCE
Xianying Xu,
xyingxu@163.com

SPECIALTY SECTION
This article was submitted to Drylands,
a section of the journal
Frontiers in Environmental Science

RECEIVED 02 May 2022
ACCEPTED 14 September 2022
PUBLISHED 31 October 2022

CITATION
Zhao P, Xu X, Tang J and Jiang S (2022),
Relationship between species
distribution of sandy alpine grasslands
and microtopography in the source
regions of Yangtze river.
Front. Environ. Sci. 10:934483.
doi: 10.3389/fenvs.2022.934483

COPYRIGHT
© 2022 Zhao, Xu, Tang and Jiang. This is
an open-access article distributed
under the terms of the [Creative
Commons Attribution License \(CC BY\)](#).
The use, distribution or reproduction in
other forums is permitted, provided the
original author(s) and the copyright
owner(s) are credited and that the
original publication in this journal is
cited, in accordance with accepted
academic practice. No use, distribution
or reproduction is permitted which does
not comply with these terms.

Relationship between species distribution of sandy alpine grasslands and microtopography in the source regions of Yangtze river

Peng Zhao^{1,2,3}, Xianying Xu^{1,4*}, Jinnian Tang⁴ and
Shengxiu Jiang¹

¹State Key Laboratory Breeding Base of Desertification and Aeolian Sand Disaster Combating, Gansu Desert Control Research Institute, Lanzhou, China, ²Key Laboratory of Desert and Desertification, Chinese Academy of Sciences, Lanzhou, China, ³Collaborative Innovation Center for Western Ecological Safety, Lanzhou University, Lanzhou, China, ⁴Gansu Minqin National Field Observation & Research Station on Ecosystem of Desert Grassland, Minqin, China

Dynamic of sandy alpine grasslands affect the progress and reversal of desertification in source regions of the Yangtze Rivers. To understand geomorphic driving mechanism of species distribution pattern, we examined the species compositions and delineated the most important landform factors influencing species distribution of sandy alpine grassland using two-way indicator species analysis (TWINSPAN), detrended correspondence analysis (DCA), and canonical correspondence analysis (CCA). Field survey were conducted in summer of 2016 using stratified random methods in hilly sloped lands, floodplains, foothills, and valley land of study region. In total, 29 plant species grouped into 27 genera and 16 families were identified. *Leymus secalinus*, *Elymus dahuricus* and *Corispermum declinatum* are the dominant species of sandy alpine grassland communities in different microtopography. The present vegetation reflected xerosere character, which indicated that desertification of alpine grassland is in progress. Standard frequency distribution of species varied with different microtopography, the proportion of dominant species was generally lower than rare species, and the vegetation community was in a highly successional stage. Seven groups were distinguished through TWINSPAN, distribution of which in the DCA ordination graph showed species with similar ecotype is clustered together. The results of the CCA ordination revealed that slope and aspect are the dominant factors among microtopography determining the species distribution of sandy alpine grassland.

KEYWORDS

species distribution, TWINSPAN, DCA, CCA, microtopography, sandy alpine grassland

Introduction

The Qinghai-Tibet Plateau is the concentrated and largest distribution area of Alpine Grassland in the world (Miehe et al., 2011). It is also an important gene pool of alpine biological resources and one of the 34 hot spots of global biodiversity conservation. Alpine grassland is not only an important pasture for herdsman in Qinghai-Tibet Plateau, but also has many ecological services, such as soil and water conservation, climate regulation and so on, which affect the ecological security of the surrounding areas and even the central and eastern part of China. However, affected by global climate change and human activities, the Tibetan Plateau has become the key area of desertification development in recent decades (Dong, 1999; Yan et al., 2000; Cui and Graf 2009; Gao et al., 2015). Specifically, climate warming, permafrost thawing, over-grazing and drainage of water systems all have been responsible for the aeolian desertification (Xue et al., 2009; Dong et al., 2010; Yang et al., 2010). Vegetation is the most common and most reliable stabilizer of shifting sand. Its dynamics are essential to the development and adverse processes of desertification in the Tibetan Plateau (Yan et al., 2004; Duran and Herrmann 2006). The degradation of soil and vegetation in desertified grassland interacts with negative feedback effects (Zhao et al., 2012). With the development of desertification, species compositions and productivity of vegetation change obviously (Zhao et al., 2011). Meanwhile, soil coarsening, looseness, organic matter, and nutrient content decreased, habitat heterogeneity increased, shrub invasion was obvious, and community structure tended to be simplified (Xu and Lv, 2011). Degeneration of grassland led to desertification and frequently induced dust storms (Wang et al., 2008). In 2010, the area of wind erosion land was 374,785 km², accounting for 15% of the total plateau (Dong et al., 2017). The degradation of alpine grassland and decline of productivity caused by desertification seriously threatened the ecological security of the Tibetan Plateau.

The interaction between landforms and vegetation processes are more developmentally intertwined at multiple spatial and temporal scales (Okin et al., 2006; Stallins 2006). The fluidity of sand draft activity in the aeolian landform affects the succession of vegetation by reshaping the micro-geomorphology (Zhao and Wang, 2005). Topography determines the strategies of colonization and survival of plant communities (Hernández-Cordero et al., 2015), vegetation association and succession patterns (Hesp et al., 2011). Under certain small-scale conditions of climate and soil, topographical elements (slope, aspect, slope position) indirectly affect plant growth dynamics and species distribution through redistribution of light, accumulated temperature, soil moisture and nutrients (Fand et al., 2012). The micro-geomorphological changes in the grassland have obvious effects on habitat heterogeneity (Urant et al., 2008). The difference of sand draft activity and soil moisture, pH, and total salt content in different parts of dune is an important influencing factor for the difference of plant communities in paradise sand dunes and *Nitraria tangutorum* brushwood (Zhang, et al., 2017). The fixation of dunes resulted in a closer interspecific relationship between the

lowland plants (Wang, et al., 2010). However, the relationship and mechanism between physical processes of desertification, especially aeolian micro-geomorphology and biological processes, are not clear (Wang J. B. et al., 2013). Thus, it is pressing need to examine species-landforms relationship of sandy alpine grassland for combating the desertification in source regions of the Yangtse rivers.

To this end, this paper focused on the compositions and distribution of desertified alpine grassland in different microtopography with methods of quantitative ecology. We hope to reveal the most important topographic factor affecting the patterns of sandy alpine grassland, and provide scientific basis for the restoration of sandy alpine grassland in the Yangtze River source.

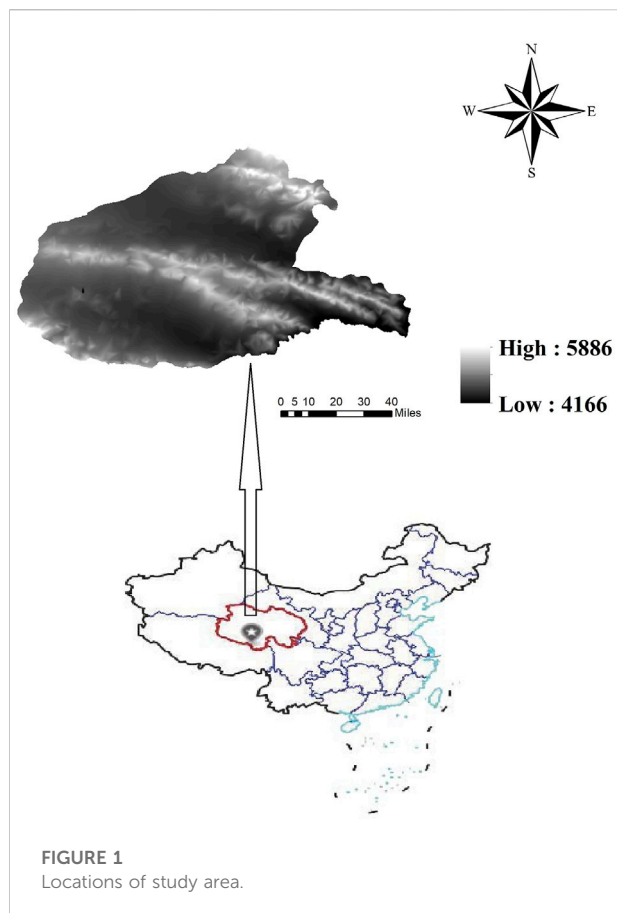
Data and methods

Discription of the study area

Since the implementation of ecological protection and construction project, the regional ecological environment of three river sources area have been significantly improved, and the degradation trend of grassland has been basically controlled. However, the degradation of grassland in the Yellow River and the Yangtze River is still relatively severe. Grassland degradation in Maduo County and Qumalai County being the most obvious (Xu, et al., 2017). Located in the southwestern part of Qinghai Province, Qumalai County is the main source of water conservation in the two major river systems in China. The average elevation in the county is more than 4,500 m, the annual average temperature is -3.3°C, and the average annual precipitation is 380–470 mm, which is an alpine continental climate. The degradation of alpine grassland caused by desertification in Qumalai county is serious. Based on the demonstration project of desertification control of Qinghai Provincial Forestry Department in 2016, the comprehensive recovery experiment of engineering and seeding was carried out in the desertification area of Qidukou alpine grassland. According to the law of sand draft activity in the study area, the HDPE sand barrier was laid to fix the mobile sand dunes. In the spring, *Poa annua*, *Elymus sibiricus*, and *Elymus dahuricus* were planted in the sand barrier area to artificially restore sandy grassland. The grassland types are mainly *Stipa steppe* and alpine meadow. The dominant species are *Kobresia pygmaea*, *Stipa breviflora*, *Stipa purpurea*, and *Orinus kokonorica*, accompanied by *Potentilla bifurca*, *p. annua*, *Carex tristachya*, *Leontopodium nanum*, *Oxytropis ochrocephala* (Du et al., 2010).

Experiment design

The field survey was carried out in the hilly sloppy lands, floodplain, foothill and valley land of typical micro-landform in sandy alpine grassland (Figure 1). Three repeated transect were set for each typical micro-geomorphology area. The length of the



transect is determined by the size of the micro-geomorphic unit. 1 m × 1 m quadrat was set every 5 m in each transect, and a total of 60 quadrats are investigated. The compass is used to record the slope, slope aspect. Latitude, longitude, and altitude of the quadrat were measured by GPS.

Data processing

The importance value (IV) is used as the dominance index of species in the community and calculated as: $I_{iv} = (R_c + R_f + R_d)/3$, where I_{iv} is the importance value index, R_c is the relative cover, R_f is the relative frequency, and R_d is the relative density. The frequency is defined as the number of squares appearing the plant species in the transect divided by the total number of squares, and the species appearing only in one or two squares is defined as a rare species. Referring to the Danish scholar C. Rainier's research method, the standard frequency distribution map of the species is drawn, and the species with a standard frequency of 1%–20% are classified into the A grade, and 21%–40% are classified into the B grade, 41%–60% is C, 61%–80% is D, and 81%–100% is E (Simpson, 1949). The terrain factor includes elevation, slope, aspect and slope

position, and a matrix of 60 × 4 environmental factors is established. The slope position assignment rules: 1-river valley flat beach; 2-downhill position; 3- mid-slope position; 4 -upper slope position; The aspect assignment rules: 1-represent leeward slope, 2-windward slope, 3-flatland. The slope is measured directly by the compass.

The classification was based on the important values of the species represented by the average values of the three samples. The vegetation assemblages were classified by TWINSpan (two-way indicator species analysis) in WinTWINS version 2.3. To identify the correlation of floristic data with environmental gradients, DCA (Detrended correspondence analysis), CCA (Canonical Correlation Analysis) ordination was carried out using the program Canoco5.0 for Windows. Species important values and environmental variables, including elevation, slope, aspect, and slope position, which were log transformed before statistical analysis to ensure homogeneity of variance. Manual forward selection through a Monte Carlo permutation test with 499 permutations ($p < 0.05$ significance) was performed to select the environmental variables explaining species composition. Species which occurred once only were omitted from the analysis.

Results

Characteristics of plant communities

In total, 29 plant species belonging to 27 genera and 16 families were identified (Table 1). At the family level, Gramineae, Compositae, Scrophulariaceae were larger families, accounting for 17.24% (5 species), 11.1% (3 species), 11.1% (3 species). Vegetation composition varies significantly under different topographic conditions. The number of plant species in hilly sloppy is up to 18 and in foothill is at least 14. *L. chinensis*, *E. dahuricus* and *C. declinatum* are the dominant species of sandy alpine grassland in the source regions of Yangtze River.

The standard frequency distribution of species based on the *C. Raunkiaer* methods is shown in (Figure 2). The number of grade species in hilly sloppy land, floodplain, foothill, valley land ranked as A > B > D, A > C > B = D = E, A > B = C > E, A > B > C = D = E respectively. The lack of E-class species is implying that the community of hilly sloppy land is in a high succession stage. In terms of species composition, the proportion of dominant species is lower than rare species. There are 2 species appearing in C, D, and E grades of four landforms, which is *L. secalinus* and *E. dahuricus*, the average frequency of which are 40% or more, respectively. There are four kinds of B-class species with an average frequency between 20% and 40%, which are *E. altotibetica*, *K. royleana*, *C. declinatum*, and *A. tenuifolia*. The rare species accounted for 48.23% of the total species.

TABLE 1 Species important value of sandy alpine grassland community in different microtopography.

Species names	Family	Micro geomorphic type		Foothill	Valley land
		Hilly_sloppy lands	Floodplain		
<i>Leymus secalinus</i>	Poaceae	31.27	50.62	43.36	44.20
<i>Avena sativa</i>	Poaceae	1.39	—	—	—
<i>Elymus sibiricus</i>	Poaceae	10.94	0.37	—	6.41
<i>Elymus dahuricus</i>	Poaceae	8.56	13.99	10.44	4.09
<i>Poa annua</i>	Poaceae	0.68	—	—	8.47
<i>Saussurea woodiana</i>	Compositae	4.68	3.00	5.70	1.36
<i>Heteropappus altaicus</i>	Compositae	3.48	1.59	—	2.66
<i>Ajania tenuifolia</i>	Compositae	0.24	6.35	4.07	0.65
<i>Lagotis brevifolia</i>	Scrophulariaceae	0.88	0.41	—	—
<i>Pedicularis longiflora</i>	Scrophulariaceae	1.27	—	—	2.09
<i>Lancea tibetica</i>	Scrophulariaceae	—	—	10.72	—
<i>Corispermum declinatum</i>	Chenopodiaceae	16.30	2.87	—	8.44
<i>Chenopodium iljinii</i>	Chenopodiaceae	—	—	—	0.27
<i>Polygonum sibiricum</i>	Polygonaceae	—	3.25	1.30	1.04
<i>Polygonum macrophyllum</i>	Polygonaceae	—	0.94	—	—
<i>Hedinia tibetica</i>	Brassicaceae	—	0.26	1.89	—
<i>Arabis pendula</i>	Brassicaceae	2.61	—	—	—
<i>Thalictrum alpinum</i>	Ranunculaceae	0.14	—	—	—
<i>Ranunculus tanguticus</i>	Ranunculaceae	—	—	—	0.33
<i>Corydalis trachycarpa</i>	Papaveraceae	1.63	—	—	—
<i>Hypecoum leptocarpum</i>	Papaveraceae	—	2.16	—	2.78
<i>Lonicera minuta</i>	Caprifoliaceae	—	1.77	1.86	—
<i>Thermopsis alpina</i>	Leguminosae	1.61	5.35	2.84	0.98
<i>Dracocephalum heterophyllum</i>	Labiatae	—	—	1.22	—
<i>Euphorbia altotibetica</i>	Euphorbiaceae	5.56	—	2.21	3.51
<i>Potentilla bigurca</i>	Polygonaceae	3.29	3.15	5.15	—
<i>Moicroula tangutica</i>	Boraginaceae	—	—	—	0.60
<i>Allium cyaneum</i>	Liliaceae	—	2.29	0.94	—
<i>Kobresia royleana</i>	Cyperaceae	5.75	1.71	8.29	12.12
Total number of species		18	17	14	17

Classification of plant community

Based on the 3rd level of division in TWINSpan classification, seven interpretable groups of plant communities were discriminated (Figure 3). The plant communities were separated into main associations: AssI. *L.secalinus*+*H. altaicus*+*S. woodiana* mainly distributed on the bottom and leeward of sandy hilly sloppy land, accompanying species include *E. altotibetica*, *P. bifurca*, and *P. annua*. AssII. *L. secalinus*+*K. royleana*+ *C. declinatum* mainly grow on upper part and windward of sandy hilly sloppy land, accompanying species include *E. altotibetica*, *P. bifurca*, and *Lancea tibetica*. AssIII. *L. secalinus*+*E. dahuricus*+*A. tenuifolia* represented the habitat of sandy floodplain, accompanied by *C. declinatum*, *A. cyaneum*, *P. sibiricum*, *S. woodiana*, and *K. royleana*. AssIV. *L.*

secalinus+*Thermopsis alpina* mainly distributed in top of sandy hilly sloppy land, and accompanied by *C. declinatum*, *P. longiflora*. AssV. *E. sibiricus*+*P. annua* grow on the leeward of sandy foothill, accompanying species include *L. secalinus*, *E. dahuricus*, *C. declinatum* and *K. royleana*. AssVI. *Elymus sibiricus*+*E. dahuricus* mainly distributed in the leeward of sandy gully land, and companied by *C. declinatum*, *C. trachycarpa* and *L. brevifolia*. AssVII. *C. declinatum* distributed in the windward of sandy gully land

Ordination of plant community

It was well known that DCA can be used to estimate the variation of species composition along the environment gradient,

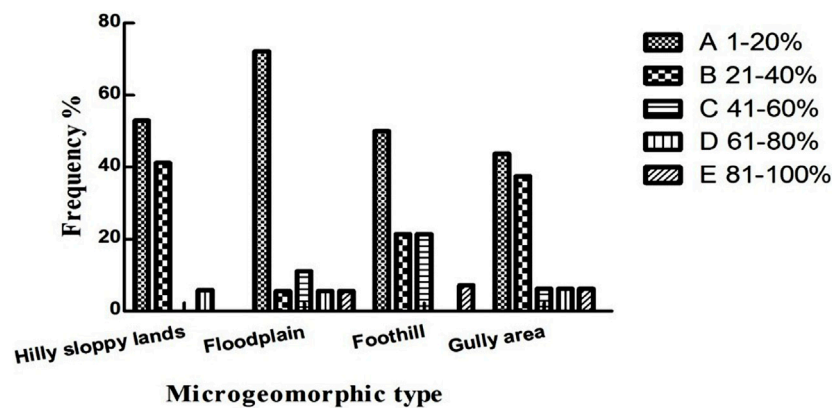


FIGURE 2
The distribution of standard frequency of species referring to the Raunkiaer's law.

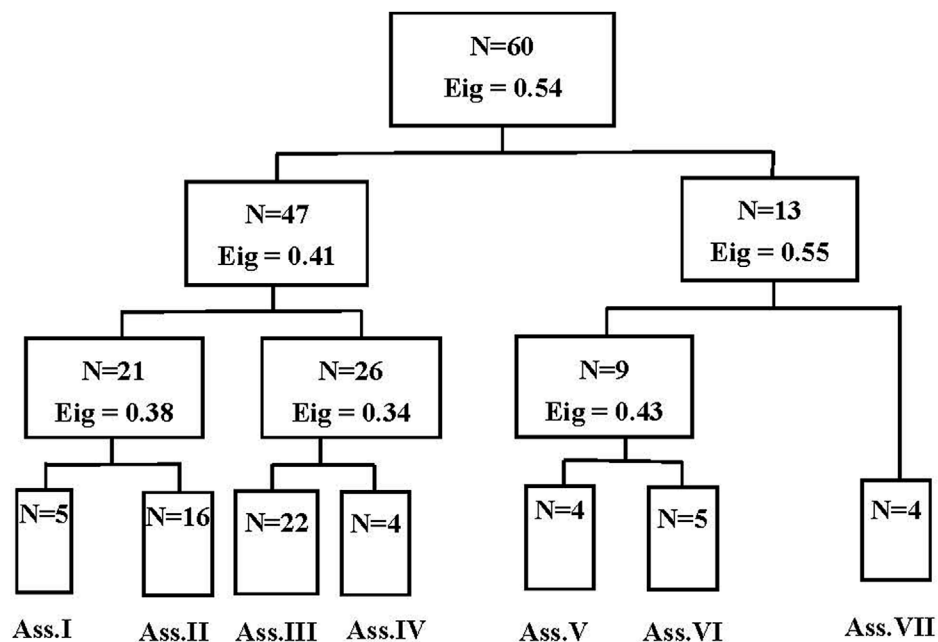


FIGURE 3
Dendrogram of TWINSpan (two-way indicator species analysis) classification for plant species. (Note: Eig = Eigenvalue).

providing gradient length reference for communities' ordination. The cluster types obtained by TWINSpan classification are basically consistent with the DCA ordination. The DCA results show that the eigenvalues of the four ordination axes are 0.56, 0.28, 0.23, and 0.17, respectively. The eigenvalues of the first two ordination axes are large, showing important ecological significance (Figure 4). The DCA ordination of sandy alpine communities shows that the maximum gradient length is 3.93

(Table 2). When the DCA gradient length was between 3 and 4, there was no difference between linear and unimodal models in the community's ordination. Therefore, CCA was selected to identify the relationship between species distribution and environmental factors.

The results of Monte Carlo test show that all the canonical ordination axes pass the statistical test ($F = 1.85$, $p = 0.002$), indicating that the topographic factor has a significant impact on

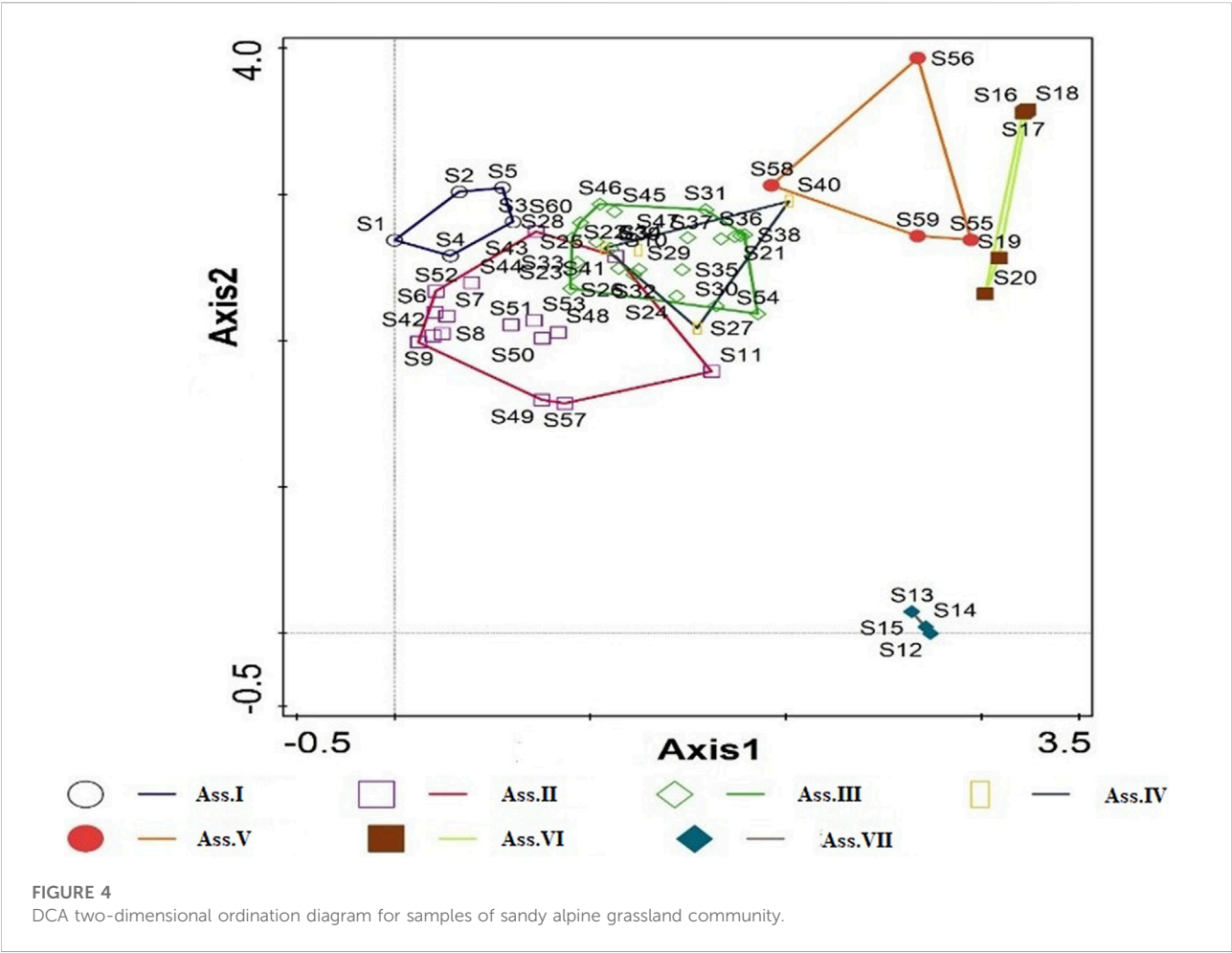


FIGURE 4 DCA two-dimensional ordination diagram for samples of sandy alpine grassland community.

TABLE 2 The DCA analysis of the species variance of sandy alpine grassland communities.

Axis	Axis I	Axis II	Axis III	Axis IV
Eigenvalues	0.56	0.28	0.23	0.17
Explained variation (cumulative)	16.4	24.71	31.46	36.44
Gradient length	3.24	3.93	2.44	2.06

the distribution of plant species in the Qidukou sandy alpine grasslands. The axes of CCA ordination represent the gradient changes of different topographic factors. According to the correlation between topographic factors and CCA ordination axis, altitude, slope, aspect and slope position are significantly positively correlated with the CCA axis I. The correlation size is graded as slope > slope position > altitude > aspect, indicating that the CCA axis I mainly reflects the gradient change of the slope. The aspect, altitude, slope, and slope position were significantly positively correlated with the CCA axis II. The correlation order was sorted as aspect > altitude > slope >

slope position, indicating that the CCA axis2 mainly represented the aspect gradient (Table 3). The results of forward selection show that the slope is the most important topographical factor for the distribution of plant species in the sandy alpine grasslands, followed by the aspect, altitude, and slope position (Table 4).

The CCA ordination of species-environmental factor visually indicates the relationship between the species distribution of sandy alpine grassland and topographic factors (Figure 5). The first two axis of CCA ordination represents the slope and aspect gradient. *A. pendula*, *E. altotibetica*, *K. royleana* and *P. longiflora*

TABLE 3 The CCA analysis of the species variance of sandy alpine grassland communities.

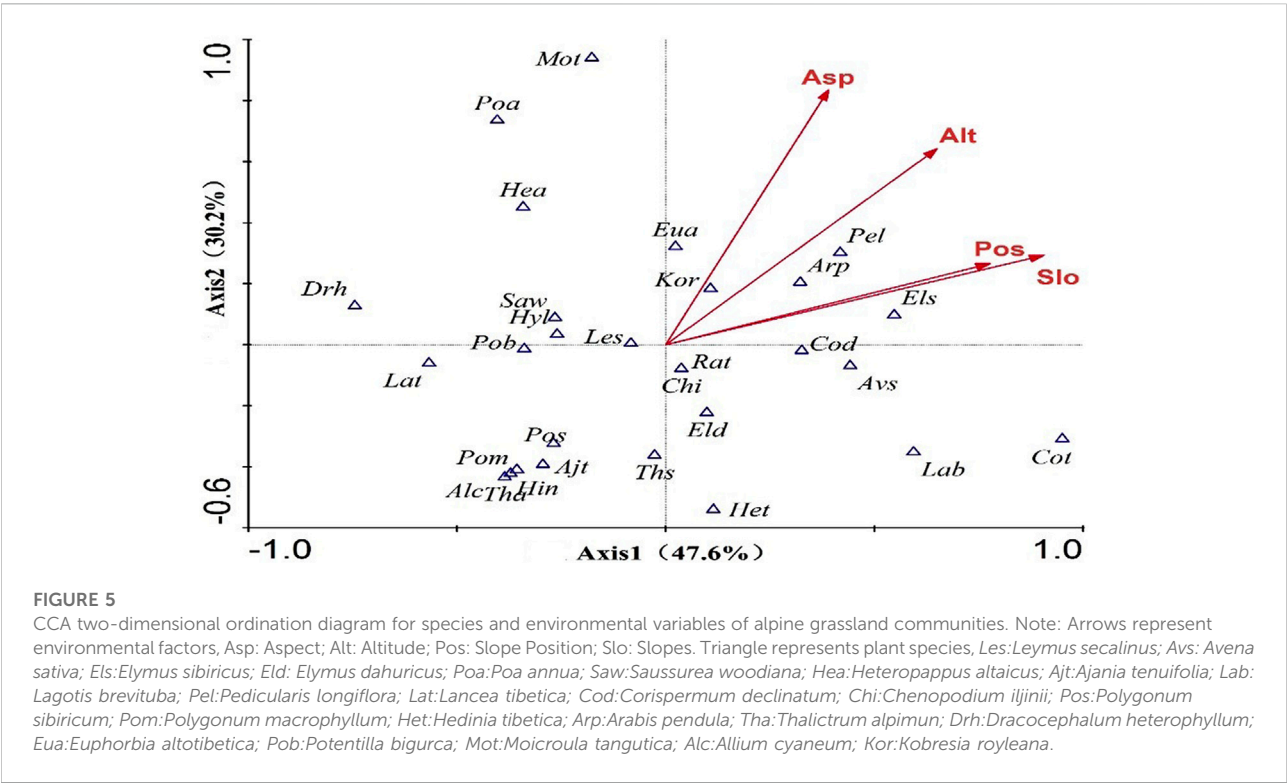
Axis	Axis I	Axis II	Axis III	Axis IV
Environmental variables				
Altitude	0.65**	0.64**	−0.062	0.4**
Slope	0.91**	0.29*	0.26*	−0.16
Aspect	0.39**	0.83**	0.39**	0.05
Slope position	0.78**	0.27*	0.50**	0.27*
Eigenvalues	0.22	0.14	0.08	0.03
Species-environment correlations	0.64	0.71	0.45	0.40
Cumulative percentage variance of species	5.6	9.2	11.2	11.8
Cumulative percentage variance relation between species and environment factors	47.6	77.8	94.3	100
Test of significance of all canonical axes	$F = 1.848$	$p = 0.002$		

** $p < 0.01$; * $p < 0.05$.

TABLE 4 Rank of importance and significance test of environmental factors.

Environmental factor	Importance rank	Variance explains of environmental factors	F	p
Slope	1	0.2	3.11	0.002**
Aspect	2	0.13	2.2	0.022*
Altitude	3	0.06	0.98	0.436
Slope position	4	0.07	1.04	0.412

* $p < 0.05$, ** $p < 0.01$.



are distributed on the upper right side of the CCA ordination diagram, which is greatly affected by slope and aspect. The *D. heterophyllum*, *P. bifurca*, and *L. tibetica* are distributed at the left end of the first axis, its distribution is less affected by slope. The *C. declinatum* and *L. brevituba* are distributed on the lower right side of the CCA ordination diagram, which is greatly affected by the slope. *P. annua*, *M. tibetica*, *A. cyaneum*, *A. tenuifolia* and *L. minuta* are located at the lower and left of the CCA ordination, which is less affected by slope and aspect, and is mainly distributed in the flat floodplain.

Discussion

Characteristics of sandy alpine grassland communities

Plants are the most sensitive and intuitive signs in all stages of desertification development. The development of desertification is closely linked to the changes in vegetation and succession simultaneously (Shao, et al., 1988). The retrograde and progressive succession of plant communities essentially correspond to the positive and negative processes of desertification (Zhao and Zhao 2000). With the increase of desertification degree, the density of soil seed bank decreased, the community diversity decreased significantly, and the grassland vegetation showed ecological adaptability to cold, drought and grazing stress (Zhao et al., 2003). The community structure tends to be simple, and the dominant species and associated species of typical alpine meadows gradually withdraw from the community, while the species adapted to sandy deserts gradually occupy the dominant position in the community, and the shrub invasion is obvious (Li et al., 2014). Succession transition pattern of hygrophytes, mesophytes, and xerophytes was appeared in the communities (Wang T. et al., 2013). With the increase of grassland desertification, the vegetation composition changed, the perennial herb plants gradually decreased, and the annual herbaceous plants showed a trend of increasing. The moderate desertification stage is an important turning point for the change of grassland plant community characteristics (Mao et al., 2014). The sandy alpine grassland community in Qidukou of the Yangtze River source region showed similar law: 29 plant species belonged to 16 families and 27 genera, and single species families accounted for 27.59%. Drought-tolerant plant species such as *L. chinensis*, *A. tenuifolia*, and *C. declinatum* have gradually replaced zonal grassland plants such as *S. woodiana*, *p. bifurca*, and *P. longiflora*, and the proportion of dominant species is lower than that of rare species and annual herb. Mainly, the vegetation community is in a high succession stage. The gradual decrease of edible pastures such as Gramineae and Cyperaceae and the sharp increase of forb cover reflect the basic characteristics of vegetation changes during the

degradation succession of alpine meadows (Wang X. M., 2013). The dominant species of *L. chinensis* in the desertified grassland of Qidukou is distributed in large quantities, which is similar to the law of vegetation differentiation of the sandy alpine grassland in the Ruergai (Li et al., 2013). The desertification of grassland has led to the expansion of semi-fixed sand area and patchy distribution. As a typical clonal plant, *L. chinensis* is a representative and widely distributed rhizomatous grass in sandy habitat, and the bare sand patchy formed by wind erosion is used as a resource for rhizome expansion. As the grassland degradation process intensifies, the *L. chinensis* population is dominated by the aggregative pattern, which reflects the cooperative relationship between the species (Ren and Zhao, 2013). The expansion of *L. chinensis*, the emergence of indicator species such as the poisonous weeds *A. tenuifolia*, and psammophyte *C. declinatum*, indicate that the desertification of the alpine grassland in Qidukou is progressing, and the vegetation community is succeeding in the direction of xerophytes.

Relationship between vegetation and desertification

The desertification of alpine grassland is a process of soil coarse texture, desiccation and poor fertility, accompanied by a decrease in soil carbon sequestration potential (Jin et al., 2015). The wind erosion and aeolian landforms formed by sand drift activity are important carriers for the survival and development of sandy vegetation. During the strong sand activity period, fine particulate matter is transported, eroded, surface roughened, fixed, and semi-fixed dunes evolve to semi-flow and mobile dunes, and wind erosion takes away the fine particulate matter required for vegetation growth (Chepil and Woodruff 1963). During the weak sand activity period, fine particulate matter slowly accumulates around the vegetation, and promotes the development of vegetation (Lancaster and Baas 1998). Wind erosion and sand burial regulate photosynthetic and transpiration rate through leaf water potential, leaf water content and stomatal conductance, and ultimately affect the water use efficiency of *Alhagi sparsifolia*. As the degree of sand fixation increases, *Corispermum patelliforme* tend to use more resources and energy for reproductive growth (Ma et al., 2014). The aeolian landform process is closely related to soil and vegetation succession changes at different spatial and temporal scales (Okin et al., 2006), forming a complex dynamic and crossfeed biogeography system (Hesp et al., 2011).

Driving mechanism of vegetation succession

Soil seed banks play an important role in community succession, renewal, and ecological restoration in desert steppe

areas. In the same climatic zone, topography has a direct impact on soil seed bank, which ultimately leads to changes in vegetation patterns. The reserves of soil seed bank from the top to the bottom slope show an overall increase trend (Han et al., 2014). With the fixation of sand dunes, the density of soil seed banks gradually increased, species diversity increased, and species distribution became more uniform. Dune types and slope positions lead to different soil seed bank densities (Zhao et al., 2007; Yu et al., 2015). With the increase of desertification degree, the density of soil seed bank decreased, the community diversity decreased significantly, and the grassland vegetation showed ecological adaptability to cold, drought and grazing stress (Zhao et al., 2003). The contribution rate of seed bank to vegetation restoration of sand dune ecosystem varies with dune types. The coupling relationship between natural physical process of dune ecosystem and seed bank is an important research direction in the future (Tang and Liu 2012). The aeolian landform process regulates the species distribution of grassland vegetation communities by affecting soil nutrients, leaf water physiology, individual survival strategies and seed bank density (He et al., 2009). This study found that the standard frequency distribution of species varies in different topography. The proportion of dominant species is lower than that of rare species. The species diversity in study region ranked as hilly sloppy lands > floodplain = valley land > foothill, reflecting an important role of the micro-geomorphology in the species distribution of sandy grassland communities.

In general, topographic factors include altitude, slope, aspect, slope position affecting the distribution pattern of species through the redistribution of matter and energy (Cantón et al., 2004), and is also an important factor affecting the process of aeolian landforms. Slope is the driving force of water and soil nutrient flow in the horizontal direction, and has a significant impact on soil thickness and physical and chemical properties. The slope increases the component force of the soil particles along the slope, which affects the wind erosion of the slope surface (He et al., 2010). The rate of wind erosion increases with the slope, which caused the spatial heterogeneity of vegetation in the windward of fixed dune (Zhao et al., 2011). The results of the research on alpine meadows in the source area of the Lantsang is consistent with this paper that slope is the most important topographic factor for the distribution of plant species in the sandy alpine (Zhang et al., 2012). Aspect affects the composition and distribution of vegetation community by affecting light, temperature, and soil nutrients (Xu 2016). The quantitative characteristics and diversity index of herbaceous vegetation on the leeward slope were larger than that of the windward slope in the Hunshadake Sandy Land (Bai et al., 2015). The aspect and slope position of the dunes have significant effects on the alpha diversity of the herbaceous plants and the spatiotemporal pattern of β diversity in the Gurbantunggut desert (Jia et al., 2018). The

soil moisture conditions in the interdune are the best, followed by the middle slope and the lowest on the top slope (Huang et al., 2009). Due to the influence of microtopography, rainfall recharge is the highest in the lowland. Soil water at dune top and up slope was in deficit during no rain for long time (Zhou et al., 2017). In the alpine meadow of Tibetan Plateau, the physical and chemical properties of soils under different topography have significant effects on the functional traits and diversity of plant communities (Li 2016). This study showed that slope and aspect have a significant impact on the species distribution of desertified grassland. In summary, due to the differences in research scales and regional natural geographical conditions, the topographical factors of altitude, slope, aspect, and slope position have different effects on the distribution of plant species.

Conclusion

The community structure of desertified grassland is simple. *L. chinensis*, *E. dahuricus* and *C. declinatum* are the dominant species of sandy alpine grassland in the source regions of Yangtze River. The species composition of sandy grassland is varied with microtopography. The proportion of dominant species is lower than rare species, suggesting that the community is in a high succession stage. The expansion of *C. declinatum* indicates that the desertification of the alpine grassland is progressing, and the vegetation community is succeeding in the direction of xerophytic. CCA ordination reflected that slope and aspect are the dominant factors among microtopography determining the species distribution of sandy alpine grassland.

The artificial restoration and reconstruction of sandy alpine grassland should firstly pay attention to the selection and utilization of native species, and then fully exploit the potential of soil seed bank in grassland restoration. Finally, the relationship between aeolian landform process and vegetation succession and favorable natural landforms for grassland restoration should be considered. Based on the aeolian landform, the comprehensive measures of engineering and biology are combined to achieve the restoration of sandy alpine grasslands.

Data availability statement

The raw data supporting the conclusion of this article will be made available by the authors, without undue reservation.

Author contributions

PZ and XX conceived and designed the experiments; JT and SJ performed the sample collection; and PZ analyzed the data and

wrote the paper. All authors read and approved the paper before submission.

Funding

This work was financially supported by the National Key R&D Program of China [grant No.2017YFC0504804], the National Natural Science Foundation of China (Grant Nos. 42207109, 32060246), the Gansu Province Youth Science and Technology Talents Lifting Project (2020-104-17), Longyuan Youth Innovation and Entrepreneurship Talents Project (2022LQGR21), the Open Project of Key Laboratory of Desert and Desertification, Chinese Academy of Sciences (KLDD-2020-017) and the Qingshan Guard Action Project of China Environmental Protection Foundation (CEPFQS202169-21).

References

- Bai, H. M., Li, G. T., Ma, J. J., Li, Y. J., and Liang, T. Y. (2015). Differentiation of micro-landform vegetation characteristics in Hunshadake sandy land. *North. Horticulture* 17, 53–57. (in Chinese). doi:10.11937/bfy.201517014
- Cantón, Y., Del Barrio, G., Solé-Benet, A., and Lázaro, R. (2004). Topographic controls on the spatial distribution of ground cover in the Tabernas badlands of SE Spain. *Catena* 55 (3), 341–365. doi:10.1016/S0341-8162(03)00108-5
- Chepil, W. S., and Woodruff, N. P. (1963). The physics of wind erosion and its control. *Adv. Agron.* 15, 211–302. doi:10.1016/S0065-2113(08)60400-9
- Cui, X. F., and Graf, H. (2009). Recent land cover changes on the Tibetan plateau: A review. *Clim. Change* 94, 47–61. doi:10.1007/s10584-009-9556-8
- Dong, Y. X. (1999). Progresses and problems in research on sandy desertification in qinghai-xizang plateau. *J. desert Res.* 19 (3), 251–255. (in Chinese). doi:10.3321/j.issn:1000-694X.1999.03.012
- Dong, Z. B., Hu, G. Y., Qian, G. Q., Lu, J. F., Zhang, Z. C., Luo, W. Y., et al. (2017). High-altitude aeolian research on the Tibetan Plateau. *Rev. Geophys.* 55 (4), 864–901. doi:10.1002/2017rg000585
- Dong, Z. B., Hu, G. Y., Yan, C. Z., Wang, W. L., and Lu, J. F. (2010). Aeolian desertification and its causes in the zoige plateau of China's Qinghai-Tibetan plateau. *Environ. Earth Sci.* 59, 1731–1740. doi:10.1007/s12665-009-0155-9
- Du, Y. G., Cui, J. Y., Ge, J. S., Zhao, X. D., Ren, J., and Wang, Y. (2010). Community characteristics study on alpine grassland in source regions of three rivers. *Pratacultural Sci.* 27 (3), 9–14. (in Chinese).
- Duran, O., and Herrmann, H. J. (2006). Vegetation against dune mobility. *Phys. Rev. Lett.* 97 (18), 188001. doi:10.1103/PhysRevLett.97.188001
- Fand, K., Song, N. P., Wei, L., and An, H. (2012). Spatiotemporal distribution of soil moisture content and aboveground biomass under different terrains in desert steppe. *Arid Zone Res.* 29 (4), 641–647. (in Chinese). doi:10.13866/j.azr.2012.04.012
- Gao, Y. H., Li, X., Leung, L. R., Chen, D. L., and Xu, J. W. (2015). Aridity changes in the Tibetan Plateau in a warming climate. *Environ. Res. Lett.* 10 (3), 034013. doi:10.1088/1748-9326/10/3/034013
- Han, R. Y., Chen, Y. Y., and Li, W. X. (2014). The distribution and relationships of ground vegetation, soil seed bank and soil water content of fixed sand under different micro-landform condition. *Pratacultural Sci.* 31 (10), 1825–1832. doi:10.11829/j.issn.1001-0629.2014-0164. (in Chinese).
- He, J. J., Tang, Z. J., and Cai, Q. G. (2010). Study on changing laws of soil wind erosion by wind tunnel experiment in Agro-pastoral area of Inner Mongolia. *J. Soil Water Conservation* 24 (4), 35–39. (in Chinese). doi:10.13870/j.cnki.stbcx.2010.04.017
- He, Y. H., Zhao, H. L., Liu, X. P., Zhao, X. Y., Li, Y. L., and Zhao, W. (2009). Reproductive allocation and its relationship with the size of *Corispermum elongatum* in different sandy habitats. *Arid Zone Res.* 26 (1), 59–64. (in Chinese). doi:10.3724/sp.j.1148.2009.00059
- Hernández-Cordero, A. I., Hernández-Calvento, L., and Perez-Chacon Espino, E. (2015). Relationship between vegetation dynamics and dune mobility in an arid transgressive coastal system, Maspalomas, Canary Islands. *Geomorphology* 238, 160–176. doi:10.1016/j.geomorph.2015.03.012
- Hesp, P., Martinez, M., da Silva, G. M., Rodríguez-Revelo, N., Gutierrez, E., Humanes, A., et al. (2011). Transgressive dunefield landforms and vegetation associations, Doña Juana, Veracruz, Mexico. *Earth Surf. Process. Landf.* 36, 285–295. doi:10.1002/esp.2035
- Huang, G., Zhao, X. Y., Huang, Y. X., and Su, Y. G. (2009). Soil moisture dynamics of artificial *Caragana microphylla* shrub at different topographical sites in Horqin land. *Chin. J. Appl. Ecol.* 20 (3), 555–561. (in Chinese). doi:10.13287/j.1001-9332.20090108
- Jia, F. Q., Ren, J. J., and Zhang, Y. M. (2018). Effect of slope aspect and terrain of sand dune on herbaceous diversity in Gurbantunggut desert. *Chin. J. Ecol.* 37 (1), 26–34. (in Chinese). doi:10.13292/j.1000-4890.201801.031
- Jin, H. X., He, F. L., Li, C. L., Han, S. H., and Wang, Q. Q. (2015). Vegetation characteristics, abundance of soil microbes, and soil physico-chemical properties in desertified alpine meadows of Maqu. *Acta Pratacultural Sin.* 24 (11), 20–28. (in Chinese). doi:10.11686/cyxb201513
- Lancaster, N., and Baas, A. (1998). Influence of vegetation cover on sand transport by wind: Field studies at Owens Lake, California. *Earth Surf. Process. Landf.* 23 (1), 69–82. doi:10.1002/(sici)1096-9837(199801)23:1<69::aid-esp823>3.0.co;2-g(199801)23:1<69::Aid-esp823>3.0.Co;2-g
- Li, C. L., Xu, X. Y., Jin, H. X., Wang, D. Z., and Li, J. J. (2014). Community structures and plant diversities in the desertification process of Maqu alpine meadow in Gansu. *Acta eco. Sin.* 34 (14), 3953–3961. (in Chinese). doi:10.5846/stxb201212021725
- Li, X. L., Gao, J., Brierley, G., Qiao, Y. M., Zhang, J., and Yang, Y. W. (2013). Rangeland degradation on the Tibetan plateau: Implications for rehabilitation. *Land Degrad. Dev.* 24 (1), 72–80. doi:10.1002/ldr.1108
- Li, Z. (2016). *Plant functional traits and functional diversity response to topographical changes*. Lanzhou: Lanzhou University.
- Ma, Y., Wang, X. Q., Zhang, B., Liu, J. H., Han, Z. Y., and Tang, G. L. (2014). Effects of wind erosion and sand burial on water relations and photosynthesis in *Alhagi sparsifolia* in the southern edge of the Taklimakan Desert. *Chin. J. Plant Ecol.* 38 (5), 491–498. (in Chinese). doi:10.3724/SP.J.1258.2014.00045
- Mao, S. H., Xie, Y. Z., and Xu, D. M. (2014). Impact of grassland desertification on vegetation and soil properties in Yanchi county of Ningxia Hui Autonomous region. *Bull. soil water conservation* 34 (1), 34–39. (in Chinese). doi:10.13961/j.cnki.stbctb.2014.01.060
- Miehe, G., Bach, K., Miehe, S., Kluge, Y., Yang, Y. P., La, D., et al. (2011). Alpine steppe plant communities of the Tibetan highlands. *Appl. Veg. Sci.* 14, 547–560. doi:10.1111/j.1654-109X.2011.01147.x
- Okin, G. S., Gillette, D. A., and Herrick, J. E. (2006). Multi-scale controls on and consequences of aeolian Processes in landscape change in arid and semi-arid environments. *J. Arid Environ.* 65, 253–275. doi:10.1016/j.jaridenv.2005.06.029

Conflict of interest

The authors declare that the research was conducted in the absence of any commercial or financial relationships that could be construed as a potential conflict of interest.

Publisher's note

All claims expressed in this article are solely those of the authors and do not necessarily represent those of their affiliated organizations, or those of the publisher, the editors and the reviewers. Any product that may be evaluated in this article, or claim that may be made by its manufacturer, is not guaranteed or endorsed by the publisher.

- Ren, H., and Zhao, C. Z. (2013). Spatial pattern and competition relationship of *Stellera chamaejasme* and *Aneurolepidium dasystachys* population in degraded alpine grassland. *Acta eco. Sin.* 33 (2), 435–442. (in Chinese). doi:10.5846/stxb201112031850
- Shao, L. Y., Dong, G. R., and Lu, F. G. (1988). Developmental and adverse process of steppe desertification and law of vegetation succession in Gonghe Basin. *J. Desert Res.* 8 (1), 30–40. (in Chinese).
- Simpson, E. H. (1949). Measurement of diversity. *Nature* 163 (4148), 688. doi:10.1038/163688a0
- Stallins, J. A. (2006). Geomorphology and ecology: Unifying themes for complex systems in biogeomorphology. *Geomorphology* 77, 207–216. doi:10.1016/j.geomorph.2006.01.005
- Tang, Y., and Liu, Z. M. (2012). Advances, trends and challenges in seed bank research for sand dune ecosystems. *Chin. J. Plant Ecol.* 36 (8), 891–898. (in Chinese). doi:10.3724/SP.J.1258.2012.00891
- Urant, S., Zhang, D. P., Wu, X. D., Yang, R. R., and Huang, X. W. (2008). Analysis on plant communities in a depression in Hulunbuir sandy meadow grassland, Inner Mongolia, China. *J. Desert Res.* 28 (6), 1125–1129. (in Chinese).
- Wang, H., Zhou, X. L., Wang, C. G., Fu, H., Zhang, F., and Ren, J. Z. (2008). Eco-environmental degradation in the northeastern margin of the Qinghai-Tibetan Plateau and comprehensive ecological protection planning. *Environ. Geol.* 55 (5), 1135–1147. doi:10.1007/s00254-007-1061-7
- Wang, J. B., Zhang, D. Z., Cao, G. M., and Tian, Q. (2013). Regional characteristics of the alpine meadow degradation succession on the Qinghai-Tibetan plateau. *Acta Prataculturae Sin.* 22 (2), 1–10.
- Wang, T., Tu, W. G., Xi, H., Li, Y. D., Tang, X. F., and Yang, Y. C. (2013). Study on vegetation and soil characteristics of desertification grassland in northwest Sichuan. *Acta Agrestia Sin.* 21 (4), 650–657. doi:10.11733/j.issn.1007-0435.2013.04.004
- Wang, X. M., Liu, Z. M., Liu, B., and Yan, S. G. (2010). Interspecific associations of plants in interdune lowland of mobile and stabilized dunes in eastern Inner Mongolia of China. *J. Ecol.* 29 (1), 16–21. (in Chinese). doi:10.13292/j.1000-4890.2010.0039
- Wang, X. M. (2013). Sandy desertification: Borne on the wind. *Chin. Sci. Bull.* 58 (20), 2395–2403. doi:10.1007/s11434-013-5771-9
- Xu, C. L. (2016). Variations in vegetation composition and nutrient characteristics related to aspect in an alpine meadow in the northeast margin of the Qinghai-Tibet plateau. *Acta Prataculturae Sin.* 25 (4), 26–35. (in Chinese). doi:10.11686/cyxb2015481
- Xu, X. L., Wang, L., Li, J., and Cai, H. Y. (2017). Analysis of the grassland restoration trend and degradation situation in the “Three-River Headwaters” region since the implementation of ecological project. *J. Geo-information Sci.* 19 (1), 50–58. (in Chinese). doi:10.3724/SP.J.1047.2017.00050
- Xu, Y. M., and Lv, S. H. (2011). Effects of wind erosion desertification on the biodiversity of grassland vegetation of Hulunbuir steppe. *J. Arid Land Resour. Environ.* 25 (4), 133–137. doi:10.13448/j.cnki.jalre.2011.04.026
- Xue, X., Guo, J., Han, B. S. A., Sun, Q. W., and Liu, L. C. (2009). The effect of climate warming and permafrost thaw on desertification in the Qinghai-Tibetan Plateau. *Geomorphology* 108, 182–190. doi:10.1016/j.geomorph.2009.01.004
- Yan, P., Dong, G. R., Su, Z. Z., and Zhang, D. D. (2004). Desertification problems in the Yangtze River source area, China. *Land Degrad. Dev.* 15 (2), 177–182. doi:10.1002/ldr.602
- Yan, P., Dong, G., Zhang, X., and Zhang, Y. (2000). Preliminary results of the study on wind erosion in the Qinghai-Tibetan Plateau using ¹³⁷Cs technique. *Chin. Sci. Bull.* 45, 1019–1025. doi:10.1007/BF02884984
- Yang, M., Nelson, F., Shiklomanov, N., Guo, D., and Wan, D. (2010). Permafrost degradation and its environmental effects on the Tibetan plateau: A review of recent research. *Earth-Science Rev.* 103, 31–44. doi:10.1016/j.earscirev.2010.07.002
- Yu, J., Gao, L., Yan, Z. J., and Wang, S. Q. (2015). Characteristics of soil seed bank of sand dune in different succession stages in the eastern KUBUQI desert. *Chin. J. Grassl.* 37 (4), 80–85. (in Chinese).
- Zhang, C. S., Xie, G. D., Bao, W. K., Chen, L., Pei, S., and Fan, Na. (2012). Effects of topographic factors on the plant species richness and distribution pattern of alpine meadow in source region of Lancang river, southwest China. *Chin. J. Ecol.* 31 (11), 2762–2774. (in Chinese). doi:10.13292/j.1000-4890.2012.0443
- Zhang, P., Kang, J. L., Yuan, Z., Tang, J., Hao, L. X., and Jin, L. (2017). Similarities and difference of the plant communities on two vegetation-dunes and their response to dune morphology. *Acta Ecol. Sin.* 37 (23), 7920–7927. (in Chinese). doi:10.5846/stxb201610262182
- Zhao, C. Y., and Wang, T. (2005). Current research status and prospects of vegetation succession on sandy land during its desertification process in semiarid regions of China. *Chin. J. Ecol.* 24 (11), 1343–1346. (in Chinese). doi:10.13292/j.1000-4890.2005.0157
- Zhao, C. Y., Wang, T., Dong, Z. B., Zhao, X. Y., and Xue, X. (2007). Plant diversity and its relationship with habitat in Korqin sandy land. *Pratacultural Sci.* 24 (10), 11–18. (in Chinese).
- Zhao, G. H., Dan, Z. T. Q., and Wei, X. H. (2012). A review grassland desertification characteristic of Qinghai-Tibet Plateau. *Grassl. Turf* 32 (5), 83–89. (in Chinese). doi:10.13817/j.cnki.cyyyp.2012.05.020
- Zhao, H. L., Zhou, R. L., Wang, J., Zhao, X. Y., and Zhang, D. H. (2011). Desertification process and its mechanism of steppe vegetation in the Hulunbuir sandy steppe, Inner Mongolia. *Arid Zone Res.* 28 (4), 565–571. (in Chinese). doi:10.3724/SP.J.1011.2011.00110
- Zhao, L. Y., Li, F. R., and Wang, X. Z. (2003). Characteristics of soil seed bank and standing vegetation change in sandy grasslands along a desertification gradient. *Acta Ecol. Sin.* 23 (9), 1745–1756. (in Chinese).
- Zhao, L. Y., and Zhao, H. L. (2000). A brief review on vegetation succession research in desertification processes of China. *J. Desert Res.* 20 (1), 8–15. (in Chinese).
- Zhou, X. Y., Yang, T. T., Wang, Z. A., Guan, D. X., Yuan, F. H., and Wu, J. B. (2017). Soil water distribution before and after a rainfall event at sand dune-interdunes in Horqin sandy land, northern China. *Chin. J. Ecol.* 36 (1), 157–163. (in Chinese). doi:10.13292/j.1000-4890.201701.008



OPEN ACCESS

EDITED BY
Guang-Lei Gao,
Beijing Forestry University, China

REVIEWED BY
Wei Shi,
Xinjiang Institute of Ecology and
Geography (CAS), China
Ziyuan Zhou,
Chinese Academy of Forestry, China

*CORRESPONDENCE
Mahdiah Ebrahimi,
maebrahimi2007@uoz.ac.ir

SPECIALTY SECTION
This article was submitted to Drylands,
a section of the journal
Frontiers in Environmental Science

RECEIVED 22 March 2022
ACCEPTED 01 November 2022
PUBLISHED 21 November 2022

CITATION
Ebrahimi M and Saberi M (2022), The
relationship between succession and
reclamation of desertified areas in
artificial forests of *Calligonum* spp. in an
arid desert of southeastern Iran.
Front. Environ. Sci. 10:901962.
doi: 10.3389/fenvs.2022.901962

COPYRIGHT
© 2022 Ebrahimi and Saberi. This is an
open-access article distributed under
the terms of the [Creative Commons
Attribution License \(CC BY\)](https://creativecommons.org/licenses/by/4.0/). The use,
distribution or reproduction in other
forums is permitted, provided the
original author(s) and the copyright
owner(s) are credited and that the
original publication in this journal is
cited, in accordance with accepted
academic practice. No use, distribution
or reproduction is permitted which does
not comply with these terms.

The relationship between succession and reclamation of desertified areas in artificial forests of *Calligonum* spp. in an arid desert of southeastern Iran

Mahdiah Ebrahimi* and Morteza Saberi

Department of Range and Watershed Management, Faculty of Water and Soil, University of Zabol, Zabol, Iran

This research investigates the association between the succession and restoration of degraded land in the southeast of Iran with artificial *Calligonum* forests regarding vegetation changes, soil properties, carbon (C) and nitrogen (N) pools in vegetation and soil. Eight forestry sites were selected, aged 1, 4, 6, 9, 11, 16, 25, and 30 years. Observations indicated that vegetation percentage, density, frequency, richness, and diversity of species substantially increased ($p < 0.01$). The highest percentage of vegetation (80.30%), density (62.70 n ha^{-1}), richness (14.15), and diversity (0.90) was observed in the 30-year site. At the end of the succession phase under study (the 25- and 30-year sites), the variation trend of vegetation was steady. As the age of the forests increased, the soil nutrient values increased significantly during succession ($p < 0.01$), even though acidity and electrical conductivity (EC) did not change significantly over time ($p > 0.01$). In the early stages of succession, the soil's C and N pools (aerial biomass, root, and litter) did not increase significantly ($p > 0.01$). Over time, however, C and N pools of the soil and plants increased (the highest amounts were seen in the 30-year site). The results indicated a significant difference in the soil and vegetation properties in the forestry sites. In general, planting native species and the succession of vegetation can play an effective role in preserving the environment in degraded lands and increasing the C and N pools.

KEYWORDS

arid rangelands, vegetation succession, species richness, carbon pool, soil degradation

Introduction

The Iranian Plateau's arid and semi-arid regions' climatic characteristics have led to sensitive and fragile conditions. In these areas, soil erosion and desertification are among the processes directly or indirectly threatening water and soil resources strongly. The restoration of vegetation in degraded rangelands can have a considerable effect on reducing soil erosion and preventing further land degradation (Ebrahimi et al., 2019).

Accordingly, forestry plans have been conducted throughout Iran to revive desert rangelands and degraded lands (Rigi Pardad et al., 2021).

Forestry practices in Iran involve covering the soil surface using plant species adaptable to arid climatic conditions. For instance, several species, such as *Calligonum polygonoides* L., *C. bungei* Boiss, and *C. comosum* (L'Her), have been widely cultured for forestry and desertification control (Amiraslani and Dragovich, 2011; Rigi Pardad et al., 2021). However, cultivating native, non-native, and adaptable species in arid lands to revive vegetation requires a great deal of analysis and assessment (Ebrahimi et al., 2019). These programs should study the effect of cultivated species on the soil and vegetation where they are planted. Selecting the appropriate species for forestry to revive vegetation and conserve soil and water resources are the main components of forestry (Hashemi Rad et al., 2018). Plants affect soil by altering its physical and chemical properties. The soil properties and food reserves strongly depend on the type of vegetation (Rigi Pardad et al., 2021).

Programs for restoring vegetation in arid areas have multiple objectives: creating secondary succession (Ebrahimi et al., 2019; Udayana et al., 2019), curbing wind and water erosion, improving soil quality and fertility, increasing carbon (C) and nitrogen (N) storage in aerial and below-ground plant biomass, cleaning the air, reducing greenhouse gases, and ultimately increasing the plant production. Therefore, restoring vegetation can play a substantial role in sustainable development and ecosystem health (Cao et al., 2011; An et al., 2019; Udayana et al., 2019; Hu et al., 2020). Given the insufficient precipitation in arid areas and the subsequent lack of plant biomass, increasing biomass volume by cultivating adaptable plants can boost the ecosystem's power to elevate C and N pools in the soil, reinforce vegetation and soil, and contribute to C and N sequestration (UNDP, 2000; Ritchie, 2020; Tessema et al., 2020).

CO₂ and NO are among the most well-known greenhouse gases, whose atmospheric concentration increases due to increased industrial activities, leading to abnormal global warming and depletion of the Earth's ozone layer (Conant et al., 2017; Hashemi Rad et al., 2018). The slightest change in the amount of C and N pools increases the amount of atmospheric C and N levels (Chapuis-Lardy et al., 2007; Hu et al., 2020; Tessema et al., 2020; Yang et al., 2020). Accordingly, the global community entered into the Kyoto Treaty in December 1997 in an extensive effort to reduce greenhouse gas emissions. One of the stressed ideas in this treaty is the attempt to reduce the atmospheric levels of greenhouse gases by preserving and creating vegetation and sequestration of C and N (Mehdipour et al., 2007; Rigi Pardad et al., 2021). C and N sequestration refers to a set of processes in which additional atmospheric concentrations of C and N are captured and stored in plant biomass and soil (Rigi Pardad, 2021). Semi-arid and arid rangelands are a great option for C and N sequestration.

Moreover, increasing biomass in these areas has several advantages by reducing sequestration costs. With these advantages, international organizations such as the FAO and the UNDP have selected these areas as sites for implementing C sequestration programs (Veramesh et al., 2010). In preliminary studies in Iran, the UNDP reported that the C sequestration volume by forestry in arid and desert rangelands predominantly vegetated with *Haloxylon* spp equals 14 ton ha⁻¹ after 20 years, reaching 21 ton ha⁻¹ in 50 years by proper management (Abedi et al., 2008).

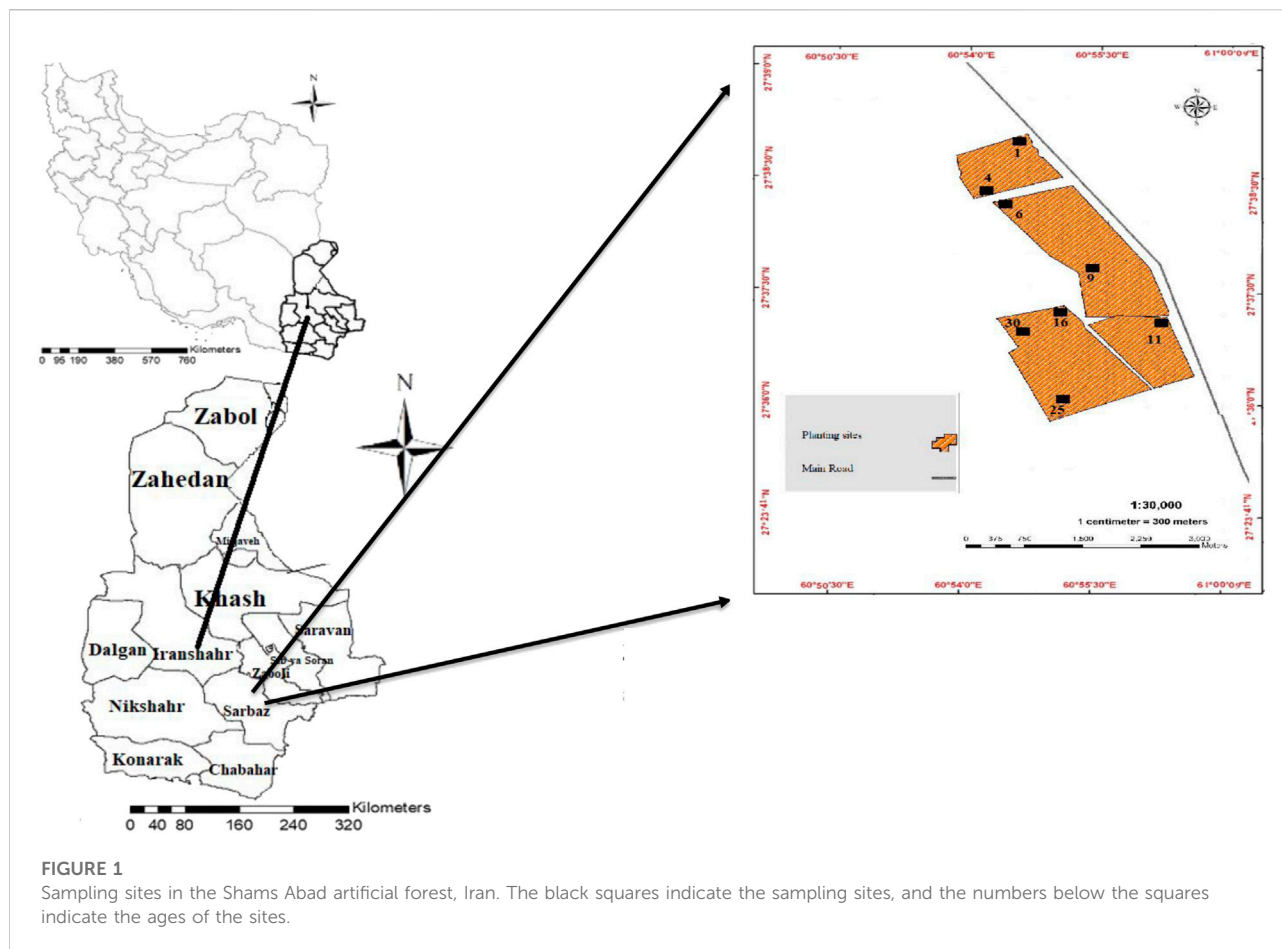
Arid rangelands have excellent potential for storing C and N (Conant et al., 2017; Tessema et al., 2020). Studies on the changes in C and N pools in arid rangelands cultivated with woody plants indicate that compared to other lands, arid rangelands display a significant increase in C and N pools due to biological reactions (Ritchie, 2020; Tessema et al., 2020). This increase can be attributed to the direct relationship between fluctuations in biomass generation with C and N pools in a region and the influential role of related management models (Tessema et al., 2020). Shams Abad is a desert region and one of the prominent locations known for wind erosion in Sistan and Baluchestan, Iran. Large parts of Shams Abad have been cultivated with perennial species, leading to considerable changes in the local ecosystem. Nonetheless, research on the effect of forestry in Iran's degraded and desert regions on conserving biodiversity, soil properties, and C and N pools is rare.

This study was carried out to find out how afforestation changed the vegetation cover and the C and N pools of plant-soil in the vegetation communities in the arid desert steppe of Iran. We aimed to evaluate the plant variety and richness of afforestation succession in the arid area of southeastern Sistan and Baluchestan, Iran, and to investigate the influence of afforestation on native plant species, *C. polygonoides* L., *C. bungei* Boiss and *C. comosum* L'Her., on plant-soil C and N reservoirs. Our hypothesis is that 1) *Calligonum* planting aids in the development of plant species and soil fertility, and 2) soil fertility in the initial phase does not change significantly compared to the middle phase.

Material and methods

Study area

The artificial forests in the Shams Abad Desert (between latitude 27°9'31"–27°29'10"N and between longitude 60°10'32"–60°37'19"E), Sistan and Baluchestan, Iran, were selected as the study site, with an area of 112,350.30 ha (Figure 1). With less than 80 mm of annual rainfall, the area has a hot and dry environment. There have been drastic variations in rainfall over the years. Extreme rainfall volatility leads to severe instabilities of annual fodder production. A large portion of rainfall occurs during December, January, and



February in the form of rainstorms, leading to torrents as water cannot penetrate the soil due to the region's light soil texture and lack of vegetation. In other months, especially during spring and summer, the region suffers absolute aridity, a condition where only deep-rooted plants with extensive roots capable of maintaining their relationship with in-depth soil moisture can survive. It is only natural that under such conditions, the seedlings of native plants, which experience significant growth following the generous winter rainfalls, stop growing as they are deprived of access to the moisture below the surface when the rainfalls stop and cause the soil to lose its surface moisture. The seedlings thus shrivel and perish in hot weather and summer aridity. Thus, it is challenging to replace native plants perishing due to various factors. The average temperature of the area is 30°C. The minimum and maximum temperature the region experiences is −8°C and 57°C, respectively, recorded in December and July. On most summer days, the temperature exceeds 50°C, hampering any form of vital plant activities for a relatively long period. In addition to rainfall and temperature, winds and storms are factors that can restrict vegetation (Report of Rangeland Improvement, 2018).

The assessment of forestry area

In this study, the selected forestry sites were cultivated with the following species: *C. polygonoides* L., *C. bungei* Boiss, and *C. comosum* (L'Her). The species were aged 1, 4, 6, 9, 11, 16, 25, and 30 years. The vegetation was thoroughly analyzed in a specific 1-ha area in each site. In March 2019, data were gathered using a randomized complete block design (RCBD). The plant species were identified and named in the Botany Laboratory of the University of Zabol. The identified plants and assigned nomenclatures were matched with those in the studies by Rechinger et al. (1984), Rechinger et al. (1988). The chorotype of plants was matched with that in the study by Zohary (1963). Low-age sites (1, 4, 6, and 9 years) were protected against livestock grazing. However, livestock grazing was permissible in sites aged 11, 16, 25, and 30 years (sheep and goats). A total of 40 sample stands with 100 m × 100 m dimensions were selected to determine the changes in plant populations (five stands were assigned to each site). Quadrats (2 m × 3 m, 5 m × 5 m, 5 m × 5 m, 6 m × 6 m, 8 m × 8 m, 10 m × 10 m, 15 m × 15 m, 20 m × 20 m for 1, 4, 6, 9, 11, 16, 25, and 30 ages, respectively) were used

to measure vegetation characteristics in each stand along 100-m transect lines by the systematic random sampling method (75 quadrats per stand). In general, 120 transects were sampled. The distance between the transect lines was 10 m.

The visual estimation method was used to estimate the percentages of vegetation and bare soil. The number of species in a sampled area was used to calculate the density of species (Ebrahimi et al., 2016). The relative density factors (RD), relative cover factors (RC), and relative frequency factors (RF) were used to compute the importance values (IV) of species. The characteristics of a dominant plant species may be derived from these characteristics. The relative density of a plant species is the ratio of its density to the overall density. An area or sample of vegetation may be defined as having a relative cover of a certain species in proportion to the cover of total plant species. Species frequency as a percentage of total plant cover is known as the relative frequency (Khosravi et al., 2017). Species richness was estimated by quantifying species per quadrat.

The formula $H' = -\sum_{i=1}^S p_i \cdot \ln p_i$ was used to determine the plant species' diversity. In this formula, p_i is the percent of points in a line where plant species i was found (Khosravi et al., 2017). Pielou's J index ($H'/\ln S$) was used to measure evenness, where S is the number of species that were sampled in each quadrat.

Plant C and N pools measurement

In each age class, inside the quadrat, the aerial parts (stems and leaves) related to the growth of the current year's *Calligonum*, related species, and all the litters under the canopy cover were extracted. To ensure minimum degradation of vegetation, plant species were collected in three quadrats in each age class. At 45-cm soil depth in each quadrat, below-ground biomass was collected using the root auger (25 cm diameter). The samples were spread on a tray to remove the soil around the roots. In each age class, all aerial organs, roots, and litters were dried (70°C for 48 h) to determine dry mass. Total plant N was measured using the modified Kjeldahl method (Bremner, 1996), and organic plant C was measured using the method of Nelson and Sommers (1982).

Measuring soil properties

Soil samples at 45-cm depth were collected from under the shrubs' canopy cover. At the same time, biomass samples were collected from roots and the lines between the shrubs (10–15 m distance) inside the quadrates. In case the quadrats had no shrubs, the plants nearest to the quadrats were selected. In each age class, a total of 15 soil samples were collected at random. A 2-mm sieve plate was used to separate soil samples that had been air-dried.

The laser diffractometry method (LDM) was used to determine the soil texture (Wang et al., 2012). The saturated soil-paste method (Thomas, 1996) was used to determine the acidity (pH) using a pH meter. The EC was measured using an EC meter (Rhoades, 1996). Total nitrogen (N) was measured using the Kjeldahl method (Bremner, 1996). The available phosphorus (P) was determined using the Olsen method via a spectrophotometer (Bray and Kurtz, 1954). The available potassium (K) was measured using a flame photometry device (Knudsen et al., 1982). Soil organic matter (OM) was measured based on the method of Lo et al. (2011), and the bulk density (BD) of soil was measured using the volumetric ring method (Wu et al., 2010). The soil organic C pool was determined using the equation: $C_p = BD \times SOC \times D$ (Deng et al., 2013; Wang et al., 2014). In this equation, C_p is the soil organic C pool (kg m^{-2}), BD (g cm^{-3}) denotes the bulk density of the soil, SOC is an abbreviation for soil organic C content (g kg^{-1}), and D (cm) denotes the thickness of the soil layer tested. The soil N pool was calculated using the following equation: $N_p = BD \times TN \times D$ (Deng et al., 2013; Wang et al., 2014). In this equation, N_p (kg m^{-2}) is the soil N pool, BD (g cm^{-3}) is soil bulk density, and TN (g kg^{-1}) is the total soil N content.

Data analysis

After studying the outlier values, verifying normal distribution, and testing homogeneity of variance, data analysis was conducted with a randomized complete block design (RCBD) in SPSS (Ver. 20.0) to investigate any significant difference among the age groups. To compare mean pairs, Duncan's multiple range test (DMRT) was used. The values of indexes, including richness, evenness, and diversity, were calculated using the PAST data analyzer. The main trends in reclamation ages were described by fitting polynomial functions to vegetation indices using the curve fit feature in the SPSS (Ver. 20.0) software package.

Results

Vegetation changes

In the study sites, 15 plant species, including ten families and three genera, were listed (Table 1). The maximum number of plant species (15 species, Figure 2A), genera (13 genera, Figure 2B), and family (ten families, Figure 2C) was in the 25- and 30-year age classes. The lowest number of species (five species, Figure 2A), genus (three genera, Figure 2B), and family (three families, Figure 2C) was related to the age class of 1 year. The highest frequency was, respectively, seen in *Polygonaceae* (20%), *Amaranthaceae* (20%), and *Fabaceae*

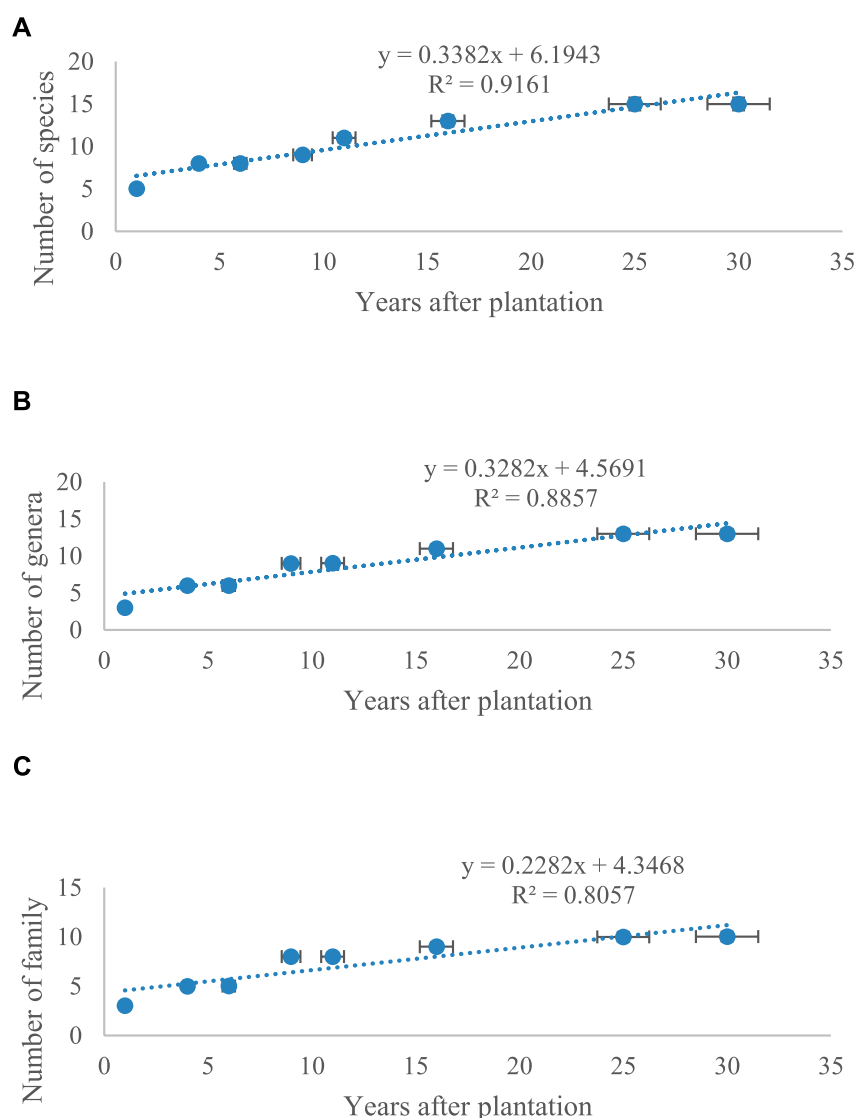
TABLE 1 Plant species composition in the eight study areas (1, 4, 6, 9, 11, 16, 25, and 30 years after afforestation).

Species	Family	Growth form	Life history	Chorotype	1 year		4 years		6 years		9 years		11 years		16 years		25 years		30 years	
					Presence/ Absence	IV (%)	Presence/ Absence	IV (%)	Presence/ Absence	IV (%)	Presence/ Absence	IV (%)	Presence/ Absence	IV (%)	Presence/ Absence	IV (%)	Presence/ Absence	IV (%)	Presence/ Absence	IV (%)
<i>Hammada salicornica</i> (Moq.) Iljin	Amaranthaceae	Ph	P	IT-SA	1	31.57	1	12.31	1	33.18	1	37.39	1	27.48	1	29.31	1	30.49	1	44.48
<i>C. polygonoides</i> L.	Polygonaceae	Ph	P	IT-SS	1	32.40	1	40.00	1	60.10	1	65.59	1	69.10	1	72.13	1	75.10	1	77.10
<i>Calligonum bungei</i> Boiss.	Polygonaceae	Ph	P	IT-SS	1	34.14	1	39.11	1	51.19	1	66.59	1	76.10	1	79.12	1	80.19	1	82.24
<i>Calligonum comosum</i> L'Hér.	Polygonaceae	Ph	P	IT-SS	1	33.26	1	42.28	1	50.43	1	67.59	1	74.25	1	76.15	1	79.20	1	80.25
<i>Prosopis cineraria</i> (L.) Druce	Fabaceae	Ph	P	SS	1	27.34	1	30.07	1	1.23	1	35.07	1	33.34	1	35.12	1	35.30	1	40.21
<i>Ziziphus spina-christii</i> (L.) Willd.	Rhamnaceae	Ph	P	SS	0	0	1	3.32	1	4.27	1	3.32	1	3.32	1	4.77	1	5.30	1	12.67
<i>Tamarix macrocarpa</i> (Ehrenb.) Bge.	Tamaricaceae	Ph	P	IT-SS	0	0	0	0	0	0	1	23.44	1	1.83	1	5.10	1	5.75	1	10.83
<i>Periploca aphylla</i> Decne.	Asclepiadaceae	Ph	P	SS	0	0	0	0	0	0	1	2.19	1	2.19	1	3.42	1	14.89	1	20.21
<i>Peganum harmala</i> L. PEGHA.	Nitrariaceae	F	P	IT-M-SS	0	0	0	0	0	0	1	3.44	1	11.23	1	10.23	1	29.91	1	29.13
<i>Alhagi camelorum</i> Fisch. ex DC	Fabaceae	Sh	P	IT	0	0	0	0	0	0	1	6.12	1	12.33	1	9.21	1	19.78	1	20.33
<i>Suaeda fruticosa</i> (L.) Forssk.	Amaranthaceae	Sh	P	IT-SS-SA	0	0	0	0	0	0	0	0	0	0	1	2.78	1	16.76	1	18.11
<i>Gymnocarpus decandrus</i> Forssk.	Caryophyllaceae	Sh	P	SS	0	0	0	0	0	0	0	0	1	6.19	1	7.00	1	15.43	1	16.22
<i>Rhazya stricta</i> Decne.	Apocynaceae	Sh	P	IT-SS-M	0	0	0	0	0	0	0	0	0	0	1	3.21	1	13.18	1	14.22
<i>Chenopodium album</i> subsp. L.	Amaranthaceae	F	A	C	0	0	1	2.44	1	5.78	0	0	0	0	0	3.45	1	21.99	1	23.42
<i>Tribulus terrestris</i> L.	Zygophyllaceae	B	A	PR	0	0	1	4.76	1	5.23	1	5.44	0	0	0	6.12	1	13.10	1	15.67

P, perennial; A, annual; Ph, phanerophyte; F, forb; Sh, shrub; B, bush.

1 and 0 indicate the presence and absence of a plant species, respectively.

M, Mediterranean; SA, Saharo-Arabian; C, Cosmopolitan; IT, Irano-Turanian; SS, Sahara-Sindian; PR, poly regional (Pontic and Irano-Anatoli, Irano-Touranian, Europe-Siberian, and Mediterranean).

**FIGURE 2**

Variations of vegetation properties in the eight *Calligonum* planting sites. (A) Number of species, (B) genera, and (C) families. Vertical bars show standard errors.

(13%) families. Most species were perennials (86.66%). Annuals had an insignificant share (13.33%) in the forestry sites. A chorological study (Table 1) showed that the largest proportion of the flora belongs to the Sahara-Sindian elements (60%), followed by Irano-Turanian (20%) and Saharo-Arabian (15%).

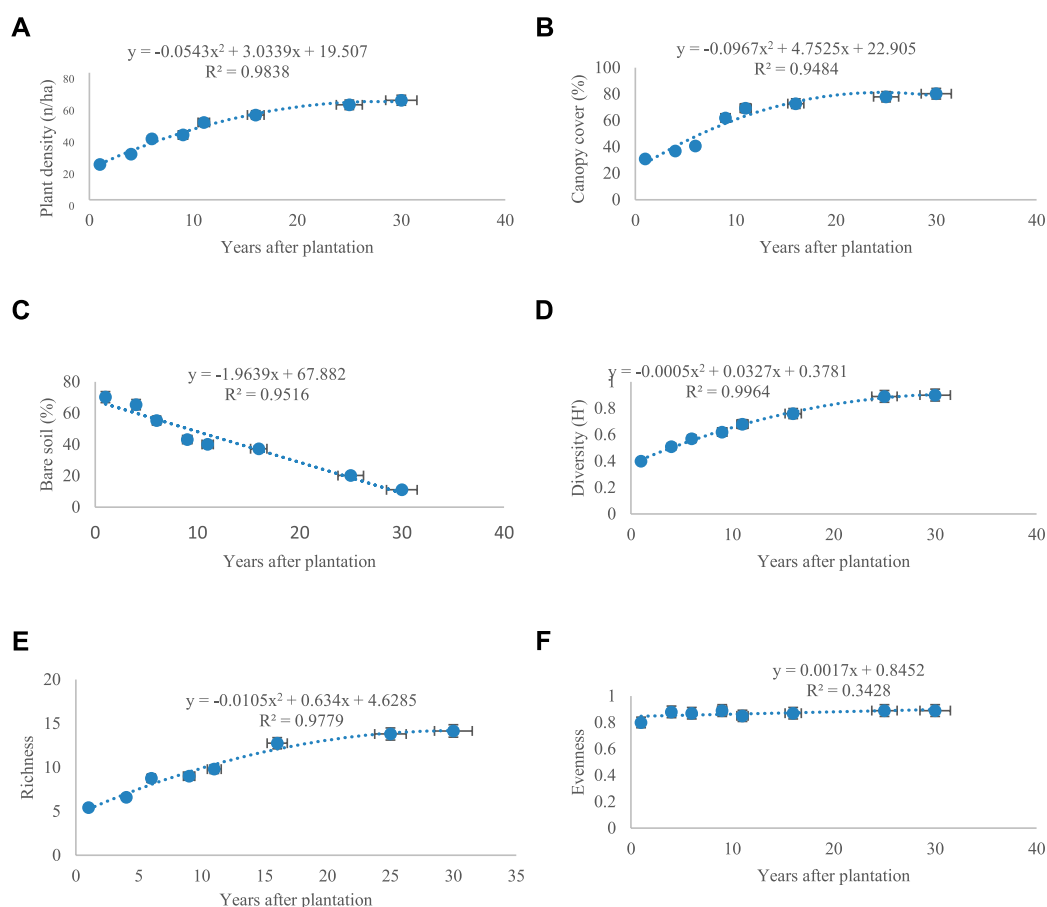
According to importance value (IV), the following species were predominant in all sites: *C. polygonoides*, *C. Bungei*, and *C. comosum*, and with the increasing age from 1 year to 30 years, vegetation cover (Figure 3A) and density (Figure 3B) displayed an ascending trend.

The maximum and minimum percentage of vegetation cover was seen in the 30-year site (80.30%) and the 1-year site (30.90%),

respectively (Figure 3A). Vegetation percentage had an almost constant trend from the 16-year site to 30-year site.

The density of species increased from 22.30 n ha⁻¹ in the 1-year site to 62.70 n ha⁻¹ in the 30-year site (Figure 3A). The density of species in the 25- and 30-year sites displayed a steady trend. In lands cultivated with *Calligonum*, the bare soil (Figure 3C) decreased significantly over time ($p < 0.01$). The highest amount of litter was seen in the 30-year age class. The results indicated that cultivating *Calligonum* significantly elevated the diversity (Figure 3D) and richness (Figure 3E) of species in the region ($p < 0.01$).

In contrast, evenness (Figure 3F) did not change significantly in the age classes in the study ($p > 0.01$). The 30-year age group

**FIGURE 3**

Vegetation characteristics in the eight *Calligonum* planting sites. (A) Plant density, (B) canopy cover, (C) bare soil, (D) diversity (H'), (E) richness, and (F) evenness. Vertical bars show standard error.

displayed the highest diversity (0.9) and richness (14.15). The 9- and 11-year age classes did not differ significantly ($p > 0.01$) in terms of richness and diversity, indicating that restoring vegetation in arid regions with harsh climatic conditions is time-consuming. Vegetation in disturbed land prone to wind erosion excellently responded to biological restoration with significant changes, thus confirming the primary hypothesis of the study.

Soil properties changes

Changes in soil properties and C and N pools in artificial forests re-vegetated with *Calligonum* in the period of 1–30 years have been shown in Table 2. Our findings showed that soil acidity changes were insignificant ($p > 0.01$). The results indicated that EC under and between the canopy cover did not change significantly over time ($p > 0.01$), despite the lower EC

between the canopy cover of *Calligonum* plants compared to the inter-canopy cover of plants mass, indicating a significant difference ($p < 0.01$). Over time, as the re-vegetated forests aged, soil fertility factors including organic matter, N, P, and K increased significantly ($p < 0.01$). The lowest recorded amounts of organic matter, N, P, and K were observed at the initial phase (1-year) of restoration. The highest values of the parameters were recorded at the end of the period. The amount of soil organic matter in the 30-year site was approximately 3.09 times (under the canopy cover of *Calligonum*) greater than the beginning of the succession phase (1-year). At the end of the phase, the N, P, and K levels were 12, 6.44, and 6.84 times greater than those at the beginning of the succession phase. The level of the N pool followed the same pattern. N and C pool levels were the highest amounts underneath the *Calligonum* canopies in the area that underwent succession for 30 years than in the area that underwent treatment of 1-year. Moreover, the changes in the C and N pool levels were not significant among the 1- and 4-year

TABLE 2 Characteristics of soil under canopy (UC) and inter canopy (IC) in the eight *Calligonum* planting sites.

Planting age		OM (%)	N (g kg ⁻¹)	P (mg kg ⁻¹)	K (mg kg ⁻¹)	ECe (dSm ⁻¹)	pH	CaCO ₃ (g kg ⁻¹)	C pool (ton ha ⁻¹)	N pool (ton ha ⁻¹)	Texture
1	UC	3.00 ± 0.01 ^{Aj}	0.10 ± 0.01 ^{Al}	2.22 ± 0.01 ^{Alk}	80.50 ± 9.98 ^{An}	5.00 ± 0.01 ^{Aa}	8.00 ± 0.50 ^{Aa}	383.50 ± 3.50 ^{Aa}	2.00 ± 0.01 ^{Ac}	0.80 ± 0.01 ^{Af}	Sandy
	IC	2.10 ± 0.01 ^{Bk}	0.10 ± 0.01 ^{Al}	2.00 ± 0.01 ^{Bk}	55.43 ± 9.98 ^{Bo}	4.00 ± 0.01 ^{Ab}	8.00 ± 0.53 ^{Aa}	386.00 ± 3.55 ^{Aa}	1.30 ± 0.01 ^{Bd}	0.30 ± 0.01 ^{Bj}	
4	UC	3.50 ± 0.01 ^{Aj}	0.25 ± 0.01 ^{Alk}	3.33 ± 0.01 ^{Aj}	110.00 ± 9.98 ^{Am}	5.00 ± 0.01 ^{Aa}	8.30 ± 0.52 ^{Aa}	384.50 ± 3.60 ^{Aa}	3.34 ± 0.01 ^{Ad}	1.20 ± 0.01 ^{Ac}	Sandy
	IC	2.20 ± 0.01 ^{Bk}	0.10 ± 0.01 ^{Bl}	2.78 ± 0.01 ^{Bk}	85.60 ± 9.98 ^{Bn}	4.00 ± 0.02 ^{Ab}	8.20 ± 0.50 ^{Aa}	395.00 ± 3.64 ^{Aa}	1.75.30 ± 0.01 ^{Bd}	0.46.30 ± 0.01 ^{Bj}	
6	UC	4.35 ± 0.01 ^{Af}	0.35 ± 0.01 ^{Aj}	4.35 ± 0.01 ^{Af}	150.32 ± 9.98 ^{Alk}	5.21 ± 0.01 ^{Aa}	8.53 ± 0.37 ^{Aa}	372.90 ± 3.43 ^{Aa}	4.44 ± 0.01 ^{Ad}	2.20 ± 0.01 ^{Ad}	Sandy
	IC	3.40 ± 0.01 ^{Bj}	0.20 ± 0.01 ^{Bk}	3.21 ± 0.01 ^{Bj}	100.30 ± 9.98 ^{Bm}	4.00 ± 0.01 ^{Ab}	8.30 ± 0.50 ^{Aa}	380.90 ± 3.45 ^{Aa}	2.50 ± 0.01 ^{Bd}	0.83 ± 0.01 ^{Bf}	
9	UC	5.62 ± 0.01 ^{Ac}	0.50 ± 0.01 ^{Ad}	5.62 ± 0.01 ^{Ac}	230.50 ± 9.98 ^{Ac}	5.29 ± 0.01 ^{Aa}	8.62 ± 0.40 ^{Aa}	377.70 ± 3.48 ^{Aa}	6.62 ± 0.01 ^{Ad}	2.78 ± 0.01 ^{Ad}	Sandy
	IC	4.10 ± 0.01 ^{Bf}	0.30 ± 0.01 ^{Bf}	4.30 ± 0.01 ^{Bf}	140.32 ± 9.98 ^{Bl}	4.00 ± 0.01 ^{Ab}	8.45 ± 0.52 ^{Aa}	383.60 ± 3.48 ^{Aa}	3.65 ± 0.01 ^{Bd}	1.34 ± 0.01 ^{Be}	
11	UC	6.30 ± 0.01 ^{Ad}	0.64 ± 0.01 ^{Ac}	6.30 ± 0.01 ^{Ad}	260.83 ± 9.98 ^{Ad}	5.00 ± 0.02 ^{Aa}	8.70 ± 0.30 ^{Aa}	361.20 ± 3.37 ^{Aa}	7.65 ± 0.01 ^{Ad}	2.90 ± 0.01 ^{Ad}	Loamy sand
	IC	4.50 ± 0.01 ^{Bf}	0.37 ± 0.01 ^{Bf}	5.00 ± 0.01 ^{Be}	170.30 ± 9.98 ^{Bj}	4.27 ± 0.01 ^{Ab}	8.45 ± 0.31 ^{Aa}	363.20 ± 3.36 ^{Aa}	4.30 ± 0.01 ^{Bd}	1.70 ± 0.01 ^{Be}	
16	UC	7.50 ± 0.01 ^{Ac}	0.75 ± 0.01 ^{Ac}	7.50 ± 0.01 ^{Ac}	300.40 ± 9.98 ^{Ac}	5.13 ± 0.01 ^{Aa}	8.76 ± 0.30 ^{Aa}	369.40 ± 3.40 ^{Aa}	9.50 ± 0.01 ^{Ad}	3.36 ± 0.01 ^{Ac}	Loamy sand
	IC	5.23 ± 0.01 ^{Be}	0.46 ± 0.01 ^{Be}	5.89 ± 0.01 ^{Be}	190.50 ± 9.98 ^{Bf}	4.32 ± 0.01 ^{Ab}	8.53 ± 0.25 ^{Aa}	369.40 ± 3.40 ^{Aa}	6.54 ± 0.01 ^{Bd}	2.00 ± 0.01 ^{Bd}	
25	UC	8.30 ± 0.01 ^{Ab}	0.80 ± 0.01 ^{Ab}	9.30 ± 0.01 ^{Ab}	400.30 ± 9.98 ^{Ab}	5.20 ± 0.04 ^{Aa}	8.86 ± 0.13 ^{Aa}	343.50 ± 3.33 ^{Aa}	19.30 ± 0.01 ^{Ad}	4.78 ± 0.01 ^{Ab}	Loamy sand
	IC	6.50 ± 0.01 ^{Bd}	0.52 ± 0.01 ^{Bd}	7.30 ± 0.01 ^{Bc}	250.50 ± 9.98 ^{Bd}	4.00 ± 0.01 ^{Ab}	8.60 ± 0.15 ^{Aa}	346.70 ± 3.34 ^{Aa}	13.21 ± 0.01 ^{Bd}	2.76 ± 0.01 ^{Bd}	
30	UC	9.27 ± 0.01 ^{Aa}	1.20 ± 0.01 ^{Aa}	14.30 ± 0.01 ^{Aa}	550.67 ± 9.98 ^{Aa}	5.23 ± 0.02 ^{Aa}	8.86 ± 0.23 ^{Aa}	347.90 ± 3.30 ^{Aa}	23.29 ± 0.01 ^{Ad}	6.64 ± 0.01 ^{Aa}	Loamy sand
	IC	7.42 ± 0.01 ^{Bc}	0.83 ± 0.01 ^{Bb}	9.54 ± 0.01 ^{Bb}	300.12 ± 9.98 ^{Bc}	4.00 ± 0.01 ^{Ab}	8.60 ± 0.25 ^{Aa}	351.60 ± 3.30 ^{Aa}	17.29 ± 0.01 ^{Bd}	4.32 ± 0.01 ^{Bb}	

*Each column has different capital case letters indicating significant changes between the under canopy and inter canopy of the same afforestation years (t-test). Each column has different lowercase letters indicating significant changes between the under canopy and inter canopy of the various afforestation years ($p < 0.05$, *post-hoc* Duncan test). Means ± SE.

sites. The soil surface layer in the 30 years' *Calligonum*-planted area exhibited higher silt and clay than the other areas (Table 2).

C and N pools variations

The amounts of C pool in aerial biomass, roots, and litter in artificial forests cultivated with *Calligonum* are shown in Table 3. The results showed that the C pool in aerial biomass, roots, and litters at the beginning of the phase was 1.30, 1.50, and 0.21 ton ha⁻¹, respectively, an insignificant difference with the 4-year class ($p > 0.01$). Over time, the C pool increased substantially ($p < 0.01$). The maximum C pool was observed in the 30-year class. Notably, the C pool showed an ascending trend at the end of the study period. In contrast, soil C storage showed a steady trend. Over time, the N pool in aerial biomass, roots, and litters

increased significantly as the re-vegetated forests aged ($p < 0.01$) (Table 4). The lowest N pool was observed at the beginning of the study period. Like C pool results, the N pool at the initial phase (1-year) did not change significantly compared to the 4-year age class ($p > 0.01$). Over time, the N pool in aerial biomass, roots, and litters increased significantly as the re-vegetated forests aged ($p < 0.01$) (Table 4). Maximum C and N pools in all age classes were observed in roots, aerial biomass, and litters, respectively, showing a significant difference ($p < 0.01$).

Discussion

The changes in plant communities and ecological processes extend the ecological niche and increase the capturing of seeds

TABLE 3 Plant C pool (ton ha⁻¹) in the eight *Calligonum* planting sites.

Planting age		Above-ground biomass	Below-ground biomass	Litter
1	UC	1.30 ± 0.01 ^{Al-B}	1.50 ± 0.01 ^{Al-A}	0.21 ± 0.01 ^{Al-C}
	IC	0.50 ± 0.01 ^{Bn-B}	0.84 ± 0.01 ^{Bn-A}	0.10 ± 0.01 ^{Bm-C}
4	UC	1.50 ± 0.01 ^{Al-B}	1.90 ± 0.01 ^{Ak-A}	0.33 ± 0.01 ^{Al-C}
	IC	1.07 ± 0.01 ^{Bm-B}	1.10 ± 0.01 ^{Bm-A}	0.23 ± 0.01 ^{Bl-C}
6	UC	1.89 ± 0.01 ^{Ak-B}	2.70 ± 0.01 ^{Aj-A}	0.70 ± 0.01 ^{Ak-C}
	IC	1.20 ± 0.01 ^{Bl-B}	1.89 ± 0.01 ^{Bk-A}	0.60 ± 0.01 ^{Bk-C}
9	UC	3.62 ± 0.01 ^{Af-B}	3.50 ± 0.01 ^{Af-A}	0.87 ± 0.01 ^{Aj-C}
	IC	2.50 ± 0.01 ^{Bj-B}	2.65 ± 0.01 ^{Bj-A}	0.80 ± 0.01 ^{Aj-C}
11	UC	4.30 ± 0.01 ^{Ae-B}	5.64 ± 0.01 ^{Ae-A}	1.30 ± 0.01 ^{Ae-C}
	IC	3.32 ± 0.01 ^{Bf-B}	3.89 ± 0.01 ^{Bf-A}	1.00 ± 0.01 ^{Bf-C}
16	UC	6.82 ± 0.01 ^{Ad-B}	8.75 ± 0.01 ^{Ad-A}	1.90 ± 0.01 ^{Ad-C}
	IC	4.23 ± 0.01 ^{Be-B}	5.46 ± 0.01 ^{Be-A}	1.73 ± 0.01 ^{Ad-C}
25	UC	10.69 ± 0.01 ^{Ab-B}	13.80 ± 0.01 ^{Ab-A}	2.67 ± 0.01 ^{Ac-C}
	IC	6.45 ± 0.01 ^{Bc-B}	7.52 ± 0.01 ^{Bd-A}	2.30 ± 0.01 ^{Ac-C}
30	UC	14.27 ± 0.01 ^{Aa-B}	17.56 ± 0.01 ^{Aa-A}	4.30 ± 0.01 ^{Aa-C}
	IC	9.42 ± 0.01 ^{Bb-B}	10.83 ± 0.01 ^{Bc-A}	3.42 ± 0.01 ^{Bb-C}

^aEach column has different capital case letters indicating significant changes between the under canopy and inter canopy of the same afforestation years (t-test). Each column has different lowercase letters indicating significant changes between the under canopy and inter canopy of the various afforestation years ($p < 0.05$, *post hoc* Duncan test). Each row has capital case letters after the space line indicating significant change among litter, above-ground, and below-ground. Means ± SE.

TABLE 4 Plant N pool (ton ha⁻¹) in the eight *Calligonum* planting sites.

Planting age		Above-ground biomass	Below-ground biomass	Litter
1	UC	6.33 ± 1.01 ^{Al-B}	7.52 ± 1.01 ^{Al-A}	5.21 ± 1.00 ^{Al-C}
	IC	4.53 ± 1.01 ^{Bn-B}	7.86 ± 1.01 ^{Bn-A}	5.10 ± 1.00 ^{Bm-C}
4	UC	6.53 ± 1.01 ^{Al-B}	7.92 ± 1.01 ^{Ak-A}	5.33 ± 1.00 ^{Al-C}
	IC	6.09 ± 1.01 ^{Bm-B}	7.12 ± 1.01 ^{Bm-A}	5.23 ± 1.00 ^{Bl-C}
6	UC	6.93 ± 1.01 ^{Ak-B}	8.72 ± 1.01 ^{Aj-A}	5.70 ± 1.00 ^{Ak-C}
	IC	6.20 ± 1.01 ^{Bl-B}	7.91 ± 1.01 ^{Bk-A}	5.60 ± 1.00 ^{Bk-C}
9	UC	8.65 ± 1.01 ^{Af-B}	9.52 ± 1.01 ^{Af-A}	5.87 ± 1.00 ^{Aj-C}
	IC	7.53 ± 2.01 ^{Bj-B}	8.67 ± 1.01 ^{Bj-A}	5.80 ± 1.00 ^{Aj-C}
11	UC	9.30 ± 2.01 ^{Ae-B}	11.66 ± 2.0 ^{Ae-A}	6.30 ± 2.00 ^{Ae-C}
	IC	8.35 ± 2.01 ^{Bf-B}	9.91 ± 2.01 ^{Bf-A}	6.00 ± 2.00 ^{Bf-C}
16	UC	11.85 ± 2.01 ^{Ad-B}	14.77 ± 2.01 ^{Ad-A}	6.90 ± 2.00 ^{Ad-C}
	IC	9.26 ± 2.01 ^{Be-B}	11.48 ± 3.01 ^{Be-A}	6.73 ± 2.00 ^{Ad-C}
25	UC	15.72 ± 3.01 ^{Ab-B}	19.82 ± 4.01 ^{Ab-A}	7.67 ± 2.00 ^{Ac-C}
	IC	11.48 ± 3.01 ^{Bc-B}	13.54 ± 4.01 ^{Bd-A}	7.30 ± 2.00 ^{Ac-C}
30	UC	19.30 ± 4.01 ^{Aa-B}	23.58 ± 5.01 ^{Aa-A}	9.30 ± 2.00 ^{Aa-C}
	IC	14.45 ± 4.01 ^{Bb-B}	16.85 ± 4.01 ^{Bc-A}	8.42 ± 2.00 ^{Bb-C}

^aEach column has different capital case letters indicating significant changes between the under canopy and inter canopy of the same afforestation years (t-test). Each column has different lowercase letters indicating significant changes between the under canopy and inter canopy of the various afforestation years ($p < 0.05$, *post hoc* Duncan test). Each row has capital case letters after the space line indicating significant change among litter, above-ground, and below-ground. Means ± SE.

(Jules et al., 2008; Suganuma et al., 2014). These changes facilitate the distribution of new plant species and lead to the establishment of suitable species in later stages of succession (Liu et al., 2015). Forestry provides appropriate habitats where

plants can grow in arid and desert regions (Amici et al., 2012). Established species can improve environmental conditions worldwide (Ebrahimi et al., 2019). The microclimate created in the understory of the cultivated species reduces the effect of

extreme sunlight; the temperature under the canopy cover of these plants is low, thus reducing the evapotranspiration and, subsequently, water demand in these areas compared to vegetation-free areas (Ebrahimi et al., 2019; Moghbeli et al., 2021). In the study, shrub and forb cover are plant structures that increased due to the planting and establishment of *Calligonum* species in the afforested area. These species rapidly increase biomass and provide a diverse canopy and vertical structure. In addition, increasing the canopy helped to increase the substrate coverage (Moghbeli et al., 2021).

Furthermore, the established plant species in re-vegetated areas help extend plant species in arid and desert areas by capturing the seeds of plant species (Aghababaei et al., 2017). The bushes and shrubs function as seed distributors by conserving wind-scattered seeds, thus increasing the quantity and diversity of plants. The seedlings of other plants can be established under the shade of these bushes, allowing herbaceous species to create colonies and attain sustainability (Hamidi et al., 2020; Moghbeli et al., 2021). Improved conditions and reduced soil erosion due to developments in plant communities increase the soil fertility and permeability, creating a suitable context for seed germination, seedlings' growth, and enhanced efficiency of plants in nutrient- and water-poor environments (Su et al., 2002; Zehtabian et al., 2006; Khosravi et al., 2017).

The 30-year site had the lowest bare soil percentage. It can be attributed to the *C. comosum* mass growing in large communities, covering the soil surface. Therefore, the percentage of canopy increases as the forestry sites age. Multiple research studies have indicated that increasing the quantity and diversity of plant species is among the most positive effects of biological measures in combating desertification (Zehtabian et al., 2006). The cultivation of *Haloxylon* in Shandan, Sistan and Baluchestan, Iran, confirmed that the quantity and diversity of plant species in the region increased significantly as the age of the re-vegetated forests increased (Ebrahimi et al., 2019). Pouyafar and Asgari Moghadam (2006) studied the environmental effects of oil mulch. They concluded that cultivating *H. aphyllum* significantly increases vegetation, species composition, and below-ground biomass. Teymuri Majnabadi et al. (2020) studied the effect of succession on the performance of desert rangelands in Iran. This study confirmed that succession has significantly improved the conditions of microhabitats for the growth of herbaceous plants in degraded desert lands.

Species composition and diversity are some of the essential characteristics of ecosystems; thus, vegetation diversity should be considered in the re-vegetation period (Brancalion et al., 2010). Johnston (2011) discussed coastal ecosystems in Sacramento, California, USA. He reported that species that can foster favorable conditions for other plants through succession are more critical than cultivating various species not resistant to harsh conditions. Our findings indicated that forestry helped enrich vegetation and provided better growth conditions for the

plants to produce seeds. Over time, as the forestry sites aged, the emergence of other plant species was observed, increasing richness and diversity substantially. Strauss (2000) examined artificial forests in Australia and reported that forestry with native species substantially enriches native species in the re-vegetated forests. Ebrahimi et al. (2019) evaluated species composition of artificial forests in Sistan and Baluchestan and demonstrated that the diversity reaches a maximum amid succession. Ruiz-Jaen and Aide (2005) examined plant structure and diversity in Sabana Seca, Puerto Rico, in mid-successional re-vegetated forests. They concluded that plant diversity increases significantly over time.

In this study, the perennial species in the 30-year site displayed the highest growth in population. Increased plant density and diversity can be helpful for ecosystem composition (Teymuri Majnabadi et al., 2020; Moghbeli et al., 2021). The planted shrubs and trees can capture and store mineral and water nutrients in the soil and increase soil fertility (Mofidi et al., 2013; Ebrahimi et al., 2019). These plants can also protect bush species under the canopy cover against extreme sunlight and temperatures in arid regions (Khosravi et al., 2017). The fertile soil and microclimate under the shrubs function as fertile resources for low-height herbaceous plants (Moghbeli et al., 2021). These resources are vital for reviving desert lands since they establish natural substitutes by facilitating the growth of other plants (Ebrahimi et al., 2019). Research studies have shown that biodiversity consistently increases as the succession continues due to the increase in ecosystem complexity (Ruiz-Jaen and Aide, 2005; Jafarian et al., 2014). Aghababaei et al. (2017) examined the process of diversifying plant species from the beginning of Iran's forest re-vegetation projects. They concluded that the introduction of additional species increases diversity after 25 years.

Livestock grazed on *C. comosum* sites aged 11, 16, 25, and 30 years. An average grazing rate increases the richness and diversity of species (Khosravi et al., 2017; Moghbeli et al., 2021). Omar (1991) discussed vegetation changes in Kuwait's arid rangelands. He showed that fully protected rangelands, that is, long-term protection programs (10 years), display signs of rangeland degradation. Diversity and richness at the beginning of the succession phase can be attributed to the high dynamics of a limited number of annuals. High dynamics is an essential structural feature at the beginning of the succession phase (Liu et al., 2015). Moreover, the low quantity of species, diversity, and richness at the beginning of the succession phase in younger sites compared to older sites can be attributed to preventing grazing (El-Keblawy and Ksiksi, 2005; Ebrahimi et al., 2019). Therefore, it can be concluded that well-managed grazing is one of many tools for modifying rangelands and forest understory in modified areas.

The results indicated that re-vegetating desert land with *Calligonum* improved soil fertility in the region. The establishment of plant species in arid lands with harsh

conditions significantly increased the soil N, P, and K under the crown of plants. The results of the researchers showed that the *Calligonum* species improves the soil structure, and the establishment of plant species increases the nutrients in the soil such as N, P, and K, and with the development of plants, the organic matter of the soil also increases significantly (Biabani, 2016). Zehtabian et al. (2006) reported that planting *Calligonum* in Semnan strengthened soil structure and increased soil N, P, and K. The increased diversity and frequency of perennials can be partially attributed to greater soil fertility. The increase in soil nutrient levels under the canopy cover of plants indicates the accumulation of litter, roots, and further root-related activities (Jozefowska et al., 2017). Two factors can activate this mechanism: First, improved vegetation in the region, resulting in decreased wind erosion. Vegetation can capture nutrients and particles carried by the wind. Second, higher nutrient levels are considerably associated with soil roots and adding root mass to the soil (Jozefowska et al., 2017; Yuuan et al., 2018).

We found that soil nutrient value gradually increased during succession; the maximum soil nutrient value was calculated in the 30-year site. This result confirms the second hypothesis presented in the Introduction section. The higher soil fertility in sites with higher ages can be partly explained by increased litter accumulation resulting in increased organic matter and nutrients in the soil due to increased vegetation canopy (Jozefowska et al., 2017; Yuuan et al., 2018; Teymuri Majnabadi et al., 2020).

In sites with higher ages, more extensive canopy covers will allow livestock to access more nutrients. Trees and shrubs with long lifespan increase soil fertility more than the annuals. This increase can be due to the immediate elimination of nutrients stored under canopy cover by the wind in sites with lower age (Cheng et al., 2004).

It should be noted that the biological restoration in arid areas where extreme sunlight and temperatures (high evapotranspiration) limit plant growth can increase vegetation and reduce exposure to sunlight in the space under plant species, hence lowering soil temperature and water loss. Moreover, higher amounts of plant litter and organic matter further increase water storage in the soil. Thus, more litter in low-age areas will result in higher soil fertility (Frouz and Novakova, 2005; Frouz et al., 2008; Ebrahimi et al., 2019).

The results showed that soil EC increased with the age of forests. This increase, however, was insignificant. This increase in EC, especially under the canopy cover, can be due to soluble salts generated by litter accumulation (Jafarian et al., 2014; Lalozaei et al., 2016). Biabani (2016) stated that *Calligonum* has increased soil EC in Iranshahr deserts, Iran.

The results indicated that organic C and N pools in the soil under the canopy were higher than between the canopy, which can be attributed to the higher percentage of the canopy of plant species, litter, and the higher root mass under the canopy, increasing organic C and N pools in surface soil by causing aerial organs and litter to decompose. Consequently, plant

textures become an important source of organic soil C. These plant textures can gradually be transferred to the soil and undergo chemical and biological changes. The maximum C and N pools in the soil and plants were observed in the 25- and 30-year sites. In areas with more vegetation, the amounts of plant textures transferred to the soil will be higher; thus, there will be greater organic matter and, subsequently, N and C pools (Shirzai et al., 2020). Most of the C and N pools in the soil were elevated to the under canopy of sites. The high amount of C and N pools under canopy of *Calligonum* may be due to the fact that most of the organic matter in the soil, related to the decomposition of dead roots and the conversion of microbial biomass to organic matter, which is located at the surface layer soil under canopy of plants (Dianati Tilaki et al., 2009). Dong et al. (2014) reported that large amounts of plant litter in the top soil increase the C stored in this layer of soil compared to deep soil. Woomer et al. (2004) showed that approximately 60% of organic carbon is stored at a soil depth of 20 cm under canopy of plants. Soil C pool is positively correlated to organic matter (Garten and Charles, 2002). This result shows the positive effect of vegetation development in the studied sites.

The results showed that the amounts of C and N pools in the below-ground biomass were higher than those in the above-ground biomass. The reason for this can be attributed to the high amount of woody tissue in the roots compared to the above-ground parts of the plants (Capuana, 2020; Rigi Pardad et al., 2021). In arid rangelands, below-ground biomass of the plants has the largest proportion of total biomass, while above-ground biomass has a small proportion of the total plant biomass (Joneidi Jafari et al., 2013). Plant organs with woody tissue have a greater ability to store C and N (Motamedi et al., 2020). In this regard, other studies have acknowledged that the woodier the tissues in the plant, the greater the plant's ability to uptake C and N (Motamedi et al., 2020; Tessema et al., 2020). Increasing the share of the root increases C and N entrance into the soil (Moghbeli et al., 2021). The type of plant species and even different organs of a plant have different potentials for C and N pools. In fact, the performance of plants to store carbon is a function of various factors such as morphological traits, including plant root height, canopy cover, plant density, plant distribution pattern, topographic characteristics, physical and chemical properties of the soil, and management factors (such as livestock grazing and rangeland exclusion) (Conti and Diaz, 2013; Mirlashkari, 2016). Expansion of vegetation cover will lead to reducing and modifying the amount of CO₂ in the atmosphere by increasing photosynthetic levels and eventually increasing the level of C uptake (Souri et al., 2020). Mirlashkari (2016), in the investigation of the impacts of exclusion on the soil C and N pool in the Jonabad rangeland of Zahedan, Iran, reported that C and N pools were higher in the site with higher plant biomass than the grazed area.

- Amici, V., Rocchini, D., Geri, F., Bacaro, G., Marcantonio, M., and Chiarucci, A. (2012). Effects of an afforestation process on plant species richness: A retrogressive analysis. *Ecol. Complex.* 9, 55–62. doi:10.1016/j.ecocom.2011.11.006
- Amiraslani, F., and Dragovich, D. (2011). Combating desertification in Iran over the last 50 years: An overview of changing approaches. *J. Environ. Manage.* 92, 1–13. doi:10.1016/j.jenvman.2010.08.012
- An, H., Tang, Z., Keesstra, S., and Zhouping, S. (2019). Impact of desertification on soil and plant nutrient stoichiometry in a desert grassland. *Sci. Rep.* 9, 9422. doi:10.1038/s41598-019-45927-0
- Biabani, Z. (2016). *The Relationship between succession and reclamation of vegetation cover and soil in afforestation with Calligonum spp. (Case study: Desert Land of Bampur)*. Iran: M.Sc Thesis, University of Zabol. (In Persian).
- Brancalion, P. H. S., Rodrigues, R. R., Gandolfi, S., Kageyama, P. Y., Nave, A. G., Gandara, F. B., et al. (2010). Instrumentos legais podem contribuir para a restauração de florestas tropicais biodiversas. *Rev. Arvore* 34, 455–470. doi:10.1590/s0100-67622010000300010
- Bray, R. H., and Kurtz, L. T. (1954). Determination of total, organic and available forms of phosphorus in soils. *Eur. J. Soil Sci.* 39–46.50, 1,
- Bremner, J. M. (1996). Nitrogen total, in *Methods of soil analysis*. Editor J. M. Bartels (Madison, WI: Soil Science Society of America), 1085–1122.
- Cao, C. Y., Jiang, S. Y., Ying, Z., Zhang, F. X., and Han, X. S. (2011). Spatial variability of soil nutrients and microbiological properties after the establishment of leguminous shrub *Caragana micro-phylla* Lam. Plantation on sand dune in the Horqin sandy land of Northeast China. *Ecol. Eng.* 37, 1467–1475. doi:10.1016/j.ecoleng.2011.03.012
- Capuana, M. (2020). A review of the performance of woody and herbaceous ornamental plants for phytoremediation in urban areas. *Jforest* 13 (2), 139–151. doi:10.3832/ijfor3242-013
- Chapuis-Lardy, L., Wrage, N., Metay, A., Chotte, J., and Bernoux, M. (2007). Soils, a sink for N₂O? A review. *Glob. Change Biol. Bioenergy* 13, 1–17. doi:10.1111/j.1365-2486.2006.01280.x
- Cheng, X., An, S., Liu, S., and Li, G. (2004). Micro-scale spatial heterogeneity and the loss of carbon, nitrogen and phosphorus in degraded grassland in Ordos Plateau, north Western China. *Plant Soil* 259, 29–37. doi:10.1023/b:plso.0000020948.66471.2b
- Conant, R. T., Cerri, C. E. P., Osborne, B. B., and Paustian, K. (2017). Grassland management impacts on soil carbon stocks: A new synthesis. *Ecol. Appl.* 27 (2), 662–668. doi:10.1002/eap.1473
- Conti, G., and Diaz, S. (2013). Plant functional diversity and carbon storage - an empirical test in semi-arid forest ecosystems. *J. Ecol.* 101 (1), 18–28. doi:10.1111/1365-2745.12012
- Deng, L., Shangguan, Z. P., and Sweeney, S. (2013). Changes in soil carbon and nitrogen following land abandonment of farmland on the Loess plateau, China. *PLoS One* 8, e71923. doi:10.1371/journal.pone.0071923
- Dianati Tilaki, G. H., Naghi pour borj, A. A., Tavakkoli, H., Haidarian Agha khani, M., and Saeed Afkhamoshara, M. R. (2009). Effect of enclosure on soil and plant carbon sequestration in semi-arid rangeland of northern Khorasan. *J. Iran. Range Manag. Soc.* 3, 668–679.
- Dong, W., Gao-Lin, W., Yuan-Jun, Z., and Zhi-Huam, S. (2014). Grazing exclusion effects on above- and below-ground C and N pools of typical grassland on the Loess Plateau (China). *Catena* 123, 120–113.
- Ebrahimi, M., Khosravi, H., and Rigi, M. (2016). Short-term grazing exclusion from heavy livestock rangelands affects vegetation cover and soil properties in natural ecosystems of southeastern Iran. *Ecol. Eng.* 95, 10–18. doi:10.1016/j.ecoleng.2016.06.069
- Ebrahimi, M., Mohammadi, F., Fakhireh, A., and Bameri, A. (2019). Effects of *Haloxylon* spp. of different age classes on vegetation cover and soil properties on an arid desert steppe in Iran. *Pedosphere* 29 (5), 619–631. doi:10.1016/s1002-0160(17)60378-3
- El-Keblawy, A., and Ksiksi, T. (2005). Artificial forests as conservation sites for the native flora of the UAE. *For. Ecol. Manage.*, 213, 288–296. doi:10.1016/j.foreco.2005.03.058
- Frouz, J., and Novakova, A. (2005). Development of soil microbial properties in topsoil layer during spontaneous succession in heaps after Brown coal mining in relation to humus microstructure development. *Geoderma* 129, 54–64. doi:10.1016/j.geoderma.2004.12.033
- Frouz, J., Prach, K., Pizl, V., Hanel, L., Sary, J., Tajovsky, K., et al. (2008). Interactions between soil development, vegetation and soil fauna during spontaneous succession in post mining sites. *Eur. J. Soil Biol.* 44, 109–121. doi:10.1016/j.ejsobi.2007.09.002
- Garten, J., and Charles, T. (2002). Soil carbon storage beneath recently established tree plantations in Tennessee and South Carolina, USA. *Biomass Bioenergy* 23 (2), 93–102. doi:10.1016/s0961-9534(02)00033-8
- Hamidi, N., and Attarrosan, S. (2020). Effect of *Albizia lebbek* (L.) Benth forestry on plant species diversity and physicochemical characteristics of soil in the warm and dry desert climate. *J. Plant Ecosyst. Conservation* 8 (16), 173–199.
- Hashemi Rad, M., Ebrahimi, M., and Shirmohammadi, E. (2018). Land use change effects on plant and soil properties in a mountainous region of Iran. *J. Environ. Sci. Manag.* 21 (2), 47–56. doi:10.47125/jesam/2018_2/07
- Hu, Y., Han, Y., and Zhang, Y. (2020). Land desertification and its influencing factors in Kazakhstan. *J. Arid. Environ.* 180, 104203. doi:10.1016/j.jaridenv.2020.104203
- Report of Rangeland Improvement (2018). *Agriculture and natural*.
- Jafarian, A., Jafari, M., and Tavili, M. (2014). Assessment of *Haloxylon* plantation effects for desert reclamation with emphasis on substratum's soil and vegetation properties in Kale Shoor of Sabzevar region, Iran. *Range Desert Res.* 21, 51–61. (In Persian).
- Johnston, D. B. (2011). Movement of weed seeds in reclamation areas. *Restor. Ecol.* 19, 446–449. doi:10.1111/j.1526-100x.2011.00785.x
- Joneidi Jafari, H. (2013). Relationship between root biomass and soil organic carbon: Case Study of arid shrub lands of Semnan province. *Desert* 18, 173–176.
- Jozefowska, A., Pietrzykowski, M., Wos, B., Cajthaml, T., and Frouz, J. (2017). The effects of tree species and substrate on carbon sequestration and chemical and biological properties in reforested post-mining soils. *Geoderma* 292, 9–16. doi:10.1016/j.geoderma.2017.01.008
- Jules, M. J., Sawyer, J. O., and Jules, E. S. (2008). Assessing the relationships between stand development and understory vegetation using a 420-year chronosequence. *For. Ecol. Manage.* 255, 2384–2393. doi:10.1016/j.foreco.2007.12.042
- Khosravi, H., Ebrahimi, M., and Rigi, M. (2017). Effects of rangeland exclusion on plant cover and soil properties in a steppe rangeland of Southeastern Iran. *Arid Land Res. Manag.* 31, 352–371. doi:10.1080/15324982.2017.1310147
- Knudsen, D., Peterson, G. A., and Pratt, P. (1982). "Lithium, sodium and potassium," in *Methods of soil analysis*. Editor A. L. Page (Madison, WI: American Society of Agronomy), 225–246.
- Lalozaei, A., Dahmardeh Ghaleno, M. R., and Ebrahimi, M. (2016). Effect of the tree windbreakers of *Tamarix* and *Eucalyptus* on some physical and chemical properties of soil in Hamoon Plain. *J. Watershed Eng. Manag.* 7 (4), 536–542.
- Liu, B., Zhao, W., Liu, Z., Yang, Y., Luo, W., Zhou, H., et al. (2015). Changes in species diversity, aboveground biomass, and vegetation cover along an afforestation successional gradient in a semiarid desert steppe of China. *Ecol. Eng.* 81, 301–311. doi:10.1016/j.ecoleng.2015.04.014
- Lo, I., Tsang, D., Yip, T., Wang, F., and Zhang, W. H. (2011). Influence of injection conditions on EDDS-flushing of metal-contaminated soil. *J. Hazard. Mat.* 192, 667–675. doi:10.1016/j.jhazmat.2011.05.067
- Mehdipour, I., Landi, A., and Amerikha, H. (2007). *Comparison the effect of land use on CO₂ emissions in north of Khuzestan*. Karaj: 10th conference on soil science of Iran.
- Mirlashkari, F. (2016). The Impact of long-term grazing exclusion and different grazing intensity on some vegetation characteristics, soil carbon pool and nitrogen pool in Joonabad rangeland-Zahedan. *Ph.D.*, University of Zabol, Iran. (In Persian)
- Mofidi, M., Jafari, M., Tavili, A., Rashtbari, M., and Alijanpour, A. (2013). Grazing exclusion effect on soil and vegetation properties in imam kandi rangelands, Iran. *Arid Land Res. Manag.* 27, 32–40. doi:10.1080/15324982.2012.719575
- Moghbeli, Z., Ebrahimi, M., and Shirmohammadi, E. (2021). Effects of different livestock grazing intensities on plant cover, soil properties, and above and below ground C and N pools in arid ecosystems (Jiroft rangeland, Iran). *Environ. Resour. Res.* 9 (1), 13–30.
- Mohammadi, T., Dastorani, M. T., Azimzadeh, H. R., and Jafarpour, A. (2018). Study of watershed management biological practices on soil carbon sequestration (case study: Kelesan Watershed-Fars Province). *Iran. J. Watershed Manag. Sci. Eng.* 12 (41), 31–40. (In Persian).
- Motamedi, J., Ebrahimi, Sh., and Sheidai Karkaj, E. (2020). Relationship between carbon storage of *Astragalus brachyanus* species with plant characteristics, habitat characteristics and rangeland management, Rajan, West Azerbaijan. *J. Range Watershed Manag.* 73 (2), 423–438. (In Persian).
- Nelson, D. W., and Sommers, L. E. (1982). "Total carbon, organic carbon and organic matter," in *Methods of soil analysis*. Editors A. L. Page, R. H. Miller, and D. R. Keeney (Madison, WI: American Society of Agronomy and Soil Science Society of American), 1–129.

- Omar, S. A. (1991). Dynamics of range plants following 10 years of protection in arid rangelands of Kuwait. *J. Arid. Environ.* 21, 99–111. doi:10.1016/s0140-1963(18)30732-8
- Pouyafar, A. M., and Asgari Moghadam, Z. (2006). Investigation of the environmental impacts of oil mulch application. *Rangel. For. J.* 70, 36–41. (In Persian).
- Rechinger, K. H., Ali, S. I., Browicz, K., Chrtkova-Zertova, A., Heller, D., Heyn, C. C., et al. (1984). "Papilionaceae II," in *Flora iranica*. Editor K. H. Rechinger (Graz: Akademische Druck U Verlagsanstalt), 65–77.
- Rechinger, K. H., Melzheimer, V., Moschl, W., and Schiman-Czeika, H. (1988). "Caryophyllaceae II," in *Flora iranica*. Editor K. H. Rechinger (Graz: Akademische Druck U Verlagsanstalt), 344–351.
- Resources Center. *Sistan Baluchestan*, 155p. (In Persian).
- Rhoades, J. D. (1996). "Salinity: Electrical conductivity and total dissolved solids," in *Methods of soil analysis*. Editor A. L. Page (Madison, WI: American Society of Agronomy), 417–435.
- Rigi Pardad, M., Ebrahimi, M., and Erfani, M. (2021). Carbon pool capacity of plant species *Calligonum comosum* L. and *Haloxylon ammodendron* (C.A.Mey.) bunge in Mirjaveh plain. *Environmental Resources Research*. 9(2), 267–276.
- Ritchie, M. E. (2020). Grazing Management, forage production and soil carbon dynamics. *Resources* 9, 49. doi:10.3390/resources9040049
- Ruiz-Jaen, M. C., and Aide, T. M. (2005). Vegetation structure, species diversity and ecosystem processes as measures of restoration success. *For. Ecol. Manage.* 218, 159–173. doi:10.1016/j.foreco.2005.07.008
- Shirzai, M., Ebrahimi, M., and Saberi, M. (2020). *The 7th scientific congress on the development and promotion of architecture and urbanism in Iran*, Carbon sequestration in *Artemisia sieberi*, Leuchonassi rangeland of zahedan city
- Souri, M., Fayyaz, M., Kamali, N., Ashuri, P., and Nateghi, S. (2020). The carbon storage capacity of the *Artemisia sieberi* under the enclosure (Kalat Sadat Abad, Sabzevar city). *J. Plant Res. Iran. J. Biol.* 32 (4), 736–748. (In Persian).
- Strauss, S. Y. (2001). Benefits and risks of biotic exchange between Eucalyptus plantations and native Australian forests. *Austral Ecol.* 26, 447–457. doi:10.1046/j.1442-9993.2001.01136.x
- Su, Y. Z., Zhao, H. L., and Zhang, T. H. (2002). Influencing mechanism of several shrubs and subshrubs on soil fertility in Keerqin sandy land. *Chin. J. Appl. Ecol.* 13, 802–806.
- Suganuma, M. S., de Assis, G. B., and Durigan, G. (2014). Changes in plant species composition and functional traits along the successional trajectory of a restored patch of Atlantic Forest. *Community Ecol.* 15, 27–36. doi:10.1556/comec.15.2014.1.3
- Tessema, B., Sommer, R., Piikki, K., Soderstrom, M., Namirembe, S., Notenbaert, A., et al. (2020). Potential for soil organic carbon sequestration in grasslands in east african countries: A review. *Grassl. Sci.* 66, 135–144. doi:10.1111/grs.12267
- Teymuri Majnabadi, J., Ramak, P., and Karimian, V. (2020). Effect of temporal succession of biological restoration on desert rangeland (case study; khaf rangelands, khorasan razavi province). *J. Range Watershed Manag.* 27 (3), 657–664. (In Persian).
- Thomas, G. W. (1996). "Soil pH and soil acidity," in *Methods of soil analysis*. Editor J. M. Bartels (Madison, WI: Soil Science Society of America), 475–490.
- Udayana, C., Skarpe, C., Solberg, S., Mathisen, K. M., and Andreassen, H. P. (2019). Soil properties after forest rehabilitation by planting teak and mahogany in Java, Indonesia. *For. Sci. Technol.* 15 (4), 230–237. doi:10.1080/21580103.2019.1673220
- UNDP (2000). *Carbon sequestration in the desertified rangelands of Hossein Abad, through community based Management, program coordination*, 1–7.
- Veramesh, S., Hoseini, M., Abdi, N., and Akbaria, M. (2010). Increment of soil carbon sequestration due to forestation and its relation with some physical and chemical factors of soil. *Iran. J. For.* 2 (1), 91–102.
- Wang, A., Luo, C., Yang, R., Chen, Y., Shen, Z., and Li, X. (2012). Metal leaching along soil profiles after the EDDS application-A field study. *Environ. Pollut.* 164, 204–210. doi:10.1016/j.envpol.2012.01.031
- Wang, D., Wu, G. L., Zhu, Y. J., and Shi, Z. H. (2014). Grazing exclusion effects on above- and below ground C and N pools of typical grassland on the Loess Plateau (China). *Catena* 123, 113–120. doi:10.1016/j.catena.2014.07.018
- Woomer, P. L., Tourc, A., and Sall, M. (2004). Carbon stocks in Senegal's sahel transition zone. *J. Arid. Environ.* 59 (3), 499–510. doi:10.1016/j.jaridenv.2004.03.027
- Wu, G. L., Liu, Z. H., Zhang, L., Chen, J. M., and Hu, T. M. (2010). Long-term fencing improved soil properties and soil organic carbon storage in an alpine swamp meadow of Western China. *Plant Soil* 332, 331–337. doi:10.1007/s11104-010-0299-0
- Yang, X., Xu, M., Zhao, Y., Bao, T., Ren, W., and Shi, Y. (2020). Trampling disturbance of biocrust enhances soil carbon emission. *Rangel. Ecol. Manag.* 73 (4), 501–510. doi:10.1016/j.rama.2020.02.005
- Yuan, Y., Zhao, Z., Niu, S., Li, X., Wang, Y., and Bai, Z., (2006). *The effects of Haloxylon aphyllum and Calligonum comosum species in stabilization and reclamation of sand dunes of Rezaabad, Semnan province. Desert*, 165, 72167–79175. Reclamation promotes the succession of the soil and vegetation in opencast coal mine: A case study from *Robinia pseudoacacia* reclaimed forests, pingshuo mine, China *Catena*
- Zohary, M. (1963). On the geobotanical structure of Iran. *Bull. Res. Council. Isr. Sect. D. Bot.* 11, 35–38.



OPEN ACCESS

EDITED BY
Hamid Gholami,
University of Hormozgan, Iran

REVIEWED BY
Shuisen Chen,
Guangzhou Institute of Geography,
China
Gustavo Lyra,
Universidade Federal Rural do Rio de
Janeiro, Brazil

*CORRESPONDENCE
Farhad Zolfaghari,
zol.farhad@gmail.com

SPECIALTY SECTION
This article was submitted to Drylands,
a section of the journal
Frontiers in Environmental Science

RECEIVED 23 March 2022
ACCEPTED 03 November 2022
PUBLISHED 28 November 2022

CITATION
Zolfaghari F, Azarnivand H, Khosravi H,
Zehtabian G and Sigaroudi SK (2022),
Monitoring the severity of degradation
and desertification by remote sensing
(case study: Hamoun
International Wetland).
Front. Environ. Sci. 10:902687.
doi: 10.3389/fenvs.2022.902687

COPYRIGHT
© 2022 Zolfaghari, Azarnivand, Khosravi,
Zehtabian and Sigaroudi. This is an
open-access article distributed under
the terms of the [Creative Commons
Attribution License \(CC BY\)](#). The use,
distribution or reproduction in other
forums is permitted, provided the
original author(s) and the copyright
owner(s) are credited and that the
original publication in this journal is
cited, in accordance with accepted
academic practice. No use, distribution
or reproduction is permitted which does
not comply with these terms.

Monitoring the severity of degradation and desertification by remote sensing (case study: Hamoun International Wetland)

Farhad Zolfaghari^{1*}, Hossein Azarnivand², Hasan Khosravi²,
Gholamreza Zehtabian² and Shahram Khalighi Sigaroudi²

¹Higher Education Complex of Saravan, Saravan, Baluchestan, Iran, ²Faculty of Natural Resources
University of Tehran, Tehran, Karaj, Iran

Monitoring degradation in arid and semi-arid areas is one of the main concerns for governments, given the growing degradation trend. Meanwhile, detecting the areas subjected to degradation requiring management in the shortest time and at the lowest cost is a necessity, especially in border areas such as Hamoun Wetland, located between Iran and Afghanistan. Albedo and normalized difference vegetation index (NDVI) were calculated using remote sensing technology to monitor the degradation intensity in different periods (August 1999, 2009, 2015, and 2020). Change vector analysis in brightness and greenness indices for 1999 and 2020 was used to determine the changes in intensity. Linear regression was run between albedo and NDVI. Finally, degradation intensity (DI) map was developed to monitor degradation intensity. A confusion matrix was created between the change vector analysis (CVA) and the albedo–NDVI model to evaluate the accuracy of the map obtained from this model for 1,476 pixels of different classes. The linear regression between NDVI and albedo showed a negative correlation between indices ($R = -0.849$). The results showed an increase for the regions with null, low, and medium degradation intensity, while an expansion was observed for the regions with severe and extreme degradation. The confusion matrix results indicated the high accuracy (0.705) of the degradation intensity model for the study area. These changes were about 52.01% from 1999 to 2009, 7.07% from 2009 to 2015, 56.26% from 1999 to 2015, and 55.15% from 2015 to 2020. Additionally, the average rate of changes in degradation intensity between 1999 and 2020 was 13.11%.

KEYWORDS

monitoring, degradation, albedo, NDVI, Hamoun Wetland

1 Introduction

Vegetation changes are closely related to desertification. Thus, vegetation index is one of the main factors in recognizing desertification processes. On the other hand, a decrease in vegetation cover and biomass is correlated with soil degradation, leading to increased surface albedo (Cordeiro et al., 2015). Changes in vegetation affect the level of surface

albedo (Myhre and Myhre, 2003), and different vegetation covers represent different albedo values (Kang and Hong, 2008). Albedo has the potential to monitor ecosystem performance changes in arid regions and provides warning of the beginning of desertification (Zhao et al., 2018). Meanwhile, surface albedo is one of the most important components causing surface radiation balance (BdaS et al., 2016). Albedo determines the energy budget in micrometeorological conditions, including temperature and aridity of a land (Goudei and Middleton, 2006). Increasing land surface albedo implies degradation of land quality (Piña et al., 2016), and vegetation can be considered one of the most important key components in reducing the effects of erosion and desertification in arid areas. Desertification development and vegetation cover change are among the factors causing changes in albedo. Surface albedo is defined as the ratio of the total radiation from the Earth's surface to total incoming solar radiation, which often has a wavelength range of 0.3–3 μm . It is one of the most important factors controlling the energy available throughout the day with surface change processes (Houldcroft et al., 2009). Therefore, it can be said that the change in vegetation affects the surface albedo and desertification occurs with the destruction of vegetation, and the surface albedo increases in the degraded areas (Zhao et al., 2018). Zongyi et al. (2011) presented the albedo–NDVI model for monitoring desertification (Zongyi et al., 2011). They showed that albedo and NDVI could well reflect the desertification intensity. Vegetation, the combination of water and heat and their changes, and desertified areas could be easily detected using multi-spectral remote sensing information. Remote sensing-based vegetation indices and land surface albedo are two preferable indicators for monitoring the degradation process (Zhao et al., 2018).

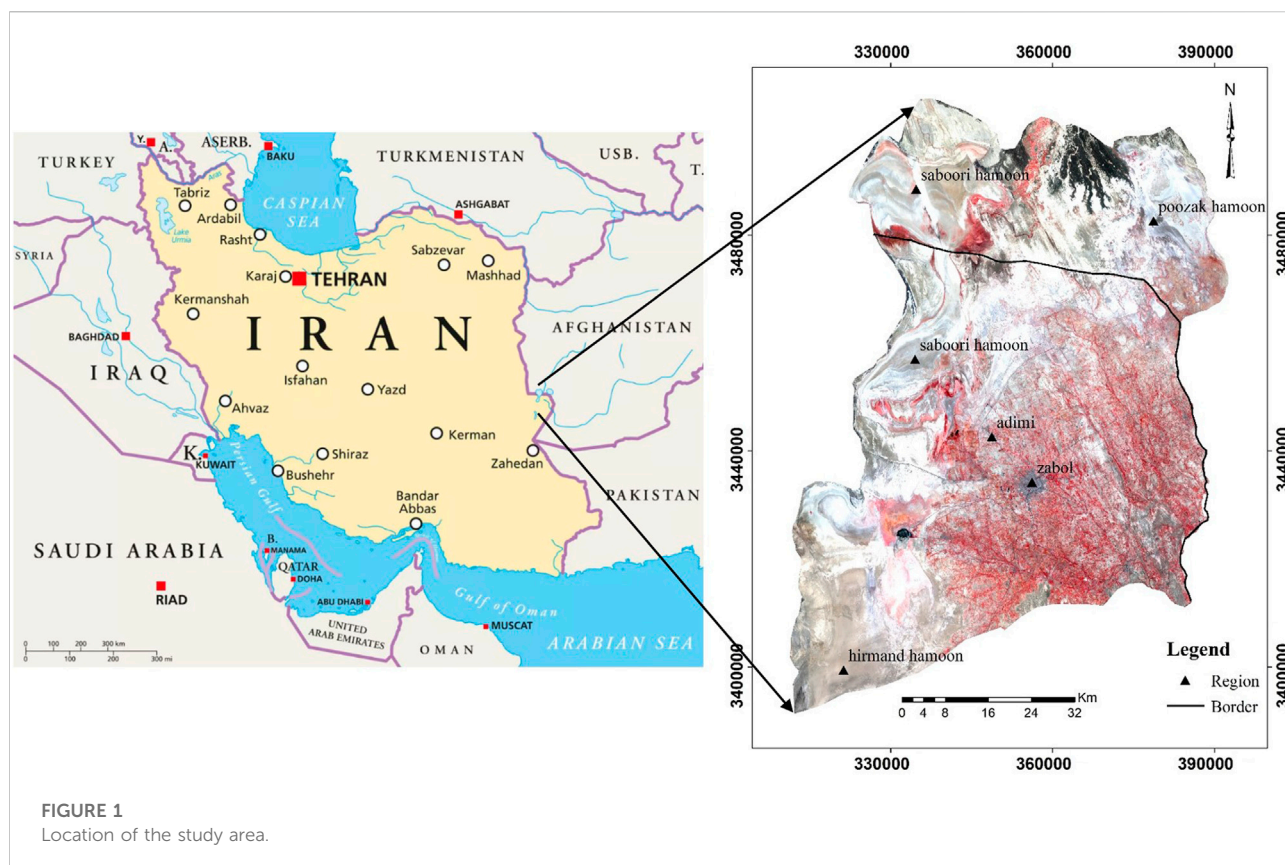
Pan and Li (2013) selected three different groups, namely, vegetation, water, and bare soil, based on the spectral mixture analysis model (Pan and Li, 2013). They assessed the status of desertification based on the temporal-spectral feature of vegetation and surface albedo components derived from Landsat satellite images. Karnieli et al. (2014) examined the changes in NDVI and albedo indices for four periods using the change vector analysis (CVA) technique to understand the spatial-temporal dynamics of the environmental processes (Karnieli et al., 2014). They used four different Landsat images and showed the changes for each time step during the studied period. Cordeiro et al. (2015) estimated the indices affecting desertification in Natal County using the SEBAL algorithm, albedo, vegetation cover, and surface temperature indices with the help of remote sensing technology (Cordeiro et al., 2015). Lamchin et al. (2016) developed a quantitative model on a local scale using remote sensing data to evaluate land cover changes and desertification (Lamchin et al., 2016). They examined the land surface status for vegetation biomass, landscape pattern, and micrometeorology using NDVI, the Topsoil Grain Size Index (TGSi), and the albedo index. Pina

et al. (2016) extracted NDVI, BSI, and the albedo index from Landsat satellite images using remote sensing (Piña et al., 2016). They applied the CVA model to define the direction and value of these indices for determining either degradation or progress of land surface status in different periods. Additionally, they determined the desertification rate index based on the relationship between NDVI and albedo.

Han et al. (2015) calculated the MSAVI, FVC, and TVDI, and land surface temperature plus surface albedo to evaluate desertification using Landsat images by applying the geographic information system (Han et al., 2015). They used these indices to analyze the spatiotemporal pattern of desertification in different periods. Querino et al. (2016) analyzed the spatiotemporal dynamics of the normalized difference vegetation index (NDVI), leaf area index (LAI), surface albedo, and temperature in two different vegetation covers, preserved and deforested areas (Querino et al., 2016). They showed that the forest conversion implies a decreased NDVI and LAI and an increased surface albedo plus surface temperature.

Different methods have been presented to assess and classify desertification intensity levels in Hamoun International Wetland (Fozuni, 2007; Mohammad Ghasemi et al., 2008; Parvariasl et al., 2010; Zolfaghari et al., 2011; Eftekhari et al., 2015). Most of them have suffered many problems such as high costs, expansive areas, and lack of access to areas beyond the political boundaries of Iran due to political and security issues. On the other hand, previous studies have been based on the NDVI or other vegetation indices. The relationship between vegetation changes and albedo has been neglected or sparsely studied with regard to desertification in this region and other areas in Iran. With an area of about 15,197 km^2 , Hamoun International Wetland is located in the southeastern part of Iran, extending as a belt around the Sistan region with more than 400,000 people. Dried Hamoun Lake contains large amounts of erodible sediment, conducive to wind erosion and dust (Choobari et al., 2014). For ecological risk control of degradation in larger arid and semi-arid areas, using remote sensing with the extraction of the albedo and vegetation index is appropriate (Wei et al., 2020). The indices are simple and easy to obtain, which is conducive for quantitative analysis, evaluation, and monitoring of degradation rate (Wu et al., 2019).

Thus, it is necessary to use inexpensive and quick methods to monitor this area's degradation and land cover changes. Detecting degradation areas for implementing appropriate management plans with the minimum cost and within the shortest time is of priority for governments and communities involved. To achieve this goal and identify the degradation areas in different periods, albedo indices and NDVI can be used to monitor and prepare degradation intensity maps. Because of its simplicity in detecting damaged areas within the shortest time with the lowest cost, this model, as a simple and innovative method, can serve as an alternative to the many methods presented for identifying desert areas that require extensive



field operations, especially in large border areas located between countries and where field access to the areas is not safe. Despite the importance of Hamoun Wetland, most field studies on the status of this particular geographical area are difficult and rare due to its location between Iran and Afghanistan and the conflicts in Afghanistan (UNEP, 2002; FAO, 2015). Therefore, most studies have focused on the Iranian part of the wetland, and parts of the wetland located in Afghanistan have been less studied. Less has been studied about degraded areas in Hamoun International Wetland due to recent droughts and lack of access to a part of the wetland in Afghanistan. Degradation intensity was evaluated during different periods based on remote sensing technology in this study.

2 Materials and methods

2.1 Study area

With about 15,197 km², Hamoun International Wetland is situated in southeast Iran. The area of Hamoun International Wetland in Iran is 62,095 ha, while it is 66,478 ha in Afghanistan (Kariminazar et al., 2010) (Figure 1). The area is characterized by even topography occurring between 30° 5' – 31° 28' N and 60° 15' – 61° 50' E (Kariminazar et al., 2010). Hamoun

International Wetland is one of the most ecologically valuable areas in Iran (Scott and Smart, 1992). According to the long-term statistics of the Zabol synoptic station, the mean long-term rainfall in this region is 61.1 mm, about 44% occurring in winter. The mean long-term temperature is 26.6°C, and the mean monthly temperatures of the warmest (July) and coldest months (January) are 41.4°C and 2.4°C, respectively. Based on long-term data, the maximum mean wind speed occurs in June, July, August, and September, while the lowest mean wind speed happens in December (Zolfaghari et al., 2011).

2.2 Research methodology

In this study, the steps to monitor degradation in the Hamoun International Wetland were as follows:

Step 1: Satellite images were prepared, and image preparation processes were performed.

Step 2: NDVI was calculated using reflectance bands and albedo index based on the SEBAL algorithm.

Step 3: The area's degradation equation and degradation intensity map were prepared.

Step 4: Brightness and greenness indices for 16 August 1999 and 17 August 2020 were calculated to determine the intensity changes using vector analysis.

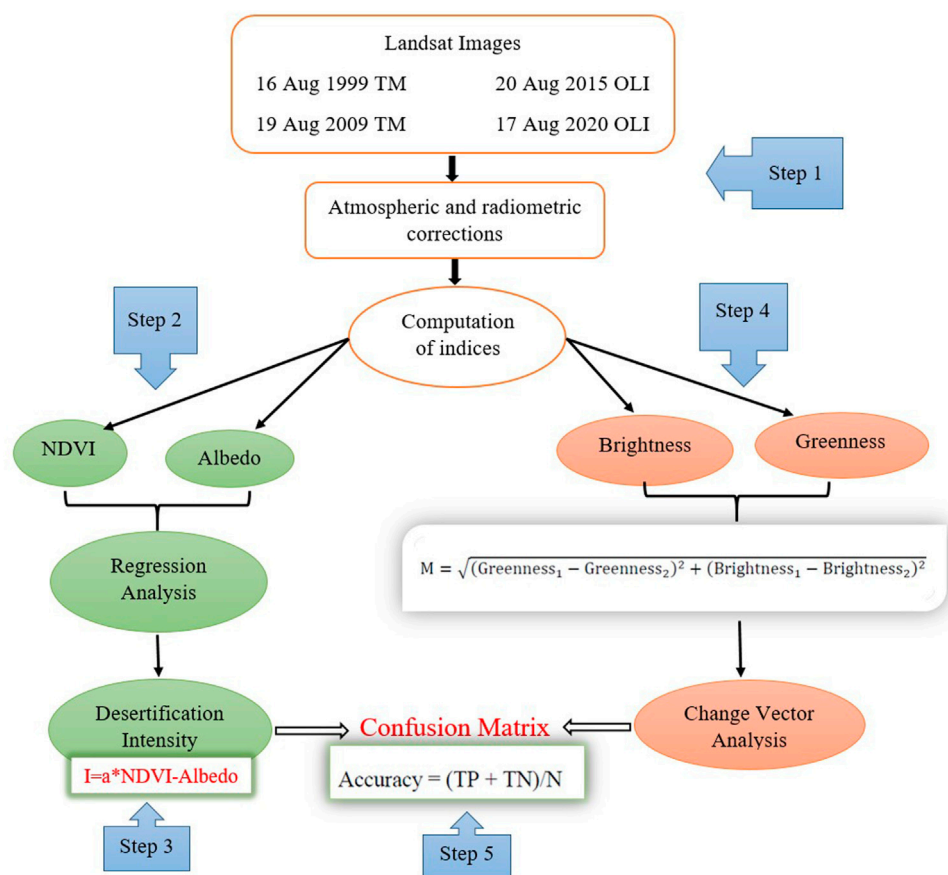


FIGURE 2

Steps in determining the intensity of degradation based on the albedo-NDVI model. N, condition negative; TP, true positive; TN, true negative; M, magnitude of change; I, intensity of degradation; greenness 1, 2, DN values of greenness from 1999 and 2020; brightness 1, 2, DN values of brightness from 1999 and 2020.

Step 5: The precision of the prepared map was assessed by controlling the points obtained from step 4, and a confusion matrix was formed.

In step 1, satellite data related to Landsat 8, OLI sensor, on 17 August 2020, 20 August 2015, and Landsat Thematic Mapper 5 (TM) for 16 August 1999, and 19 August 2009 (Path 157-Row 38 and Path 157-Row 39), with a completely clear sky, were downloaded from <http://earthexplorer.usgs.gov/>.

For proper image efficiency and reduction of sensor error and to increase the image quality before calculating the required indices, first, the DN value for each band must be converted into spectral radiance and then to spectral reflectance (Lamchin et al., 2016). This operation was carried out according to Landsat 8 manual (Landsat 8, 2015). The flowchart and different steps of determining the intensity of degradation based on the albedo-NDVI model and change vector analysis are shown in Figure 2. In this study, summer season (August) was selected to reduce the error caused by surface soil moisture. Another reason was the

absence of annual plant species in this season since the soil surface is dry and contains only permanent species that play a very important role in soil stability and protection.

2.3 NDVI-albedo model

2.3.1 Calculation of the indices

Normalized difference vegetation index (NDVI) are among the most important indicators, defined as the ratio of reflectivity measured in visible red radiation (red band) to near-infrared reflectance (NIR band). Since NDVI are highly affected by chlorophyll absorption in evergreen leafy cover and vegetation density and the contrast between vegetation and soil is highest in red and near-infrared bands, NDVI were selected (Cai et al., 2010; Khosravi et al., 2017). This index was estimated according to Eq. 1.

$$\text{NDVI} = (\text{NIR} - \text{R}) / (\text{NIR} + \text{R}), \quad (1)$$

where NIR is the near-infrared band and R is the red band.

In this study, for the calculation of the water index, we used MNDWI (Modified Normalized Difference Water Index) to distinguish water bodies (Wu et al., 2019). The MNDWI was calculated using Equation 2.

$$\text{MNDWI} = \frac{(\text{Green} - \text{NIR})}{(\text{Green} + \text{NIR})}, \quad (2)$$

where green is the green band and NIR is the near-infrared band.

Another important index is surface albedo, defined as the ratio of the reflected radiation to the incident shortwave radiation. The surface albedo was calculated using Eq. 3 (Allen et al., 2002).

$$\alpha = \frac{\alpha_{\text{toa}} - \alpha_{\text{path-radiance}}}{\tau_{\text{sw}}^2}, \quad (3)$$

where

$\alpha_{\text{path-radiance}}$ is the average portion of the incoming solar radiation across all bands which is back-scattered to the satellite before it reaches the earth's surface, with the values for $\alpha_{\text{path-radiance}}$ ranging between 0.025 and 0.04 according to the SEBAL model; its value was set at 0.03 in this study (Allen et al., 2002).

α_{toa} is the above-atmospheric albedo and is calculated through Eq. 4 (Allen et al., 2002).

$$\alpha_{\text{toa}} = \sum (\omega_{\lambda} * \rho_{\lambda}), \quad (4)$$

where

ω_{λ} is the weighted coefficients for non-thermal bands and ρ_{λ} is the spectral reflectivity of each band.

The weighted coefficients for non-thermal bands can be calculated from Eq. 5 (Allen et al., 2002).

$$\omega_{\lambda} = \frac{\text{ESUN}_{\lambda}}{\sum \text{ESUN}_{\lambda}}, \quad (5)$$

where ESUN_{λ} is the solar exo-atmospheric irradiance for each band.

τ_{sw} is the atmospheric transitivity, which is a part of the incident radiation transmitted by the atmosphere, and represents the effects of the atmosphere. Given that this effect exists for both incoming and outgoing radiation, its square is used to calculate the surface albedo. For a clear and dry sky, it is calculated using Eq. 6 (Allen et al., 2002).

$$\tau_{\text{sw}} = 0.75 + 2 * 10^{-5} * Z, \quad (6)$$

where Z is elevation above sea level (m).

In step 3, to develop a degradation map, the NDVI and albedo indices were normalized. For processing normalization data, the maximum and minimum values of NDVI and albedo in the study area were found, they were used for data normalization processing based on Eqs 7 and 8, and then a linear regression was taken between these two indices (Zongyi et al., 2011; Han et al., 2015).

$$\text{NDVI}_N = \left(\frac{\text{NDVI} - \text{NDVI}_{\min}}{\text{NDVI}_{\max} - \text{NDVI}_{\min}} \right) \times 100 \quad (7)$$

$$\text{Albedo}_N = \left(\frac{\text{Albedo} - \text{Albedo}_{\min}}{\text{Albedo}_{\max} - \text{Albedo}_{\min}} \right) \times 100 \quad (8)$$

The slope coefficient of the regression line between NDVI and albedo indices was calculated to achieve the degradation intensity equation, and the resulting equation was applied to determine the degradation intensity. The relationship obtained from the linear regression between NDVI and albedo is given as Eq. 9:

$$\text{Albedo} = -0.8491 * \text{NDVI} + 0.6573. \quad (9)$$

To evaluate the degradation intensity of the study area, Eq. 10 was used (Zongyi et al., 2011; Lamchin et al., 2016):

$$\text{DI} = a * \text{NDVI} - \text{Albedo}. \quad (10)$$

In this equation, DI represents the degradation intensity, and the a value is the slope of the orthogonal lines found in the NDVI-albedo relationship, or in this study, 0.8491 (1/1.177 Eq. 9). The degradation index based on the Jenks natural breaks index was classified into five classes (null, low, moderate, severe, and extreme) using ArcGIS10.8 software (Han et al., 2015; Han et al., 2015; Piña et al., 2016; Wei et al., 2020).

2.4 Change vector analysis model

The change vector analysis model was applied to multi-temporal data to compare the differences in intensity of change in times (Ali Baig et al., 2014). The tasseled cap greenness and brightness were used for two successive periods 1999 and 2020.

The magnitude of change was calculated by Eq. 11 to evaluate the intensity of change between 1999 and 2020.

$$M = \sqrt{(\text{Greenness}_{1999} - \text{Greenness}_{2020})^2 + (\text{Brightness}_{1999} - \text{Brightness}_{2020})^2} \quad (11)$$

The coefficient used for Landsat 8 (OLI) and Landsat 5 (TM) to evaluate the greenness and brightness of the study area is shown in Supplementary Tables S1, S2 (Khosravi et al., 2017).

Eventually, 1,476 pixels of different classes were selected randomly (Table 1), and a confusion matrix was created between the map prepared by the NDVI-albedo model and the change vector analysis derived from brightness and greenness indices to calculate the kappa coefficient accuracy.

3 Results

3.1 Variation of albedo index

Evaluation and classification by the natural breaks method using ArcGIS10.8 revealed that the albedo index for August 1999, 2009, 2015, and 2020 was variable (Supplementary Figures S1,

TABLE 1 Percentage of pixels selected in each class.

Class	Extreme	Sever	Moderate	Low	Null
No. of pixel	337	455	333	261	90
Percent	22.8	30.8	22.6	17.7	6.1

TABLE 2 Results from the study of albedo and NDVI.

NDVI			Albedo index			Year
Average	High	Low	Average	High	Low	
0.021	0.60	−0.75	0.38	0.63	0.06	1999
0.14	0.67	−0.25	0.41	0.70	0.14	2009
0.10	0.63	−0.26	0.48	0.81	0.11	2015
0.13	0.63	−0.26	0.28	0.45	0.13	2020

S2). The albedo index in the four periods showed the range of 0.06–0.63 in August 1999, 0.14–0.7 in August 2009, 0.11–0.81 in August 2015, and 0.13–0.45 in August 2020. The maximum albedo increased from 1999 to 2015, but in 2020, it decreased due to floods in parts of the wetland (Table 2). Additionally, the average albedo index in the region was variable from 1999 to 2020.

The results also showed that the highest albedo value occurred in the northern, northwestern, and western parts of the wetland (Saburi and Puzak Hamoun), indicating vegetation decline and destruction of Hamoun International Wetland during the years. The results of the classification of albedo classes in the study area using the Jenks natural breaks method are presented in Table 2.

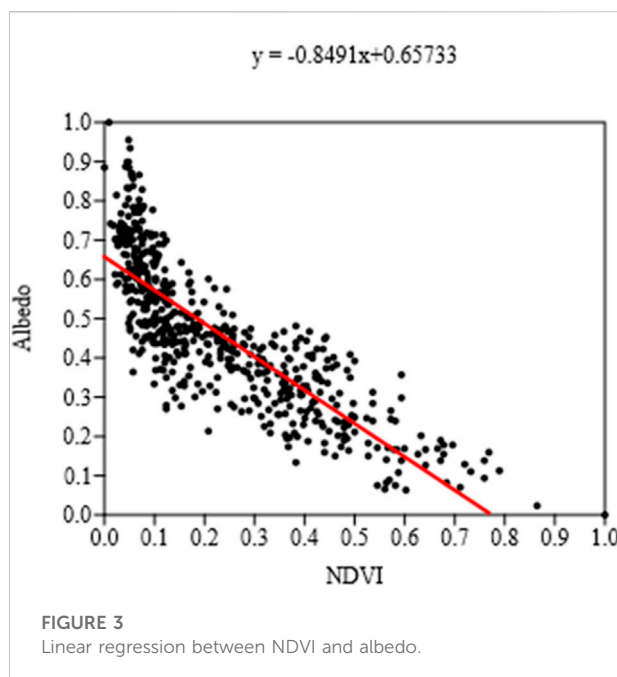
3.2 Variation of NDVI

The NDVI estimations for August 1999, 2009, 2015, and 2020 are shown in Supplementary Figures S3, S4 for a comparative study of the changing trend.

According to NDVI classification using ArcGIS10.8, the range was between −0.75 and +0.60 in August 1999 and between −0.25 and +0.67 in August 2009. It was between −0.26 and +0.63 in August 2015 (Table 2).

The higher minimum in 1999 was due to the upper water level in Hamoun Wetland, and during the years, the water level has decreased, and the minimum range has also decreased.

The linear regression between NDVI and albedo is shown in Figure 3. The regression between the NDVI and albedo showed a high correlation between these two indices, with the coefficient of



determination $R^2 = 0.72$ and the negative correlation coefficient $R = -0.849$.

3.3 Degradation intensity map (August 1999)

Evaluation of degradation intensity based on the albedo–NDVI model in the study area in August 1999 showed 28.72% of the study area was classified in the severe degradation class and 31.79% was in the extreme one (Figure 4, Supplementary Table S3). Based on the degradation intensity map results, severe and extreme degradation intensities were observed in parts of the wetland that has been already dried up. This year, 10.22% of the study area was covered with water (Figure 5A).

3.4 Degradation intensity map (August 2009)

Evaluation of degradation intensity based on the albedo–NDVI model in the study area in August 2009 showed that 7.89% was classified as severe degradation intensity and 35.59% was in the extreme class (Figure 4, Supplementary Table S3). Based on the degradation intensity map, severe and extreme degradation intensities were observed in some parts of the wetland and the central and agricultural land in the study area (Figure 5B).

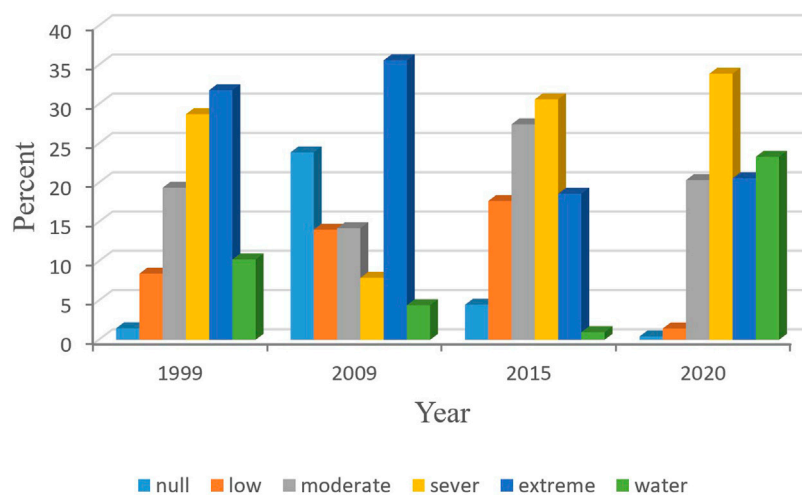


FIGURE 4
Degradation intensity percent for study periods.

3.5 Degradation intensity map (August 2015)

Evaluation of degradation intensity based on the albedo–NDVI model in the study area in August 2015 showed 30.62% of the area in the severe degradation intensity and 18.60% in the extreme class. Approximately all wetland area was dry and without water (Figure 4, Supplementary Table S3). Additionally, severe and extreme degradation intensities were observed in the north and west of the studied region, which indicated the wetland area (Figure 5C).

3.6 Degradation intensity map (August 2020)

Evaluation of degradation intensity based on the albedo–NDVI model in the study area in August 2020 showed 33.88% of the area in the severe degradation intensity and 20.57% in the extreme class (Figure 4, Supplementary Table S3). Moreover, severe and extreme degradation intensities were observed in the north and west of the studied region. Due to the flooding of the wetland in 2020, the extreme degradation class decreased (Figure 5D). The description of degradation intensity classes is shown in Table 3.

3.7 Degradation intensity changes from 1999 to 2020

The rate changes in degradation intensity classes around the studied period 1999–2020 showed that 3.72% of the area without

degradation and 2.88% of the area with low degradation intensity have decreased. Also, the area of severe degradation class has increased by 6.36 percent, and the area of extreme degradation class has decreased by 8.44%. Due to the flooding of the wetland in 2020, the highest degradation intensity in the study area occurred from 2015 to 2020. In the four studied periods, the regions without degradation, with low degradation, and with medium degradation decreased, but those with severe and extreme intensity increased. The average of changes in all classes was about +5.81% for 1999–2009, +3.43% for 2009–2015, +9.24% for 1999–2015, –13.11% for 1999–2020, –18.92% for 2009–2020, and –22.35% for 2015–2020 (Table 4).

3.8 The intensity of changes from 1999 to 2020

The results of the evaluation of the intensity changes based on the change vector analyses showed that 56.16% of the area had extreme changes, and the highest level of changes occurred in the wetland area (Figure 6). Table 5 shows the intensity change classification from 1999 to 2020.

3.9 Degradation intensity map accuracy

The confusion matrix between the degradation intensity map obtained from the albedo–NDVI model and the degradation based on the linear coefficient of variation derived from brightness and greenness indices was used to evaluate the accuracy of the degradation intensity map classification. The

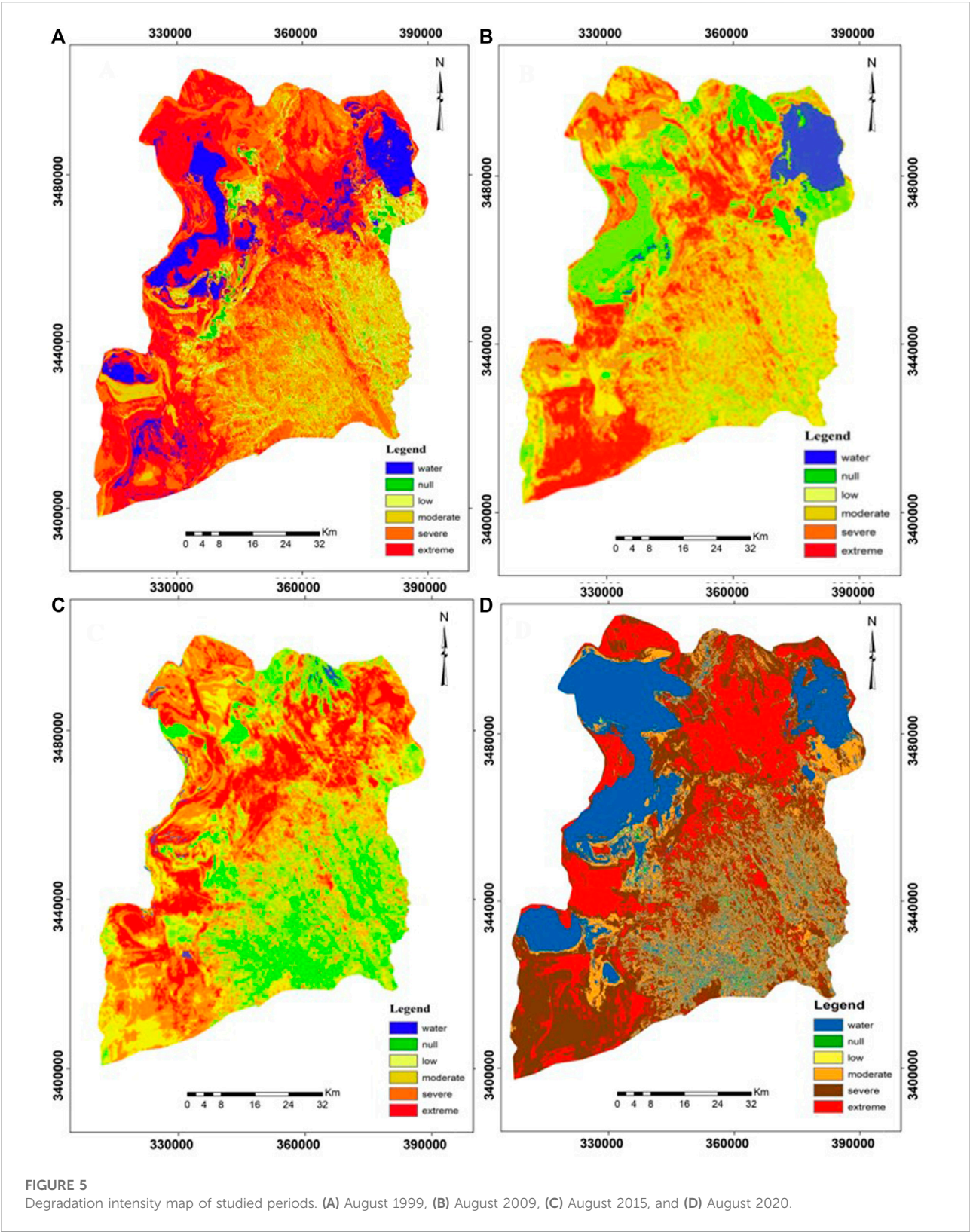


FIGURE 5
Degradation intensity map of studied periods. (A) August 1999, (B) August 2009, (C) August 2015, and (D) August 2020.

confusion matrix for 1,476 pixels showed that the kappa coefficient was 0.705 (Table 6).

4 Discussion

In this research, we studied the degradation intensity of a region using a remote sensing technique based on spectral reflectance from the earth’s surface.

A linear regression analysis between NDVI and the albedo index showed a negative and strong relationship ($r = -0.849$), consistent with the results presented by Pan and Li (2013), Karnieli et al. (2014), and Piña et al. (2016). Increased NDVI is accompanied by a decline in albedo, where areas with high albedo indicate vegetation degradation and bare soil. In the study area, due to frequent droughts, drying of Lake Hamoun, and high evaporation intensity, vegetation is one of the points of desertification, consistent with the study of Zolfaghari et al.

TABLE 3 Description of different degradation intensities in the study area.




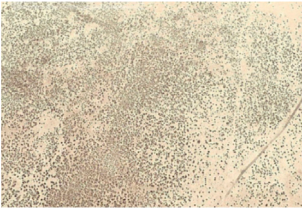

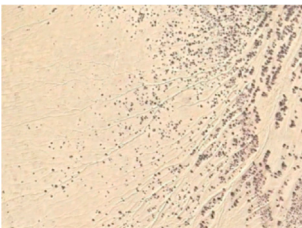


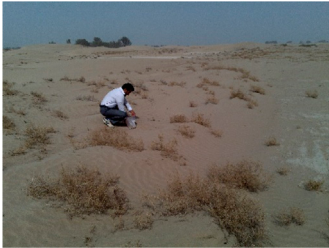
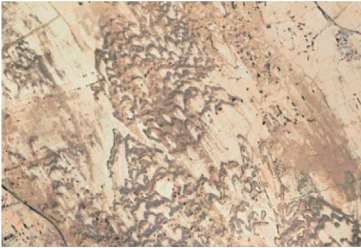
Class	Field image	Google Earth image	Description
1—Null: non-degradation			It is located generally in the south and east of the study area. The dominant vegetation in this class is <i>Tamarix aphylla</i> and <i>Alhagi camelorum</i> . These areas are supplied by the flooding of the Helmand River (Zolfaghari et al., 2019)
2—Low			These areas mainly refer to moderate class of degradation. The dominant vegetation in this class is <i>Desmostachya bipinnata</i> (Zolfaghari et al., 2019)
3—Moderate			Abandoned lands and destroyed agricultural land are in this class, and its vegetation is sparse <i>Tamarix</i> trees (Zolfaghari et al., 2019)
4—Severe			This category refers to zones with hard clay lands with very low <i>Tamarix</i> and halophyte vegetation. Severe degradation intensity was observed in the northern and western parts of the studied region located in Saburi Hamoun. This grade of degradation includes playa fans with fine sediment (Zolfaghari et al., 2019)
5—Extreme			This class corresponds to the dense sand dunes, eroded marl terrace, and low vein combined with claypan and basin hole. It is located generally in a large part of Saburi and Puzak Hamoun in Iran and Afghanistan; the area is dry, and the soil is bare due to the prevailing drought conditions in the wetland. Except for a few spots of scattered vegetation, the triple hamouns are affected by wind erosion (Zolfaghari et al., 2019)

TABLE 4 Percentage of changes in degradation intensity classes in the study periods (1999–2020).

Water	Extreme	Severe	Medium	Low	Null	Intensity class year
10.22	31.79	28.72	19.37	8.43	1.47	1999
4.41	35.59	7.89	14.21	14.02	23.88	2009
0.98	18.60	30.62	27.44	17.68	4.68	2015
23.32	20.57	33.88	20.34	1.45	0.43	2020
−5.8	+3.8	−20.83	−5.16	+5.59	+22.41	Rate of changes between 1999 and 2009
−9.24	−13.19	+1.9	+8.07	+9.25	+3.21	Rate of changes between 1999 and 2015
+13.11	−11.22	+5.16	+0.97	−6.98	−1.04	Rate of changes between 1999 and 2020
−3.43	−16.99	+22.73	+13.23	+3.66	−19.2	Rate of changes between 2009 and 2015
+18.91	−15.02	+25.99	+6.13	−12.57	−23.45	Rate of changes between 2009 and 2020
+22.34	+1.97	+3.26	−7.1	−16.23	−4.25	Rate of changes between 2015 and 2020
+5.98	−8.44	+6.36	+2.69	−2.88	−3.72	Average

(2013). The degradation intensity map of the study area in 1999 revealed that the classes with the highest degradation intensity were observed in parts of the wetland that dried up, and there was no extreme class in the study area. In total, 28.72% of the area was classified into the severe degradation class and 31.79% into the extreme class. Evaluation of the degradation intensity map obtained from the albedo–NDVI for 2015 showed that 76.66% of the study area had an extreme, severe, and moderate degradation intensity class. A total of 49.22% of the area had an extreme and severe class, consistent with the results reported by Zolfaghari et al. (2011). As expected, the severe and extreme degradation classes in the proposed maps correspond to the areas with the minimum NDVI and the maximum albedo. Evaluation of the degradation intensity maps in 1999 and 2009 showed that 60.51% and 43.48% of the study area had severe and extreme degradation classes. One of the main reasons for the very high percentage of destruction in 1999 is the dryness of a large part of Saburi Hamoun in Afghanistan, as shown in Figure 5A. The rate of changes in degradation intensity classes showed that the highest intensity of changes occurred between 2015 and 2020 with 22.35% because a large part of Saburi and Puzak Hamoun in Iran and Afghanistan is dry, and the soil is bare due to the prevailing drought conditions in the wetland. Except for a few spots of scattered vegetation, the triple hamouns are affected by wind erosion. It is consistent with the studies of Rashki et al. (2015). Additionally, the rate of changes in degradation intensity classes between 2009 and 2020 was 18.92% and between 2009 and 2015 was 3.43%. It was 13.11% between 1999 and 2020, 9.24% between 1999 and 2015, and 5.81% between 1999 and 2009. The results showed that 22.32% of null areas, 17.28% of areas with low degradation, and 50.62% of areas with extreme degradation were reduced from 1999 to 2020. Meanwhile, 16.14% and 38.21% were added to areas with moderate and severe degradation classes, respectively. Additionally, the map of degradation intensity classes showed

that the highest degradation intensity is related to the northern, northwestern, and western parts of Hamoun International Wetland, corresponding to areas of the three hamouns that are dry and where the dust rises into the air (Rashki et al., 2015). Therefore, it can be said that albedo is one of the main parameters for inland studies whose effects on the environment should be discussed. Additionally, the maps prepared for albedo distribution (Supplementary Figures S1, S2) and NDVI classification (Supplementary Figures S3, S4) indicated that the lowest NDVI and the highest albedo value occurred in the northern and western parts of the study area, coinciding with the most intense degradation class. NDVI is among the indices sensitive to viable and healthy vegetation. The vegetation distribution map showed that over 65% of the study area was characterized by an NDVI of less than 0.15, representing bare soil. The results reported by Zolfaghari et al. (2011) of a part of the Sistan region revealed that vegetation indices were among the indices for determining desertification (Zolfaghari et al., 2011). Additionally, based on the surface albedo distribution map, 43% of the region had an albedo value larger than 0.45. To evaluate the relationship between these two indices, we selected 600 points randomly where the regression correlation between the NDVI and albedo index showed a negative and robust correlation coefficient with a value of $r = 0.849$. These were compatible with the studies by Zongyi et al. (2011), Pan and Li (2013), Cordeiro et al. (2015), and Querino et al. (2016). Investigation of the degradation intensity map of the albedo index and NDVI indicated that 79.88, 57.69, 76.66, and 74.79% of the study area were found to belong to very intense, intense, and moderate degradation classes for 1999, 2009, 2015, and 2020, respectively. Over 49% of the region is characterized by very intense and intense degradation classes for 1999, 2015, and 2020, confirming the results reported by Zolfaghari et al. (2011). Additionally, according to Supplementary Figures S1, S2, and S4, intense and very intense degradation classes corresponded with areas with

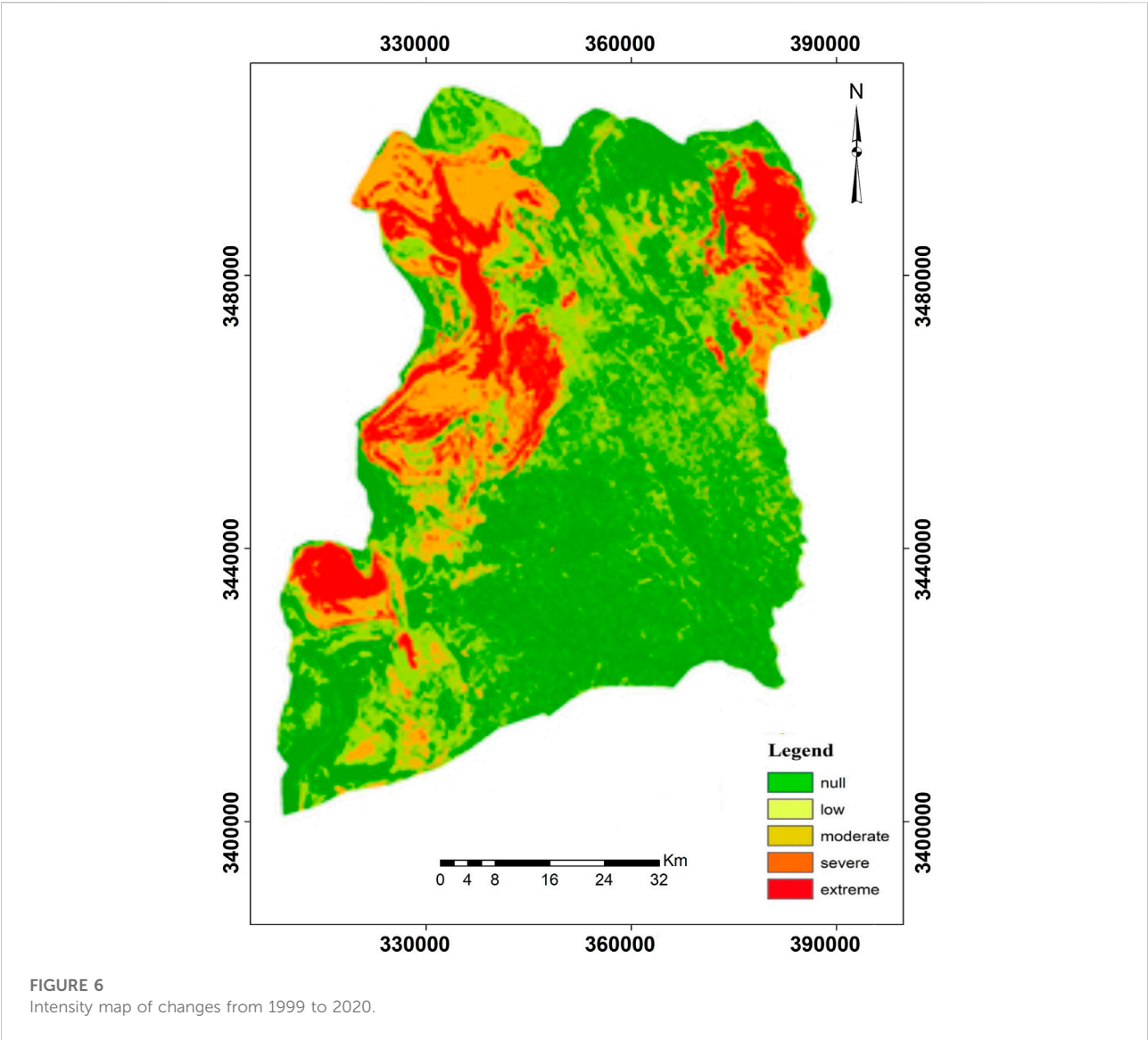


TABLE 5 Intensity change classification from 1999 to 2020.

Percentage	Area (ha)	Intensity of change	Row
22.34	27,639.36	Low change	1
14.13	17,475.3	Moderate change	2
7.37	9,120.06	High change	3
56.16	69,462.36	Extreme change	4

the minimum NDVI and maximum albedo values. In this study, it was found that the value of surface albedo in each area is influenced by the characteristics of that area. The map of degradation intensity classes indicated that the highest degradation intensity occurred in the northern, northwestern,

TABLE 6 Results of the confusion matrix.

N = 1,476	Predicted NO	Predicted YES
Actual NO	TN = 81	FP = 325
Actual YES	FN = 28	TP = 1,042

According to Pina et al. (2016), a coefficient between 0.7 and 0.85 indicates high compliance (Piña et al., 2016). So, we can say that the classification of desertification intensity based on the albedo-NDVI model in the study area has acceptable compliance with the degradation intensity changes that occurred in the same period.

and western parts of the Hamoun International Wetland. Thus, albedo is one of the important parameters in land use-related studies that should be discussed further due to its environmental impacts.

5 Conclusion

Results of the different periods showed that the areas without degradation and with low intensity of degradation decreased and were added to those with severe class from 1999 to 2020. However, the area of extreme class fluctuated and did not follow a general trend due to fluctuations in water and the level of dewatering of the wetland. When the surface of the wetland dries up, the surface of the land is free of moisture and vegetation and classified as extreme degradation class because the rate of albedo increases and the NDVI decreases. Additionally, when the wetland is flooded, the degradation area is highly reduced. Unlike expectations, the land area without any degradation increased in 2009 due to the temporarily created vegetation.

In summary, the results obtained are as follows:

1. The highest intensity of degradation occurred outside Iran between Hamoun Puzak and Saburi inside Afghanistan during the study period, consistent with the highest albedo and the lowest NDVI in these areas.
2. The highest intensity of changes in Saburi, Puzak, and Helmand hamouns occurred during the study period due to the presence of water or drought in Hamoun International Wetland.
3. The intensity of the changes based on the change vector analysis between 1999 and 2020 also showed that the most severe changes occurred in the range of the triple hamouns.
4. Degradation intensity maps (with Kappa coefficients ranging from 0.7 to 0.85) prepared using the albedo–NDVI model, are highly accurate compared to the maps derived from the change vector analysis models.
5. Monitoring of degraded areas with lack of access to the field can be done with this technique with high accuracy.
6. The development and use of this model may be a new step toward identifying and monitoring degradation in remote areas and determining dust sources in areas prone to wind erosion.

References

- Ali Baig, M. H., Zhang, L., Shuai, T., and Tong, Q. (2014). Derivation of a tasseled cap transformation based on Landsat 8 at-satellite reflectance. *Remote Sens. Lett.* 5 (5), 423–431. doi:10.1080/2150704X.2014.915434
- Allen, R., Tasumi, M., and Trezza, R. (2002). *SEBAL (surface energy balance algorithms for land)-advanced training and user's manual-idaho implementation, version 1.0*.
- BdaS, Bernardo, Alexandra, C. B., Celia, C. B., MmdeO, Leidjane, Suzana, M. G. L. M., and Bernardo, B. J. (2016). Procedures for calculation of the albedo with OLI-Landsat 8 images: Application to the Brazilian semi-arid. *Rev. Bras. Eng. Agric. Ambient.* 20 (1), 3–8. doi:10.1590/1807-1929/agriambi.v20n1p3-8
- Cai, G., Du, M., and Liu, Y. (2010). Regional drought monitoring and analyzing using MODIS data—A case study in yunnan province. *Proc. 4th IFIP Int. Fed. Inf. Process.* 345, 243–251.
- Chooari, O., Zawar, R. P., and Sturman, A. (2014). The wind of 120 days and dust storm activity over the Sistan Basin. *Atmos. Res.* 143, 328–341. doi:10.1016/j.atmosres.2014.02.001
- Cordeiro, M. C., Santos, N. A., Silva, V. M. A., Luiz, D. M., and Silva, V. P. R. (2015). Case study: Identification of desertification in the years 1999, 2006, and 2011 in mossoró-rn. *Jour. Hyp. Rem. Sen.* 4, 101–106. doi:10.29150/jhrs.v5.4.p101-106
- Eftekhari, R., Shahriyari, A. R., and Ekhtesasi, M. R. (2015). Assessment and mapping of current and potential desertification using MICD Model with emphasis on wind erosion criteria in the southwest of Hirmand city. *J. Dev. Geogr.* 38, 139–150.
- FAO (2015). *Analysis on water availability and uses in Afghanistan river basins: Water accounting through remote sensing (WA+) in Helmand River Basin*. FAO Project TCP/AFG/3402, 50.
- Fozuni, L. (2007). *Evaluation of the current status of desertification Sistan plain using modify MEDALUS Model with emphasis on wind and water erosion criteria*. Master's degree in desertification thesis. The University of Zabol.
- Goudei, A. S., and Middleton, N. J. (2006). *Desert dust in the global System*. Heidelberg: Springer Verlag, 1–287.

Data availability statement

The original contributions presented in the study are included in the article/[Supplementary Material](#); further inquiries can be directed to the corresponding author.

Author contributions

FZ: formal analysis and writing the original draft. HKh: methodology. HA: conceptualization. GhZ: data curation. SKS: software.

Conflict of interest

The authors declare that the research was conducted in the absence of any commercial or financial relationships that could be construed as a potential conflict of interest.

Publisher's note

All claims expressed in this article are solely those of the authors and do not necessarily represent those of their affiliated organizations, or those of the publisher, the editors, and the reviewers. Any product that may be evaluated in this article, or claim that may be made by its manufacturer, is not guaranteed or endorsed by the publisher.

Supplementary material

The Supplementary Material for this article can be found online at: <https://www.frontiersin.org/articles/10.3389/fenvs.2022.902687/full#supplementary-material>

- Han, L., Zhang, Z., Zhang, Q., and Wan, X. (2015). Desertification assessments in the Hexi corridor of northern China's Gansu Province by remote sensing. *Nat. Hazards (Dordr)*. 75, 2715–2731. doi:10.1007/s11069-014-1457-0
- Houldcroft, C. J., Grey, W. F., Barnsley, M., Taylor, C. M., Los, S. O., and North, P. R. J. (2009). New vegetation albedo parameters and global fields of soil background albedo derived from MODIS for use in a climate model. *J. Hydrometeorol.* 10, 183–198. doi:10.1175/2008JHM1021.1
- Kang, H., and Hong, S. (2008). An assessment of the land surface parameters on the simulated regional climate circulations: The 1997 and 1998 East Asian summer monsoon cases. *J. Geophys. Res.* 113, D15121. doi:10.1029/2007jd009499
- Kariminazar, M., Mosaaedi, A., and Moghadamnia, A. R. (2010). Investigation of climatic factors affecting the occurrence of drought (Case Study of Zabol Region). *J. Water Soil Conservation* 17 (1), 145–158.
- Karnieli, A., Qin, Z., Wu, B., Panov, N., and Yan, F. (2014). Spatio-temporal dynamics of land-use and land-cover in the mu us sandy land, China, using the change vector analysis technique. *Remote Sens.* 6, 9316–9339. doi:10.3390/rs6109316
- Khosravi, H., Haydari, E., Shekoohizadegan, S., and Zareie, S. (2017). Assessment the effect of drought on vegetation in desert area using Landsat data. *Egypt. J. Remote Sens. Space Sci.* 20, S3–S12. doi:10.1016/j.ejrs.2016.11.007
- Lamchin, M., Lee, J. Y., Lee, W. K., Lee, E. J., Kim, M., Lim, C. H., et al. (2016). Assessment of land cover change and desertification using remote sensing technology in a local region of Mongolia. *Adv. Space Res.* 57 (1), 64–77. doi:10.1016/j.asr.2015.10.006
- LANDSAT 8 (L8) Data users handbook, (2015). The Landsat 8 Data User's Handbook is a living document prepared by the U.S. Geological Survey Landsat Project Science Office at the Earth Resources Observation and Science (EROS) Center in Sioux Falls, Greenbelt, Maryland: Zanter LSOS CCB Chair USGS. Version 1.0.
- Mohammad Ghasemi, S., GhR, Zehtabian, and Ahmadi, H. (2008). Assessment of desertification intensity based on water index using MEDALUS methodology. *Pajouhesh Sazandegi* 80, 59–67.
- Myhre, G., and Myhre, A. (2003). Uncertainties in radiative forcing due to surface albedo changes caused by land-use changes. *J. Clim.* 16, 1511–1524. doi:10.1175/1520-0442-16.10.1511
- Pan, J., and Li, T. (2013). Extracting desertification from Landsat TM imagery based on spectral mixture analysis and Albedo- Vegetation feature space. *Nat. Hazards (Dordr)*. 68, 915–927. doi:10.1007/s11069-013-0665-3
- Parvariasl, H., Pahlavanravi, A., and Moghaddamnia, A. R. (2010). Assessing desertification hazard in Neiyatak region using ESAs Model. *J. Iran Nat. Resour.* 2, 42–54.
- Piña, R. B., Diaz-Delgado, C., Mastachi-Loza, C. A., and González-Sosa, E. (2016). Integration of remote sensing techniques for monitoring desertification in Mexico. *Hum. Ecol. Risk Assess. Int. J.* 22, 1323–1340. doi:10.1080/10807039.2016.1169914
- Querino, C. A. S., Beneditti, C. A., Machado, N. G., Silva, M. J. G., da Silva Querino, J. K. A., dos Santos Neto, L. A., et al. (2016). Spatiotemporal NDVI, LAI, albedo, and surface temperature dynamics in the southwest of the Brazilian Amazon forest. *J. Appl. Remote Sens.* 10 (2), 026007. doi:10.1117/1.JRS.10.026007
- Rashki, A., Kaskaoutis, D. G., Francois, P., Kosmopoulos, P. G., and Legrand, M. (2015). Dust- storm dynamics over Sistan region, Iran: Seasonality, transport characteristics and affected areas. *Aeolian Res.* 16, 35–48. doi:10.1016/j.aeolia.2014.10.003
- Scott, D. A., and Smart, M. (1992). Wetlands of the sistán basin, south caspian, and fars, islamic republic of Iran. *Ramsar Conv. Monit. Proced. Rep. No.*, Gland, Switzerland: Ramsar Convention Bureau 26, 53.
- UNEP (2002). *Sistan oasis parched by drought*, Geneva: UNEP/DEWP/GRID-Geneva, 11–21. 87 pp
- Wei, H., Wang, J., and Han, B. (2020). Desertification information extraction along the China-Mongolia railway supported by multisource feature space and geographical zoning modeling. *IEEE J. Sel. Top. Appl. Earth Obs. Remote Sens.* 13, 392–402. doi:10.1109/jstars.2019.2962830
- Wu, Zh, Lei, Sh, Bian, Zh, Huang, J., and Zhang, Y. (2019). Study of the desertification index based on the albedo-MSAVI feature space for semi-arid steppe region. *Environ. Earth Sci.* 78 (6), 232. doi:10.1007/s12665-019-8111-9
- Zhao, Y., Wang, X., Novillo, C. J., Arrogante-Funes, P., Vázquez-Jiménez, R., and Maestre, F. T. (2018). Albedo estimated from remote sensing correlates with ecosystem multifunctionality in global drylands. *J. Arid. Environ.* 157, 116–123. doi:10.1016/j.jaridenv.2018.05.010
- Zolfaghari, F., Khosravi, H., Shahriyari, A., Jabbari, M., and Abolhasani, A. (2019). Hierarchical cluster analysis to identify the homogeneous desertification management units. *PLoS ONE* 14 (12), 0226355–e226421. doi:10.1371/journal.pone.0226355
- Zolfaghari, F., Shahriyari, A., and Fakhireh, A. (2013). Evaluate the effect of vegetation cover on land degradation process using IMDPA model and GIS (Case study: Sistan plain). *J. Appl. RS GIS Tech. Nat. Resour. Sci.* 4 (1), 69–77.
- Zolfaghari, F., Shahriyari, A., Fakhireh, A., Rashki, A. R., Noori, S., and Khosravi, H. (2011). Assessment of desertification potential using IMDPA model in Sistan plain. *Watershed Manag. Res.* 9, 97–107.
- Zongyi, M., Yaowen, X., Jizong, J., Linlin, L., and Xiangqian, W. (2011). The construction and application of an albedo-NDVI based desertification monitoring model. *Procedia Environ. Sci.* 10, 2029–2035. doi:10.1016/j.proenv.2011.09.318

Frontiers in Environmental Science

Explores the anthropogenic impact on our natural world

An innovative journal that advances knowledge of the natural world and its intersections with human society. It supports the formulation of policies that lead to a more inhabitable and sustainable world.

Discover the latest Research Topics

[See more →](#)

Frontiers

Avenue du Tribunal-Fédéral 34
1005 Lausanne, Switzerland
frontiersin.org

Contact us

+41 (0)21 510 17 00
frontiersin.org/about/contact

